Advances in Meteorology

Observations and Modeling of the Climatic Impact of Land-Use Changes 2014

Guest Editors: Xiangzheng Deng, R. B. Singh, Qun'ou Jiang, Jinwei Dong, and Hongbo Su

Observations and Modeling of the Climatic Impact of Land-Use Changes 2014

Advances in Meteorology

Observations and Modeling of the Climatic Impact of Land-Use Changes 2014

Guest Editors: Xiangzheng Deng, R. B. Singh, Qun'ou Jiang, Jinwei Dong, and Hongbo Su

Editorial Board

Contents

Hindawi Publishing Corporation
Advances in Meteorology
Volume 2015, Article ID 592636, 2 pages
http://dx.doi.org/10.1155/2015/592636

Editorial

Observations and Modeling of the Climatic Impact of Land-Use Changes 2014

Xiangzheng Deng,[1] R. B. Singh,[2] Qun'ou Jiang,[3] Jinwei Dong,[4] and Hongbo Su[5]

[1]*Institute of Geographic Sciences and Natural Resources Research, Chinese Academy of Sciences (CAS), Beijing 100101, China*
[2]*Department of Geography, Delhi School of Economics, University of Delhi, Delhi 110007, India*
[3]*School of Soil and Water Conservation, Beijing Forestry University, Beijing 100038, China*
[4]*Department of Microbiology and Plant Biology, Center for Spatial Analysis, University of Oklahoma, Norman, OK 73019, USA*
[5]*Department of Civil, Environmental and Geomatics Engineering, Florida Atlantic University, Boca Raton, FL 33431-0991, USA*

Correspondence should be addressed to Xiangzheng Deng; dengxz.ccap@gmail.com

Received 4 May 2015; Accepted 4 May 2015

Land Use and Cover Change (LUCC) is synthetically driven by a combination of natural and human induced factors including urbanization, grassland degradation, cultivated land reclamation, deforestation, and geological hazards. LUCC has been observed at different spatial and temporal scales in the context of regional or global climate changes. At the same time, LUCC can respond to and make an important impact on the global or regional climate changes. For example, LUCC directly changes the land surface conditions, such as albedo, roughness, and imperviousness, and indirectly changes the aerosol and compositions in the atmosphere, which in turn will change the energy balance and mass exchanges at the land and atmospheric interface. Study of the climatic impact of LUCC is of interest to both scientists and policy makers. Investigation of the interaction between LUCC and climate changes is a hot research topic in the scientific community, although it remains a challenging task because of the strong coupling between LUCC and climate changes. For example, to correctly interpret long term data records of surface temperature observations from meteorological stations, the site locations have to be distinguished between rural areas and urban areas. To improve our understanding of the climatic impact of LUCC, we need to develop more observation techniques, observation datasets, and modeling frameworks to support the data analysis, decision making of LUCC.

The studies included in this special issue cover diversified areas in LUCC and climate changes. The first category of the studies is on observation techniques and observation datasets related to LUCC and the climatic impact. Y. Li et al. observed the different impact of land use patterns on the evapotranspiration for a grassland ecosystem. B. Yang et al. studied the impact of body of water in a city on the heat island effect using satellite based land surface temperature observations. Their finding is, the area and spatial locations of the body of water can be optimized to maximize the cooling effects from the waters in urban areas. X. Che et al. developed a method to downscale the MODIS surface reflectance to improve the extraction of body of water. X. Yao et al. used the LUCC data in 20 years to study the impact on regional temperature and precipitation in the middle and lower reaches of the Yangtze River. It was revealed that the impact of LUCC on regional temperature is significant, but not on regional precipitation in this region. W. Hu et al. investigated the relationship between the land use intensity and the surface temperature changes in the Dongting Lake area, China, from year 2001 to year 2010 based on the datasets derived from Landsat TM. It was reported that the surface temperature was more sensitive to the land use intensity in low altitude areas than in high altitude areas.

The second category of studies in this special issue is on the modeling of LUCC and the climatic impact. M. Wang and X. Yan used two methods named the "urban minus rural" and the "observation minus reanalysis" to quantify the potential impact of the urbanization in the Beijing-Tianjing-Hebei metropolitan area on the regional temperature changes. Seasonal patterns of the regional temperature changes were simulated and it was found out that the latter

method performed relatively better in this case study. F. Wu et al. did scenario analysis of potential climate changes and LUCC in Heihe River Basin of China using the Soil and Water Assessment Tool (SWAT) and investigated the hydrological impact in different scenarios. Z. Wang et al. used a structural equation model to study the impact of LUCC on the regional climate in Southern China. F. Wu et al. used a hydrologic model and scenario analyses to quantify the impact of forest area changes in the head-water area of a river basin on the water yield variation. Z. Li et al. used the binary panel logit regression to separate the impact of LUCC, economic development, and climate change on the land degradation represented by the NDVI.

This special issue also includes a category of studies on adaptation/management of LUCC and the regional climate changes. X. Mao et al. investigated the efficiency of using constructed wetlands to remove the pollutant from the agricultural wastewater. The seasonal variation of the purification efficiency was reported in their study. X. Deng et al. identified the water scarcity issue for an ecologically fragile area in a river basin in northwestern China and proposed solutions to adapt to the regional climate changes. W. Song et al. assessed the different impact of two vital ecological policies (Grain-for-Green and Grain-for-Blue) on the ecosystem service values based on the net primary productivity and soil erosion. D. Lin and Y. Lin used an empirical analysis to model the game situation and analyze the game behaviors of stakeholders of voluntary forest carbon offset projects in China. They concluded that a win-win solution can be achieved through the joint participation and a compromise in the voluntary forest carbon offset projects. C. Shi et al. developed a system to optimize the land use zoning to maximize the ecosystem service values under scenarios of LUCC and climate changes for the middle reaches of Heihe River Basin in North China. G. Jin et al. employed the fuzzy weight of evidence model to assess the land use suitability in a mountain area to avoid the potential geological hazards in a scenario of rapid urbanization in Yunan Province, China. D. Yuan et al. presented a method to establish the feasibility of Certified Emission Reduction (CER) quantitative evaluation, in order to implement the Clean Development Mechanism (CDM) at the United Nations Framework Convention on Climate Change (UNFCCC).

All the papers in this special issue presented a collection of latest research results in the field of observations and modeling of the climatic impact of land-use changes. This special issue is intended to advance our understanding of the mechanisms and impacts of LUCC on climate change and even the human well-being. We are quite optimistic that these articles would be of great interest to the readers of this journal and will be of help to address the new emerging challenges in this field.

Acknowledgments

As guest editors of this special issue, we would like to thank all the authors for their contributions to this volume. Special mention of thanks and appreciation is due to the international panel of reviewers for making their expertise available for evaluation of the manuscripts.

Xiangzheng Deng
R. B. Singh
Qun'ou Jiang
Jinwei Dong
Hongbo Su

Hindawi Publishing Corporation
Advances in Meteorology
Volume 2015, Article ID 563673, 10 pages
http://dx.doi.org/10.1155/2015/563673

Research Article

Impacts of Land Use Change on the Regional Climate: A Structural Equation Modeling Study in Southern China

Zhanqi Wang, Bingqing Li, and Jun Yang

School of Public Administration, China University of Geosciences, Wuhan 430074, China

Correspondence should be addressed to Zhanqi Wang; zhqwang@cug.edu.cn

Received 17 September 2014; Revised 17 February 2015; Accepted 23 February 2015

Academic Editor: Jinwei Dong

With the frequent human activities operating on the earth, the impacts of land use change on the regional climate are increasingly perceptible. Under the background of the rapid urbanization, understanding the impacts of land use change on the regional climate change is vital and significant. In this study, we investigated the relationships between land use change and regional climate change through a structural equation model. Southern China was selected as the study area for its rapid urbanization and different structure of land use among its counties. The results indicate that the path coefficients of "vegetation," "Urban and surrounding area," and "other" to "climate" are −0.42, 0.20, and 0.46, respectively. Adding vegetation area is the main method to mitigate regional climate change. Urban and surrounding area and other areas influence regional climate by increasing temperature and precipitation to a certain extent. Adding grassland and forestry, restraining sprawl of built-up area, and making the most use of unused land are efficient ways to mitigate the regional climate change in Southern China. The results can provide feasible recommendations to land use policy maker.

1. Introduction

Human activities have played a dominant role in land use change, especially in the recent decades [1]. With acceleration of urbanization and industrialization, the average income and living standard have been improved obviously. Hence, the increasing material demands have led to rapid build-up area expansion and resources development, all of which have largely influenced the land use structure [2]. Firstly, the phenomenon that a large number of rural population transfer to the city continuously adds the demand for living and production room, which has a lot of land surrounding cities replaced by asphalt, metal, buildings, vegetative cover, and other anthropogenic lands [2, 3]. Secondly, in order to feed more people, forestry and grassland will be cultivated and nature land would be changed into cultivated and built-up land. Consequently, the land surface is changed significantly to provide more resources and room for human beings. The land use change, caused by human activities mentioned above, has generated a series of ecological and climatic problems and aroused widespread concern among scholars. So far, a great number of researches have documented the relationship of land use change and regional climate change. For example, Pielke Sr. pointed out that land use change played a first-order role in climate-forcing effect [1]. Cai and Kalnay put forward the view that two-thirds of warming over the past four decades was caused by land use change [4]. The Intergovernmental Panel on Climate Change reported that the addition of artificial land could raise the greenhouse gas in the air by fossil fuel burning, which contributed to the change of average temperature [5]. Deng et al. thought that land use and cover change could influence the ecosystems at local, regional, and global scales and affected climate change in the direct or indirect way [6]. Conversely, climate can influence the urban development, growth of vegetation, and production of cultivated land, among others. The climate change is one of the most important agents in the change of land use.

Now, it is widely accepted that the impacts of land use change on the regional climate change include two aspects which are biogeophysics and biogeochemistry [7]. The biogeophysical effects refer to the change of physical parameters such as surface roughness, albedo, reflective and surface hydrology and vegetation transpiration characteristics. These

parameters are known for having close connection to the regional precipitation and temperature [8]. Meanwhile, the biogeochemical effects mainly refer to altering the chemical composition of atmosphere [9]. There are a lot of literatures which had contributed to the research of carbon and nitrogen storage during the process of land use change [10–13], which have significant impacts on the composition of atmosphere.

For those complicated relations between land surface's physical, chemical, and biological characteristics, the contributions of land use change to the regional climate system are different and some uncertainties are still existing in the current stage of investigation [14–16]. Massive methods are being applied to identify the impacts. For instance, the regional climate model which has high resolution can simulate the current climate and climate change by describing the change in boundary conditions of the land surface so as to analyze the effects of land use change on regional climate change [15, 17]. Reliable land use information is necessary in the regional climate model. Keeping the capacity of analyzing the radiation, energy, water, and dynamics interaction between atmosphere and land surface, the land surface model is used to integrate with regional climate model [6]. Furthermore, land use change evaluation models such as econometric model, agent-based model, scenario development, and their integration are invited to assess and simulate the land use change and regional climate in the future [18–21]. Referring to previous researches, it is obvious that most of them study the impacts between land use change and regional climate through land surface parameters such as evapotranspiration, roughness, and leaf area index. However, the quantitative analysis by the data of land use and regional climate is insufficient. Hence, we think that the relationship between panel data of land use and regional climate can be revealed by empirical statistical method, which is helpful to recognize the impacts of land use change on regional climate.

Taking advantage of abundant forestry and water resources, Southern China is experiencing the fast growth of population and rapid development of economy. Since Southern China is facing the crucial period of accelerating industrialization and urbanization, the urban development and land use structure are quite different among the counties. It will vary the regional climate environment further. Considering its typical climatic condition, rapid urbanization, and significant differences of land use structure among counties, Southern China was selected as the case study area. Therefore, in this study, the impacts of land use change on the regional climate in Southern China were quantitatively analyzed from the county level. And based on a statistical model, the effect significance and direction of each land use classification are assessed. The results can be used to provide certain reference for the decisions making of land use planning and policy so as to mitigate the regional climate change by land use change in the area.

2. Data and Methodology

2.1. Study Area. Southern China (located between 18°10′N~26°24′N and 104°26′E~117°20′E) is one of the seven geographic partitions in China. The study area has a total land area of 451900 km^2 covering three provinces which are Guangdong Province, the Guangxi Zhuang Autonomous Region, and Hainan Province (Figure 1). It is not just an important grain production base but also an excellent base of tropical crops in China.

As a typical tropic and subtropics monsoon climate region, Southern China keeps the characteristics of rain, high temperature, and being evergreen. Its average temperature and precipitation are about 16.5°C~25.9°C and 1000~2600 mm, respectively. For the rich sunshine and water resources, its lush plants account for 63.71% of the total area in 2005, most of which involve tropical rain forestry, monsoon forestry, and subtropical monsoon evergreen broad-leaved forestry. In recent years, the concerns of resources' rational use and protection have widely spread. Therefore, afforestation has been carried out frequently in Southern China.

With the rapid development of economy, the imbalanced development of agriculture, industry, and service industry results in the remarkable land use change in Southern China. Additionally, the imbalanced regional development causes the huge differences of regional land use. The irrational development and utilization of land resources have led to regional climate change to a certain extent. According to the temperature and precipitation data from meteorological observation station, it is clear that the temperature in Southern China coastal area is rising and the annual precipitation in southern China varies periodically. In order to optimize land use structure and mitigate the regional climate change, a series of plans were implemented, for example, ecological restoration projects [22]. Therefore, the exploration of land use change's impact mechanism on regional climate is significant and helpful to the policy making and sustainable development.

2.2. SEM (Structural Equation Model Analyses Variables' Relations by Covariance Matrix). Variables can be divided into four kinds: exogenous latent variables, endogenous latent variables, exogenous observed variables, and endogenous observed variables. Observed variables generally refer to objectives. By contrast, latent variables are difficult to be observed directly but can be indicated by several related observed variables. This new multivariate statistical analysis method integrated by traditional factor analysis and path analysis mainly describes two kinds of relationships: the relationships between latent and related observed variables and the relationships among latent variables [23, 24]. To solve questions mentioned above, SEM is divided into measurement component and structural component. The measurement component deals with the measurement errors and relationships between latent and related observed variables [25]. It specifies latent variables as some linear functions of their observed variables. The structural component's function is to capture the impacts of exogenous latent variables on endogenous latent variables and the impacts of endogenous latent variables upon one another [26]. The based equations are as follows:

$$\text{SEM} \begin{cases} \text{measurement component} & \begin{cases} Y = \bigwedge_Y \eta + \varepsilon \\ X = \bigwedge_X \xi + \delta \end{cases} \\ \text{structural component} & \eta = B\eta + \Gamma\xi + \zeta, \end{cases} \quad (1)$$

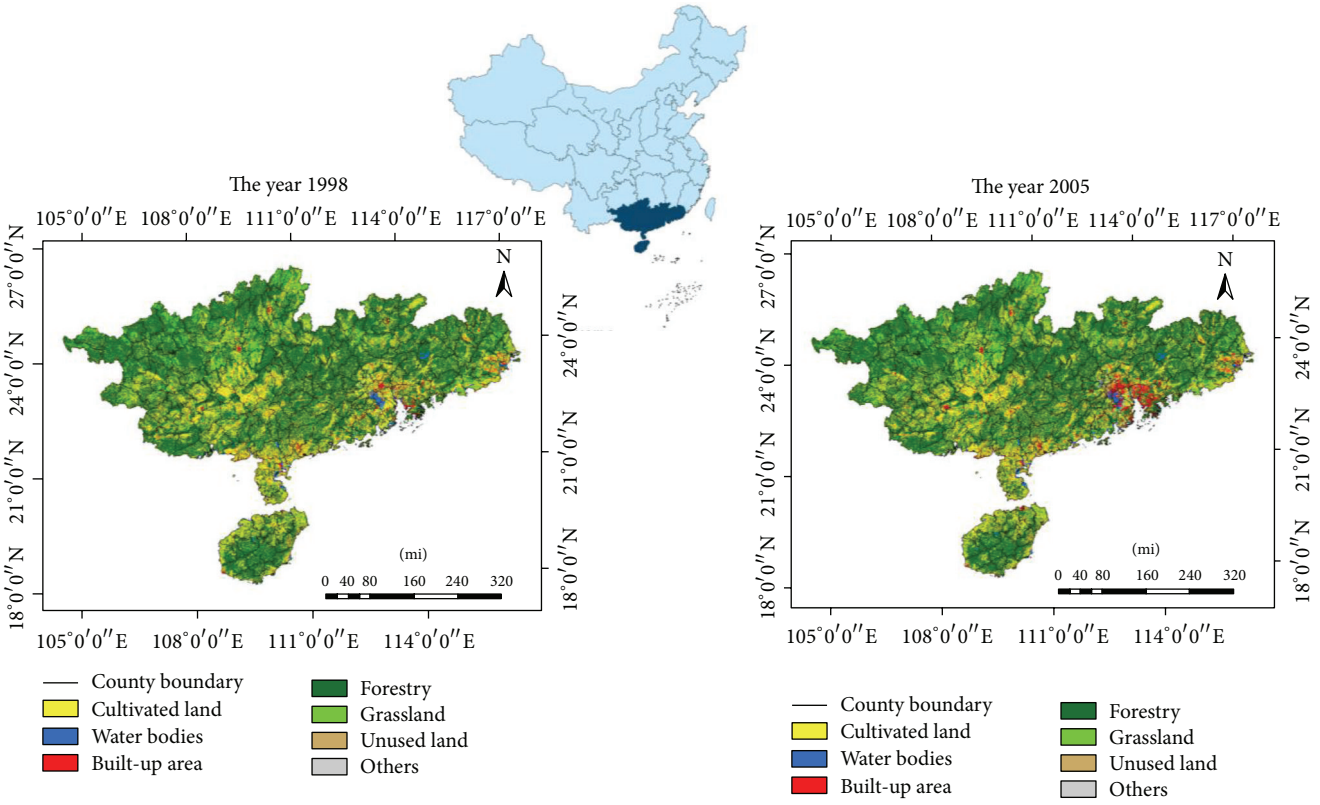

Figure 1: Location and the land use structure of Southern China.

where Y is endogenous observed variable, X is exogenous observed variable, η are endogenous latent variables, ξ are exogenous latent variables, and ε, δ are the measurement errors of Y and X, respectively. $\wedge_Y$, $\wedge_X$ are the relationships between latent and corresponding observed variables; B is the relationship among endogenous latent variables; Γ is the impact of exogenous latent variable on endogenous latent variable; ζ is the residual of η, reflecting the irresoluble parts. Figure 2 is the sketch of SEM. These ellipses represent latent variables; the rectangles represent observed variables; the lines (called paths) indicate that there are relationships between variables; arrows show the effect direction; "*a*-*b*" are path coefficients and "*c*–*h*" are factor loadings. Path coefficients and factor loadings are main research objects used in measuring relationships. Generally, an SEM can have any number of latent and observed variables.

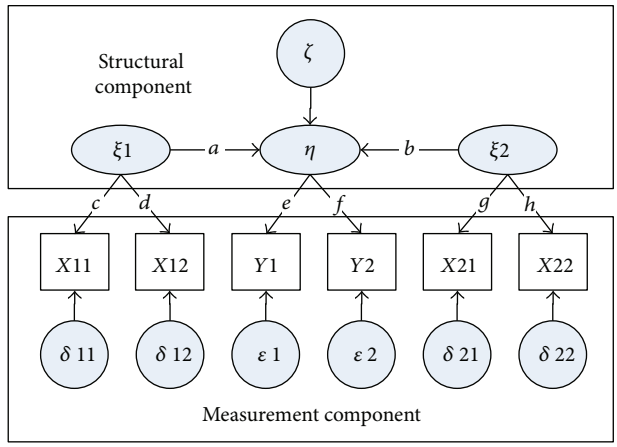

Figure 2: The sketch of SEM.

Compared with other traditional analysis methods, the SEM has the advantages of [26, 27]: (1) estimating multiple and interrelated dependence relationships at the same time; (2) allowing the measurement errors in the latent and observed variables; (3) the ability of dealing with unobserved variables making the model more flexible in application; (4) setting the entire relationship and goodness-of-fit; (5) handling nonnormal data; (6) accounting for missing data. Although SEM is mainly used in psychometrics and questionnaire analysis, it is worth noting that the model is being increasingly used in construction-related studies, where latent variables and measurement errors exist in regression model [28]. Because there are measurement errors and a series of interrelated unobserved variables in the assumptions, the SEM is applied in this research.

The implementation of SEM includes three steps [29]. Due to the fact that SEM is obtained by the modification of existing hypothesis, the first step is to put forward a hypothesis SEM based on the advance verification of data structure. The verification estimates the relationships of observed variables and can be gotten by principal component

analysis. Secondly, confirmatory factor analysis (CFA) is used to test the validity of hypothesis' measurement component. According to goodness-of-fit indices and theoretical meanings of variables, CFA will modify paths and fit model repeatedly until suitable corresponding relationships between latent and observed variables can be obtained. Finally, structural component is modified by the same method. Therefore, the factor loadings and path coefficients are explored. Most of the time, measurement and structural component are adjusting at the same time to get a more scientific model.

2.3. Data and Processing. The changes of land use and climate in Southern China were quantified by the differences between the years 1988 and 2005. The data used in the research mainly include (1) land use data of Southern China in the years 1988 and 2005 and (2) meteorological data in the years 1987 to 1989 and 2004 to 2006.

Firstly, the land use data (with a spatial resolution of 1 km × 1 km) were extracted from remote sensing digital images of the US landsat TM/ETM satellite, which were obtained from the Resources and Environment Data Center of the Chinese Academy of Science. According to United States Geological Survey Classification, the land use was interpreted into seven parts of cultivated land, forestry, grassland, built-up area, water bodies, unused land, and others (most is the extension for coastline). The land use of each county was obtained by above data and administrative area boundary of the counties of Southern China.

Secondly, we used surface temperature and precipitation to reflect the regional meteorology. The original data were collected from meteorology stations. Kriging interpolation algorithm estimates unknown samples by original data and the distribution and spatial structure of samples. Compared with other methods, it reflects samples' spatial structure and takes the chance to work with extreme data. So it is good in regional estimation of temperature and precipitation. With about 60 meteorological stations in the study area and more than 30 around it (Figure 3), the original data were interpolated into 1 km resolution grid data by Kriging [30]. The climates of the years 1988 and 2005 were indicated by the average values of the years 1987 to 1989 and 2004 to 2006, respectively. Afterward, we counted the annual average temperature and precipitation of each county by arithmetic average method.

We can see from the above data that the land use of Southern China had changed greatly from 1988 to 2005. Cultivated land and built-up area had reduced 3859 km^2 and increased 4369 km^2, accounting for 3.57% and 36.88% of their total, respectively. Their changes were significant. Additionally, unused land, grassland, water bodies, and forestry had reduced 489 km^2, 1490 km^2, 35 km^2, and 349 km^2, accounting for 60.59%, 4.78%, 0.28%, and 0.12%, respectively. In addition to the built-up area, they were all reduced to a certain degree. The proportion of unused land was the most obvious. From 1988 to 2005, the annual average temperature and precipitation of Southern China had changed 0.67°C and

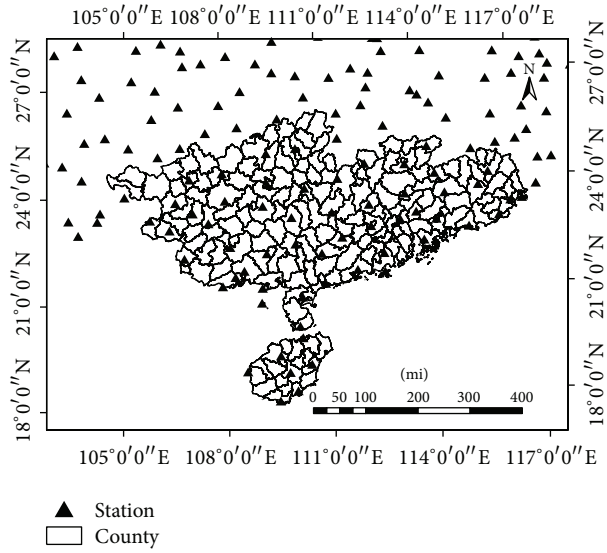

Figure 3: The distribution of meteorological station.

46.33 mm. There was obviously upward trend in annual average temperature. However, the annual average precipitation fluctuated frequently and showed no obvious trend.

Principal component analysis is an important way to get the basic SEM hypothesis which is put forward based on the advance verification of data structure. Principal component analysis' dimensionality reduction function is to replace the original variables by fewer variables. The new variables contain most information of original variables. Comparing the different relationship coefficient between original and new variables, we can classify the original variables and conclude the new variables' meanings. Therefore, the data structure is clearly defined and SEM hypothesis can be constructed.

The strong correlation among variables is necessary for principal component analysis. Kaiser-Meyer-Olkin (KMO) determines the correlation through comparing the simple and partial correlation coefficient. The greater value indicates the stronger correlation. Bartlett test of sphericity is testing the independent character of variables by correlation coefficients matrix. The two tests are usually used to examine the appropriateness of data for principal component analysis performance. It is often suggested that KMO value should be of 0.5 as a minimal level and Bartlett test should be significant. For the land use data, the KMO valuing 0.594 and significant Bartlett test result were proving that the data were suitable for principal component analysis.

The principal component analysis of the land use data was carried out by statistics software SPSS, whose result was shown in Table 1. The "1," "2," and "3" represented the three principal components. The rotated component matrix which consisted of the numbers below the three principal components was presenting how close correlations between variables and principal components were. The number was called the factor loading of variable on principal component. Considering the closest correlation, each variable was classified to a principal component. Finally,

Table 1: Rotated component matrix of principal component analysis.

	Principal component		
	1	2	3
Cultivated land	0.746	0.025	0.422
Forestry	−0.048	−0.071	0.837
Grassland	−0.065	−0.026	0.817
Water bodies	0.788	0.265	−0.132
Built-up area	0.823	0.015	−0.257
Unused land	0.158	0.939	−0.050
Others	0.065	0.953	−0.046

Notes: (1) principal component analysis was used; (2) orthogonal rotation method with Kaiser standardized was used and converged after four time iterations.

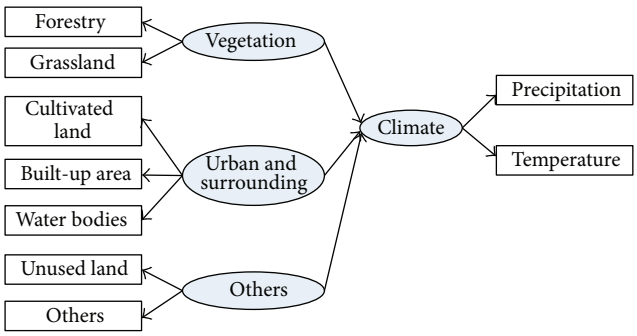

Figure 4: The basic hypothesis of structural equation model.

the land use classifications were divided into three parts: (1) vegetation area, including forestry and grassland; (2) urban and surrounding area, including cultivated land, built-up area, and water bodies; (3) other areas, including unused land and others. The cumulative contribution rate of the three principal components was 77.03%, which judged the possession of original information. Generally, cultivated land is related to vegetation. However, from the perspective of change, the cultivated land has closer relationship to built-up area. This is because cultivated land keeps the capacity of feeding. For the convenience of travelling, built-up area is surrounded by cultivated land. The production of cultivated land also should satisfy the need of humanity. Consequently, cultivated land and built-up were classified into one principal component which was called the urban and surrounding area.

The basic SEM hypothesis of the research is shown in Figure 4. The research took each county as a sample, so the sample size is 194. Based on above analysis, we regarded county's land use classifications as exogenous observed variables, regarded county's annual average temperature and precipitation as endogenous observed variables, regarded the three principal components as exogenous latent variables, and regarded climate as endogenous latent variable. The SEM reflected the relationships among above observed and latent variables.

2.4. Reliability Analysis. Reliability analysis is the foundation of this study's scientific benefit and properties. Reliability is used to test whether several variables can be used to explain the question together. So, it is also called the consistency of data. Before SEM analysis, the index of Cronbach's alpha is frequently used to investigate the consistency and reliability of measurements. When the Cronbach's alpha is greater than 0.7, these data are suitable for SEM analysis [23, 29, 31]. Obtaining standard data by statistics software SPSS, the Cronbach's alpha value of above data was calculated. The value of 0.734 indicated that the data could be used for SEM analysis.

3. Result and Discussion

The software LISREL 8.80 was used to confirm and modify the basic hypothesis in our research. As an important statistical method, the maximum likelihood estimation method keeps the optimal characters of unbiasedness, consistency, and efficiency. The result will not be influenced by the unit of measurement [32]. Taking advantage of these characters, the maximum likelihood estimation method was selected as the fitting way. After fitting, model was estimated by goodness-of-fit indices. Some modifications which included adding and deleting paths took place based on the path coefficients, T-values, modification indices, and the meaning of each variable. Finally, we got the suitable structural equation model which revealed the impacts of land use change on the regional climate in Southern China.

3.1. Confirmatory Factor Analysis. By the confirmatory factor analysis, we got the path coefficients between observed variables and latent variables as well as the measurement errors of the observed variables. Considering that a large amount of literature had confirmed that precipitation and temperature were the key variables to reflect the area climate [16, 33], this confirmatory factor analysis was mainly attributed to the path between land use classifications and the three principal components. There were many indices involved in the assessment of overall goodness-of-fit of SEM, of which we selected the following important seven indices as evaluation criteria [34, 35]. These indices measured the difference between the sample's covariance matrix and model-implied covariance matrix. Their meanings, equations, and criteria are shown in Table 2.

During the process of model modification, we deleted the path whose T-value was less than 1.96 and added the path by modification indices. Notably, all of the modifications were combined with proper theory analysis. As the result, the paths of "vegetation" → "cultivated land" and "vegetation" → "water bodies" were added to get a better fitting measurement model. The expansion of built-up area is based on the decrease of cultivated land due to the fact that the built-up area is surrounded by cultivated land. To satisfy the need of food, grassland, and forestry will be transformed to cultivated land. Therefore, the cultivated land has close relationship with "vegetation" and "urban and surrounding." Consequently, the path of "vegetation" → "cultivated land" was added. The land use maps (Figure 1) showed that the built-up area was always developed with water bodies, which kept the ability to reduce

Table 2: The meanings and equations of indices of the goodness-of-fit.

Index	Meaning	Equation	Criterion
χ^2/df	χ^2 is impacted by the difference between sample and model-implied matrices. The small χ^2 represents the good fitting of model and samples. Degree of freedom (df) is the number of independent variables. Considering that χ^2 is too sensitive to sample size, χ^2/df is selected as a relative chi-square value	—	<5
P	The probability of error. P value and result's credibility will change in the opposite direction. If $P < 0.05$, the result is meaningful	—	<0.005
GFI	Goodness-of-fit presents the proportion of covariance in sample explained by implied model. Greater GFI means the good explanation of dependent variables by independent variables	$1 - \frac{tr[(E^{-1}S - I)^2]}{tr[(E^{-1}S)^2]}$	>0.9
CFI	Comparative fit index can avoid the underestimation of fit in small samples. It also tests the difference between the worst (independence) model and model of interest	$1 - \frac{\max(\chi_T^2 - \mathrm{df}_T, 0)}{\max(\chi_N^2 - \mathrm{df}_N, \chi_T^2 - \mathrm{df}_T, 0)}$	>0.9
RMSEA	Root mean square error of approximation estimates the discrepancy between model-implied and true population covariance matrix per degree of freedom	$\mathrm{Sqrt}\left\{\frac{\max[(\chi^2 - \mathrm{df})/(N-1), 0]}{\mathrm{df}}\right\}$	<0.08
RMR	Root mean square residual tests one kind of mean of residual	$\mathrm{Sqrt}\left[\frac{2\Sigma\Sigma(s_{ij} - e_{ij})^2}{p(p+1)}\right]$	<0.05
NFI	Normed fit index reflects the proportion of worst (independence) model χ^2 explained by model of interest	$\frac{\chi_N^2 - \chi_T^2}{\chi_N^2}$	>0.9

Notes: N is sample's size, p is number of variables, s_{ij} is sample's relation coefficient, e_{ij} is model-implied relation coefficient, S is sample's covariance matrix, E is model-implied covariance matrix, I is identity matrix, χ_N^2 is chi-square of worst (independence) model, χ_T^2 is chi-square of model of interest, df_N is worst (independence) model's degree of freedom, and df_T is model of interest's degree of freedom.

temperature and influence precipitation in Southern China. Hence, water bodies have close relationship with "vegetation" and "urban and surrounding." So the path of "vegetation" → "water bodies" was also added.

3.2. Structural Equation Modeling. As a good measurement model was obtained in the confirmatory factor analysis, the relationships among four latent variables in hypothesis were tested in structural model. There was no need for path modification. Therefore, we got the final structural equation model of the impacts of land use change on the regional climate (Figure 5). The numbers ranging from 0 to 1 on the lines of latent variables refer to observed variables presenting the standardized factor loading, which could reflect the related direction and significance. The numbers next to the arrows pointed to observed variables presenting the errors of observed variables. The numbers on the line between latent variables, which made up the main part of structural model, were called the standardized path coefficient.

Table 3 shows the measurement and structural component's estimate models, errors, T-values, and corresponding significance. Different from standardized factor loading and path coefficient in Figure 5, the coefficient of estimate models reflected the quantitative relationship between data. If T-value was larger than 1.96 and P was below 0.001, the path is significant. The SEM was composed of nine measurement equations and one structural equation. Accordingly, in addition to the path "Urban and surrounding" → "Climate," all the path coefficients had passed the significant test. It is widely known that the development of urban leads to climate change, so we did not delete this path. Therefore, we thought the SEM was valid. Table 3 is helpful to deepen the understanding of variables' relationships and test the significance of each path. However, because the standard coefficient is comparable, the analysis of the result is based on Figure 5.

Table 4 presents the results of goodness-of-fit of confirmatory factor analysis and structural equation modeling. All paths were based on theoretical analysis. For the confirmatory factor analysis and structural equation modeling, it showed that their χ^2/df, P value, GFI CFI, RMR, and NFI fell well within their acceptable ranges but RMSEA was slightly out of its limit. This might be caused by weaker linkage between "urban and surrounding area" with "climate." On the one hand, the goodness-of-fit measure indices are sensitive to sample size and easy to be underestimated when sample size is relatively small [26]. On the other hand, like other statistical analyses, the statistical relationship or association cannot prove the must-be relationship but simply provides support to the logical and intuitive belief influence between the data [35]. So the best model should be established based on the proper theory and the result of goodness-of-fit. According to above analysis, we considered that this SEM whose indices were

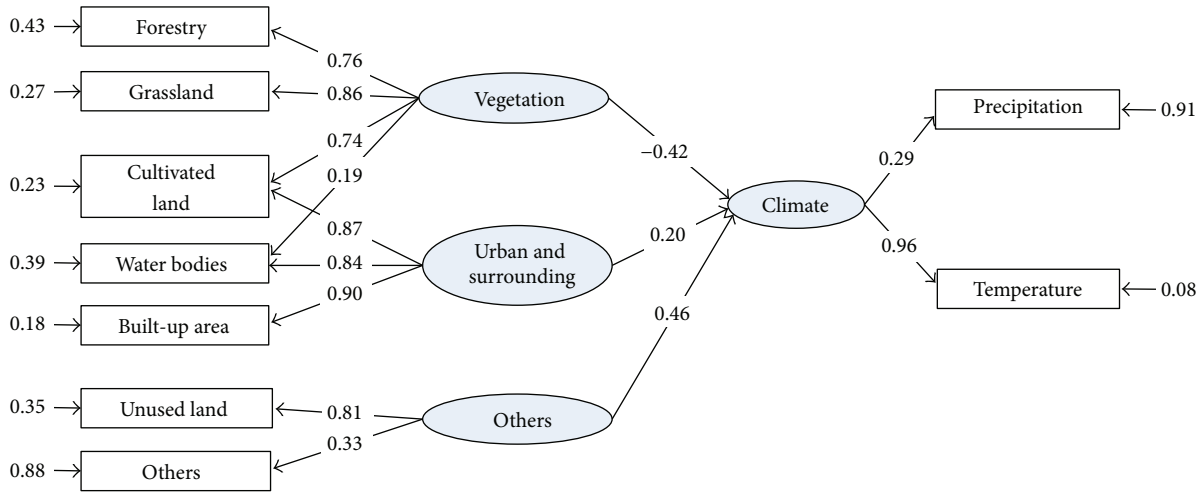

Figure 5: The structural equation model of the impacts of land use change on climate.

Table 3: The measurement and structural equations estimated by LISREL.

Component	Estimate model	Error	t-value	Significance
Measurement component	Forestry = 0.76 × vegetation	0.43	11.52	$P < 0.001$
	Grassland = 0.86 × vegetation	0.27	13.49	$P < 0.001$
	Cultivated land = 0.74 × vegetation + 0.87 × urban and surrounding	0.23	10.26 11.90	$P < 0.001$
	Water bodies = 0.19 × vegetation + 0.84 × urban and surrounding	0.39	2.97 11.96	$P < 0.001$
	Built-up area = 0.91 × urban and surrounding	0.18	15.36	$P < 0.001$
	Unused land = 0.81 × other	0.35	6.24	$P < 0.001$
	Others = 0.33 × other	0.88	3.92	$P < 0.001$
	Precipitation = 0.29 × climate	0.91	—	—
	Temperature = 0.95 × climate	0.08	3.07	$P < 0.001$
Structural component	Climate = −0.42 × vegetation + 0.20 × urban and surrounding + 0.46 × other	0.38	−2.74 1.46 2.34	$P < 0.001$ $P < 0.005$ $P < 0.001$

Table 4: The result of goodness-of-fit.

goodness-of-fit measure	χ^2/df	P	GFI	CFI	RMSEA	RMR	NFI
Indices of confirmatory factor analysis	2.43	0.0007	0.95	0.96	0.086	0.045	0.94
Indices of structural equation modeling	2.40	0.0006	0.95	0.96	0.085	0.044	0.93

below but close to the criteria was acceptable. Consequently, the SEM was valid.

The standard factor loading and path coefficient revealed the significance and direction of relationships among the nine observed variables and four latent variables. The path coefficient of "vegetation" to "climate" (−0.42) proved that vegetation area had dramatically negative impact on the regional climate change. That is to say, the addition of forestry, grassland, cultivated land, and water bodies could reduce the temperature and precipitation effectively. The path coefficient of "urban and surrounding" to "climate" (0.20) proved that the urban and surrounding area had positive impact on the climate change. Accordingly, the addition of cultivated land, water bodies, and built-up area could rise the temperature and precipitation to a certain extent. The path coefficient of "other" to "climate" (0.46) showed that other areas had positive impact on climate change, and the significance of effects was almost the same as "urban and surrounding." We thought this path coefficient was abnormal.

3.3. Analysis of SEM. The objective of this research is to carry out the quantitative impacts of land use change on

the regional climate by a statistical model, so as to provide scientific understanding of the relationship between land use change and regional climate change to policy makers. According to the factor loadings, path coefficients of measurement, and structural models, we summed the opinions as follows.

(1) The structural model displays that all the three parts of vegetation area, urban and surrounding area, and other areas can impact regional climate to a certain extent. Compared with other two parts, vegetation area has negative relationship with regional climate change. First of all, adding vegetation area in low latitude area can mitigate temperature rise by affecting planetary energetic, atmospheric composition and hydrologic cycle [36]. Additionally, in coastal province, cities with high temperature increase their precipitation by evaporation and atmospheric circulation; thus the change of temperature and precipitation in Southern China has the same direction. Above analyses and the result of previous researches clearly indicate that decrease of vegetation resulting from deforestation and urbanization would make the temperature and precipitation increase in low latitude area [37, 38]. Urban and surrounding area has positive relationship with climate change. Urban has a large number of heaters, motor vehicle, and other energy consuming devices, which transmit a lot of heat to air. Furthermore, a large number of buildings and roads increase heat capacity and conductivity of land. Therefore, adding urban and surrounding area leads to higher temperature. This result can be used to explain the urban heat island effect. The structural model shows that other areas which mainly include unused land and the extension for coastline have positive effects on regional climate change. Because the change of unused land was highly different among counties, the coefficient between "other" and "climate" calculated by SEM is relatively big. Referring to the land use change of Southern China in 1988 and 2005, unused land had reduced 489 km^2, accounting for 60.59%, which was the most significant change. A large proportion of unused land was changed to built-up area. Consequently, we think what this path indicates is that the rapid development of built-up area leads to the great climate change.

(2) The relationships between seven exogenous observed variables and three exogenous latent variables can be revealed in measurement model. Firstly, "forestry," "grassland," and "cultivated land" have strong and positive linkages with "vegetation," but the linkage between "water bodies" and "vegetation" is weaker relatively. Forestry, grassland, and cultivated land belong to vegetation area which keeps the characteristic of affecting a series of parameters of earth's surface. However, water bodies mitigate regional temperature and precipitation mainly by evaporation. Compared with the sea, the effect of evaporation of inland water bodies is less obvious, which results in the weaker link of water bodies in Southern China. Secondly, "built-up area," "cultivated land," and "water bodies" have strong and positive linkages with "urban and surrounding." Generally, the urban and surrounding area almost refers to the built-up area. In order to satisfy human's needs for food and water resources, the areas of cultivated land and water bodies have the trend to keep the same change direction with built-up area. This can be used to explain why the three variables are all related to "urban and surrounding," and "cultivated land" and "water bodies" have positive and slightly weaker relationships with "urban and surrounding" in SEM. Both unused land and others have positive linkages with other areas. Because unused land's distribution is much wider and larger than the extension of coastline, the SEM displays that "unused land" has closer linkage with "others."

(3) The urbanization of Southern China had changed the land use structure to a great extent, which had caused the obviously regional climate change. In the procession of slowing down the regional climate change, addition of vegetation is playing the most important role. For the majority of study area has been occupied by forestry which is much larger than grassland, the regional climate change is slightly less sensitive to deforestation than grassland development when they change the same area. The cultivated land and water bodies have the functions of mitigating regional climate change and feeding. Due to their weaker comprehensive impacts, the reclamation of grassland and forestry is against the mitigation of regional temperature and precipitation change. During the urbanization, the policy makers had put forward a series of efficient measures to protect the total amount of cultivated land such as land consolidation, land requisition-compensation balance, and land increase and decrease linked. We think the reasonable scales of cultivated land and water bodies should be judged by requirement. The change of unused land to vegetation can mitigate the regional climate change obviously. However, the change of unused land to built-up area can slightly mitigate the regional climate. This may be because the utilization of unused land can decrease the occupancy of vegetation. Hence, under the background of land intensive and sustainable use, taking full use of unused land plays an important role in mitigating the increasing temperature and precipitation.

4. Conclusion

In this paper, we applied SEM to analyze the impacts mechanism of land use change on the regional climate from the county level. Southern China was selected as case study area due to its typical climatic conditions, obvious land use conversion, and unbalanced regional development among counties. The contribution of this paper is to explore the potential relationship and effects between land use change and regional climate change by the application of SEM. This method is worth spreading. Besides, the identification of the relationship is helpful to generate land use policy options for authorities in Southern China. The conclusions of this research were summarized as follows.

Firstly, it is demonstrated that adding vegetation area is a significant effective way to mitigate regional climate change by reducing temperature and precipitation. Adding urban and surrounding area which enhances temperature and precipitation can affect regional climate to a certain extent. It seems that rapid urbanization contributes to the regional climate change of Southern China in recent decades.

The influence of city expansion is relatively weaker. From the analysis of statistical data, other areas which mainly include unused land and extension of coastline show the significant and positive effect on the regional climate change. This path also reveals the positive relationship between city expansion and climate change.

Secondly, forestry and grassland both have strong linkages with vegetation area, which indicates the climate change can be mitigated by afforestation and adding grassland area. There is a significant and positive relationship between built-up area and urban and surrounding area. Accordingly, restraining sprawl of built-up area and adopting the strategy of sustainable development are important methods to mitigate regional climate change. Possessing the characteristics of mitigating regional climate change and feeding, cultivated land and water bodies both have relationships with vegetation area and urban and surrounding area. However, the suitable scales of them depend on the demand of humanity. Other lands mainly point to unused land in the study area, which can be used to ease the reduction of vegetation area caused by urbanization. This is a good way to solve the conflict between urban development and regional climate change.

It needs to be mentioned, however, that there are still some limitations in the research. For example, the result of good-of-fit is defective. In particular, it is because the relationship revealed by panel data is only a "probable and performance" relationship. That is to say, the structural equation model should be analyzed and applied based on theories and practices. To solve the problem, more data and variables are needed for the sample to improve model fit. Furthermore, the comparison among multitemporal data is helpful to get more credible results.

Conflict of Interests

The authors declare that there is no conflict of interests regarding the publication of this paper.

Acknowledgments

The research presented in this paper was supported by the National Basic Research Program of China (973 Program) (no. 2010CB950904). The data were collected by the Resources and Environment Data Center of the Chinese Academy of Science. The authors are grateful to Xiangzheng Deng for helpful comments on the early draft of the paper and to the editor and reviewers for their valuable comments and suggestions.

References

[1] R. A. Pielke Sr., "Land use and climate change," *Science*, vol. 310, no. 5754, pp. 1625–1626, 2005.

[2] J. Zhan, J. Huang, T. Zhao, X. Geng, and Y. Xiong, "Modeling the impacts of urbanization on regional climate change: a case study in the beijing-tianjin-tangshan metropolitan area," *Advances in Meteorology*, vol. 2013, Article ID 849479, 8 pages, 2013.

[3] Q. Weng, "Fractal analysis of satellite-detected urban heat island effect," *Photogrammetric Engineering and Remote Sensing*, vol. 69, no. 5, pp. 555–566, 2003.

[4] M. Cai and E. Kalnay, "Climate (communication arising) Impact of land-use change on climate," *Nature*, vol. 427, no. 6971, pp. 213–214, 2004.

[5] R. Pachauri and A. Reisinger, *IPCC Fourth Assessment Report*, Intergovernmental Panel on Climate Change(IPCC), Geneva, Switzerland, 2007.

[6] X. Deng, C. Zhao, and H. Yan, "Systematic modeling of impacts of land use and land cover changes on regional climate: a review," *Advances in Meteorology*, vol. 2013, Article ID 317678, 11 pages, 2013.

[7] J. J. Feddema, K. W. Oleson, G. B. Bonan et al., "Atmospheric science: the importance of land-cover change in simulating future climates," *Science*, vol. 310, no. 5754, pp. 1674–1678, 2005.

[8] R. A. Betts, P. D. Falloon, K. K. Goldewijk, and N. Ramankutty, "Biogeophysical effects of land use on climate: model simulations of radiative forcing and large-scale temperature change," *Agricultural and Forest Meteorology*, vol. 142, no. 2–4, pp. 216–233, 2007.

[9] J. Liu and X. Deng, "Impacts and mitigation of climate change on Chinese cities," *Current Opinion in Environmental Sustainability*, vol. 3, no. 3, pp. 188–192, 2011.

[10] J. D. Aber and C. T. Driscoll, "Effects of land use, climate variation, and *N* deposition on *N* cycling and C storage in northern hardwood forests," *Global Biogeochemical Cycles*, vol. 11, no. 4, pp. 639–648, 1997.

[11] L. P. Rosa, S. K. Ribeiro, M. S. Muylaert, and C. P. de Campos, "Comments on the Brazilian proposal and contributions to global temperature increase with different climate responses-CO_2 emissions due to fossil fuels, CO_2 emissions due to land use change," *Energy Policy*, vol. 32, no. 13, pp. 1499–1510, 2004.

[12] S. Queguiner, E. Martin, S. Lafont, J.-C. Calvet, S. Faroux, and P. Quintana-Seguí, "Impact of the use of a CO_2 responsive land surface model in simulating the effect of climate change on the hydrology of French Mediterranean basins," *Natural Hazards and Earth System Science*, vol. 11, no. 10, pp. 2803–2816, 2011.

[13] J. Dong, X. Xiao, S. Sheldon et al., "A 50-m forest cover map in Southeast Asia from ALOS/PALSAR and its application on forest fragmentation assessment," *PLoS ONE*, vol. 9, no. 1, Article ID e85801, 2014.

[14] V. K. Arora and A. Montenegro, "Small temperature benefits provided by realistic afforestation efforts," *Nature Geoscience*, vol. 4, no. 8, pp. 514–518, 2011.

[15] A. Kattenberg, F. Giorgi, H. Grassl et al., "Climate models-projections of future climate," in *Climate Change 1995: The Science of Climate Change, Contribution of Working Group I to the Second Assessment Report of the Intergovernmental Panel on Climate Change*, pp. 285–357, 1996.

[16] X. Gao, Y. Luo, W. Lin, Z. Zhao, and F. Giorgi, "Simulation of effects of land use change on climate in China by a regional climate model," *Advances in Atmospheric Sciences*, vol. 20, no. 4, pp. 583–592, 2003.

[17] H. Von Storch, E. Zorita, and U. Cubasch, "Downscaling of global climate change estimates to regional scales: an application to Iberian rainfall in wintertime," *Journal of Climate*, vol. 6, no. 6, pp. 1161–1171, 1993.

[18] R. B. Matthews, N. G. Gilbert, A. Roach, J. G. Polhill, and N. M. Gotts, "Agent-based land-use models: a review of applications," *Landscape Ecology*, vol. 22, no. 10, pp. 1447–1459, 2007.

[19] W. D. Solecki and C. Oliveri, "Downscaling climate change scenarios in an urban land use change model," *Journal of Environmental Management*, vol. 72, no. 1-2, pp. 105–115, 2004.

[20] G. B. Bonan, "Effects of land use on the climate of the United States," *Climatic Change*, vol. 37, no. 3, pp. 449–486, 1997.

[21] R. N. Lubowskia, A. J. Plantingab, and R. N. Stavins, "Land-use change and carbon sinks: econometric estimation of the carbon sequestration supply function," *Journal of Environmental Economics and Management*, vol. 51, no. 2, pp. 135–152, 2006.

[22] Y. Qin, H. Yan, J. Liu, J. Dong, J. Chen, and X. Xiao, "Impacts of ecological restoration projects on agricultural productivity in China," *Journal of Geographical Sciences*, vol. 23, no. 3, pp. 404–416, 2013.

[23] S.-C. Huang, S.-L. Lo, and Y.-C. Lin, "Application of a fuzzy cognitive map based on a structural equation model for the identification of limitations to the development of wind power," *Energy Policy*, vol. 63, pp. 851–861, 2013.

[24] X.-Y. Song, F. Chen, and Z.-H. Lu, "A Bayesian semiparametric dynamic two-level structural equation model for analyzing non-normal longitudinal data," *Journal of Multivariate Analysis*, vol. 121, pp. 87–108, 2013.

[25] S. P. Washington, M. G. Karlaftis, and F. L. Mannering, *Statistical and econometric methods for transportation data analysis*, Chapman and Hall, Boca Raton, Fla, USA, 2nd edition, 2011.

[26] T. F. Golob, "Structural equation modeling for travel behavior research," *Transportation Research Part B: Methodological*, vol. 37, no. 1, pp. 1–25, 2003.

[27] R. B. Keline, *Principles and Practice of Structural Equation Modeling*, The Guilford Press, New York, NY, USA, 2005.

[28] S. Rabe-Hesketh, A. Skrondal, and A. Pickles, "Generalized multilevel structural equation modeling," *Psychometrika*, vol. 69, no. 2, pp. 167–190, 2004.

[29] H. L. Dang, E. Li, I. Nuberg, and J. Bruwer, "Understanding farmers' adaptation intention to climate change: a structural equation modelling study in the Mekong Delta, Vietnam," *Environmental Science & Policy*, vol. 41, pp. 11–22, 2014.

[30] M. R. Holdaway, "Spatial modeling and interpolation of monthly temperature using kriging," *Climate Research*, vol. 6, no. 3, pp. 215–225, 1996.

[31] J.-H. Wu, S.-C. Wang, and L.-M. Lin, "Mobile computing acceptance factors in the healthcare industry: a structural equation model," *International Journal of Medical Informatics*, vol. 76, no. 1, pp. 66–77, 2007.

[32] S.-Y. Lee and H.-T. Zhu, "Maximum likelihood estimation of nonlinear structural equation models," *Psychometrika*, vol. 67, no. 2, pp. 189–210, 2002.

[33] J. Al-Bakri, A. Suleiman, F. Abdulla, and J. Ayad, "Potential impact of climate change on rainfed agriculture of a semi-arid basin in Jordan," *Physics and Chemistry of the Earth*, vol. 36, no. 5-6, pp. 125–134, 2011.

[34] X. Cao, P. L. Mokhtarian, and S. L. Handy, "Do changes in neighborhood characteristics lead to changes in travel behavior? A structural equations modeling approach," *Transportation*, vol. 34, no. 5, pp. 535–556, 2007.

[35] B. Xiong, M. Skitmore, B. Xia, M. A. Masrom, K. Ye, and A. Bridge, "Examining the influence of participant performance factors on contractor satisfaction: a structural equation model," *International Journal of Project Management*, vol. 32, no. 3, pp. 482–491, 2014.

[36] G. B. Bonan, "Forests and climate change: forcings, feedbacks, and the climate benefits of forests," *Science*, vol. 320, no. 5882, pp. 1444–1449, 2008.

[37] S. A. Changnon Jr., "Rainfall changes in summer caused by St. Louis," *Science*, vol. 205, no. 4404, pp. 402–404, 1979.

[38] S. D. Chow and C. Chang, "Shanghai urban influences on humidity and precipitation distribution," *GeoJournal*, vol. 8, no. 3, pp. 201–204, 1997.

Hindawi Publishing Corporation
Advances in Meteorology
Volume 2015, Article ID 395094, 10 pages
http://dx.doi.org/10.1155/2015/395094

Research Article

Impact of Urbanization and Land-Use Change on Surface Climate in Middle and Lower Reaches of the Yangtze River, 1988–2008

Xiaowei Yao,[1,2] Zhanqi Wang,[1] and Hua Wang[2]

[1] *School of Public Administration, China University of Geosciences, Wuhan 430074, China*
[2] *Faculty of Earth Resources, China University of Geosciences, Wuhan 430074, China*

Correspondence should be addressed to Zhanqi Wang; zhqwang@cug.edu.cn

Received 17 September 2014; Revised 12 January 2015; Accepted 20 January 2015

Academic Editor: R. B. Singh

Land-use/land cover change (LUCC) is one of the fundamental causes of global environmental change. In recent years, understanding the regional climate impact of LUCC has become a hot-discussed topic worldwide. Some studies have explored LUCC impact on regional climate in specific cities, provinces, or farming areas. However, the quick-urbanized areas, which are highly influenced by human activities, have the most severe land-use changes in developing countries, and their climatic impact cannot be ignored. This study aims to identify the impact of land-use change coupled with urbanization on regional temperature and precipitation in the metropolitan areas of middle and lower reaches of the Yangtze River in China by means of spatial analysis and numeric methods. Based on the exploration of land-use change and climate change during 1988–2008, the impact of land-use transition from non-built-up area to built-up area on temperature and precipitation was analyzed. The results indicated that the land-use conversion has affected the regional temperature with an increasing effect in the study area, while the influence on precipitation was not so significant. The results can provide useful information for spatial planning policies in consideration of regional climate change.

1. Introduction

It is widely recognized that land-use/cover change (LUCC) at local, regional, and global scales is one of the crucial driving factors of global climate change [1, 2]. According to the fourth assessment report of Intergovernmental Panel on Climate Change (IPCC) in 2007, human activities, such as urbanization and agriculture, accounted for 90% of global warming [3]. This has been of great concern because innumerable consequent changes were produced on the earth. Some important researches showed that human-induced LUCC was one of the key factors which influence the regional climate [4–8]. LUCC exerts influences on the local and regional climate systems via biogeochemical and biogeophysical feedback mechanisms [9, 10]. The biogeochemical impact of land-use change on the climate is produced by changing atmospheric concentrations of greenhouse gases (GHGs). In this way of feedback mechanism, LUCC mainly changes the carbon and nutrient cycling in the terrestrial ecosystem and affects the GHGs and aerosol exchange between surface and atmosphere [11]. The GHGs from agricultural land-uses, for instance, are estimated to account for 10–20% of the total global anthropogenic emissions, which has raised a wide range of concern about LUCC impact on climate change [12]. Besides, land-use change also plays an important role in climatic system by means of biogeophyisical effects. The biogeophyisical feedback mechanism basically manifests the changes of physical features of the earth's surface such as roughness, surface albedo, soil moisture, and vegetation coverage and structure, which influence the radiation, heat, and moisture exchange process between the surface and the atmosphere [13]. These effects directly result in the changes of surface temperature, humidity, wind speed, and precipitation, accordingly bringing more complex climate at large scales [14, 15]. As the direct indicators of biogeophyisical feedback mechanism, land surface temperature and precipitation are useful observational

evidence, so that they are widely applied to measure the climate changes [16–19]. And the land-use change data also produces great effect in the climate change assessment.

As an important source of considerable human activities, urbanization causes changes of the land-use/cover over the urban areas [20]. Many experiments have been conducted to understand that there is close relationship between urbanization and climate change [21]. The research by Kalnay and Cai, for instance, suggested that half of the observed decrease in diurnal temperature range is due to urban and other land-use changes [6]. Zhang et al. [22] simulated the influence of urbanization on climate in the Yangtze River Delta by the application of weather research and forecasting (WRF) model and found out that the conversion of rural land (mostly irrigated cropland) to urban land cover results in significant changes to the near-surface temperature, humidity, wind speed, and precipitation. Observations by Liao et al. [23] revealed that, by utilizing WRF/Chem model and MODIS data, intensive building clusters in mega cities in the Yangtze River Delta form the urban canopy layers and modify the surface energy budgets and surface roughness, which change thermal and dynamic characteristics of the surface layer. Both simulative and numerical analysis suggest that urban growth-driven land-use change significantly influences the surface heat balance, exchange of water vapor, and momentum between the atmosphere and the surface layer and consequently results in the changes of regional weather, especially the rainfalls [24–27]. But arguments on the effects of urban development on large-scale warming climate still exist [28]. At local scales, a lot of researches have been implemented focusing on urban heat island (UHI), which is a widely concerned issue [29]. Case studies by observations and remote sensing images such as Miao et al. [30] and Wu et al. [31] on Chinese cities and Singh et al. [20] on Delhi of India showed that the UHI generally took place in various types of cities in different regions, and the cases of extreme rainfall weather got increased [32, 33].

Although there have been considerable reports of current researches, there is still much unknown about the impact of regional land-use change and urbanization on climate change. As the surface physical, chemical, and biological characters vary greatly across regions, the climatic influences of urbanization and land-use change vary correspondingly [14]. Due to the lack of data and knowledge, it has been widely recognized that this issue is of great importance for further exploration and discussion [34].

Since the overall economic reforms in the mid-1980s, China has experienced unprecedented urbanization. Cities in China started to face increasing climate risks [35, 36]. The middle and lower reaches of the Yangtze River are one of the most developed regions across the country. Tens of big and medium sized cities are located along or near the Yangtze River, which are interconnected to consist of a considerable "Yangtze River Economic Belt" in the eastern and central China. There have been studies on the impact of LUCC on regional climate [22, 23, 37], in some specific cities like Wuhan [31] and specific provinces like Jiangxi [38]. However, some physical characteristics such as elevation, latitude, or landforms may be ignored when investigating a specific city or province. In this study, we selected the metropolitan areas along the middle and lower reaches of the Yangtze River as the study area. The research would be of great significance because, on one hand, it could provide regional comparison analysis of climate changes resulting from land-use changes; on the other, it could be a guide to alleviating the climatic risks in the rapid urbanization process.

2. Data and Methodology

2.1. Study Area. The metropolitan area in the middle and lower reaches of the Yangtze River is located in 110°15′ ~ 123°25′E, 26°03′ ~33°25′N with a total area of 4.82×10^5 km^2. It stretches across seven provincial regions from west to east, covering the central and east of Hubei, the northeast of Hunan, the north of Jiangxi, the central and south of Anhui, the south of Jiangsu, the north of Zhejiang, and entire Shanghai. In this region, there are tens of big cities such as Yichang, Yueyang, Nanchang, Hefei, Nanjing, Suzhou, and Hangzhou, involving Wuhan metropolitan, Changsha metropolitan, Poyang Lake metropolitan, Yangtze-side metropolitan Region of Anhui, and Yangtze River Delta metropolitan (Figure 1).

Mainly located in the Yangtze Plain with part of South Yangtze hills at this latitude, this area belongs to subtropical monsoon climate and subtropical moist monsoon climate region. Owing to moderate rainfall and sunlight, and with abundant amount of water resources, it is a fertile region which is famous for rice cultivation and fishery. It is an important grain producing area in China that plays a key role in the national agricultural industry. In addition, with the obvious locational superiority and favorable industrial and commercial basis, it is also one of the most dynamic economic regions across the country. Demographically, the proportion of urban population to permanent population in the study area also increased at an unprecedented speed since it rose from 19.8% in 1990 to 38.9% in 2000,and then to 49.3% in 2008 in the seven provinces, according to the official statistical data launched by National Bureau of Statistics of China and the involved provinces. At the same time, the regional land-use has changed severely. According to the land-use data extracted from remote sensing images, the total area of cultivated land was 215913 km^2 in the late 1980s, which decreased by 13292 km^2 to 202621 km^2 in the year of 2008. In contrast, the amount of built-up area grew significantly from 19135 km^2 to 30008 km^2 during this period, which was almost 56.8% more than that in the year of 1988. Except for the water bodies increasing from 36654 km^2 to 38528 km^2 during 1988–2008, the areas of forestry, grassland, and unused area all slightly decreased. Consequently, it is of great significance to explore the changes of built-up area and their influence on regional climate.

2.2. Data and Methods. The data used in this paper was collected from the data center of Chinese Academy of Sciences (CAS). It mainly included land-use data and meteorological data of the study area.

Land-use data was extracted from the Chinese subset of the Global Land Cover Characteristics database. The dataset is on the basis of land-use maps at the scale of 1 : 100 000,

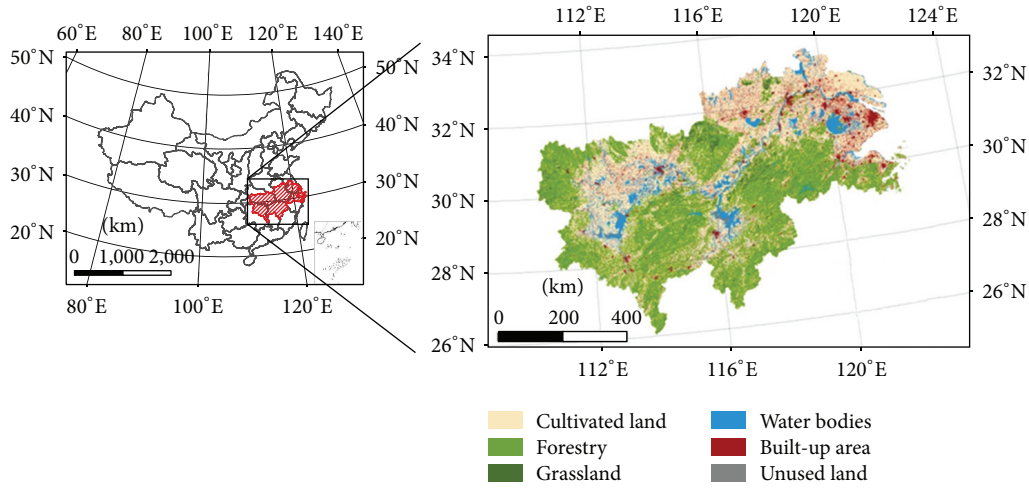

Figure 1: Location of the study area and the land cover, 2008.

using the classification system of 6 classes of first level and 25 classes of second level, which relied on interpretation of Landsat TM imagery and ground survey of 2000 with high level of accuracy (about 98.7% of the average degree of interpretation accuracy and 97.6% of comparing the changing patches of land-use between two periods) [39]. The land-use data involved in this study was originally generated with 1 km grid scale in the years of 1988, 1995, 2000, 2005, and 2008 with Albers projection, which is believed to be an effective kind of data that can provide sufficient information for the regional land-use change monitoring [40].

The meteorological data during 1988–2008 was collected from meteorological stations of China Meteorological Administration, including the annual near-surface temperature and annual average precipitation. Based on the observational data acquired from the 756 observation stations distributed across China's mainland (Figure 2), the 3-year average data was calculated to represent the temperature/precipitation in the specific time points including 1988, 1995, 2000, 2005, and 2008. Then the observational data were interpolated into 1 km resolution grid data with Kriging Interpolation algorithm and were uniformly projected with Albers projection so that they could be spatially matched with land-use change data. During interpolation with temperature data, terrain conditions of the study area were taken into consideration. Therefore, the temperature data was first adjusted to the sea level. After interpolation, the digital elevation model (DEM) was applied to correct the data by 0.6°C per 100 m in height.

In order to explore the climatic impact of land-use change during the fast urbanization process, the land-use conversion matrix was first applied to calculate the total amount of conversion from non-built-up area to built-up area in each period of time. It is a fundamental tool in analysis of land-use change [41]. The conversion matrix was simplified here because only the changes from non-built-up area to built-up area were discussed in this paper (Table 1).

After the land-use conversions and the changes of temperature and precipitation during the study period were evaluated by gird on the ArcINFO platform, numerical analysis was applied to examine their relationship. The parameter of E could be used to describe the responses of climate changes to the land-use conversion. For each type of land-use conversion, consider the following:

$$E_t = \frac{\sum_1^m \Delta I_t}{M}, \qquad E_p = \frac{\sum_1^n \Delta I_p}{N}, \tag{1}$$

where E refers to the effects of land-use conversion to built-up area on temperature and precipitation, t and p refer to temperature and precipitation, respectively, ΔI represents the changes of the temperature/precipitation where conversion from non-built-up area to built-up area occurred, m and n mean the number of temperature/precipitation that changed, and M and N are the total amount of each land-use conversion type.

The research diagram for data handling and analysis is shown in Figure 3.

Table 1: Land-use conversion matrix for non-built-up area to built-up area.

		$T1$				
		CU	FO	GR	WA	UN
$T2$	BU	S_{CU2BU} P_{CU2BU}	S_{FO2BU} P_{FO2BU}	S_{GR2BU} P_{GR2BU}	S_{WA2BU} P_{WA2BU}	S_{UN2BU} P_{UN2BU}

Note: CU, FO, GR, WA, UN, and BU refer to cultivated land, forestry, grassland, water bodies, unused land, and built-up area, respectively. S and P refer to the area and proportion of conversion from each land cover to built-up area, respectively, during $T1$ to $T2$. Hence, S_{CU2BU} represents the amount of conversion from cultivated land to built-up area during the time $T1$ to $T2$, and P_{CU2BU} refers to the conversion rate from cultivated land to built-up area during the time $T1$ to $T2$, and so on, which is calculated with the following equation: $P_{CU2BU} = (S_{CU2BU} - S_{CU})/S_{CU} \times 100\%$.

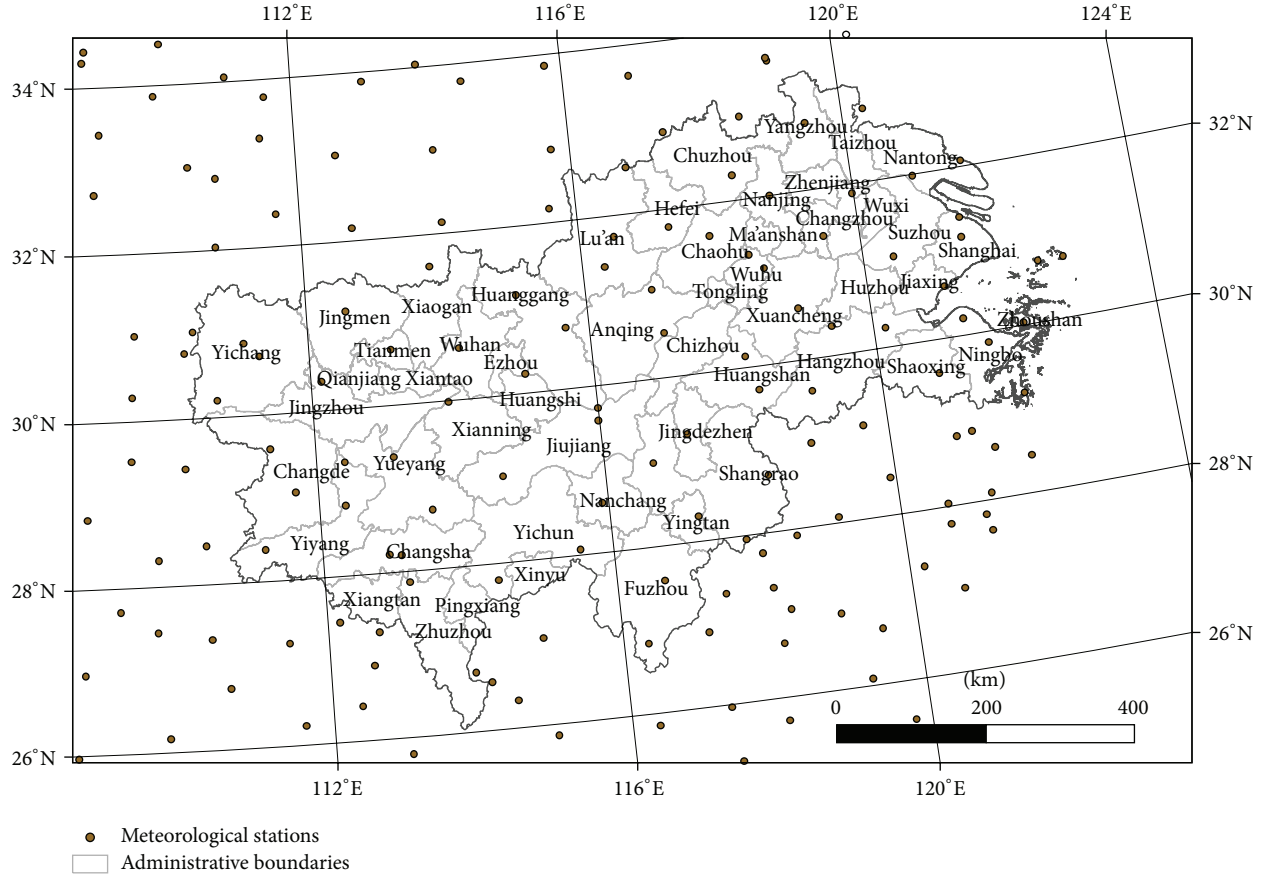

Figure 2: Distribution of the meteorological stations used for interpolation within and around the study area.

Table 2: Land-use conversion from non-built-up to built-up area, 1988–2008 (area unit: ten thousand hectares).

Period/land-use conversion		CU2BU	FO2BU	GR2BU	WA2BU	UN2BU
1988–1995	Area	147.62	16.12	1.65	12.08	0.30
	Proportion	6.84%	0.84%	1.02%	3.30%	1.47%
1995–2000	Area	134.27	12.53	0.85	7.70	0.13
	Proportion	6.33%	0.65%	0.52%	2.12%	0.66%
2000–2005	Area	161.13	18.62	1.81	11.40	0.18
	Proportion	7.62%	0.97%	1.12%	3.04%	0.88%
2005–2008	Area	170.91	26.71	2.48	19.09	0.37
	Proportion	8.28%	1.39%	1.54%	4.93%	2.11%

Note: the data was calculated according to land-use conversion matrix introduced in Table 1.

3. Results and Discussion

3.1. Spatiotemporal Changes of Built-Up Area Expansion during 1988–2008. According to the land cover data, the amount of built-up areas and the conversion from other land cover types could be calculated. The overall area of built-up areas in the metropolitans of the middle and lower reaches of the Yangtze River grew from 19135 km^2 to 30008 km^2. It can obviously be seen that the main conversion type to built-up area in the region was the conversion from cultivated land (Table 2).

Temporally, despite the areas of land cover conversion fluctuating in 1995–2005, the annual conversions of each type in the four periods were speeding significantly except for the conversion of grassland, water bodies, and unused land in 1995–2000. The years of 2005–2008 were the most prominent time that built-up area expanded while occupying other five land covers. During these three years, about 8.28% of the cultivated land and 4.93% of the water bodies were lost and the proportion of built-up area increased from 5.64% in 2005 to 6.24% in 2008. In the year of 1988, however, the percentage of the built-up area was just 3.97% (Figure 4).

Spatially, most of the built-up areas were distributed in a zigzag manner along with the Yangtze River, with Shanghai metropolitan as the center (Figure 5). Another part of the built-up areas was located in the south of the Yangtze River,

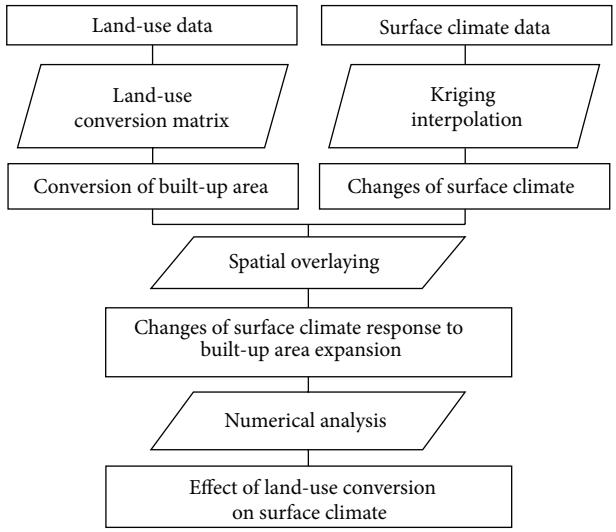

Figure 3: Research diagram for data handling and analysis.

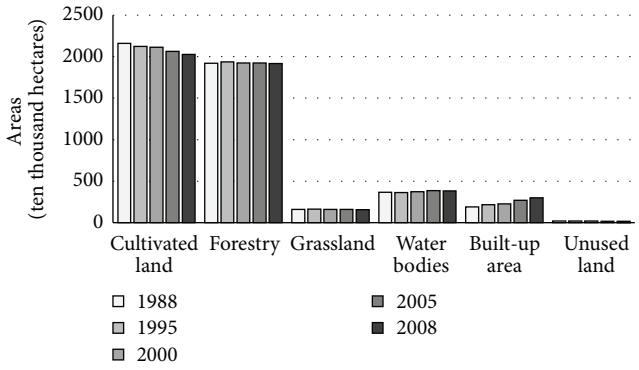

Figure 4: Structures of land-use in the middle and lower reaches of the Yangtze River, 1988–2008.

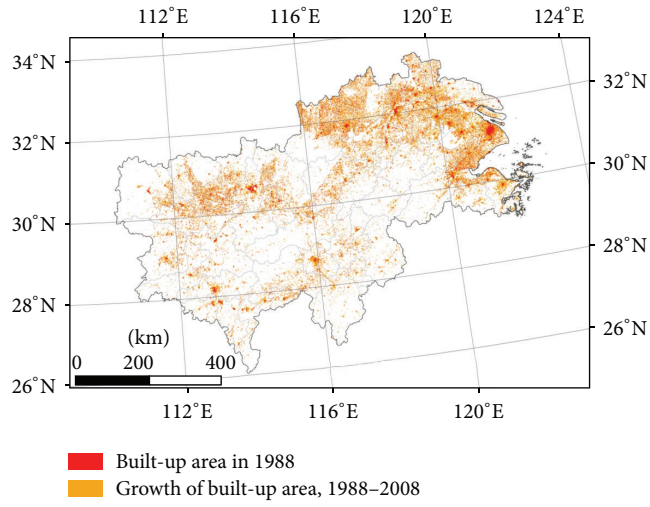

Figure 5: Distribution of built-up area, 1988–2008.

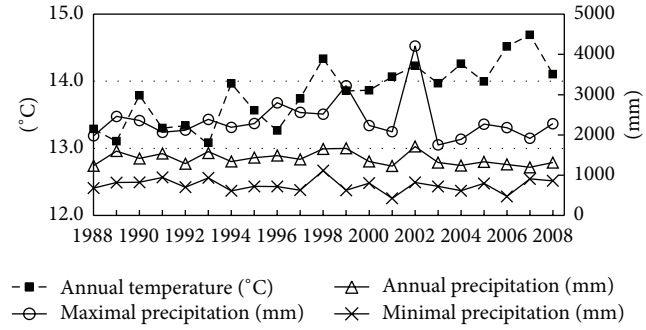

Figure 6: Temporal changes of temperature and precipitation in the study area, 1988–2008.

with Changsha and Nanchang as the centers. By dividing the study area into two parts including the middle reaches metropolitan region and the lower reaches metropolitan region, we could make out that approximately 64% of land-use conversions were found in the lower reaches metropolitan region, even though the area accounted for about 42% of the overall region. In the middle reaches metropolitan region, the average proportion of cultivated land conversion in the total conversion types was 72.8%, followed by 16.8% of forestry conversion and about 9% of water bodies conversion, respectively, whose trends were on the rolling rise. In the lower reaches metropolitan region, the average proportion of cultivated land conversion in the total conversion types dominated in 88.3% with a descending trend since 2000. The ratios of conversion from water bodies and forestry were both about 5% before 2005, but with a slight increasing trend to over 7% during 2005–2008.

3.2. Spatiotemporal Changes of the Regional Climates during 1988–2008. Generally, there were distinct changes in annual average temperature and precipitation in the metropolitans of middle and lower reaches of the Yangtze River from 1988 to 2008. The temperature showed an increasing trend in fluctuations in the study area, with the average temperature rising from 13.3°C in 1988 to 14.1°C in 2008 (Figure 6). Most of the regions had an increase of the annual temperature, except a tiny part of the hilly areas such as the north of Yichang and the south of Zhuzhou having a slight decrease of 0–1.5°C. The maximal rise of temperature that almost reached 6.7°C took place in the Hangzhou metropolitan, the west part of Yichang in Hubei Province, and the southeast corner of Shangrao in Jiangxi Province. Besides, the temperature basically increased 2.4–4.9°C in the majority of other parts of the region, including Shanghai, Nanjing, Wuhan, and Changsha metropolitans (Figure 7(a)).

At the same time, the annual precipitation in the study area did not show a significant rising or descending trend (Figure 6). The peak with 1713.7 mm appeared in the year of 2002, and then the amount of rainfall fluctuated at a relatively lower level from 2003 to 2008. In addition, the changes of precipitation varied greatly across the area. On one side, the rainfalls showed a rising trend in the majority part of the region, with the maximum increase of 76.7 mm in the north-central part of Huangshan. On the other side, they

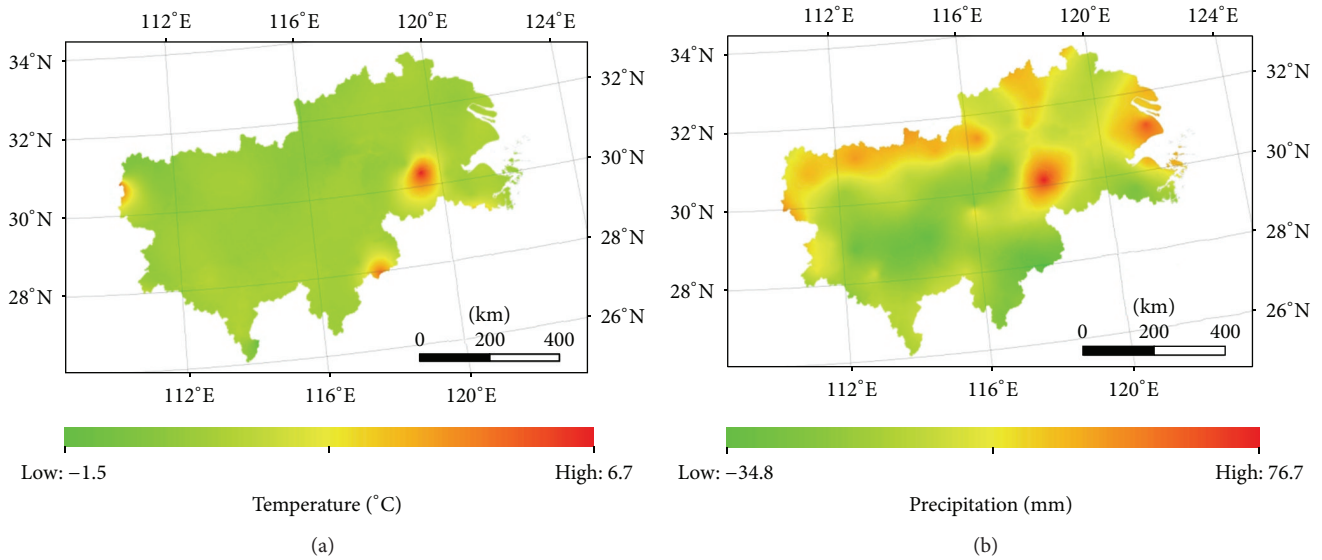

Figure 7: Changes in spatial distribution of annual average temperature (a) and precipitation (b) in the middle and lower reaches of the Yangtze River, 1988–2008.

showed a downward variation in the north part of Hunan, the southeast of Hubei, the southwest of Anhui, the east of Jiangxi, and east areas of Hangzhou, with the maximal decrease of 34.8 mm. According to the results mentioned above, it can be concluded that the process of urbanization in this region has affected the regional climate to a certain extent (Figure 7(b)).

3.3. Effects of Land-Use Conversion on Temperature and Precipitation. We overlaid the built-up area growth maps with the climate change maps, and the variations of the climate responses to the land-use change showed significant differences in spatial distribution (Figure 8). Most of the metropolitan areas including the interior of Jianghan Plain, Wuhan, Changsha, Nanchang, Hefei, and the Yangtze River Delta Region got warmer in 1995 than in 1988 while a mass of cultivated land surrounding these cities and towns was lost due to urbanization. Part of the nearby water bodies, especially in Wuhan and so forth, was also turned to built-up area. When the trends of built-up area expansion and cultivated land loss kept going on for the next over 10 years, the changes of the temperature varied across the region. The urbanized areas with upward temperatures were not as concentrated as they were in the late 1980s; besides, fluctuations with downward temperatures occurred in some of the metropolitans such as Shanghai (Figures 8(a), 8(b), 8(c), and 8(d)).

The precipitation in spatial distribution significance across the region was not very obvious compared to the match of temperature with land-use change. The amounts of rainfall increased around Shanghai but decreased in Nanjing and Hefei metropolitans in 1988–1995. Another typical fluctuation was found in Nanchang metropolitan, the north of Jiangxi. The precipitation in this region went up in 1988–1995 and 2000–2005 but sharply cut down in 1995–2000 and 2005–2008 (Figures 8(e), 8(f), 8(g), and 8(h)).

The calculation results of E showed the relativity of urbanizing land-use change with regional climate which matched the spatial layout analysis above (Figure 8). During the four time periods, the changes of regional average temperature were basically in accordance with the impact of other four types of conversion, especially with the grassland conversion and forestry conversion, except that of unused land turning to built-up areas, but the influence of the conversions got smaller (Figure 9(a)). These observations indicated that each type of conversion from non-built-up to built-up area had a positive influence on temperature changes. As we have known that when land-use cover such as natural vegetation and crops is replaced with the nonevaporating and nontranspiring built-up areas, surface properties such as albedo and soil moisture generally become lower. These changes may have an influence on heat and moisture exchange process between the surface and atmosphere and thus result in the rise of temperature.

According to the numeric observations, the land-use conversion from non-built-up to built-up areas did not have particular significance on precipitation changes in the study area during 1988–2008 (Figure 9(b)). There were both increase and decrease in precipitation when the built-up area expanded. The changing trends of rainfall almost reacted in the opposite directions between the four periods. Among the four types of land-use change, conversion from unused land to built-up area had the most severe impact on precipitation both in positive and in negative directions during the four periods, while conversion from cultivated land to built-up areas had the least influence on it. These differences in time sequence and land conversion types indicated that there is still uncertainty about the impact of LUCC on surface climate in this region, even though there is reduction in evapotranspiration due to urbanization [20].

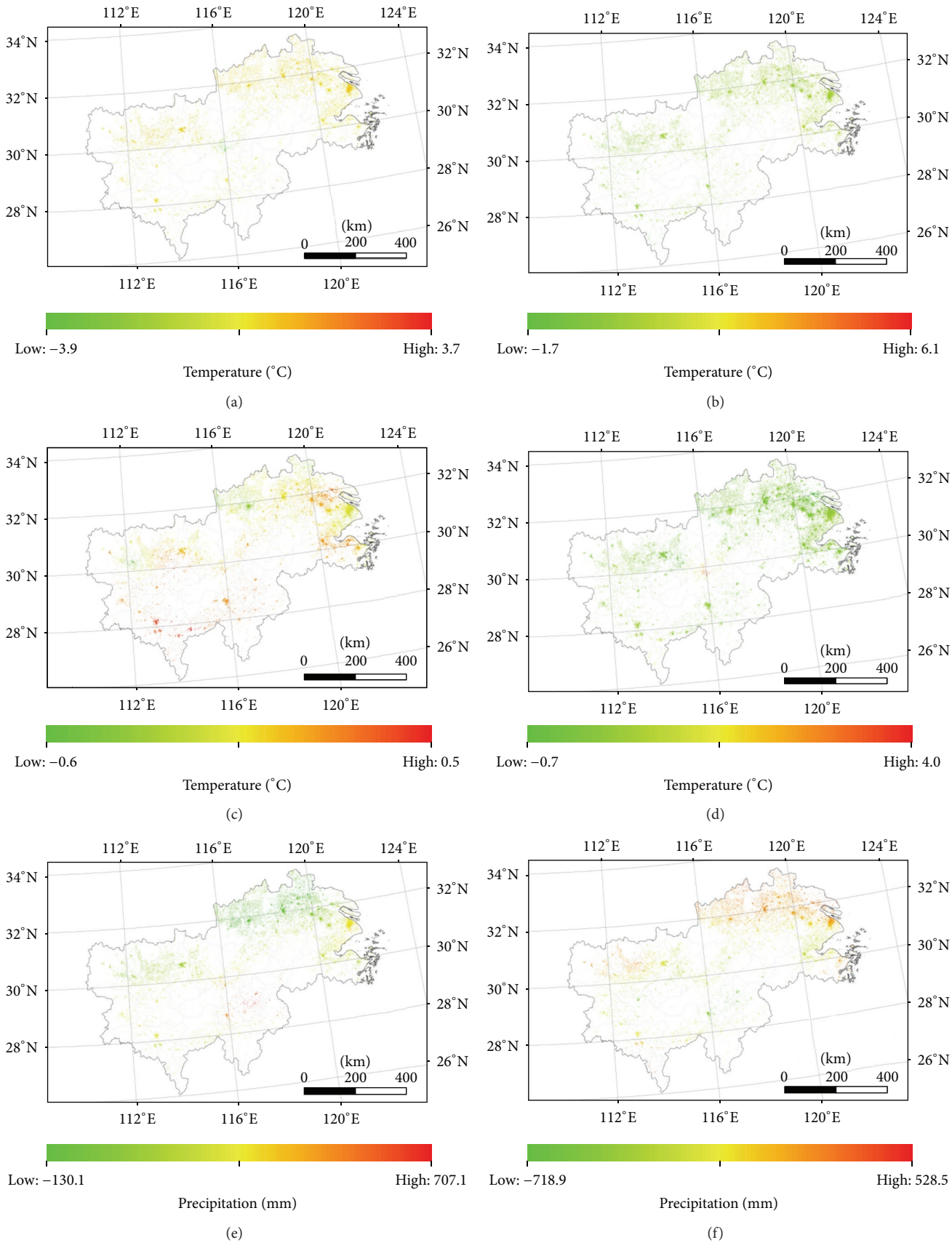

Figure 8: Continued.

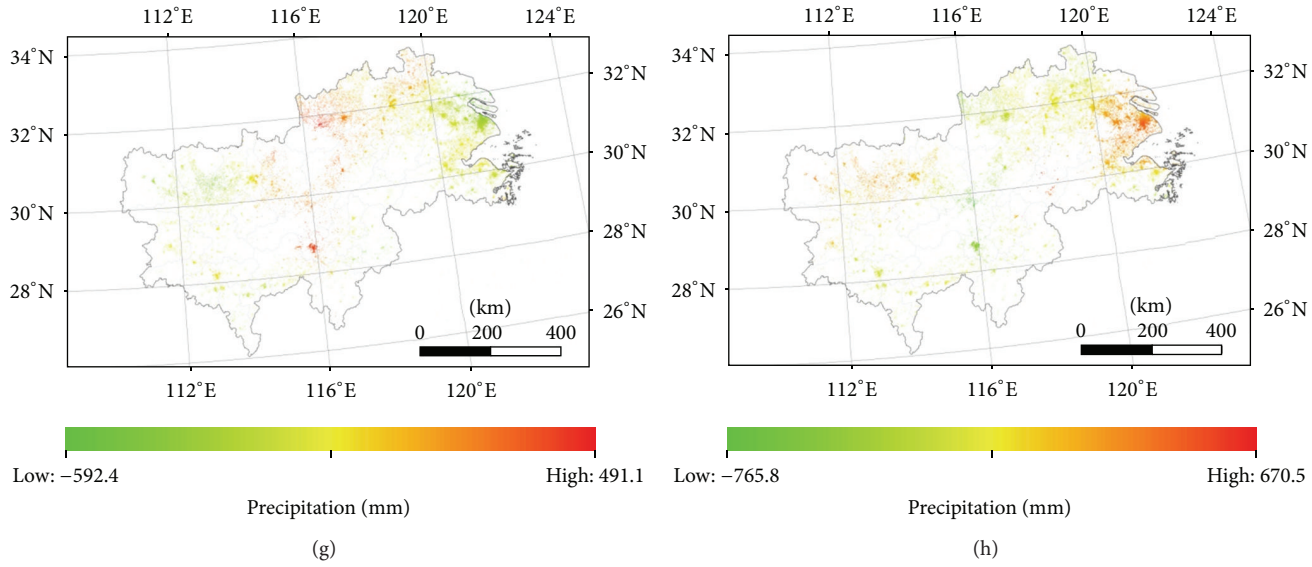

Figure 8: Variations of the temperature and precipitation response to land-use conversion from non-built-up to built-up area in periods 1988–1995 (a, e), 1995–2000 (b, f), 2000–2005 (c, g), and 2005–2008 (d, h).

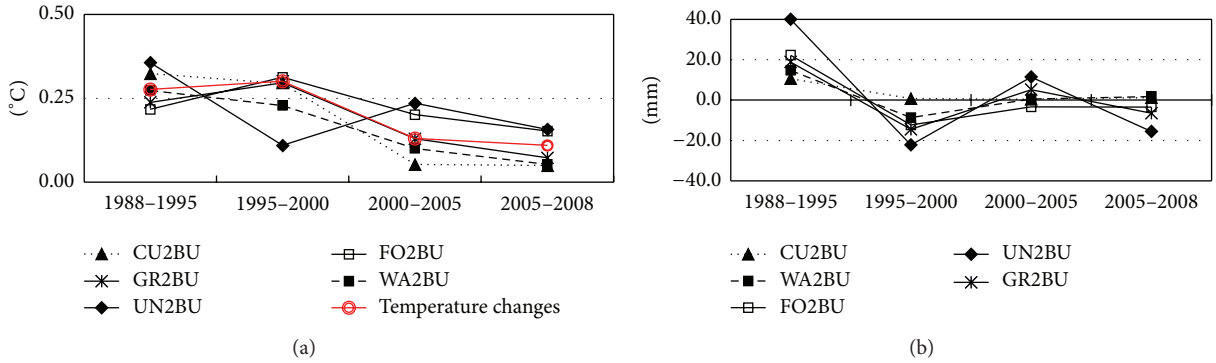

Figure 9: Changes of temperature (a) and precipitation (b) upon land-use conversions from non-built-up to built-up area.

4. Conclusions

In this paper, the impact of the land-use conversion from non-built-up areas to built-up areas on surface temperature and precipitation in the middle and lower reaches of the Yangtze River during 1988–2008 was examined by using spatial and numeric analysis. The results showed that conversion from cultivated land to built-up area was the most important type of land-use change in the region under the rapid urbanization process, which was recognized as "urbanization of land" and concentrated much of focuses from academia. The loss of water bodies was another important source that made the growth of built-ups.

The numeric results indicated that the transitions from non-built-up areas to built-up areas had positive relationship with the rising trend of regional temperature in the study area, but the effects of different conversion types in different periods were varied obviously. All the conversion types except the unused land transition have very similar impact on the changes of temperature. Within the 20-year time period, the upward and downward changing trend of regional temperature was quite in accordance with that where grassland and forestry were changed to built-up areas. These trends were increasing first and then went down significantly. The change of regional climate slightly went up from 0.28°C in 1988–1995 to 0.3°C in 1995–2000, but both the warming effects of conversion from cultivated land and from water bodies on temperature change decreased steadily in this period of time, which kept on going downwards significantly to the bottom of 0.05°C during 2005–2008. As to the regional precipitation, the results did not show much significant impact of land-use conversions from non-built-up areas to built-up areas, even though there were some researches that indicate it could result in either increasing or decreasing effect on precipitation [27, 42].

Generally, we have only focused on the physical climatic impact of transition from non-built-up to built-up areas in the urbanized area of the middle and lower reaches of the Yangtze River in this paper. The land-use change of transition from non-built-up to built-up areas influences the regional

temperature mainly by altering the land surface net radiation and latent heat flux. The results are of great value for the state governments to guide land resource distribution and urbanization policies that respond to the regional climate changes.

Although the precipitation effect was also under consideration in this research, either the positive or negative influence was observed, probably due to the limited annual statistical data or the numeric methods involved. However, trapped by the limitations and the uncertainties of full understanding of the procedure mechanisms, the regional climate change is a very complicated process and there are many other factors that may take effect. As a consequence, it is a rather challenging goal to assess and quantize the climatic effects of land-use change since various biogeophysical and biogeochemical processes interact or even offset each other on the climate change [43]. Besides, the lack of forecasting climate changes in future under the land-use change was another inadequacy of the research. And the explorations would be more notable if the simulation was added by socioeconomic indicators such as population and industries.

Conflict of Interests

The authors declare that there is no conflict of interests regarding the publication of this paper.

Acknowledgments

This research was cosupported by National Natural Science Foundation of China (Grant no. 41101535), China Postdoctoral Science Foundation funded project (Grant no. 2012M521503), and Fundamental Research Funds for the Central Universities, China University of Geosciences (Wuhan) (Grant no. CUG120861). The authors also wanted to thank China National Natural Science Funds for Distinguished Young Scholar (Grant no. 71225005) for data support.

References

[1] J. A. Foley, R. Defries, G. P. Asner et al., "Global consequences of land use," *Science*, vol. 309, no. 5734, pp. 570–574, 2005.

[2] R. A. Pielke, "Land use and climate change," *Science*, vol. 310, no. 5754, pp. 1625–1626, 2005.

[3] R. Pachauri and A. Reisinger, *IPCC Fourth Assessment Report*, IPCC, Geneva, Switzerland, 2007.

[4] G. B. Bonan, "Effects of land use on the climate of the United States," *Climatic Change*, vol. 37, no. 3, pp. 449–486, 1997.

[5] C. M. Taylor, E. F. Lambin, N. Stephenne, R. J. Harding, and R. L. H. Essery, "The influence of land use change on climate in the Sahel," *Journal of Climate*, vol. 15, no. 24, pp. 3615–3629, 2002.

[6] E. Kalnay and M. Cai, "Impact of urbanization and land-use change on climate," *Nature*, vol. 423, no. 6939, pp. 528–531, 2003.

[7] M. Cai and E. Kalnay, "Climate: impact of land-use change on climate," *Nature*, vol. 427, no. 6971, p. 214, 2004.

[8] H. Paeth, K. Born, R. Girmes, R. Podzun, and D. Jacob, "Regional climate change in tropical and Northern Africa due to greenhouse forcing and land use changes," *Journal of Climate*, vol. 22, no. 1, pp. 114–132, 2009.

[9] L. Jiang, E. J. Ma, and X. Z. Deng, "Impacts of irrigation on the heat fluxes and near-surface temperature in an inland irrigation area of Northern China," *Energies*, vol. 7, no. 3, pp. 1300–1317, 2014.

[10] P. J. Lawrence, J. J. Feddema, G. B. Bonan et al., "Simulating the biogeochemical and biogeophysical impacts of transient land cover change and wood harvest in the community climate system model (CCSM4) from 1850 to 2100," *Journal of Climate*, vol. 25, no. 9, pp. 3071–3095, 2012.

[11] K. L. Findell, E. Shevliakova, P. C. D. Milly, and R. J. Stouffer, "Modeled impact of anthropogenic land cover change on climate," *Journal of Climate*, vol. 20, no. 14, pp. 3621–3634, 2007.

[12] P. H. Verburg, K. Neumann, and L. Nol, "Challenges in using land use and land cover data for global change studies," *Global Change Biology*, vol. 17, no. 2, pp. 974–989, 2011.

[13] P. J. Grutzen and M. O. Andreae, "Biomass burning in the tropics: impact on atmospheric chemistry and biogeochemical cycles," *Science*, vol. 250, no. 4988, pp. 1669–1678, 1990.

[14] X. Deng, C. Zhao, and H. Yan, "Systematic modeling of impacts of land use and land cover changes on regional climate: a review," *Advances in Meteorology*, vol. 2013, Article ID 317678, 11 pages, 2013.

[15] X. Deng, C. Zhao, Y. Lin et al., "Downscaling the impacts of large-scale LUCC on surface temperature along with IPCC RCPs: a global perspective," *Energies*, vol. 7, no. 4, pp. 2720–2739, 2014.

[16] F. Wang and Q. S. Ge, "Estimation of urbanization bias in observed surface temperature change in China from 1980 to 2009 using satellite land-use data," *Chinese Science Bulletin*, vol. 57, no. 14, pp. 1708–1715, 2012.

[17] H. Y. Ding and W. Z. Shi, "Land-use/land-cover change and its influence on surface temperature: a case study in Beijing City," *International Journal of Remote Sensing*, vol. 34, no. 15, pp. 5503–5517, 2013.

[18] W. Junkermann, J. Hacker, T. Lyons, and U. Nair, "Land use change suppresses precipitation," *Atmospheric Chemistry and Physics*, vol. 9, no. 17, pp. 6531–6539, 2009.

[19] A. T. Woldemichael, F. Hossain, and R. Pielke Sr., "Impacts of postdam land use/land cover changes on modification of extreme precipitation in contrasting hydroclimate and terrain features," *Journal of Hydrometeorology*, vol. 15, no. 2, pp. 777–800, 2014.

[20] R. B. Singh, A. Grover, and J. Y. Zhan, "Inter-seasonal variations of surface temperature in the urbanized environment of Delhi using landsat thermal data," *Energies*, vol. 7, no. 3, pp. 1811–1828, 2014.

[21] R. B. Singh and C. Shi, "Advances in observation and estimation of land use impacts on climate changes: improved data, upgraded models, and case studies," *Advances in Meteorology*, vol. 2014, Article ID 748169, 14 pages, 2014.

[22] N. Zhang, Z. Q. Gao, X. M. Wang, and Y. Chen, "Modeling the impact of urbanization on the local and regional climate in Yangtze River Delta, China," *Theoretical and Applied Climatology*, vol. 102, no. 3-4, pp. 331–342, 2010.

[23] J. B. Liao, T. J. Wang, X. M. Wang et al., "Impacts of different urban canopy schemes in WRF/Chem on regional climate and air quality in Yangtze River Delta, China," *Atmospheric Research*, vol. 145-146, pp. 226–243, 2014.

[24] H. C. Wan, Z. Zhong, X. Q. Yang, and X. Q. Li, "Impact of city belt in Yangtze River Delta in China on a precipitation process in summer: a case study," *Atmospheric Research*, vol. 125-126, pp. 63–75, 2013.

[25] A. Pathirana, H. B. Denekew, W. Veerbeek, C. Zevenbergen, and A. T. Banda, "Impact of urban growth-driven landuse change on microclimate and extreme precipitation—a sensitivity study," *Atmospheric Research*, vol. 138, pp. 59–72, 2014.

[26] R. A. Memon, D. Y. C. Leung, and C.-H. Liu, "An investigation of urban heat island intensity (UHII) as an indicator of urban heating," *Atmospheric Research*, vol. 94, no. 3, pp. 491–500, 2009.

[27] C.-Y. Lin, W.-C. Chen, S. C. Liu, Y. A. Liou, G. R. Liu, and T. H. Lin, "Numerical study of the impact of urbanization on the precipitation over Taiwan," *Atmospheric Environment*, vol. 42, no. 13, pp. 2934–2947, 2008.

[28] D. E. Parker, "A demonstration that large-scale warming is not urban," *Journal of Climate*, vol. 19, no. 12, pp. 2882–2895, 2006.

[29] A. J. Arnfield, "Two decades of urban climate research: a review of turbulence, exchanges of energy and water, and the urban heat island," *International Journal of Climatology*, vol. 23, no. 1, pp. 1–26, 2003.

[30] S. G. Miao, F. Chen, M. A. LeMone, M. Tewari, Q. C. Li, and Y. C. Wang, "An observational and modeling study of characteristics of urban heat island and boundary layer structures in Beijing," *Journal of Applied Meteorology and Climatology*, vol. 48, no. 3, pp. 484–501, 2009.

[31] H. Wu, L.-P. Ye, W.-Z. Shi, and K. C. Clarke, "Assessing the effects of land use spatial structure on urban heat islands using HJ-1B remote sensing imagery in Wuhan, China," *International Journal of Applied Earth Observation and Geoinformation*, vol. 32, pp. 67–78, 2014.

[32] R. K. Kaufmann, K. C. Seto, A. Schneider, Z. Liu, L. Zhou, and W. Wang, "Climate response to rapid urban growth: evidence of a human-induced precipitation deficit," *Journal of Climate*, vol. 20, no. 10, pp. 2299–2306, 2007.

[33] Y.-Z. Cao, S. Wang, G. Zhang, J. Luo, and S. Lu, "Chemical characteristics of wet precipitation at an urban site of Guangzhou, South China," *Atmospheric Research*, vol. 94, no. 3, pp. 462–469, 2009.

[34] J. J. Feddema, K. W. Oleson, G. B. Bonan et al., "The importance of land-cover change in simulating future climates," *Science*, vol. 310, no. 5754, pp. 1674–1678, 2005.

[35] X. Deng, J. Huang, S. Rozelle, and E. Uchida, "Growth, population and industrialization, and urban land expansion of China," *Journal of Urban Economics*, vol. 63, no. 1, pp. 96–115, 2008.

[36] X. Deng and X. Bai, "Sustainable urbanization in Western China," *Environment*, vol. 56, no. 3, pp. 12–24, 2014.

[37] C. Gu, L. Hu, X. Zhang, X. Wang, and J. Guo, "Climate change and urbanization in the Yangtze River Delta," *Habitat International*, vol. 35, no. 4, pp. 544–552, 2011.

[38] Q. Wang, D. Riemann, S. Vogt, and R. Glaser, "Impacts of land cover changes on climate trends in Jiangxi province China," *International Journal of Biometeorology*, vol. 58, no. 5, pp. 645–660, 2014.

[39] M. Li, J. Wu, and X. Deng, "Identifying drivers of land use change in China: a spatial multinomial logit model analysis," *Land Economics*, vol. 89, no. 4, pp. 632–654, 2013.

[40] Z. H. Li, X. Z. Deng, J. K. Huang, and R. R. Zhang, "Critical studies on integrating land-use induced effects on climate regulation services into impact assessment for human well-being," *Advances in Meteorology*, vol. 2013, Article ID 831250, 14 pages, 2013.

[41] T. Takada, A. Miyamoto, and S. F. Hasegawa, "Derivation of a yearly transition probability matrix for land-use dynamics and its applications," *Landscape Ecology*, vol. 25, no. 4, pp. 561–572, 2010.

[42] Y. Lin, A. Liu, E. Ma, X. Li, and Q. Shi, "Impacts of future urban expansion on regional climate in the Northeast megalopolis, USA," *Advances in Meteorology*, vol. 2013, Article ID 362925, 10 pages, 2013.

[43] R. A. Pielke Sr., G. Marland, R. A. Betts et al., "The influence of land-use change and landscape dynamics on the climate system: Relevance to climate-change policy beyond the radiative effect of greenhouse gases," *Philosophical Transactions of the Royal Society A: Mathematical, Physical and Engineering Sciences*, vol. 360, no. 1797, pp. 1705–1719, 2002.

Hindawi Publishing Corporation
Advances in Meteorology
Volume 2015, Article ID 410198, 11 pages
http://dx.doi.org/10.1155/2015/410198

Research Article

Scenario-Based Impact Assessment of Land Use/Cover and Climate Changes on Watershed Hydrology in Heihe River Basin of Northwest China

Feng Wu,[1] Jinyan Zhan,[1] Hongbo Su,[2] Haiming Yan,[1] and Enjun Ma[3]

[1]*State Key Joint Laboratory of Environmental Simulation and Pollution Control, School of Environment, Beijing Normal University, Beijing 100875, China*
[2]*Key Laboratory of Water Cycle & Related Land Surface Processes, Institute of Geographic Sciences and Natural Resources Research, CAS, Beijing 100101, China*
[3]*School of Mathematics and Physics, China University of Geosciences, Wuhan 430074, China*

Correspondence should be addressed to Jinyan Zhan; zhanjy@bnu.edu.cn

Received 9 August 2014; Accepted 8 October 2014

Academic Editor: R. B. Singh

This study evaluated hydrological impacts of potential climate and land use changes in Heihe River Basin of Northwest China. The future climate data for the simulation with Soil and Water Assessment Tool (SWAT) were prepared using a dynamical downscaling method. The future land uses were simulated with the Dynamic Land Use System (DLS) model by establishing Multinomial Logistic Regression (MNL) model for six land use types. In 2006–2030, land uses in the basin will experience a significant change with a prominent increase in urban areas, a moderate increase in grassland, and a great decrease in unused land. Besides, the simulation results showed that in comparison to those during 1981–2005 the temperature and precipitation during 2006–2030 will change by +0.8°C and +10.8%, respectively. The land use change and climate change will jointly make the water yield change by +8.5%, while they will separately make the water yield change by −1.8% and +9.8%, respectively. The predicted large increase in future precipitation and the corresponding decrease in unused land will have substantial impacts on the watershed hydrology, especially on the surface runoff and streamflow. Therefore, to mitigate negative hydrological impacts and utilize positive impacts, both land use and climate changes should be considered in water resource planning for the Heihe River Basin.

1. Introduction

Climate and land use/land cover (LULC) changes are amongst the greatest global environmental pressures resulting from anthropogenic activities, both of which greatly impact the hydrological cycle [1–3]. Their impact on the hydrological cycle at the basin scale has become an important research issue in hydrology community owing to the increasingly serious water scarcity [4, 5]. The hydrological response of watersheds to climate and LULC changes is an important issue of water resource planning and management [6, 7], and the potential impacts of LULC change on the hydrological cycle must be considered by water resource managers [8, 9]. For example, the LULC changes due to urbanization and deforestation can alter the hydrological processes and lead to change of flood frequency and annual mean discharge by impacting the evapotranspiration, soil infiltration capacity, and surface and subsurface flow regimes [8, 10, 11], while climate change can alter the flow routing time and peak flows [10, 12]. It is crucial to the long-term water resource planning and management to better understand the potential impacts of climate and LULC changes on the runoff and streamflow in basins [9, 13]. In particular, effective water resource management under changing conditions requires reliable information about flows and modes that can be used to simulate flow regimes under different scenarios of changing land use and climate [6].

Separation of impacts of climate and LULC changes on the hydrological cycle is of great importance to improving the land use planning and water resource management [10, 14],

especially in arid and semiarid regions where the climate change may significantly affect the hydrological cycle [15]. The effects of LULC and climate changes on the streamflow are more evident in the arid and semiarid regions. One typical example is the Heihe River Basin in Northwest China, which is characterized by limited water resources and special hydroclimatic and physiographic conditions [16]. Understanding the hydrological responses to potential climate change is very important for developing sustainable water resource management strategies in this region. However, the impacts of urbanization and deforestation on the hydrological cycle in arid and semiarid regions have been rarely documented [17–19]. Overall, there is still very limited understanding of the separate as well as combined impacts of LULC and climate changes on regional water and energy cycles, and therefore more in-depth research is needed, especially in the arid and semiarid regions [17].

There are many studies about the hydrological impacts of land use change or climate change at the basin scale, and most of them were conducted with a hydrological model based on a series of land use data extracted from satellite images [9, 20, 21]. For example, the impacts of land use change scenarios in the Wutu watershed, North Taiwan, were assessed using the conversion of a land use model (CLUE-s) and a generalized watershed loading functions model [16]. A Soil Water Assessment Tool (SWAT) and multiple General Circulation Models (GCMs) were used to investigate the relationship between climatic and hydrological changes in the Upper Mississippi River [22]. Most of these studies assume no change in LULC [4, 23], but the impacts of climate change on hydrology vary among regions and should be investigated with regional climate change scenarios [4]. Besides, the hydrological impacts of LULC change also vary with the climatic conditions [9]. For example, water balance variables might add or subtract the impacts of climate change under varying land cover conditions. In particular, the regional LULC change can offset or magnify the changes in global average temperature and can significantly alter the impacts associated with global warming [17, 24]. In addition, some studies about the combined effects of climate and LULC changes on streamflow showed that climate change was generally more significant than LULC change in determining the basin hydrological response [25–27]. For example, climate dominates the changing streamflow in the Xinjiang River Basin of Poyang Lake, China [25]. However, the hydrological cycle in a basin is a complex process influenced by climate and the physical properties of the catchment and human activities together [4, 5]. The complexity of these factors complicates the separation between effects of land use and climatic variability on streamflow [26, 28]. Therefore, it is still a challenge to distinguish the effects of LULC change from that of concurrent climate variability [14].

This study aims to separate the impacts of climate and LULC changes on the hydrological cycle in the Heihe River Basin under future scenarios to provide some useful reference information that can be used to improve the water resource management and guarantee the sustainable development. The climatic data predicted by General Circulation Models (GCMs) under RCP 4.5 scenario were used to represent the climate change scenarios for 2006–2030, and the land use data simulated with the Dynamic Land Use System (DLS) model were used to represent the land use change scenarios. The future hydrological cycle was simulated with the SWAT based on the scenario data of climate change and land use change, the hydrological impacts of which were analyzed by comparing the simulation results under different scenarios. The results of this study can provide valuable information for guiding future water resource management in the Heihe River Basin as well as other arid and semiarid regions in China.

2. Methods

2.1. Study Area. The Heihe River Basin is the second largest inland river basin in China, which lies between 37°43′–42°41′N and 97°23′–102°72′E with a total area of 127,96 thousand km^2. This basin expands across Qinghai Province, Gansu Province, and Inner Mongolia Autonomous Region in Northwest China (Figure 1). With a total length of 821 km, the Heihe River is divided into the upper, middle, and lower reaches, where the natural and socioeconomic characteristics differ significantly. For example, the average annual precipitation is between 200 and 500 mm, less than 200 mm, and less than 50 mm in these reaches, respectively, while the annual evaporation ranges from 700 mm in the upper reach to more than 3000 mm in the lower reach [29]. Besides, the annual average temperature is 9.4°C over the last 30 years, and this basin enjoys a dry continental climate. The altitude ranges from 869 to 5542 m, with an average of 1778 m. The main land cover types are desert (57.15% of total basin area), mountains (33.16%), and oasis (8.19%) [30]. The ecosystems from the upper reach to the lower reach are linked by the hydrological cycle, but the hydrological cycle has significantly changed due to the land use change and climate change in the past decades. For example, about 65% of the irrigation water in the middle reach was extracted from the river runoff, which greatly influences the hydrological cycle of the whole basin. Therefore, a detailed and integrated simulation analysis of the water resources is critical and urgent for better water resource management in the Heihe River Basin.

2.2. Data for Model Simulation. The spatial data (i.e., topography, soil and land use), historical climate data, and hydrological data for the watershed were first prepared for the SWAT model and DLS model. The topography was represented with the 90 m resolution digital elevation model (DEM) of Shuttle Radar Topography Mission (SRTM) (http://srtm.csi.cgiar.org/) [31]. The soil data, including texture, depth, and drainage attributes, were from the Harmonized World Soil Database (HWSD) supplied by the Environmental and Ecological Science Data Center for West China (WestDC) (http://westdc.westgis.ac.cn/). The historical land use data including 25 land use types, which were derived from Landsat TM/ETM images, were provided by Data Center of Chinese Academy of Sciences (CAS) [32]. In particular, the glacier data were obtained from WestDC (http://westdc.westgis.ac.cn/), and land use properties were directly obtained from the SWAT model database (Table 1). The historical hydrological data for SWAT model calibration and validation

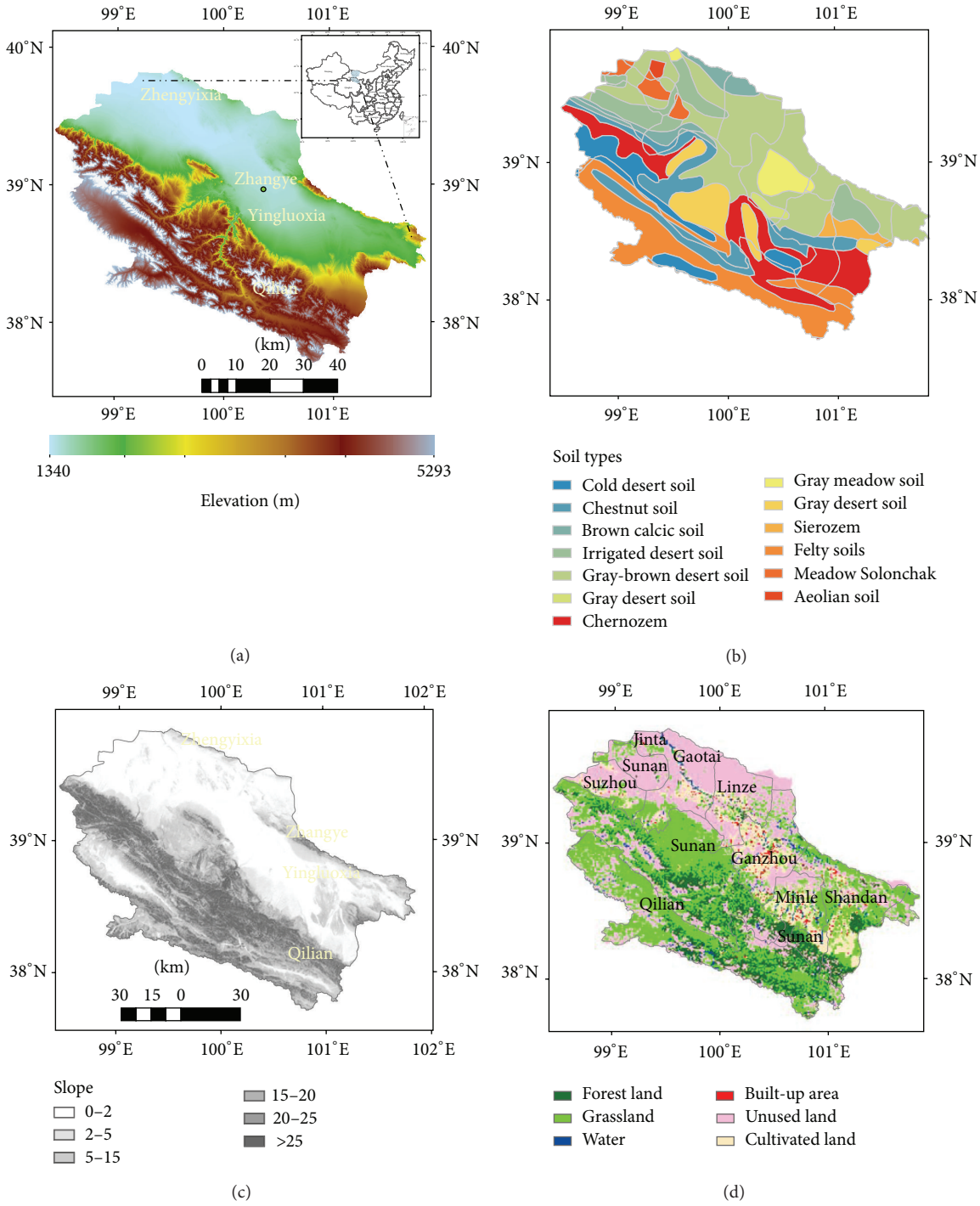

Figure 1: The upper and middle Heihe River Basin: (a) digital elevation model, (b) soil type, (c) slope, and (d) land use in 2010.

include the river flow data from four hydrological stations. The hydrological observation data, including annual data in Heihe River Basin during 1980–2010, were obtained from the hydrological yearbook provided by WestDC. The river flow data used for the model calibration and validation were provided by the Data Center of CAS. The historical daily weather data during 1980–2010 were collected from China Meteorological Administration (CMA), including daily precipitation, maximum and minimum temperatures, solar radiation, humidity, wind speed, and wind direction from 13 weather stations in or near the Heihe River Basin.

2.3. Simulation of Land Use Changes with the DLS Model. The DLS model is a set of applications used to simulate the changing process of land use system and is an effective tool for simulation of spatial-temporal land use changes to assist land

Table 1: Data used and sources.

Data type	Data sources	Scale	Description
DEM	Shuttle Radar Topography Mission (SRTM)	90 m	Elevation
Land use	Data Center of Chinese Academy of Science	1 : 100000	The classification system contains 25 categories
Soil	WestDC (http://westdc.westgis.ac.cn/)	1 : 1000000	Some parameters were calculated using a (Soil-Plant-Atmosphere-Water) Field and Pond Hydrology model
Weather	China Meteorological Administration	Daily	5 weather stations
Hydrological observation	Hydrological yearbook	Daily	4 stations
River flow	Data Center of Chinese Academy of Science	1 : 250000	River network diversion
Glacier	WestDC (http://westdc.westgis.ac.cn/)	1 : 100000	The attributes include width, length, and depth

management [33]. The DLS model consists of three modules: a spatial regression module that identifies the relationships between land uses and the influencing factors; a scenario analysis module of land use changes that determines the land demands at the regional level; a spatial disaggregation module that allocates land use changes from a regional level to the disaggregated grid cells [34, 35].

The DLS model simulates the spatial-temporal land use changes with three processes: scenario analysis of land use change, spatial regression analysis, and spatial allocation of land use changes. The first process was carried out with the scenario analysis module, which provides the data of total land demands at the annual scale during a given period. By including the scenario analyses of land use changes, a set of spatially explicit simulation results of land use change can be exported by the DLS model [36]. The total land use demands can be set by several approaches, such as trend analysis methods (e.g., linear interpolations or more sophisticated econometric models) and economic models. In this study, the total land demands during the simulation period were first determined using trend analysis methods and then were used to establish a scenario of land use change during 2006–2030.

In the spatial regression module, the relationships between land uses and influencing factors were analyzed via stepwise logistic regression analysis of past land use changes and their drivers [37]. For each grid cell, the total probability for each land use type is calculated on basis of the multinomial logistic regression at the pixel scale as follows:

$$P_{i,k} = \begin{cases} \dfrac{1}{1 + \sum_{k \neq i} e^{x_k \beta_k}} & i = k \\ \dfrac{e^{x_k \beta_k}}{1 + \sum_{k \neq i} e^{x_k \beta_k}} & i \neq k, \end{cases} \quad (1)$$

where $P_{i,k}$ is the probability of conversion from land type i to k in the cells under given driving factors; $X_1, X_2, \ldots, X_n$ represent the driving factors of climate, landform, location, population, economic growth, policy, and other categories; $\beta_1, \beta_2 \cdots \beta_n$ are the regression analysis coefficients of driving factors for further estimation.

In this study, all the data of land use and the influencing factors were prepared at the annual scale. The land use data in 2000 and 2005 were used in the logistic regression. The assumed driving factors were categorized into five groups: climate, geophysics, transportation, location, and socioeconomics. The data of these factors in the corresponding years were also prepared (Table 2).

The spatial disaggregation module is used to spatially and explicitly convert the land demands into land use changes at various locations of the study area. The spatial disaggregation is carried out in an iterative procedure based on the probability maps, conversion rules, historical land use maps, and land demands under the scenarios. The probability maps of each land use type were prepared with the logistic regression results. Besides, the rules of land use conversion were set for each land use type, whose value ranges from 0 to 1. A smaller value means one land use type is more likely to be converted to another type, and vice versa. The development-restricted areas in the study area were also specified.

2.4. Downscaling of GCM Climate Data. GCMs are arguably the best available tools for modeling future climate. Yet GCMs provide information at a resolution that is too coarse to be directly used in hydrological modeling [38]. Therefore downscaling is required to transform the low resolution GCM outputs to the high resolution climate features needed for hydrological simulation. The downscaling procedure is as follows. First, the average annual precipitation and temperature of 30 years (1980–2010) were calculated, which were adopted as a baseline for selecting the GCMs. We considered future climate change scenarios for the basin (Figure 2) by using the spatially distributed outputs from 10 GCMs under RCP 4.5 scenario. The climate projections of Max Planck Institute (MPI) were downscaled to the 3 km × 3 km grid in the study area, and bias was corrected and climate change scenarios were developed by MPI for Meteorology. The annual mean values of 10 GCM spatial data from 2006 to 2030 were calculated according to the basin perimeter, and one out of ten GCMs was also selected based on the historical trends and annual averages of temperature and precipitation. The MPI

Table 2: Results of logistical regression for the six land use types with 13 driving factors.

	Cultivated land	Forest land	Grassland	Water	Built-up area	Unused land
Slope	−0.000049	0.000121	−7.42E − 05	−7.76E − 06	−1.1E − 06	0.0000105
	(−27.52)***	(−63.65)***	(−18.89)***	(−7.24)***	(−2.07)*	(−2.64)**
Elevation	−0.000136	−3.02E − 05	0.000116	−0.0000149	−5.9E − 06	0.0000711
	(−53.82)***	(−11.13)***	(−20.8)***	(−9.76)***	(−7.85)***	(−12.56)***
Rain	−0.000045	0.0000228	0.0000419	0.0000136	1.4E − 06	−0.0000347
	(−16.09)***	(−7.61)***	(−6.79)***	(−8.05)***	−1.7	(−5.54)***
Radiation	−0.000407	0.000243	−0.000923	−8.64E − 06	1.16E − 05	0.00108
	(−24.27)***	(−13.55)***	(−24.98)***	(−0.86)	(−2.34)*	(−28.91)***
>0°C accumulated temperature	−0.0000106	0.0000127	0.000026	−3.88E − 06	−7.2E − 07	−0.0000234
	(−24.03)***	(−26.78)***	(−26.59)***	(−14.55)***	(−5.52)***	(−23.67)***
Soil organic matter	0.0685	0.232	−0.186	0.0152	−0.00655	−0.123
	(−9.38)***	(−29.64)***	(−11.58)***	(−3.46)***	(−3.03)**	(−7.52)***
pH value	0.00769	−0.0131	−0.00541	0.00171	0.000719	0.00834
	(−7.15)***	(−11.32)***	(−2.28)*	(−2.64)**	(−2.26)*	(−3.47)***
Population density	0.000247	−7.82E − 05	−3.16E − 05	0.0000206	−3.2E − 06	−0.000154
	(−32.18)***	(−9.52)***	(−1.87)	(−4.46)***	(−1.40)	(−9.00)***
Per capita GDP	0.000548	−3.08E − 05	−0.000185	−0.00002	0.000411	−0.000723
	(−76.02)***	(−3.99)***	(−11.62)***	(−4.61)***	(−192.54)***	(−44.87)***
Distance to railway	0.000193	0.000229	0.000979	0.00000653	1.72E − 05	−0.00142
	(−13.55)***	(−14.96)***	(−31.16)***	−0.76	(−4.07)***	(−44.71)***
Distance to road	−0.000221	−0.000335	0.00111	−0.000066	−1.4E − 05	−0.000477
	(−18.45)***	(−26.06)***	(−42.08)***	(−9.13)***	(−3.79)***	(−17.79)***
Distance to water source	−0.000338	0.0000239	0.000926	−0.000346	−5.2E − 06	−0.000261
	(−14.46)***	−0.95	(−17.96)***	(−24.55)***	(−0.75)	(−4.99)***
Distance to city	−0.000125	−0.000108	−0.000567	0.0000996	−2E − 05	0.00072
	(−8.11)***	(−6.58)***	(−16.76)***	(−10.78)***	(−4.31)***	(−20.98)***

Note: t statistics in parentheses; *significant at 10%; **significant at 5%; ***significant at 1%.

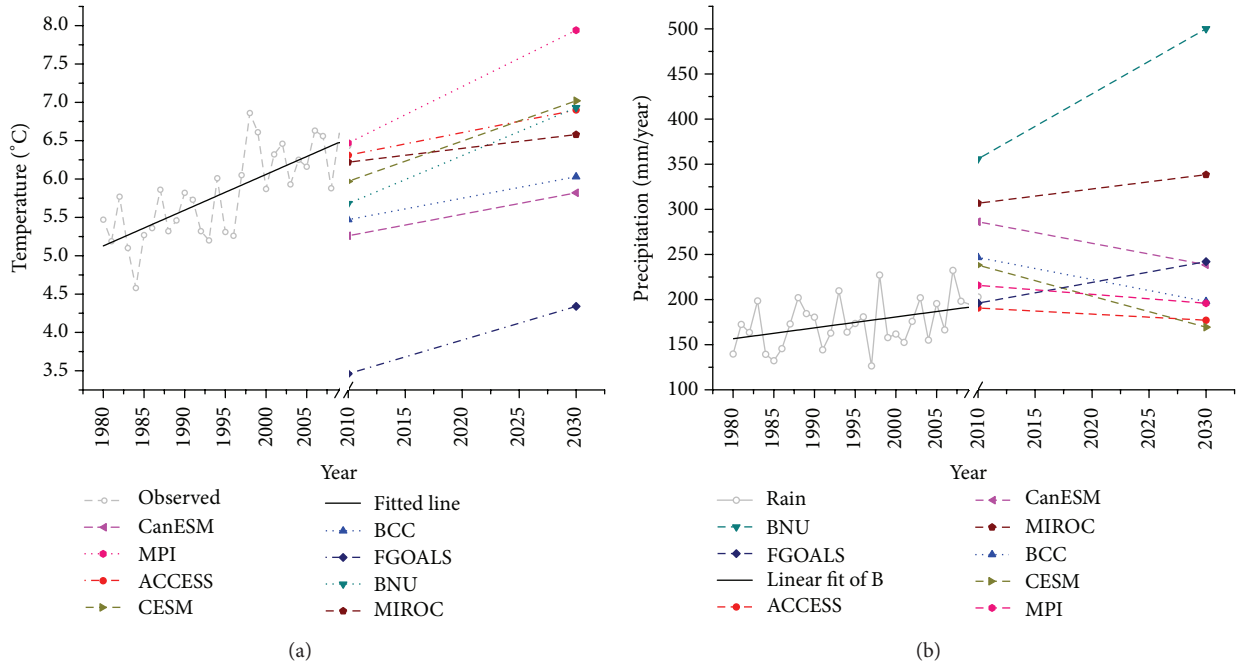

Figure 2: The trends in (a) observed (grey line; running average in black) and projected (10AR5 GCMs; colored dash lines) temperature, (b) observed and projected precipitation.

Table 3: List of calibration parameters and the optimized values.

Parameter	Description	Range	Optimized value
TLAPS	Temperature lapse rate [°C/km]	0, −10	−3.8
PLAPS	Precipitation lapse rate [mm H_2O/km]	0, 100	5.8
SFTMP	Snowfall temperature [°C]	−2, +2	0.9
SMTMP	Snow melt base temperature [°C]	−5, +5	2.1
SNOEB	Initial snow water content in elevation band [mm]	50, 230	100
TIMP	Snowpack temperature lag factor	0.38–0.62	0.49
SMFMN	Melt factor for snow on December 21 [mm H_2O/°C-day]	3.05–3.51	3.25
SMFMX	Melt factor for snow on June 21 [mm H_2O/°C-day]	5.85–6.27	6.02
SURLAG	Surface runoff lag time [days]	4.18–5.19	4.68

model was finally chosen through comparison. The result of MPI model originates in MPI, and the spatial resolution is 1.865° (LAT) × 1.875° (LON). Then the parameters in MPI GCM were transformed into the forcing data of a regional climate model in weather research and forecasting (WRF) simulation, and thereafter dynamical downscaling simulation was performed at the spatial resolution of 3 km for the period of 2006–2030. We considered the impacts of land use changes on regional climate, and the land cover data before WRF simulation were dynamically replaced with land use change data based on the simulation with the DLS model. Finally, the data simulated by the regional climate model were matched with meteorological sites, and the meteorological site data were prepared for the simulation with SWAT.

2.5. Simulation of Hydrological Cycle with the SWAT Model. The study area was first divided into subwatersheds, which were subdivided into hydrological response units (HRUs). Besides, for each subwatershed, the climate data used are taken from the GCM grid point that is the closest to its centroid. To improve performance, the SWAT model was calibrated and validated by adjusting several parameters and comparing the simulated streamflow with observed values. The most sensitive parameters were identified with the built-in sensitivity analysis tool in SWAT [39]. The daily streamflow observation data from Yingluoxia Hydrological Station in 2004 were used for calibration, and the observation data in 2005 were used for validation. It should be noted that the first three years were used as a warm-up period to mitigate the effects of unknown initial conditions, which were then excluded from the subsequent analysis. The ability of the SWAT model to replicate the temporal trends in the historical hydrological observations was assessed using the coefficient of determination (R^2), the Nash and Sutcliffe (1970) model efficiency (NSE), and the root mean square error (RMSE).

3. Result and Discussion

3.1. Calibration and Validation. The SWAT model was calibrated for 2004 and validated for 2005 using the daily streamflow observation data from four gauging stations within the study area. Finally, fifteen parameters were selected for the calibration (Table 2), which are associated with snow (SFTMP, SMTMP, SMFMX, SMFMN, and TIMP), runoff (CN2), groundwater (ALPHA_BF and GW_DELAY), soil (SOL_AWC), channel (CH_N and CH_K2), and evaporation (ESCO) processes. After the sensitivity analysis, 9 relatively more sensitive parameters were identified for the calibration. Most of the parameters were adjusted based on multiple trials, and the SWAT model was calibrated using an automatic calibration technique with the program Sequential Uncertainty Fitting Version (SUFI-2). With SUFI-2, sensitive initial and default parameters related to hydrology varied simultaneously until an optimal solution was achieved. The most sensitive parameters with their best ranges and best-fitted values are shown in Table 3. Finally, these best-fitted values were used to adjust the initial model inputs for the simulation during 2006–2030. The model was validated using daily streamflow observation data from the Yingluoxia Hydrological Station in 2005. The validation results show that the NSE is 0.78 and R^2 of the observed and simulated data is 0.81 (Figure 3), demonstrating the high behavioral performance of the SWAT model.

3.2. Future Climate under the RCP 4.5 Scenario. Based on the downscaled GCM climate data, we calculated the mean temperature and precipitation of the 9 lattice points around the grid that included Qilian meteorological station. The results were compared with the mean monthly temperatures and precipitation of the meteorological station during 1981–2005. The monthly mean temperatures of the 25 years ranged from −3 to 3°C and increased by around 0.8°C. The mean monthly precipitation ranges from −0.3% to 10% and increased by around 7.8% (Figure 4). The increase range of mean monthly precipitation is large, while the range of reduction is smaller.

3.3. Future Land Use Change Simulated with DLS. The results suggested the change in one land use type was influenced by multiple factors, and the 13 driving factors can reasonably explain the spatial patterns of all land use types. For example, the existence of forest land was significantly influenced by all the 13 driving factors, while the existence of cultivated land and grassland was affected by the altitude, distance, and soil factors. The future land uses for 2006–2030 were simulated with the DLS model by combining

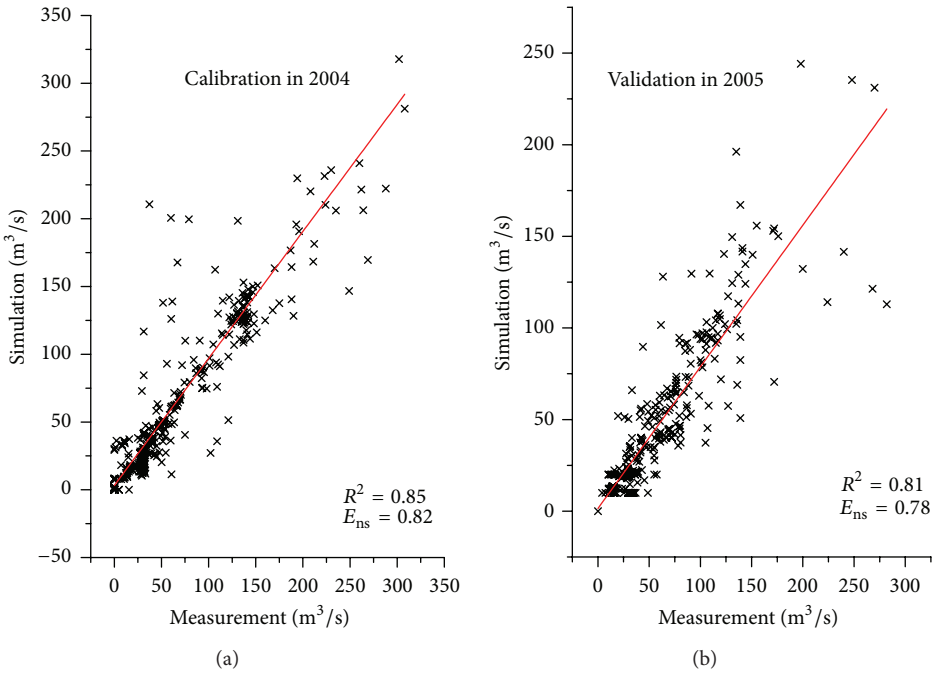

Figure 3: The calibration and validation on streamflow of the SWAT.

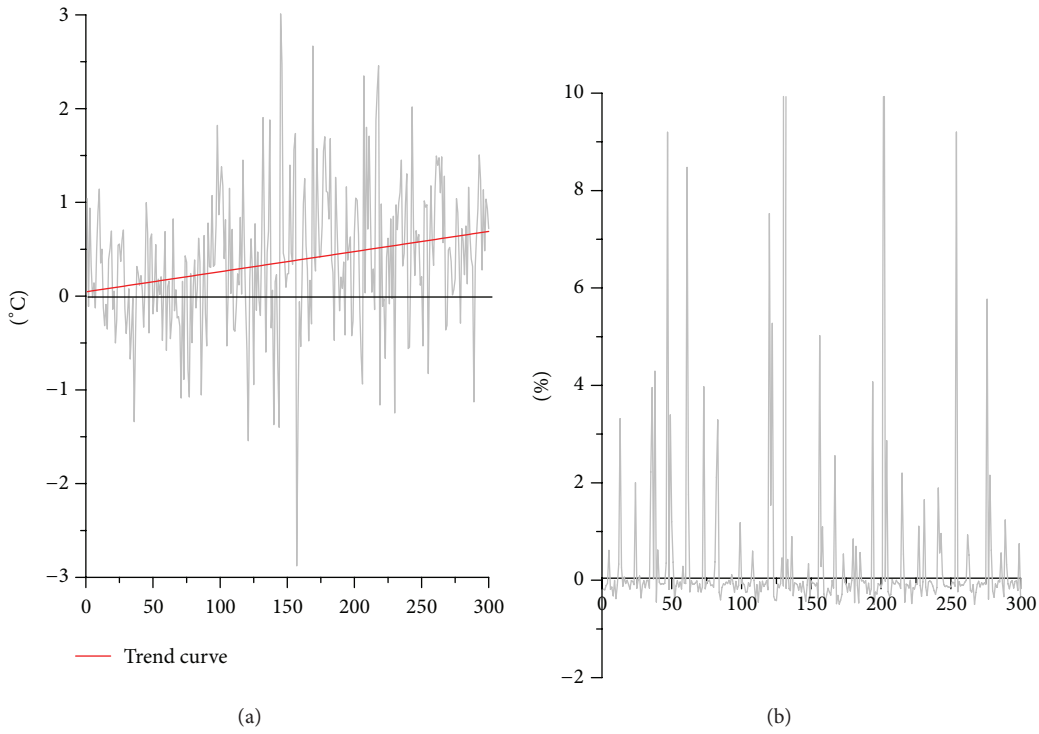

Figure 4: The difference of average monthly temperature and precipitation between 1981–2005 and 2006–2030 in Qilian Weather observed station.

the probability maps prepared with logistic regression analysis, the land demands under different scenarios, and the map of development-restricted areas. The simulation results indicated that the most dramatic land use changes during 2006–2030 will mainly occur in the upper reach and some parts of the middle reach of Heihe River Basin. Compared to 2005, the areas of forest land and unused land in 2030 will decrease by 6.2% and 1.6%, respectively, while the areas of built-up land, cultivated land, and grassland will increase by 1.7%, 1.3%, and 4.8%, respectively (Figure 5). The significant

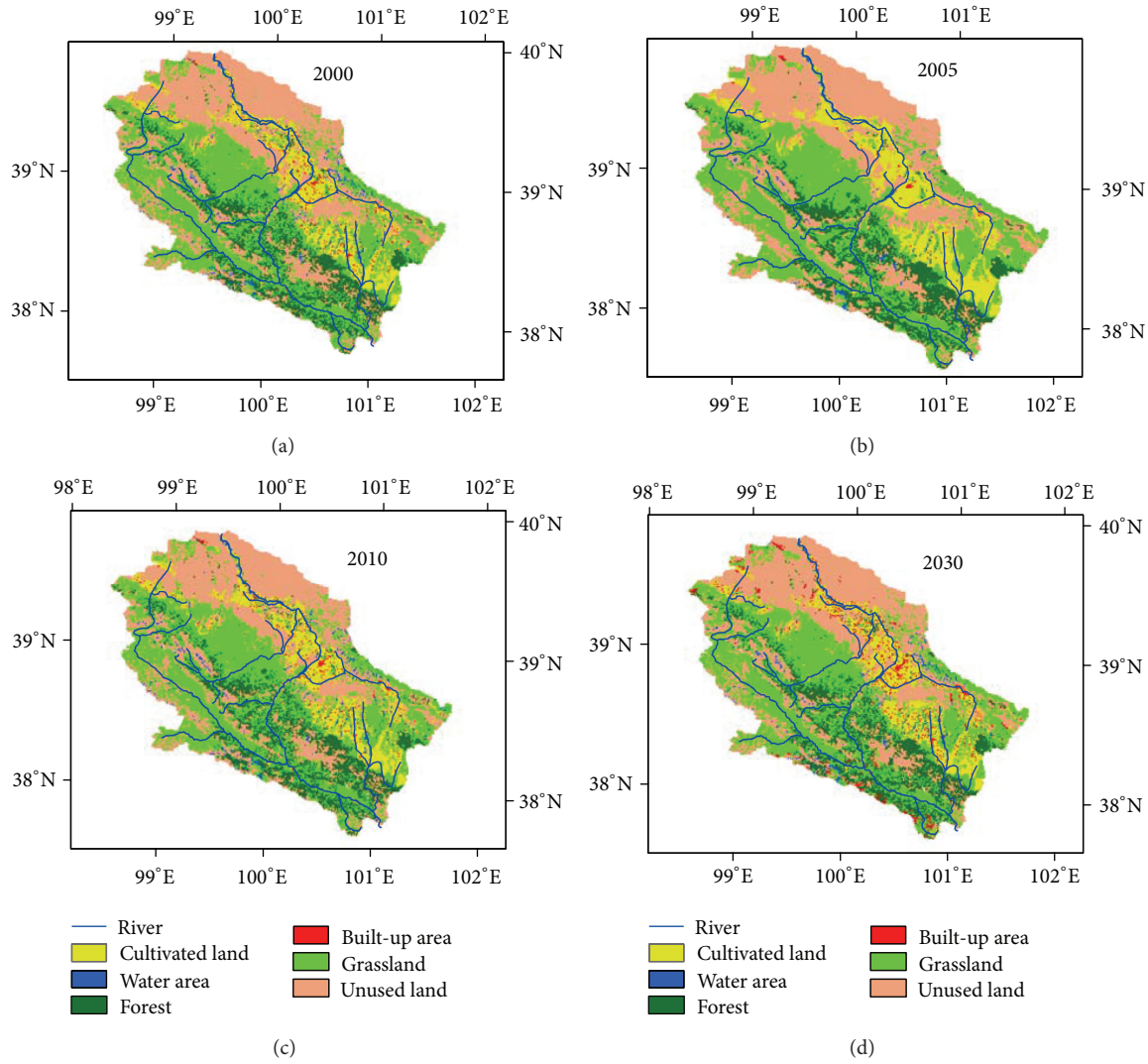

Figure 5: Comparison of the land uses interpreted in 2000, 2005 and simulated in 2010, 2030.

increase of grassland area may mainly result from the steady pasture construction, and this uptrend may continue in the future owing to the increasing demand for pasture products.

3.4. Impacts of Climate and Land Use Changes on Watershed Hydrology. Four simulation experiments were designed based on the land use data and climate data. In the baseline experiment for the period during 1981–2005, the water yield was simulated with the land use data in 2000, 2005 and the weather station observations during 1981–2005 (Figure 6(b)). Then three scenarios for the period during 2006–2030 were designed based on the land use and climate change (Figure 6(a)), the results from which were compared with that in the baseline experiment. In the first scenario during 2006–2030, the water yield was simulation with the land use data in 2010 and 2030, temperature data during 2006–2030, and the precipitation data during 1981–2005. The simulation result shows that the impacts of future land use change on the water yield vary with seasons, and the land use change will have negative overall influence on the water yield, with an influence degree of −1.8% according to the annual mean water yield.

The second scenario during 2006–2030 was based on scenarios of temperature and land use changes. The second experiment used the land use data in 2010 and 2030, scenario data of temperature during 2006–2030, and precipitation data during 1981–2005. The analysis of climate change scenarios shows that the average temperature will rise by 0.8°C between 1981–2005 and 2006–2030. The simulation result in the second experiment shows that the land use and temperature changes will make the water yield change by 0.6%–1.1%, the change range of which is relatively smaller compared to the simulation results under the scenario with only land use change. The reasons may be that the temperature rise and melting of a small amount of snow slightly offset the adverse effects of land use change. At the same time, the higher

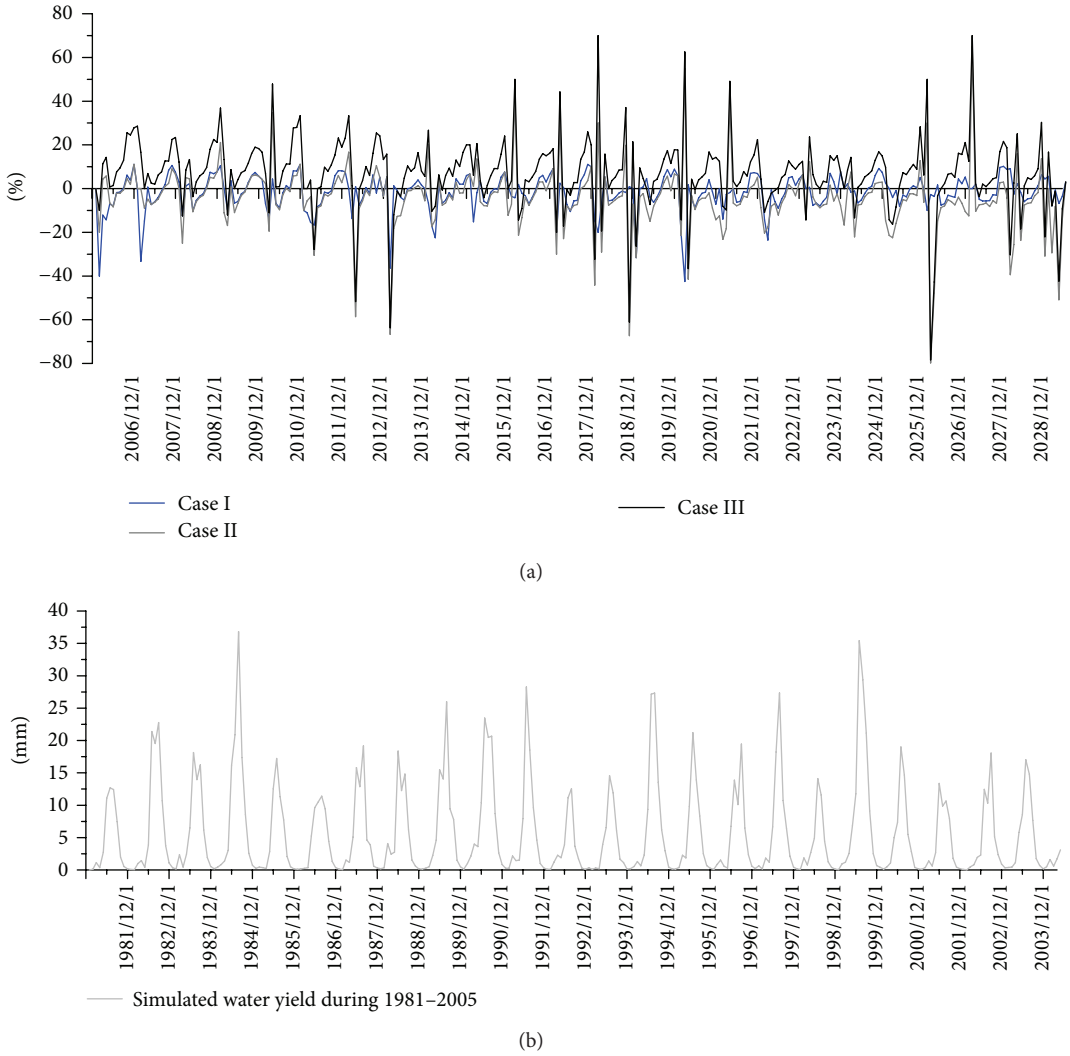

Figure 6: Comparison of water yields under three scenarios.

temperatures will result in more winter precipitation in the form of rain rather than snow, leading to the hydrologic consequences including increased winter discharge, a shift in the spring snowmelt peak to earlier in the season, and decreased summer discharge.

The third scenario during 2006–2030 involves scenarios of changes in all of land use, temperature, and precipitation. The land use data in 2010 and 2030 and temperature and precipitation data during 2006–2030 were used under the third scenario. The simulation result shows that these three factors jointly have positive impacts on the water yield, making the basin water yield increase by about 9.8%. The increase of the basin water yield is mainly caused by the change in precipitation, which will increase by around 10.8% during 2006–2030 in comparison to that during 1981–2005. Overall, the simulation results suggest that the basin water yield will increase in the future under different scenarios of climate and land use changes.

4. Discussion and Conclusions

In the Heihe River Basin, the upper reaches are featured with the generation and use of blue water, while the lower reach and surrounding areas are characterized by natural ecosystems and a low population density. LULC is defined as syndromes of human activities such as agriculture, forestry, and building construction, and most of previous studies only focused on the hydrological influence of LULC change in the upper reach. The separation between hydrological impacts of land use and climate changes has never been studied in the upper and middle reaches of the Heihe River Basin. However, we argue that studying the hydrological processes in the upper and middle reaches is essential since water supply to the lower reach is impacted by both the climate change and human activities in the upper and middle reaches.

In this study, we analyzed the impacts of potential climate and land use changes on the water yield in the upper and

middle reaches of Heihe River Basin based on the simulation with the SWAT model. The results show that the water yield was more affected by climate change than by land use change. This indicates that the predicted increase in precipitation will exert more significant impacts on the watershed hydrology than the predicted land use changes will. However, the analysis of the projected streamflow changes shows that there are higher uncertainties in the dry season compared with the wet season in the simulation with the hydrological model and GCMs climate data. It is difficult to accurately project the hydrological changes since there are various uncertainties associated with the future Green House Gas (GHG) emission scenarios, GCM structure, downscaling method, LULC, and hydrological models. In particular, water resource managers are generally confronted with complex problems in sustainable management and conservation of water resources due to the uncertainties in the future hydrological projection under climate and land use changes. It is therefore crucial to consider both land use and climate changes in water resource planning for the Heihe River Basin so as to mitigate their negative hydrological impacts, and more valuable information may be provided to the water resource managers if these uncertainties in the future hydrological projection can be effectively reduced through advanced modeling and research.

Conflict of Interests

The authors declare that there is no conflict of interests regarding the publication of this paper.

Acknowledgments

This research was financially supported by the major research plan of the National Natural Science Foundation of China (Grant no. 91325302), National Basic Research Program of China (973 Program) (no. 2010CB950904), and the National Natural Science Funds of China for Distinguished Young Scholar (Grant no. 71225005).

References

[1] Z. Žalud, M. Trnka, M. Dubrovský, P. Hlavinka, D. Semerádová, and E. Kocmánková, "Climate change impacts on selected aspects of the Czech agricultural production," *Plant Protection Science*, vol. 45, pp. S11–S19, 2009.

[2] E. Lorencová, J. Frélichová, E. Nelson, and D. Vačkář, "Past and future impacts of land use and climate change on agricultural ecosystem services in the Czech Republic," *Land Use Policy*, vol. 33, pp. 183–194, 2013.

[3] R. Mahmood, A. I. Quintanar, G. Conner et al., "Impacts of land use/land cover change on climate and future research priorities," *Bulletin of the American Meteorological Society*, vol. 91, no. 1, pp. 37–46, 2010.

[4] Z. Ma, S. Kang, L. Zhang, L. Tong, and X. Su, "Analysis of impacts of climate variability and human activity on streamflow for a river basin in arid region of northwest China," *Journal of Hydrology*, vol. 352, no. 3-4, pp. 239–249, 2008.

[5] B. R. Scanlon, I. Jolly, M. Sophocleous, and L. Zhang, "Global impacts of conversions from natural to agricultural ecosystems on water resources: quantity versus quality," *Water Resources Research*, vol. 43, no. 3, Article ID W03437, 2007.

[6] L. M. Mango, A. M. Melesse, M. E. McClain, D. Gann, and S. G. Setegn, "Land use and climate change impacts on the hydrology of the upper Mara River Basin, Kenya: results of a modeling study to support better resource management," *Hydrology and Earth System Sciences*, vol. 15, no. 7, pp. 2245–2258, 2011.

[7] C. J. Vörösmarty, P. Green, J. Salisbury, and R. B. Lammers, "Global water resources: vulnerability from climate change and population growth," *Science*, vol. 289, no. 5477, pp. 284–288, 2000.

[8] S. Qi, G. Sun, Y. Wang, S. G. McNulty, and J. A. M. Myers, "Streamflow response to climate and landuse changes in a coastal watershed in North Carolina," *Transactions of the ASABE*, vol. 52, no. 3, pp. 739–749, 2009.

[9] J. Kim, J. Choi, C. Choi, and S. Park, "Impacts of changes in climate and land use/land cover under IPCC RCP scenarios on streamflow in the Hoeya River Basin, Korea," *Science of the Total Environment*, vol. 452-453, pp. 181–195, 2013.

[10] Z. Li, W.-Z. Liu, X.-C. Zhang, and F.-L. Zheng, "Impacts of land use change and climate variability on hydrology in an agricultural catchment on the Loess Plateau of China," *Journal of Hydrology*, vol. 377, no. 1-2, pp. 35–42, 2009.

[11] R. W. Skaggs, D. M. Amatya, G. Chescheir, C. Blanton, and J. Gilliam, "Effect of drainage and management practices on hydrology of pine plantation," in *Proceedings of the International Conference on Hydrology and Management of Forested Wetlands*, 2006.

[12] T. D. Prowse, S. Beltaos, J. T. Gardner et al., "Climate change, flow regulation and land-use effects on the hydrology of the Peace-Athabasca-Slave system; Findings from the Northern Rivers Ecosystem Initiative," *Environmental Monitoring and Assessment*, vol. 113, no. 1–3, pp. 167–197, 2006.

[13] B. Dixon and J. Earls, "Effects of urbanization on streamflow using SWAT with real and simulated meteorological data," *Applied Geography*, vol. 35, no. 1-2, pp. 174–190, 2012.

[14] E. Lioubimtseva, R. Cole, J. M. Adams, and G. Kapustin, "Impacts of climate and land-cover changes in arid lands of Central Asia," *Journal of Arid Environments*, vol. 62, no. 2, pp. 285–308, 2005.

[15] Z. Wang, D. L. Ficklin, Y. Zhang, and M. Zhang, "Impact of climate change on streamflow in the arid Shiyang River Basin of northwest China," *Hydrological Processes*, vol. 26, no. 18, pp. 2733–2744, 2012.

[16] D. R. D'Agostino, L. G. Trisorio, N. Lamaddalena, and R. Ragab, "Assessing the results of scenarios of climate and land use changes on the hydrology of an Italian catchment: modelling study," *Hydrological Processes*, vol. 24, no. 19, pp. 2693–2704, 2010.

[17] V. Mishra, K. A. Cherkauer, D. Niyogi et al., "A regional scale assessment of land use/land cover and climatic changes on water and energy cycle in the upper Midwest United States," *International Journal of Climatology*, vol. 30, no. 13, pp. 2025–2044, 2010.

[18] J. A. Vano, J. A. Foley, C. J. Kucharik, and M. T. Coe, "Evaluating the seasonal and interannual variations in water balance in Northern Wisconsin using a land surface model," *Journal of Geophysical Research G: Biogeosciences*, vol. 111, no. 2, 2006.

[19] D. Mao and K. A. Cherkauer, "Impacts of land-use change on hydrologic responses in the Great Lakes region," *Journal of Hydrology*, vol. 374, no. 1-2, pp. 71–82, 2009.

[20] J.-Y. Park, M.-J. Park, M.-J. H.-K. Joh et al., "Assessment of MIROC3.2 hires climate and clue-s land use change impacts on watershed hydrology using Swat," *Transactions of the ASABE*, vol. 54, no. 5, pp. 1713–1724, 2011.

[21] S. J. Kim, H. J. Kwon, G. A. Park, and M. S. Lee, "Assessment of land-use impact on streamflow via a grid-based modelling approach including paddy fields," *Hydrological Processes*, vol. 19, no. 19, pp. 3801–3817, 2005.

[22] E. Lu, E. S. Takle, and J. Manoj, "The relationships between climatic and hydrological changes in the upper Mississippi river basin: a SWAT and multi-GCM study," *Journal of Hydrometeorology*, vol. 11, no. 2, pp. 437–451, 2010.

[23] L. Liu, Z. Liu, X. Ren, T. Fischer, and Y. Xu, "Hydrological impacts of climate change in the Yellow River Basin for the 21st century using hydrological model and statistical downscaling model," *Quaternary International*, vol. 244, no. 2, pp. 211–220, 2011.

[24] S. Fall, D. Niyogi, A. Gluhovsky, R. A. Pielke, E. Kalnay, and G. Rochon, "Impacts of land use land cover on temperature trends over the continental United States: assessment using the North American Regional Reanalysis," *International Journal of Climatology*, vol. 30, no. 13, pp. 1980–1993, 2010.

[25] H. Guo, Q. Hu, and T. Jiang, "Annual and seasonal streamflow responses to climate and land-cover changes in the Poyang Lake basin, China," *Journal of Hydrology*, vol. 355, no. 1–4, pp. 106–122, 2008.

[26] L. Tang, D. Yang, H. Hu, and B. Gao, "Detecting the effect of land-use change on streamflow, sediment and nutrient losses by distributed hydrological simulation," *Journal of Hydrology*, vol. 409, no. 1-2, pp. 172–182, 2011.

[27] M. D. Tomer and K. E. Schilling, "A simple approach to distinguish land-use and climate-change effects on watershed hydrology," *Journal of Hydrology*, vol. 376, no. 1-2, pp. 24–33, 2009.

[28] P. F. Juckem, R. J. Hunt, M. P. Anderson, and D. M. Robertson, "Effects of climate and land management change on streamflow in the driftless area of Wisconsin," *Journal of Hydrology*, vol. 355, no. 1–4, pp. 123–130, 2008.

[29] Q. Feng, G. D. Cheng, and K. N. Endo, "Towards sustainable development of the environmentally degraded River Heihe basin, China," *Hydrological Sciences Journal*, vol. 46, no. 5, pp. 647–658, 2001.

[30] G.-D. Cheng, H.-L. Xiao, Z.-M. Xu, J.-X. Li, and M.-F. Lu, "Water issue and its countermeasure in the inland river basins of Northwest China—a case study in Heihe River Basin," *Journal of Glaciology and Geocryology*, vol. 28, no. 3, pp. 406–413, 2006.

[31] A. Jarvis, H. I. Reuter, A. Nelson, and E. Guevara, *Hole-Filled Seamless SRTM Data V3*, International Centre for Tropical Agriculture (CIAT), 2006.

[32] X. Deng, Q. Jiang, H. Su, and F. Wu, "Trace forest conversions in Northeast China with a 1-km area percentage data model," *Journal of Applied Remote Sensing*, vol. 4, no. 1, Article ID 041893, pp. 1–13, 2010.

[33] X. Deng, H. Su, and J. Zhan, "Integration of multiple data sources to simulate the dynamics of land systems," *Sensors*, vol. 8, no. 2, pp. 620–634, 2008.

[34] X. Deng, J. Liu, Y. Lin, and C. Shi, "A framework for the land use change dynamics model compatible with rcms," *Advances in Meteorology*, vol. 2013, Article ID 658941, 7 pages, 2013.

[35] X. Deng, C. Zhao, and H. Yan, "Systematic modeling of impacts of land use and land cover changes on regional climate: a review," *Advances in Meteorology*, vol. 2013, Article ID 317678, 11 pages, 2013.

[36] X. Deng, F. Yin, Y. Lin, Q. Jin, and R. Qu, "Equilibrium analyses on structural changes of land uses in Jiangxi Province," *Journal of Food, Agriculture and Environment*, vol. 10, no. 1, pp. 846–852, 2012.

[37] X. Deng, Q. Jiang, J. Zhan, S. He, and Y. Lin, "Simulation on the dynamics of forest area changes in Northeast China," *Journal of Geographical Sciences*, vol. 20, no. 4, pp. 495–509, 2010.

[38] X. Deng, C. Zhao, Y. Lin et al., "Downscaling the impacts of large-scale LUCC on surface temperature along with IPCC RCPs: a global perspective," *Energies*, vol. 7, no. 4, pp. 2720–2739, 2014.

[39] S. Neitsch, J. Arnold, J. E. A. Kiniry, R. Srinivasan, and J. Williams, "Soil and water assessment tool user's manual version 2000," GSWRL Report 02-06, 2002.

Hindawi Publishing Corporation
Advances in Meteorology
Volume 2015, Article ID 496942, 13 pages
http://dx.doi.org/10.1155/2015/496942

Research Article

Land Use Zoning for Conserving Ecosystem Services under the Impact of Climate Change: A Case Study in the Middle Reaches of the Heihe River Basin

Chenchen Shi,[1] Jinyan Zhan,[1] Yongwei Yuan,[2] Feng Wu,[1] and Zhihui Li[3,4]

[1] *State Key Laboratory of Water Environment Simulation, School of Environment, Beijing Normal University, Beijing 100875, China*
[2] *Faculty of Resources and Environmental Science, Hubei University, Wuhan, Hubei 430062, China*
[3] *Institute of Geographic Sciences and Natural Resources Research, Chinese Academy of Sciences, Beijing 100101, China*
[4] *University of Chinese Academy of Sciences, Beijing 100049, China*

Correspondence should be addressed to Jinyan Zhan; zhanjinyan.bnu@gmail.com

Received 30 June 2014; Accepted 30 July 2014

Academic Editor: Hongbo Su

Ecosystem services are the benefit human populations derive directly and indirectly from the natural environment. They suffer from both the human intervention, like land use zoning change, and natural intervention, like the climate change. Under the background of climate change, regulation services of ecosystem could be strengthened under proper land use zoning policy to mitigate the climate change. In this paper, a case study was conducted in the middle reaches of the Heihe River Basin to assess the ecosystem services conservation zoning under the change of land use associated with climate variations. The research results show the spatial impact of land use zoning on ecosystem services in the study area which are significant reference for the spatial optimization of land use zoning in preserving the key ecosystem services to mitigate the climate change. The research contributes to the growing literature in finely characterizing the ecosystem services zones altered by land use change to alleviate the impact of climate change, as there is no such systematic ecosystem zoning method before.

1. Introduction

Ecosystem services are the natural environment provision and utility the ecosystem provides upon which human-beings survival lie [1]. It is the material basis to maintain the human survival and support earth life system [2]. According to the Millennium Ecosystem Assessment (MA) [3], the ecosystem services can be mainly divided into four categories, namely, provisioning, supporting, regulating, and cultural services. The degree of human demand influences the sustaining of the ecosystem services [4]. Meanwhile, the services provided by the ecosystem directly affect the human well-being [5, 6]. Both natural and human interventions will exert great influence on the ecosystem services, which will hinder the social and economic development and have an impact on the human well-being.

Among those natural interventions of ecosystem services, climate change is likely to affect the abundance, production, distribution, and quality of ecosystems [7]. Therefore, ecosystem services, such as climate stabilization through carbon sequestration, the provision of nonirrigated forage for livestock and wildlife species, the delivery of water which supports fish for commercial and recreational sport fishing, the provision of critical habitat for biodiversity, and many other types of ecosystem services, are likely to be impacted by a changing climate [8]. And in return the ecosystem service conservation and restoration under proper land use zoning policy play a key role in climate mitigation [9].

As for human interferences that influence the ecosystem services, numerous studies have showed that land use change associated with climate variations could affect the structure and function of ecosystem and then affect the supply of ecosystem services functions [2, 10, 11]. The spatial land use allocation may affect the provision of a wide range of ecosystem services and is instrumental to their conservation and enhancement [12].

Previous studies have shown that, in order to characterize the ecological changes, monitoring landscape pattern

changes provides an indirect approach, as such changes would influence a variety of ecological processes and functions [13–15]. However, ecosystem services zoning, which aims at identifying major regional ecological environment problems and therefore establishes ecosystem services zones, seems to be a more direct way of showing the ecosystem services change associated with land use change.

Ecological function zoning is one of the hot issues among academia in the field of ecology [16]. There are various researches of ecosystem service function zoning from different research aspects [17–19]. However, these researches either focus on only one type of ecosystem [19] or are confined to land use zoning [20]. The spatial changes of the regional ecosystem service have not been reflected. And case studies of grid scale space dynamic zoning are absent.

A scientifically sound guidance is always needed for planners to reveal the mechanism of the ecological and climatic effect of land use change and additionally to promote sustainable development. In order to achieve that, it is necessary to conduct zoning characterization of the ecosystem service under the comprehensive consideration of land use and land cover change and the site condition. While there is lack of a successful model and systematic method to accomplish this goal in the academia, this paper addressed the issue by presenting a case study research aimed at empirically exploring how land use zoning will affect the ecosystem services. Different land use zoning through the time period from 1988 to 2008 was analyzed and the ecosystem services were identified and zoned by using SIZES. The SIZES can automatically generate the boundaries of the ecosystem service function zone in the case study area after the input of the raster data and therefore visually reveals the temporal and spatial variation characteristics of the regional ecosystem services. Finally, through the spatial and temporal variation of the key ecosystem services generated by SIZES, effects of the land use zoning on selected ecosystem services are then qualitatively analyzed.

The study area is located in the Heihe River Basin (HRB), China. As one of the largest inland river basins in Northeast China, it is characterized by the multiple natural landscapes and is composed by various natural geographic units. As a typical arid area, it comprises almost all the major natural characters. And the living of the residents or farmers there depends largely upon the provision of the ecosystem services. While in the middle reaches, there are 95% of the cultivated land, 91% of the population and over 80% of the production value of the whole watershed. It is the main agricultural production area of the whole region. However, in recent decades, with the strengthening of human economic activities, a series of ecological environment problems appear, such as grassland degradation, natural forest decrease, species number and glacier area reduction, land desertification and secondary salinization, and water scarcity. These problems are all associated with the land use and land cover change and the quality changes of ecological environment. The degraded ecosystem will weaken the ecosystem services function, thus influencing the social-economic development of the whole region. Therefore we selected the three cities and five counties along the middle reaches as the study area to assess the impact of LUC on ecosystem services. And the method we used will lend some credence to the related research in similar areas.

The following content of this paper is divided into four parts, namely, methodology, case study, results, and discussion and conclusions. In the methodology part, we will explicitly introduce SIZES. Thereafter, a case study of the middle reaches of the HRB is presented to elaborate the land use zoning for conserving ecosystem services under the impact of climate change in this ecological fragile region. Major results of this study are stated in the "Results" section. Finally several discussions are made to conclude this research.

2. Methodology

We built a system for identifying and zoning ecosystem services (SIZES) to identify the key ecosystem services and their spatial and temporal variation. The system is composed of the following four principal components: indicator system for ecosystem services evaluation based on analytic hierarchy process (ISESE-AHP), ranking matrix of ecosystem services based on factor analysis (RMES-FA), identification of the core ecosystem services based on principal component evaluation (ICES-PCE), and identification and zoning of ecosystem services based on unsupervised fuzzy clustering (IDES-UFC).

2.1. Principle of SIZES. SIZES delimitates the functional zones for regional ecosystem services based on core ecosystem services in the minimum consistent units. The indicator system of ecosystem services in SIZES is developed with the conceptual framework provided by MEA (2003) and the influencing factors at different spatiotemporal scales are accordingly selected. The core ecosystem services, the indicators which comprehensively represent the most important ecosystem services in a functional zone, are identified with factor analysis according to their contribution to the variance of indicators of ecosystem services. The core ecosystem services are interpreted according to the factor loading matrix obtained with the principal component method and further calculated on the 1 km × 1 km grid cells. Finally, the functional zones for ecosystem services are delimitated with fuzzy clustering analysis and critical areas for ecosystem services are identified. The procedures of SIZES are illustrated more specifically as the following.

(1) AHP-Based Indicator System for Ecosystem Services Assessment (ISESA-AHP). An assessment hierarchy is constructed to break down ecosystem services into a series of interrelated factors. Since the regional ecosystem services are influenced by various factors [8], measurable primary indicators for ecosystem services have been selected based on the analytic hierarchy process so as to integrate these various influencing factors into one model to determine their interdependencies and the perceived consequences interactively. With a conceptual framework provided by MEA [21], important influencing factors of ecosystem services are elicited according to the driving mechanism of regional ecosystem services. There are four levels in this assessment hierarchy, that is, the overall goal at the top, criteria and subcriteria in the middle, and the measurable primary indicators at the bottom. During the

process of selecting primary indicators of regional ecosystem services, three principles are followed: (1) the indicators characterizing ecosystem services are easy to access; (2) the selected indicators should cover all the aspects of regional ecosystem services; and (3) the selected indicators should be coherent with the upper-layer indicators.

(2) FA-Based Extraction of the Core Ecosystem Services (ECES-FA). Factor analysis is used to summarize and aggregate the aforementioned primary indicators of ecosystem services into a few principal components (PCs) that represent certain core ecosystem services. It describes the variance of primary indicators of ecosystem services in terms of potentially fewer comprehensive indicators, that is, PCs. The PCs for a data set are defined as linear combinations of variables that account for the maximum variance within the entire data set and are orthogonal to each other. With the correlation matrix of standardized data of primary indicators of ecosystem services, the eigenvalues, that is, the contribution of core ecosystem services to the variance of primary indicators of ecosystem services, are calculated and their corresponding eigenvectors are obtained. The contribution rate of each PC and its cumulative contribution rates are also calculated. It is assumed that the PCs with higher contribution rate represent better core ecosystem services. Only the PCs with the cumulative contribution rate reaching a certain threshold are retained. The threshold is generally set to be above 60%. Therefore, only the PCs with the cumulative contribution reaching above 60% are retained and used to represent the core ecosystem services in SIZES.

(3) PCM-Based Ranking Matrix of Ecosystem Services (RMES-PCM). The relative importance of primary indicators to the core ecosystem services is analyzed with RMES-PCM, a ranking matrix based on the factor loading matrix obtained with principal component method (PCM). The factor loading reflects the correlation between one primary indicator and one certain PC. The core ecosystem services are identified and interpreted with the primary indicators with the heavy factor loading; a correlation matrix involving these primary indicators was used as an input for the analysis instead of a covariance matrix, resulting in normalized PCM. Since there may be no representative indicators of the PCs, it is necessary to conduct factor rotation so as to obtain satisfactory PCs. The eigenvalues are used as a criterion for selecting PCs for the factor rotation. Only PCs with eigenvalues above 1 are retained and subjected to varimax rotation for maximizing the correlation between primary indicators and PCs [22]. The RMES-PCM is obtained by sorting the primary indicators of ecosystem services according to their factor loadings in descending order. The relative importance of primary indicators of ecosystem services to PCs is ranked to represent certain core ecosystem services.

With RMES-PCM, the core ecosystem services can be identified and interpreted according to the most important primary indicators of ecosystem services. The factor scores of the retained PCs are calculated at each 1 km × 1 km grid cell to spatially represent the core ecosystem services. The factor score can be calculated with many methods, such as the regression estimation method, Bartlett estimation method, and Thomson estimation method. SIZES adopts Bartlett estimation method and spatially represents the core ecosystem services on 1 km × 1 km grid cells in the study area with the factor score.

(4) UFC-Based Zonation of Ecosystem Services (ZES-UFC). With the core ecosystem services represented at 1 km × 1 km grid cells, the functional zones for ecosystem services are delimitated with unsupervised fuzzy clustering (UFC) algorithm, which is based on the modified fuzzy c-means algorithm and maximum likelihood estimation (MLE). The minimum consistent units (samples) are coherent in the type of core ecosystem services and they are classified into clusters with unsupervised optimal fuzzy clustering algorithm. The core ecosystem services of samples within one cluster are more similar to each other than that belonging to different clusters, where the similarity is defined by a distance measure. This partition approach defines the cluster to which each sample belongs, using the elements of the membership matrix. Each sample is attached with different degrees of membership to each cluster. The initial centers of each partition are found with the fuzzy c-means with the Euclidean distance and the fuzzy c-means with the exponential (or MLE) distance are used for precise modeling of the Gaussian mixture in the samples. The number of clusters is determined by finding the partition with minimum number of Gaussian clusters. Specifically, the number of clusters is determined by beginning with one group at the center of data and adding another group with each iteration process at a location in which membership in the previous groups is small, while examining the partition validity criteria until reaching the maximal number of groups. Finally the number of clusters providing maximal validity criteria measurements is chosen for optimal partition.

2.2. Function Modules Embedded in SIZES. The procedures mentioned above are realized with four function modules in SIZES, that is, MIES (module for identifying ecosystem services), MRES (module for ranking ecosystem services), MECES (module for identifying the core ecosystem services), and MZES (module for zoning ecosystem services).

2.2.1. Module for Identifying Ecosystem Services (MIES). MIES mainly consists of an indicator system for ecosystem services, representing interaction processes between ecosystem services and influencing factors, and enabling interactive access to SIZES. There are four indicators that fit broadly at the top level in this indicator system, namely, supporting, provisioning, regulating, and cultural services. Since the indicators at lower levels may vary among different researches, users of SIZES may recode the program and set these indicators by specifying input parameters and the system will dynamically track the input indicators. Users may also access the online help system, clarifying the underlying assumptions and formal definitions of parameters used in this software. Within MIES of SIZES, each cell (1 km × 1 km) is assigned with multilayer values to represent attributes of each factor (e.g., NPP and land quality). With the 1-kilometer

(km) grid pixel data model, MIES can combine, analyze, and interpret the multiple and hierarchical spatial factors efficiently in consideration of maintenance and improvement of ecosystem services.

2.2.2. Module for Extracting the Core Ecosystem Services (MECES). MECES aims to extract the PCs that represent the core ecosystem services according to established criteria with factor analysis. The core ecosystem services are extracted with the following steps.

(1) Assessment matrix for ecosystem services is calculated with

$$X = \left[x_{ij}\right]_{n\times p} = \begin{bmatrix} x_{11} & x_{12} & \cdots & x_{1p} \\ x_{21} & x_{22} & \cdots & x_{2p} \\ \vdots & \vdots & \cdots & \vdots \\ x_{n1} & x_{n2} & \cdots & x_{np} \end{bmatrix}, \quad (1)$$

where x_{ij} is the value of the jth ($j = 1, 2, \ldots, p$) variable of ecosystem services on the ith ($i = 1, 2, \ldots, p$) grid cell. The vector on the ith ($i = 1, 2, \ldots, n$) grid cell can be presented by $X_i = (x_{i1}, x_{i2}, \ldots, x_{ip})'$.

(2) Sample deviation matrix is constructed with

$$E = \sum_{i=1}^{n}\left(X_i - \overline{X}\right)\left(X_i - \overline{X}\right)' \triangleq (e_{kl}), \quad (2)$$

where $\overline{X} = (1/n)\sum_{i=1}^{n} X_i = (\overline{x}_1, \overline{x}_1, \ldots, \overline{x}_1)'$.

(3) Sample correlation matrix is calculated as

$$R = \left(\frac{e_{kl}}{e_{kk}e_{ll}}\right), \quad k, l = 1, 2, \ldots, p. \quad (3)$$

(4) The eigenvalues and corresponding eigenvectors are obtained with following steps.

The eigenvalue λ_i ($i = 1, 2, \ldots, p$) of the equation ($|\lambda I - R| = 0$) is obtained with the Jacobi method and the values are ranked as $\lambda_1 \geq \lambda_2 \geq \cdots \geq \lambda_p \geq 0$. Then l_i ($i = 1, 2, \ldots, p$), the eigenvector of the corresponding eigenvalue λ_i, is calculated. Concurrently, the condition should agree with $\|l_i\| = 1$; that is, $\sum_{j=1}^{p} {l_{ij}}^2 = 1$, where l_{ij} is the jth of vector (l_{ij}). Then the ith PC is $Z_i = l_i X$.

(5) The eigenvalues represent the contributions of these PCs to the variance of primary indicators of ecosystem services. The contribution rate of PCs is calculated with $m_i = \lambda_i / \sum_{j=1}^{p} \lambda_j$. The PCs are sorted according to their contribution rate in descending order and then their cumulative contribution rate is calculated with $\sum_{k=1}^{i} m_i$. When the cumulative contribution rate of the PCs satisfies $\sum_{k=1}^{i} m_i \geq \delta$, where δ is set to be 60%, the first m PCs are selected to represent the core ecosystem services.

2.2.3. Module for Ranking Ecosystem Services (MRES). MRES determines the relative importance of primary indicators to the core ecosystem services with RMES-PCM. The interface of MRES embedded in SIZES is shown in Figure 2. The factor loading matrix is obtained with the PCM. The factor loading vector is calculated with

$$a_i = \sqrt{\lambda_i} l_i \quad (i = 1, 2, \ldots, p), \quad (4)$$

where λ_i is the eigenvalue corresponding to the ith retained PC and l_i is its corresponding orthonormal eigenvector. The factor loading matrix is $A = (a_1, \ldots, a_p)$. The varimax rotation is conducted for maximizing the correlation between primary indicators and PCs for making the representative variables of PCs more prominent. The RMES-PCM is then obtained by sorting the primary indicators of ecosystem services in the factor loading matrix according to their factor loadings in descending order. With RMES-PCM, the core ecosystem services can be identified and interpreted according to the primary indicators of ecosystem services with the factor loading. Finally, SIZES calculates the factor scores of core ecosystem services with Bartlett method and spatially represents the core ecosystem services on 1 km × 1 km grid cells with their factor scores.

2.2.4. Module for Zoning Ecosystem Services (MZES). MZES utilizes unsupervised fuzzy clustering (UFC) analysis to delimitate and generate functional zones for ecosystem services. The steps of delimitating functional zones for ecosystem services with unsupervised fuzzy clustering analysis are as follows.

(1) Calculate the average value of all data records:

$$P = \frac{1}{m}\sum_{i=1}^{m} X_i \quad (5)$$

and set the number of clusters (c) to be one; that is, $c = 1$.

(2) Let $U_{ki-\text{old}} = 0$ ($U_{ki-\text{old}}$ = previous U_{ki}).

The basic fuzzy c-means algorithm (FCM).

(3) Calculate the Euclidean distance (for all i, k):

$$d^2\left(P_k, X_i\right) = \left[\left(P_k - X_i\right)^T \cdot \left(P_k - X_i\right)\right]. \quad (6)$$

(4) Calculate the degree of membership (U_{ki}) of all data records in all clusters (for all i, k):

$$U_{ki} = \frac{1/d^2\left(P_k, X_i\right)}{\sum_{j=1}^{c}\left(1/d^2\left(P_j, X_i\right)\right)}. \quad (7)$$

(5) Compute the new set of cluster centers, $P_{1\to k}$ (for all k):

$$P_k = \frac{\sum_{i=1}^{m} {U_{ki}}^2 X_i}{\sum_{i=1}^{m} {U_{ki}}^2}. \quad (8)$$

(6) If $\max_{k,i}[|U_{ki} - (U_{ki-\text{old}})|] > \varepsilon$, then $U_{ki-\text{old}} = U_{ki}$: go to Step 3, or else a loop is started and continues Step 6.

The modified fuzzy c-means algorithm based on MLE (FMLE).

(7) Compute the MLE distance.

The sum of memberships within the kth cluster (the a priori probability of the kth cluster) is

$$A_k = \frac{1}{m}\sum_{i=1}^{m} U_{ki}. \tag{9}$$

The fuzzy covariance matrix of the kth cluster is

$$F_k = \frac{\sum_{i=1}^{m} U_{ki}\,(P_k - X_i)\,(P_k - X_i)^T}{\sum_{i=1}^{m} U_{ki}}. \tag{10}$$

The fuzzy hypervolume of the kth cluster is

$$H_k = \left[\det\left(F_k\right)\right]^{1/2}. \tag{11}$$

Then the MLE distance (for all i, k) is

$$d^2\left(P_k, X_i\right) = \frac{H_k}{A_k}\exp\left[\left(P_k - X_i\right)^T \cdot F_k^{-1} \cdot \frac{\left(P_k - X_i\right)}{2}\right]. \tag{12}$$

(8) Repeat Steps 4 and 5 using the MLE distance.

(9) If $\max_{k,i}[|U_{ki} - (U_{ki-\text{old}})|] > \varepsilon$, $U_{ki-\text{old}} = U_{ki}$, go to Step 7; if not, continue.

(10) Compute the partition and average density validity criteria for choosing the optional number of clusters. For instance, the partition density criterion definition is

$$\text{PD}\,(c) = \frac{\sum_{j=1}^{c} A_j}{\sum_{j=1}^{c} H_j}. \tag{13}$$

(11) Create an imaginary center that has the same distance (very far) from all data records, for instance, by choosing the initial distance to the new cluster as

$$d^2\left(P_{k+1}, X_i\right) = 10 \cdot \text{variance}\,(X) \quad (i = 1, \ldots, m). \tag{14}$$

(12) Let $c = c + 1$. If $c \le c_{\max}$ ($c_{\max}$ is the maximum feasible number of clusters in the data), $U_{ki-\text{old}} = 0$ and go to Step 4; or else, the UFC algorithm is completed.

The matrices U and P created in Step 9 are the required output of the UFC algorithm.

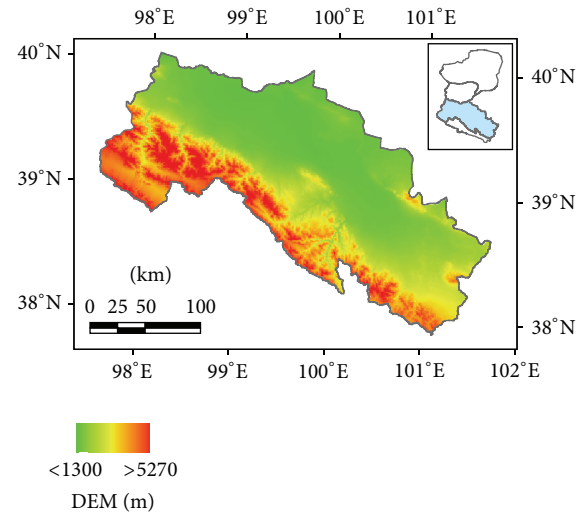

Figure 1: Location and geographic boundaries of the middle reaches of the HRB.

3. Case Study in the Heihe River Basin

3.1. Study Area. The Heihe River Basin, with an altitude between 2000 m and 5500 m, is one of the largest inland river basins in Western China, which stretches over 821 km and covers an area of 142.9 thousand km^2. It is characterized by the multiple natural landscapes of ice, river, lake, oasis, and desert and is composed by the natural geographic units of high mountain snow-ice zone, plain oasis zone, and Gobi desert zone. As a typical arid area, it comprises almost all the major natural characters and therefore possesses various ecosystem services. And the living of the residents or farmers depends largely upon the provision of the ecosystem services. In the middle reaches, the runoff has been fully used, while 95% of the cultivated land, 91% of the population, and over 80% of the production value of the whole watershed gathered here. It is the main agricultural production area of the whole region. Both human and natural interventions will exert great influence on the ecosystem services, which will hinder the social and economic development and thus impact the human well-being.

In this situation, climate change plays a key role in altering the provision service of the middle reaches and the region depends largely on the regulating services of ecosystem to mitigate this change. Therefore investigating how the land use zoning could conserve the ecosystem service and thus counter the impact of climate change is of great significance in this area. So we selected the three cities and five counties along the middle reaches as the study area (Figure 1).

Identifying the general characteristics of the regional ecological environment is of great significance to the rational regional ecosystem service function identification. In the middle reaches, the key ecological environment problems are land desertification and salinization and water pollution. Besides, due to the lack of monitoring and control measures, the condition is getting worse. The reduction of grassland area caused by the massive land reclamation as well as overgrazing leads to the grassland degradation. The unreasonable

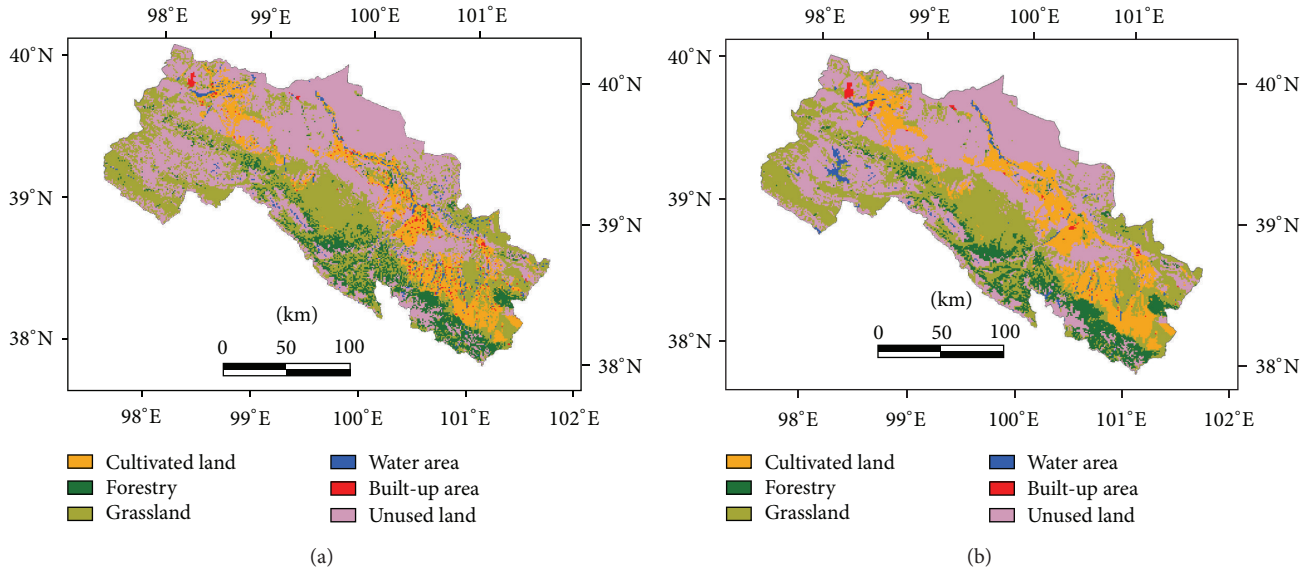

Figure 2: (a) Land use patterns of middle reaches of the HRB in 1988 and (b) land use patterns of middle reaches of the HRB in 2008.

industrial structure not only limited the regional economy development, but also worsened the supply and demand contradictions of the water resources, leading to further problems such as land desertification and salinization.

3.2. Data Selection. The selection of the ecosystem services is based on the characteristics of the study area mentioned above and is under the guidance of MA, which has been systematically elaborated in Section 2.1, "(1) AHP-based indicator system for ecosystem services evaluation" part. In this study, we divided the ecosystem services in the middle reaches of HRB into three major categories, namely, provisioning services, regulating services, and supporting services. And in each category, there are subcategories and further items, each being relevant to the land use change process that characterizes this study; thus an index system of the key ecosystem services of the HRB was built (Tables 1 and 2). Given the fact that the cultural services function is difficult to quantify, this research did not take the cultural function into consideration.

In this study, the information about land use change was derived from the remote sensing images of the HRB in the years of 1988, 1955, 2000, and 2008 through the human-computer interactive interpretation (Figure 2). And the information can be used as the basic data for analyzing the different land use zoning.

3.3. Data Processing. Our study uses a land cover classification data set developed by the Chinese Academy of Sciences (CAS) [23, 24] as the background data for spatially identifying the ecosystem services. The data set is derived from Landsat TM/ETM images of bands 3, 4, and 5 with a spatial resolution of 30 m × 30 m. And the classification contains 6 types of land uses/covers, including cultivated land, forestry, grassland, water area, built-up area, and unused land [25].

3.3.1. Raster Data Processing. The identification of the key ecosystem services function is based on the raster data model. The indicators of the ecosystem services function are characterized by multi-source and multi-scale. Therefore, the 1 km area percentage data [26, 27] (Figure 3) is an expressive way of data integration and fusion in monitoring, forecasting, and analyzing the regional ecosystem services changes. The procedure to generate the 1 km area percentage data set includes four steps. The first step is to generate a vector map of land cover and land use changes during the study period at a scale of 1 : 100,000 based on the remote sensing Landsat TM/ETM data. The second step is to generate a 1 km FISHNET vector map georeferenced to a boundary map of the study area at a scale of 1 : 100,000. Each cell of the generated 1 km FISHNET vector map owns a unique ID. The third step is to overlay the vector map of land cover and land use changes with the 1 km FISHNET vector map. This is done by aggregating converted areas in each 1 km grid identified by cell IDs of the 1 km FISHNET vector map in the TABLE module of ArcGIS software. Finally, the area percentage vector data are transformed into grid raster data to identify the conversion direction and intensity. The design of working flow insists on no loss of area information. Without special notification, the statistical area of cultivated land according to the GRID data is survey area by satellite remote sensing data, which can be called "gross area."

3.3.2. Indicator Data Processing. Among the indicators that are needed in the identification of the key ecosystem services (Figure 4), the raster data of the net primary production are provided by the CAS. The data sources and processing methods of other indicators are listed below.

(1) Food, water, and fuelwood supply: in order to precisely characterize the supply of grain, water, and fuelwood in each cell, in this research, we use the

Table 1: Key ecosystem services indicators in the HRB.

Categories	Subcategories	Indicators and description
Provisioning services	Food	Cultivated land percentage %
	Fresh water	Water area percentage %
	Fuelwood	Forestry area percentage %
Regulating services	Climate regulating	Air temperature: mean annual temperature (0.1°C)
		Temperature departure
		Precipitation departure
		Cumulated temperature (>10°C) Annually cumulated temperature of daily mean Air temperature above 10°C (0.1°C)
		Sunshine hours: sunshine hours rectifying the spatial variability of solar radiation
		Sunshine hours departure
	Species diversity	Landscape diversity index (Shannon diversity index)
Supporting services	Soil formation	Loam proportion %
		Slope: terrain slope derived from DEM (0.01 degrees)
	Nutrient cycling	Soil phosphorus content %
	Primary production	Net primary production gC $m^{-2}yr^{-1}$
	Grassland area	Grassland percentage %

Table 2: Descriptive statistics of key ecosystem services indicators in the Heihe River Basin.

Variable	Unit	Mean	Std. Dev.	Min	Max
Cultivated land	%	5.52	1873.59	0	100
Water area	%	4.49	1616.67	0	100
Grassland	%	16.79	3091.04	0	100
Forestry area	%	1.12	660.01	0	100
Air temperature	°C	0.51	2.54	0	0.96
Temperature departure	°C	0	2.52	−5.59	4.27
Precipitation departure	mm	0	75.04	−137.93	213.55
Cumulated temperature	°C	2479.10	733.29	461.29	3942.56
Sunshine hours	h	8.33	0.35	7.31	9.30
Sunshine hours departure	h	$-2.85e-15$	0.31	−1.00	0.76
Landscape diversity index	—	−37.81	116.46	−460.52	460.52
Loam proportion	%	22.50	6.37	4	34
Slope	0.01°	4.72	5.53	0	60.57
Soil phosphorus content	%	0.07	0.01	0.02	0.08
Net primary production	gC $m^{-2}yr^{-1}$	97.54	112.16	0	897

Note: total observation: 161584.

percentage of the cultivated land, water area, and forestry to indicate these provisions. The 1 km area percentage data processing method is shown above in Figure 3.

(2) Climate variables: all the climatic variables are generated from the site-based observations from the China Meteorological Administration. The spline interpolation algorithm is employed to make the surface data of climatic variables acquired at observation stations [28, 29]. The values for the climatic variables during simulation period are estimated using the space-time stochastic model [30].

(3) Landscape diversity index: we selected the Shannon diversity index to measure the landscape diversity index [31].

The Shannon diversity index (H) is expressed as [32]

$$H = \sum_i p_i \ln(p_i), \tag{15}$$

where p_i is the share of land use type i in total area of the landscape.

(4) Soil data [33]: soil data were from multiple sources. Firstly, the specific soil survey points were

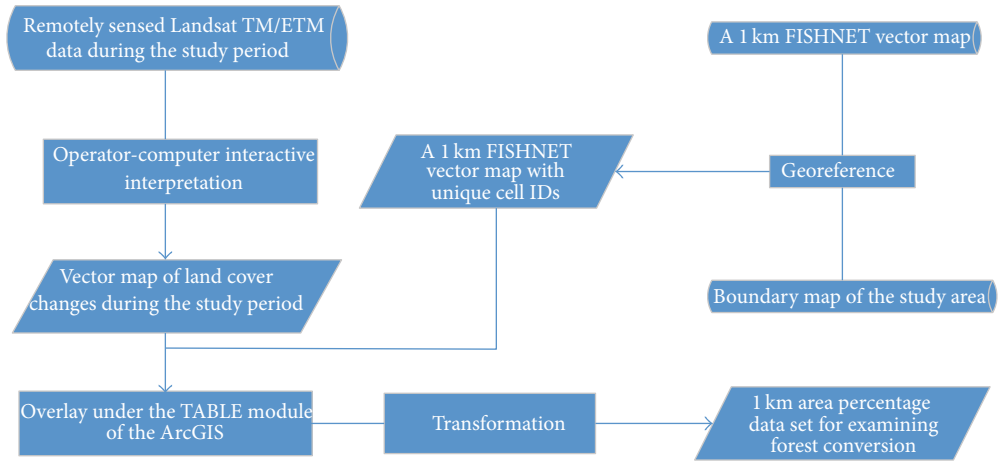

Figure 3: Flowchart of generating 1 km area percentage data set of land use changes.

calibrated on local administrative division base map, based on carefully comparing the information on National Secondary Soil Survey data and 1 : 250000 topographic maps. Secondly, an Albert projection value for specific soil survey point was assigned onto the map and generated a soil survey base map. After that, soil attribute data were linked onto soil survey base map by using the Kring interpolation algorithm and generated spatial soil data encompassing soil type and physicochemical characters. Finally, these soil data were saved as ArcGIS Grid format, with soil type, soil depth, soil organic content, and soil texture information.

(5) Elevation data: the elevation data were derived from China 1 : 250000 digital elevation models, with a spatial resolution of 50 m. Average slope information was extracted on each 1 km × 1 km plot by GIS spatial analyzing function; then it was used as basic information for land suitability evaluation.

4. Results

4.1. Land Use Change. Land use changes, which are mainly caused by human activities, are the major driving force of the ecosystem services changes. The land use changes in the study area from 1988 to 2008 (Table 3) were characterized by a general increase of cultivated land, with a decrease in forestry, grassland, and water area. Built-up area recorded the most significant expansion, being the result of rapid urbanization. Among all six types of land use, the unused land accounts for the largest proportion in all of the four study time periods, which is composed mainly by alp and desert and concentrated mainly in the north part of the region, where the major ecosystem service there is climate regulating services.

As for the transformation of land use types (Table 4) characterizing the ecosystem structure changes, we can see that the increased cultivated land mainly comes from grassland and used land. During this process, though the ecosystem service of the cultivated land is strengthened, the grassland's ecosystem services, which are also crucial in providing provision and supporting services, are impaired. Therefore, in land use zoning, it is important to consider not only the amount of the land use conversion but also the direction of the conversion among various land use types.

The spatial land use change (Figure 5) mainly occurred in the midnorth, midcentral, and midsouth area, which could explain the boundary shifting of the ecosystem services zone in these areas. Through studying the historical land use zoning policy and its impact on ecosystem services, we aim at optimizing the spatial planning of land use to conserve ecosystem services under the impact of climate change.

4.2. Ecosystem Service Zoning Change. In identifying and zoning of ecosystem services, firstly, we applied the analytic hierarchy process to build an indicator system (Table 1) with the conceptual framework provided by MEA for ecosystem services assessment with 15 indicators that proved to be the major driving forces of ecosystem services in the middle reaches of the HRB. The data of these indices were then spatially represented with the 1-kilometer (km) grid pixel data model. Then using a correlation matrix, factors with eigenvalues >1 were retained, and factors were subjected to varimax rotation to maximize the correlation between factors and measured attributes. The magnitude of the eigenvalues was used as a criterion for interpreting the relationship between ecosystem services and factors. Afterwards, to summarize and aggregate the selected ecosystem services attributes, a principal component evaluation was performed on the aforementioned variables. We assumed that principal components receiving a high contribution best represented the core ecosystem services. Therefore, we retained only the principal components with a cumulative contribution greater than 60%. An unsupervised fuzzy clustering algorithm was then performed using values for the retained principal components to develop the functional zones for ecosystem services, with subsequent valuing of each 1 km grid cell after the iterations reaching their threshold. Finally, we grouped data in clusters, where within each cluster the data exhibit similarity. Besides, in this paper, the center of gravity of

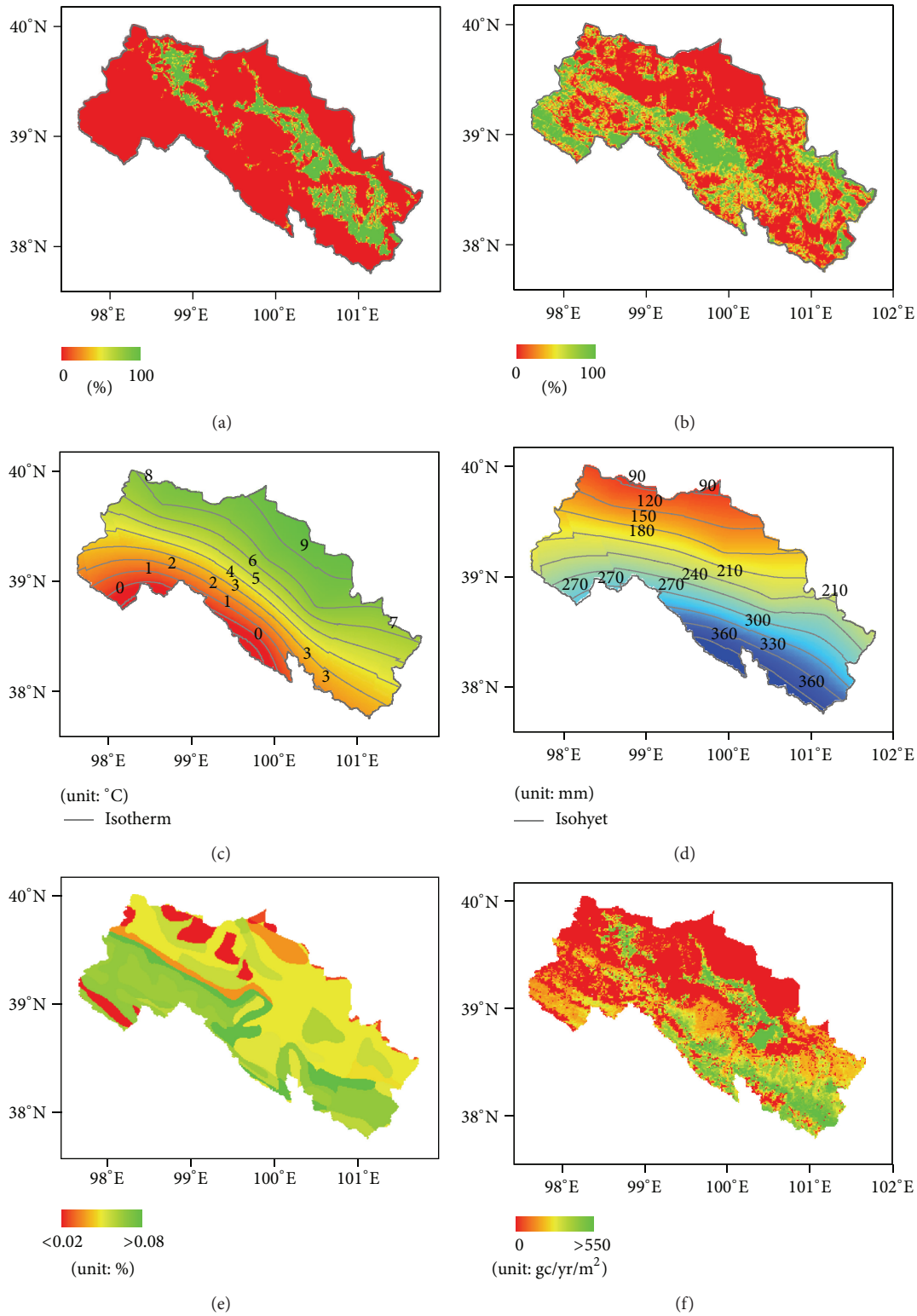

Figure 4: Spatial dispersion and characterization of the ecosystem services indicators, (a) cultivated land percentage, (b) grassland area percentage, (c) air temperature, (d) precipitation, (e) soil phosphorus content, and (f) net primary production.

Table 3: Land use changes during 1988–2008 (unit: km^2).

Land use type	1988	1995	2000	2008	Change rate during 1988–2008 (%)
Cultivated land	4650	4290	4814	5194	11.70
Forestry	3509	3575	3538	3505	−0.11
Grassland	13382	13642	13186	13269	−0.84
Water area	739	1075	750	701	−5.14
Built-up area	390	365	419	466	19.49
Unused land	17718	17446	17686	17239	−2.70

Note: change rate during (R) 1988–2008 is calculated based on the following formula: $R = (B - A)/A * 100\%$; A represents the area of each type of land in 1988 and B represents the area of each type of land in 2008.

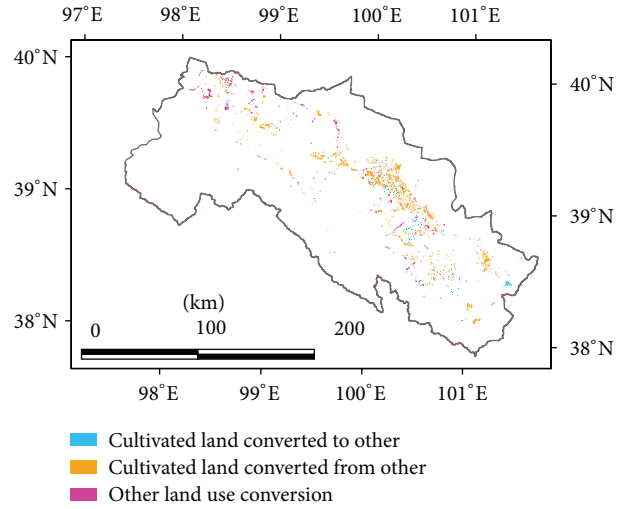

Figure 5: Spatial land use changes during 1988–2008.

Table 4: Land use transformation matrix during 1988–2008 (unit: km^2).

	1	2	3	4	5	6
1		1.84	42.61	2.16	23.41	4.06
2	24.99		14.63	0.06	0.34	2.95
3	345.92	6.46		3.71	7.15	10.28
4	45.23	0	5.44		0.98	5.35
5						
6	201.16	2.77	41.41	12.99	31.83	

Note: 1: cultivated land, 2: forestry, 3: grassland, 4: water area, 5: built-up area, and 6: unused land.

each service zone in each time is generated in the ArcGIS to analyze the shifts of center of gravity (Figure 7).

In 1988 and 1995, there are five major clusters, namely, climate regulating function, food provision function, nutrient cycling supporting function, soil supporting function, and supporting function. The name of each cluster is determined according to the above mentioned principal component analysis within each cluster. Similarly, four clusters have been identified in 2000 and 2008, which are climate regulating function, food provision function, soil supporting function, and supporting function.

Each functional zone involves one kind of ecosystem services, which is displayed with different zoning boundaries. The functional zones for ecosystem service obtained with SIZES comprehensively reflect the spatial clusters of ecosystem services in the middle reaches of the HRB. There were some uncertainties, but the result obtained with the SIZES still reflected the conditions of local ecosystem services in the HRB; the result indicated the boundaries of functional zones for ecosystem services were conspicuously different from the administrative boundaries (Figure 6). The functional zones generally expand across several counties; there is generally one major kind of ecosystem services as well as several kinds of secondary ecosystem services in each county.

The ecosystem service zoning results (Figure 6) showed that, during 1988–2008, the middle reaches maintained the climate regulating function, which is the major function of the area mainly distributed in the north region. It plays a key role in mitigating the climate change. The boundaries of the climate regulation service zone changed slightly and the center of gravity (Figure 7) changed the most among all the other services in this region, which is a result of the changing in land use structure and climate and its own fragile ecological condition in the northern part.

The food provision function zone is mainly concentrated in the cultivated land area. From 1988 to 1995, the food provision function is decreasing in response to the cultivated land degradation during the same time period. And by 2008, this provision increased with the expansion of the cultivated land area. The center of gravity also shifted between each two of the study time period, though being the slightest shift among others. In 2000, a large area of fuelwood supply function zone occurred in the southern part, which is considered as the result of forestry land increase.

The supporting function showed an overall declining trend characterized by boundary shrinking, which is the result of the net primary production loss and the decreased soil function due to the forestry and grassland reduction. In the southern part, the shift from supporting function to fuelwood provision function after 2000 is the result of the

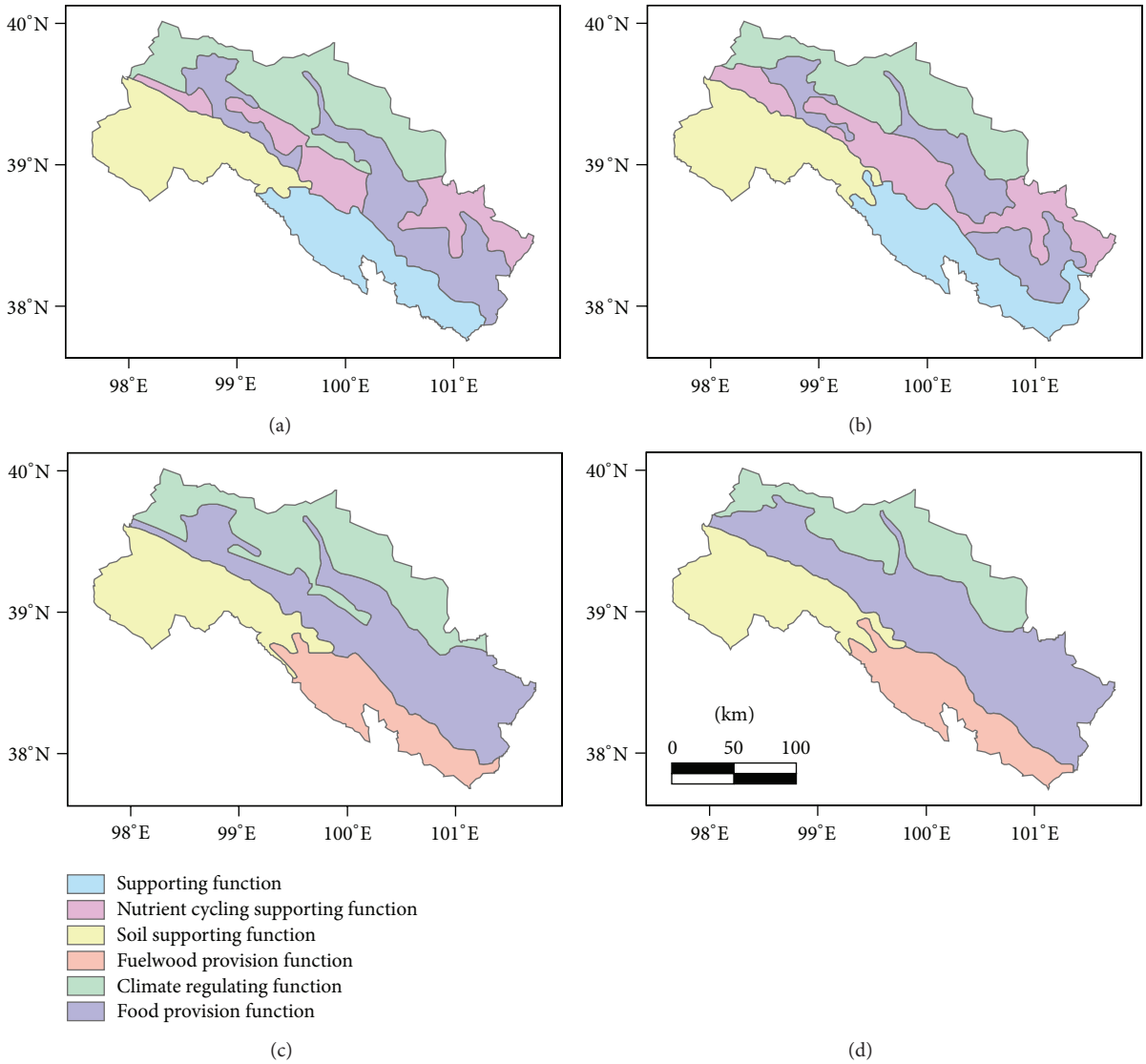

Figure 6: Ecosystem service zoning of middle reaches of the HRB in the years of (a) 1988, (b) 1995, (c) 2000, and (d) 2008.

forestry increase in this region; fuelwood provision took place as the major ecosystem service.

5. Discussion and Conclusions

This paper used a model to identify and zone the ecosystem services to explore the land use zoning on ecosystem services in climate mitigation. The research contributes to the growing literature in finely characterizing the ecosystem services zones via land use zoning to mitigate the impact of climate change, as there is no such systematic ecosystem zoning method before.

The application of SIZES proves capable of automatically identifying the boundary of ecosystem service function zone. The method of ecosystem services spatial clustering at watershed scale can be applied in other regions. Though in our study in the middle reaches of HRB we focused on the climate regulation ecosystem services, our method can be further applied in other regions to explore their specific typical ecosystem services. And the results will provide scientific basis for the formulation of regional ecosystem services development planning and ecosystem adaptive management decision. However, the spatial mapping capability of the software needs to be further strengthened.

As one of the largest inland river basins, the provision of the ecosystem services in the HRB is of great significance to the production and life of the local residents. And the regulating services are of crucial importance for this ecological fragile region to counter the impact of climate change. In this research, the impact of land use change on ecosystem services was explored in the middle reaches of the HRB. Through the identification of the ecosystem service, we recognize that, in the middle reaches of the HRB, it is important to protect the provision and regulating services, especially given the fragile ecology in this region. We identify that it is a direct and effective way of land use zoning to protect the key

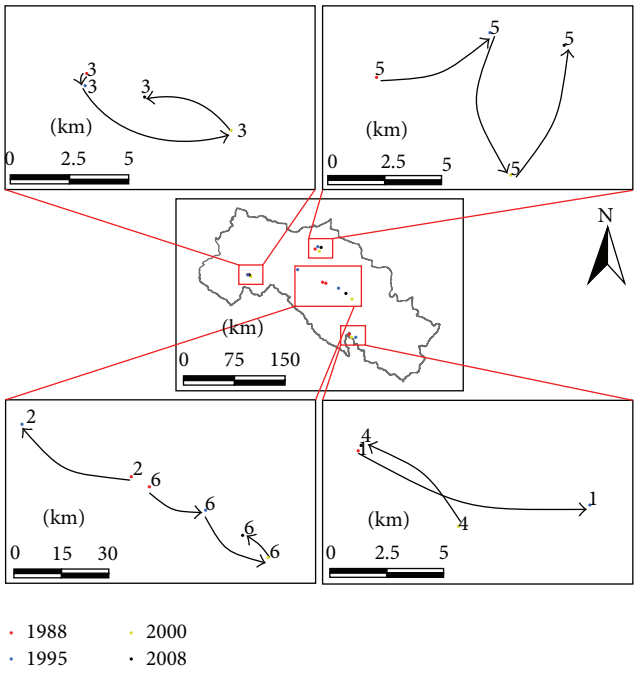

FIGURE 7: Spatial shifts of the center of gravity of ecosystem service zones. Note: 1: supporting function, 2: nutrient cycling supporting function, 3: soil supporting function, 4: fuelwood provision function, 5: climate regulating function, and 6: food provision function.

ecosystem service and raise the provision and regulating function.

Identifying major regional ecological environment problems and thereafter establishing the prioritized ecosystem conservation zone are of practical significance. In the middle reaches of the HRB, the major provision function of ecosystem is food provision function, which is mainly concentrated in the cultivated land area and is strengthened with the expansion of cultivated land during the studied time period. In 2000, a large area of fuelwood provision function zone occurred in the southern part, which is considered as the result of forestry land increase. The supporting services mainly occurred in the grassland and water area and show a general trend of degradation, as a result of the net primary production loss and the decreased soil function due to the forestry and grassland reduction. The major regulation service in this study area is climate regulation services, mainly concentrated in the northern desert, Gobi, and grassland area. The conservation of major ecosystem services should be prioritized. And land use zoning serves as an effective way to protect the key ecosystem services.

Conflict of Interests

The authors declare that there is no conflict of interests regarding the publication of this paper.

Acknowledgments

This research was financially supported by the major research plan of the National Natural Science Funds of China for Distinguished Young Scholar (Grant no. 71225005), the National Natural Science Foundation of China (Grant no. 91325302), and the National Key Programme for Developing Basic Science in China (Grant no. 2010CB950900).

References

[1] G. C. Daily, S. Alexander, P. R. Ehrlich et al., *Ecosystem Services: Benefits Supplied to Human Societies by Natural Ecosystems*, Ecological Society of America, Washington, DC, USA, 1997.

[2] R. Costanza, R. D'Arge, R. de Groot et al., "The value of the world's ecosystem services and natural capital," *Nature*, vol. 387, no. 6630, pp. 253–260, 1997.

[3] M. E. Assessment, *Ecosystems and Human Well-Being*, Island Press, Washington, DC, USA, 2005.

[4] B. Burkhard, F. Kroll, S. Nedkov, and F. Müller, "Mapping ecosystem service supply, demand and budgets," *Ecological Indicators*, vol. 21, pp. 17–29, 2012.

[5] S. J. Jordan, S. E. Hayes, D. Yoskowitz et al., "Accounting for natural resources and environmental sustainability: linking ecosystem services to human well-being," *Environmental Science and Technology*, vol. 44, no. 5, pp. 1530–1536, 2010.

[6] Millennium Ecosystem Assessment (Ma), *Ecosystems and Human Well-Being*, Island Press, Washington DC, USA, 2005.

[7] O. J. Schmitz, E. Post, C. E. Burns, and K. M. Johnston, "Ecosystem responses to global climate change: moving beyond color mapping," *BioScience*, vol. 53, no. 12, pp. 1199–1205, 2003.

[8] M. R. Shaw, L. Pendleton, D. R. Cameron et al., "The impact of climate change on California's ecosystem services," *Climatic Change*, vol. 109, no. 1, pp. 465–484, 2011.

[9] L. Huang, X. Xu, Q. Shao, and J. Liu, "Improving carbon mitigation potential through grassland ecosystem restoration under climatic change in Northeastern Tibetan Plateau," *Advances in Meteorology*, vol. 2014, Article ID 379306, 11 pages, 2014.

[10] M. D. B. Watanabe and E. Ortega, "Dynamic emergy accounting of water and carbon ecosystem services: a model to simulate the impacts of land-use change," *Ecological Modelling*, vol. 271, pp. 113–131, 2014.

[11] M. J. Metzger, M. D. A. Rounsevell, L. Acosta-Michlik, R. Leemans, and D. Schröter, "The vulnerability of ecosystem services to land use change," *Agriculture, Ecosystems and Environment*, vol. 114, no. 1, pp. 69–85, 2006.

[12] S.-H. Wang, S.-L. Huang, and W. W. Budd, "Integrated ecosystem model for simulating land use allocation," *Ecological Modelling*, vol. 227, pp. 46–55, 2012.

[13] Y. Weng, "Spatiotemporal changes of landscape pattern in response to urbanization," *Landscape and Urban Planning*, vol. 81, no. 4, pp. 341–353, 2007.

[14] M. K. Shrestha, A. M. York, C. G. Boone, and S. Zhang, "Land fragmentation due to rapid urbanization in the Phoenix Metropolitan Area: analyzing the spatiotemporal patterns and drivers," *Applied Geography*, vol. 32, no. 2, pp. 522–531, 2012.

[15] J. Solon, "Spatial context of urbanization: landscape pattern and changes between 1950 and 1990 in the Warsaw metropolitan area, Poland," *Landscape and Urban Planning*, vol. 93, no. 3-4, pp. 250–261, 2009.

[16] Q. Fang, L. Zhang, H. Hong, L. Zhang, and F. Bristow, "Ecological function zoning for environmental planning at different levels," *Environment, Development and Sustainability*, vol. 10, no. 1, pp. 41–49, 2008.

[17] V. K. Shitikov, L. A. Vykhristyuk, V. N. Pautova, and T. D. Zinchenko, "Comprehensive ecological zoning of the Kuibyshev Reservoir," *Water Resources*, vol. 34, no. 4, pp. 450–458, 2007.

[18] M. del Carmen Sabatini, A. Verdiell, R. M. Rodríguez Iglesias, and M. Vidal, "A quantitative method for zoning of protected areas and its spatial ecological implications," *Journal of Environmental Management*, vol. 83, no. 2, pp. 198–206, 2007.

[19] T. Kara and M. Guler, "Agro-ecological zoning by GIS: a case study of the Bafra and Carsamba plains in Turkey," *Asian Journal of Chemistry*, vol. 19, no. 3, pp. 2277–2284, 2007.

[20] C. A. Dehring and M. S. Lind, "Residential land-use controls and land values: zoning and covenant interactions," *Land Economics*, vol. 83, no. 4, pp. 445–457, 2007.

[21] S. N. Gosling, "The likelihood and potential impact of future change in the large-scale climate-earth system on ecosystem services," *Environmental Science and Policy*, vol. 27, pp. S15–S31, 2013.

[22] C. Fezzi, I. Bateman, T. Askew et al., "Valuing provisioning ecosystem services in agriculture: the impact of climate change on food production in the United Kingdom," *Environmental & Resource Economics*, vol. 57, no. 2, pp. 197–214, 2014.

[23] J. Liu, M. Liu, D. Zhuang, Z. Zhang, and X. Deng, "Study on spatial pattern of land-use change in China during 1995–2000," *Science in China D: Earth Sciences*, vol. 46, no. 4, pp. 373–384, 2003.

[24] X. Deng, H. Su, and J. Zhan, "Integration of multiple data sources to simulate the dynamics of land systems," *Sensors*, vol. 8, no. 2, pp. 620–634, 2008.

[25] J. Liu, Z. Zhang, X. Xu et al., "Spatial patterns and driving forces of land use change in China during the early 21st century," *Journal of Geographical Sciences*, vol. 20, no. 4, pp. 483–494, 2010.

[26] X. Deng, Q. Jiang, H. Su, and F. Wu, "Trace forest conversions in Northeast China with a 1-km area percentage data model," *Journal of Applied Remote Sensing*, vol. 4, no. 1, Article ID 041893, 2010.

[27] X. Deng, J. Huang, Q. Huang, S. Rozelle, and J. Gibson, "Do roads lead to grassland degradation or restoration? A case study in Inner Mongolia, China," *Environment and Development Economics*, vol. 16, no. 6, pp. 751–773, 2011.

[28] D. T. Price, D. W. McKenney, I. A. Nalder, M. F. Hutchinson, and J. L. Kesteven, "A comparison of two statistical methods for spatial interpolation of Canadian monthly mean climate data," *Agricultural and Forest Meteorology*, vol. 101, no. 2-3, pp. 81–94, 2000.

[29] S. J. Jeffrey, J. O. Carter, K. B. Moodie, and A. R. Beswick, "Using spatial interpolation to construct a comprehensive archive of Australian climate data," *Environmental Modelling & Software*, vol. 16, no. 4, pp. 309–330, 2001.

[30] M. F. Hutchinson, "Stochastic space-time weather models from ground-based data," *Agricultural and Forest Meteorology*, vol. 73, no. 3-4, pp. 237–264, 1995.

[31] K. Zhou, J. Huang, X. Deng et al., "Effects of land use and insecticides on natural enemies of aphids in cotton: first evidence from smallholder agriculture in the North China Plain," *Agriculture, Ecosystems & Environment*, vol. 183, pp. 176–184, 2014.

[32] L. Jost, "Entropy and diversity," *Oikos*, vol. 113, no. 2, pp. 363–375, 2006.

[33] W. Wu, J. Huang, and X. Deng, "Potential land for plantation of Jatropha curcas as feedstocks for biodiesel in China," *Science China D: Earth Sciences*, vol. 53, no. 1, pp. 120–127, 2010.

Hindawi Publishing Corporation
Advances in Meteorology
Volume 2015, Article ID 213534, 10 pages
http://dx.doi.org/10.1155/2015/213534

Research Article

Impacts of Grain-for-Green and Grain-for-Blue Policies on Valued Ecosystem Services in Shandong Province, China

Wei Song,[1] Xiangzheng Deng,[1,2] Bing Liu,[3] Zhaohua Li,[4] and Gui Jin[4]

[1] *Key Laboratory of Land Surface Pattern and Simulation, Institute of Geographic Sciences and Natural Resources Research, Chinese Academy of Sciences, Beijing 100101, China*
[2] *Center for Chinese Agricultural Policy, Chinese Academy of Sciences, Beijing 100101, China*
[3] *College of Geomatics, Shandong University of Science and Technology, Qingdao, Shandong 266590, China*
[4] *Resources and Environmental Science, Hubei University, Wuhan, Hubei 430062, China*

Correspondence should be addressed to Xiangzheng Deng; dengxz.ccap@gmail.com

Received 13 September 2014; Accepted 20 December 2014

Academic Editor: Jinwei Dong

China launched a series of ecological restoration policies to mitigate its severe environmental challenges in the late 1990s. From the beginning, the effects and influences of the ecological restoration policies have been hotly debated. In the present study, we assessed the effects of two vital ecological restoration policies (Grain-for-Green and Grain-for-Blue) on valued ecosystem services in Shandong province. A new method based on the net primary productivity and soil erosion was developed to assess the ecosystem service value. In the areas implementing the Grain-for-Green and Grain-for-Blue policies, the ecosystem service value increased by 24.01% and 43.10% during 2000–2008, respectively. However, comparing to the average increase of ecosystem service value (46.00%) in the whole of Shandong province in the same period, Grain-for-Green and Grain-for-Blue did not significantly improve overall ecosystem services. The ecological restoration policy led to significant tradeoffs in ecosystem services. Grain-for-Green improved the ecosystem service function of nutrient cycling, organic material provision, and regulation of gases but decreased that of water conservation. Grain-for-Blue increased the water conservation function but led to a reduction in the function of soil conservation and nutrient cycling.

1. Introduction

Over the past 50 years, 60% of worldwide ecosystem services have degraded due to social and economic development [1]. In China, ecological degradation is also extensive; for example, 23% of the area in China has suffered ecological degradation [2]. The economic loss from ecological degradation accounted for over 13% of the national gross domestic product [3]. Awakening to the severe effects of ecological degradation, the Chinese government implemented two ecological restoration policies at the end of the 1990s, that is, the Grain-for-Green policy and Grain-for-Blue policy.

The Grain-for-Green policy, the largest land retirement/afforestation program in China, was launched in 1999 to mitigate land degradation (soil erosion) by returning steeply sloping cultivated land to forest area or grassland [2, 4–7]. The Grain-for-Blue policy was launched in 1998, aiming to return cultivated land to water areas, that is, relinquishing the cultivated land at the periphery of water areas [8–11].

Policy can affect decision making and change the ways people utilize and manage ecosystems [12]. Evaluating the consequences of a policy is a critical lesson from the Millennium Ecosystem Assessment [13]. In recent years, the policy research interest in ecosystems has focused on the policy tools [14, 15], policy impacts [16–18], policy incentives [19], policy option [20], policy assessment approach [21], and policy making [22, 23]. For example, Brady et al. [24] modeled the impacts of agricultural policy on ecosystem services using an agent-based approach; Bronner et al. [25] assessed the impacts of US stream compensatory mitigation policy on ecosystem functions and services; Geneletti [26] assessed the impacts of alternative land use zoning policies on future ecosystem services; Simpson [27] estimated the effects of conservation policy on ecosystems.

As an effective approach to recognize the multiple benefits provided by ecosystems, the work of economic valuation of ecosystem services has been widely conducted since 1990 [28, 29]. These works cover the method developed in valuating ecosystem services and the estimation of ecosystem service value in different regions and ecosystems. One of the most notable assessments of ecosystem service value (ESV) was conducted by Costanza et al. [30, 31], who estimated 17 ESV provided by 16 dominant global biomes using a market valuation method. Other researchers also estimated ESV of tropical forests [32–36] and protected areas [37–39], endangered species management [40, 41], and different biological resources [28, 42–44].

Although Grain-for-Green and Grain-for-Blue have been implemented over 10 years in China, few works have been conducted to assess the ecological impacts of the two ecological restoration policies particularly from the perspective of changes in ESV. In this paper, we evaluated the effects of Grain-for-Green and Grain-for-Blue on ESV by a newly developed approach. Specifically, the aims of this paper are to (a) examine land use change in Shandong province during 2000–2008, (b) assess the changes in ESV, and (c) estimate the effects of Grain-for-Green and Grain-for-Blue on ESV.

2. Study Area and Data Sources

2.1. Study Area. Shandong province, located on the eastern edge of the North China Plain (114°19′–122°43′E, 34°22′–38°15′N) and the lower reaches of the Yellow River, is a coastal province in China (Figure 1). It covers a total area of over 151,100 km^2 with plains terrain accounting for 55%, mountainous area for 15.5%, and hilly area for 13.2% (Figure 1). The northwest, west, and southwest of the Shandong are all part of the North China Plain. The central region of the province is mountainous, with Mount Tai being the most prominent. Shandong province lies in the warm-temperate zone with a continental monsoon climate.

2.2. Data Sources. The land use maps of Shandong province in 2000 and 2008 were obtained from the Institute of Geographic Sciences and Natural Resources Research of the Chinese Academy of Sciences [45]. The maps were interpreted from Landsat TM (Thematic Mapper) satellite images by the human-machine interactive approach. The average accuracy of the maps is over 95% [46]. The land use was divided into six primary types and 25 subclasses [47, 48].

The net primary productivity (NPP) data in Shandong are the products of EOS/MODIS of NASA. The Normalized Difference Vegetation Index (NDVI) data are sourced from SPOT-vegetation with a temporal step of 10 days. The data formats of NPP and NDVI are all 1 km grid. Precipitation and temperature in Shandong province were gained from the China Meteorological Data Sharing Service System (http://cdc.cma.gov.cn/home.do) and interpolated in spatial. The soil nutrients data such as the contents of N, P, K, and organic matter were taken from the soil map generated from the second soil survey of China. The actual evapotranspiration data, which were calculated by IBIS model with a temporal step of 8 days, were sourced from the China Data Sharing Infrastructure of Earth Systems Science.

3. Method

3.1. Value Quantification of Ecosystem Services. The method for assessing ESV can be summarized into two categories, that is, the primary data based method and proxy based method [49]. The primary data based method directly assesses the ESV according to the primary data from the study area. For the complicated calculation process, many models have been developed to assess ESV, for example, InVEST, ARIES, SoLVES, and MIMES. The proxy based method assesses ESV by assigning each biome a value. One of the most representative proxy based methods was developed by Costanza et al. [31]. The merit of the primary data based method is high accuracy while the demerit is the complexity. Since running ESV models usually needs numerous parameters, the primary data based method is usually not convenient. The merit of the proxy based method is the convenience while the accuracy of this method is usually challenged.

In this paper, we developed a novel method to assess ESV. The method is one of the primary data based methods. However, since the calculation of ESV in this method is based on remote sensing data such as NPP, the calculation process is very convenient. Considering data accessibility and technique feasibility, we estimated five kinds of ESV, that is, values for provision of organic material, nutrient cycling, soil conservation, water conservation, and regulation of gases.

3.2. Assessment of the Value of Provision of Organic Material. The value of organic material of an ecosystem was assessed by NPP. The equation is as follows:

$$V_{\mathrm{om}} = \sum \mathrm{NPP}\,(x) \times P_{\mathrm{om}},$$
$$P_{\mathrm{om}} = \mathrm{NPP}\,(x) \times 2.2 \times 0.67 \times P_{\mathrm{sc}}, \quad (1)$$

where V_{om} is the value of provision of organic material; NPP(x) is the organic material produced in x pixel; P_{sc} is the price of standard coal in 2000.

3.3. Assessment of the Value of Nutrient Cycling. We utilized the saved inputs due to nutrient cycling in agricultural production to assess the value of nutrient cycling. The formula is as follows:

$$V_{\mathrm{nc}} = \sum V_{\mathrm{nc}_i}\,(x) = \sum \mathrm{NPP}\,(x) \times R_{i1} \times R_{i2} \times P_i, \quad (2)$$

where V_{nc} is the value of nutrient cycling in an ecosystem; i is the nutrient elements of N (nitrogen), P (phosphorus), or K (potassium); NPP(x) is the organic material produced in x pixel; $V_{\mathrm{nc}_i}(x)$ is the accumulated value of N, P, and K; R_{i1} is the distribution rate of nutrient elements of N, P, and K in organic material in different ecosystems; R_{i2} is the converted coefficients of N, P, and K to corresponding chemical fertilizer; P_i is the chemical fertilizer price of N, P, and K in 2000.

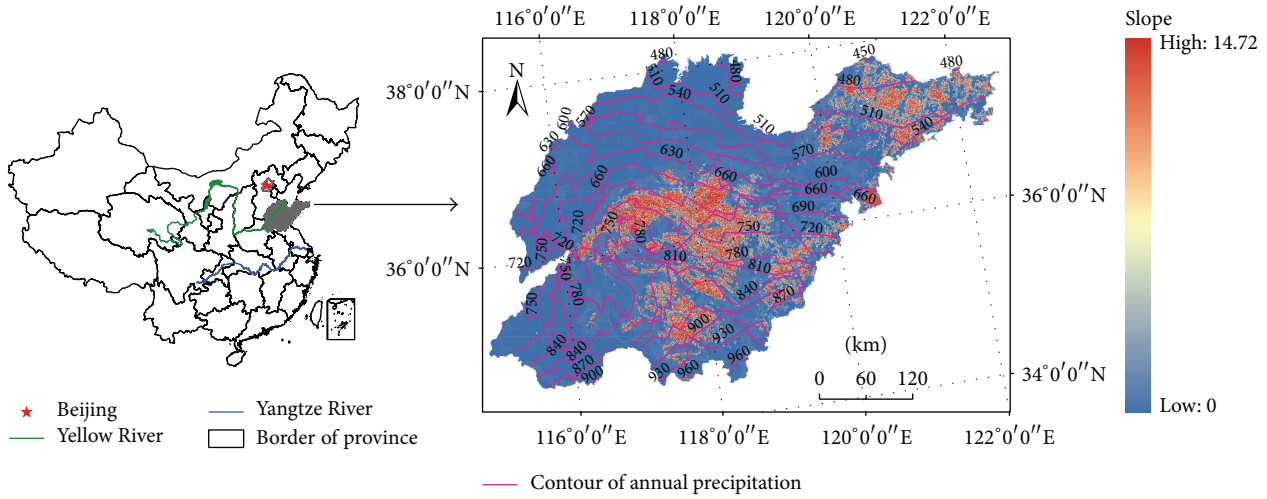

Figure 1: Slope and precipitation of Shandong province, China.

3.4. Assessment of the Value of Water Conservation. The function of water conservation of an ecosystem is similar to that of a reservoir. Therefore, we utilized the average construction cost of a reservoir to assess the value of water conservation. The formula is as follows:

$$V_{\text{wc}} = \sum V(x) \times P_w, \tag{3}$$

where V_{wc} is the value of water conservation; $V(x)$ is the water conservation amount in x pixel; P_w is the average cost of reservoir construction in 2000.

According to the difference in underlying surface, we utilized two different approaches to assess the water conservation amount of an ecosystem. When the underlying surface is soil, the equation is as follows:

$$V_s(x) = \sum P_{\text{mean}}(x) \times K_w \times R_w, \tag{4}$$

where $V_s(x)$ is the annual water conservation amount in x pixel; $P_{\text{mean}}(x)$ is the monthly precipitation in x pixel; K_w is the ratio of runoff generated from precipitation. R_w is the coefficient of reducing runoff by comparison with bare land without vegetation. R_w of cultivated land, woodland, and grassland are valued as 0.4, 0.29, and 0.24, respectively, while R_w of other land use types are valued as 0 [50].

When the underlying surface of an ecosystem is an area of water, the equation is as follows:

$$V_{\text{wc}}(x) = \sum \left(P_{\text{mean}}(x) - ET_a(x)\right), \tag{5}$$

where $V_{\text{wc}}(x)$ is the annual water conservation amount in x pixel; $P_{\text{mean}}(x)$ is the monthly precipitation in x pixel; $ET_a(x)$ is the monthly actual evaporation in x pixel.

3.5. Assessment of the Value of Soil Conservation. Soil erosion usually leads to three different kinds of value loss in an ecosystem, that is, a reduction in soil fertility, river channel sedimentation, and loss of top soil. Therefore, the assessment of the value of soil conservation is composed of three sections:

$$V_{ac} = V_{ef} + V_{en} + V_{es}, \tag{6}$$

where V_{ac} is the value of soil conservation; V_{ef} is the value of soil fertility conservation; V_{en} is the value of reducing soil sedimentation in a river channel; V_{es} is the value of the loss of top soil.

3.5.1. Assessment of the Soil Conservation Amount. The soil erosion amount without any vegetation is viewed as the potential soil erosion amount. The soil erosion amount that actually occurred is looked on as the actual soil erosion amount. The difference between the amount of potential soil erosion and actual erosion is the soil conservation amount. The soil erosion was assessed by Universal Soil Loss Equation:

$$\begin{aligned} A_p &= R \times K \times L \times S, \\ A_v &= R \times K \times L \times S \times C \times P, \\ A_c &= A_p - A_v, \end{aligned} \tag{7}$$

where A_p is the amount of potential soil erosion; A_v is the amount of actual soil erosion; A_c is the soil conservation amount; K is the soil erodible factor; L is the slope length; S is the slope factor; C is the vegetation and crop management factor; P is the soil conservation measure factor. Detailed parameters of R, K, L, S, C, and P were referenced from Wischmeier [51], Renard et al. [52], Flanagan et al. [53], Kuok et al. [54], and Renard and Foster [55].

3.5.2. Assessment of the Value of Soil Fertility Conservation. N, P, and K are the three most important nutrients in soil. Soil erosion could lead to the nutrients' losses and a decrease in soil fertility. Thus, we estimated the value of soil fertility

conservation by assessing the nutrient element value of the soil conservation amount. The equation is as follows:

$$V_{ef} = \sum A_c(x) \times C_i \times P_i, \quad (8)$$

where V_{ef} is the value of soil fertility conservation; $A_c(x)$ is the soil conservation amount in x pixel; C_i is the price of N, P, and K fertilizer in 2000.

3.5.3. Assessment of the Value of the Loss of Top Soil. The value of the loss of top soil was assessed by calculating the value of conserved land where soil erosion has been avoided due to the protection of vegetation coverage in an ecosystem. The formula is as follows:

$$V_{es} = \frac{\sum A_c(x) \times P_f}{D_{\text{soil}} \times T_{\text{soil}}}, \quad (9)$$

where V_{es} is the value of the loss of top soil; $A_c(x)$ is the soil conservation amount in x pixel; D_{soil} is the soil density; P_f is the economic benefits of forest planting which is valued as 26,400 CNY/km^2·Year; T_{soil} is the average soil thickness.

3.5.4. Assessment of the Value of Reducing Soil Sedimentation in a River Channel. In China, about 24% of sediments from soil erosion are deposited in reservoirs, lakes, and rivers according to the research of Ouyang et al. [56]. Thus, the value of reducing soil sedimentation in a river channel was assessed as follows:

$$V_{en} = \frac{\sum A_c(x) \times 0.24 \times P_w}{D_{\text{soil}}}, \quad (10)$$

where V_{en} is the value of reducing the soil sedimentation in a river channel; P_w is the construction cost of a reservoir per unit; $A_c(x)$ is the quantity of soil conserved; D_{soil} is the soil density.

3.6. Assessment of the Value of Regulation of Gases. The value of regulation of gases was assessed on the basis of the functions of CO_2 absorption and O_2 generation. The equation is as follows:

$$V_{gr} = \sum 1.62 \times \text{NPP}(x) \times P_{CO_2} + \sum 1.2 \times \text{NPP}(x) \times P_{O_2}, \quad (11)$$

where V_{gr} is the value of regulation of gases NPP(x) is the organic material in x pixel; according to the photosynthesis and breathing reaction equation, it can be deduced that producing 1 g dry matter absorbs 1.62 g CO_2 and releases 1.2 g O_2; P_{CO_2} is the price of carbon tax, valued as 7.39×10^{-4} CNY/g C; P_{O_2} is the price of producing O_2, valued as 8.8×10^{-4} CNY/g C.

4. Results

4.1. Changes in Land Use. In 2000, cultivated land in Shandong province comprised 67.62% of the total area, followed by built-up areas (12.62%), grassland (8.72%), forestry area (6.44%), water area (3.44%), and unused land (1.17%).

Shandong province experienced drastic land use changes during 2000–2008. The features of land use change in Shandong were the expansion of built-up areas, reclamation of unused land, and drastic conversions in water areas. Due to rapid urbanization, urban built-up areas expanded by 56.13%, with the built-up area increasing from 301,939 ha to 471,418 ha. However, unused land shrank by 16.54% due to reclamation (Figure 2). Both drastic increase and decrease occurred in the water areas. For example, reservoirs/ponds and streams/rivers significantly increased by 42.30% and 5.67%, respectively, while beach and shore, lakes, and bottomland decreased by 53.46%, 23.66%, and 21.99%, respectively.

During 2000–2008, the conversion from cultivated land to built-up area reached 235,256 ha, contributing to 45.00% of the total conversions, followed by the conversion from cultivated land to water areas (42,236 ha) and from grassland to cultivated land areas (33,112 ha).

4.2. Changes in Value of Ecosystem Services. The ESV of Shandong was as high as 267.53 billion CNY in 2000. The value of regulation of gases contributed to 38.69% of the total ESV, followed by the values of soil conservation (34.83%), water conservation (16.69%), nutrient cycling (5.05%), and organic material provision (4.73%). The ESV per unit in Shandong ranged from 0 to 71.07 CNY/m^2, with an average value of 1.76 CNY/m^2 (Figure 3). The value of organic material provision per unit ranged from 0 to 0.37 CNY/m^2 while the values of regulating gases, nutrient cycling, and soil conservation ranged from 0 to 2.90 CNY/m^2, from 0 to 0.52 CNY/m^2, and from 0 to 69.36 CNY/m^2, respectively. The average values of regulating gases, organic material provision, water conservation, nutrient cycling, and soil conservation are 0.68 CNY/m^2, 0.08 CNY/m^2, 0.29 CNY/m^2, 0.09 CNY/m^2, and 0.61 CNY/m^2, respectively in 2000.

In spatial, total ESV is high in central and eastern Shandong while low in northern and western Shandong (Figure 3). The spatial feature of soil conservation value is similar to that of total ESV. The spatial distribution of organic material provision value, gases regulating value, and nutrient cycling value all gradually decreased from the northeast to the southwest. However, the value of water conservation gradually decreased from the southwest to the northeast.

In 2008, the ESV of Shandong province reached 390.59 billion CNY, with an increase of 46.00% compared to 2000. The soil conservation value increased by 71.64 billion CNY contributing to 58.21% of the total increase. Values of regulating gases, water conservation, nutrient cycling, and organic material provision increased by 37.40 billion CNY, 4.23 billion CNY, 5.00 billion CNY, and 4.80 billion CNY, respectively, contributing 30.39%, 3.44%, 4.06%, and 3.90% of the total increase, respectively. In 2008, the average ESV per unit of regulating of gases, water conservation, soil conservation, nutrient cycling, and organic material provision reached 0.93 CNY/m^2, 0.32 CNY/m^2, 1.09 CNY/m^2, 0.12 CNY/m^2, and 0.12 CNY/m^2, respectively. The total average ESV per unit is 2.58 CNY/m^2.

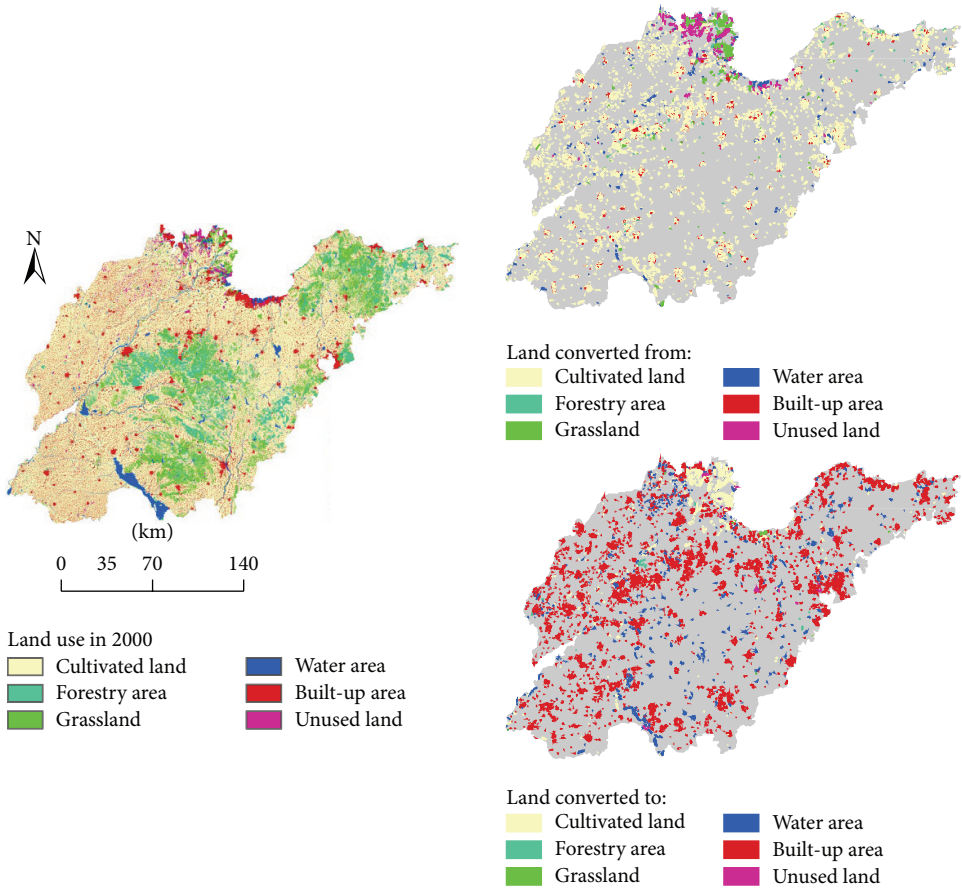

Figure 2: Land use changes in Shandong province during 2000–2008.

In spatial, total ESV and value of soil conservation significantly increased in central and eastern Shandong province. In these areas, mountains (Figure 4) are the dominant topography. The changes in value of organic material provision, regulating gases, and nutrient cycling all significantly increased in eastern Shandong while decreased in the coastal zone of Shandong. Water conservation value significantly increased in water areas.

4.3. Changes in Value of Ecosystem Services in Response to Land Use. One of the most important consequences of land use change is land use conversion. During 2000–2008, 40.57×10^4 ha of land in total in Shandong experienced conversions. The ESV of these converted lands in 2000 was 3.78 billion CNY while that in 2008 was 3.81 billion CNY, showing an increase of 0.74% (Figure 5).

However, conversions from other land use types to built-up areas significantly decreased the ESV in Shandong. The conversion from cultivated land to built-up areas reduced the ESV by 54.75 million CNY, contributing 89.49% of the ESV loss from land use conversion. Conversion from water areas, forestry areas, grassland, and unused to built-up areas increased by 2418.54×10^4 CNY, 1322.89×10^4 CNY, 1283.96×10^4 CNY, and 932.15×10^4 CNY, respectively (Figure 5). The conversion from water areas to unused land also led to a decrease of 469.42×10^4 CNY. Other kinds of land use conversion do not lead to a decrease in ESV.

4.4. Impacts of Ecological Restoration on Ecosystem Services. The vital consequences of the two ecological restoration policies on land use are the conversions from cultivated land to forestry area/grassland and to water areas. Theoretically, if the sites implementing the two ecological restoration policies in spatial are known, changes in ESV in these areas during 2000–2008 could be viewed as the effects of the two ecological restoration policies. However, information is lacking on the location and the degree of implementation for the two ecological restoration policies in Shandong. It should be noted that the starting time of our research was 2000 when the two ecological restoration policies had just been launched. Furthermore, during 2000–2008, no other policies were implemented to drive the conversion from cultivated land to grassland, forestry area, or water areas. Most of the conservations from cultivated land to grassland/forestry area or water area during 2000–2008 could be similarly looked upon as the consequence of the Grain-for-Green and Grain-for-Blue policies.

Accordingly, we assessed the impacts of Grain-for-Green and Grain-for-Blue on changes in ESV. Grain-for-Green in total added an ESV of 5.19×10^6 CNY, while Grain-for-Blue

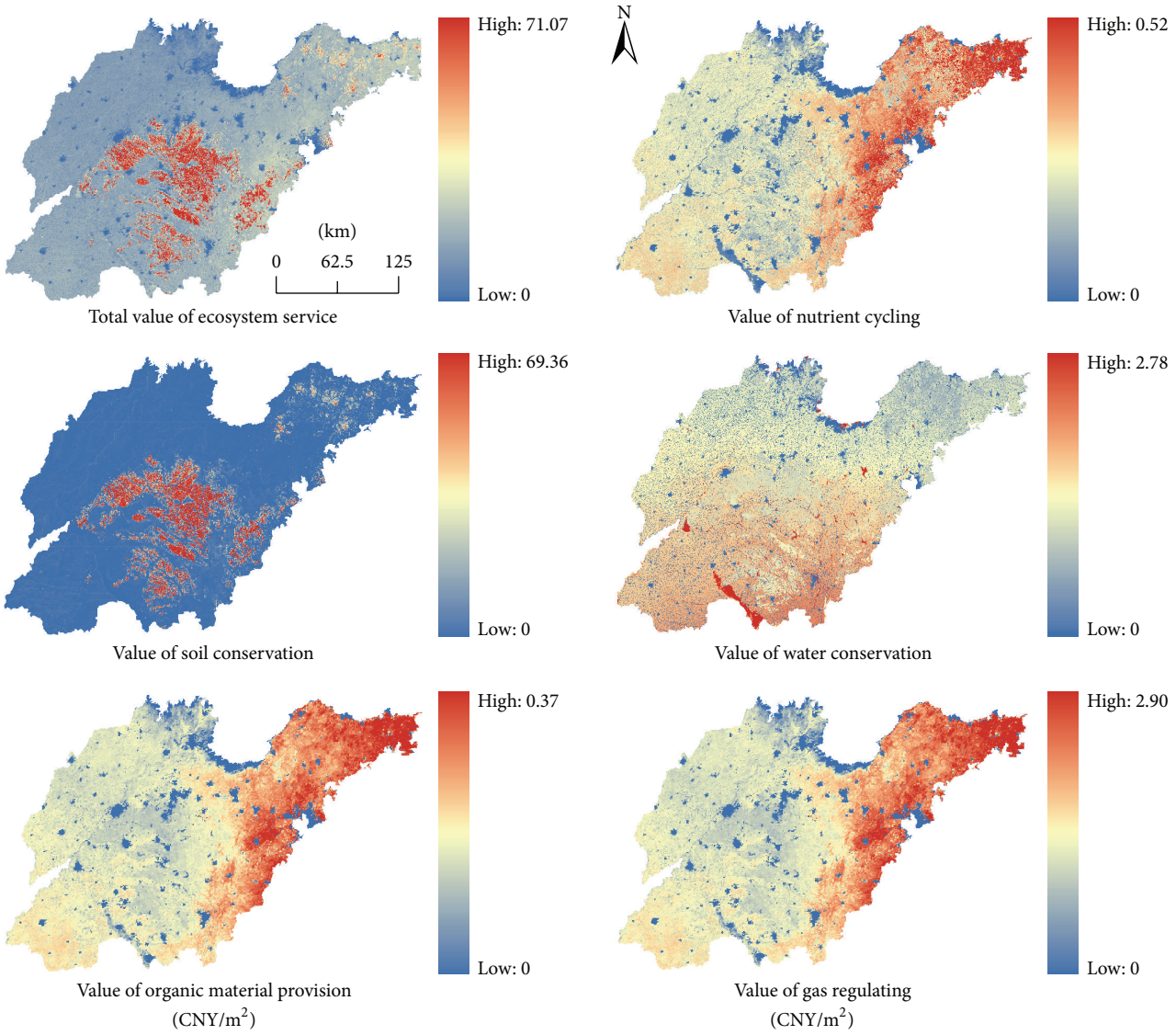

Figure 3: Value of ecosystem services in Shandong in 2000.

led to an increase of ESV of 206.77 × 10^6 CNY (Table 1). The two ecological restoration policies in total led to an increase of 42.30% in ESV. The ESV per unit increased from 1.23 CNY/m^2 in 2000 to 1.53 CNY/m^2 in 2008 due to the implementation of Grain-for-Green. The ESV per unit increased from 1.14 CNY/m^2 in 2000 to 1.63 CNY/m^2 in 2008 due to the implementation of Grain-for-Blue. The effects of Grain-for-Blue on ecosystem services seem better than those of Grain-for-Green.

The two ecological restoration policies produced different results for the ecosystem service value. For the Grain-for-Green policy, the value of nutrient cycling, regulating gases, organic material provision, and soil conservation increased by 64.12%, 38.98%, 40.00%, and 18.25%, respectively, while the value of water conservation decreased by 21.48% (Table 2). For the Grain-for-Blue policy, the value of water conservation significantly increased by 103.12%, followed by the increase in regulating gases (23.60%) and organic material provision (25.72%). However, the values of soil conservation and nutrient cycling decreased by 100.00% and 56.20%.

5. Discussions and Conclusion

The main objective of Grain-for-Green was to restore forests and grasslands in an effort to control soil erosion in China from 1998. In this paper, we found that the values of soil conservation increased by 18.25% due to Grain-for-Green during 2000–2008. However, the value of soil conservation in the whole of Shandong province increased by 76.87% during the same period. Grain-for-Green in Shandong does not significantly reduce soil erosion. The reason could be that Grain-for-Green in Shandong was mainly implemented in low sloping areas where soil erosion is not significant. The

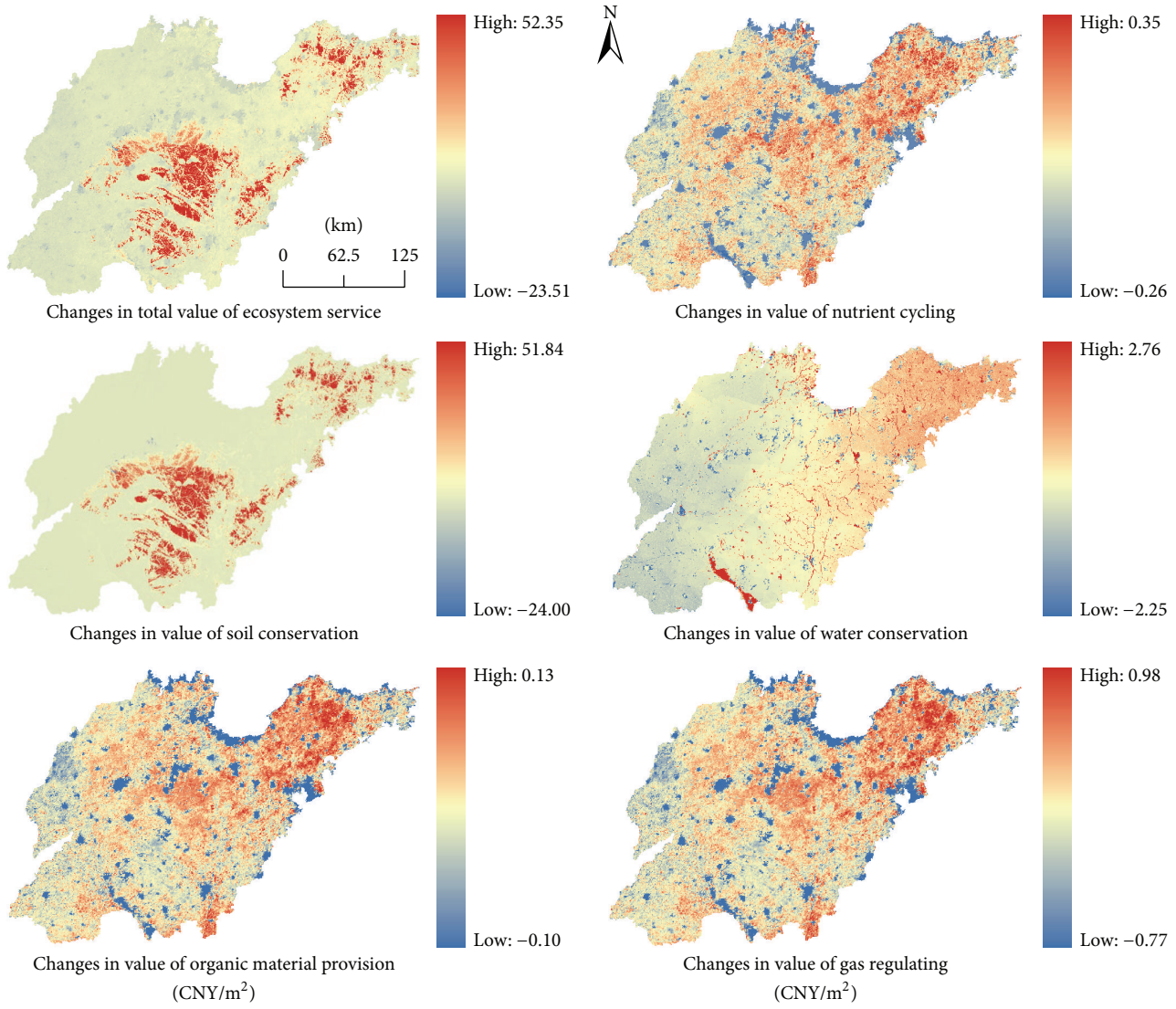

Figure 4: Changes in value of ecosystem services in Shandong during 2000–2008.

Table 1: Changes in ESV in response to ecological restoration policies.

Policy	Total value ($\times 10^6$ CNY)			Value per unit (CNY/m^2)			Change percentage (%)
	2000	2008	Change	2000	2008	Change	
Grain-for-Green	21.36	26.55	5.19	1.23	1.53	0.30	24.30
Grain-for-Blue	479.68	686.45	206.77	1.14	1.63	0.49	43.11
Total	**501.04**	**713.00**	**211.96**	**1.141**	**1.62**	**0.48**	**42.30**

implementation of Grain-for-Green in these areas has limited positive effects on controlling soil erosion.

In comparison to the soil conservation value, Grain-for-Green did improve the ecosystem service function of nutrient cycling, organic material provision, and regulating gases. During 2000–2008, the values of nutrient cycling, organic material provision, and regulating gases increased by 64.12%, 40.00%, and 38.98%, respectively, in the areas implementing Grain-for-Green, but increased by 37.02%, 37.90%, and 36.13%, respectively, in the whole of Shandong. The ESV of the areas implementing the Grain-for-Blue policy increased by 43.10% during 2000–2008. The increase in water conservation value accounted for most of the added ESV. In the same period, the value of water conservation in the whole of Shandong increased by 16.69%, while it increased by 103.12% in Grain-for-Blue areas. Grain-for-Blue significantly improved the ecosystem service function of water conservation due to the improvement of the water regulating function in water areas.

We assessed five kinds of ecosystem service values in Shandong province. The ecological restoration policies led to significant tradeoffs in ESV. Although Grain-for-Green

Table 2: Changes in different ecosystem service values in response to ecological restoration policies.

Policy	Ecosystem service value	2000 (10^4 CNY)	2008 (10^4 CNY)	Change percentage (%)
Grain-for-Green	Regulating gases	1169.29	1625.10	38.98
	Water conservation	554.92	435.71	−21.48
	Soil conservation	101.31	119.80	18.25
	Nutrient cycling	166.66	273.53	64.12
	Organic material provision	143.36	200.71	40.00
	Total	**2135.54**	**2654.85**	**24.32**
Grain-for-Blue	Regulating gases	20550.32	25399.44	23.60
	Water conservation	19239.73	39079.81	103.12
	Soil conservation	3300.42	0.00	−100.00
	Nutrient cycling	2400.89	1051.63	−56.20
	Organic material provision	2476.81	3113.85	25.72
	Total	**47968.17**	**68644.73**	**43.10**

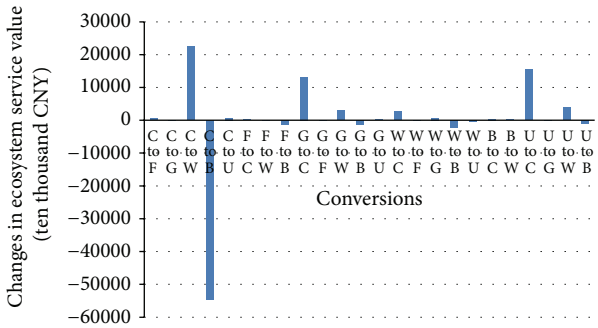

Figure 5: Changes in ESV due to land use conversions. Notes: C, F, G, W, B, and U are cultivated land, forestry area, grassland, water area, built-up area, and unused land, respectively; C to F means the conversion from cultivated land to forestry, and similarly for the others.

improved the ecosystem service function of nutrient cycling, organic material provision, and regulating gases, it also decreased the ecosystem service function of water conservation. Grain-for-Blue increased the ecological service function of water conservation but led to a decrease in soil conservation (100%) and the nutrient cycling function (56.20%).

Ecosystems comprise several different ecosystem service functions. A single ecological restoration policy cannot improve all the ecosystem service functions. Thus, we argue that integral ecological restoration policy should be adopted in ecological restoration. For example, when implementing Grain-for-Green in sloping areas, a water conservation project, such as rainfall collection, should be adopted simultaneously. Rainfall collection can not only improve the irrigation condition of farmland but also improve the water conservation function. When implementing the Grain-for-Blue policy, a soil conservation project (such as afforestation) should also be considered. Furthermore, close attention must be given to the suitability of the policy. For example, Grain-for-Green in plain areas is of no benefit to the overall improvement of the ecosystem service function and should be strictly limited to sloping areas.

Most of the maps (e.g., NPP, NDVI) utilized to assess the changes in ESV in this paper are 1 km grid maps. The resolution of these maps could be too low at the provincial scale. In addition, owing to a lack of suitable method and data, we did not assess the ESV of regulating waste which is one of the most important ecosystem services of water areas. Thus, the ESV of water areas assessed in this paper could be underestimated. For the same reason, we also did not assess the ESV of the culture function which could also generate some uncertainty in the results for ESV.

Conflict of Interests

The authors declare that there is no conflict of interests regarding the publication of this paper.

Acknowledgments

This work was supported by the National Natural Science Funds of China for Distinguished Young Scholars (Grant no. 71225005), the National Natural Science Foundation of China (Grant nos. 41071343 and 41171434), and the Key Project in the National Science & Technology Pillar Program of China (no. 2013BAC03B00).

References

[1] W. V. Reid, H. A. Mooney, A. Cropper et al., *Ecosystems and Human Well-Being: Synthesis*, Millennium Ecosystem Assessment, Island Press, Washington, DC, USA, 2005.

[2] Y. H. Lü, B. J. Fu, X. M. Feng et al., "A policy-driven large scale ecological restoration: quantifying ecosystem services changes in the loess plateau of China," *PLoS ONE*, vol. 7, no. 2, Article ID e31782, 2012.

[3] M. Shi, G. Ma, and Y. Shi, "How much real cost has China paid for its economic growth?" *Sustainability Science*, vol. 6, no. 2, pp. 135–149, 2011.

[4] W. Song and B. C. Pijanowski, "The effects of China's cultivated land balance program on potential land productivity at a national scale," *Applied Geography*, vol. 46, pp. 158–170, 2013.

[5] W. Song, "Decoupling cultivated land loss by construction occupation from economic growth in Beijing," *Habitat International*, vol. 43, pp. 198–205, 2014.

[6] X. Q. Jia, B. J. Fu, X. M. Feng, G. H. Hou, Y. Liu, and X. F. Wang, "The tradeoff and synergy between ecosystem services in the Grain-for-Green areas in Northern Shaanxi, China," *Ecological Indicators*, vol. 43, pp. 103–113, 2014.

[7] W. Song and M. L. Liu, "Assessment of decoupling between rural settlement area and rural population in China," *Land Use Policy*, vol. 39, pp. 331–341, 2014.

[8] R. A. Logsdon and I. Chaubey, "A quantitative approach to evaluating ecosystem services," *Ecological Modelling*, vol. 257, pp. 57–65, 2013.

[9] J. A. Foley, R. DeFries, G. P. Asner et al., "Global consequences of land use," *Science*, vol. 309, no. 5734, pp. 570–574, 2005.

[10] M. J. Metzger, M. D. A. Rounsevell, L. Acosta-Michlik, R. Leemans, and D. Schröter, "The vulnerability of ecosystem services to land use change," *Agriculture, Ecosystems and Environment*, vol. 114, no. 1, pp. 69–85, 2006.

[11] E. Nelson, H. Sander, P. Hawthorne et al., "Projecting global land-use change and its effect on ecosystem service provision and biodiversity with simple models," *PLoS ONE*, vol. 5, no. 12, Article ID e14327, 2010.

[12] W. J. Sutherland, T. Gardner, T. L. Bogich et al., "Solution scanning as a key policy tool: identifying management interventions to help maintain and enhance regulating ecosystem services," *Ecology and Society*, vol. 19, no. 2, article 3, 2014.

[13] C. Perrings, A. Duraiappah, A. Larigauderie, and H. Mooney, "The biodiversity and ecosystem services science-policy interface," *Science*, vol. 331, no. 6021, pp. 1139–1140, 2011.

[14] R. J. Kemkes, J. Farley, and C. J. Koliba, "Determining when payments are an effective policy approach to ecosystem service provision," *Ecological Economics*, vol. 69, no. 11, pp. 2069–2074, 2010.

[15] J. Börner, A. Mendoza, and S. A. Vosti, "Ecosystem services, agriculture, and rural poverty in the Eastern Brazilian Amazon: interrelationships and policy prescriptions," *Ecological Economics*, vol. 64, no. 2, pp. 356–373, 2007.

[16] B. J. Fu, M. Forsius, and J. Liu, "Ecosystem services: climate change and policy impacts editorial overview," *Current Opinion in Environmental Sustainability*, vol. 5, no. 1, pp. 1–3, 2013.

[17] P. J. Ferraro, K. Lawlor, K. L. Mullan, and S. K. Pattanayak, "Forest figures: ecosystem services valuation and policy evaluation in developing countries," *Review of Environmental Economics and Policy*, vol. 6, no. 1, pp. 20–44, 2012.

[18] P. Kumar, S. E. Esen, and M. Yashiro, "Linking ecosystem services to strategic environmental assessment in development policies," *Environmental Impact Assessment Review*, vol. 40, pp. 75–81, 2013.

[19] L. E. Barry, R. T. Yao, D. R. Harrison, U. H. Paragahawewa, and D. J. Pannell, "Enhancing ecosystem services through afforestation: how policy can help," *Land Use Policy*, vol. 39, pp. 135–145, 2014.

[20] A. Jordan and D. Russel, "Embedding the concept of ecosystem services? The utilisation of ecological knowledge in different policy venues," *Environment and Planning C: Government and Policy*, vol. 32, no. 2, pp. 192–207, 2014.

[21] F. J. Sijtsma, C. M. van der Heide, and A. van Hinsberg, "Beyond monetary measurement: how to evaluate projects and policies using the ecosystem services framework," *Environmental Science & Policy*, vol. 32, pp. 14–25, 2013.

[22] J. Hauck, C. Görg, R. Varjopuro, O. Ratamäki, and K. Jax, "Benefits and limitations of the ecosystem services concept in environmental policy and decision making: some stakeholder perspectives," *Environmental Science and Policy*, vol. 25, pp. 13–21, 2013.

[23] K. Helming, K. Diehl, D. Geneletti, and H. Wiggering, "Mainstreaming ecosystem services in European policy impact assessment," *Environmental Impact Assessment Review*, vol. 40, pp. 82–87, 2013.

[24] M. Brady, C. Sahrbacher, K. Kellermann, and K. Happe, "An agent-based approach to modeling impacts of agricultural policy on land use, biodiversity and ecosystem services," *Landscape Ecology*, vol. 27, no. 9, pp. 1363–1381, 2012.

[25] C. E. Bronner, A. M. Bartlett, S. L. Whiteway, D. C. Lambert, S. J. Bennett, and A. J. Rabideau, "An assessment of U.S. stream compensatory mitigation policy: necessary changes to protect ecosystem functions and services," *Journal of the American Water Resources Association*, vol. 49, no. 2, pp. 449–462, 2013.

[26] D. Geneletti, "Assessing the impact of alternative land-use zoning policies on future ecosystem services," *Environmental Impact Assessment Review*, vol. 40, pp. 25–35, 2013.

[27] R. D. Simpson, "Ecosystem services as substitute inputs: basic results and important implications for conservation policy," *Ecological Economics*, vol. 98, pp. 102–108, 2014.

[28] B. Zhao, U. Kreuter, B. Li, Z. Ma, J. Chen, and N. Nakagoshi, "An ecosystem service value assessment of land-use change on Chongming Island, China," *Land Use Policy*, vol. 21, no. 2, pp. 139–148, 2004.

[29] Z. Guo, X. Xiao, Y. Gan, and Y. Zheng, "Ecosystem functions, services and their values—a case study in Xingshan County of China," *Ecological Economics*, vol. 38, no. 1, pp. 141–154, 2001.

[30] R. Costanza, R. d'Arge, R. de Groot et al., "The value of the world's ecosystem services and natural capital (Reprinted from Nature, vol. 387, no. 6630, pp. 253–260, 1997)," *Ecological Economics*, vol. 25, no. 1, pp. 3–15, 1998.

[31] R. Costanza, R. D'Arge, R. De Groot et al., "The value of the world's ecosystem services and natural capital," *Nature*, vol. 387, no. 6630, pp. 253–260, 1997.

[32] C. M. Peters, A. H. Gentry, and R. O. Mendelsohn, "Valuation of an Amazonian rainforest," *Nature*, vol. 339, no. 6227, pp. 655–656, 1989.

[33] D. Tobias and R. Mendelsohn, "Valuing ecotourism in a tropical rain-forest reserve," *AMBIO*, vol. 20, no. 2, pp. 91–93, 1991.

[34] K. Chopra, "The value of non-timber forest products: an estimation for tropical deciduous forests in India," *Economic Botany*, vol. 47, no. 3, pp. 251–257, 1993.

[35] K. N. Ninan and M. Inoue, "Valuing forest ecosystem services: what we know and what we don't," *Ecological Economics*, vol. 93, pp. 137–149, 2013.

[36] J. O. Kenter, T. Hyde, M. Christie, and I. Fazey, "The importance of deliberation in valuing ecosystem services in developing countries-Evidence from the Solomon Islands," *Global Environmental Change*, vol. 21, no. 2, pp. 505–521, 2011.

[37] S. Silvestri, L. Zaibet, M. Y. Said, and S. C. Kifugo, "Valuing ecosystem services for conservation and development purposes: a case study from Kenya," *Environmental Science and Policy*, vol. 31, pp. 23–33, 2013.

[38] M. L. Mann, R. K. Kaufmann, D. M. Bauer, S. Gopal, J. G. Baldwin, and M. Del Carmen Vera-Diaz, "Ecosystem service value and agricultural conversion in the Amazon: implications for policy intervention," *Environmental and Resource Economics*, vol. 53, no. 2, pp. 279–295, 2012.

[39] R. L. Deal, B. Cochran, and G. LaRocco, "Bundling of ecosystem services to increase forestland value and enhance sustainable forest management," *Forest Policy and Economics*, vol. 17, pp. 69–76, 2012.

[40] W. F. Hyde and K. R. Kanel, *The Marginal Cost of Endangered Species Management*, IUCN, Cambridge, UK, 1994.

[41] R. Kramer and M. Munasinghe, *Valuing a Protected Tropical Forest: A Case Study in Madagascar*, IUCN, Cambridge, UK, 1994.

[42] P. C. L. White, K. W. Gregory, P. J. Lindley, and G. Richards, "Economic values of threatened mammals in Britain: a case study of the otter *Lutra lutra* and the water vole *Arvicola terrestris*," *Biological Conservation*, vol. 82, no. 3, pp. 345–354, 1997.

[43] M. M. Gardiner, C. E. Burkman, and S. P. Prajzner, "The value of urban vacant land to support arthropod biodiversity and ecosystem services," *Environmental Entomology*, vol. 42, no. 6, pp. 1123–1136, 2013.

[44] C. White, C. Costello, B. E. Kendall, and C. J. Brown, "The value of coordinated management of interacting ecosystem services," *Ecology Letters*, vol. 15, no. 6, pp. 509–519, 2012.

[45] X. Z. Deng, J. K. Huang, E. Uchida, S. Rozelle, and J. Gibson, "Pressure cookers or pressure valves: do roads lead to deforestation in China?" *Journal of Environmental Economics and Management*, vol. 61, no. 1, pp. 79–94, 2011.

[46] J. Y. Liu, M. L. Liu, H. Q. Tian et al., "Spatial and temporal patterns of China's cropland during 1990–2000: an analysis based on Landsat TM data," *Remote Sensing of Environment*, vol. 98, no. 4, pp. 442–456, 2005.

[47] X. Deng, J. Huang, S. Rozelle, and E. Uchida, "Economic growth and the expansion of urban land in China," *Urban Studies*, vol. 47, no. 4, pp. 813–843, 2010.

[48] X. Deng, Q. Jiang, H. Su, and F. Wu, "Trace forest conversions in Northeast China with a 1-km area percentage data model," *Journal of Applied Remote Sensing*, vol. 4, no. 1, Article ID 041893, 2010.

[49] S. Su, D. Li, Y. Hu, R. Xiao, and Y. Zhang, "Spatially non-stationary response of ecosystem service value changes to urbanization in Shanghai, China," *Ecological Indicators*, vol. 45, pp. 332–339, 2014.

[50] W. Guo, *Valuation of ecosystem services based on remote sensing and landscape pattern optimization in Beijing [Ph.D. thesis]*, Beijing Forestry University, Beijing, China, 2012.

[51] W. H. Wischmeier, "A soil erodibility nomograph for farm land and construction," *Journal of Soil and Water Conservation*, vol. 26, pp. 189–193, 1971.

[52] K. G. Renard, G. R. Foster, and G. A. Weesies, *Predicting Soil Erosion by Water: A Guide to Conservation Planning with the Revised Universal Soil Loss Equation (RUSLE)*, Handbook no. 703, U.S. Department of Agriculture, Washington, DC, USA, 1997.

[53] D. C. Flanagan, G. R. Foster, W. H. Neibling, and J. P. Burt, "Simplified equations for filter strip design," *Transactions of the American Society of Agricultural Engineers*, vol. 32, no. 6, pp. 2001–2007, 1989.

[54] K. K. K. Kuok, D. Y. S. Mah, and P. C. Chiu, "Evaluation of C and P factors in universal soil loss equation on trapping sediment: case study of Santubong River," *Journal of Water Resource and Protection*, vol. 5, no. 12, pp. 1149–1154, 2013.

[55] K. G. Renard and G. R. Foster, "Soil conservation: principles of erosion by water," in *Dryland Agriculture*, H. E. Dregne and W. O. Willis, Eds., pp. 155–176, American Society of Agronomy, Soil Science Society of America, Madison, Wis, USA, 1983.

[56] Z. Y. Ouyang, X. K. Wang, and H. Miao, "A primary study on Chinese terrestrial ecosystem services and their ecological-economic values," *Acta Ecological Sinica*, vol. 19, pp. 607–613, 1999.

Hindawi Publishing Corporation
Advances in Meteorology
Volume 2015, Article ID 848795, 9 pages
http://dx.doi.org/10.1155/2015/848795

Research Article

Land Use Suitability Assessment in Low-Slope Hilly Regions under the Impact of Urbanization in Yunnan, China

Gui Jin,[1] Zhaohua Li,[1] Qiaowen Lin,[2] Chenchen Shi,[3] Bing Liu,[4] and Lina Yao[5]

[1] *Faculty of Resources and Environmental Science, Hubei University, Wuhan, Hubei 430062, China*
[2] *School of Public Administration, China University of Geosciences, Wuhan 430074, China*
[3] *State Key Laboratory of Water Environment Simulation, School of Environment, Beijing Normal University, Beijing 100875, China*
[4] *College of Geomatics, Shandong University of Science and Technology, No. 579 Qianwangang Road, Economic & Technical Development Zone, Qingdao, Shandong 266590, China*
[5] *Institute of Geographic Sciences and Natural Resources Research, Chinese Academy of Sciences, Chaoyang District, Beijing 100101, China*

Correspondence should be addressed to Zhaohua Li; zli@hubu.edu.cn

Received 19 September 2014; Accepted 13 December 2014

Academic Editor: Jinwei Dong

Nowadays, the conflict between land development and land conservation has become increasingly serious in China. The plan called "town of mountain" is carried out in many nonplain areas to alleviate the conflict. To avoid geological disasters and ecological risks in those areas, land use suitability assessment is of great importance. In this paper, the fuzzy weight of evidence model is applied into land use suitability assessment in low-slope hilly regions in Yunnan, China. Fuzzy weight of evidences is calculated to determine 9 map layers. Finally, posterior probabilities are modified after synthesizing each map layer, which are used to generate a land use suitability map. The results show that 9.33%, 26.18%, 45.98%, and 18.51% of low-slope hilly regions are separately highly suitable, moderately suitable, marginally suitable, and unsuitable for development. Besides, highly and moderately suitable areas are mainly located in towns with excellent natural and socioeconomic conditions. The largest areas which are marginally suitable for development are most widely distributed. Unsuitable areas are mainly distributed far away from towns and water sources. The findings of the research will promote the rational use and scientific management of the land.

1. Introduction

Due to the rapid urbanization in China [1], the demand for built-up land both in urban and rural areas has been dramatically increased with the shrinking of arable land [2–4]. The conflict between land development and land conservation has become increasingly serious [5–8]. Under the most stringent farmland protection system in China, the strategy of developing low-slope hilly regions is carried out to alleviate the conflict [9]. The concept of low-slope hilly regions is put forward under the demand for land resources in mountain area with the social and economic development and urbanization construction. It refers to contiguously distributed land with slopes less than 25 degrees in the majority of hilly areas as well as unused low mountains and hills which can be used by town construction in the mountain area. It mainly includes a variety of reserved land types such as unused land, abandoned garden, and inefficient forest, which are mostly distributed in the regions with little plain and inadequate protection of cultivated land. Currently, there is a shortage of land available for the development of cities and towns in China [10, 11]. However, low-slope hilly regions account for a relatively large proportion of the available land. Current land use in China, such as a small amount of land per person, intense exploitation of land development, and shortage of reserved land, has limited the development of regional economy and society [12, 13]. Therefore, it is a good way to alleviate the conflict between land and people in the developed regions with high pressure of protecting arable land by optimally using low-slope hilly land [14]. Compared to the plain areas, low-slope hilly land has the lower ecological carrying capacity and higher

ecological sensitivity. Lack of good understanding of low-slope hilly land and objective evaluation of development activities will bring enormous environmental disturbance and destruction, resulting in serious or even irreversible consequences on the structure and function of ecosystems, biodiversity, and landscape in this area [15, 16]. Therefore, it is of great significance to do the suitability assessment in low-slope hilly land and classify development levels in order to ensure the orderly development of it [17–19]. Since a framework for land evaluation reported by the Food and Agriculture Organization (FAO), the research of land use suitability assessment receives more and more attention. The theory, method, and specific scheme on land use suitability evaluation are also improved constantly. Currently, scholars usually carry out land suitability assessment in different regions [16, 20–22]. However, the screening of evaluation factor and the determination method of factor weight are both significant on the influence of the cultivated land suitability assessment. On the one hand, the evaluation factor is different in different areas such as the plateau region, hilly area, and flood plain area, and the emphasis of the research is different. Accordingly, on the other hand, the calculation method of factor weight can be divided into two categories [12, 23, 24]: one is the mathematical logical reasoning based on knowledge and rules, containing the comprehensive index method and Fuzzy-AHP methods; this kind of methodology has higher dependency on knowledge and then makes the result more subjective. The other one is the data driven mechanism based on adaptive system such as neural network method. But its reasoning process is cumbersome and its algorithm is complex, which cannot effectively use existing knowledge and often leads to the fact that it is hard to explain the acquired rules. In view of the special natural and social economic conditions in Yunnan region, this paper determines the factor weights by the fuzzy weight of evidence model to avoid subjective influence, multiple collinear interference, and complex model algorithm. The paper provides a scientific basis for urbanization and optimal allocation of land through evaluating the development suitability levels of low-slope hilly resources (not including the ecological preservation areas) such as unused land, woodland, and grassland.

2. Study Area

Yunnan province (97°31′~106°11′W, 21°8′~29°15′N) is a low-latitude inland, spreading about 394,000 square kilometers which accounts for 4.11 percent of total area in China (Figure 1) . It comprises mainly mountains, plateaus, hills, and small basins. Mountains and plateaus occupy around 94% of the province. Much of the province lies within the subtropical highland. There is little variance in annual temperature but a large diurnal temperature range. It has distinct wet and dry seasons. The temperature changes greatly with the terrain. Due to the interaction of climate, biology, geology, topography, and so on, various types of soil are formed. It is characterized by the vertical distribution of soil. The area of red soil accounts for 50% of the province. Rainfall is unevenly distributed in terms of seasons and regions [25]. Yunnan province, with strong intensity in urban land use, is one of the provinces where mountain towns are widespread in China. Therefore, it is an inevitable choice for urbanization development to moderately develop the low-slope hilly regions in Yunnan province.

3. Materials and Methods

3.1. Data Acquisition. The main data in this study includes meteorological data mainly referring to daily average temperature in 2010 and rainfall in Yunnan province. These data were derived from the daily observation data of meteorological stations maintained by the China Meteorological Administration. Current land use data with the scale 1 : 100,000 in 2010 of Yunnan province (http://www.resdc.cn) is also used, which contains data regarding all land use types such as built-up land, woodland, grassland, and unused land. Terrain data with the scale 1 : 25,000 in Yunnan province is from Data Sharing Infrastructure of Earth System Science in China (http://www.geodata.cn/Portal/metadata/viewMetadata.jsp?id=100101-11221). The outcome of overall land use plan (2006–2020) in Yunnan province which derived from the Office of Land and Resources in Yunnan province is used by the research.

ArcGIS10.0 is used to process Kriging interpolation on the rainfall distribution and average temperature distributions with meteorological data, which results in creating an annual rainfall distribution map and an annual temperature distribution map. Topographic data are used to generate digital elevation model (DEM) (whose spatial resolution is 1 km × 1 km) and a slope map. Buffer zones of water sources and state roads are obtained later. Therefore, based on the optimum distance, a map of distance to water and a map of distance to state roads are obtained, respectively. Interpolation analysis is done through socio-economic data, which generates a map of GDP per capita and a population distribution map in Yunnan in the grid with cells of 1 × 1 square kilometers [26–28]. The proportion of plain areas is obtained through land use data in Yunnan province [29]. With the help of geoscience data analysis system, the existing built-up land parcels in Yunnan are extracted as training samples suitable for construction and are used to make a distribution map of the sample. It should be noted that GeoDAS4.2 was developed by the Geomatics Research Group at York University, and it is a GIS software that synthesizes the fuzzy weight of evidence model, fractal model, spatial statistics, artificial intelligence, and other modern data processing techniques (http://www.yorku.ca/yul/gazette/past/archive/2002/030602/current.htm). A sampling interval of 1 km × 1 km pixels is determined as the unit of area according to the minimum shape and size of the parcel of evaluation objects. Each map layer is saved in the form of GRID.

3.2. Research Methods. Fuzzy weight of evidence is evolved from weight of evidence which is firstly used in medical diagnosis without considering the space. Since 1980s, Agterberg et al. [30, 31] had modified this method and applied it

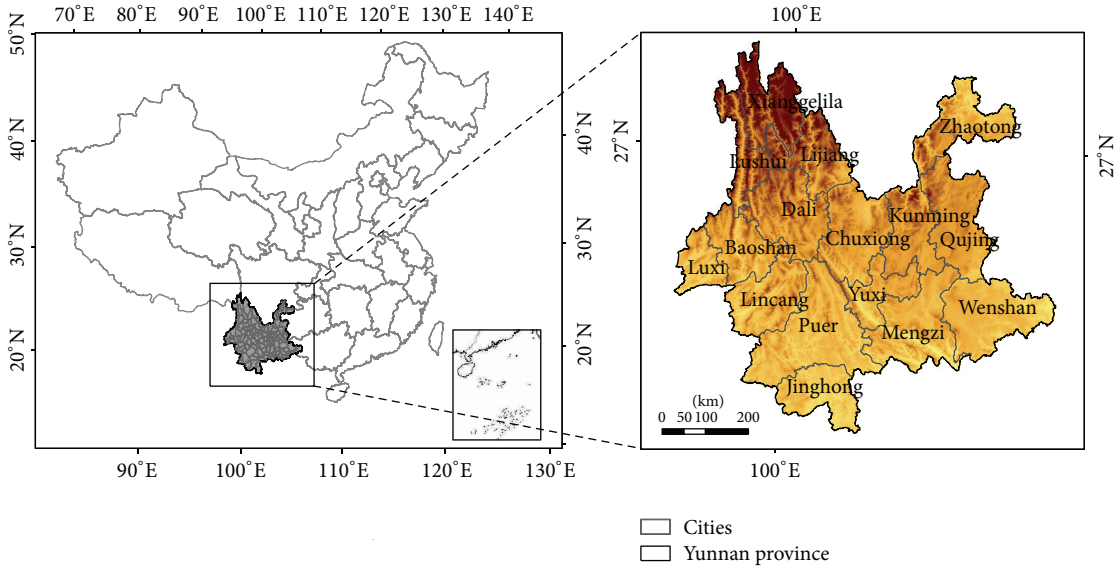

Figure 1: Location and DEM of Yunnan province.

on mineral forecast. Since this method can be applicable to integrate multiple information and spatial decision support systems, it has been applied in the evaluation on various mineral resources, geological disaster risk assessment, and environmental evaluation in recent years.

3.2.1. The Principle of the Method. Weight of evidence method is a log-linear model under a Bayesian probability criterion. A priori probabilities are firstly calculated. Then conditional probabilities are calculated under a certain geological evidence model. Weight of evidence method includes posterior logit model, the general weight of evidence model, fuzzy weight of evidence model, and weighted weight of evidence model. The principle of the method is as follows [32–34].

(1) Calculate A Priori Probabilities. Suppose total area of the study area T is $A(T)$ which is divided into cells of a fixed area u. D is the event to be predicted. It follows that there are $N(T) = A(T)/u$ cells totally in the study area where $A(\,)$ represents the area and $N(\,)$ is the number of cells. Therefore, the frequency of events D in the study area T is $N(D)$. The probability of the event is

$$P(D) = \frac{N(D)}{T(D)}, \tag{1}$$

where $P(D)$ is the a priori probability, and the occurrence can be expressed as $O(D) = P(D)/(1 - P(D))$.

(2) Calculate Weight of Evidence. Any weight of evidence (the map layer) x is binary. Its weight is defined as

$$W^{+} = \ln\left[\frac{P(B/D)}{P\left(B/\overline{D}\right)}\right],$$

$$W^{-} = \ln\left[\frac{P\left(\overline{B}/D\right)}{P\left(\overline{B}/\overline{D}\right)}\right], \tag{2}$$

where W^{+} and W^{-} represent the weight for presence of B and weight for absence of $\overline{B}$, respectively. $P(B/D) = N(B \cap D)/N(D)$ denotes the probability of selected weight of evidence D in any unit cell of B, where $N(B \cap D)$ stands for the occurrence of weight in B and $N(D)$ is the total number of occurrence in the study area. Other equations can be explained in the same way.

(3) Calculate Posterior Probability. If there is n number of weights which are independent of each other on the occurrence, the probability of the occurrence of any cell in the study area can be expressed by the posterior probability logarithm which is expressed as follows:

$$\ln O\left(D \mid B_1^k \cap B_2^k \cap B_3^k \cdots B_n^k\right) = \sum_{m=1}^{n} W_m^k + \ln O(D), \tag{3}$$

where $m = (1, 2, 3, \ldots n)$, and k indicates the presence and absence of the weight, namely,

$$W_m^k = \begin{cases} W_m^{+} \\ W_m^{-} \\ 0, \end{cases} \tag{4}$$

where W_m^{+} is the weight for presence of weight m. W_m^{-} is the weight for absence of weight m. 0 is the weight for missing of weight m. Accordingly, the posterior probability can be expressed as

$$P = \frac{O}{(1 + O)}. \tag{5}$$

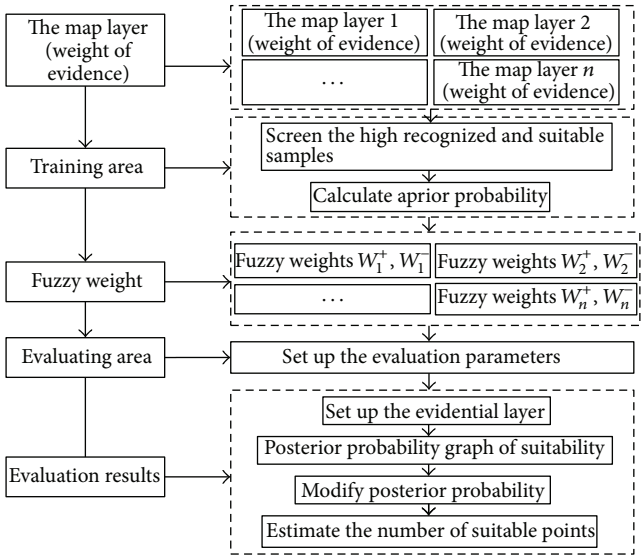

Figure 2: Flowchart of fuzzy weight of evidence.

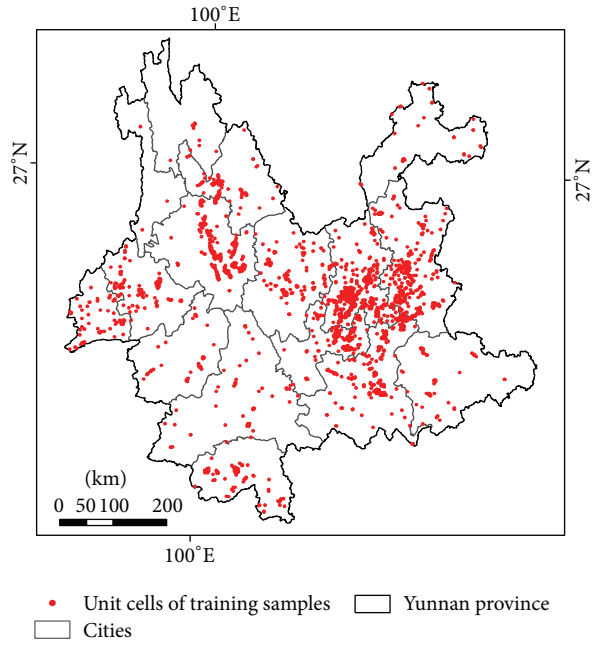

Figure 3: Distribution of training samples.

(4) Membership Function. Weight of evidence approach will result in loss of data while doing binary process for map layers which will affect the accuracy of assessment. Cheng and Agterberg [35] have developed a fuzzy weight of evidence approach which automatically copes with the missing data on discrete layers. Fuzzy weight of evidence uses ambiguity membership of layers which is determined by membership function to deal with multiclassification layers. Multivalued fuzzy membership function $0 \leq u(x) \leq 1$ is used to fit training samples. The weight of evidence is calculated in the end.

3.2.2. Procedures. The procedures of fuzzy weight of evidence (Figure 2) are as follows. (1) Identify research objectives, such as suitability of the development of the low-slope hilly regions; select the samples and calculate the a priori probabilities. (2) Determine the spatial layer related to the target; screen indicators; and establish an index system. (3) Extract map layers related to the target; use fuzzy membership functions to represent the credibility of the map layer. (4) Calculate the weight of fuzzy map layer; determine the value of the map layer; and screen indicators. (5) Integrate multiple fuzzy map layers and calculate a priori probabilities in order to obtain a suitability map in low-slope hilly regions. (6) Modify posterior probabilities; test the model; and make an interpretation for suitability distribution.

4. Results and Analysis

4.1. Training Samples and A Priori Probabilities. That selected training samples should follow two principles. (1) The training samples should be the given information approved by the public and the relevant departments. (2) The training samples should distribute widely in the research area. According to current land use data in Yunnan province, the existing built-up land parcels in Yunnan province are taken as samples suitable for urban development. The priori probability can be known by integrating (1) that the total number of unit cells of training samples is 2332 (Figure 3).There are 220,084 unit cells in the whole areas. The priori probability is 0.010596.

4.2. Fuzzy Map Layers and Weight of Evidence. The selection of evaluation factors is under the principle of dissimilarity, stability, and reality. On the basis of previous research on land use suitability assessment in low-slope hilly regions and built-up land, the evaluation index system of land use suitability assessment in low-slope hilly regions mainly refers to climate, topography, geography, and socioeconomic conditions. Impact factors include temperature, rainfall, elevation, slope, proportion of plain area, distance to water, distance to state roads, population distribution, and GDP per capita (Figure 4).

Each fuzzy weight of evidence is calculated by GeoDAS4.2. The influence of individual factors on the incident can be known which leads to the objective decision on choosing evaluation factors. Final map layers and parameters of fuzzy weights of evidence can be seen in Table 1 through (2) and multivalued fuzzy membership function.

4.3. The Posterior Probability and Its Modification. These map layers are synthesized and the posterior probability map in Yunnan is calculated by (5). Then the posterior probability map of land use suitability in low-slope hilly regions in Yunnan is made by taking reserved land parcels in low-slope hilly regions as the crop box (Figure 5). Posterior probabilities are affected by the setting of the unit cell. However, they do not affect the distribution of posterior probabilities. Therefore, posterior probabilities do not represent the probability of occurrences but the distribution after occurrences.

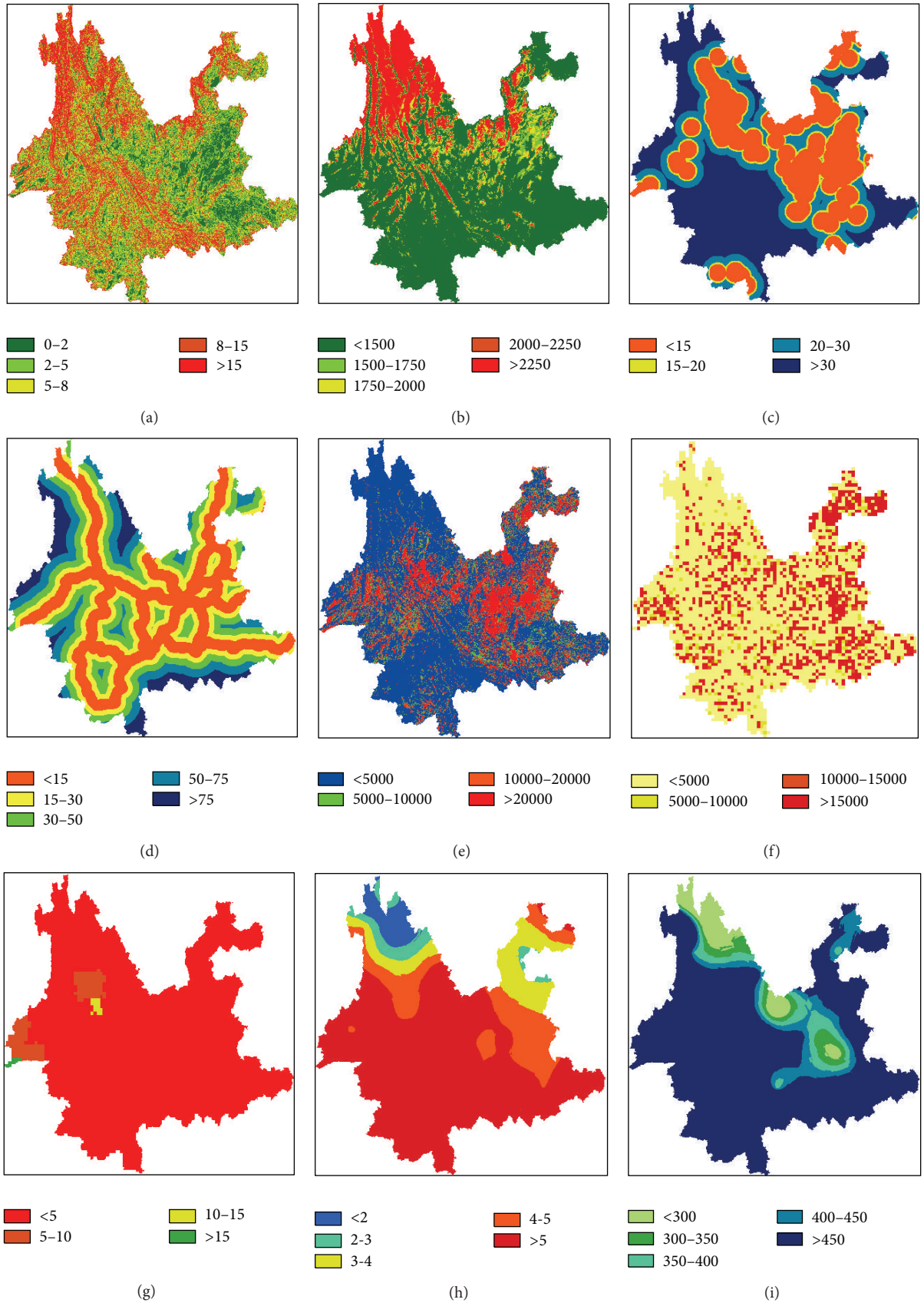

Figure 4: Nine-factor maps. (a) Slope (°); (b) elevation (m); (c) distance to water (Km); (d) distance to state roads (Km); (e) GDP per capita (Yuan); (f) population (person); (g) proportion of plain areas (%); (h) annual average temperature (°C); (i) annual rainfall (mm).

Table 1: Parameters of fuzzy weights of evidence for each map layer.

	Classification value	W^+	W^-	C	STDEV	T	MSF	FW	S(FW)	T(FW)
Slope/(°)	0~2	1.38	−0.69	2.07	0.04	49.10	1.00	1.38	0.03	49.62
	2~5	0.68	−1.21	1.89	0.05	34.35	0.60	1.03	0.08	13.50
	5~8	0.36	−1.44	1.79	0.07	24.30	0.38	0.68	0.12	5.91
	8~15	0.09	−2.03	2.12	0.19	11.32	0.15	−0.06	0.16	−0.37
	>15						0.00	−2.03	0.19	−10.92
Elevation (m)	<1500	0.28	−0.82	1.10	0.06	19.37	1.00	0.28	0.02	12.18
	1500~1750	0.24	−1.15	1.38	0.07	18.99	0.80	0.22	0.03	6.28
	1750~2000	0.20	−1.69	1.89	0.11	17.52	0.68	0.17	0.05	3.40
	2000~2250	0.17	−2.16	2.32	0.15	15.59	0.40	−0.03	0.09	−0.29
	>2250						0.00	−2.16	0.15	−14.62
Distance to water/km	<15	0.83	−1.17	2.00	0.05	38.85	1.0	0.83	0.02	35.72
	15~20	0.71	−1.26	1.97	0.06	35.39	0.8	0.61	0.02	26.25
	20~30	0.41	−1.49	1.90	0.07	26.06	0.4	−0.01	0.04	−0.19
	>30						0.0	−1.49	0.07	−21.43
Distance to state roads/km	<15	0.72	−0.79	1.51	0.05	33.35	1.00	0.72	0.02	29.02
	15~30	0.42	−1.20	1.62	0.06	26.05	0.68	0.63	0.06	11.12
	30~50	0.18	−1.31	1.49	0.09	16.66	0.40	0.46	0.10	4.51
	50~75	0.07	−1.64	1.71	0.17	10.02	0.20	0.16	0.14	1.15
	>75						0.00	−1.64	0.17	−9.71
GDP per capita/Yuan	<5000						0.00	−2.24	0.08	−28.60
	5000~10000	1.00	−2.24	3.24	0.08	39.85	0.40	−0.19	0.05	−3.92
	10000~20000	1.31	−1.97	3.28	0.07	48.71	0.85	1.10	0.02	48.67
	>20000	1.60	−1.74	3.34	0.06	56.64	1.00	1.60	0.02	70.40
Population/person	<5000	0.01	−0.77	0.78	0.22	3.55	0.0	−0.38	0.03	−12.26
	5000~10000	0.52	−0.39	0.91	0.04	21.71	0.6	0.11	0.02	5.18
	10000~15000	0.58	−0.36	0.94	0.04	22.62	0.8	0.35	0.03	13.78
	>15000	0.65	−0.34	0.99	0.04	23.84	1.0	0.65	0.03	21.21
Proportion of plain areas/%	<5	0.00	−1.38	1.38	0.58	2.38	0.0	−0.04	0.02	−1.74
	5~10	0.59	−0.04	0.64	0.07	8.60	0.4	−0.02	0.05	−0.39
	10~15	1.77	−0.03	1.80	0.12	14.74	1.0	1.77	0.12	14.75
	>15	0.80	0.00	0.81	0.34	2.40	1.0	1.77	0.12	14.75
Annual average temperature/°C	<2						0.00	−2.16	0.30	−7.18
	2~3	0.04	−2.17	2.20	0.30	7.28	0.65	0.05	0.11	0.46
	3~4	0.07	−1.85	1.92	0.19	10.29	1.00	0.07	0.02	3.36
	4~5	0.12	−0.86	0.98	0.08	12.55	1.00	0.07	0.02	3.36
	>5	−0.33	0.44	−0.77	0.04	−18.62	1.00	0.07	0.02	3.36
Annual rainfall/mm	<300						0.0	−1.40	0.27	−5.25
	300~350						0.0	−1.40	0.27	−5.25
	350~400	0.02	−1.40	1.42	0.27	5.31	0.3	−0.09	0.19	−0.50
	400~450	0.02	−0.47	0.49	0.11	4.39	0.8	−0.05	0.06	−0.91
	>500	−0.05	0.23	−0.27	0.05	−5.16	1.0	−0.05	0.02	−2.00

W^+: positive weight; W^-: negative weight; C: contrast of $W^+ - W^-$; STDEV: standard deviation of C; T: significance level; MSF: membership; FW: fuzzy weight; S(FW): standard deviation of fuzzy weight; T(FW): significance of fuzzy weight. Among them, GDP is the present value of 2010.

The map layer of fuzzy weight of evidence model is required to meet the needs of conditional independence. However, in reality, it is very difficult to achieve this which inevitably results in the deviation of posterior probabilities. The modified posterior probability can overcome the deficit of less accurate estimation on appropriate points.

Data tests of the linear function correction, logarithmic function correction, and exponential function correction are carried out with the help of GeoDAS4.2's posterior probability correction module. Ultimately, exponential function model $Y = 0.12x^{0.96}$ with optimal fitting degree is determined. After the modification of the posterior probability, the

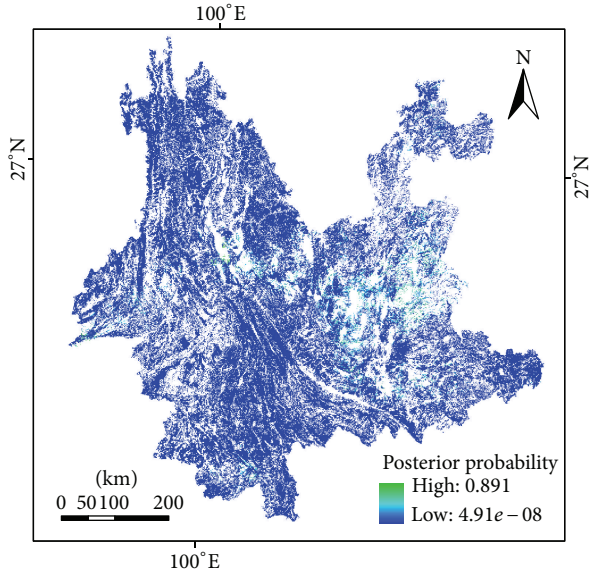

Figure 5: Posterior probability map of land use suitability.

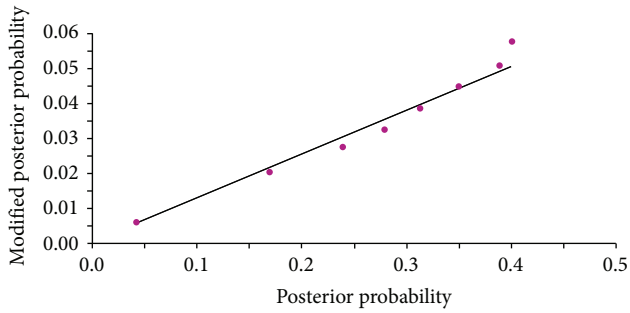

Figure 6: Modification on posterior probabilities.

coefficient of determination R is equal to 0.98. Procedures and results of the modification are shown in Figures 6 and 7.

4.4. Classification of Land Use Suitability in Low-Slope Hilly Regions. The posterior probability map is modified according to an exponential function model, which is used to create the modified posterior probability map. On the basis of this, the distribution frequency of modified posterior probabilities is analyzed. Distribution frequency curve is used. Finally, land use suitability in low-slope hilly regions in Yunnan province is divided into four levels (Table 2, Figure 8) according to obvious inflection point of the frequency curve and parameters of the weight of evidence of those evaluation factors.

There are four levels in terms of land use suitability in low-slope hilly regions in the study area: highly suitable, moderately suitable, marginally suitable, and unsuitable. (1) 9.33% of the land is highly suitable for development, mostly distributed in Kunming, Lijiang, Dali Bai autonomous prefecture, Qujing, and so on. Spatially, highly suitable areas are mainly located around cities where its terrain is relatively

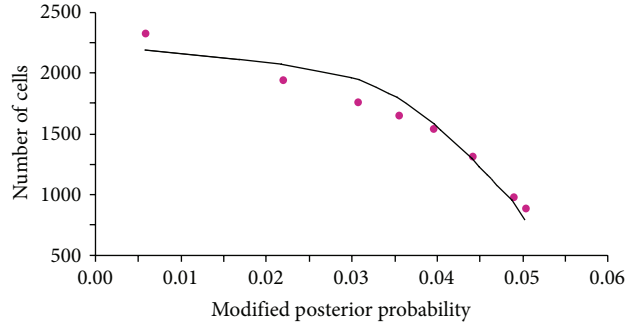

Figure 7: Modified posterior probabilities of land use suitability and numbers of corresponding points.

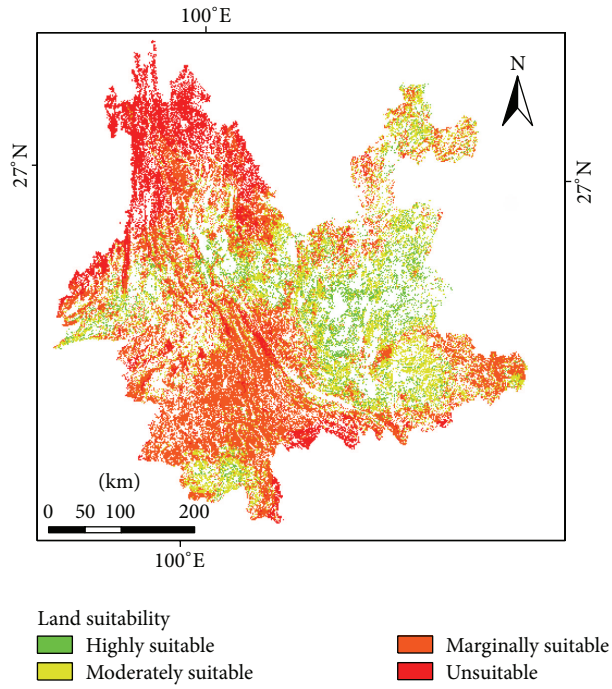

Figure 8: Classification map of land use suitability in low-slope hilly regions in Yunnan.

flat with slopes below 5 degrees and altitude mostly below 1500 m. The plain area accounts for more than 15% of the total area. Usually, the distance to water and state roads is no more than 15 km. GDP per capita is higher than 20,000 yuan. It is densely populated with 1,500 people/km^2. Its average annual temperatures are relatively high with abundant rainfall. (2) 26.18% of land is moderately suitable where it still has good natural resource and socioeconomic conditions with slopes ranging from 5 degrees to 8 degrees. It is close to towns. GDP per capita ranging from about 10,000 to 20,000 yuan is high. The population is relatively concentrated in these areas with a population density of 10,000 to 15,000 people/km^2. It has adequate rainfall and pleasant weather suitable for living. (3) 45.98% of land is marginally suitable for development. It is widely spread. Compared with highly suitable and moderately suitable areas, basic conditions in this area are relatively poor. However, it has strong potential for transformation,

Table 2: Classification of land use suitability in low-slope hilly regions in Yunnan.

Modified posterior probability	Suitability level	Numbers of cells	Description	Percentage of area/%
>0.01047~0.10860	Level 1	20315	Highly suitable	9.33
>0.00050~0.10467	Level 2	56997	Moderately suitable	26.18
>0.00002~0.00050	Level 3	100131	Marginally suitable	45.98
<0.00002	Level 4	40309	Unsuitable	18.51

which can be the main source of future development for some time. Therefore, its development potential, the overall size, and spatial layout should be the focus of policy makers. (4) 18.51% of land is unsuitable for development. These areas are more dispersed with slopes above 15 degrees in general and altitude mostly above 2200 m. The proportion of plain area is less than 5% of the total area. It is far away from water resources and state roads. GDP per capita is low and population density is relatively small. It is far away from cities and towns. It is not suitable for living due to the relatively unpleasant weather. At the same time, it is prone to geological disasters and ecological risks, inappropriate for development and construction. In summary, the four levels of the suitability assessment in low-slope hilly regions in Yunnan province can provide a basis for the priority of development in these regions. Under the consideration of social-economic development, urbanization, and ecological safety, the paper offers strategies to develop low-slope hilly regions, which focus on the exploration of unused land and give preferential protection to woodland and grassland. In addition, comparing the results of this paper with the achievement of the outcome of overall land use plan, it can be known that, as far as quantity structure is concerned, it is quite scientific and reasonable that the area of highly suitable resources of low-slope hilly regions is much larger than the built-up land index of the planning phase (2006–2020); as for the spatial distribution, the layout of the built-up land in the planning phase is basically consistent with the highly suitable low-slope hilly regions or is distributed in its perimeter zone.

5. Conclusion and Discussion

Due to global climate change and urbanization in China, the conflict between land development and land conservation has become increasingly serious [36]. The development of low-slope hilly regions is an important measure to alleviate the conflict. This paper takes Yunnan province as a typical case study, integrating natural geographical features and elements of human geography in Yunnan province to analyze land use suitability of low-slope hilly regions in Yunnan province and avoid potential geological disasters and ecological risks in those regions. Land use suitability of low-slope hilly regions in Yunnan province is evaluated by analyzing some factors referring to climate, topography, geography, society, and economy. Nine map layers regarding temperature, rainfall, elevation, slope, proportion of plain areas, distance to water, distance to state roads, population distribution, and GDP per capita are selected. The results show that (1) 9.33% of low-slope hilly regions in Yunnan are highly suitable for development. 26.18% of land is moderately suitable. 45.98% of land is generally suitable. The remaining 18.51% of land is unsuitable for development. This outcome of spatial distribution of low-slope hilly land in Yunnan province can finally optimize the size and layout of low-slope hilly land and promote the rational use of it. However, it is worth mentioning that not only the suitability of natural quality should be considered, but also some factors such as social and economic suitability, ecological suitability, and land policy should be taken into consideration. The related research will provide references for the plan of "town of mountain" in Yunnan and for the development of low-slope hilly land in Yunnan province. As for the model used in this study, it should be pointed out that training samples chosen in the study must be highly recognized appropriate points to ensure scientific results. Therefore, future research should pay more attention to how to ensure diversification of the given sources and improve the accuracy of given information.

Conflict of Interests

The authors declare no conflict of interests.

Acknowledgments

This research was financially supported by the major research plan of the National Natural Science Foundation of China (Grant no. 91325302), the National Natural Science Funds of China for Distinguished Young Scholar (Grant no. 71225005), and National Key Programme for Developing Basic Science in China (Grant no. 2010CB950900).

References

[1] R. Lal, "Soil carbon sequestration impacts on global climate change and food security," *Science*, vol. 304, no. 5677, pp. 1623–1627, 2004.

[2] G. C. S. Lin and S. P. S. Ho, "China's land resources and land-use change: insights from the 1996 land survey," *Land Use Policy*, vol. 20, no. 2, pp. 87–107, 2003.

[3] Y. Xie, Y. Mei, T. Guangjin, and X. Xuerong, "Socio-economic driving forces of arable land conversion: a case study of Wuxian City, China," *Global Environmental Change*, vol. 15, no. 3, pp. 238–252, 2005.

[4] P. Hao, S. Geertman, P. Hooimeijer, and R. Sliuzas, "The land-use diversity in urban villages in Shenzhen," *Environment and Planning A*, vol. 44, no. 11, pp. 2742–2764, 2012.

[5] L. Jiang, X. Deng, and K. C. Seto, "Multi-level modeling of urban expansion and cultivated land conversion for urban hotspot counties in China," *Landscape and Urban Planning*, vol. 108, no. 2–4, pp. 131–139, 2012.

[6] L. Jiang, X. Deng, and K. C. Seto, "The impact of urban expansion on agricultural land use intensity in China," *Land Use Policy*, vol. 35, pp. 33–39, 2013.

[7] E. Keys and W. J. McConnell, "Global change and the intensification of agriculture in the tropics," *Global Environmental Change*, vol. 15, no. 4, pp. 320–337, 2005.

[8] I. Eng, "The rise of manufacturing towns: externally driven industrialization and urban development in the Pearl River Delta of China," *International Journal of Urban and Regional Research*, vol. 21, no. 4, pp. 554–568, 1997.

[9] Y. Liu and Y. Li, "Environment: China's land creation project stands firm," *Nature*, vol. 511, no. 7510, article 410, 2014.

[10] J. Liu, J. Zhan, and X. Deng, "Spatio-temporal patterns and driving forces of urban land expansion in China during the economic reform era," *Ambio*, vol. 34, no. 6, pp. 450–455, 2005.

[11] X. Deng, J. Huang, S. Rozelle, and E. Uchida, "Economic growth and the expansion of urban land in China," *Urban Studies*, vol. 47, no. 4, pp. 813–843, 2010.

[12] J. Gong, Y. Liu, and W. Chen, "Land suitability evaluation for development using a matter-element model: a case study in Zengcheng, Guangzhou, China," *Land Use Policy*, vol. 29, no. 2, pp. 464–472, 2012.

[13] J. S. Jeong, L. García-Moruno, and J. Hernández-Blanco, "A site planning approach for rural buildings into a landscape using a spatial multi-criteria decision analysis methodology," *Land Use Policy*, vol. 32, pp. 108–118, 2013.

[14] P. La Greca, D. La Rosa, F. Martinico, and R. Privitera, "Agricultural and green infrastructures: the role of non-urbanised areas for eco-sustainable planning in a metropolitan region," *Environmental Pollution*, vol. 159, no. 8-9, pp. 2193–2202, 2011.

[15] R. S. Sicat, E. J. M. Carranza, and U. B. Nidumolu, "Fuzzy modeling of farmers' knowledge for land suitability classification," *Agricultural Systems*, vol. 83, no. 1, pp. 49–75, 2005.

[16] T. V. Reshmidevi, T. I. Eldho, and R. Jana, "A GIS-integrated fuzzy rule-based inference system for land suitability evaluation in agricultural watersheds," *Agricultural Systems*, vol. 101, no. 1-2, pp. 101–109, 2009.

[17] J. Malczewski, "Ordered weighted averaging with fuzzy quantifiers: GIS-based multicriteria evaluation for land-use suitability analysis," *International Journal of Applied Earth Observation and Geoinformation*, vol. 8, no. 4, pp. 270–277, 2006.

[18] J. Marull, J. Pino, J. M. Mallarach, and M. J. Cordobilla, "A land suitability index for strategic environmental assessment in metropolitan areas," *Landscape and Urban Planning*, vol. 81, no. 3, pp. 200–212, 2007.

[19] R. J. Zomer, A. Trabucco, D. A. Bossio, and L. V. Verchot, "Climate change mitigation: a spatial analysis of global land suitability for clean development mechanism afforestation and reforestation," *Agriculture, Ecosystems and Environment*, vol. 126, no. 1-2, pp. 67–80, 2008.

[20] S. V. Bobade, B. P. Bhaskar, M. S. Gaikwad et al., "A GIS-based land use suitability assessment in Seoni district, Madhya Pradesh, India," *Tropical Ecology*, vol. 51, no. 1, pp. 41–54, 2010.

[21] D. D'haeze, J. Deckers, D. Raes, T. A. Phong, and H. V. Loi, "Environmental and socio-economic impacts of institutional reforms on the agricultural sector of Vietnam: land suitability assessment for Robusta coffee in the Dak Gan region," *Agriculture, Ecosystems & Environment*, vol. 105, no. 1-2, pp. 59–76, 2005.

[22] Y.-S. Liu, J.-Y. Wang, and L.-Y. Guo, "GIS-based assessment of land suitability for optimal allocation in the Qinling Mountains, China," *Pedosphere*, vol. 16, no. 5, pp. 579–586, 2006.

[23] Y. Chen, J. Yu, and S. Khan, "Spatial sensitivity analysis of multi-criteria weights in GIS-based land suitability evaluation," *Environmental Modelling and Software*, vol. 25, no. 12, pp. 1582–1591, 2010.

[24] O. Marinoni, "A discussion on the computational limitations of outranking methods for land-use suitability assessment," *International Journal of Geographical Information Science*, vol. 20, no. 1, pp. 69–87, 2006.

[25] C. Zhao, X. Deng, Y. Yuan, H. Yan, and H. Liang, "Prediction of drought risk based on the WRF model in Yunnan province of China," *Advances in Meteorology*, vol. 2013, Article ID 295856, 9 pages, 2013.

[26] X. Deng, H. Su, and J. Zhan, "Integration of multiple data sources to simulate the dynamics of land systems," *Sensors*, vol. 8, no. 2, pp. 620–634, 2008.

[27] X. Deng, J. Huang, Q. Huang, S. Rozelle, and J. Gibson, "Do roads lead to grassland degradation or restoration? A case study in Inner Mongolia, China," *Environment and Development Economics*, vol. 16, no. 6, pp. 751–773, 2011.

[28] X. Deng, J. Huang, E. Uchida, S. Rozelle, and J. Gibson, "Pressure cookers or pressure valves: do roads lead to deforestation in China?" *Journal of Environmental Economics and Management*, vol. 61, no. 1, pp. 79–94, 2011.

[29] X. Deng, J. Huang, S. Rozelle, and E. Uchida, "Growth, population and industrialization, and urban land expansion of China," *Journal of Urban Economics*, vol. 63, no. 1, pp. 96–115, 2008.

[30] F. P. Agterberg, "Computer programs for mineral exploration," *Science*, vol. 245, no. 4913, pp. 76–81, 1989.

[31] F. Agterberg, G. Bonham-Carter, Q. Cheng, and D. Wright, "Weights of evidence modeling and weighted logistic regression for mineral potential mapping," *Computers in Geology*, vol. 25, pp. 13–32, 1993.

[32] F. P. Agterberg and Q. Cheng, "Conditional independence test for weights-of-evidence modeling," *Natural Resources Research*, vol. 11, no. 4, pp. 249–255, 2002.

[33] F. Agterberg, "A modified weights-of-evidence method for regional mineral resource estimation," *Natural Resources Research*, vol. 20, no. 2, pp. 95–101, 2011.

[34] G. Jin, Z. Wang, X. Hu, S. Hu, and D. Zhang, "Land suitability evaluation in Qinghai-Tibet Plateau based on fuzzy weight of evidence model," *Transactions of the Chinese Society of Agricultural Engineering*, vol. 29, no. 18, pp. 241–250, 2013 (Chinese).

[35] Q. Cheng and F. P. Agterberg, "Fuzzy weights of evidence method and its application in mineral potential mapping," *Natural Resources Research*, vol. 8, no. 1, pp. 27–35, 1999.

[36] J. Luo, J. Zhan, Y. Lin, and C. Zhao, "An equilibrium analysis of the land use structure in the Yunnan Province, China," *Frontiers of Earth Science*, 2014.

Hindawi Publishing Corporation
Advances in Meteorology
Volume 2015, Article ID 786764, 8 pages
http://dx.doi.org/10.1155/2015/786764

Research Article

Water Yield Variation due to Forestry Change in the Head-Water Area of Heihe River Basin, Northwest China

Feng Wu,[1] Jinyan Zhan,[1] Jiancheng Chen,[2] Chao He,[2] and Qian Zhang[3,4]

[1] *State Key Laboratory of Water Environment Simulation, School of Environment, Beijing Normal University, Beijing 100875, China*
[2] *School of Economics and Management, Beijing Forestry University, Beijing 100083, China*
[3] *Institute of Geographic Science and Natural Resource Research, CAS, Beijing 100101, China*
[4] *Center for Chinese Agricultural Policy, CAS, Beijing 100101, China*

Correspondence should be addressed to Jinyan Zhan; zhanjy.bnu@gmail.com

Received 19 September 2014; Accepted 12 December 2014

Academic Editor: Hongbo Su

Understanding the effects of forestation on the hydrological process is crucial to protecting water resources. In this study, the upstream Heihe River Basin is selected as the study area, which is the water source area of the whole basin. The grassland and forest are the main land use types, the proportion of which in the total land area is 21% and 50%, respectively. Firstly, a scenario of forestation was designed with the actual land cover data in 1980. Then a scenario with simulated land cover data in 1980 was established, in which the forest area increases by 12%. Thereafter a hydrological simulation was carried out with the actual and simulated land cover maps and the climate observation data during 1980–2010. The results suggested that the total water yield increased by 12.57 mm under the scenario with land use change during 1980–2010 compared with the simulation with the actual land cover in 1980. However, the results also indicated that the surface runoff reduced by 22.17 mm during the same period, indicating the forest land has "sponge" effects on the water resource in the mountainous watershed. These results may provide important information that supports operational practices, such as forest regeneration programs and watershed restoration.

1. Introduction

Forestation has been encouraged worldwide for providing the ecosystem services. Understanding the effects of forestation is crucial to balance many ecosystem services provided by the forests (i.e., regulating seasonal flows, enhancing the availability of water resources, and ensuring water environment) [1, 2]. The relationship between forests and water resources is a critical issue which must be accorded with high priority. A key challenge faced by the land, forest, and water managers is how to maximize the wide range of forest benefits without detriment to water resources and ecosystem functions. To address this challenge, there is an urgent need for a better understanding of the interactions between forests/trees and water, also for awareness raising and capacity building in forest hydrology, and for embedding this knowledge and the research findings in policies. The successful forestation programs which are implemented in China have improved the ecological as well as environmental conditions and have gained wide attention of many researchers and highlighted the relationship between forestation and water yields [3]. Forestation in upstream watershed is deemed as the most effective measure to enhance water availability for agriculture, industrial, and domestic uses [4]. However, some studies suggested that the hydrological benefits from forests in respect of increasing water yield and regulating dry season flow have been exaggerated [5–7]. Researchers even questioned the wisdom of having the forest as land cover to increase water yield in downstream regions [8]. Meanwhile, researchers also argued that the effects of forestation on runoff are not stationary [9]. A quantitative assessment of the hydrological effects of forestation, especially on the water yield, is therefore crucial for improving the forestation and water resource management to guarantee the sustainable forestry development within the arid or semiarid regions [10].

The hydrological effects of forestation of degraded land in the dry region have important implications for local and regional hydrological services, but such issues have

been relatively less studied when compared to the issue of impacts of forest conversion [11]. Scientists from forestry and environmental sciences disciplines emphasized the significance of forests in regulating runoff and controlling soil erosion [1, 3, 12]. While scientists from other fields, for example, geography, climatology, and agriculture, argued that forests only have limited effects on water budgets and controlling flood [11, 13]. Overall, the relationship between forestation/reforestation and water yield is still a controversial issue. A central concept in the "traditional" view of the role of forests is the "sponge" effect of the tree roots, forest litter, and soil. It has been ever claimed that the tree roots soak up water during wet periods and release it slowly and evenly during the dry season to maintain water supplies [14]. The debate was endless because there were no convincing field data from research on forest hydrology, especially in China. Most literature suggested that the effects of forestation on annual flow are largely on the base flow, which is an important component of annual water yield for most forested watersheds. Some may conclude that forests increased base flow because the trees help to increase infiltration [9], while others may argue that forests used more water and thus reduced the base flow [2]. However, the hydrological consequences of forestation on degraded lands are not well studied in the forest hydrology research [2, 3].

Catchment parameters have great influence on responses of the water budget and runoff to forestation. The magnitude of effects of forestation on annual water yield varies as a function of vegetation, climate, soil, and management practices [8]. Hydrological models, for example, the soil and water assessment tool (SWAT), allow for simulating the hydrological effects of these catchment parameters, which can help to understand the effects of forestation on water yields in entire basin. The SWAT has been widely used in the water quantity and quality assessments at a wide range of scales and environmental conditions [15, 16]. For example, applications of SWAT have been reported in rural [17, 18], more urbanized [19], and also coastal watersheds [20]. In addition, the SWAT has been successfully used to simulate the hydrological processes in the small upstream watershed of the Heihe River Basin [21, 22]. In this study, the SWAT model, which includes the components such as soil and vegetation, is used to analyze the effects of forestation on the water yield.

2. Study Area

The Heihe River Basin is located in a typical arid region of Northwest China that suffers from serious water scarcity. The annual precipitation is over 200 mm in regions above 2000 m in elevation and increases by 10.9~15.9 mm for every 100 m increase in elevation. The geography varied greatly in Heihe River Basin with the average altitude over 1200 m [21]. The main soil types in the watershed are alpine meadow soil, alpine steppe soil, frigid desert soil, gray cinnamonic soil, and gray-brown desert soil. The Heihe River Basin is divided into the upper, middle, and lower reaches, which differ significantly in the natural and socioeconomic characteristics. For example, the average annual precipitation in the upper, middle, and lower reaches is 200 mm to 600 mm, less than 200 mm, and less than 50 mm, respectively, while the annual evaporation ranges from 500 mm in the upper reach to over 3000 mm in the lower reach [23]. Besides, the ecosystem patterns range from alpine ecosystems on the south Qilian Mountain in the upstream to the oases at the Hexi Corridor in midstream basin and to the deserts in the north downstream basin [24, 25].

The Qilian Mountains with remarkably vertical landscape is the water source area, where the ecosystem patterns ranging from low to high altitude include dry shrubbery grassland, forest grassland, subalpine shrubbery meadow, alpine cold-and-desert meadow, and alpine permafrost-snow-ice. Being an important regional headwater area, the upstream Heihe River Basin is selected as the study area, where the elevation ranges from 2000 m to about 5500 m (Figure 1). The area of the upstream is about 11145 km^2. The dominant land use types are forestland and grassland, occupying nearly 21% and 50% of the total area, respectively. Picea crassifolia is the major species covering about 76.8% of the forest in upstream of Heihe River Basin.

3. Data and Methodology

SWAT is a semidistributed hydrological model based on geography and natural hydrological processes at the watershed scale. SWAT subdivides an entire watershed into subwatersheds connected with a river network and into smaller units that is called hydrological response units (HRUs). Each HRU represents a combination of land use, soil, and slope. HRUs are assumed to be nonspatially distributed with no interaction or dependency [26]. Major model components of SWAT include weather, hydrology, temperature and properties of soil, plant nutrients and growth, pesticides, bacteria, and land management [26]. The meteorological variables in SWAT include precipitation, temperature, wind speed, solar radiation, and relative humidity in daily or subdaily time steps. The model uses readily available inputs efficiently for computing the large watersheds and is capable of simulating long-term yields for determining impacts of land management practices [27]. SWAT allows a number of different physical processes to be simulated in a basin. The hydrological routine of SWAT actually and also potentially consists of discharge, snow melting, and evapotranspiration. SWAT has been successfully applied worldwide to solve many environmental issues in water quality and quantity studies [28, 29].

This study addressed the processes related to vegetation interception, infiltration, transpiration, and evaporation in the dry watersheds. Data used in this study are presented in Table 1. The 30 m resolution Landsat TM images in 1980 were downloaded from the United States Geological Survey (USGS) website (http://earthexplorer.usgs.gov/) for mapping the land cover types in the upstream of the HRB in 1980. The collected images have already been georeferenced, and these images were then radiometrically corrected using the calibration utility for Landsat in ENVI 4.7 software package. The preprocessed images were subsequently clipped with the boundary of the study area. Supervised classification method was used to classify the land cover types in 1980.

Table 1: Data used and sources information.

Data type	Data source	Scale	Description
DEM	Shuttle radar topography mission (SRTM)	90 m	Elevation
Soil	Regional database (http://westdc.westgis.ac.cn/)	1 : 1000000	(Soil-Plant-Atmosphere-Water) Field and Pond Hydrology model was used to calculate some parameters
Weather	China Meteorological Administration (daily)		13 weather stations
Hydrological observation	Hydrologic yearbook (daily)		4 stations
River flow	Data Center of Chinese Academy of Science	1 : 250000	River network-diversion

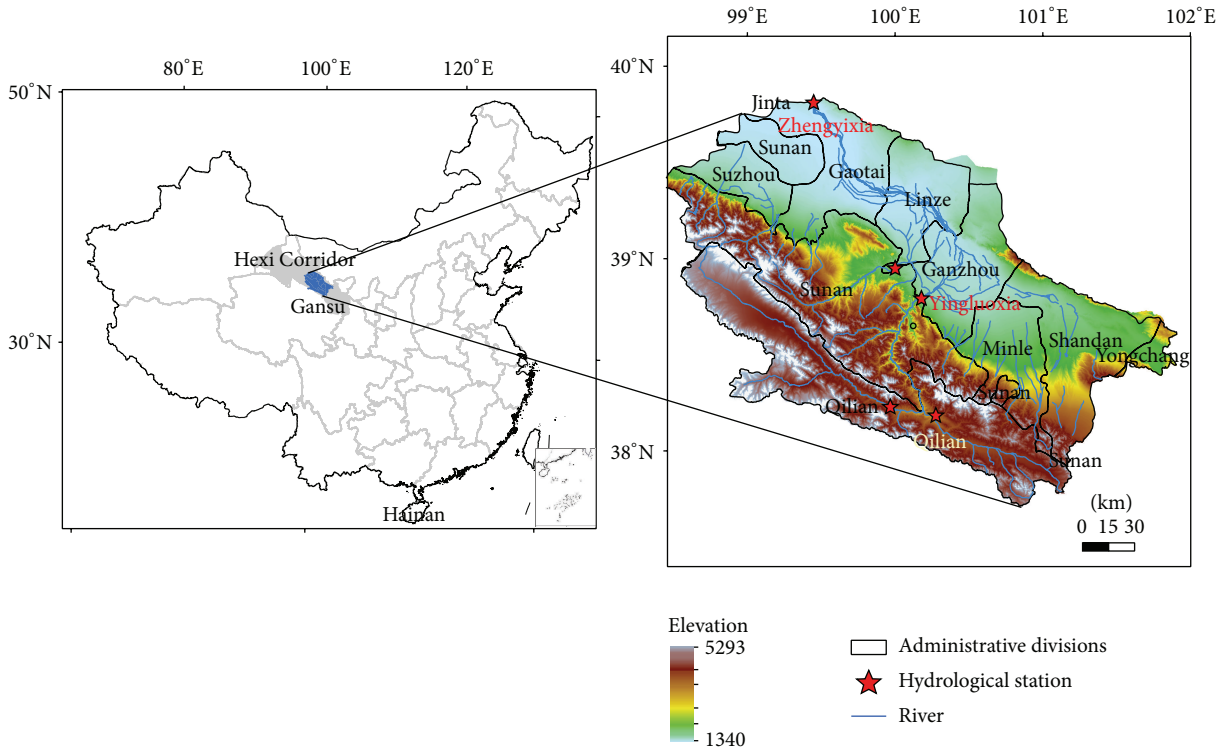

Figure 1: Location of administration region and hydrological station in the Heihe River Basin.

The Chinese Land Resource Classification System, from Data Center of Chinese Academy of Science, was used as the classification scheme to categorize the pixels of the image [30, 31]. The classification system includes cultivated land, forestland, grassland, water, urban, and/or built-up area, and unused land. In this study, a baseline scenario of forestation was designed on the basis of the land cover in 1980, in which the forestry proportion is 21%. Then a scenario was established with the simulated land cover data in 1980, in which the forest area increases by 12% compared to the actual land cover data in 1980. The regions with land use conversion are mainly located in the middle and west part of the study area (Figure 2). The precipitation data of Qilian weather station was also used to analyze the trend of precipitation. From 1980 to 2010, the precipitation showed a significantly upward trend, increasing at an average rate of 1.79 mm·year^{-1}, and the annual average temperature significantly increased by 0.06°C·year^{-1} (Figure 3).

The hydrological routines within SWAT account for vegetation physical processes (e.g., infiltration, evaporation, plant uptake, lateral flows, and percolation) and ground water flows. As precipitation descends, it may be intercepted and held in the vegetation canopy or fall to the soil surface. Water on the soil surface will infiltrate into the soil profile or flow overland as runoff. The hydrological cycle that is simulated by SWAT is based on the water balance equation:

$$SW_t = SW_0 + \sum_{t=1}^{t} \left(R_{day}(i) - Q_{surf}(i) - E_{sub}(i) - w_{seep}(i) - Q_{gw}(i)\right), \quad (1)$$

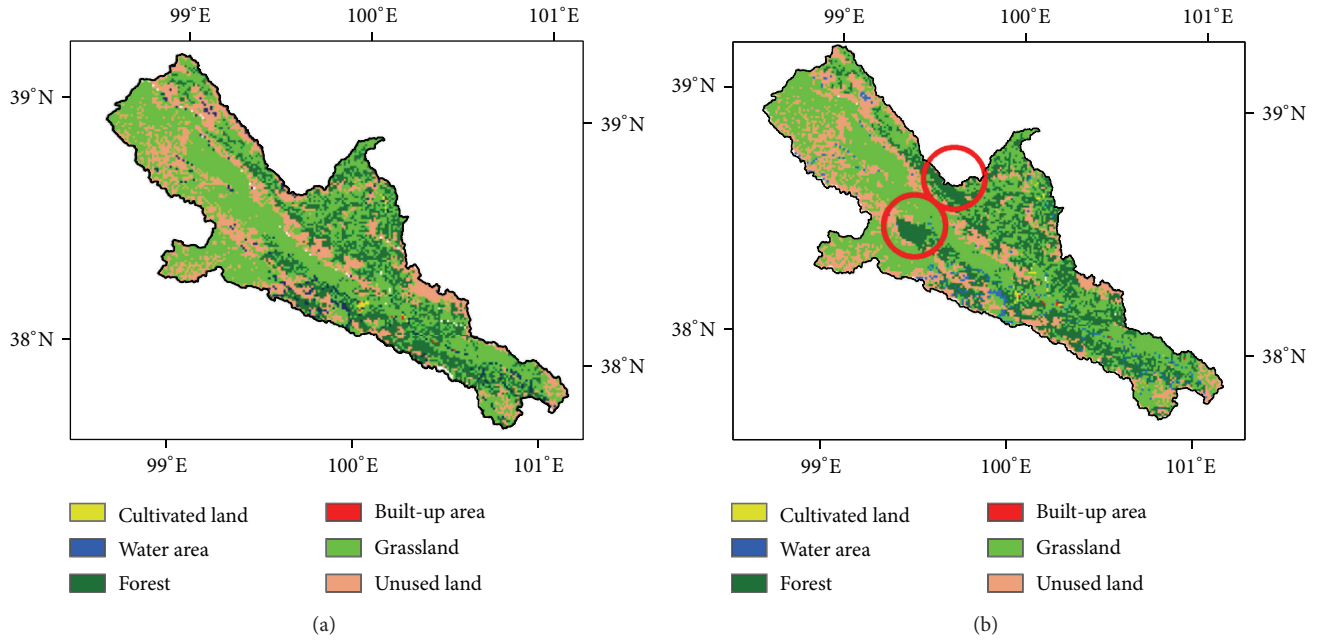

Figure 2: The land use map in the upstream of Heihe River Basin: (a) 1980; (b) scenario based simulated map.

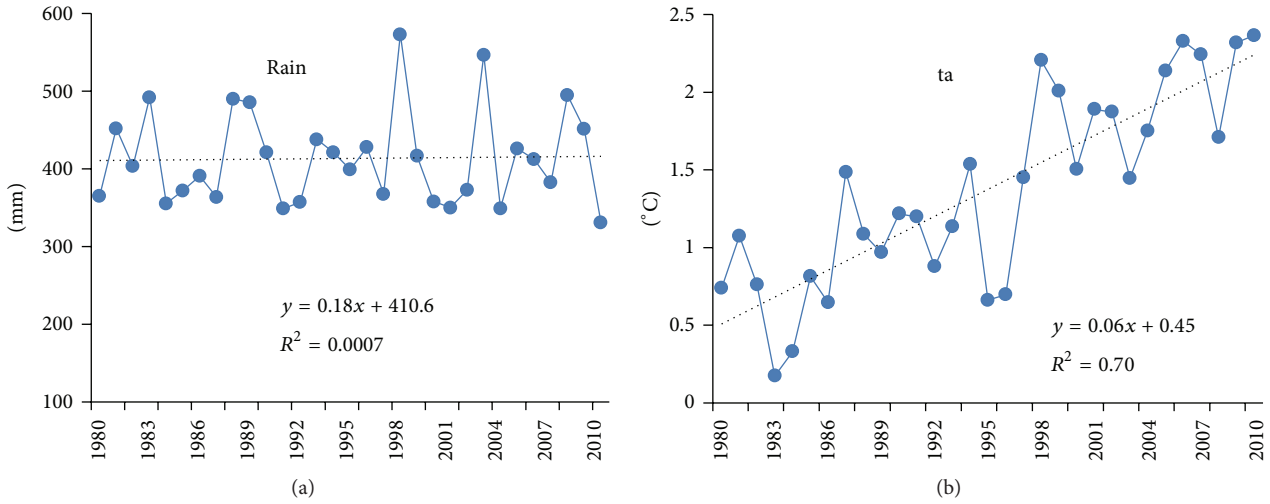

Figure 3: The change trend of precipitation and temperature at Qilan weather station during 1980–2010.

where SW_t is the final soil water content (mm H_2O), SW_0 is the initial soil water content on day i (mm H_2O), t is the time (days), R_{day} is the amount of precipitation on day i (mm H_2O), Q_{surf} is the amount of surface runoff on day i (mm H_2O), E_{sub} is the amount of evapotranspiration on day i (mm H_2O), w_{seep} is the amount of water entering the vadose zone from the soil profile on day i (mm H_2O), and Q_{gw} is the amount of return flow on day i (mm H_2O).

The role of forest vegetation in influencing hydrological processes can be well analyzed with the SWAT model. The canopy storage value and the leaf area index are used in the SWAT model to compute the maximum storage at any time in the growth cycle of the land cover. SWAT utilizes a single plant growth model to simulate all types of land cover. This model is able to differentiate between annual and perennial plants. When the evaporation is computed, water is firstly removed from canopy storage. Plant transpiration is simulated as a linear function of potential evapotranspiration and leaf area index. SWAT allows the maximum amount of water held in canopy storage to vary from day to day as a function of leaf area index:

$$\text{can}_{\text{day}} = \text{can}_{\text{mx}} \times \frac{\text{LAI}}{\text{LAI}_{\text{mx}}}, \quad (2)$$

where can_{day} is the amount of water that can be trapped in canopy on a given day (mm H_2O), can_{mx} is the maximum amount of water that can be trapped in canopy on a given day (mm H_2O), and LAI is the leaf area index of the

canopy. For the other potential evapotranspiration methods, transpiration is calculated as follows:

$$E_t = \frac{E_0' \times \mathrm{LAI}}{3.0} \quad 0 \le \mathrm{LAI} \le 3.0,$$
$$E_t = E_0' \quad \mathrm{LAI} > 3.0, \tag{3}$$

where E_t is the maximum transpiration on a given day (mm H_2O), E_0' is the potential evapotranspiration adjusted for evaporation of free water in the canopy (mm H_2O), and LAI is the leaf area index.

The Penman-Monteith equation combines components that account for energy needed to sustain evaporation and the strength required to remove the water vapor and aerodynamic and surface resistance terms. Consider

$$\lambda E = \frac{\Delta \times (H_{\mathrm{net}} - G) + \rho_{\mathrm{air}} \times C_P \times \left[e_z^0 - e_z\right] / r_a}{\Delta + \gamma \times (1 + \gamma_c/\gamma_a)}, \tag{4}$$

where λE is the latent heat flux density (MJ·m^{-2}·d^{-1}), E is the depth rate evaporation (mm·d^{-1}), Δ refers to the slop of the saturation vapor pressure-temperature curve, de/dT (kpa·°C^{-1}), H_{net} is the net radiation (MJ·m^{-2} d^{-1}), G is the heat flux density to the ground, ρ_{air} is the air density, C_P is the specific heat at constant pressure (MJ·kg^{-1}·°C^{-1}), e_z^0 is the saturation vapor pressure of air at height z, e_z is water vapor pressure at height z (kpa), γ is the psychometric constant (kpa·°C^{-1}), γ_c is the plant canopy resistance (s·m^{-1}), and γ_a is the diffusion resistance of the air layer (s·m^{-1}). Studies of the canopy resistance have shown that the canopy resistance for a well-watered reference crop can be estimated by dividing the minimum surface resistance for a single leaf by one-half of the canopy leaf area index:

$$\gamma_c = \frac{\gamma_e}{0.5 \times \mathrm{LAI}}, \tag{5}$$

where γ_c is the canopy resistance (s/m) and γ_e is the minimum effective stomatal resistance of a single leaf (s/m).

A standard hydrological model performance criterion has been proposed. In this study, Nash-Sutcliffe coefficient (E_{ns}) and coefficient of determination (R^2) were used as model performance indices. Model performance was high when $E_{\mathrm{ns}} > 0.5$ and $R^2 > 0.8$. Here, E_{ns} is the relationship strength between observed value $Q_{o,i}$ and simulated value $Q_{m,i}$ at time t. E_{ns} lies between $-\infty$ and +1, and in this study E_{ns} should be closer to +1. The square of Pearson's product moment correlation, R^2, represents the proportions of total variance of measured data that can be explained by simulated data, and the model performance is higher when R^2 is closer to 1. Consider

$$E_{\mathrm{ns}} = 1 - \frac{\sum_{i=1}^{n} \left(Q_{o,i} - Q_{m,i}\right)^2}{\sum_{i=1}^{n} \left(Q_{o,i} - \overline{Q}_o\right)^2},$$
$$R^2 = \frac{\left[\sum_{i=1}^{n} \left(Q_{o,i} - \overline{Q}_o\right)\left(Q_{m,i} - \overline{Q}_m\right)\right]^2}{\sum_{i=1}^{n} \left(Q_{o,i} - \overline{Q}_o\right)^2 \sum_{i=1}^{n} \left(Q_{m,i} - \overline{Q}_m\right)^2}, \tag{6}$$

where E_{ns} is the Nash-Sutcliffe coefficient, $Q_{o,i}$ is the observed runoff in i years, $Q_{m,i}$ the simulated runoff in i years, and n is the length of the time series. The closer the E_{ns} and R^2 is to 1, the more accurate the model prediction is.

4. Results

We simulated the effect of forestation on water yield using the SWAT model which couples the vegetation and physical processes. The SWAT model was calibrated according to the daily observation data records during 1980–1990 from Yingluoxia Hydrological Station, which is an outlet of the upstream area and the simulation results were validated with the daily observation records during 1990–2000. Some parameters were updated after the calibration. Both calibration of the model and validation of the simulation results show that the SWAT model performed well in simulating the hydrological process in the upstream area of the Heihe River Basin. The coefficients in (6) were determined with eligible evaluation of calibration and validation. The results showed that R^2 reached 0.72 and 0.70 for the calibration as well as the validation periods, respectively. With regard to the model performance, the E_{ns} values for the calibration and validation periods (0.80 and 0.79, resp.) correspond to "good" and "good," respectively (Figure 4). The two coefficients of validation were lower than the calibration period, the reason for which is the use of the land use map in 1980. Moreover, by comparing the simulation results with the observation records from Yingluoxia Hydrological Station, we cannot reject the significance of the parameters of the SWAT model, indicating the model is suited for simulating the water balance in the upstream area of the Heihe River Basin.

The intervals of the most sensitive parameters were identified and the most appropriate values are eventually shown in Table 2. The temperature lapse rate (TLAPS) is the most sensitive parameter, and it is directly related to the melting process of snow and glacier. Snow melting occurs mostly from March to June in a subwatershed. The snow melting factor on June 21 was parameterized to be SMFMX, which is the maximum melting rate; any increase of SMFMX drives rapid snow melting. The snow temperature lag factor TIMP is also linked with SMFMX because it is based on the previous situation. Along with TIMP surface water lag time, SURLAG plays an important role in influencing the model performance as a melted snow routing process is related to the geology of the watershed, where the melted water mainly flows to the surface runoff covering the impervious rock formations. SMTMP is sensitive since it indicates the starting and ending of melting of snow and glacier, the availability of snow melting on a specific day, and the model-simulated streamflow, especially their peak values, are significantly influenced by the variation of SMTMP. Some parameters were updated after the calibration, and both calibration of the model and validation of the simulation results show that the model performed well in simulating the runoff variation due to glacier melting and climate change in upstream Heihe River Basin.

Streamflow production may be related to the differences in climatic pattern, meteorological conditions, species

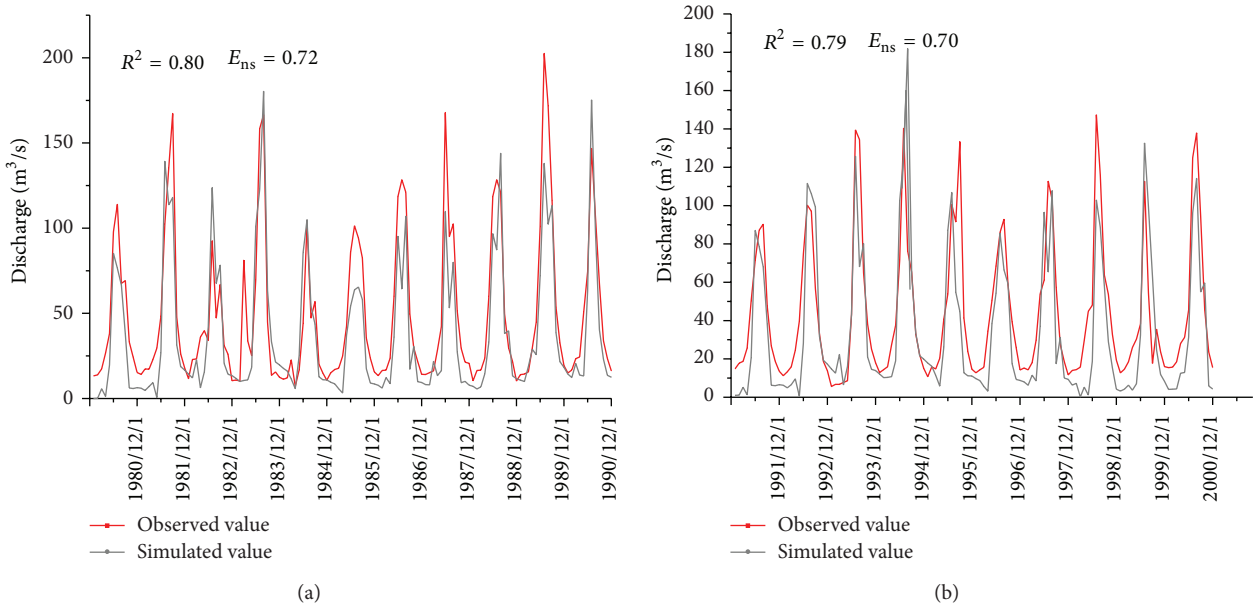

Figure 4: The calibration and validation of monthly discharge at the Yingluoxia hydrological station, observed versus simulated using the SWAT.

Table 2: Ranges and values of the most sensitive parameters in SWAT model.

Parameters	Descriptions	Ranges	Values
CN_2	SCS curve number	−20%~20%	+6.32%
Sol_k	Saturated hydrological conductivity	−20%–20%	+11.56%
Escno	Evaporation compensation factor	0~1.0	0.83
SFTMP	Snowfall temperature	−2.0~2.0°C	0.9°C
Sol_z	Depth from soil surface to bottom of layer	−20%–20%	+3.65%
Sol_Awc	Available soil water content	−20%–20%	−0.35%
GWQMN	Threshold depth of water in the shallow aquifer required for return flow to occur	0–500 mm	306.5
ALPHA_BF	Base flow alpha factor	0.00~1.00	0.07

composition, canopy structure, and morphological characteristics of tree leaves, branches, and bark. Canopy rainfall interception varied from 14.7 to 31.8% of total rainfall, depending upon stand characteristics of different land cover type. Forest canopy interception was also affected by rainfall characteristics, which generally decreases with the rainfall amount and intensity. Evapotranspiration (ET), including physical evaporation and biological transpiration, is a significant component of forest water budgets, ranging in 80–90% of the total rainfall in the region. As expected, the actual amount of ET raised due to the increase of temperature and rainfall, whereas the amount of ET is relatively low in the mountainous watershed. ET from a forest is generally higher than that from pasture or bare land. However, ET is about 600 mm in the forest cover in the upstream area of the Heihe River Basin, which is far lower than that in those regions covered by grassland or unused land. The ET/PET ratio of native grasslands declined as the fastest, followed by pine woodlands, shrub lands, alfalfa, and croplands. Pine woodland's low ET/PET ratios were mainly caused by its higher runoff due to soil compaction resulting from soil desiccation.

Previous studies have shown that the effect of forestation on water yield may differ among regions due to the difference in the topography, soil properties, and climate conditions [32]. The simulation results in this study suggest that the monthly average water yield has generally increased, with an increment of 15.7 mm during 1980–2010 (Figure 5). The increase of water yield mainly happened in summer, while the decrease of water yield mainly occurred in winter. This may be due to the water conservation function of the forests. The study area is located in the mountain area with an altitude of approximately 3000 m, where the annual rainfall is about 600 mm and the slope is generally very high, and the forests intercept a large proportion of rainfall. The forest has a more powerful conservation function compared to the grassland, and it is more difficult to generate runoff in the forest than in the grassland. The results of the two simulation experiments show that the monthly average runoff decreased by 22.12 mm when the forest area increased during 1980–2010. In addition, the simulation results show that the interflow declined dramatically, the monthly average value of which decreased by approximately 500 mm during 1980–2010. This may be due to the difference in the moisture

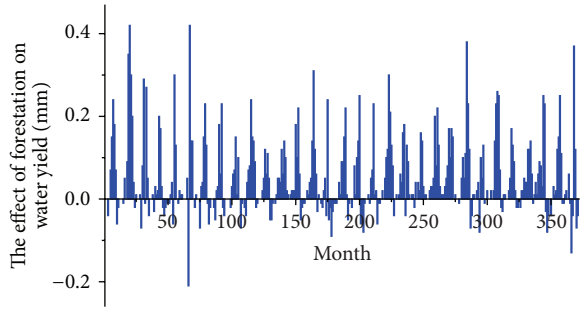

Figure 5: The difference of water yield between forestation scenario and baseline during 1980–2010.

infiltration between forests and grasslands. The surface roots of forests can absorb more surface moisture and keep the shallow soil moist. By comparison, the surface roots of grasslands are generally very shallow, which can promote the infiltration of rainfall into the soil.

The results of this study may not coincide with that of some research about the relationship between forestation and water yield. A recent review also shows that reforestation can cause decreased water yield [9]. However, the belief is based on the assumption of a constant relationship between precipitation and ET; that is, a reduced ET can logically lead to a gain of water yield. However, if this assumption is not true or if the relationship between precipitation and ET varies over time and space, the simple logic may be not tenable. Besides, forestation practices may cause the decrease of annual water yield due to the increase of ET. For any statistical tests, streamflow data must be first naturalized to account for other water uses. Moreover, the majority of the statistical studies are experiments at the plot scale, whereas there are few watershed-scale studies. Therefore, using ET information to infer water yield may not always be correct.

It is difficult to accurately simulate the hydrological processes because they are influenced by a myriad of biophysical factors. The results of this study suggest that the effect of forestation on water yield differs in different areas, and the forestation has positive effects on the water yield in the mountainous area. Several influential studies have also demonstrated the uncertainty and variability of forestation on potential hydrological responses across China due to the large differences in climate and soil conditions [33]. At the same time, most studies have focused on understanding whether forests are important in influencing water protection and soil erosion, and almost none of them have aimed at determining what percentage of forested land in a watershed or a landscape must be protected in order to minimize negative impacts on water resources. This question is important and must be answered in order to provide reference information for designing and implementing sustainable forest management practices.

5. Conclusion

The study concludes that there was a significant positive relationship between forestation and water yield in the upstream area of the Heihe River Basin during 1980–2010. The annual water yield increased by 1.2 mm when the forest cover increased by 1%. The result also suggested that the surface runoff have reduced 1.8 mm with every 1% increase in the forest cover. Besides, although forestation generally reduces runoff, the effects of forestation on the water yield may vary greatly in different regions due to the differences in topography, soil, and climatic conditions. The results of this study are different from that of some previous studies, but all studies have demonstrated that forests play an important, positive role in reducing surface runoff and peak streamflow. In spite of inconsistent results from those studies about forestation and the hydrological processes, the simulation experiment continues to allow us to build a solid foundation in understanding the interactions between forests and hydrological processes. It can be beneficial to improving the sustainable forest management to apply the hydrological models in regions where there are sufficient data since this approach allows us to evaluate the impacts of different forest management scenarios on hydrology within a short time.

Conflict of Interests

The authors declare that there is no conflict of interests regarding the publication of this paper.

Acknowledgments

This research was financially supported by the National Natural Science Funds of China for Distinguished Young Scholar (Grant no. 71225005), the major research plan of the National Natural Science Foundation of China (Grant no. 91325302), and the Key Project in the National Science & Technology Pillar Program of China (no. 2013BAC03B00).

References

[1] L. Chen, J. Wang, W. Wei, B. Fu, and D. Wu, "Effects of landscape restoration on soil water storage and water use in the Loess Plateau Region, China," *Forest Ecology and Management*, vol. 259, no. 7, pp. 1291–1298, 2010.

[2] Z.-J. Wang, J.-Y. Jiao, Y. Su, and Y. Chen, "The efficiency of large-scale afforestation with fish-scale pits for revegetation and soil erosion control in the steppe zone on the hill-gully Loess Plateau," *CATENA*, vol. 115, pp. 159–167, 2014.

[3] H. Bi, B. Liu, J. Wu, L. Yun, Z. Chen, and Z. Cui, "Effects of precipitation and landuse on runoff during the past 50 years in a typical watershed in Loess Plateau, China," *International Journal of Sediment Research*, vol. 24, no. 3, pp. 352–364, 2009.

[4] S. Singh and A. Mishra, "Spatiotemporal analysis of the effects of forest covers on water yield in the Western Ghats of peninsular India," *Journal of Hydrology*, vol. 446-447, pp. 24–34, 2012.

[5] S. W. Trimble, F. H. Weirich, and B. L. Hoag, "Reforestation and the reduction of water yield on the southern Piedmont since circa 1940," *Water Resources Research*, vol. 23, no. 3, pp. 425–437, 1987.

[6] A. K. Sikka, J. S. Samra, V. N. Sharda, P. Samraj, and V. Lakshmanan, "Low flow and high flow responses to converting natural grassland into bluegum (*Eucalyptus globulus*) in Nilgiris

watersheds of South India," *Journal of Hydrology*, vol. 270, no. 1-2, pp. 12–26, 2003.

[7] M. Robinson, "30 years of forest hydrology changes at Coalburn: water balance and extreme flows," *Hydrology and Earth System Sciences*, vol. 2, no. 2-3, pp. 233–238, 1998.

[8] I. R. Calder, "Assessing the water use of short vegetation and forests: development of the hydrological land use change (HYLUC) model," *Water Resources Research*, vol. 39, no. 11, p. 1318, 2003.

[9] D. F. Scott, L. A. Bruijnzeel, R. A. Vertessy, and I. R. Calder, "Hydrology: impacts of forest plantations on streamflow," in *Encyclopedia of Forest Sciences*, J. Burley, Ed., pp. 367–377, Elsevier, Oxford, UK, 2004.

[10] Y. Wang, P. Yu, K.-H. Feger et al., "Annual runoff and evapotranspiration of forestlands and non-forestlands in selected basins of the Loess Plateau of China," *Ecohydrology*, vol. 4, no. 2, pp. 277–287, 2011.

[11] P. Yu, Y. Wang, A. Du et al., "The effect of site conditions on flow after forestation in a dryland region of China," *Agricultural and Forest Meteorology*, vol. 178-179, pp. 66–74, 2013.

[12] L. Deng, Z.-P. Shangguan, and R. Li, "Effects of the grain-for-green program on soil erosion in China," *International Journal of Sediment Research*, vol. 27, no. 1, pp. 120–127, 2012.

[13] J. Krishnaswamy, M. Bonell, B. Venkatesh et al., "The groundwater recharge response and hydrologic services of tropical humid forest ecosystems to use and reforestation: support for the 'infiltration-evapotranspiration trade-off hypothesis'," *Journal of Hydrology*, vol. 498, pp. 191–209, 2013.

[14] N. Myers, "Tropical moist forests: over-exploited and under-utilized?" *Forest Ecology and Management*, vol. 6, no. 1, pp. 59–79, 1983.

[15] C. R. Castillo, İ. Güneralp, and B. Güneralp, "Influence of changes in developed land and precipitation on hydrology of a coastal Texas watershed," *Applied Geography*, vol. 47, pp. 154–167, 2014.

[16] M. Faramarzi, K. C. Abbaspour, R. Schulin, and H. Yang, "Modelling blue and green water resources availability in Iran," *Hydrological Processes*, vol. 23, no. 3, pp. 486–501, 2009.

[17] K. Kirsch, A. Kirsch, and J. Arnold, "Predicting sediment and phosphorus loads in the Rock River basin using SWAT," *Transactions of the ASAE*, vol. 45, no. 6, pp. 1757–1769, 2002.

[18] A. Saleh, J. G. Arnold, P. W. Gassman et al., "Application of SWAT for the upper North Bosque River watershed," *Transactions of the American Society of Agricultural Engineers*, vol. 43, no. 5, pp. 1077–1087, 2000.

[19] J. Franczyk and H. Chang, "The effects of climate change and urbanization on the runoff of the Rock Creek basin in the Portland metropolitan area, Oregon, USA," *Hydrological Processes*, vol. 23, no. 6, pp. 805–815, 2009.

[20] T. Lee, R. Srinivasan, J. Moon, and N. Omani, "Estimation of fresh water inflow to bays from gaged and ungaged watersheds," *Applied Engineering in Agriculture*, vol. 27, no. 6, pp. 917–923, 2011.

[21] Q. Huang and W. Zhang, "Improvement and application of GIS-based distributed SWAT hydrological modeling on high altitude, cold, semi-arid catchment of Heihe River Basin, China," *Journal of Nanjing Forestry University (Natural Sciences Edition)*, vol. 28, pp. 22–26, 2004.

[22] Z. Li, *Runoff simulation in the upper reaches of Heihe River Basin and uncertainty anakysis in hydrological modeling [Ph.D. thesis]*, Beijing Normal University, Beijing, China, 2009.

[23] Q. Feng, G. D. Cheng, and K. N. Endo, "Towards sustainable development of the environmentally degraded River Heihe basin, China," *Hydrological Sciences Journal*, vol. 46, no. 5, pp. 647–658, 2001.

[24] Z. Li, Z. Xu, Q. Shao, and J. Yang, "Parameter estimation and uncertainty analysis of SWAT model in upper reaches of the Heihe river basin," *Hydrological Processes*, vol. 23, no. 19, pp. 2744–2753, 2009.

[25] N. L. Wang, S. B. Zhang, J. Q. He, J. C. Pu, X. B. Wu, and X. Jiang, "Tracing the major source area of the mountainous runoff generation of the Heihe River in northwest China using stable isotope technique," *Chinese Science Bulletin*, vol. 54, no. 16, pp. 2751–2757, 2009.

[26] S. Neitsch, J. Arnold, J. Kiniry, and J. R. Williams, "Soil and water assessment tool: theoretical documentation, version 2005," 2005.

[27] J. G. Arnold, R. Srinivasan, R. S. Muttiah, and P. M. Allen, "Continental scale simulation of the hydrologic balance," *Journal of the American Water Resources Association*, vol. 35, no. 5, pp. 1037–1051, 1999.

[28] S. M. Pradhanang, A. Anandhi, R. Mukundan et al., "Application of SWAT model to assess snowpack development and streamflow in the Cannonsville watershed, New York, USA," *Hydrological Processes*, vol. 25, no. 21, pp. 3268–3277, 2011.

[29] E. Varanou, E. Gkouvatsou, E. Baltas, and M. Mimikou, "Quantity and quality integrated catchment modeling under climate change with use of soil and water assessment tool model," *Journal of Hydrologic Engineering*, vol. 7, no. 3, pp. 228–244, 2002.

[30] X. Deng, H. Su, and J. Zhan, "Integration of multiple data sources to simulate the dynamics of land systems," *Sensors*, vol. 8, no. 2, pp. 620–634, 2008.

[31] X. Deng, J. Liu, Y. Lin, and C. Shi, "A framework for the land use change dynamics model compatible with RCMs," *Advances in Meteorology*, vol. 2013, Article ID 658941, 7 pages, 2013.

[32] X. Deng, Q. Jiang, J. Zhan, S. He, and Y. Lin, "Simulation on the dynamics of forest area changes in Northeast China," *Journal of Geographical Sciences*, vol. 20, no. 4, pp. 495–509, 2010.

[33] X. Wei, S. Liu, G. Zhou, and C. Wang, "Hydrological processes in major types of Chinese forest," *Hydrological Processes*, vol. 19, no. 1, pp. 63–75, 2005.

Hindawi Publishing Corporation
Advances in Meteorology
Volume 2015, Article ID 976370, 11 pages
http://dx.doi.org/10.1155/2015/976370

Research Article

Analysis of Climate and Land Use Changes Impacts on Land Degradation in the North China Plain

Zhihui Li,[1,2,3] Xiangzheng Deng,[1,2] Fang Yin,[4] and Cuiyuan Yang[5]

[1] *Institute of Geographic Sciences and Natural Resources Research, Chinese Academy of Sciences, Beijing 100101, China*
[2] *Center for Chinese Agricultural Policy, Chinese Academy of Sciences, Beijing 100101, China*
[3] *University of Chinese Academy of Sciences, Beijing 100049, China*
[4] *Leibniz Institute of Agricultural Development in Transition Economies (IAMO), Theodor-Lieser Street 2, 06120 Halle (Saale), Germany*
[5] *College of Geomatics, Shandong University of Science and Technology, Qingdao, Shandong 266590, China*

Correspondence should be addressed to Xiangzheng Deng; dengxz.ccap@gmail.com

Received 19 September 2014; Accepted 6 December 2014

Academic Editor: R. B. Singh

Land degradation is a complex process which involves both the natural ecosystem and the socioeconomic system, among which climate and land use changes are the two predominant driving factors. To comprehensively and quantitatively analyze the land degradation process, this paper employed the Normalized Difference Vegetation Index (NDVI) as a proxy to assess land degradation and further applied the binary panel logit regression model to analyze the impacts of the driving factors on land degradation in the North China Plain. The results revealed that an increase in rainfall and temperature would significantly and positively contribute to the land improvement, and conversion from cultivated land to grassland and forest land showed positive relationship with land improvement, while conversion to built-up area will lead to land degradation. Besides, human agricultural intensification represented by fertilizer utilization will help to improve the land quality. The economic development may exert positive impacts on land quality to alleviate land degradation, although the rural economic development and agricultural production will exert negative impacts on the land and lead to land degradation. Infrastructure construction would modify the land surface and further resulted in land degradation. The findings of the research will provide scientific information for sustainable land management.

1. Introduction

Land degradation has become a critical issue worldwide, especially in the developing countries, which leads to great concerns about food security. To improve livelihoods of human beings and to keep sustainable development of human society, healthy land ecosystems are basically essential elements. However, the key services of good quality land and their true values have been usually taken for granted and underestimated, leading to serious land degradation, which not only deteriorates the ecosystem services but also hinders regional sustainable development. Land degradation means a significant reduction of the productive capacity of land. It is an interactive process involving various casual factors, among which climate changes, land use/cover changes, and human dominated land management play a significant role [1–4]. Land degradation involves two interlocking complex systems, the natural ecosystem and the human social system, and both changes in biophysical natural ecosystem and socioeconomic conditions will affect the land degradation process [5]. Natural forces affect land degradation through periodic stresses of extreme and persistent climatic events. Human activities also contribute to land degradation through deforestation, removal of natural vegetation, and urban sprawl that lead to land use/cover changes; unsustainable agricultural land use management practices, such as use and abuse of fertilizer, pesticide, and heavy machinery; and overgrazing, improper crop rotation, poor irrigation practices, and so forth [6].

In comparison to other regions, land degradation afflicts China more seriously in terms of the extent, intensity, economic impacts, and affected population [7]. China accounts for 22% of the world's population but only 6.4% of the global

land area and 7.2% of the global cultivated land area. Agricultural production is an important issue that always plagues the national economy and livelihood of citizens [8]. However, the rapid population growth and urbanization, unreasonable human utilization, and influence of natural factors have caused degradation of 5.392 million km^2 of land, which accounts for about 56.2% of the total national area [9]. Only 1.3 million km^2 of land is suitable for cultivation in China, which accounts for about 14% of the total national land area. The land degradation has involved more than half of the total cultivated land area and further exerts more pressure on the economic benefits of agricultural production and food security. Besides, as the cultivated land degradation will directly affect the potential land productivity, more inputs such as fertilizer and irrigation water will be needed in order to get the same production as well as yield level, which will increase the production cost [10]. In addition, the structural change and pattern succession of the land system resulting from land conversions will undoubtedly lead to changes in the suitability and quality of land and directly influence land productivity [11]. Hence sustainable productive land management is crucial for the country's long-term agricultural economy.

China is a large country with significant spatial variation of natural/climatic conditions and diverse socioeconomic characteristics. For example, the eastern, central, and western part of China have different population density, industrial structure, per capita income, and so forth. The difference among regions will affect the land use, leading to difference in the way and extent of economic use of land resources [12]. The North China Plain has been one of the most productive agricultural bases in China for thousands of years. It is of great significance to quantitatively measure the intensity and spatial pattern of land degradation and analyze the driving mechanisms, which can provide information for sustainable land management to ensure the food safety in the North China Plain.

In order to provide information for sustainable land management, it is necessary to quantitatively clarify the impacts of major natural and socioeconomic driving forces on land degradation. The recent development of remote sensing techniques (RS) and geographic information system (GIS) techniques has enhanced the capabilities to obtain and handle spatial information on the heterogeneities of land surface characteristics. The integration of RS and GIS technologies has been proven to be an efficient approach and has been successfully used in various investigations for land degradation assessment. Land degradation is a long-term process indicating the loss of ecosystem function and productivity. For quantitative analysis of land degradation, satellite measurements of the Normalized Difference Vegetation Index (NDVI), which is the most widely used proxy for vegetation cover and production, have been widely applied in studies of land degradation from the field scale to national and global scales [7, 13–15]. Therefore, the objective of this study is to explore the spatial pattern and temporal variation of land degradation based on NDVI in the North China Plain and then to analyze the impact mechanisms of a set of natural and socioeconomic driving forces on land degradation, with the application of the binary panel logit regression model.

2. Data Processing and Analyses

2.1. An Overview of the North China Plain. The North China Plain (32°08′–40°16′N, 112°10′–122°40′E) is one of the most significant grain production regions of China. It covers two metropolises (Beijing and Tianjin) and five provinces including Anhui, Hebei, Henan, Jiangsu, and Shandong. As it is an alluvial plain developed by the intermittent flooding of the Huanghe, Huaihe, and Haihe rivers, it is also known as Huang-Huai-Hai Plain in China (Figure 1).

As estimated with the remote sensing data derived from the Landsat TM and ETM+ images in the year 2008, the cultivated land accounts for about 68% of the total land area of the North China Plain (Figure 2). There is a semiarid to semihumid warm temperate climate in the North China Plain, with the average annual temperature of 10°C–15°C and annual rainfall of 500–800 mm. It is evident that the North China Plain is suitable for developing rain-fed agriculture and planting a variety of crops and fruit trees. Meanwhile, it is conducive to mechanization and irrigation with its natural conditions of a flat terrain, deep soil, and contiguous land concentration. All of these unique conditions have made the North China Plain a major agricultural region and a significant commodity base for grain, cotton, meat, and oil in China [16].

However, the rapid population growth and urban land expansion have led to serious cultivated land loss and environmental degradation in the North China Plain. Many researches showed that the conversion from cultivated land to other types of land led to the decrease of cultivated land in the North China Plain [11, 16, 17]. Among the researches, Shi et al. (2013) pointed out that the area of cropland abandonment was much greater than the area of cropland reclamation in the North China Plain [17]. Besides, the quality of cultivated land converted to other land use types is generally higher than that of the cultivated land converted from other land use types [11]. As a result, the shrinkage of cultivated land in the North China Plain will exert great impact on the land quality. How to improve land productivity is becoming vital for the improvement of agricultural production. In addition, though the statistic data showed that the grain yields were increasing, it is due to the additional investment into the agricultural production. In this regard, it is an urgent issue to study how to make scientific policy and sustainable land management measures to rationally regulate the land conversion and control land degradation to improve the productivity of the remaining resources in the agricultural sector.

2.2. Data Preparation. According to previous studies, driving factors of land degradation are complex, among which biophysical causes (including topography that determines soil erosion hazard and climatic conditions, such as rainfall and temperature) and land use change (such as deforestation, desertification resulting from unsustainable land management practices) are major direct contributors to land

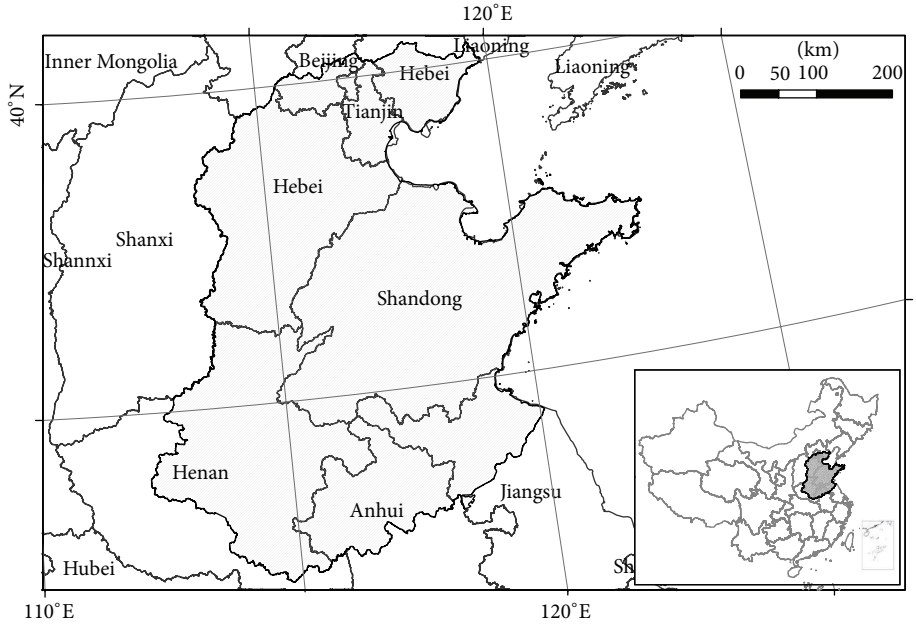

Figure 1: Location of the North China Plain.

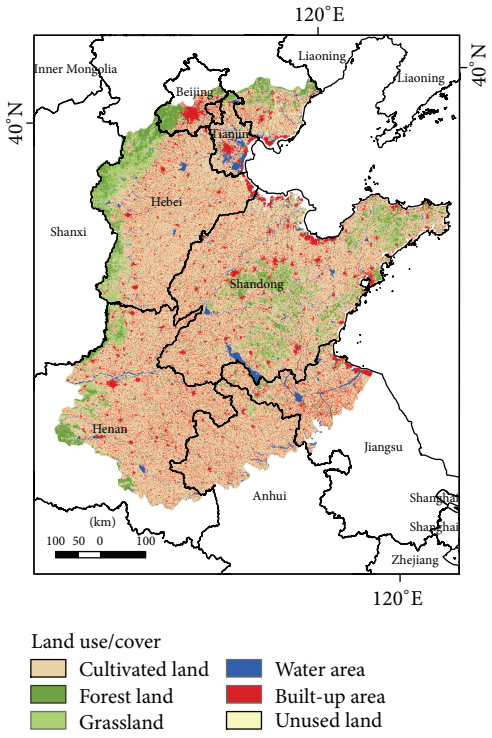

Figure 2: Land use pattern of the North China Plain in the year 2008.

degradation, while the underlying causes of land degradation include population density, economic development, land tenure, and access to agricultural extension, and infrastructure. Thus, in order to analyze the situation of agricultural production and impact mechanisms of climate and land use changes integrated with socioeconomic factors on cultivated land degradation in the North China Plain, we collected the NDVI data, land use datasets, climatic data, socioeconomic statistical data, and other geophysical data of the years 2000–2008.

NDVI. NDVI is one of the most commonly used indicators for vegetation monitoring [18, 19]. Many previous studies have used the NDVI and other measures based on the NDVI

as indicators of changes in ecosystem productivity and land degradation, which showed that NDVI is strongly correlated with the green vegetation coverage [20]. Though there are some limitations and criticisms related to the use of this measure, NDVI remains the only dataset available at the global level and the only dataset that reliably provides information about the condition of the aboveground biomass [21, 22]. In this study, we used the remote sensing data of NDVI to measure the land degradation. Before 2006, the NDVI data was obtained from the GIMMS NDVI dataset produced by the GLCF (Global Land Cover Facility) research group at the University of Maryland from July 1981 to December 2006, with a spatial resolution of 8 km by 8 km and a temporal resolution of 15 days. The NDVI data after the year 2006 was derived from SPOT VEGETATION data (ten-day ensembles) which were derived from a dataset developed over the period from April 1998 to December 2010, with a spatial resolution of l km by l km. Based on the period when the two datasets overlapped (1998 to 2006), we conducted data processing according to the previous experience of Yin et al. (2014) [23]. Firstly, correlation analysis between the maximum monthly NDVI and other factors was performed, following which a linear regression equation was established to extend the GIMMS (Global Inventory Modeling and Mapping Studies) dataset from 2007 to 2008. This helps to eliminate any sensor errors in the other two datasets [24]. To ensure the data quality, reliable and internationally recognized data pretreatment processes were used [25]. In order to eliminate cloud contamination effects and the noise caused by other atmospheric phenomena, we included a smoothing method proposed by Chen et al. [26] based on the Savitzky-Golay filter. Finally, we clipped the NDVI data of the North China Plain during the period from the year 2000 to 2008.

Land Use. The land use data came from the land use database of the Resources and Environment Scientific Data Center, Chinese Academy of Sciences [11, 27, 28]. The database was constructed from remotely sensed digital images by the US Landsat TM/ETM satellite with a spatial resolution of 30 by 30 meters. Further the land use data are upscaled to 1 by 1 kilometer. The data that was analyzed in this study covered the years 2000 and 2008.

Climatic Data. The climatic data, mainly including temperature and rainfall from the year 2000 to 2008, were derived from the daily records of 117 observation stations covering the entire area of the North China Plain, which were maintained by the China Meteorological Administration. A spline interpolation using the coupling-fitted thin plate interpolation method was chosen to interpolate the meteorological data [29]. Based on the climatic dependence on topography, climatic variables were interpolated with spatial resolution of 1 by l kilometer [30]. At a broader scale, temperature declined roughly with the increasing elevation at a typical standard lapse rate of 6.5°C per 1 kilometer [31], so the interpolated air temperature data were adjusted to the sea level according to the altitudinal correction factors based on the digital elevation model (DEM) dataset.

Soil Organic Matter. The soil fertility map of the study area was clipped from the soil map of China provided by the Institute of Soil Science, Chinese Academy of Sciences. It was based on the maps on the scale of 1 : 4,000,000 from the Second National Soil Survey of China for Soil Organic Matter (SOM).

Socioeconomic Statistical Data. In this study, we collected and processed the socioeconomic data of 385 major counties in the North China Plain at a county level for the period of the years 2000–2008, including the gross domestic production (GDP), population, rural farmers' per capita income, fertilizer utilization, pesticide utilization, farm machinery, total grain production, and total grain sown area, which were all acquired from socioeconomic statistical yearbooks published by National Statistical Bureau of China.

Geophysical Data. The geophysical data is also closely related with the land productivity. In this specific study, the geographic factors mainly include elevation and average slope, the data of which were derived from China's Digital Elevation Model dataset supplied by the National Geomatics Center of China. Another part of the geophysical data was the proximity variables, including the distance from each grid to the nearest expressway or highway and other ways, which were incorporated to measure the impacts of the infrastructure construction on the land degradation.

2.3. Primary Analysis

Changes of Grain Production. We analyzed the changes of grain production and the relationship between total grain production and grain yield (kg/ha) of the North China Plain during the years 2000–2008. The spatial distribution of grain yield at municipality or county level in the years 2000, 2005, and 2008 is shown in Figure 3. The grains mainly included wheat and maize, but some rice, soybean, and tuber crops were also included.

During the period of the years 2000–2008, annual total grain production of the selected counties of the North China Plain increased by more than 40%, and the average grain yield increased from 4994 to 5986 kg/ha (with an increasing rate of 20%). The time-series changing trend of the total grain production is similar to that of the average grain yield, and therefore the increase of agricultural production can be mainly ascribed to the increase in the average grain yield (Figure 4). The time-series change of grain yield from year 2000 to 2008 can be divided into two periods. Firstly, the average grain yield decreased after the year 2000 because of a decrease in grain price. Secondly, the price of grain increased again through governmental support after the year 2003, which made the average yields recover again.

Also, we showed that the application rates of fertilizer and pesticide increased with fluctuations from 525 to 622 kg/ha and from 12.6 to 16.2 kg/ha during the period of the years 2000–2008, respectively. The application rate of the farm machinery also showed an increasing trend (Figure 5). The increases of the application of farm machinery, fertilizer, and pesticide can be the key determinants of the increase in crop

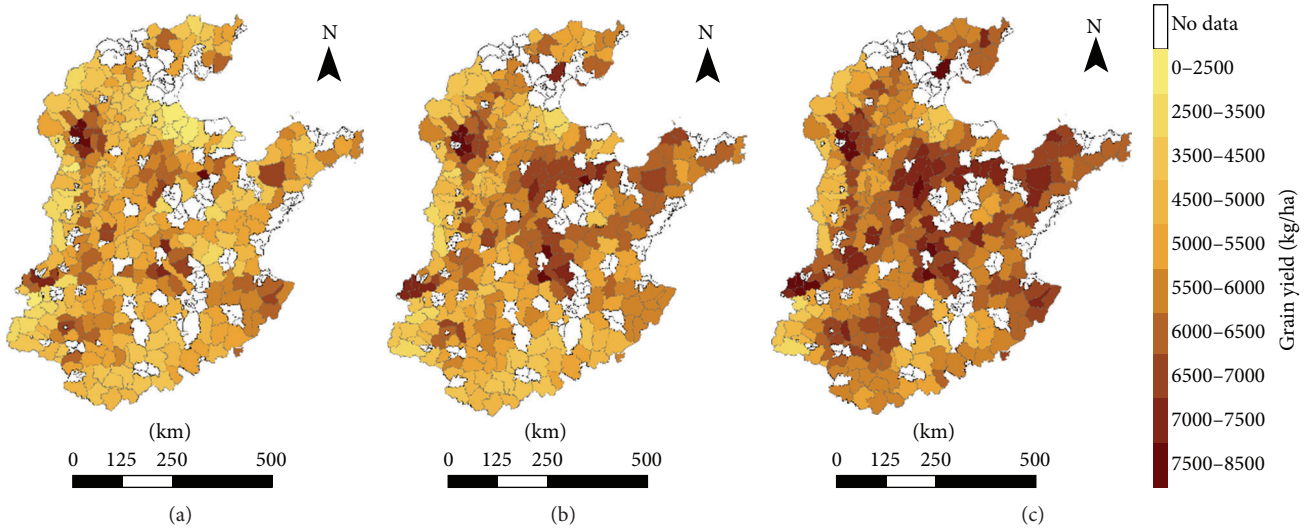

Figure 3: County-level grain yield of the North China Plain, (a) 2000, (b) 2005, and (c) 2008.

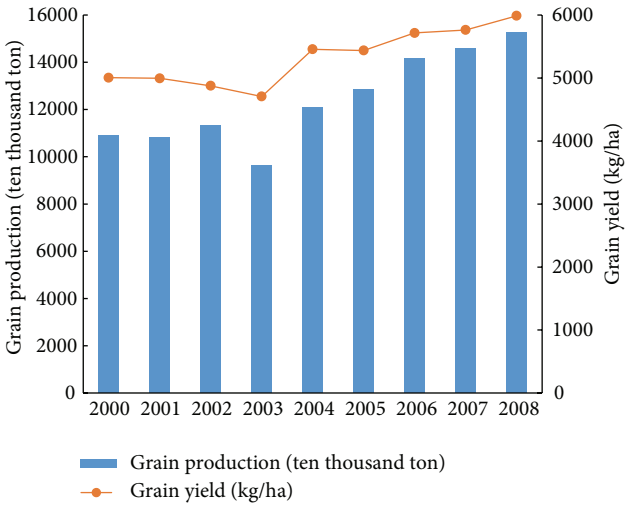

Figure 4: Relationship between grain production and grain yield of the North China Plain, 2000–2008.

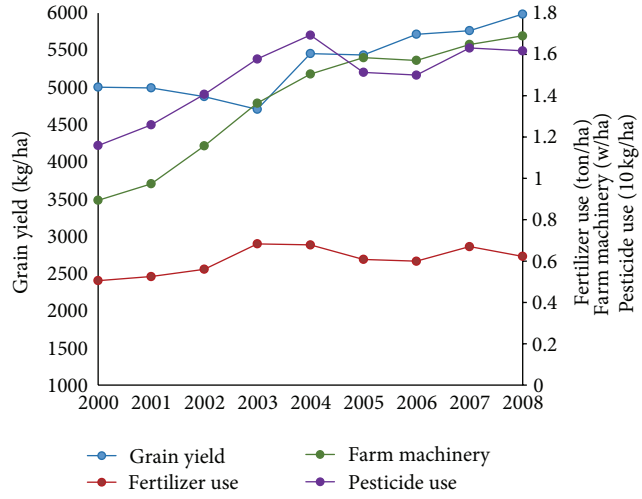

Figure 5: Changes of grain yield, fertilizer use, pesticide use, and farm machinery application of the North China Plain, 2000–2008.

yield; however, further increases in fertilizer and pesticide application are unlikely to be as effective as they previously were in increasing the grain yields because of the gradually diminishing return rate.

Trends in NDVI. The annual average greenness (represented with NDVI) is chosen as the standard proxy of annual average biomass productivity, which generally fluctuates with the rainfall. The NDVI calculated using remote sensing image data currently is one of the most commonly used indicators to monitor regional or global vegetation and the ecosystem and is the best instruction factor to reflect vegetation growth conditions and coverage [32]. In this study, the cultivated land degradation areas were identified with a sequence of analyses of the NDVI data. The result shows that the annual average NDVI of the North China Plain showed an overall increasing trend during the years 2001–2004. About 90% of the study area's annual average NDVI experienced an increasing trend. While only 5% of the study area's annual average NDVI showed a decreasing trend, which was distributed in the Shandong Province (Figure 6(a)). In comparison, during the years 2004–2008, about 80% of the study area's annual average NDVI experienced a decreasing trend, with only 19% of the study area's annual average NDVI showed an increasing trend (Figure 6(b)). Besides, the annual average NDVI in some areas showed first increasing and then decreasing trend during the years 2000–2008. Overall, the annual average NDVI showed an increasing trend in most parts of the whole study area during the years 2000–2008 (Figure 6(c)).

Land Use Changes. During the years 2000–2008, the land use change is mainly dominated by the conversion from

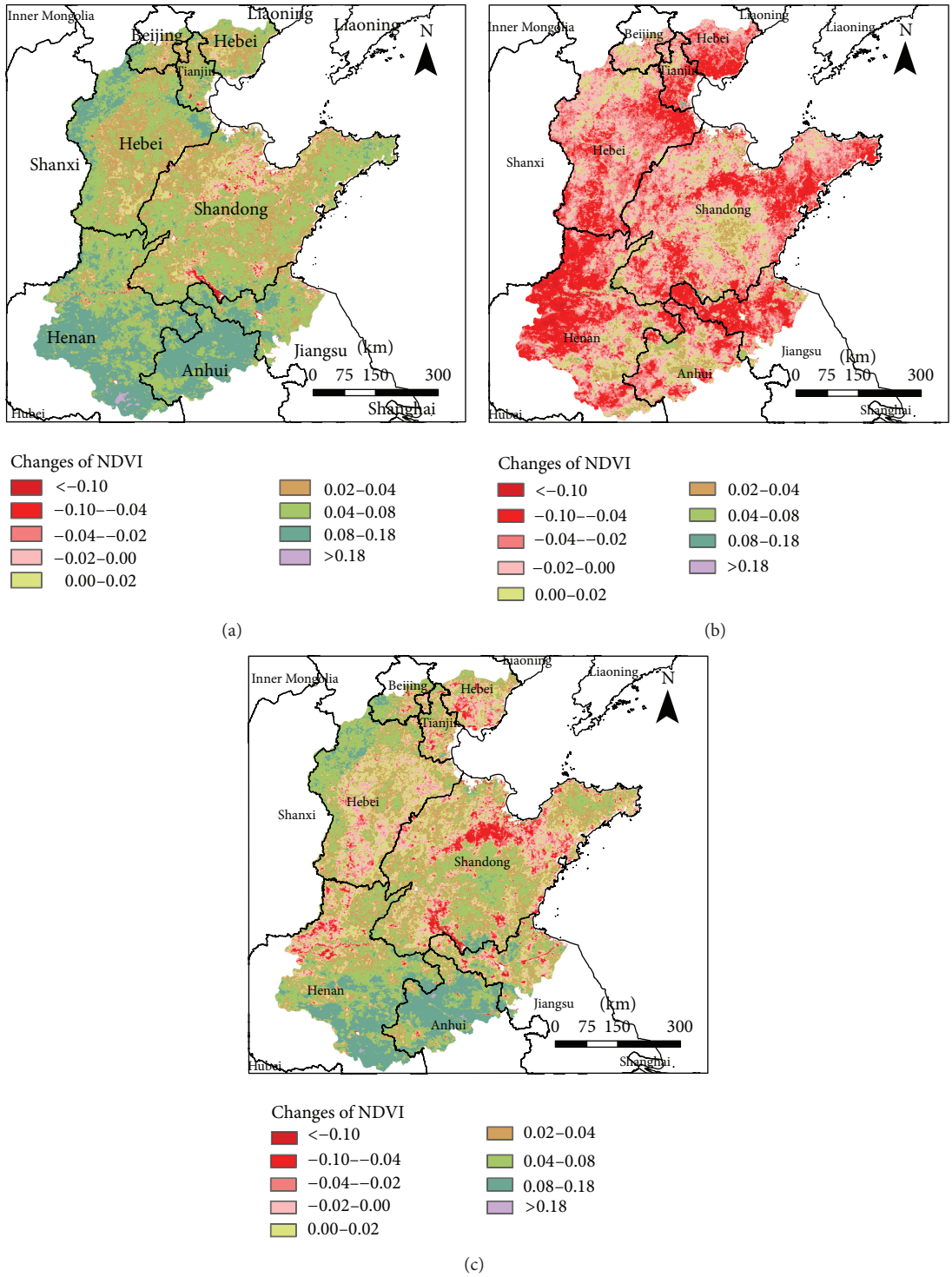

Figure 6: Changes of NDVI of the North China Plain during (a) 2000–2004; (b) 2004–2008; and (c) 2000–2008.

cultivated land to other land use types, especially the conversion from cultivated land to built-up land. As cultivated land is the major land use types in the study area, thus we focus on the cultivated land conversion. In the North China Plain, cultivated land is mainly converted to built-up land (67%), forest land (9.1%), and grassland (12.4%) (Figure 7).

2.4. Associations between Climate Factors and Land Degradation. We investigated the relationship between NDVI (from year 2000 to 2008) and climate factors. The relationship between NDVI and climate indicators is widely analyzed in many previous studies, which have confirmed that vegetation changes are closely related to changes in the climate factors

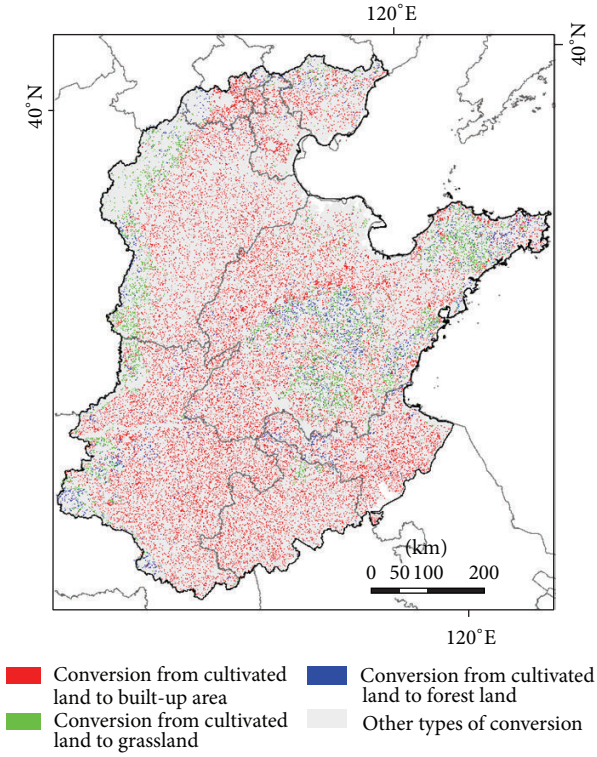

Figure 7: Land conversion from cultivated land to three major land use types during 2000–2008.

at the global or regional scale. In particular, it is widely acknowledged that the temperature and rainfall are the most significant factors influencing the ecosystem characteristics and distribution. We sampled the value of the NDVI, rainfall, and temperature and calculated their annual average values in the whole North China Plain. The mean NDVI, temperature, and rainfall for the study area were plotted along a nine-year time series (Figure 8). Figure 8 visually showed that the average NDVI experienced a fluctuated increasing trend, and the average rainfall and temperature slightly showed an increasing trend with some fluctuations.

Specifically, to study the responses of NDVI to the climate change, we analyzed the spatial correlation of NDVI with rainfall and temperature using the correlation analysis at the pixel scale. Figure 9 showed the spatial distribution of the correlation of NDVI with rainfall and temperature, respectively. It shows that the rainfall has a strong effect on NDVI, and there was a positive correlation between rainfall and NDVI in most parts of the study area, especially in the northern part of the study area where it showed a high correlation. As to the relationship between NDVI and temperature, there was generally a positive relationship between NDVI and temperature, which only in the northern part of the study area showed negative relationships.

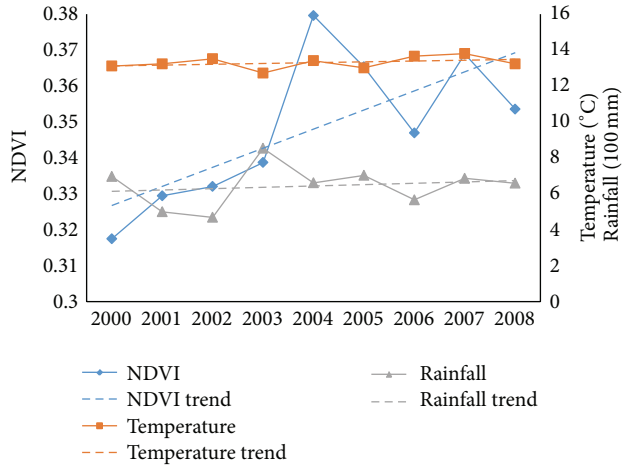

Figure 8: Changing trend of spatially aggregated annual NDVI, rainfall, and temperature.

3. Assessments of the Driving Forces of Land Degradation

The causes of land degradation are numerous, interrelated, and complex. The relationship between direct and underlying causes of land degradation is complex also, and the impact of underlying factors is context specific [33]. Quite often, the same cause may lead to diverging consequences in different contexts because of its varying interactions with other proximate and underlying causes of land degradation. This implies that targeting only one underlying factor is not sufficient in itself to address land degradation. It is necessary to take into account a number of underlying and proximate factors when designing policies to prevent or mitigate land degradation. For our model specification, it is essential to

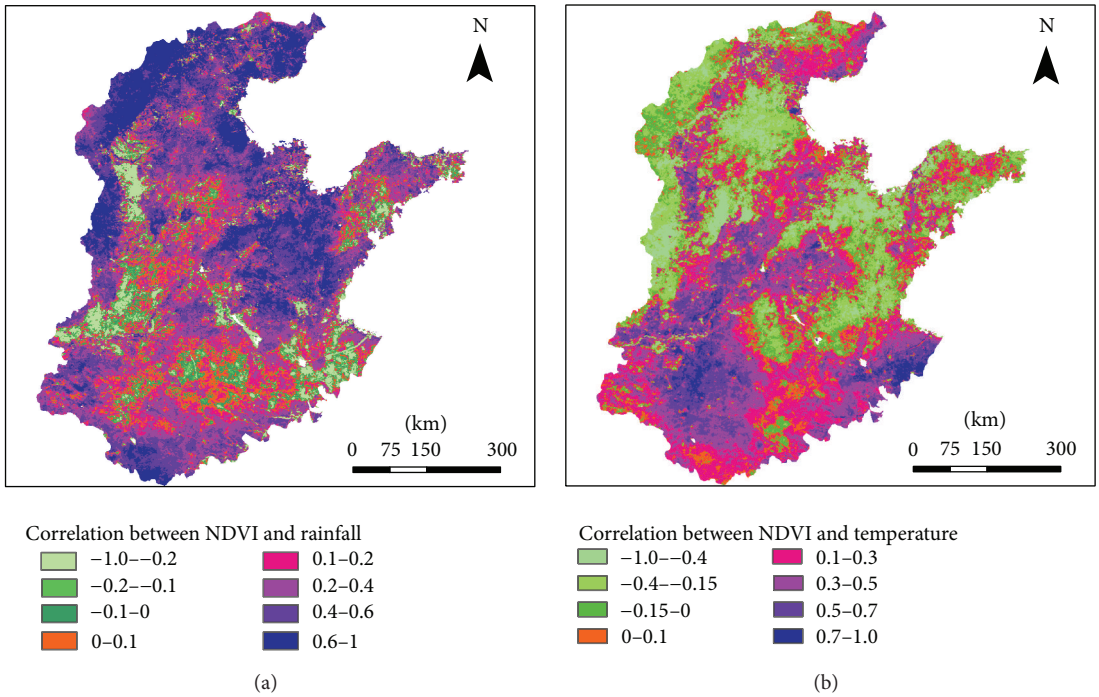

FIGURE 9: Spatial patterns of correlation (a) between annual average NDVI and rainfall and (b) between annual average NDVI and temperature at the pixel level in the North China Plain.

identify the effects of various combinations and interactions of underlying and proximate causes of land degradation in a robust manner rather than only analyze the individual cause of land degradation. In this regard, we try to identify the key underlying and proximate causes of land degradation. In this part, we conducted econometric analysis of the causes of land degradation in the North China Plain with the binary logistic regression model.

We constructed the model for estimating causes of land degradation or land improvement at the county level, using annualized data, and the model specification is as follows:

$$\text{Logit}\, Y_t = \beta_0 + \beta_1 \Delta x_{1t} + \beta_2 \Delta x_{2t} + \beta_3 x_3 + \beta_4 x_4 + \varepsilon_{it}, \quad (1)$$

where $Y_t = 1$, if $\text{NDVI}_t - \text{NDVI}_{t-1} \geq 0$ and $Y_t = 0$ if $\text{NDVI}_t - \text{NDVI}_{t-1} < 0$; x_{1t} = a vector of biophysical causes of land degradation (e.g., climate conditions, topography, and soil fertility constraints); x_{2t} = a vector of demographic and socioeconomic causes of land degradation (e.g., population density, per capita GDP, rural farmers' per capita income, agricultural intensification); x_3 = a vector of variables representing access to infrastructure services (e.g., distance to expressway, distance to high way, and distance to other ways); and x_4 = a vector of variables representing land use changes (e.g., county-level percentage of land conversion from cultivated land to built-up land, forest land, and grassland during the years 2000–2008).

Y_t is a binary variable that is being used to identify whether land degradation happens; if Y_t equals or is larger than zero, then we assume that there happens land improvement; otherwise there happens land degradation. Furthermore, we applied a binary panel logit regression model to simultaneously study the relationship between land degradation conditions and all other variables. Table 1 illustrates the results of the regression. The results are to be interpreted with extreme caution due to the complex and multidirectional relationship between NDVI changes and the selected variables. Note that the results might not indicate a causal relationship but only an association between NDVI and the selected biophysical and socioeconomic variables [21].

The climate changes are significantly related with the land degradation conditions which are represented by the changes in NDVI. As expected, increments in temperature and rainfall are positively related with the increases in NDVI, and increases in temperature and rainfall will significantly contribute to land improvement. Land use change is also the major driving force of land degradation. The results showed that the conversion from cultivated land to grassland and forest land will contribute to land improvement, which corresponded to increase in NDVI, while the conversion from cultivated land to built-up land would lead to land degradation. Among the land conversions, only the conversion from cultivated land to grassland significantly affects the land degradation. In comparison, climate change plays a much more important role than land use change in land degradation. Besides, agricultural intensification represented by fertilizer utilization is significantly and positively related with land improvement, as fertilizer application increases soil carbon [34], which could correspond to an increase in NDVI. Increases in the population density would lead to land degradation but not significantly. According to the previous studies, the impact of population density on land degradation is ambiguous, while our results suggested that there would

Table 1: Results for binary panel logistic regression analyses for the biophysical and socioeconomic driving forces of land degradation.

Land degradation conditions Y (1 represents land improvement and 0 represents land degradation)	Coef.
ΔRainfall (mm)	3.221***
ΔTemperature (°C)	1.025***
Percentage of land conversion from cultivated land to built-up land (%)	−0.326
Percentage of land conversion from cultivated land to forest land (%)	1.788
Percentage of land conversion from cultivated land to grassland (%)	8.507*
ΔFertilizer utilization per unit area (kg/ha)	0.506**
ΔPopulation density (ten thousand people/km^2)	−11.282
ΔRural farmers' per capita income (ten thousand yuan)	−0.076
ΔPer capita gross domestic production (ten thousand yuan)	0.0004
ΔShare of production value of agriculture animal husbandry and fishery in GDP (%)	−1.672*
DEM (km)	3.214
Slope (degree)	−0.018
Soil organic matter (%)	0.446***
Distance to highway (km)	0.002*
_cons	0.032

Note: *significant at the 10% level; **significant at the 5% level; and ***significant at the 1% level.

be more serious land degradation in areas with higher population density [35]. The population growth will lead to increasing demand for housing and other facilities, which in turn can lead to increase of impervious surface as a result of urban development and infrastructure construction and deforestation. Rapid economic development, which can be represented by changes in the per capita GDP, shows that an increase in both GDP and NDVI had positive impacts on land quality, suggesting the role the ecosystem service could play in economic growth and prosperity. Economic development would stimulate the land improvement, but such impacts were not significant, while the rural economic development, represented by rural farmers' per capita income, showed negative relationship with land improvement, suggesting that the NDVI will decrease as the rural farmer's income increase. It may be due to the fact that rural economic growth develops at the cost of intensive land use practice, which contributes to environmental degradation further leading to the land degradation. In addition, the increases in the share of the primary industry (agriculture, animal husbandry, and fishery) in GDP significantly corresponded to the decrease in NDVI. As production value of the agriculture increases mostly resulted from the investment into agricultural production, such as fertilizer, pesticide, and farm machinery, not from natural land quality improvement. In addition, the geographic and topographic factors also affect the land degradation. As to the topographical factors, the results showed that the higher the elevation and the slower the slope, the less serious the land degradation. The impact of elevation was not significant, while it may suggest that, in the areas with higher elevation, there would be less impacts of anthropogenic factors on the land degradation. The slope had clear significant impacts on land degradation, suggesting that steep slopes would lead to land degradation more easily, as steep slope regions were more vulnerable to severe water-induced soil erosion. As to the soil fertility represented by soil organic matter, the results showed that the higher the soil fertility was, the less the possibility of land degradation is. Besides, the distance to highway was significantly positively related with land improvement, which suggested that the larger distances to road network meant that there was less human disturbance, less infrastructure development, and land use changes, which would exert less impacts on the land degradation.

4. Conclusions and Discussions

Land degradation or improvement is an outcome of many highly interlinked direct and underlying causes, including natural, socioeconomic, and related agricultural practices. In China, many types of land degradation are occurring, such as grassland degradation, deforestation, and cultivated land degradation. In this paper, we conducted an empirical study in the North China Plain and analyzed the basic grain production changes, the changing trend of NDVI, the spatial pattern of relationship between climatic factors and NDVI. Further taking NDVI as a proxy for land degradation and improvement, we applied an econometric model to analyze the causes of land degradation.

According to the analyses, both the grain production and grain yield of the North China Plain showed an increasing trend during the years 2000–2008; however, estimation based on the remotely sensed NDVI data showed that the North China Plain still experienced land degradation. Degraded areas have been expending in the northern part of the study area, though many parts of the study area showed land improvement. Based on the correlation analysis, the increases in temperature and rainfall corresponded to the increase in NDVI in most parts of the North China Plain, though some parts of the study area showed negative correlation between NDVI and temperature and rainfall. Further, according to the binary panel logistic regression analysis, the results showed there were strong impacts of some key biophysical and socioeconomic variables on land degradation. Some of these relationships were consistent with conclusions in previous case studies, while others showed complex differences. The results for climate factors were not surprising, and increase in temperature and rainfall would contribute to land improvement. Different land use changes exert different impacts on land degradation. Unsurprisingly, increasing of forest land and grassland would benefit land quality, while urban expansion would lead to land degradation. Our estimation results about the positive effects of agricultural intensification represented by fertilizer utilization on land degradation were also as expected, and the soil organic matter was also a crucial positive factor for land quality conservation. Rural economic and agricultural development may lead to land

degradation. The rural economic and agricultural production growth exerted negative impacts on land quality, which means the development of rural economy and agricultural production led to land degradation. The increases in rural farmers' per capita income and primary production value ratio did not result in the improvement of land quality, which may be due to the overexploitation of land with insufficient investment into the land conservation. In this regard, an effective response to land degradation needs increasing incentives of farmers to conserve their cultivated land and improve their access to the knowledge and inputs that are required for proper conservation. Promotion of such land improvements should be a development policy priority. During the process to promote rural economic development, the governments should also focus on the monitoring and assessment of land quality and make measures to improve land quality, and such improvement measures should be designed together with farmers to meet their prior needs and use appropriate techniques according to the local economic and social conditions. In addition, increasing accessibility to infrastructures may also have negative effects on land quality. Infrastructure development is the basis for regional prosperity, and a booming economy will result in more construction of infrastructure. The expansion of basic infrastructure of transportation such as roads, railways, and airports can further take up land resources and further result in land overexploitation and degradation. The covering of the soil surface with impervious materials as a result of urban development and infrastructure construction is known as soil sealing. Sealing of the soil and land consumption are closely interrelated; when natural, seminatural, and cultivated land is covered by impervious surfaces and structures, this will degrade soil functions or cause their loss. To reduce the impacts of infrastructure construction on land quality, the local government should take the assessment of land degradation into consideration during the construction of infrastructures.

Based on the above analysis results, to achieve sustainable land management, climate changes should be monitored so as to make adaptation measures to mitigate the impacts of climate changes on land quality; along with the socioeconomic development, investments and better land management for improving land quality should be definitely encouraged through appropriate policy measures; human activities that change the land surface, such as infrastructure constructions, should be regulated on the basis of the assessment of impacts on land quality, and corresponding land conservation measures should be taken during the construction process.

Conflict of Interests

The authors declare that there is no conflict of interests regarding the publication of this paper.

Acknowledgments

This research was financially supported by China National Natural Science Funds for Distinguished Young Scholar (Grant no. 71225005). The data support from the National Natural Science Foundation of China (Grant no. 41171434) and the National Key Program for Developing Basic Science in China (Grant no. 2012CB955700) was also greatly appreciated.

References

[1] S. Bajocco, A. de Angelis, L. Perini, A. Ferrara, and L. Salvati, "The impact of land use/land cover changes on land degradation dynamics: a Mediterranean case study," *Environmental Management*, vol. 49, no. 5, pp. 980–989, 2012.

[2] E. B. Barbier, "The economic determinants of land degradation in developing countries," *Philosophical Transactions of the Royal Society B: Biological Sciences*, vol. 352, no. 1356, pp. 891–899, 1997.

[3] M. V. Sivakumar and N. Ndiang'ui, *Climate and Land Degradation*, Springer, 2007.

[4] E. Symeonakis, A. Calvo-Cases, and E. Arnau-Rosalen, "Land use change and land degradation in southeastern Mediterranean Spain," *Environmental Management*, vol. 40, no. 1, pp. 80–94, 2007.

[5] Millennium Ecosystem Assessment, *Ecosystems and Human Well-Being: Desertification Synthesis*, World Resources Institute, 2005.

[6] WMO, *Cliamte and Land Degradation*, World Meteorological Organization, 2005.

[7] Z. Bai and D. Dent, "Recent land degradation and improvement in China," *Ambio*, vol. 38, no. 3, pp. 150–156, 2009.

[8] X. Deng, J. Huang, S. Rozelle, and E. Uchida, "Growth, population and industrialization, and urban land expansion of China," *Journal of Urban Economics*, vol. 63, no. 1, pp. 96–115, 2008.

[9] F. Long, Introduction to the resources status in China-Land resources Jingchengnew.cn, 2013 (Chinese), http://www.jingchengw.cn/new/20130411/4927.htm.

[10] H. Li, Z. Liu, L. Zheng, and Y. Lei, "Resilience analysis for agricultural systems of North China plain based on a dynamic system model," *Scientia Agricola*, vol. 68, no. 1, pp. 8–17, 2011.

[11] X. Deng, J. Huang, S. Rozelle, and E. Uchida, "Cultivated land conversion and potential agricultural productivity in China," *Land Use Policy*, vol. 23, no. 4, pp. 372–384, 2006.

[12] H. Long, G. Tang, X. Li, and G. K. Heilig, "Socio-economic driving forces of land-use change in Kunshan, the Yangtze River Delta economic area of China," *Journal of Environmental Management*, vol. 83, no. 3, pp. 351–364, 2007.

[13] G. N. Bastin, G. Pickup, and G. Pearce, "Utility of AVHRR data for land degradation assessment: a case study," *International Journal of Remote Sensing*, vol. 16, no. 4, pp. 651–672, 1995.

[14] K. J. Wessels, S. D. Prince, P. E. Frost, and D. van Zyl, "Assessing the effects of human-induced land degradation in the former homelands of northern South Africa with a 1 km AVHRR NDVI time-series," *Remote Sensing of Environment*, vol. 91, no. 1, pp. 47–67, 2004.

[15] D. Singh, M. S. P. Meirelles, G. A. Costa, I. Herlin, J. P. Berroir, and E. F. Silva, "Environmental degradation analysis using NOAA/AVHRR data," *Advances in Space Research*, vol. 37, no. 4, pp. 720–727, 2006.

[16] Q. Jiang, X. Deng, J. Zhan, and S. He, "Estimation of land production and its response to cultivated land conversion in North China Plain," *Chinese Geographical Science*, vol. 21, no. 6, pp. 685–694, 2011.

[17] W. Shi, F. Tao, and J. Liu, "Changes in quantity and quality of cropland and the implications for grain production in the

Huang-Huai-Hai Plain of China," *Food Security*, vol. 5, no. 1, pp. 69–82, 2013.

[18] C. J. Tucker, "Red and photographic infrared linear combinations for monitoring vegetation," *Remote Sensing of Environment*, vol. 8, no. 2, pp. 127–150, 1979.

[19] C. J. Tucker, H. E. Dregne, and W. W. Newcomb, "Expansion and contraction of the Sahara desert from 1980 to 1990," *Science*, vol. 253, no. 5017, pp. 299–301, 1991.

[20] M. Elhag and S. Walker, "Impact of climate variability on vegetative cover in the Butana area of Sudan," *African Journal of Ecology*, vol. 47, supplement 1, pp. 11–16, 2009.

[21] E. Nkonya, N. Gerber, P. Baumgartner et al., *ZEF Discussion Papers on Development Policy*, 2011.

[22] Z. G. Bai, D. L. Dent, L. Olsson, and M. E. Schaepman, "Proxy global assessment of land degradation," *Soil Use and Management*, vol. 24, no. 3, pp. 223–234, 2008.

[23] F. Yin, X. Deng, Q. Jin, Y. Yuan, and C. Zhao, "The impacts of climate change and human activities on grassland productivity in Qinghai Province, China," *Frontiers of Earth Science*, vol. 8, no. 1, pp. 93–103, 2014.

[24] G. Zhang, X. Xu, C. Zhou, H. Zhang, and H. Ouyang, "Responses of grassland vegetation to climatic variations on different temporal scales in Hulun Buir Grassland in the past 30 years," *Journal of Geographical Sciences*, vol. 21, no. 4, pp. 634–650, 2011.

[25] J. R. G. Townshend, C. Justice, D. Skole et al., "The 1km resolution global data set: needs of the International Geosphere Biosphere Programme," *International Journal of Remote Sensing*, vol. 15, no. 17, pp. 3417–3441, 1994.

[26] J. Chen, P. Jönsson, M. Tamura, Z. Gu, B. Matsushita, and L. Eklundh, "A simple method for reconstructing a high-quality NDVI time-series data set based on the Savitzky-Golay filter," *Remote Sensing of Environment*, vol. 91, no. 3-4, pp. 332–344, 2004.

[27] J. Liu, M. Liu, D. Zhuang, Z. Zhang, and X. Deng, "Study on spatial pattern of land-use change in China during 1995–2000," *Science in China Series D: Earth Sciences*, vol. 46, no. 4, pp. 373–384, 2003.

[28] J. Liu, Z. Zhang, X. Xu et al., "Spatial patterns and driving forces of land use change in China during the early 21st century," *Journal of Geographical Sciences*, vol. 20, no. 4, pp. 483–494, 2010.

[29] M. F. Hutchinson and P. E. Gessler, "Splines—more than just a smooth interpolator," *Geoderma*, vol. 62, no. 1–3, pp. 45–67, 1994.

[30] D. Xiangzheng, *Simulation of Land System Dynamics*, China Land Press, Beijing, China, 2008, (Chinese).

[31] P. A. Hancock and M. F. Hutchinson, "Spatial interpolation of large climate data sets using bivariate thin plate smoothing splines," *Environmental Modelling & Software*, vol. 21, no. 12, pp. 1684–1694, 2006.

[32] X. Zhang, Q. Ge, and J. Zheng, "Impacts and lags of global warming on vegetation in Beijing for the last 50 years based on remotely sensed data and phonological information," *Chinese Journal of Ecology*, vol. 24, no. 2, pp. 123–130, 2005.

[33] E. Nkonya, N. Gerber, J. von Braun, and A. de Pinto, "Economics of land degradation," IFPRI Issue Brief 68, 2011.

[34] P. L. G. Vlek, G. Rodríguez-Kuhl, and R. Sommer, "Energy use and CO_2 production in tropical agriculture and means and strategies for reduction or mitigation," *Environment, Development and Sustainability*, vol. 6, no. 1-2, pp. 213–233, 2004.

[35] S. J. Scherr, "A downward spiral? Research evidence on the relationship between poverty and natural resource degradation," *Food Policy*, vol. 25, no. 4, pp. 479–498, 2000.

Hindawi Publishing Corporation
Advances in Meteorology
Volume 2015, Article ID 452603, 12 pages
http://dx.doi.org/10.1155/2015/452603

Research Article

Influence of Land Use Patterns on Evapotranspiration and Its Components in a Temperate Grassland Ecosystem

Yuzhe Li,[1,2] Jiangwen Fan,[1] Zhongmin Hu,[3] Quanqin Shao,[1] Liangxia Zhang,[1,2] and Hailing Yu[1,2]

[1] *Key Laboratory of Land Surface Pattern and Simulation, Institute of Geographical Sciences and Natural Resources Research, Chinese Academy of Sciences, Beijing 100101, China*
[2] *University of Chinese Academy of Sciences, Beijing 100049, China*
[3] *Key Laboratory of Ecosystem Network Observation and Modeling, Synthesis Research Center of Chinese Ecosystem Research Network, Institute of Geographic Sciences and Natural Resources Research, Chinese Academy of Sciences, Beijing 100101, China*

Correspondence should be addressed to Jiangwen Fan; fanjw@igsnrr.ac.cn

Received 18 September 2014; Accepted 9 December 2014

Academic Editor: Jinwei Dong

To better understand variation in response of components of ecosystem evapotranspiration (ET) to grassland use differences, we selected three typical land use patterns in a temperate steppe area: grazed steppe (G), steppe with grazers excluded (GE), and steppe cultivated to cropland (C). ET was divided into its components evaporation (E) and canopy transpiration (T) using herbicide and a chamber attached to a portable infrared gas analyzer (Li-6400). The results indicated that daily water consumption by ET in G was 3.30 kg m^{-2} d^{-1}; compared with G, ET increased significantly in GE at 13.4% and showed a trend of 6.73% increase in C. Daily water consumption by E increased 24.3% in GE relative to G, and C showed 20.2% more than GE. At 0.46, E/ET in C was significantly higher than G at 0.35. Air temperature and the vapor pressure deficit were closely correlated with variation in diurnal ET, E, and T. The leaf area index (LAI) was also positively correlated with daily ET and E varied among grassland use patterns and explained variation in E/ET (81%). Thus, variation in LAI strongly influences the overall magnitude of ecosystem ET and the composition of its components under different grassland use patterns.

1. Introduction

Large-scale changes in land use are strongly connected to global climate change [1–3]. In recent years, changes in land use patterns in large areas of grassland in Northern China [4] have altered surface vegetation cover [5] and, as a result, significantly influenced the ecosystem and regional environment [6]. Grazed steppe covers the majority of grassland area in the European-Asian continent [7]. In Northern China, grazing by livestock has long been the major anthropogenic influence on the temperate grassland ecosystem. In recent years, however, grassland destruction by sandstorms has increased environmental protection awareness and government input for grassland restoration in China, resulting in a rapid increase in steppe area where grazing is excluded [1]. In contrast, in response to crop-planting limits and the need for economic benefit, a large grassland area in the pastoral-farming ecotone of the steppe in China has been converted to cropland [8]. By altering vegetation, original soil structure, and microclimate, changes in grassland use may affect overall ecosystem evapotranspiration (ET), as well as its components soil surface evaporation by vapor loss (E) and canopy vapor consumption by transpiration (T). These processes contribute to carbon uptake [9].

Water is a critical limiting factor in arid and semiarid grassland area in Northern China and influences productivity and regional climate [10, 11]. ET is related to a number of ecosystem processes, including photosynthesis, soil moisture, and latent heat transfer [12] and plays an important role in global energy and water cycles [8]. The magnitude and dynamics of ET differ with changes in vegetation traits, meteorological conditions, and soil characteristics [13]. Therefore,

it is important to investigate how change in grassland use patterns in the Northern China steppe has altered local vapor budget and water balances, thereby influencing natural ecological functions in these grasslands [14, 15] and impacting regional climate.

Previous work on ET has been conducted primarily using the eddy covariance system [15–17] and the lysimeter [18]. The eddy covariance system can record ET automatically over long durations, but, because of its whole-ecosystem scale [19], it is difficult to distinguish differences in water flux among local sites. This problem can be resolved by using a chamber attached to a portable infrared analyzer [20–22], which is more suitable for measuring flux of adjacent plots. Thus it can be used to determine the influence of the land use type on water exchange within an ecosystem. In addition, few previous studies have correctly divided ET into soil evaporation (E) and transpiration (T) [8], resulting in difficulty uncovering underlying mechanisms of variation in ET [23, 24]. However, with a fine treatment such as clipping, portable infrared gas analyzers measured the contribution of E to total ET [25]. Measuring the components of ET (E and T) is key not only to understand mechanisms underlying variation in ecosystem ET with grassland use patterns [23] but also to help resolve uncertainties in modeling simulation of ET or latent heat and thereby to increase simulation precision [25, 26].

We used herbicide rather than clipping and removing the vegetation to more accurately divide ecosystem ET into canopy T and surface E, as killing the vegetation with herbicide leaves the structure intact, largely maintaining the original level of shading. Specifically, we aimed to (i) understand the effect of the varied grassland use patterns on the components of ET and the daily vapor transfer between the ecosystem and the atmosphere and (ii) investigate the mechanisms underlying changes in ET and its composition among different grassland use patterns in the steppe.

2. Materials and Methods

2.1. Study Area. This study was conducted on *Stipa grandis*, a dominant grass of the temperate steppe, at Xilinhot, Inner Mongolia, Northern China (43°32′24.06″N, 116°33′41.76″E, elevation 1250 m). The study site is located at 500 km north to Beijing and is considered as an important sand source of Beijing (Figure 1). Between 1982 and 2004, mean annual temperature was 0.6°C, and mean monthly temperature ranged from −21.4°C (January) to 18.5°C (July) [20]. Mean annual precipitation was 350 mm, mainly falling from June to August during the main growth period. The weather is mainly dry and windy, and the soils are chestnut or chernozem soil. Data of the main meteorological parameters during the experimental period (August 2012) are shown in Figure 2.

2.2. Observation Design. Three types of land use in adjacent areas were selected for study: grazed steppe (G), steppe with grazers excluded (GE), and steppe cultivated to cropland (C). G is a typical steppe that has been grazed by sheep and horses for more than 20 years. GE is steppe where herbivores have been excluded since 1979 and a large amount of plant litter remains on the ground. The original land use and community structure of C were similar to G until 5 years prior to the study, when the land was cultivated for wheat cropping. No irrigation is applied to cropped areas. Organic manure was applied prior to crop planting, and 240 kg hm^{-2} effective fertilizer (N 110 kg/ha, P_2O_5 70 kg/ha, and K_2O 60 kg/ha) was applied in two applications during crop growth. At the center of the grazed steppe (G) (43°32′24.06″N, 116°33′41.76″E), an eddy covariance system was set up to measure the water, carbon, and heat exchange between the

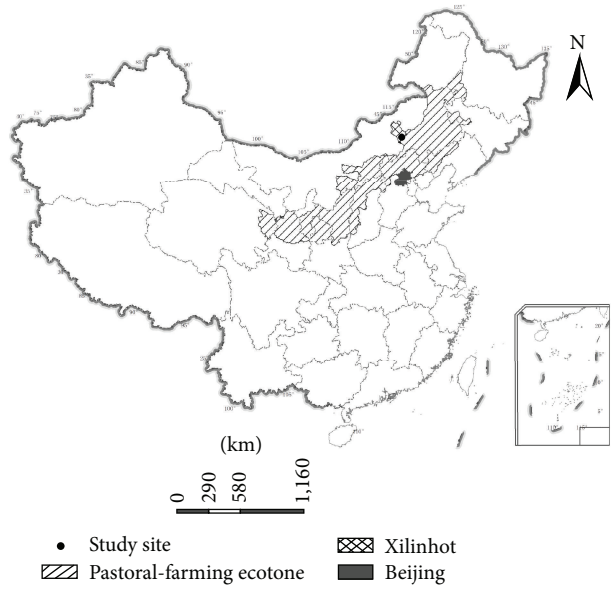

Figure 1: The location of the study area and the pastoral-farming ecotone in Northern China.

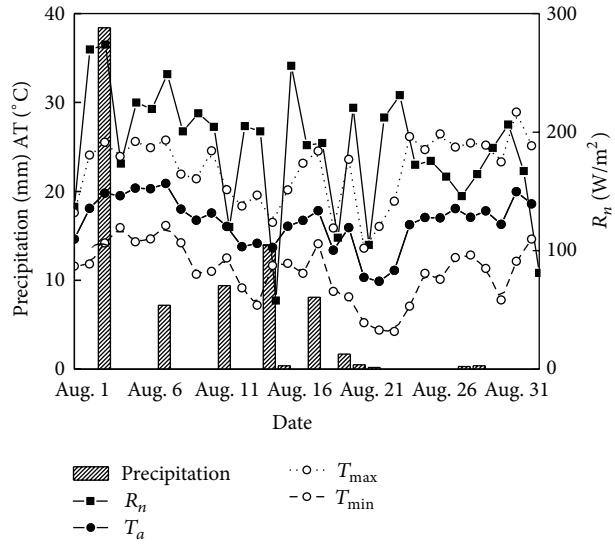

Figure 2: Daily precipitation, air temperature (T_a, daily mean; T_{max}, daily maximum; T_{min}, daily minimum) and net radiation (R_n) during the experimental period from 1 August to 31 August 2012 in a typical temperate steppe at Xilinhot, Inner Mongolia.

Table 1: Microclimate characteristics of land use types (LT) and vegetation cover treatments (TR).

LT/Tr	ST (°C)	SM (%)	AT (°C)	VPD
G				
DS	20.68 ± 0.81^{a}	21.98 ± 0.81^{a}	21.84 ± 1.00^{a}	1.72 ± 0.14^{a}
CL	20.94 ± 0.37^{a}	21.34 ± 0.78^{a}	21.89 ± 1.02^{a}	1.78 ± 0.16^{a}
CK	19.82 ± 0.71^{ab}	21.91 ± 0.79^{a}	21.79 ± 1.02^{a}	1.68 ± 0.13^{a}
GE				
DS	17.69 ± 0.55^{bc}	26.10 ± 0.56^{bc}	21.71 ± 1.05^{a}	1.76 ± 0.16^{a}
CL	18.47 ± 0.32^{b}	22.83 ± 0.67^{ab}	22.01 ± 1.08^{a}	1.81 ± 0.16^{a}
CK	17.25 ± 0.46^{c}	24.41 ± 0.30^{b}	21.63 ± 0.97^{a}	1.68 ± 0.14^{a}
C				
DS	18.76 ± 0.26^{abc}	27.09 ± 0.51^{c}	23.15 ± 0.89^{a}	1.29 ± 0.14^{a}
CL	20.55 ± 0.37^{a}	24.23 ± 0.44^{b}	23.39 ± 0.90^{a}	1.28 ± 0.14^{a}
CK	18.17 ± 0.42^{bc}	26.33 ± 0.14^{c}	23.09 ± 0.86^{a}	1.22 ± 0.13^{a}

Different letters in the same column indicate statistical differences at $P < 0.05$. ST, soil temperature; SM, soil moisture; AT, air temperature; VPD, vapor deficit; CK, control; DS, dry standing; Cl, clipped.

ecosystem and atmosphere. The flux tower was positioned more than 800 m from the boundaries of GE and C.

The study area was set up using a randomized block design. Within each type of land use, there were four replicate blocks (3.5 m × 3.5 m with 5 m space between blocks). Four 1 m × 1 m plots were randomly arranged within each block, with 1.5 m between plots. Two weeks before observation began, one plot in each block (DS) was randomly selected and sprayed with herbicide (41% glyphosate, diluted with water 150 times). All vegetation in these plots withered in 2 days, but the canopy remained standing and dry throughout the observation period. Another plot in each block (CL) was chosen in which the aboveground tissue was removed by clipping, following the procedure used in previous studies [20, 23]. The third randomly selected plot in each block served as the control plot (CK) to which no further treatment was administered. The fourth plot was used for destructive sampling to determine the community characteristics of each block, including above/belowground biomass, leaf area index (LAI), and soil properties.

For determination of ET, we found that the herbicide method (DS) resulted in shading and surface roughness more similar to the control plots (CK) than the commonly used clipping method [20, 23] (CL), providing more realistic evaporation and microclimate conditions. Thus, the DS method provides a more accurate determination of ecosystem E, consequently improving the accuracy of separating T from ET. This method assumes that transpiration in herbicide-sprayed plots (DS) was completely suppressed by withering of all living plant tissues. Thus, vapor exchange in DS plots would mainly come from earth surface evaporation (E). Plant transpiration (T) was calculated by subtracting E in the DS treatment from ET in the control. Of the different observational methods to partition the components of soil evaporation (E) and canopy transpiration (T) from ecosystem ET, our approach appears to be the most accurate, as it disturbs the original environmental conditions the least (Table 1) and avoids the influence of air advection or large eddies [15, 18, 23].

2.3. Vapor Flux Measurements. Two weeks before observations began, a square metal base rim (50 cm × 50 cm in area, 10 cm in height with 3 cm aboveground) was installed in each of the three types of observed plot (CK, CL, and DS) for the measurement of the vapor exchange rate. The vapor exchange rate was determined by a cubic chamber (50 cm × 50 cm × 50 cm) attached to an infrared gas analyzer (IRGA, LI-6400, LiCor, Lincoln, NE, USA). When measurements commenced, thirty consecutive recordings of vapor concentrations were taken for each placed chamber at 1 s intervals during 30 s periods. H_2O flux rates were calculated from the time courses of changing concentrations. The fluxes of E were directly determined in the treatments of DS, and the fluxes of ET were determined in CK plots. This static-chamber method has been used and validated in previous studies [23]. One temperature probe at the center measured air temperature (AT) and another pushed into the soil aside the chamber measured soil temperature (ST) at 5 cm depth. The soil moisture (SM) was measured with a portable soil moisture device (TDR100, Spectrum, Plainfield, IL, USA).

The water exchange ET and E rates were calculated based on the formula [20, 23]

$$F_h = \frac{1000 V P_{\text{av}}}{RS\left(T_{\text{av}} + 273\right)} \times \frac{dc}{dt}, \tag{1}$$

where F_h is H_2O flux (mmol m^{-2} s^{-1}, positive F_h values represent ecosystem vapor release and negative represent vapor condensation); V is the chamber volume (m^3), P_{av} is the average pressure (kPa), R is the ideal gas constant (8.314 J mol^{-1} K^{-1}), S is the surface area covered by chamber (m^2), T_{av} is the average temperature (°C) during the measurement, and dc/dt is the slope of linear least squares regression of H_2O concentration by time.

The transpiration rate (T) was calculated by the difference between ET and E:

$$\text{T} = \text{ET} - \text{E}. \tag{2}$$

Observations were conducted on clear sunny days during the peak in live grassland biomass (August). Observations

Table 2: Community characteristics of the three land uses.

Use pattern	Grazing (G)	Grazing exclusion (GE)	Cultivation to cropland (C)
Constructive species	*Stipa grandis*	*Stipa grandis*	*Triticum aestivum*
Average cover (%)	56.3 ± 2.4^a	95.0 ± 2.0^b	93.8 ± 1.25^b
Average height (cm)	14.75 ± 0.95^a	56.25 ± 5.54^b	89.0 ± 1.29^c
Soil organic carbon (g/kg)	11.98 ± 1.73^a	15.10 ± 1.89^b	19.77 ± 1.05^c
Soil bulk density (g/cm^3)	1.63 ± 0.02^a	1.37 ± 0.06^b	1.29 ± 0.02^b
Leaf area index (LAI)	0.42 ± 0.03^a	0.68 ± 0.05^a	1.33 ± 0.13^b
Total biomass (kg $*$ s^{-1})	2.04 ± 0.14^a	3.01 ± 1.38^b	1.02 ± 0.06^c
Above/underground biomass (%)	3.73 ± 0.20^a	5.95 ± 0.29^b	64.50 ± 2.24^c
C4 total biomass (%)	32.98 ± 1.70^a	6.10 ± 2.26^b	0^c
Litter fall (g/m^2)	1.60 ± 0.55^a	84.81 ± 4.47^b	10.98 ± 1.00^c
Species abundance (S)	7.25 ± 0.63^a	4.00 ± 0.41^b	2.25 ± 0.25^c

Mean ± standard; the different letters in the same row signify significant changes between them ($P < 0.05$).

were conducted continuously through the day at 1-hour intervals over 12 days. During each day, measurements were taken within one land use type to ensure similar weather conditions within an ecosystem to maintain comparability of data. Thus each land use or ecosystem type (C, G, and GE) had 4 replicate days of observation.

Daily vapor exchange (E, T, and ET) in each of the three ecosystems was calculated from the H_2O flux rates obtained with the portable infrared gas analyzers using the following equation:

$$\text{Daily water exchange} = \int_{0:00}^{24:00} F_h * 18 * 10^{-6} \left(\text{kg } H_2O\right), \tag{3}$$

where F_h is the H_2O flux (mmol m^{-2} s^{-1}, positive F_h values represent ecosystem vapor release and negative values represent vapor uptake).

2.4. Measurement of Community Characteristics. Species composition, average height, and plant cover were measured in the 12 observational plots in each of the three different land uses of steppe (G, GE, and C). Aboveground biomass was measured with the clipping method, and underground biomass was measured with the root drill method [4]. LAI was measured using the method proposed by Miao et al. [8].

2.5. Data Analysis. Origin 8.0 was used for figure drawing and SPSS 12.0 was used for data analysis. Three one-way ANOVAs followed by Duncan tests were used to analyze the differences of ecosystem microclimates and community and soil characteristics among the three land uses. Paired t-tests compared the diurnal dynamics of ecosystem vapor exchange within each of the three types of land use. One-way ANOVAs and Duncan tests analyzed the mean daily accumulated E, T, and ET among the three land uses. Linear regression analysis compared the consistency of ET measurements between the eddy covariance system and the portable infrared chamber method. Linear regression analysis was used to evaluate the relationships of ET and its composition E/ET on environmental factors.

3. Results

3.1. Microclimate and Community Characteristics of Land Use Types. Soil temperature of G was significantly higher than that of GE. At 2.5% less than GE and 4.42% less than C, G had the lowest soil moisture (Table 1). Land use also significantly affected soil condition but had little effect on aerial microclimate factors including temperature and VPD. Clipping did not cause marked microclimate change in G blocks, but, in GE and C blocks, CL plots had increased temperatures and reduced soil moisture relative to CK plots (Table 1). There were no significant differences of microclimate factors between paired DS and CK plots.

Land use pattern substantially influenced the grassland community characteristics. Total biomass in C and G was significantly lower than in GE (Table 2). The proportion of the aboveground biomass and biomass of C4 plants also varied significantly among the three types of land use (Table 2). Litter fall was significantly higher in GE than in G or C. The LAI was the lowest in G, with 300% higher LAI in C and 62% higher in GE (Table 2). The influence of land use on soil properties was visible in the soil organic carbon (Table 2, $P < 0.05$) and bulk density.

3.2. Components of ET in Response to Different Land Uses. The daily dynamics of E, T, and ET among the different land uses of grassland steppe were generally represented by a unimodal curve that peaked around midday (Figures 3(a)–3(c)), although a minor midday depression in T (Figure 3(b)) may have driven a similar trend in ET (Figure 3(c)).

GE and C both tend to increase the average daily ET of the grazed steppe, which was 3.30 kg m^{-2} d^{-1} (Figure 4). Cultivation significantly increased ecosystem ET 13.4% over that of grazed steppe (3.74 kg m^{-2} d^{-1}; $P < 0.05$), whereas the change in grazing exclusion (3.52 kg m^{-2} d^{-1}; $P < 0.05$) was not significant.

Land use type did not significantly affect T ($P > 0.05$) but increased rates of E relative to C in G and GE (24.3% and 40.2%, resp.) ($P < 0.05$). Consequently, variation in E was the driving cause of differences in ET among the three grassland uses (Figures 3(a) and 4(a)). The proportion of

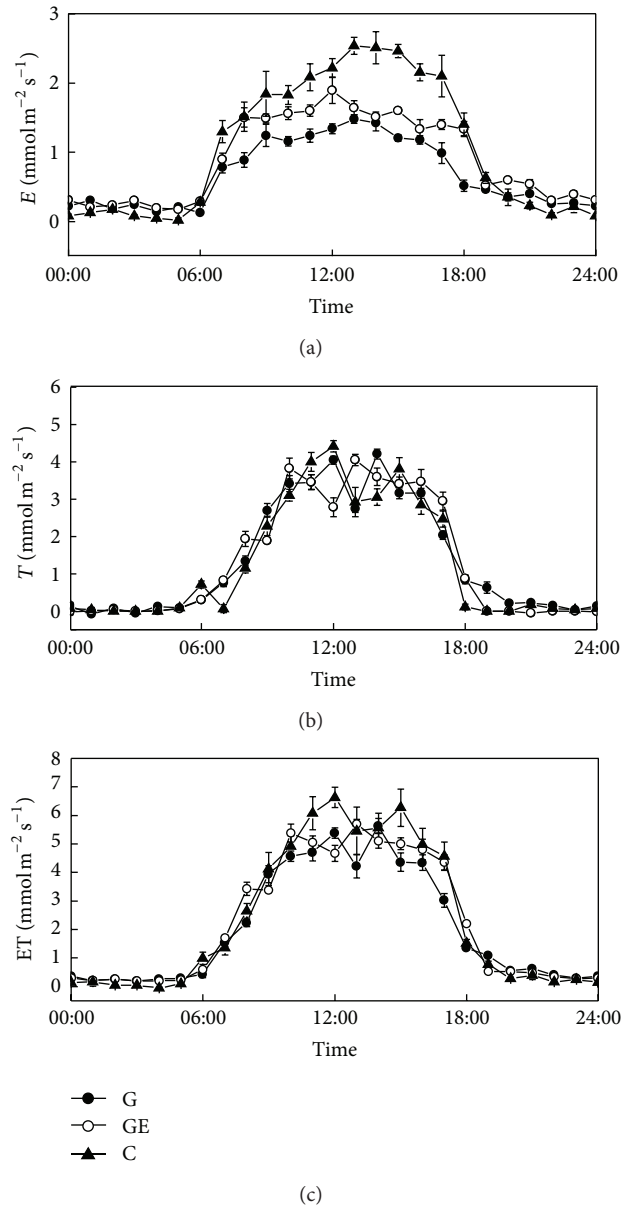

Figure 3: Daily dynamics of vapor exchange composition of different land uses during the peak growing period. (a) Evaporation (E); (b) transpiration (T); (c) evapotranspiration (ET). Error bar was 1 SE. G; grazing; GE, grazing excluded; C, crop.

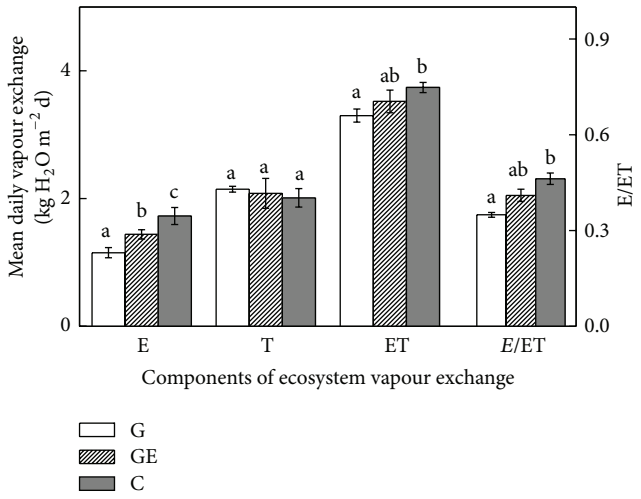

Figure 4: Compositions of mean daily ecosystem vapor consumption (E, T, ET, and E/ET) for different steppe grassland uses. The values represent the daily mean values (means ± 1 SE) in the peak growing period. Different letters in each bar group indicate significant difference ($P < 0.05$). G, grazing; GE, grazing excluded; C, crop.

evaporation to total vapor consumption (E/ET, Figure 4) of C was significantly increased in comparison with G ($P < 0.05$).

3.3. Relationships between Components of ET and Microclimate Factors. The components (E, T) of total ecosystem vapor consumption (ET) were significantly correlated with AT and VPD among different grassland uses (Figures 5(a)–5(f), $P < 0.001$). AT explained a large proportion of the variance in ET among the types of steppe land uses (Figure 5(a), 81–83%).

Variation among the grassland uses in sensitivity of the components of ET to microclimate factors was reflected by differences in their regression slopes. The sensitivity of T to VPD (Figure 5(f), 0.14–0.16) and AT (Figure 5(c), 1.20–1.31) did not differ substantially among the three land uses. However, crop cultivation increased the sensitivity of E to AT by 160% relative to grazed steppe (Figure 5(b)). Moreover, in GE and C plots, the slope of the regression of E to VPD was 1.4 and 3.3 times that of grazed plots, respectively (Figure 5(e)). The differential sensitivity of E led to a variable overall response of ET to VPD and AT among the three grassland uses. ET responded more strongly to AT (Figure 5(a)) and VPD (Figure 5(d)) in cultivated plots than grazed or grazer exclusion plots.

3.4. Relationships between Components of ET and Community Traits. Variation in each of the community traits (aboveground biomass, LAI, soil bulk density, and mean soil moisture) was significantly linearly correlated with mean daily vapor consumption by E and ET among different patterns of grassland use (Figure 6, all $P < 0.01$). In particular, a large proportion of the variance in both ET and E were explained by LAI (78–87%) and soil moisture (89–90%). Trends of linear correlation between ET and biomass, LAI, soil bulk density, and soil moisture were consistent with those of E. There were no significant relationships between T and aboveground biomass, LAI, soil bulk density, or soil moisture (Figure 6, $P > 0.05$).

3.5. Mechanisms Underlying Variance in E/ET among Steppe Grassland Uses. Linear correlations between mean daily vapor consumption and mean daily E/ET were significant for both E (Figure 7(a), $P < 0.001$) and T (Figure 7(b), $P < 0.05$), though the relationship was stronger for E. Additionally, mean daily water consumption by E explained

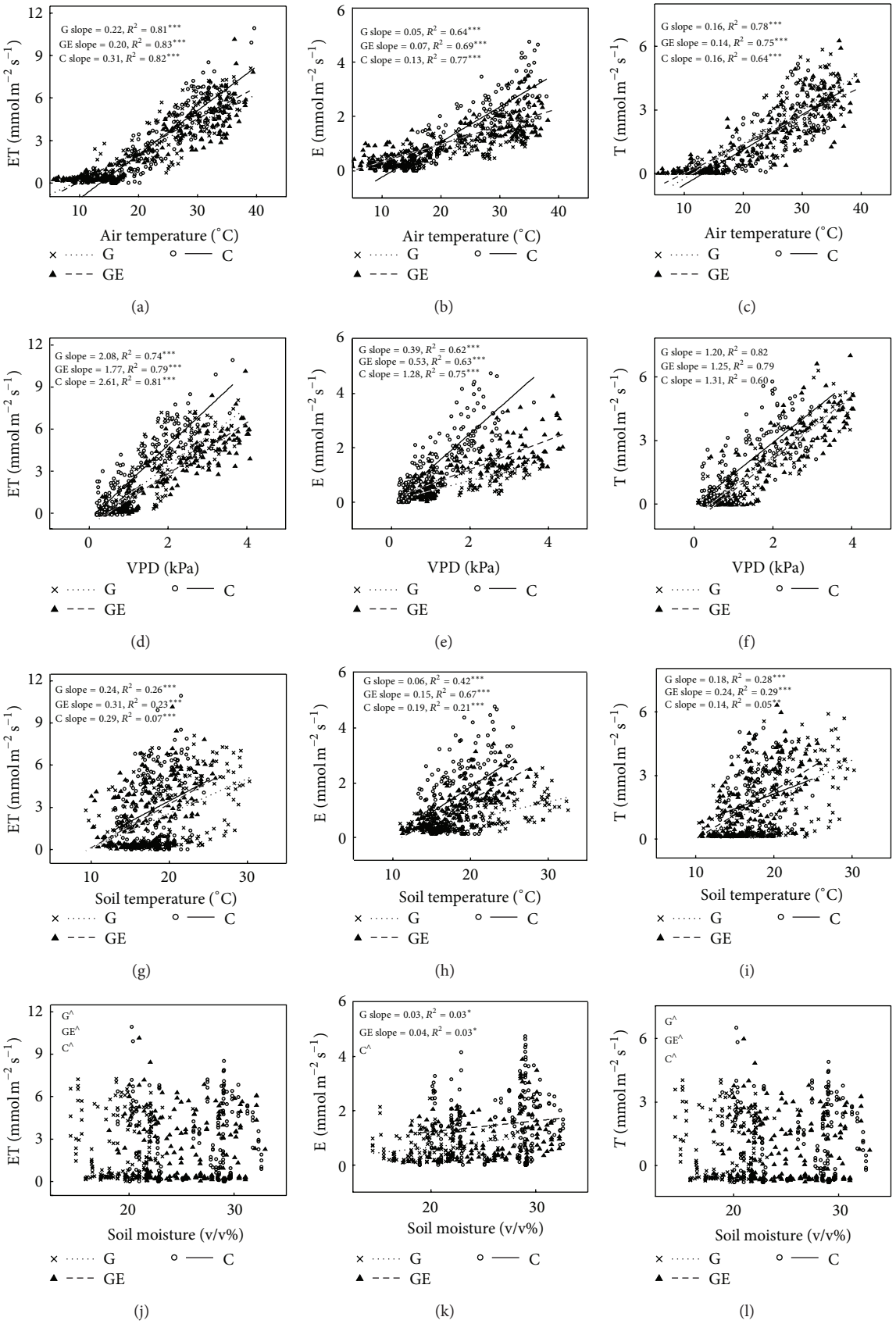

Figure 5: Relationships between microclimate factors (AT, VPD, ST, and SM) on vapor exchange rates (ET, E, and T) across the three land uses of steppe. R^2 and probabilities of regressions are shown; $^{\wedge}P > 0.05$; $^{*}P < 0.05$; $^{**}P < 0.01$; $^{***}P < 0.001$. G, grazing; GE, grazing excluded; C, crop.

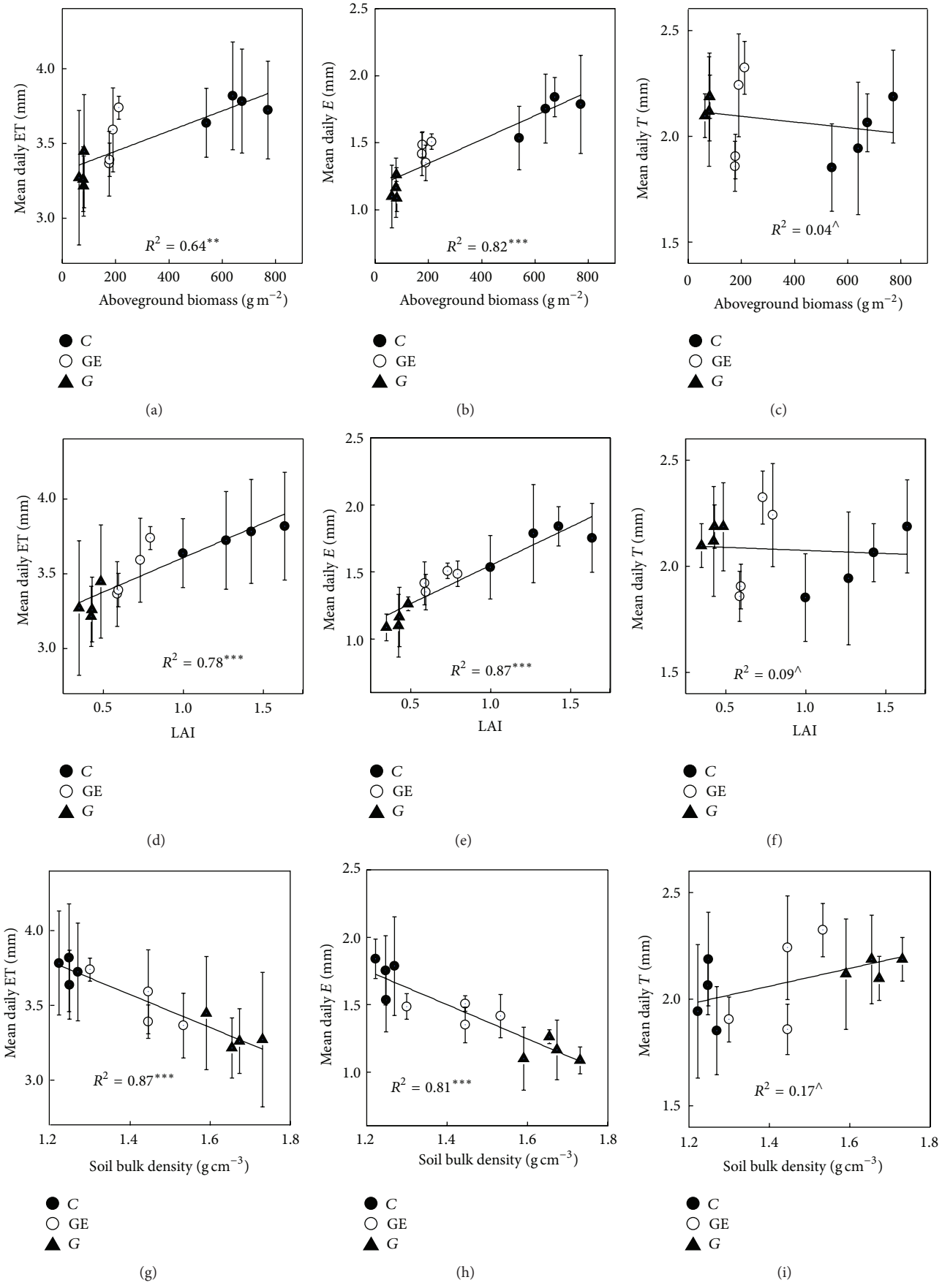

Figure 6: Continued.

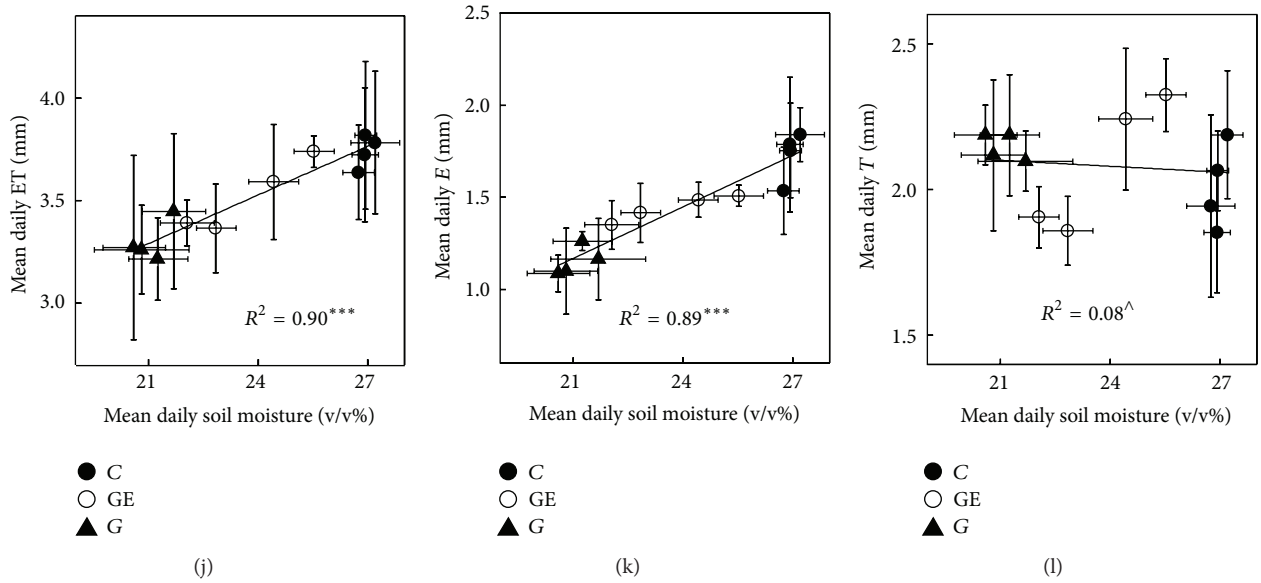

Figure 6: Relationships between mean daily water consumption components (E, T, and ET) on aboveground biomass, leaf area index (LAI), soil bulk density, and soil moisture across the three different steppe land uses. Error bar in WUE was 1 SE. R^2 and probabilities of regressions are shown; $^{\wedge}P > 0.05$; $^{*}P < 0.05$; $^{**}P < 0.01$; $^{***}P < 0.001$. G, grazing; GE, grazing excluded; C, crop.

three times more variance in E/ET than T (90% versus 30%). LAI (Figure 7(c)) and soil moisture (Figure 7(d)) were also positively correlated with E/ET, while the relationship between LAI and soil moisture depended on the level of LAI. When LAI was less than 1, soil moisture was positively linearly correlated with LAI, but values of LAI larger than 1 did not stimulate corresponding increases in soil moisture (Figure 7(e)).

4. Discussion

4.1. Effect of Grassland Use Types on the Components of ET. Because ecosystem ET takes away heat from the earth surface through latent heat transport, variation in ET with different grassland uses may alter the energy budget and consequently affect the regional climate [8]. ET rates determined by converted latent heat measurements taken by the eddy covariance system were highly correlated with ET rates measured using the chamber method (Figure 8, $P < 0.01$), confirming the reliability of chamber-measured vapor exchange rates. In addition, our measurements of ET rates in the three different patterns of grassland use were comparable to relevant previous work and modeled data for adjacent areas [1, 8, 26]. Though the chamber-measured ET rates were highly correlated with eddy covariance methods, yet there are uncertainties, which are caused by the measurement devices, in ET compositions (E and T). The certain deviation in this method is due to the chamber. Since the chamber blocked the natural wind, this should cause underestimate of surface E and lead to a certain overestimate of T rates.

Previous research has shown that different land uses can significantly change community structure [27, 28], soil properties [29, 30], and microclimate conditions [31–33], which may be correlated with ecosystem vapor exchange [34–37]. Consistent with this previous work [8, 24], our study demonstrated that cultivation and exclusion of grazing increased ET, the total vapor consumption of an ecosystem. Our examination of the individual components of ET revealed that it was evaporation (Figure 4, $P < 0.05$), not transpiration (Figure 4, $P > 0.05$), that caused the variance in ET among the different land uses of the steppe (Figure 4, Figure 6). Although few previous experimental studies in grassland ecosystems have separated ET into E and T [25], a study doing so in an agricultural ecosystem also found that changes in E were more important than those in T in driving patterns of ET, among different crop species [24].

Despite the suggestion of previous large-scale studies including cross regional simulations [26, 37] and long-term observations [8] that vegetation with higher LAI should have lower E/ET, our findings corroborated those of another regional study [24], showing that E/ET was higher in land use types with higher LAI in adjacent areas (Figure 4). These contrasting results demonstrate that the components of ET may respond variably to increases in LAI depending on the spatial and temporal scale of the study. The positive relationship between E/ET and LAI in our study (Figure 7(c)) may be owing to the shading effect of redundant LAI. During the peak growing season, when LAI reaches its maximum, an individual plant in any grassland use type has redundant leaves which are shaded by those newer and higher leaves of its own. Thus, in those land uses with higher LAI, the increase of LAI just enhanced the shading; ineffective leaves would not contribute substantially to an increase in canopy T. In contrast, increased shading in communities with a larger LAI would result in higher soil moisture. In arid and semiarid areas, where water supply is a limiting factor of E [26], increased soil moisture would stimulate higher rates of surface E.

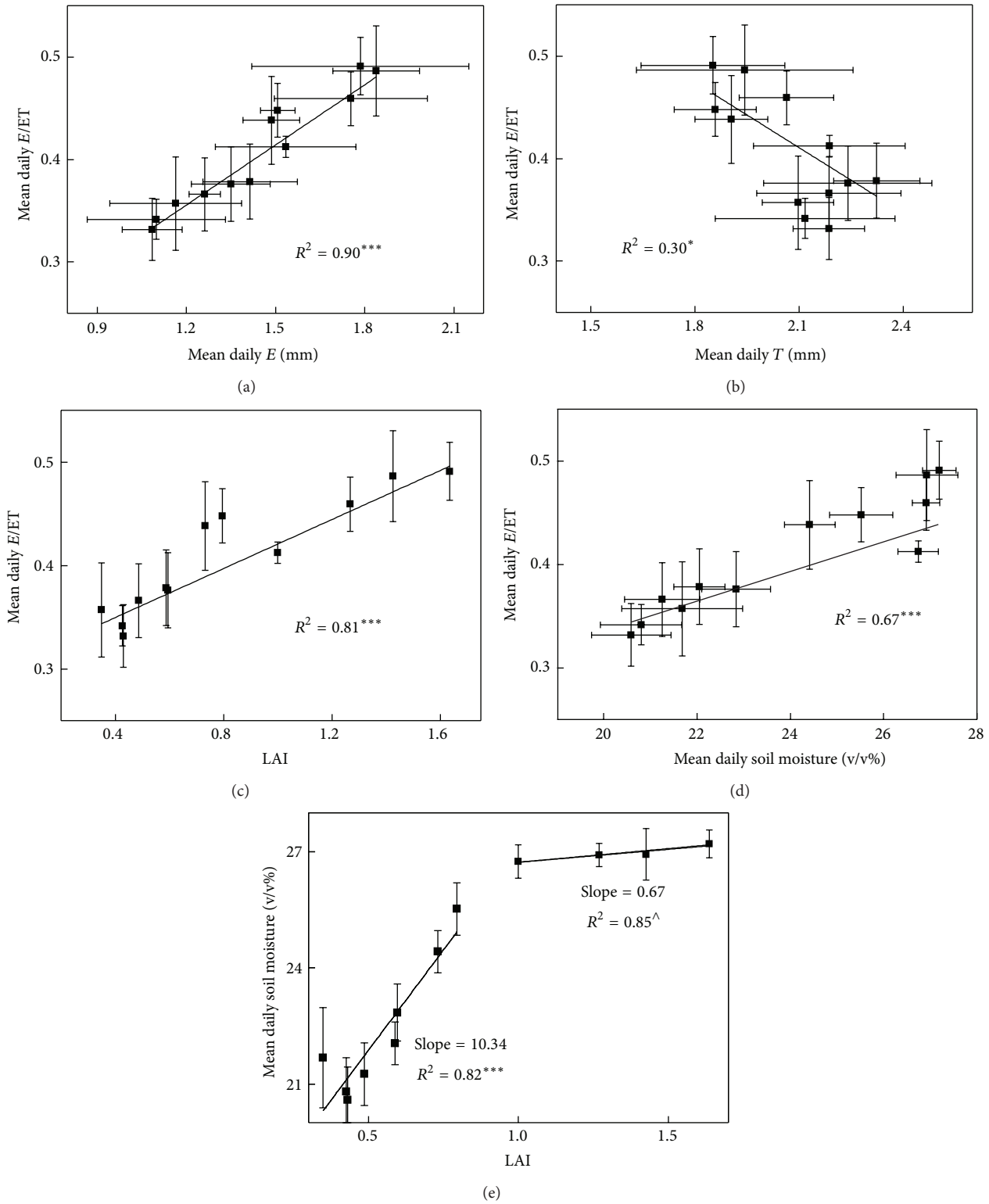

Figure 7: Relationships between mean daily E/ET and mean daily (a) E, (b) T, (c) LAI, and (d) soil moisture and (e) the relationship between LAI and mean daily soil moisture. $^{\wedge}P > 0.05$; $^{*}P < 0.05$; $^{**}P < 0.01$; $^{***}P < 0.001$.

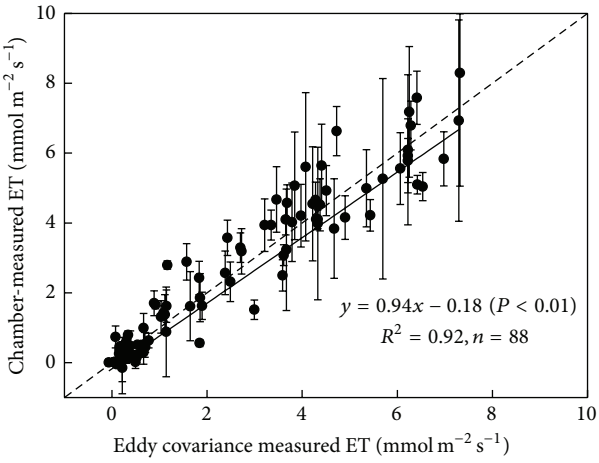

Figure 8: Comparison of the ecosystem vapor exchange (ET) obtained by the chamber method and the eddy covariance system. Data were obtained from the eddy covariance system located in the center of grazed grassland (G).

Relative to grazed areas, grazer exclusion and cultivation both tended to increase ecosystem ET (Figure 4), which facilitates water transfer from the grassland to the atmosphere. Despite similar effects on ET, these two patterns of grassland use (GE, C) may have differing effects on regional climate. Elevated rates of ET would increase regional precipitation in both types of systems, but the larger mass of accumulated litter in grasslands with grazers excluded (Table 2) would increase rainfall absorption and infiltration, reducing water loss by overflow and evaporation. In contrast, without accumulated litter (Table 2), lower rainfall infiltration in cultivated steppe [8] would reduce ground water supplementation, and ground water may eventually be exhausted by elevated vapor loss (Figure 4). Thus, long-term cultivation of steppe may intensify drought and cause damage to regional ground water stores, whereas grazer exclusion may increase soil moisture content sustainably, with corresponding effects on regional climate through increased precipitation and humidity.

4.2. Factors Driving the Variation of Components of ET among Patterns of Grassland Use. In arid and semiarid areas, soil water content is a key factor controlling vapor loss [8, 23], and previous studies have shown that soil moisture is closely related to ET and E [20, 23, 31]. Similarly, in this study, variation in soil moisture among different land uses explained 90% and 89% of the mean daily ET (Figure 6(j)) and E (Figure 6(k)), respectively. Additionally, we found that soil moisture variation among patterns of grassland use may be caused by changes in LAI with land use (Table 2). This was demonstrated by strong positive relationships of LAI and soil moisture (Figure 7(e)), where LAI explained 95% of soil moisture variation, and may also underlie the close correlations of LAI with ET (Figure 6(d)) and E (Figure 6(e)). Furthermore, significant relationships of ET and E with aboveground biomass and soil bulk density may be because these community traits are inherently related to LAI (Figure 6). In contrast to previous work conducted on large spatial and temporal scales [26, 31], we found no significant relationships between LAI and T (Figure 6(f)). Comparison of these studies with our work and similar findings in an agricultural system [24] suggest that the influence of LAI on vapor consumption may vary with scale.

Few studies have been conducted on the daily dynamics and controlling factors of ecosystem ET and its components. At the large spatial and temporal scale, evidence suggests that change in ET may be closely related to some microclimate factors and soil traits, such as VPD, air temperature, soil temperature, and soil moisture [23, 26, 31]. Consistent with previous conclusions, we found that VPD and air temperature were significantly related to ET, E, and T (Figure 5). In particular, AT explained 80% of the variation in ET rates among varied land uses (Figure 5(a)). However, unlike previous studies [23, 31], changes in soil temperature and moisture were not correlated with E and T (Figure 5). Instead, we suggest that soil moisture may contribute to vapor exchange regulation indirectly. Since soil water supply ability varies with soil moisture, we assumed that soil moisture may be the primary factor controlling the regression slope of E and ET with AT and VPD under different grassland use patterns.

E/ET, the contribution of E (rather than T) to total ecosystem vapor consumption (ET) [24, 38], is an important trait of water vapor exchange and the ecosystem in general [39]. Measurements of E/ET in this study (approximately 0.4, Figure 4) were comparable with those obtained by modeling [37] and experimental observation [31] in similar ecosystems. Variation in mean daily E (Figure 7(a)) and T (Figure 7(b)) both significantly affected E/ET, although E explained three times more variation in E/ET than T. Thus, variation in surface vapor consumption (E) was more important in controlling patterns of E/ET among grassland use types. Moreover, because soil moisture directly regulates E [10], soil moisture was also significantly positively related to E/ET (Figure 7(d)). Finally, change in LAI with varying patterns of land use was a significant predictor of soil moisture (Figure 7(e)), which is similar to Xu et al.'s result [32]. Consequently, LAI explained 81% of the variation in E/ET (Figure 7(c)). These results corroborate the conclusions of a previous modeling study [26] that LAI is a primary community characteristic involved in regulation of the components of ecosystem ET.

5. Conclusions

Land use changes in grasslands of temperate steppe ecosystems, such as cultivation and grazing exclusion, may significantly influence vegetation and soil properties as well as some microclimate factors. Thus, variation in grassland use may have large effects on the vapor budget. Our results indicated that grassland cultivation and grazing exclusion both tend to increase ecosystem ET, with a significant increase in cultivated steppe. Differential litter accumulation and resultant infiltration of rainfall to ground water among grassland uses suggest that large-scale cultivation may intensify aridity of the

steppe area in Northern China, while the grazing exclusion may gradually alleviate local arid conditions. Division of ET into its components indicated that changes in ET in cultivated and grazer excluded grassland were primarily caused by elevated E, while T did not increase significantly. Through shading, variation in LAI with land use type substantially influenced the soil moisture, thus acting as a key regulator of E and even ET and E/ET in the ecosystem. Consequently, LAI is the primary regulating factor of the magnitude and composition of grassland-atmosphere vapor exchange under different grassland uses. These observed results would help reduce the uncertainty of relevant models in simulating ET and the surface energy budget and provide significant reference for the land use management to alleviate the climate change.

Conflict of Interests

The authors declare that there is no conflict of interests regarding the publication of this paper.

Acknowledgments

This research was jointly funded by the State Key Technologies R&D Program (Grant no. 2013BAC03B04), the Natural Sciences Foundation of China (41301043), the Funding for Talent Young Scientists of IGSNRR (2013RC203), and the National "973" Project (no. 2010CB950902). In addition, the authors thank Dr. Ning Jia for her help in improving their figures, as well as the editor and two anonymous reviewers for their constructive comments, which helped them to improve the paper.

References

[1] S. Chen, J. Chen, G. Lin et al., "Energy balance and partition in Inner Mongolia steppe ecosystems with different land use types," *Agricultural and Forest Meteorology*, vol. 149, no. 11, pp. 1800–1809, 2009.

[2] IPCC, *Climate Change 2007: The Physical Science Basis*, Contribution of Working Group I to the Fourth Assessment Report of the Intergovernmental Panel on Climate Change, edited by S. Solomon, D. Qin, M. Manning, Z. Chen, M. Marquis, K. B. Averyt, M. Tignor and H. L. Mille, Cambridge University Press, Cambridge, UK, 2007.

[3] J. Liu, M. Liu, D. Zhuang, Z. Zhang, and X. Deng, "Study on spatial pattern of land-use change in China during 1995–2000," *Science in China, Series D: Earth Sciences*, vol. 46, no. 4, pp. 373–384, 2003.

[4] Y.-Z. Li, J.-W. Fan, L.-X. Zhang, J. Di, G.-F. Liu, and J. Li, "The impact of different land use and management on community composition , species diversity and productivity in a typical temperate grassland," *Acta Pratacultuae Sinica*, vol. 22, no. 1, pp. 1–9, 2013.

[5] L. Jiyuan and B. Aoser, "Study on spatial-temporal feature of modern land use change in China: using remote sensing techniques," *Quaternary Sciences*, vol. 20, no. 3, pp. 229–239, 2000.

[6] W. Tao, "Land use and sandy desertification in the north China," *Journal of Desert Research*, vol. 20, no. 2, pp. 103–107, 2000.

[7] R. Lal, "Land use and soil management effects on soil organic matter dynamics on Alfisols in Western Nigeria," in *Soil Processes and the Carbon Cycle*, pp. 109–126, CRC Press, Boca Raton, Fla, USA, 1997.

[8] H. Miao, S. Chen, J. Chen et al., "Cultivation and grazing altered evapotranspiration and dynamics in Inner Mongolia steppes," *Agricultural and Forest Meteorology*, vol. 149, no. 11, pp. 1810–1819, 2009.

[9] J. M. Wraith, D. A. Johnson, R. J. Hanks, and D. V. Sisson, "Soil and plant water relations in a crested wheatgrass pasture: response to spring grazing by cattle," *Oecologia*, vol. 73, no. 4, pp. 573–578, 1987.

[10] W. Bai, S. Wan, S. Niu et al., "Increased temperature and precipitation interact to affect root production, mortality, and turnover in a temperate steppe: implications for ecosystem C cycling," *Global Change Biology*, vol. 16, no. 4, pp. 1306–1316, 2010.

[11] Y. Bai, J. Wu, Q. Xing et al., "Primary production and rain use efficiency across a precipitation gradient on the Mongolia plateau," *Ecology*, vol. 89, no. 8, pp. 2140–2153, 2008.

[12] L. A. Wever, L. B. Flanagan, and P. J. Carlson, "Seasonal and interannual variation in evapotranspiration, energy balance and surface conductance in a northern temperate grassland," *Agricultural and Forest Meteorology*, vol. 112, no. 1, pp. 31–49, 2002.

[13] D. D. Baldocchi, L. Xu, and N. Kiang, "How plant functional-type, weather, seasonal drought, and soil physical properties alter water and energy fluxes of an oak-grass savanna and an annual grassland," *Agricultural and Forest Meteorology*, vol. 123, no. 1-2, pp. 13–39, 2004.

[14] D. J. Bremer, L. M. Auen, J. M. Ham, and C. E. Owensby, "Evapotranspiration in a prairie ecosystem: effects of grazing by cattle," *Agronomy Journal*, vol. 93, no. 2, pp. 338–348, 2001.

[15] D. G. Williams, W. Cable, K. Hultine et al., "Evapotranspiration components determined by stable isotope, sap flow and eddy covariance techniques," *Agricultural and Forest Meteorology*, vol. 125, no. 3-4, pp. 241–258, 2004.

[16] L. B. Hutley, A. P. O'Grady, and D. Eamus, "Monsoonal influences on evapotranspiration of savanna vegetation of northern Australia," *Oecologia*, vol. 126, no. 3, pp. 434–443, 2001.

[17] J. F. Reynolds, P. R. Kemp, and J. D. Tenhunen, "Effects of long-term rainfall variability on evapotranspiration and soil water distribution in the Chihuahuan Desert: a modeling analysis," *Plant Ecology*, vol. 150, no. 1-2, pp. 145–159, 2000.

[18] C. Liu, X. Zhang, and Y. Zhang, "Determination of daily evaporation and evapotranspiration of winter wheat and maize by large-scale weighing lysimeter and micro-lysimeter," *Agricultural and Forest Meteorology*, vol. 111, no. 2, pp. 109–120, 2002.

[19] D. D. Baldocchi, "Assessing the eddy covariance technique for evaluating carbon dioxide exchange rates of ecosystems: past, present and future," *Global Change Biology*, vol. 9, no. 4, pp. 479–492, 2003.

[20] S. Chen, G. Lin, J. Huang, and G. D. Jenerette, "Dependence of carbon sequestration on the differential responses of ecosystem photosynthesis and respiration to rain pulses in a semiarid steppe," *Global Change Biology*, vol. 15, no. 10, pp. 2450–2461, 2009.

[21] R. L. Scott, T. E. Huxman, W. L. Cable, and W. E. Emmerich, "Partitioning of evapotranspiration and its relation to carbon dioxide exchange in a Chihuahuan Desert shrubland," *Hydrological Processes*, vol. 20, no. 15, pp. 3227–3243, 2006.

[22] L. B. Flanagan, E. J. Sharp, and M. G. Letts, "Response of plant biomass and soil respiration to experimental warming and precipitation manipulation in a Northern Great Plains grassland," *Agricultural and Forest Meteorology*, vol. 173, pp. 40–52, 2013.

[23] S. Niu, X. Xing, Z. Zhang et al., "Water-use efficiency in response to climate change: from leaf to ecosystem in a temperate steppe," *Global Change Biology*, vol. 17, no. 2, pp. 1073–1082, 2011.

[24] P. Béziat, V. Rivalland, T. Tallec et al., "Evaluation of a simple approach for crop evapotranspiration partitioning and analysis of the water budget distribution for several crop species," *Agricultural and Forest Meteorology*, vol. 177, pp. 46–56, 2013.

[25] D. Kool, N. Agam, N. Lazarovitch, J. L. Heitman, T. J. Sauer, and A. Ben-Gal, "A review of approaches for evapotranspiration partitioning," *Agricultural and Forest Meteorology*, vol. 184, pp. 56–70, 2014.

[26] Z. Hu, G. Yu, Y. Zhou et al., "Partitioning of evapotranspiration and its controls in four grassland ecosystems: application of a two-source model," *Agricultural and Forest Meteorology*, vol. 149, no. 9, pp. 1410–1420, 2009.

[27] P. Schönbach, H. Wan, M. Gierus et al., "Grassland responses to grazing: effects of grazing intensity and management system in an Inner Mongolian steppe ecosystem," *Plant and Soil*, vol. 340, no. 1-2, pp. 103–115, 2011.

[28] T. A. Day and J. K. Detling, "Water relations of *Agropyron smithii* and *Bouteloua gracilis* and community evapotranspiration following long-term grazing by prairie dogs," *The American Midland Naturalist*, vol. 132, no. 2, pp. 381–392, 1994.

[29] A. N. Nunes, A. C. de Almeida, and C. O. A. Coelho, "Impacts of land use and cover type on runoff and soil erosion in a marginal area of Portugal," *Applied Geography*, vol. 31, no. 2, pp. 687–699, 2011.

[30] F. Shi, H. Chen, Y. Wu, and N. Wu, "Effects of livestock exclusion on vegetation and soil properties under two topographic habitats in an alpine meadow on the eastern Qinghai-Tibetan Plateau," *Polish Journal of Ecology*, vol. 58, no. 1, pp. 125–133, 2010.

[31] S. Niu, M. Wu, Y. Han, J. Xia, L. Li, and S. Wan, "Water-mediated responses of ecosystem carbon fluxes to climatic change in a temperate steppe," *New Phytologist*, vol. 177, no. 1, pp. 209–219, 2008.

[32] X. Xu, R. A. Sherry, S. Niu, D. Li, and Y. Luo, "Net primary productivity and rain-use efficiency as affected by warming, altered precipitation, and clipping in a mixed-grass prairie," *Global Change Biology*, vol. 19, no. 9, pp. 2753–2764, 2013.

[33] S. Niu, H. Yang, Z. Zhang et al., "Non-additive effects of water and nitrogen addition on ecosystem carbon exchange in a temperate steppe," *Ecosystems*, vol. 12, no. 6, pp. 915–926, 2009.

[34] T. F. Keenan, D. Y. Hollinger, G. Bohrer et al., "Increase in forest water-use efficiency as atmospheric carbon dioxide concentrations rise," *Nature*, vol. 499, no. 7458, pp. 324–327, 2013.

[35] T. E. Huxman, M. D. Smith, P. A. Fay et al., "Convergence across biomes to a common rain-use efficiency," *Nature*, vol. 429, no. 6992, pp. 651–654, 2004.

[36] A. K. Knapp and M. D. Smith, "Variation among biomes in temporal dynamics of aboveground primary production," *Science*, vol. 291, no. 5503, pp. 481–484, 2001.

[37] Z. Hu, G. Yu, Y. Fu et al., "Effects of vegetation control on ecosystem water use efficiency within and among four grassland ecosystems in China," *Global Change Biology*, vol. 14, no. 7, pp. 1609–1619, 2008.

[38] W. K. Lauenroth and J. B. Bradford, "Ecohydrology and the partitioning AET between transpiration and evaporation in a semiarid steppe," *Ecosystems*, vol. 9, no. 5, pp. 756–767, 2006.

[39] C. Brümmer, T. A. Black, R. S. Jassal et al., "How climate and vegetation type influence evapotranspiration and water use efficiency in Canadian forest, peatland and grassland ecosystems," *Agricultural and Forest Meteorology*, vol. 153, pp. 14–30, 2012.

Hindawi Publishing Corporation
Advances in Meteorology
Volume 2015, Article ID 424291, 13 pages
http://dx.doi.org/10.1155/2015/424291

Research Article

Downscaling MODIS Surface Reflectance to Improve Water Body Extraction

Xianghong Che,[1,2] Min Feng,[3] Hao Jiang,[1] Jia Song,[1] and Bei Jia[2]

[1]*State Key Laboratory of Resources and Environmental Information System, Institute of Geographic Sciences and Natural Resources Research, Chinese Academy of Sciences, Beijing 100101, China*
[2]*College of Mining Engineering, Taiyuan University of Technology, Taiyuan 030024, China*
[3]*Global Land Cover Facility, Department of Geographical Sciences, University of Maryland, College Park, MD 20742, USA*

Correspondence should be addressed to Min Feng; fengm@umd.edu

Received 19 September 2014; Revised 29 December 2014; Accepted 20 January 2015

Academic Editor: R. B. Singh

Inland surface water is essential to terrestrial ecosystems and human civilization. Accurate mapping of surface water dynamic is vital for both scientific research and policy-driven applications. MODIS provides twice observation per day, making it perfect for monitoring temporal water dynamic. Although MODIS provides two bands at 250 m resolution, accurately deriving water area always depends on observations from the spectral bands with 500 m resolution, which limits its discrimination ability over small lakes and rivers. The paper presents an automated method for downscaling the 500 m MODIS surface reflectance (SR) to 250 m to improve the spatial discrimination of water body extraction. The method has been tested at Co Ngoin and Co Bangkog in Qinghai-Tibet plateau. The downscaled SR and the derived water bodies were compared to SR and water body mapped from Landsat-7 ETM+ images were acquired on the same date. Consistency metrics were calculated to measure their agreement and disagreement. The comparisons indicated that the downscaled MODIS SR showed significant improvement over the original 500 m observations when compared with Landsat-7 ETM+ SR, and both commission and omission errors were reduced in the derived 250 m water bodies.

1. Introduction

Inland surface water bodies include fresh and saline lakes, rivers, and reservoirs in the land. Although inland surface water only covers a small portion of global land, it is essential to terrestrial ecosystems and human civilization. For example, the distribution of surface water in space and its dynamic over time would greatly alter the Earth's surface conditions and influence the general circulation of the atmosphere [1, 2]. On the other hand, by influencing the hydrological cycle and water phase variability, variations in temperature and precipitation strongly affect lakes and glaciers. They would also impose some feedback on the climate system and affect the environment of human beings [3, 4]. Thus, the expansion and shrinkage of lakes are related to many environmental and ecological issues and are important factors that must be considered in human socioeconomic development [5]. Particularly, in the mountain regions, as the alpine hydrologic environment has been minimally disturbed by human activities, such as agricultural settlements and irrigation, the high altitude lakes are sensitive to the changes in air temperature, precipitation, snow-glacier melt, and soil frost degradation [6]. Because of the remoteness and inaccessibility of the lakes in mountain regions, remote sensing provides quick views of land from distance and has been proven to be the most effective way for mapping surface water in terms of spatial distribution and dynamic [7]. Data acquired from many remote sensing sensors, such as Landsat-5 TM (Thematic Mapper), Landsat-7 ETM+ (Enhanced Thematic Mapper Plus) and MODIS (Moderate Resolution Imaging Spectroradiometer), have been used for water mapping [8]. Although remote sensing data with higher spatial resolution (e.g., Landsat-5 TM and Landsat-7 ETM+) are able to delineate smaller water bodies, its long repeating time (16 days) limits it from

catching rapid water dynamic due to seasonal or extreme weather events, such as heavy rainfall [9]. The long repeating time also makes it difficult to observe the water body progress especially in cloudy areas due to its vulnerability to cloud contaminations [10]. Quick repeating remote sensing sensors, such as MODIS on board of Terra and Aqua, are able to catch water body changes precisely with their high temporal resolutions, making it particularly suitable for detecting water body dynamic for large areas [11]. The downside of MODIS is the low spatial resolution. MODIS has only two 250 m bands, but water bodies are usually detected at 500 m since they require Green or SWIR bands at 500 m resolution, unless combining other high resolution reference data. Ji et al. found that the Normalized Difference Water Index (NDWI) calculated from Green and SWIR with shorter wavelength region (1.2 to 1.8 um) had the most stable threshold to delineate surface water features [12]. Soti et al. suggested that among several water indices, two middle infrared-based indices (MNDWI—Modified Normalized Difference Water Index and NDWI) were most efficient for locating and monitoring temporary ponds in arid lands [13]. Another example is the production of the MODIS water mask data set (MOD44W) by combining MODIS 250 m bands and 90 m SRTM water body dataset [14]. However, previous studies have suggested that there are possible relationships between the 250 m bands and other 500 m MODIS bands, and such relationships can be used for improving the spatial resolution with MODIS data downscaled to 250 m. For example, Discrete Wavelet Transform (DWT) fusion method by decomposing high resolution images and inverse DWT was used to generate other related high resolution images. However, DWT fusion method had lower visual interpretation [15]. Trishchenko et al. proposed an adaptive regression model for every generic scene type (vegetation, desert/barren land, snow, water and cloud), relating MODIS band3–7 with band1, band2 and Normalized Difference Vegetation Index (NDVI) to obtain band3-7 SR at 250 m. The adaptive regression model was mainly built on MODIS MOD 02-Level-1B calibrated and geo-located at-aperture radiances product (MOD02HKM/MOD02QKM) without atmospheric conditions correction [16]. Therefore, to build an adaptive regression model, atmospheric correction aimed to adjust for atmospheric scattering and absorption effects and a generic land cover classification were needed, which required complicated processing steps and much time [17].

This paper presents a downscaling method based on the modified adaptive regression model towards extracting water bodies from MODIS SR at 250 m resolution. The method was applied to the MODIS image acquired in Co Ngoin and Co Bangkog in the Tibetan Plateau. Finally, we make comparison between the extracted water area at original 500 m, downscaled 250 m and water mask visually interpreted from Landsat-7 ETM+ data acquired on the same date.

2. Study Area and Data Sources

2.1. Study Area. The Qinghai-Tibet plateau (QTP) is located in central Asia, with an average elevation over 4,000 m and is called "the Third Pole" of the Earth and "Asian water tower" because of the thousands of lakes formed by water melted from the large glaciers in QTP [18]. Among all the lakes in QTP, Co Ngoin and Co Bangkog located in the center of the plateau is selected as the study area to represent the lakes in QTP, primarily because their complex shapes and shorelines are perfect for investigating the improvement after incasing the spatial discrimination (Figure 1). Both Co Ngoin (31°24′–31°32′N and 91°28′–91°33′E) and Co Bangkog (31°40′–31°47′N and 89°26′–89°39′E) are located in the basin of Selin. The area of Co Ngoin is 61.3 km^2 and supplied by rivers in its southwest. Average annual temperature in the lake catchment is −2.0~0.0°C, and the annual evaporation is around 1,000 mm. Annual precipitation fluctuates between 300 and 600 mm,. and more than 80% annual precipitation concentrates between May to September and falls mainly as hailstorms [19]. Co Bangkog is about 90 km^2 in area and the average annual temperature in the lake catchment is −2.0~ −1.0°C. The annual precipitation is 308.33 mm and the annual evaporation is around 2238.6 mm. More thunderstorms and hail concentrate in July and August [20]. In rainy seasons, regional continuous precipitation could result in the expansion and shrinkage of lake area over several days in QTP. For example, there was twice continuous precipitation in the period of both from August 31 to September 5th and from September 16 to 17 for Zhuonai lake, which led to the dramatic extension of lake area. After flooding, the area of Zhuonai lake declined steeply [21]. MODIS provides twice observation per day, making it particularly suitable for detecting water body rapid dynamic.

2.2. Data Sources. The MODIS sensor on the Terra and Aqua satellites has viewing swath width of 2,330 km and a revisit period of one day with 36 spectral bands ranging in wavelength from 0.4 μm to 14.4 μm. The sensor takes observations at R and NIR bands at a nominal resolution of 250 m at nadir, five bands at 500 m, and the remaining 29 bands at 1 km (Table 1) [22]. MOD09GA provides MODIS $B_{1–7}$ daily SR at 500 m resolution and 1 km observation and geo-location statistics. MOD09GQ provides MODIS $B_{1\text{-}2}$ daily SR at 250 m resolution in conjunction with the MOD09GA where important quality and viewing geometry information is stored [23]. The two products are distributed in the Sinusoidal (SIN) projection and HDF-EOS format. The global coverage of the datasets is divided into 648 tiles. The data were downloaded from http://modis.gsfc.nasa.gov/.

The Landsat-7 ETM+ image acquired on the same dates as MODIS data was collected for validating the results because: (1) The Terra MODIS and Landsat-7 are in the same orbit, with MODIS Terra nadir observations occurring approximately 15 min after Landsat-7 observations while the orbit of Landsat-5 is greatly different from MODIS Terra which may lead to disagreements on SR due to Bidirectional Reflectance Distribution Function (BRDF) effect [24]; (2) The MODIS bands have been proven to be comparable and strongly agree with the 6 Landsat-7 ETM+ multispectral bands [25] (Table 1). We only use the Landsat-7 ETM+ SR acquired before 2003 to avoid the scan-line corrector (SLC) off issue.

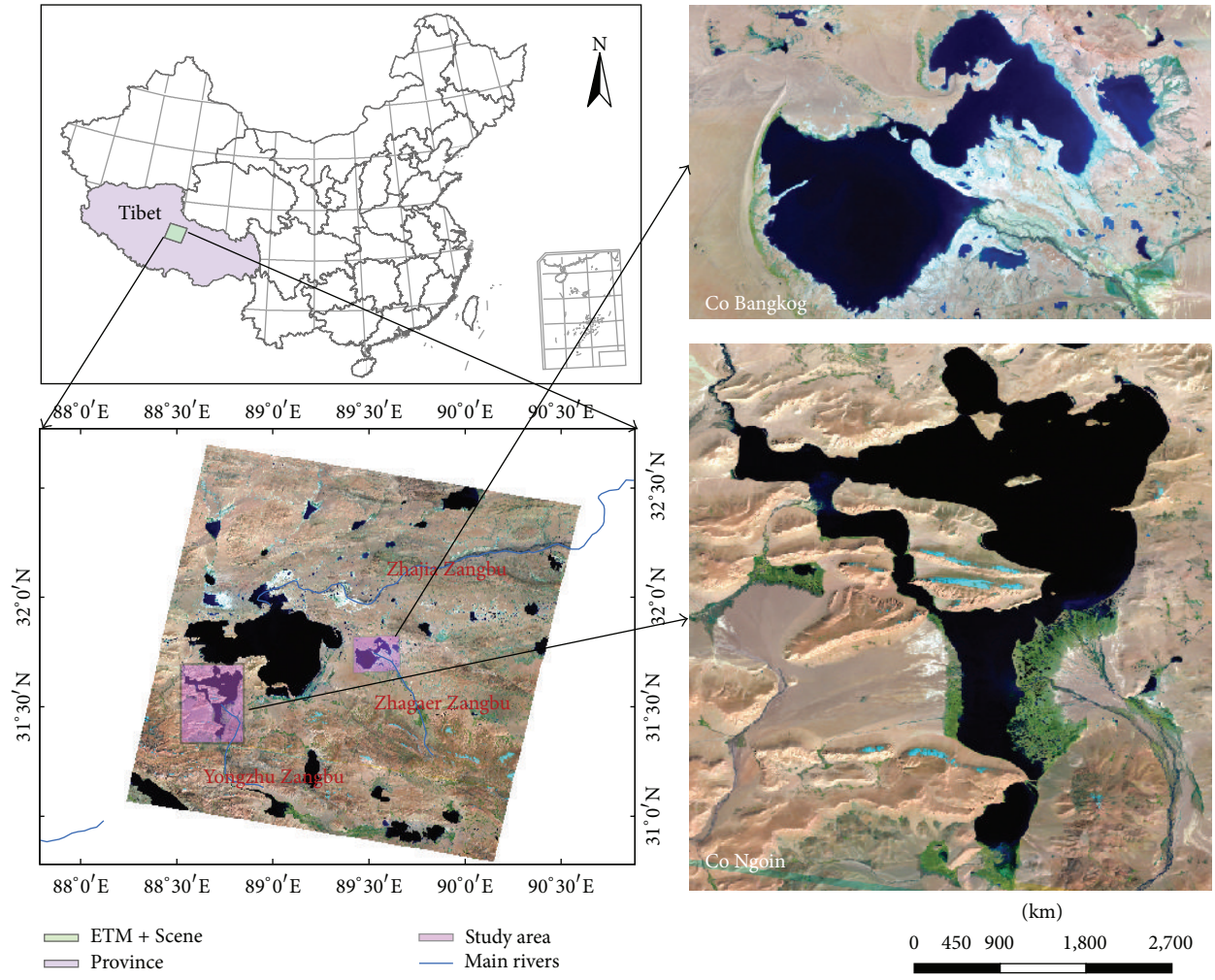

Figure 1: Locations of Co Ngoin and Co Bangkog (RGB543 TM image).

Table 1: Bands information comparison of MODIS[a] and Landsat-7 ETM+[b].

Acquisition date		7 October 2000				
Band	MODIS band	MODIS resolution (m)	MODIS bandwidth (nm)	Landsat-7 ETM+ Band	ETM+ resolution (m)	ETM+ bandwidth (nm)
R	1(B_1)	250	620–670	3	30	630–690
NIR	2(B_2)	250	841–876	4	30	780–900
B	3(B_3)	500	459–479	1	30	450–520
G	4(B_4)	500	545–565	2	30	530–610
SWIR1	6(B_6)	500	1628–1652	5	30	1550–1750
SWIR2	7(B_7)	500	2105–2155	7	30	2090–2350

[a] http://www.gscloud.cn/userfiles/file/MOD09_UserGuide.pdf.
[b] http://landsathandbook.gsfc.nasa.gov/pdfs/Landsat7_Handbook.pdf.

The coincident Landsat-7 ETM+ SR (http://www.landcover.org/data/gls_SR/), had been preprocessed by Landsat ecosystem disturbance adaptive processing system (LEDAPS, version 1.2.0) algorithm to compensate for atmospheric scattering and absorption effects [26].

3. Methodology

3.1. Downscaling Method. Based on the nonlinear correlation between MODIS B_3 to B_7 and B_1, B_2 and NDVI [27], a regression model is designed to calculate regression parameters for

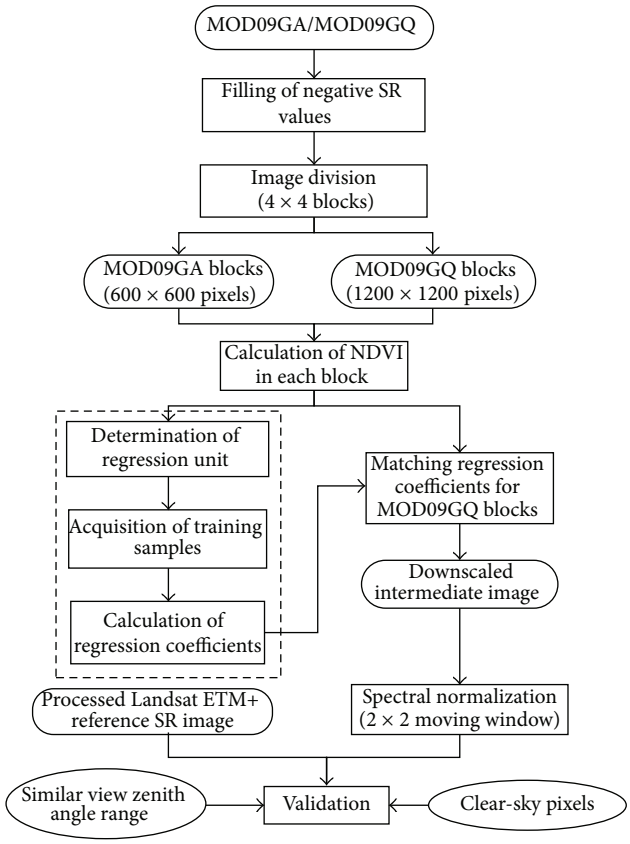

Figure 2: The flow chart for the downscaled method.

500 m resolution, which is then applied to MODIS 250 m B_1 and B_2 to predict corresponding B_{3-7} SR (Equation (1)). The logic and sequence of operations for this processing scheme (Figure 2) as follows:

$$B_{i(3-7)} = a_{0,i} + \left(a_{1,i}B_1 + a_{2,i}B_2\right)\left(1 + a_{3,i}\mathrm{NDVI}\right), \quad (1)$$

where NDVI $= (B_2 - B_1)/(B_2 + B_1)$ and B_i is the observed reflectance for band i.

Step 1 (data blocking). A few negative SR values resulted from atmospheric correction algorithm [23] were firstly filled with 1. To minimize the impact of vegetation diversity across different climatic and ecological zones, latitudinal variation of surface properties, and sun-view geometry effects on the SR prediction, each MOD09GA tile was equally divided into blocks (4 × 4) where pixels within the NDVI range of 0.1 as homogeneous land cover type were in the same regression units. Similar processes were applied to corresponding MOD09GQ tile as well.

Step 2 (training samples collection). To build the model precisely, three sampling rules were applied: (1) pixels with cloud contaminations and detector problem, identified by the 1 km QA layer in MOD09GA [23], were filtered; (2) heterogeneous pixels were excluded. Specifically, a window of 3 × 3 MODIS pixels was used to calculate the value range of each centered pixel as the difference between the maximum and the minimum values of the 9 MODIS pixels. A MODIS pixel was homogeneous if the value range was less than a predefined threshold value tested by Feng et al. [28]; (3) for the regression unit without adequate homogeneous samples, these samples were then pooled with other homogeneous samples within corresponding block to form an ensemble training sample.

Step 3 (regression coefficients calculation). In each regression unit, taking B_1, B_2, and NDVI as independent variables and B_3 to B_7 as dependent variables separately at 500 m resolution, regression coefficients were derived using the nonlinear least-squares method of Press et al. [29]. Subsequently, according to the NDVI, each pixel at 250 m resolution was matched to specific regression coefficients within the parallel blocks. Pixels with NDVI values out of the range of NDVI at 500 m resolution were assigned to coefficients related to nearest maximum or minimum NDVI at 500 m. The matched regression coefficients finally were applied to MODIS 250 m B_1 and B_2 SR to generate the surrogate intermediate B_3 to B_7 SR at 250 m.

Step 4 (spectral normalization). A simple 2 × 2 active window for preserving the radiometric consistency was utilized to average SR values of four pixels at 250 m to the corresponding pixel SR at the original 500 m resolution.

3.2. Water Extraction Based on Multiple Water Indexes. Water body extraction is mainly based on the visible, near-infrared and shortwave-infrared band reflectance difference in water from other land cover types (e.g., vegetation, soil, and resident region) [30]. For example, NDWI proposed by Mcfeeters took advantage of the obvious difference of reflectance in the visible green and near-infrared wavelengths (Equation (2)) [31]. However, Xu discovered that the reflectance of water in the shortwave-infrared band is generally a little lower to augment the difference with the visible green in comparison with near-infrared band, hence MNDWI was proposed to detect water body (Equation (3)) [32]. Consider

$$\mathrm{NDWI} = \frac{\mathrm{CH4} - \mathrm{CH2}}{\mathrm{CH4} + \mathrm{CH2}} \quad (2)$$

$$\mathrm{MNDWI} = \frac{\mathrm{CH4} - \mathrm{CH6}}{\mathrm{CH4} + \mathrm{CH6}}, \quad (3)$$

where CH2, CH4, and CH6 are near-infrared, visible green, shortwave-infrared band reflectance in MODIS, respectively.

To our knowledge, single NDWI or MNDWI is difficult to distinguish water from other features. For example, shallow or low quality water bodies showing weak water character in the multispectral bands, are difficult to be identified. Hill shade and shadow may also show similar spectral profile and cause errors in water extraction. Therefore, water body extraction model built in this paper integrates NDWI and MNDWI with spectral relation between near-infrared, shortwave-infrared band [33]. More specifically, typical water bodies were identified using a stable threshold value of NDWI (0.1). Since MNDWI is more sensitive to water bodies and ice and snow, it was used to extract ice and snow of the QTP region [34]. Finally, unlike other features (such as vegetation and soil), water

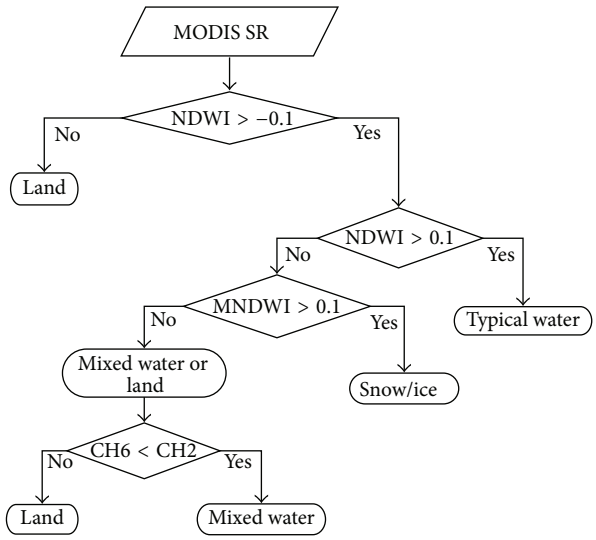

Figure 3: Flow chart of lake detection with multiple water indexes.

in the short-wave infrared reflectivity is lower than the near infrared wave band, thus spectral relation between short-wave infrared and near infrared band can distinguish the difference between water and land mixed pixels [35]. Figure 3 presents the steps of the water detection process.

3.3. Implementation and Sharing of the Methods. The method was implemented using C and Python programming languages. Open-source libraries, that is, GDAL/OGR (http://www.gdal.org/), PROJ4 (http://trac.osgeo.org/proj/), NumPy (http://www.numpy.org/), Matplotlib (http://matplotlib.org/), were integrated into the implementation to avoid using commercial software and also to enable application on multiple platforms, for example, Linux, Windows. The method implementation has also been standardized and deployed on a model sharing platform to promote applications of the method in the scientific research communities. The shared model can be called and interacted through predefined protocols, such as the Open Geospatial Consortium (OGC) Web Processing Service (WPS) standard. Detail of the model sharing can be found in [36].

4. Validation

To evaluate the performance of MODIS downscaling method, it was applied to MODIS SR acquired in Co Ngoin and Co Bangkog, and the results were compared to simultaneously acquired Landsat-7 ETM+ SR. The Landsat-7 ETM+ SR was aggregated to match the MODIS spatial resolution for comparisons. Water bodies extracted from the original and downscaled MODIS SR data were compared to water body visually interpreted from Landsat-7 ETM+ images. Confusion matrix was calculated to measure their agreement.

4.1. MODIS-Landsat-7 ETM+ SR Comparison. The original and downscaled images were compared to coincident Landsat-7 ETM+ SR, respectively. When comparing the results derived from MODIS to Landsat, the Landsat pixels were aggregated to MODIS projection and pixel footprint for comparison to minimize the error caused by reprojection. The Landsat data is distributed at 30-m resolution in Universal Transverse Mercator (UTM) projection. The area of a 250-m MODIS pixel is roughly 64 times of a Landsat pixel. In order to match the coverage of each MODIS pixel more accurately, the four corners of each MODIS pixel are used to draw a polygon, which represents the footprint of the MODIS pixel. The polygon was re-projected to Landsat UTM projection, and only Landsat pixels located within the polygon were used for calculate an average reflectance value for the corresponding MODIS pixel, which was then compared to the SR value of the MODIS. Additionally, MODIS has a wider view than Landsat-7. To avoid disagreement caused by view zenith angles differences, cloud and shadow, only the cloud-free pixels with view zenith angles within the view zenith angle range of the Landsat-7 (i.e., ±7.5° from nadir) were used in the comparison.

Consistency metrics were calculated to measure the agreement and disagreement between the original and downscaled MODIS SR and aggregated Landsat-7 ETM+ SR. These evaluation metrics were quantified by Mean Absolute Error (MAE), Root-Mean-Squared Difference (RMSD) recommended by Willmott [37]. Consider

$$\mathrm{MAE} = \sum_{i=1}^{n} \frac{\left|M_i - L_i\right|}{n}, \tag{4}$$

where M_i and L_i are the measured SR values for MODIS and aggregated Landsat-7 ETM+, n is the count of joint observations in the sample. In order to reduce uncertainties of MODIS and Landsat-7 ETM+ SR values, the linear relationship ($M = \alpha + \beta L$) between M and L was modeled by Reduced Major Axis (RMA) regression to calculate the parameters α (intercept), β (slope), and R^2 (correlation coefficient). Consider

$$\begin{aligned} \beta &= \pm\left(S_{ML}\right) \\ &\cdot \left(\frac{S_M}{S_L} = \pm\left(\frac{1}{n-1} \sum_{i=1}^{n} \left(M_i - \overline{M}\right)\left(L_i - \overline{L}\right) \right) \right. \\ &\left. \cdot \sqrt{\frac{\sum_{i=1}^{n} \left(M_i - \overline{M}\right)^2}{\sum_{i=1}^{n} \left(L_i - \overline{L}\right)^2}} \right)^{1/2} \\ \alpha &= \overline{M} - \beta \overline{L} \end{aligned} \tag{5}$$

$$R^2 = \frac{{S_{ML}}^2}{S_M S_L} = \frac{\left(\sum_{i=1}^{n} \left(M_i - \overline{M}\right)\left(L_i - \overline{L}\right)\right)^2}{\left(\sum_{i=1}^{n} \left(M_i - \overline{M}\right)^2\right)\left(\sum_{i=1}^{n} \left(L_i - \overline{L}\right)^2\right)},$$

where $\overline{M}$, S_M, $\overline{L}$, and S_L are mean and sample variance of M and L, respectively, and S_{ML} is covariance of M and L. Consider

$$\mathrm{MSE}_s = \sum_{i=1}^{n} \frac{\left(\widehat{M}_i - L_i\right)^2}{n}$$
$$\mathrm{MSE}_u = \sum_{i=1}^{n} \frac{\left(M_i - \widehat{M}_i\right)^2}{n}, \quad (6)$$

where $\widehat{M}_i$ is predicted MODIS SR value from a Landsat-7 ETM+-derived SR value based on the modeled correlation ($M = \alpha + \beta L$). Systematic error (MSE_s) represents the difference between the trend of MODIS-derived and Landsat-7 ETM+ SR while unsystematic error (MSE_u) accounts for the variation surrounding the trend. Therefore, MSE_s and MSE_u are aggregated to RMSD. Consider

$$\mathrm{RMSD} = \sqrt{\mathrm{MSE}_s + \mathrm{MSE}_u}. \quad (7)$$

To maintain consistent units, the square roots of MSE_s and MSE_u are reported, that is, RMSD_s and RMSD_u, in units of percent reflectance.

4.2. Accuracy Assessment of Extracted Water Bodies. The water bodies extracted from both the original and downscaled MODIS SR were compared to the water body interpreted from Landsat-7 ETM+ image to assess the improvement of the downscaled method in terms of water classification. To achieve better pixel accuracy, water map acquired from coincident Landsat-7 ETM+ images was first aggregated to MODIS spatial resolution based on the principle of dominant type by calculating the number of Landsat-7 water pixels within the extent of each sampled MODIS pixel. Detected water bodies were separately overlaid with aggregated Landsat-7 water extent to verify the content of the pixels on the MODIS image. Accuracy measures were based on confusion matrix [7], overall classification accuracy (A), percentage of omission, and commission error (E_o and E_c). Consider

$$\mathrm{A} = \frac{N_t}{N_r} \times 100\%$$
$$E_c = \frac{N_c}{N_r} \times 100\% \quad (8)$$
$$E_o = \frac{N_o}{N_r} \times 100\%,$$

where A is the accuracy of water pixels identified correctly and E_c and E_o are commission and omission error, respectively. N_r is the number of water pixels in the reference ETM+ water map, N_t is the number of water pixels detected in MODIS images, N_c is the number of land pixels misclassified as water in MODIS images, and N_o is the number of water pixels misclassified as land in MODIS images.

5. Result and Discussion

5.1. Improvement of Downscaled MODIS SR. Figure 4 presents false-color compositions (Band SWIR1, NIR and R) of downscaled 250 m MODIS SR data (Figure 4(a)), the original 500 m MODIS SR data (Figure 4(b)), and simultaneously acquired aggregated 250 m Landsat-7 ETM+ SR data (Figure 4(c)) in Co Nagoin. Figure 5 presents false-color compositions (Band SWIR1, NIR and R) of downscaled 250 m MODIS SR data (Figure 5(a)), the original 500 m MODIS SR data (Figure 5(b)), and simultaneously acquired aggregated 250 m Landsat-7 ETM+ SR data (Figure 5(c)) in Co Bangkog. Significant improvement of spatial delineation can be observed in the downscaled data than the original data. For example, in the two study areas, the lakes and islands (Figures 4(a) and 5(a)) were showing closer areas and shapes to the higher resolution Landsat-7 ETM+ reference data (Figures 4(c) and 5(c)). The white noise pixels in band 6 of the original MODIS data Figure 4(b) were fixed in the downscaled result (Figure 4(a)).

Although the downscaled data showed more detail, few uneven SR values can be observed, especially at the transition boundary of different land cover type, such as the red pixels sat at the edge of the lake and islands in the Figures 4(a) and 5(a). Further investigation revealed that the disagreements were caused by spectral normalization of the downscaled method. In this study, spectral normalization using equally weighted average method possibly led to the excessive enhancement on mixed pixels with high SR values. Theoretically, the pixel SR at 500 m can be derived from aggregating the 250 m pixels within the particular extent centered at the corresponding pixel at 500 m [38]. For mixed pixels of 500 × 500 m cell size at the edge of the lakes, SR values of the corresponding four pixels at 250 m change greatly, especially in the two MODIS SWIR bands. As a result, the equally weighted average method based on a 2 × 2 active window generally causes excessive enhancement in the pixels of higher SR and widens the distinction among neighboring pixels. This variable condition can also be confirmed in Figure 6(a) where part of pixels, especially for the two MODIS SWIR bands, tend to have higher SR values than Landsat-7 ETM+. Nevertheless, excessive enhancement has inherent advantage of identifying mixed water pixels at the edge of lakes on the ground that excessive enhancement can increase the difference between water and other land types to better detect water pixels.

The performance of the downscaling method was further assessed by comparing the MODIS and Landsat-7 ETM+ SR in density plots shown in Figure 6. Following the conclusion of the comparability of Landsat and MODIS bands proposed by Masek et al. [39], each MODIS band was compared to its Landsat-7 ETM+ solar-reflective spectral band with closer spectral range (Table 1). Figure 6(a) presents the SR comparison between the MODIS downscaled SR and aggregated Landsat-7 ETM+ SR, and Figure 6(b) displays the result of MODIS 500 m observations comparison.

Deviations between Landsat-7 ETM+ and 250 m MODIS SR, as measured by RMSD, range from 1.6 to 4.3 percentage points of reflectance. Bias (MAE) fluctuates within 1.0–2.5

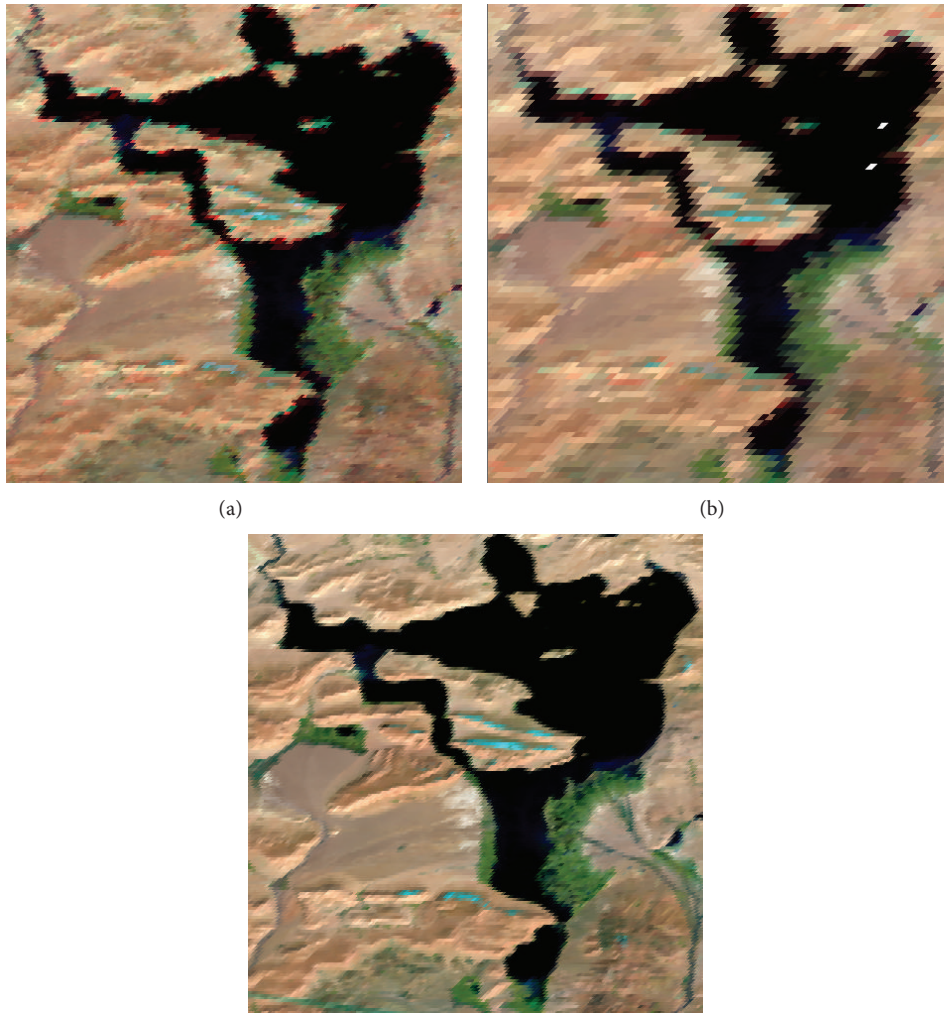

(a) (b)

(c)

Figure 4: False color composite images (621) over Co Ngoin; October 7, 2000. (a) Shows downscaled data at 250 m spatial resolution; (b) shows original data at 500 m; (c) shows Landsat-7 ETM+ image aggregated to 250 m from 30 m spatial resolution.

percentage points. Correlations at the local scale are strongly linear, with R^2 higher than 0.9 for all bands except blue band. Intercepts vary between –1.5 and 0.9, and slopes are close to 1, although outliers-boundary pixels SR of excessive enhancement for two MODIS SWIR bands (Table 2). Correspondences between 500 m MODIS SR and the coincident Landsat-7 ETM+ SR are similar to those between 250 m MODIS SR and Landsat-7 ETM+ SR, but the spread of the data are wider (Figures 6(b)), and deviations (RMSD) range from 1.9 to 4.6 percentage points (Table 2).

When comparing results at 500 m spatial resolution, R^2 is typically higher and other evaluation indicators are lower (i.e., MAE, RMSD, RMSD_s, RMSD_u), indicating that SR results at 250 m are superior to corresponding SR at 500 m. On the other hand, there are still some discrepancies in comparison to Landsat-7 ETM+ SR, particularly for two MODIS SWIR bands. Table 2 shows that two SWIR bands have higher RMSD than the other 5 bands. Wavelength differences between Landsat-7 and MODIS bands (Table 1) are likely source of the SR differences. The much narrower bandwidth of the two MODIS SWIR bands make it possible to avoid the spectral ranges with lower atmospheric transmittance that are covered by the Landsat-7 ETM+ SWIR bands [26].

5.2. Improvement of Water Body Map. Figure 7 presents the comparison of MODIS water masks and spatial error distributions in comparison to Landsat-7 ETM+ data in Co Nogin and Figure 8 is for Co Bangkog. Although the same water classification method was applied, the water map produced from the downscaled data (Figures 7(c) and 8(c)) shows more details than the map from the original MODIS data (Figures 7(d) and 8(d)). For instance, the edges of the identified lakes are smoother. Shapes of the small islands in Co Ngoin and Co Bangkog are also improved. This richer information generally matches the features that are depicted in the water body reference map well (Figures 7(b) and 8(b)).

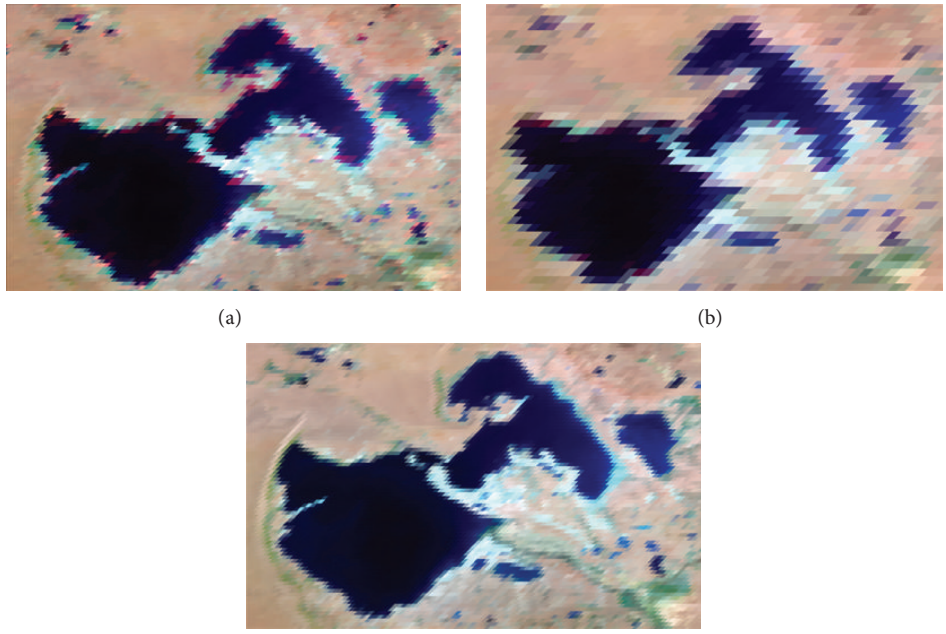

(a) (b)

(c)

Figure 5: False color composite images (621) over Co Bangkog; October 7, 2000. (a) Shows downscaled data at 250 m spatial resolution; (b) shows original data at 500 m; (c) shows Landsat-7 ETM+ image aggregated to 250 m from 30 m spatial resolution.

Table 2: Summary of comparison between MODIS original and downscaled SR estimates and coincident Landsat-7 ETM+ derived SR. Values are represented as percent reflectance (%) for intercept, RMSD, $RMSD_s$, $RMSD_u$ and MAE.

Resolution	Indicators	Red	Green	Blue	NIR	SWIR1	SWIR2
250 m	Slope	0.998	0.999	1.019	1.006	1.010	0.977
	Intercept	−0.526	−0.684	−1.533	−0.402	0.985	0.690
	R^2	0.974	0.935	0.856	0.978	0.927	0.914
	RMSD	1.661	1.783	2.026	1.862	4.240	3.763
	$RMSD_s$	0.557	0.704	1.319	0.278	1.253	0.326
	$RMSD_u$	1.565	1.638	1.538	1.841	4.051	3.748
	MAE	1.034	1.200	1.525	1.020	2.475	2.137
500 m	Slope	0.981	0.973	0.982	0.986	0.990	0.955
	Intercept	−0.211	−0.284	−1.108	0.036	1.536	1.240
	R^2	0.931	0.916	0.830	0.933	0.909	0.898
	RMSD	2.573	1.958	2.080	3.165	4.613	4.047
	$RMSD_s$	0.595	0.721	1.314	0.331	1.259	0.603
	$RMSD_u$	2.503	1.820	1.613	3.148	4.438	4.001
	MAE	1.530	1.300	1.560	1.681	2.728	2.391

Table 3: Errors of water bodies derived from the original and downscaled MODIS SR images for Co Ngoin and Co Bangkog.

Lakes	Co Ngoin		Co Bangkog	
Resolution (m)	250	500	250	500
Omission errors	4.32%	8.30%	3.45%	12.02%
Commission errors	3.14%	5.78%	8.68%	9.13%
Accurate	95.68%	91.70%	91.31%	90.87%

Apart from visual interpretation, the spatial errors were calculated and presented in Table 3. For Co Nagoin, MODIS results (5166 water pixels at 250 m and 5096 at 500 m resp.) underestimate the extent of water body compared to that of Landsat-7 ETM+ image with 5228 water pixels. Although omission (E_o) and commission error (E_c) exist in both water bodies from the original and downscaled MODIS data, both E_o and E_c at 250 m (4.32% and 3.14%) are almost cut in half in comparison to the original 500 m resolution data (8.30% and 5.78%), and overall accuracy (A) increases from 91.70% to 95.68%. For Co Bangkog, E_o is reduced slightly from 9.13% to 8.68%. E_c significantly reduces from 12.02% at 500 m to 3.45% at 250 m. Overall accuracy (A) increases from 90.87% to 91.31%.

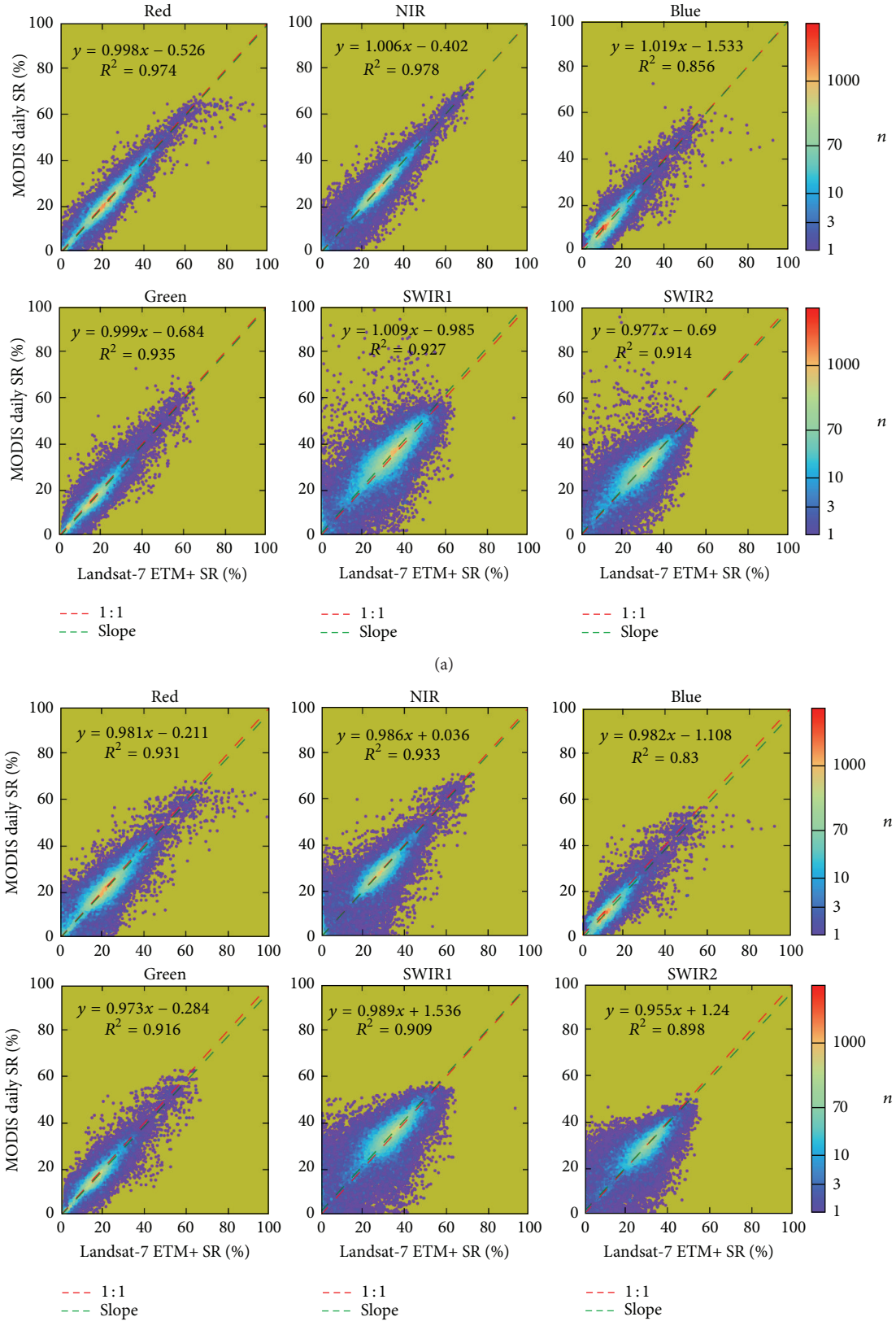

Figure 6: Density plots of comparison between Landsat-7 ETM+ aggregated to 250 m and MODIS 250 m (a) and 500 m (b).

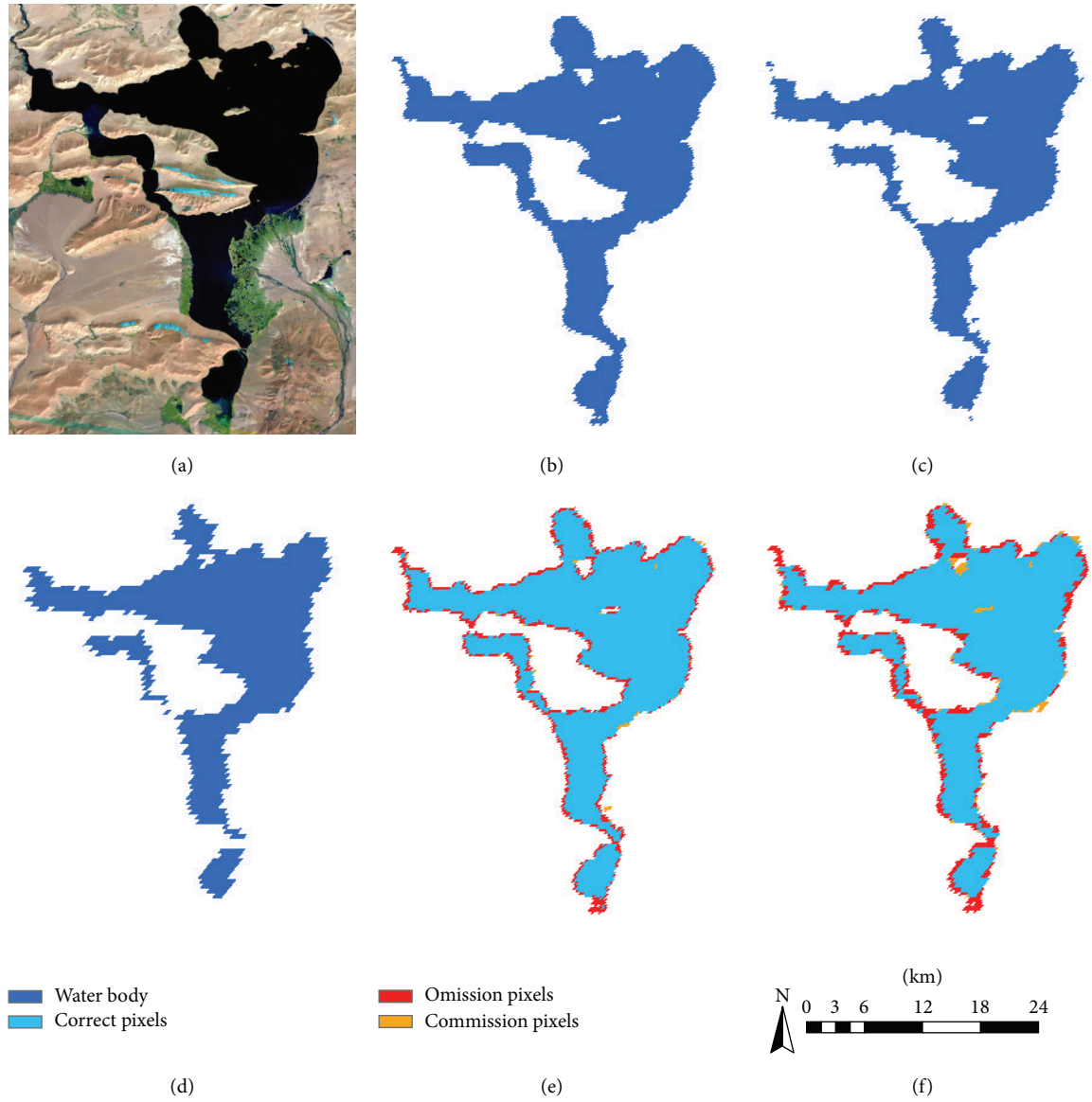

Figure 7: Visual performance in extracted water bodies and spatial errors for Co Ngoin; October 7, 2000. (a) Landsat-7 ETM+ 543 band false-color image; (b) aggregated reference water map from ETM+ image; (c) extracted result from downscaled image at 250 m; (d) extracted result from original image at 500 m; (e) result of spatial error for (c) map; (f) result of spatial error for (d) map.

6. Conclusion

In order to improve the spatial delineation of water mask detected from MODIS data, this paper presents an automated method for downscaling the original 500 m bands to 250 m for water detection. The method was applied to Co Ngoin and Co Bangkog, to extract water bodies at a higher spatial resolution. Comparisons to SR and water body extracted from simultaneously acquired Landsat-7 ETM+ image suggest the improvement over the original data in terms of downscaled SR and water classification. The edges of the lakes become smoother than the results from original MODIS image and smaller islands are delineated with clearer shape in the downscaled 250 m water body maps, as well as a higher overall accuracy and lower omission and commission error of water bodies mapping for Co Ngoin and Co Bangkog at 250 m.

The paper presented downscaled 250 m resolution SR and detected water bodies for two lakes in QTP. With two MODIS images, the results only demonstrated static representing of water extent of the two lakes on the image acquisition dates, but the success of the method enables detecting possibly daily water dynamics using MODIS Terra observations. The automated method is also expected to be applied to other lakes in QTP to meet the need for measuring water distribution and dynamic in the plateau and its surrounding areas. Further effort is needed to assess the robustness of the method for nonwater applications and water bodies in other areas beyond QTP.

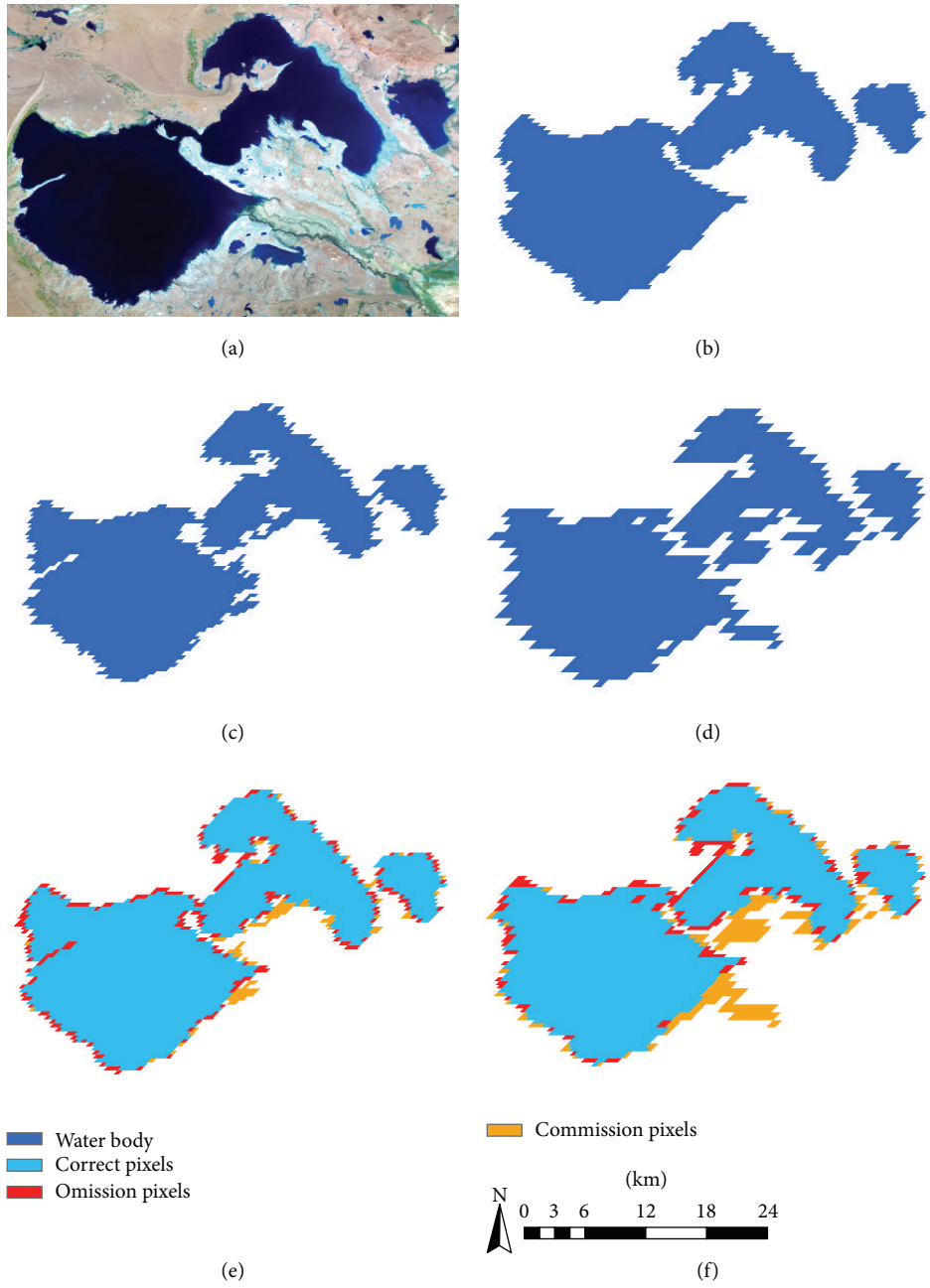

Figure 8: Visual performance in extracted water bodies and spatial errors for Co Bangkog; October 7, 2000. (a) Landsat-7 ETM+ 543 band false-color image; (b) aggregated reference water map from ETM+ image; (c) extracted result from downscaled image at 250 m; (d) extracted result from original image at 500 m; (e) result of spatial error for (c) map; (f) result of spatial error for (d) map.

Conflict of Interests

The authors declare that there is no conflict of interests regarding to the publication of this paper.

Acknowledgments

This research was financially supported by the National Natural Science Foundation of China (no. 41101364), the Key Project for the Strategic Science Plan in the Institute of Geographical Sciences and Natural Resources Research, the Chinese Academy of Sciences (no. 2012ZD010), and the China Clean Development Mechanism Fund Grant Project (no. 1214115). The authors are indebted to National Aeronautics and Space Administration (http://modis.gsfc.nasa.gov/), the US Geological Survey server (http://glovis.usgs.gov/) and the Global Land Cover Facility (http://www.landcover.org/) for providing the MODIS and Landsat-7 ETM+. Thanks are also

given to the Data Sharing Infrastructure of Earth System Science for providing the China administrative boundaries data (http://www.geodata.cn/).

References

[1] G. E. Yu and S. P. Harrison, "Holocene changes in atmospheric circulation patterns as shown by lake status changes in northern Europe," *Boreas*, vol. 24, no. 3, pp. 260–268, 1995.

[2] B. Qin, Y. Shi, and G. Yu, "Lake level fluctuations of Asia inland lakes during 18 kaBP and 6 kaBP with their significance," *Chinese Science Bulletin*, vol. 42, no. 24, pp. 2586–2595, 1997.

[3] P. Singh and L. Bengtsson, "Impact of warmer climate on melt and evaporation for the rainfed, snowfed and glacierfed basins in the Himalayan region," *Journal of Hydrology*, vol. 300, no. 1–4, pp. 140–154, 2005.

[4] S. Harrison, N. Glasser, V. Winchester, E. Haresign, C. Warren, and K. Jansson, "A glacial lake outburst flood associated with recent mountain glacier retreat, Patagonian Andes," *Holocene*, vol. 16, no. 4, pp. 611–620, 2006.

[5] J. Liu, S. Wang, S. Yu, D. Yang, and L. Zhang, "Climate warming and growth of high-elevation inland lakes on the Tibetan Plateau," *Global and Planetary Change*, vol. 67, no. 3-4, pp. 209–217, 2009.

[6] C. Song, B. Huang, and L. Ke, "Modeling and analysis of lake water storage changes on the Tibetan Plateau using multi-mission satellite data," *Remote Sensing of Environment*, vol. 135, pp. 25–35, 2013.

[7] H. Jiang, M. Feng, Y. Zhu, N. Lu, J. Huang, and T. Xiao, "An automated method for extracting rivers and lakes from Landsat imagery," *Remote Sensing*, vol. 6, no. 6, pp. 5067–5089, 2014.

[8] H. Wang and M. Ma, "A review of monitoring change in lake water areas based on remote sensing," *Remote Sensing Technology and Application*, vol. 24, no. 5, pp. 674–684, 2009.

[9] X. Xiao, S. Boles, S. Frolking et al., "Observation of flooding and rice transplanting of paddy rice fields at the site to landscape scales in China using VEGETATION sensor data," *International Journal of Remote Sensing*, vol. 23, no. 15, pp. 3009–3022, 2002.

[10] D. J. Weiss and R. L. Crabtree, "Percent surface water estimation from MODIS BRDF 16-day image composites," *Remote Sensing of Environment*, vol. 115, no. 8, pp. 2035–2046, 2011.

[11] F. Sun, Y. Zhao, P. Gong, R. Ma, and Y. Dai, "Monitoring dynamic changes of global land cover types: fluctuations of major lakes in China every 8 days during 2000–2010," *Chinese Science Bulletin*, vol. 59, no. 2, pp. 171–189, 2013.

[12] L. Ji, L. Zhang, and B. Wylie, "Analysis of dynamic thresholds for the normalized difference water index," *Photogrammetric Engineering & Remote Sensing*, vol. 75, no. 11, pp. 1307–1317, 2009.

[13] V. Soti, A. Tran, J.-S. Bailly, C. Puech, D. L. Seen, and A. Bégué, "Assessing optical earth observation systems for mapping and monitoring temporary ponds in arid areas," *International Journal of Applied Earth Observation and Geoinformation*, vol. 11, no. 5, pp. 344–351, 2009.

[14] M. Carroll, C. DiMiceli, J. Townshend, P. Noojipady, and R. Sohlberg, *UMD Global 250 Meter Land Water Mask User Guide*, 2009.

[15] S.-H. Kim, S.-J. Kang, and K.-S. Lee, "Comparison of fusion methods for generating 250 m MODIS image," *Korean Journal of Remote Sensing*, vol. 26, no. 3, pp. 305–316, 2010.

[16] A. P. Trishchenko, Y. Luo, K. V. Khlopenkov, and S. Wang, "A method to derive the multispectral surface albedo consistent with MODIS from historical AVHRR and VGT satellite data," *Journal of Applied Meteorology and Climatology*, vol. 47, no. 4, pp. 1199–1221, 2008.

[17] Y. Luo, A. P. Trishchenko, and K. V. Khlopenkov, "Developing clear-sky, cloud and cloud shadow mask for producing clear-sky composites at 250-meter spatial resolution for the seven MODIS land bands over Canada and North America," *Remote Sensing of Environment*, vol. 112, no. 12, pp. 4167–4185, 2008.

[18] G. Zhang, H. Xie, S. Kang, D. Yi, and S. F. Ackley, "Monitoring lake level changes on the Tibetan Plateau using ICESat altimetry data (2003–2009)," *Remote Sensing of Environment*, vol. 115, no. 7, pp. 1733–1742, 2011.

[19] Y. Wu, S. Wang, and X. Hou, "Chronology of Holocene lacustrine sediments in Co Ngoin, central Tibetan Plateau," *Science in China Series D: Earth Sciences*, vol. 49, no. 9, pp. 991–1001, 2006.

[20] S. M. Wang, H. S. Dou, K. Z. Chen et al., *Chinese Lakes*, Science Press, 1998.

[21] X. J. Yao, S. Y. Liu, M. P. Sun et al., "Changes of Kusai Lake in Hoh Xil Region and causes of its water overflowing," *Journal of Geographical Science*, vol. 67, no. 5, pp. 689–698, 2012.

[22] V. V. Salomonson, W. L. Barnes, P. W. Maymon, H. E. Montgomery, and H. Ostrow, "MODIS: advanced facility instrument for studies of the earth as a system," *IEEE Transactions on Geoscience and Remote Sensing*, vol. 27, no. 2, pp. 145–153, 1992.

[23] E. Vermote, S. Kotchenova, and J. Ray, *MODIS Surface Reflectance User's Guide*, MODIS Land Surface Reflectance Science Computing Facility, 2008.

[24] D. P. Roy, J. Ju, P. Lewis et al., "Multi-temporal MODIS-Landsat data fusion for relative radiometric normalization, gap filling, and prediction of Landsat data," *Remote Sensing of Environment*, vol. 112, no. 6, pp. 3112–3130, 2008.

[25] R. Irish, *Landsat-7 ETM+7 Science Data Users Handbook*, National Aeronautics and Space Administration, 2000.

[26] M. Feng, J. O. Sexton, C. Huang et al., "Global surface reflectance products from Landsat: assessment using coincident MODIS observations," *Remote Sensing of Environment*, vol. 134, pp. 276–293, 2013.

[27] A. P. Trishchenko, Y. Luo, and K. V. Khlopenkov, "A method for downscaling MODIS land channels to 250-m spatial resolution using adaptive regression and normalization," in *6th Remote Sensing for Environmental Monitoring, GIS Applications, and Geology*, vol. 6366 of *Proceedings of SPIE*, Stockholm, Sweden, October 2006.

[28] M. Feng, C. Huang, S. Channan, E. F. Vermote, J. G. Masek, and J. R. Townshend, "Quality assessment of Landsat surface reflectance products using MODIS data," *Computers and Geosciences*, vol. 38, no. 1, pp. 9–22, 2012.

[29] W. H. Press, W. Vetterling, S. A. Teukolsky et al., "Numerical recipes in FORTRAN—the art of scientific computing," *SIAM Review*, vol. 36, no. 1, pp. 149–150, 1994.

[30] S. Huang, J. Li, and M. Xu, "Water surface variations monitoring and flood hazard analysis in Dongting Lake area using long-term Terra/MODIS data time series," *Natural Hazards*, vol. 62, no. 1, pp. 93–100, 2012.

[31] S. K. Mcfeeters, "The use of the Normalized Difference Water Index (NDWI) in the delineation of open water features," *International Journal of Remote Sensing*, vol. 17, no. 7, pp. 1425–1432, 1996.

[32] H. Xu, "Modification of normalised difference water index (NDWI) to enhance open water features in remotely sensed imagery," *International Journal of Remote Sensing*, vol. 27, no. 14, pp. 3025–3033, 2006.

[33] X. H. Che, M. Feng, H. Jiang et al., "Detection and analysis of Qinghai-tibet plateau lake areas from 2000 to 2013," *Journal of Geo-Information Science*, vol. 17, no. 1, pp. 99–107, 2015.

[34] B. H. Tang, B. Shrestha, Z. L. Li et al., "Determination of snow cover from MODIS data for the Tibetan Plateau region," *International Journal of Applied Earth Observation and Geoinformation*, vol. 21, pp. 356–365, 2012.

[35] W. B. Ming, "A method to identify water body from MODIS image data in upper reach of Changjiang river," *Plateau Meteorology*, vol. 23, pp. 141–145, 2004.

[36] M. Feng, S. Liu, J. N. H. Euliss, C. Young, and D. M. Mushet, "Prototyping an online wetland ecosystem services model using open model sharing standards," *Environmental Modelling & Software*, vol. 26, no. 4, pp. 458–468, 2011.

[37] C. J. Willmott, "Some comments on the evaluation of model performance," *Bulletin of the American Meteorological Society*, vol. 63, no. 11, pp. 1309–1313, 1982.

[38] M. Nishihama, R. Wolfe, D. Solomon et al., "MODIS level 1A Earth location: algorithm theoretical basis document version 3.0," SDST-092, MODIS Science Data Support Team, 1997.

[39] J. G. Masek, E. F. Vermote, N. E. Saleous et al., "A landsat surface reflectance dataset for North America, 1990–2000," *IEEE Geoscience and Remote Sensing Letters*, vol. 3, no. 1, pp. 68–72, 2006.

Hindawi Publishing Corporation
Advances in Meteorology
Volume 2015, Article ID 279173, 13 pages
http://dx.doi.org/10.1155/2015/279173

Research Article

Identification of Water Scarcity and Providing Solutions for Adapting to Climate Changes in the Heihe River Basin of China

Xiangzheng Deng[1,2] and Chunhong Zhao[1,2,3]

[1] *Institute of Geographic and Natural Resources Research, Chinese Academy of Sciences, Beijing 100101, China*
[2] *Center for Chinese Agricultural Policy, Chinese Academy of Sciences, Beijing 100101, China*
[3] *University of Chinese Academy of Sciences, Beijing 100049, China*

Correspondence should be addressed to Xiangzheng Deng; dengxz.ccap@gmail.com

Received 30 June 2014; Accepted 18 October 2014

Academic Editor: R. B. Singh

In ecologically fragile areas with arid climate, such as the Heihe River Basin in northwestern China, sustainable social and economic development depends largely on the availability and sustainable uses of water resource. However, there is more and more serious water resource shortage and decrease of water productivity in Heihe River Basin under the influence of climate change and human activities. This paper attempts to identify the severe water scarcity under climate change and presents possible solutions for sustainable development in Heihe River Basin. Three problems that intervened land use changes, water resource, the relevant policies and institutions in Heihe River basin were identified, including (1) water scarcity along with serious contradiction between water supply and demand, (2) irrational water consumption structure along with low efficiency, and (3) deficient systems and institutions of water resource management along with unreasonable water allocation scheme. In this sense, we focused on reviewing the state of knowledge, institutions, and successful practices to cope with water scarcity at a regional extent. Possible solutions for dealing with water scarcity are explored and presented from three perspectives: (1) scientific researches needed by scientists, (2) management and institution formulation needed by governments, and (3) water resource optimal allocation by the manager at all administrative levels.

1. Introduction

In most arid and semiarid areas, water resource is the core and the linkage between the ecosystem and the economic system [1]. It not only plays a vital role in the formation, development, and stability of desert oasis, but also is a key component of the ecosystem environment and services [2]. Most of the inland rivers in China are faced with severe water resource shortage and serious ecological deterioration. The north and northwest of China account for half of the total area of China but have less than 20% of total national available water resource [2, 3]. Meanwhile, as one of the major constraints on sustainable development, water is the determining factor to maintain social production and livelihoods of the arid and semiarid region [4]. The water issue in arid and semiarid inland areas is thus receiving considerable attention worldwide [5].

Climate change emerges as one of the major forces that affect water availability in the future [6, 7]. The Intergovernmental Panel on Climate Change [8] points to the high sensitivity of semiarid and arid regions to climate, considering the already existing water stress driven by growth in agricultural, industrial, and urban demands. The need for more research on the impact of climate change on surface and ground water has been addressed by the current research [9, 10]. Meanwhile, human activities have exerted great impacts on water resource. Global urban water utilization increased over 20 times within the past century, from $200 \times 108\,m^3$ in the year 1900, to $600 \times 10^8\ m^3$ in the year 1950, to $1500 \times 10^8\ m^3$ in the year 1975, and to $4400 \times 10^8\ m^3$ in the year 2000 [11]. With continuous population growth and urbanization progresses, the availability of water with sufficient quantity and quality is one of the anticipated future problems.

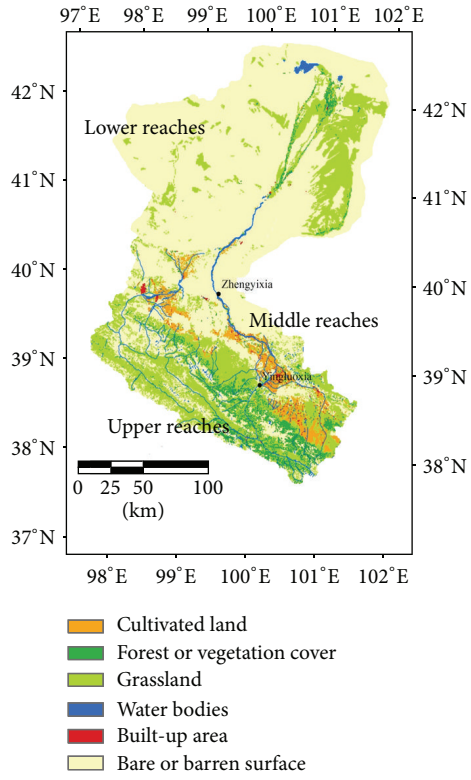

Figure 1: Location of the Heihe River Basin.

The Heihe River Basin (HRB), well-known for dry climate with intense evaporation and scarce but concentrated precipitation, is the second largest inland river basin in China (Figure 1). Some issues such as watershed management, water-saving policies, environmental degradation, and ecosystem restoration have drawn great attention, making the HRB become the ideal case study area for sustainable development of arid regions [12–15]. The main feature of the water resource of the HRB is that the runoff is produced in mountains in the upper reaches but is mostly utilized and consumed in middle reaches and lower reaches. However, water and ecological environment has experiencing rapid deterioration since the 1950s [12]. In fact, the HRB could be vulnerable to water stress under climate change because of the limited water availability and the increasing demand for water from agriculture irrigation and industry sectors.

Human activities have been the dominant factor for environmental problems of the HRB. The grassland has degraded severely due to long-time overgrazing and overcultivation in the upper reaches, while water holding capacity has decreased greatly. Meanwhile, water consumption has increased steadily, especially in the middle reaches where it is featured with remarkable economic growth. Consequently, the hydrological processes of these areas have been deeply modified by human activities, such as the expansion of irrigation, rapid population growth, and socioeconomic development [16]. On one hand, due to the high intensity of water usage in the upper and middle reaches in the HRB, the lower reaches have dried up and groundwater levels have decreased severely [12, 17]. On the other hand, with the implementation of national Policy on Integrated Development of Western China, plenty of water previously used by natural ecosystems and irrigation agriculture will be saved and used into industrial and urban systems to maintain the economic development. Generally, it has caused the imbalance in the whole interrelated system of human beings and natural resource, as well as environment, thus leading to sever ecological and socioeconomic problems in the whole region.

The sustainable development of an arid area largely depends on the availability of water from the inland rivers like the HRB of China. A number of studies analyzed the hydrological process and the water problems of the HRB [12, 13, 17, 18]. These researches have put forward some approaches and schemes for water management. However, some knowledge gaps on the spatial variability of water and water efficiency in the HRB ought to be stressed. Meanwhile, the institutions and successful practices of water management for improving water efficiency need to be integrated in the arid basin research.

The objectives of this paper are to review and identify the key issues on the HRB and present possible water management approaches for sustainable development of the HRB. The remaining parts of this paper are organized as follows. Firstly, the geographical and hydrological background of the HRB is introduced in the second section. This is followed by a brief elective review of the main water problems in the HRB in the third section, and three knowledge gaps that exist within the HRB are identified. In the fourth section, possible adaptive solutions to water problems in the HRB are discussed. We conclude by discussing the pressing matters for reforming the water management systems in the HRB and the possibility of the inspiration for other inland rivers.

2. Geographical and Hydrological Background of the Heihe River Basin

The Heihe River Basin (90°E–102°E, 37°50′N–42°40′N) is located in the north of Qilian Mountains and the middle part of the Hexi Corridor. It covers Qinghai Province, Gansu Province, and Inner Mongolia, with a river length of 821 kilometers and a catchment area of 14×10^4 km^2 (Figure 1). Heihe River breeds the prosperity and civilization of the HRB basin. The average evaporation is up to 84 mm/a. The total water resource is 2800 mm^3/a, which includes surface water 2470 mm^3/a and ground water 330 mm^3/a. From south to north, the special variation of the HRB is evident and can be divided into three subunits. The upper reaches of the HRB, located in Qilian Mountain, belong to the northern margin of the Tibet Plateau. It is the birthplace of Heihe River as well as the runoff area, with abundant rainfall, less evaporation, and cold and damp climate. Being the oasis of the Hexi Corridor and the desert plain, the middle reaches of the HRB are the key area for agriculture and they are the grain base for Gansu province. The lower reaches of HRB, north of the Langxinshan Gorge, form the oasis in Inner Mongolia, making it an essential ecosystem barrier of Northern China.

The upper reaches are the runoff producing area of the HRB. The southern Qilian Mountains, with remarkable vertical zonality, are composed of a series of parallel mountains and basins in northwest-southeast direction. The high mountain range serves as the water source for inland rivers, which flow to basins and form internal stream systems. The alpine desert accounts for 22% of the area of upper reaches. In addition, it has a length of 303 kilometers, with 68% runoff contribution rate and 85% runoff coefficient. The elevation of this area ranges from 2000 to 5500 meters and the mean annual precipitation ranges from about 250 mm in the low mountain zone to 500 mm in the high mountain zone. With an altitude of over 4000 meters, most middle and high mountains are covered with snow all year round coupled with modern glaciers, and it is the natural reservoir of Hexi Corridor. Meantime, in the area with an altitude of lower than 3000 meters, the vegetation is relatively fair and the land is covered mainly by natural ecosystems, including cold deserts, mountain forests and shrubs, alpine meadows and steppe, and ice and snow. The vegetation on Qilian Mountain is called water conservation forest because of its good regulatory role on water resource.

The middle reaches of the HRB are the runoff and water using area, which is characterized by irrigation agriculture. The irrigation area is up to 205, 230 hectares, accounting for 91% of the area of cultivated land in the whole basin. 95% of the population lives in this region and they produce over 80% of GDP for the whole region. Annual rainfall ranges from 300 mm to 100 mm, and annual potential evaporation is about 1900 mm/a. The middle Hexi Corridor, with an area of 17,000 km^2, is sandwiched between the southern Qilian Mountains and the northern Mazong Mountains. The topography is fairly smooth, and the elevation ranges from 2000 to 1000 meters, correspondent with a decrease of the mean annual precipitation from 250 mm to less than 100 mm. Irrigation agriculture is dominated by farmland vegetation. It develops very well but is based on high consumption of water. In the area where the rivers flow through, there are a series of oases with loamy soil and abundance of sunshine, making the HRB one of the five bases of national commodity grain. In addition, here various artificial oases exist, including the counties of Mingle, Shandan, Linze, Gaotai and Jinta, Zhangye, Jiuquan, and Jia Yuguan. Meanwhile, Gobi and desert are largely scattered in other areas of the HRB.

The lower reaches of the HRB are the runoff disappearing area. With a mean elevation of around 1,000 m and mean annual precipitation of 50 mm, it is mainly occupied by Gobi, desert, and bare land. The precipitation in the lower basin is only 55 mm/a, while the annual potential evaporation reaches 2300 mm/a. Ejina, covering an area of 114,000 km^2, is located at the end of the HRB and in the west of Inner Mongolia of China. The Gobi and desert occupy over 90% of the total land area of Ejina. According to the runoff data of the Langxinshan hydrological station, the discharge of the Heihe River has decreased since the year 1950, and the shortage of water caused the Ejina Oasis to shrink considerably. From the year 1960, with the decrease of discharge from the Heihe River, the oasis of Ejina began to shrink and caused a series of environmental problems. For instance, the areas of West Juyan Lake and East Juyan Lake were 267 km^2 and 35 km^2, respectively, and dried up in the year 1961 and the year 1992, respectively [19]. In addition, both overgrazing and overcultivation have resulted in severe ecological deterioration in Ejina, where rivers and lakes are drying out, groundwater table is decreasing, water quality is deteriorating, and biodiversity is degrading.

3. Water Scarcity of the Heihe River Basin

Water plays an important role in economic development and ecological balance of the middle reaches and lower reaches of the HRB. Lacking of effective coordinated water management system, the amount of water flowing into the lower reaches has continually been decreasing. As a result, the rivers and lakes dried up intensively in the lower reaches, along with declining groundwater table and a high level of water mineralization. Meanwhile, the area of vegetation coverage is reducing sharply, leading the HRB to becoming a source of dust for sandstorms in Northwestern China.

3.1. Water Scarcity along with Serious Contradiction between Supply and Demand of Water. Water scarcity is a long-standing and widespread problem in the HRB, and there is unevenly temporal and spatial water distribution. There are a series of reservoirs (one large reservoir, 9 medium size reservoirs, and 89 small reservoirs) in the basin and the total capacity is 416.9 billion m^3. Influenced by topography, altitude, and atmospheric circulation at different scale, the spatial distribution of precipitation is extremely uneven in the middle reaches and lower reaches. Generally, the annual average precipitation decreases from southeast to northwest (Figure 2). The maximum precipitation zone mainly concentrated in the upper reaches with an altitude of 2200–3000 m and an annual precipitation of 400–750 mm. In contrast, the minimum precipitation zone is the desert area of Ejina which administratively belongs to the Inner Mongolia, with an annual precipitation of 15–50 mm [20].

Aside from precipitation, water resource is mainly supplied by springs, subsurface flow, and solid glacier in Qilian Mountain [21]. There are 298 million m^3 water resource formed by ice and snow melting from the Qilian Mountain, accounting for 8% of the total amount of runoff. The previous studies have concluded that the yearly based rate of glacial retreating was around 0.60% in the HRB from 1960s to the year 2010, and this speed was significantly faster than Tianshan Mountain (0.49%/a), Geladandong (0.05%), and Naimona Nyi region (0.26%) [21]. In this sense, water scarcity is induced not only by the natural process, but also by irrational damage. The landscape structure and composition in the upper reaches of the HRB have been seriously changed, which inevitably reduced water availability in the lower reaches [21].

Meanwhile, water demand in HRB has increased considerably over the past half century. Since the year 1949, the China government has paid much attention to the development of irrigation infrastructure. By the year 1985, the number of reservoirs (the small plain reservoirs and embankments with a volume less than 100 thousand m^3 are not

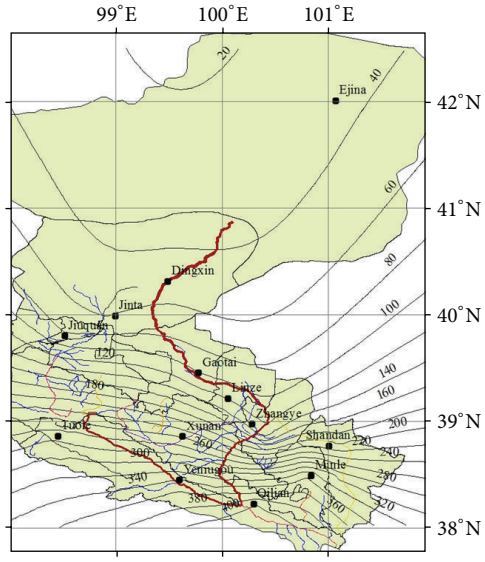

FIGURE 2: Spatial distribution of the average precipitation (mm) in the Heihe River Basin for the year 1960–2006 [20].

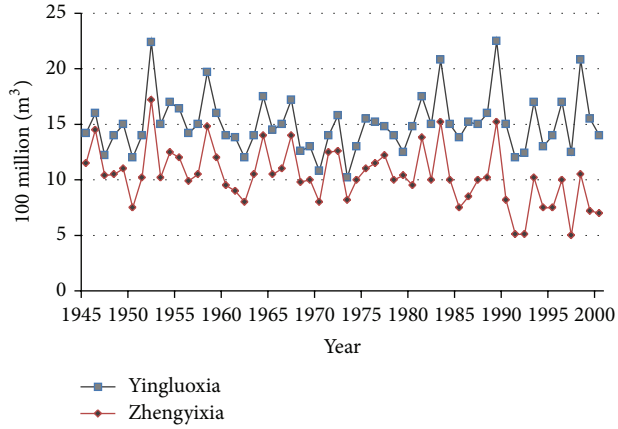

FIGURE 3: Change of the surface runoff through the Yingluoxia in the upper reaches and the Zhengyixia in the middle reaches.

accounted) in the middle reaches has come to 95, and the total storage capacity is up to 360 million m^3, 20 times more than that in the year 1949. As a result, the hydrology changed radically in the middle reaches, which is highlighted by the fact that the utilization rate of surface water increased by 19 times, the area of irrigated oasis expanded by 89.5%, and the area of desertification land increased by 4% to 11% since the year 1949. Along with utilization of the surface water, the groundwater was also been explored, and the number of motor-pumped well had doubled from the year 1985 to the year 1994 [22]. The groundwater table had been steadily decreasing due to the overpumping and the decreasing of recharges. In fact, there is a very close interconnection between the surface runoff and groundwater in the HRB because of the water distribution characteristics of HRB, which partly determined the hydrological process [16]. Last but not least, as the intermediate linkage between the surface water and the groundwater, the volume of springs also shows a decreasing tend. In addition, the average reducing rate had increased by 6.8% in the year 1981–1991 compared to the year 1960–1980 [22].

Consequently, the exploitation on surface runoff water and groundwater dramatically changed the hydrological situation of the HRB in the long historical period. All the 33 tributaries in the middle reaches no longer joined into the mean stream after 1980s, and they gradually disappeared and formed some independent irrigation oasis. The water volume of the runoff through the Zhengyixia decreased sharply in recent decades, from 1.19 billion m^3 in 1950s to merely 691 million m^3 in 1990s, and the mainstream became the seasonal river below the Zhengyixia (Figure 3). In arid region, large-scale development of irrigation agriculture induces dramatic increase of water demand. The excessive water consumption by humans has resulted in continued environmental deterioration, which has become a serious threat to sustainable development.

3.2. Irrational Water Consumption Structure along with Low Water Efficiency. Currently, the overall water consumption of all sectors in the HRB is about 3.36 billion m^3. Among them, industrial and domestic water consumption is fairly less, and agricultural water use accounts for about 95%, posing a great threat to the ecological water consumption. Indeed, groundwater has become the dominant source of water supply for irrigation in Northern China. Taking the year 2000 as an example, the annual water consumption in the HRB is 2.65 billion m^3. Specifically, the farmland irrigation consumption is 2.03 billion m^3, and the water consumption in the forestry, stock raising, and fishing sector is 489 million m^3 totally, industrial water consumption is 86 million m^3, livestock water consumption is 15 million m^3, people living consumption is 32 million m^3 (including urban public consumption), and the urban environment water consumption is two million m^3.

In terms of the spatial distribution of water consumption, it is mainly concentrated in the middle reaches, accounting for 84.1%. The water consumption in the lower reaches accounts for 13.6%, and the water consumption in the upper reaches merely accounts for 2.3% of the total water consumption. When water moves from mountains in the upper reaches to oases in the middle reaches and then disappears in the desert in the lower reaches, it courses significant differences in economic development, natural environmental bearing capacity, and ecological stability among the three reaches. The fact that population and economy mainly concentrate in the middle reaches results in the high water consumption in Shandan, Minle, Linze, Gaotai, and other regions (Table 1). Meanwhile, utilization of water resource in the year 2006 reached 95% (statistical data from the water resource department of Gansu Province), which far exceeds the rational exploitation warning line of 40% set by international consensus.

Globally, agricultural water use including irrigation accounts for about 70% of the global water and irrigated agricultural land comprises less than one fifth of the total cultivated area of the world but produces about two fifths of

Table 1: Statistics of water consumption (1000 m^3) of the Heihe River Basin by counties in the year 2000.

Region	Domestic living in cities	Domestic living in countryside	Industry	Farmland irrigation	Forest and fishing	Stock raising	City environment	Total
Qilian	417.8	353.3	1246.0	7815.6	5154.6	3305.9	38.8	18331.9
Shandan	1435.5	2702.9	15573.0	214360.0	20214.3	1300.0	138.5	255724.2
Minle	1968.3	3099.6	8771.0	404498.1	27034.0	1162.3	183.5	446716.7
Ganzhou	6371.4	6086.4	28222.1	640706.5	49352.0	4312.6	723.0	735774.0
Linze	1300.6	1993.0	13102.8	380011.4	57492.0	1109.6	119.1	455128.4
Gaotai	1591.5	2103.8	8609.9	278336.0	45154.0	1367.5	148.0	337310.7
Sunan	335.2	279.4	2434.4	24108.0	13844.4	1134.2	32.9	42168.6
Jinta	461.7	684.2	4669.2	68783.4	21100.0	418.4	41.0	96157.7
Ejina	390.9	62.9	2981.1	10136.5	249421.0	810.7	78.2	263881.2
Total	14272.8	17365.5	85609.4	2028755.5	488766.3	14921.0	1503.0	2651193.5

the world's food (Postel, 1999). Similarly, the irrigation farming in the middle reaches of the HRB has greatly contributed to the increase of food production historically and supported the large number of population of the northwestern China. In the HRB, large-scale development of irrigation farming induces dramatic increase of water demand. However, from the global perspective, food production relying on "irrigation miracle" gives significant impacts on water [23]. China's agricultural water consumption was much higher than other countries all over the world. For the ratio of daily life water usage, industrial water usage, and agricultural water, Russian is 17 : 60 : 23, Canada is 18 : 70 : 12, America is 13 : 45 : 42, and Brazil is 22 : 19 : 59, while China is 6 : 7 : 87. Therefore, there is a lot of works to do on agricultural water saving strategies in terms of water resource management.

In the HRB, agricultural water use accounted for about 94% of the total social and economic water consumption in the year 2006, but the water efficiency and the water productivity were very low. Due to people's unawareness of implementation of water-saving projects, as well as the restriction on the crop types, planting technologies, crop rotation, land management patterns, and unguaranteed maintenance costs, the water-saving renovation project cannot be effectively promoted, and leading the water demand for farmland irrigation is hard to decrease. This phenomenon is extremely predominating in the middle reaches of the HRB, where there are too many irrigation gates and plain reservoirs and where high technical irrigation engineering and exploitation of groundwater cannot be supported. All of these lead to low water efficiency and lower GDP output of per unit of water.

Water resource of the HRB can not only generate economic benefits, but also provide the ecological service function. Some scholars put forward the generalized water efficiency and point out that it not only represents the social and economic water consumption, but also represents natural ecological water consumption; it not only focuses on a single department or units water utilization process, but also pays attention to the water utilization of the whole region. A river basin is not only characterized by natural and physical processes but also related to man-made projects and management policies. In this sense, the lower reaches are rich in natural resources, but the ecological sustainability is extremely vulnerable because of limited water. The oasis is the most concentrated area of human activities in arid regions and the disturbances are happening on a large scale in this area. Therefore, the desertification process of the lower reaches of HRB exacerbated the deterioration of the ecological environment, causing the area to become a source of dust storms and threat environmental safety in northern China.

3.3. Deficient Systems and Institutions on Water Management along with Unreasonable Water Allocation Scheme. In the inland river basin, rising the water security and efficiency is of great significance, which can guarantee the water supply for livelihood and production. The situation about the low water efficiency in the HRB is far from being satisfactory. The deficiency of systems and institutions on water management as well as the unreasonable water allocation scheme becomes the primary cause of the severe water consumption in agriculture.

There are two main kinds of management strategies for community irrigation in the HRB: the collective management strategy and Water User Associations (WUAs) management strategy. For the collective management strategy mode, village leaders are in charge of the village water allocation, channel maintenance, water charges, and other relevant issues to fulfill their water management duties. In contrast, WUAs is independent water management organizations which take over the village leaders to be responsible for water allocation, channel maintenance, water charges, and other relevant issues in a specific village. In terms of the policies and measures on water demand management, there are three modes: water price, water tickets, and water rights. For the water price mode, the government would charge some fees for water services. For the water tickets mode, the farmers need to purchase water tickets from village leaders or WUAs before the farmland irrigation activities. The water rights mode refers to the water right card issued to farmers to guarantee their water consumption rights.

From the year 1992 onward, a series of water resource allocation and management policies have been implemented in China to alleviate the conflicts between natural water shortage and the high water consumption [24]. In the year

1997, the Heihe River Basin Bureau was established for special management of water resource in the HRB. With the support of scientific research from Chinese scholars, it has allocated the water resource for five times among the HRB. Unfortunately, different counties have its own management focuses and time schedules and that leads to another form of water waste.

The difficulty for a rational water allocation scheme is also constricted by the fact that the supply volume and the annual distribution of water in the lower reaches are completely subjected to the human activities in the middle reaches. In the long history, people living in the middle reaches performed irrigation agriculture (settled culture) and the people living in lower reaches performed nomadic husbandry. Even though conflict on water use between the middle reaches and lower reaches has a history of 200 years, it reached to an unprecedented situation. Since 1950s, intensive agricultural practices in the middle reaches have resulted in drastic environmental degradation in the lower reaches.

In addition, Heihe River dries up in May, June, and July and is flooded in August to October, and the water volume would reduce and even stops flowing sharply in December till the next March or April. At that time the river will be recharged. Consequently, there is a prominent contradiction between the water supply and demand in the lower reaches timely and spatially, which deteriorated by that fact that the high water demanding just happens in the dry periods [22]. Meanwhile, the water quality and water pollution caused by severe human activities cannot be ignored. In the past decades, the water scarce conditions and water quality situation have been aggravated dramatically in the lower reaches because of the large increase in agricultural fertilizer and pesticide use in the middle reaches.

4. Water Solutions of the Heihe River Basin

Considering the water scarcity character of the HRB, it is important to clarify the coupling relationship between water, ecology, and social economy, reveal the driving mechanism of the socioeconomic system on the evolution of water resource, improve the systems and institution designs for water management, and explore innovative approaches on optimal water allocation.

4.1. Research Findings on Decision Making for Water Management. There are significant differences in ecosystem structure among upper, middle, and lower reaches. Industrial and agricultural water demand in the middle reaches and ecological water consumption in the lower reaches form the mechanism of interaction of water supply and demand with the water producing in the upper reaches. Therefore, researches on the HRB should firstly focus on simulation of hydrologic process of the basin with the help of complex systematic modeling technology [25]. Granted by the "Major Research Plan on the HRB" initiated by the National Natural Science Foundation of China, Chinese scholars have conducted a series of researches, which are focused on the hydrologic process as well as the impacts of human activities on water resource. These researches basically conceptualized the basic laws of ecohydrological process in the HRB and revealed mechanisms on water cycling and ecological system evolution as well as the coupling mechanism between them.

The modeling work on the HRB is highlighted by model integration and meanly based on subregional modeling. There has been a lot of researches on hydrological process, groundwater, water resource, land use, land surface process, ecology, and social economy of the HRB based on a series of related models [12]. The model integration on the upper reaches of the HRB takes the distributed hydrological model as the core and realized the model coupling in a series of issues including the characteristics of runoff from mountainous subwatershed and the unity of atmosphere-vegetation-soil-permafrost-snow cover. As for the model integration in the middle reaches in the HRB, these researches are focused on coupling troubles among the surface water, groundwater, and the ecological models. For example, there was a study coupling SiB2 (land surface model) with aquifer flow, which significantly enhanced the capability of simulating evapotranspiration and surface-groundwater interaction and achieved systematic simulation for hydrological cycle in the middle reaches of the HRB. More comprehensively, a genuine farmland ecohydrological model was established by integrating MODFLOW (groundwater model), Hydrus-1D (soil water model), and WOFOST (crops growth model) models, coupling the land surface process module and stomatal-photosynthesis module. In addition, the model has certain capability of prediction and decision support. For instance, if the model is used to optimize irrigation system, it can save 27.27% irrigation water than the existing irrigation system. These studies have proved that the coupling model can be used to analyze ecological system and the interactions of the hydrological cycle and guide the water-saving practices on agriculture.

Another important consideration in model integration is modeling environment. It is the visual computer software platform that supports the efficient development of integration model, convenient connection among existing models or modules, module management, data pretreatment, and parameter calibration. The application of modeling environment in the integrated research of the HRB has mainly two directions. One is to use the existing international mature model to realize the coupling modeling environment to solve the key problems in integration issue. Considering the defects of existing modeling environment in the flexibility, another direction is to develop a new modeling environment. In this aspect, some Chinese scholars established the new modeling environment to explore the hydrology and land surface process. By using highly efficient and flexible module and data transfer mechanism, this environment has realized the flexible extensibility and reusability of the module. Based on this platform, some case studies of the modeling integration of the HRB have been implemented. For instance, the hydrological model TOPMODEL and the evaporation module from Noah (land surface process model) can be coupled together to make TOPMODEL be more reasonable when considering the effect of vegetation on water balance. In addition, with the help of this modeling environment, the question that "who supplies,

how much, how to fill" about water on ecological compensation of the upper reaches of the HRB has been answered.

Generally, studies in HRB meanly focused on the ecohydrological processes, water use mechanism of the typical plants, and their characteristics when responding to stress. A series of ecohydrology process model had been introduced, interpreted, or set up [26], including the Noah for ecological and hydrological processes, MODFLOW models for groundwater process, SWAT model for distributed hydrological processes, HYDRUS model, and the systematic conceptual model Gouburn-Broken Catchment for atmosphere-hydrology-vegetation interaction. At the upper reaches of the HRB, the integration research on ecohydrology process revealed the interaction mechanism between ecological system and hydrologic system, enhanced the cognition of mechanism on water resource formation and transformation, and laid the foundation for water resource evolution research under climate change. At the middle and lower reaches, the ecohydrological integration research clarified the relationship between the transformations of different kinds of water resource, illustrated the interaction and coupling mechanism between the water cycle and vegetation structure, rebuilt the spatial-temporal distribution of water resource in the historic periods, and forecasted it in the future.

However, the basin is a complete system for cooperative development and evolution of the human society as well as ecology. The HRB is an ideal case for integration study of "Water-Soil-Gas-Biology-Human" [12, 27]. Human activities have becoming the main driving force for hydrological circulation, and the social-economic water dimension rather than the natural hydrological dimension has become the driving water circulation, but researches on the former are very weak [28]. Model on either single process cannot comprehensively simulate the characterization of the process, behavior, and interaction mechanism of the whole system.

Based on the modeling and integration analysis, the Decision Support System (DSS) is vital to achieving the adaptive water management in the HRB. At present, there have been two types of DSS: research-oriented DSS and application-oriented DSS. Research-oriented DSS for the HRB is a scientific model integrating "Water-Soil-Gas-Biology-Human." It tries to integrate the expert knowledge and experience of the HRB to build a spatially explicit model with scenario analysis method. For the development of the research-oriented DSS, it has integrated multiple hydrologic models and coupled many GIS functions to support coupled work of multidisciplinary model. Also, it has made technical breakthroughs on the mismatch of the models at different spatial-temporal scales. Through providing scenario-driven decision making strategies graphically and multiobjectively and providing various auxiliary decision tools, it is expected to be a new generation of DSS for river basin integrated management. For the application-oriented DSS, some water management DSS can analyze the climate and human activities at the middle reaches of the HRB. It is also able to study the planting structure of different crops and spatial-temporal distribution of water requirement with different hydraulic engineering conditions. Finally, it can realize the simulation of water resource allocation process at multilevel (the whole basin, administrational district, and irrigation region) and evaluate the influence of varied water resource management strategies.

Taking the arid climate and the unique relationship among the three reaches of the HRB into consideration, there should be an innovative framework and research components for DSS for the HRB based on the existing studies (Figure 4). Spatially, water consumption of the HRB mainly concentrated in the middle reaches, where industrialization and urbanization are evident. Institutionally, there is a history of water right and water price system and institutions in the HRB, especially in the middle reaches where irrigation agriculture is preformed widely. Naturally, the desertification process exacerbated the deterioration of the ecology and change of oasis area. Also, the future climate change will greatly influence the hydrological process and water supple, that is, the precipitation as well as the solid glacier in the upper reaches. Therefore, as a unit of the whole scientific framework of the DDS, we should firstly comprehensively consider and make multiple scenarios analysis on the impacts of water right system reform, industrialization and urbanization, land use change, change of oasis area, and climate change on the HRB. This work can be conducted on the basis of exciting knowledge, data, and regional models. The scenarios analysis results would help to deepen and widen the recognition of the mechanism and linage of a series of factors within the ecology and economy of the arid area.

Secondly, the water resource utilization in the HRB is often confronted with the contradiction between ecological service and social and economic development. Therefore, it is necessary to realize the modeling integration between the social-economic model and ecohydrological model for the optimization of watershed management. Also, Millennium Ecosystem Assessment puts forward the idea that "regulating water supply service on ecosystem by means of economy and market is the preferred method of management." The balance between the water supply and demand is the core to integrate the social-economic model and ecohydrological model as separate module (Figure 4). The work on model integration needs to analyze the water supply capacity, water consumption structure, water efficiency, and water demand trend at multilevel (whole basin, administrational district, and irrigation region). Specifically, it needs to clarify the interaction mechanism among the water supply in the upper reaches, the industrial water consumption in middle reaches, and ecological water consumption in the lower reaches.

Further, the water management system is indispensable for the whole framework of the DDS. In practice, due to the absence of proper water management system, the conflicts among counties often arise because of competition on water use and jurisdictional mandates of the related stakeholders. An integrated watershed water management system should comprehensively consider the ecology, hydrology, and socioeconomy in the basin, in order to provide scientific support for the water security, ecological security, and sustainable development of the inland river basin. Last but not least, water optimal allocation strategies should be involved to explore the regulation measures under different natural and social scenarios. In recent years, a series of studies have been carried out on understanding the impact of human

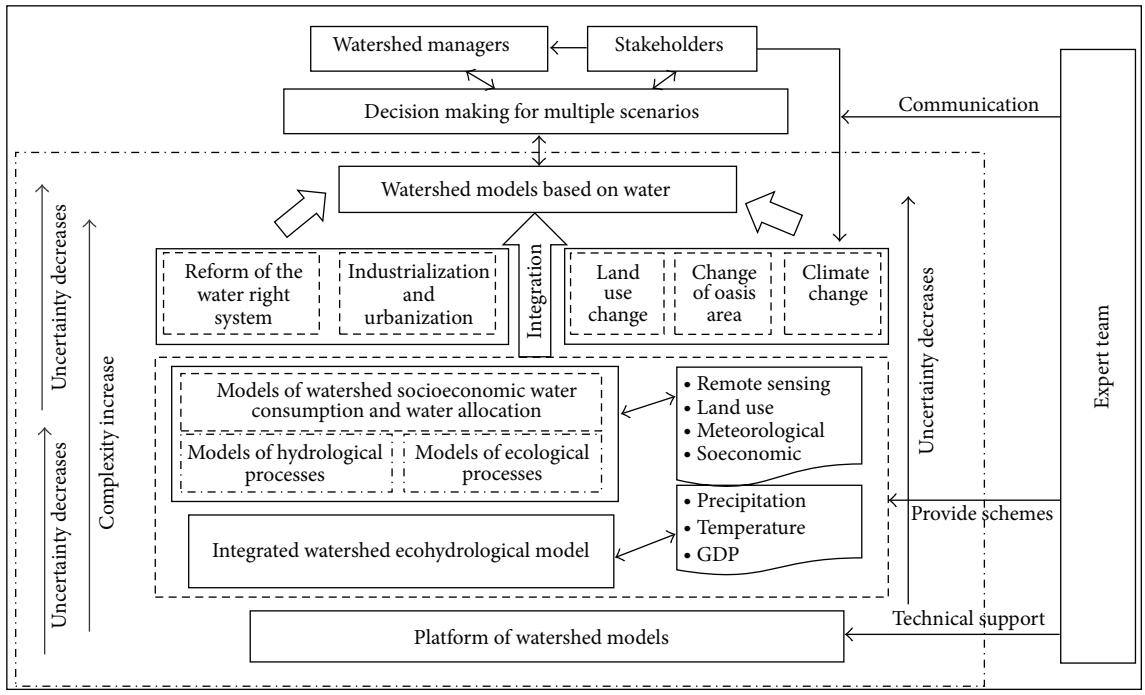

Figure 4: Framework and components for a DSS for the integrated water management in the Heihe River Basin.

activities (irrigation, livestock activities, and institutional change) on water [29]. However, compared to the study on the ecohydrological process and modeling research on the HBR, the mechanism studies water resource allocation are relatively weak. In this sense, both the system and institution design for water management and the optimal water resource allocation would be extended as follows.

4.2. Improving the System and Institution Design for Water Management. In recent years, the integrated management of the HRB has drawn great attention from Chinese government. Yellow River Conservancy Commission (YRCC) of the Ministry of Water Resources has organized a series of tasks such as "water problems and solutions of the HRB" and "ecological environment problems and solutions of the HRB," as well as "safeguard measures of water management of HRB" to improve the systems and institution design of water management. Further, Chinese government sets up Heihe River Bureau, an institution belonging to the YRCC, in the year 1999. A major task of this Bureau is to lead the project on uniform water management and water distribution throughout the HRB. Before that, water was used mainly for forest and grassland irrigation, groundwater recharge, and replenishment of the rivers in East Juyan Lake in lower reaches. Unfortunately, there has been no fundamental improvement for the water solutions.

Globally, there is a longstanding and widespread recognition that the river basin is the natural unit for water management [30, 31] (Table 2). For instance, the USA began to set up institutions to comprehensively manage river basins from 1930s. Created in the year 1933, the Tennessee Valley Authority (TVA) in 1933 is a river basin authority for the unified planning and full development of water resource on a river basin scale in order to achieve comprehensive regional socioeconomic development [30, 31]. Specifically, a far-reaching work was the Universal Soil Loss Equation (USLE), an empirical predictor for soil loss by water erosion [32]. It was built based on systematically analysis of observation data from more than 10 thousand runoff regions in 30 states in Eastern America in 30 years.

The last decades witnessed growth in research examining partnerships for integrated water resources management (IWRM) in different global regions. It is now employed globally in various physical, socioeconomic, cultural, and institutional settings. Compared to traditional approaches to water problems, IWRM takes a broader holistic view and examines a more complete range of solutions. It has promoted the water management to move into the substantial scientific research period, with good public participation mechanism and considering water, ecology, and social economy in the basin scale [33, 34]. Water management of basins in Colorado and Sacramento are based on the IWRM model. IWRM was also applied to water management practices in Murry-darling basin in Australia, River Rhine Basin, and The River Thames basin in Europe and received satisfactory results [35–37]. In addition, Arabia region paid great attention to the groundwater management and wastewater reuse and considered that IWRM must be considered when building the institutional framework; Countries belonging to the southern Africa development community (SADC) also tried to improve the water efficiency in arid area with the help of IWRM method to confront the food crisis and poverty [38].

Table 2: International water management strategies at typical watersheds and its inspirations for the Heihe River basin.

	Management modes and strategies	Inspiration
Mississippi valley in the USA	It has a comprehensive management system operated by multisectors and organizations at multilevel, including the military institutions composed of representatives from federal government and state government and nongovernmental organizations. The division of labor is clear-cut, avoiding confliction caused by duplication of work. A number of organizations at different levels to coordinate the interests of all parties concerned.	(i) Strengthening the legal system and establishing a series of watershed management regulations to constraint the behaviors from various stakeholders. (ii) Managing the whole basin that relies on subbasin as the unit by sharing information and cooperating by various institutions. (iii) Relying on the nonengineering measures, instead of engineering technology.
Murray-Darling River basin in Australia	Developed organization systems, which included three levels: the first level is the Ministerial Council in the national level, which is the highest decision-making body. The second level is the executing agency from the Ministerial Council, including the river basin committee and its office. The third level is the community advisory committee, which is responsible for communication between the council and the community and emphasizes public participation in watershed management.	(i) Authority for watershed management should be established on consultation mechanism. The full participation in proposal making is the key. An effective organization system can guarantee the implementation of the protocol. (ii) Introducing a new theory and method in the water distribution, separating the water right from the land right, and providing water for trading to formulate water market. (iii) Making the watershed management process more scientific, democratic, transparent, and fair.
Rhine River basin in the EU	This river applied international coordination and management mechanism early. Countries along the coastal signed agreements and regulations, as well as built different kinds of organization in the last centuries. The International Commission for the Protection of the Rhine (ICPR) was established in 1950 as the first intergovernmental body for protection against pollution in the Rhine and has made great success. ICPR set up supervision organizations and various professional groups and achieved remarkable success.	(i) Giving preference to prevention and source controlling and formulating detailed, standardized strict to regulate basin development. (ii) Paying emphasis on real-time monitoring and evaluation of the watershed management measures. (iii) Increasing storage capacity both in cities agriculture area to reduce water loss and soil erosion. Prohibiting development in riverbed. (iv) Presenting new concept of river ecosystem management and paying attention to the river health function and social economic factors as well as the support from modern science and technology.

One representative work on integrated river basin management is reflected in Water Framework Directive (WFD) implemented by EU in the year 2000. Taking over 10 years to develop, the objective of WFD is to build a comprehensive monitor and management system for all water bodies and develop programs and measures to formulate an up-to-date watershed management plan for dynamic water management. The basic requirement is that the watershed management plan must be comprehensively presented, making it clear that how to achieve the targets (ecological conditions, water conditions, chemical conditions, and protected scope) within the required time. In addition, it must carry on the economic analysis to effectively consider the cost and benefit of all the stakeholders as for all the measurement, making itself truly participating in watershed management planning work [39]. Although this command has been implemented for nearly 10 years, the management condition of these cross-border rivers is still in the stage of national independent development and management, and the mechanism of cooperation and negotiation within countries still needs to improve. With the rapid globalization and economic development, the development of the basin dynamics will continue to increase, so how to realize the basin management across administrative boundaries is an urgent problem.

In particular, there are some similar problems on water management among Murray-Darling River basin in Australia, the Nile River basin in Egypt, and the HRB. For instance, the responsibilities for water management in response to drought are unclear, water management authorities based on subriver basin have not paid enough attention compared to government management authority based on administrative regions, and economic and legal measurement still needs to be improved. To some extent, the comprehensive water management in Murray-Darling River basin and the Nile River basin can provide useful experiment and lessons for the water management in the HRB. The successful river management model and experience in Murray-Darling River basin include water management based on subwatershed rather than administrative regions, three-layer coordination (decision level, execution level, and coordination level), and market management strategy such as trade in water rights, as well as regular legal system based on interstate water compact. In addition, as for water management in arid region, Egypt is setting up the Nile River Forecast Center (NFC) for

controlling Nile water resource, in order to achieve the goal "maximum exploiting of existing water resource, restricting the projects that can pose a threat to water quality and water resource" by the year 2017. The prediction of river flow using the remote sensing, geography information systems, and global positioning systems (3S) technology can provide the basis for management and decision. Moreover, it emphasizes on the drainage reuse in the agricultural field and strengthens the utilization of rainfall resources through the implementation of farmland rainwater harvesting project. It reduces the rice planting area through the adjustment of planting structure and promotes drought resistant crops, thus effectively reducing the water consumption on agricultural production.

4.3. Reforming Management to Actualize the Optimal Water Allocation. Aside from scientific framework and institutions, the reform of water resource management needs investigations and studies at multiple levels to provide key parameters for DSS based on water demand of production, life, and ecology. First and foremost, it needs to carry out investigation at the irrigation district level to clarify the water management system in each irrigation district. By this method, we can evaluate the performance of the water management systems, such as "water price" and "water right." By doing so, we understand the current situation as well as the transformation character of existing water policies, and then clarify the impact mechanism on agricultural department and ecological systems. Secondly, it needs to further our research at the administrational level, calrifying the WUAs, water consuming situations, water association system, and other social economic features. The performance evaluation for WUAs can clarify the situation of WUAs (organization, incentive mechanism, and institutional arrangement) and the evolution character of the WUAs as well as its impacts on the agricultural production and the water efficiency.

Furthermore, the third level of investigations should focus on the household level to clarify water use of different crops, agricultural activities, and their socioeconomic characteristics. By doing so, we can analyze the impacts of various policy scenarios on water demand. For example, the land use patterns, labor force allocation, crop production and food security, and agricultural input-output benefits can be affected by the different land use and economic behavior of farmers in different water resource allocation scenarios. In addition, the income compensation policies, the adjustment on irrigation water price, and the progress on irrigation technologies are also related to various policy scenarios on water demand. Based on the above three levels of investigations, the useful and key parameters for the DSS can be obtained and thus can provide suggestions and recommendation for the management, institution, and policies to build a water-saving society.

As for the water efficiency in the HRB, the existing water management strategy should be improved firstly. Establishing water management system based on the theory of "water rights, water market" is an important method to improve the allocation efficiency of water. Although water managers in the middle reaches of the HRB introduce the "water right" for water resources management, the leverage function failed to play a role because of the deficient water rights trading market. Research shows that market-oriented water management framework is beneficial to allocating water and improving water efficiency [40]. How to allocate the water resource among multiple regions and industries efficiently is the vital joint of augmenting the water use efficiency to sustain the balance between ecology and economy and also within the related economies.

Research on the optimal allocation of water resource in China is to build the input-output model and the Computable General Equilibrium (CGE) model, both including the water resource account [41–43]. The extended input-output model and CGE model can be used at basin and county level to analyze the impacts of water right transformation and industrialization [44]. Other partial equilibrium models can be used to allocate the water resource among the irrigated areas according to the crop pattern, irrigation rate, and other agricultural attributes, and these are the core of the system to calculate and improve the water efficiency. Some scholars explored the effects of water market regulation strategies such as the reform of water price and the transaction of water rights through building input-output model in the Yellow River basin.

In addition, with the development of computer modeling technology, CGE model has become an effective tool to explore the effects of policies on water management. For instance, the CGE model had been used in Beijing to evaluate the economic policies on the water price and water allocation [41]. A number of indicators of water consumption were established to analyze the structural relationships between economic activities and their physical relationships with the water in Zhangye [29]. Other relevant studies at different scales include the impact of water allocation on social economy of different districts in Yellow River basin and the economic impact of South-to-North Water Diversion Project on different Administrative Region [45, 46]. The social and economic data used in most of these studies are static and on a single period, which are unfavourable for the scientific research applied to water management.

In this sense, it is necessary to build multisector dynamic CGE model for water allocation to comprehensively consider the effects of technological progress, the water rights system, water market on water demand (industrial water, ecological water, and domestic water), and water efficiency (Figure 5). The framework of CGE model should incorporate the water and land use resource as the production inputs into the production function to characterize the configuration on the water and land resources in various social and economic sectors under market price adjustment. The rationality of water rights allocation of the river basin refers to the fact that it can clarify a series of complex relationships, such as the contradiction between water supply and demand, the competition among different sectors, the water coordination among upper, middle and lower reaches, the investments about different water projects, and the benefits of economic and ecological water consumption, as well as the contemporary and future water consumption. Only in this way, can we achieve a relatively fair, acceptable water allocation scheme.

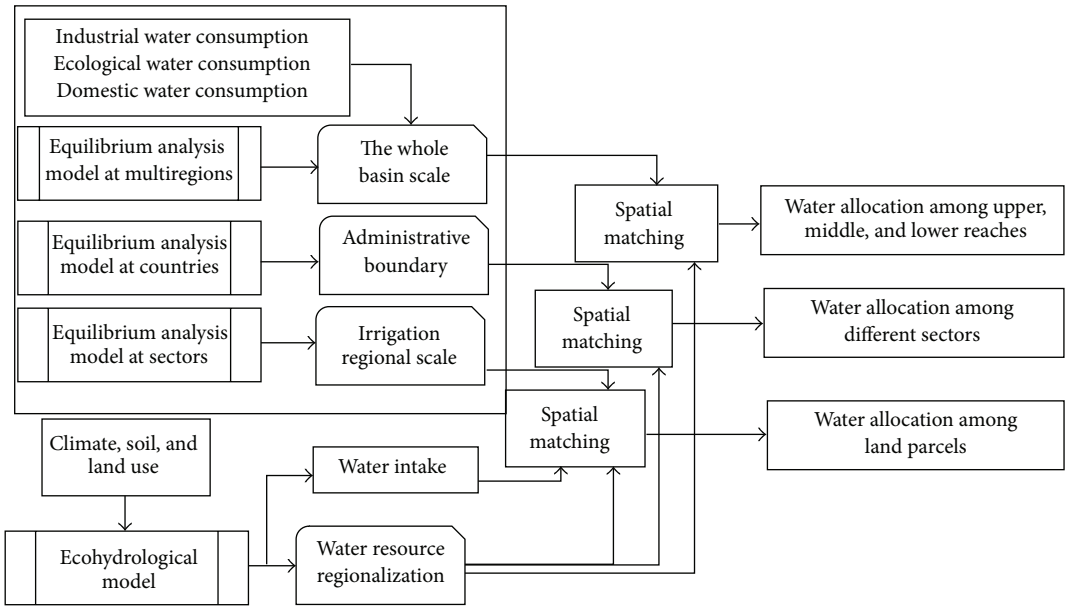

Figure 5: Multilevel water allocation strategy among irrigated area, counties, and sections of basin in the Heihe River Basin.

5. Conclusions

With high confidence to experience significant reduction in precipitation and water availability under potential climate change as indicated by the IPCC, the harmony between human being and water has become the theme of the development of river basin. As one of the largest inland river basins in Northwestern China, the HRB is characterized by fragile ecology as well as sensitive climate. Industrial and agricultural development in the middle reaches caused a decrease of incoming water and shrinking area of the Ejina Oasis in the lower reaches. Water security of the HRB is driven by multiple factors including agriculture and industry and livestock production, as well as ecology. Aside from a historical deceasing tendency in the water supply, water demand has changed dramatically during the 20th century in the HRB. Since water is a limited natural resource in the HRB, water scarcity is emerging when the demand outstrips the lands ability to provide the needed water. Sustainable development of the HRB needs a guarantee from water security, and there are a lot of emergent issues that need to be solved.

With an increasing competition for water across sectors and regions, the river basin has been recognized as the appropriate unit to analyze and confront the challenges of water management. In particular, the HRB is facing competition problems for water uses among domestic, industrial, and agricultural sectors and between users and ecological needs. Therefore, coupling of the ecohydrological model and social-economic model is to optimize the necessary premise of integrated river basin management. Generally, conflictions of priorities on water resource coupled to the severe natural conditions make it urgent to build a successful water management system for different stakeholders in the HRB. In this sense, establishing a DSS for water management is an important method to realize the adaptive water management for the sustainable development of the HBR.

Contemporarily, there are a series of worldwide researches on water management in river basin. Some counties have presented and improved their own policies and regulation measures based on their own water problems and national conditions. All of these provide some experience for integrated water management of the HRB. Nevertheless, the basin is a dynamic, multivariate unbalanced, and open dissipative "unstructured" or "semistructured" system. Considering the two dimensions (Nature-Society) driving character, for water reallocation, the existing modes and systems can not directly be copied and applied to the HRB.

Throughout studies on the HRB and other inland rivers, it can be identified that promoting water management from water demand management to water consumption management is an important direction for scientific and sustainable development of the HRB. Furthermore, from the institutional perspective, a spatially and dynamically effective water allocation scheme is a strategic need for rational and efficient use of water in the HRB. In view of the abovementioned structure and efficiency of the current water consumption situation, a pressing matter of the moment for reforming the water management systems in the HRB is to improve and the water right system based on the water demand in production, human living, and natural ecology.

In summary, it is necessary to establish an integrated water management system based on the water carrying capacity in order to provide support for the strategic decision making at watershed scale for sustainable development of the HRB. In addition, establishing an integrated model on river basin with clear physical process, powerful functions, and strong applicability has universal significance. It can also be applied to many inland basins in China, as well as other

inland river basins which are distributed in all continents of the world, account for 11.4% of the global land area, and provide significant support for sustainable development of regions with severe water shortage, fragile environment, and rapid development demand.

Conflict of Interests

The authors declare that there is no conflict of interests regarding the publication of this paper.

Acknowledgments

This research was financially supported by the major research plan of the National Natural Science Foundation of China (Grant no. 91325302) and the National Natural Science Funds of China for Distinguished Young Scholar (Grant no. 71225005).

References

[1] F. R. Rijsberman, "Water scarcity: fact or fiction?" *Agricultural Water Management*, vol. 80, no. 1–3, pp. 5–22, 2006.

[2] H. Zhou, X. Zhang, H. Xu, H. Ling, and P. Yu, "Influences of climate change and human activities on Tarim River runoffs in China over the past half century," *Environmental Earth Sciences*, vol. 67, no. 1, pp. 231–241, 2012.

[3] X.-P. Deng, L. Shan, H. Zhang, and N. C. Turner, "Improving agricultural water use efficiency in arid and semiarid areas of China," *Agricultural Water Management*, vol. 80, no. 1–3, pp. 23–40, 2006.

[4] C.-L. Fang, C. Bao, and J.-C. Huang, "Management implications to water resources constraint force on socio-economic system in rapid urbanization: a case study of the Hexi Corridor, NW China," *Water Resources Management*, vol. 21, no. 9, pp. 1613–1633, 2007.

[5] K. Bakker, "Water security: research challenges and opportunities," *Science*, vol. 337, no. 6097, pp. 914–915, 2012.

[6] B. Bates, Z. W. Kundzewicz, S. Wu, and J. Palutikof, *Climate Change and Water*, Intergovernmental Panel on Climate Change (IPCC), 2008.

[7] C. J. Vörösmarty, P. Green, J. Salisbury, and R. B. Lammers, "Global water resources: vulnerability from climate change and population growth," *Science*, vol. 289, no. 5477, pp. 284–288, 2000.

[8] IPCC, "Climate change 2007: the physical science basis," *Agenda*, vol. 6, no. 7, p. 333, 2007.

[9] J. Kim, J. Choi, C. Choi, and S. Park, "Impacts of changes in climate and land use/land cover under IPCC RCP scenarios on streamflow in the Hoeya River Basin, Korea," *Science of the Total Environment*, vol. 452-453, pp. 181–195, 2013.

[10] F. Tao, M. Yokozawa, Y. Hayashi, and E. Lin, "Future climate change, the agricultural water cycle, and agricultural production in China," *Agriculture, Ecosystems & Environment*, vol. 95, no. 1, pp. 203–215, 2003.

[11] C. Bao and C.-L. Fang, "Water resources constraint force on urbanization in water deficient regions: a case study of the Hexi Corridor, arid area of NW China," *Ecological Economics*, vol. 62, no. 3-4, pp. 508–517, 2007.

[12] G. Cheng, X. Li, W. Zhao et al., "Integrated study of the water-ecosystem-economy in the Heihe River Basin," *National Science Review*, vol. 1, no. 3, pp. 413–428, 2014.

[13] G.-D. Cheng, H.-L. Xiao, Z.-M. Xu, J.-X. Li, and M.-F. Lu, "Water issue and its countermeasure in the Inland River basins of Northwest China—a case study in Heihe River Basin," *Journal of Glaciology and Geocryology*, vol. 3, p. 016, 2006.

[14] S.-Z. Qi and F. Luo, "Water environmental degradation of the Heihe River Basin in arid Northwestern China," *Environmental Monitoring and Assessment*, vol. 108, no. 1–3, pp. 205–215, 2005.

[15] Q. Guo, Q. Feng, and J. Li, "Environmental changes after ecological water conveyance in the lower reaches of Heihe River, northwest china," *Environmental Geology*, vol. 58, no. 7, pp. 1387–1396, 2009.

[16] G. Zhu, Y. Su, C. Huang, Q. Feng, and Z. Liu, "Hydrogeochemical processes in the groundwater environment of Heihe River Basin, northwest China," *Environmental Earth Sciences*, vol. 60, no. 1, pp. 139–153, 2010.

[17] H. Xi, Q. Feng, W. Liu, J. Si, Z. Chang, and Y. Su, "The research of groundwater flow model in Ejina Basin, Northwestern China," *Environmental Earth Sciences*, vol. 60, no. 5, pp. 953–963, 2010.

[18] R. Ding, F. Wang, J. Wang, and J. Liang, "Analysis on spatial-temporal characteristics of precipitation in Heihe River Basin and forecast evaluation in recent 47 years," *Journal of Desert Research*, vol. 29, pp. 335–341, 2009.

[19] Y. H. Su, G. F. Zhu, Q. Feng, Z. Z. Li, and F. P. Zhang, "Environmental isotopic and hydrochemical study of groundwater in the Ejina Basin, Northwest China," *Environmental Geology*, vol. 58, no. 3, pp. 601–614, 2009.

[20] R. Ding, F. Wang, J. Wang, and J. Liang, "The analysis and forecast evaluation about the temporal and spatial characteristic of the precipitation in Heihe River Basin nearly 47 years," *Journal of Desert Research*, vol. 2, 2009.

[21] B. Huai, Z. Li, M. Sun, P. Zhou, and Y. Xiao, "RS analysis of glaciers change in the Heihe River Basin in the last 50 years," *Acta Geographica Sinica*, vol. 69, no. 3, pp. 365–377, 2014.

[22] G. Wang and G. Cheng, "Changes of hydrology and ecological environment during late 50 years in Heihe River Basin," *Journal of Desert Research*, vol. 18, no. 3, pp. 233–238, 1998.

[23] H. Turral, J. J. Burke, and J.-M. Faurès, *Climate Change, Water and Food Security*, Food and Agriculture Organization of the United Nations, Rome, Italy, 2011.

[24] X. Cai, "Water stress, water transfer and social equity in Northern China-Implications for policy reforms," *Journal of Environmental Management*, vol. 87, no. 1, pp. 14–25, 2008.

[25] L. J. Bracken and E. A. Oughton, "Interdisciplinarity within and beyond geography: introduction to special section," *Area*, vol. 41, no. 4, pp. 371–373, 2009.

[26] X. Li, X. Yang, Q. Gao, Y. Li, and S. Dong, "Integrative assessment of hydrological, ecological, and economic systems for water resources management at river basin scale," *Frontiers of Earth Science in China*, vol. 3, no. 2, pp. 198–207, 2009.

[27] G. Cheng, H. Xiao, C. Li, J. Ren, and S. Wang, "Water saving eco-agriculture and integrated water resources management in the Heihe River Basin, northwest China," *Advances in Earth Science*, vol. 23, no. 7, pp. 661–665, 2008.

[28] X. Li, G. Cheng, and L. Wu, "Digital Heihe River Basin. 1: an information infrastructure for the watershed science," *Advances in Earth Science*, vol. 25, no. 3, pp. 297–305, 2010.

[29] Y. Wang, H.-L. Xiao, and R.-F. Wang, "Water scarcity and water use in economic systems in Zhangye City, Northwestern China,"

Water Resources Management, vol. 23, no. 13, pp. 2655–2668, 2009.

[30] G. F. White, "A perspective of river basin development," *Law and Contemporary Problems*, vol. 22, no. 2, pp. 157–187, 1957.

[31] J. Warner, P. Wester, and A. Bolding, "Going with the flow: river basins as the natural units for water management?" *Water Policy*, vol. 10, no. 2, pp. 121–138, 2008.

[32] P. Cardei, V. Herea, V. Muraru, and R. Sfaru, "Vector representation for the soil erosion model USLE, a point of view," *Bulletin of University of Agricultural Sciences and Veterinary Medicine Cluj-Napoca. Agriculture*, vol. 66, no. 2, pp. 46–53, 2009.

[33] G. W. P. Gwp, "Integrated water resources management," Technical Advisory Committee (TAC), 2004.

[34] J. Alcamo, M. Flörke, and M. Märker, "Future long-term changes in global water resources driven by socio-economic and climatic changes," *Hydrological Sciences Journal*, vol. 52, no. 2, pp. 247–275, 2007.

[35] C. Tortajada, A. Biswas, O. Varis, and C. Tortajada, "Institutions for IWRM in Latin America," in *Integrated Water Resources Management in South and Southeast Asia*, pp. 303–324, 2004.

[36] B. Mitchell, "Integrated water resource management, institutional arrangements, and land-use planning," *Environment and Planning A*, vol. 37, no. 8, pp. 1335–1352, 2005.

[37] S. Giri, A. P. Nejadhashemi, and S. A. Woznicki, "Evaluation of targeting methods for implementation of best management practices in the Saginaw River Watershed," *Journal of Environmental Management*, vol. 103, pp. 24–40, 2012.

[38] U. Simon, R. Brüggemann, and S. Pudenz, "Aspects of decision support in water management—example Berlin and Potsdam (Germany) I—Spatially differentiated evaluation," *Water Research*, vol. 38, no. 7, pp. 1809–1816, 2004.

[39] P. Chave, *The EU Water Framework Directive*, IWA Publishing, 2001.

[40] J. J. Pigram, "Economic instruments in the management of Australia's water resources: a critical view," *International Journal of Water Resources Development*, vol. 15, no. 4, pp. 493–509, 1999.

[41] X. Deng, Y. Wang, F. Wu, T. Zhang, and Z. Li, "The integrated CGE model construction," in *Integrated River Basin Management*, SpringerBriefs in Environmental Science, pp. 57–78, Springer, Berlin, Germany, 2014.

[42] F. Wu, J. Zhan, C. Shi, and C. Zhao, "An extended inputoutput table for environmental and resources accounting," *Chinese Journal of Population Resources and Environment*, vol. 12, no. 1, pp. 33–41, 2014.

[43] Y. Zhao, X. Deng, Q. Lu, and W. Huang, "Regional rural development, nitrogen input and output in farming-grazing system and its environmental impacts—a case study of the Wuliangsuhai Catchment," *Procedia Environmental Sciences*, vol. 2, pp. 542–556, 2010.

[44] X. Deng, F. Zhang, Z. Wang, X. Li, and T. Zhang, "An extended input output table compiled for analyzing water demand and consumption at county level in China," *Sustainability*, vol. 6, no. 6, pp. 3301–3320, 2014.

[45] M. Berrittella, K. Rehdanz, R. Roson, and R. S. J. Tol, "The economic impact of water taxes: a computable general equilibrium analysis with an international data set," *Water Policy*, vol. 10, no. 3, pp. 259–271, 2008.

[46] S. Feng, L. X. Li, Z. G. Duan, and J. L. Zhang, "Assessing the impacts of South-to-North Water Transfer Project with decision support systems," *Decision Support Systems*, vol. 42, no. 4, pp. 1989–2003, 2007.

Hindawi Publishing Corporation
Advances in Meteorology
Volume 2015, Article ID 632151, 11 pages
http://dx.doi.org/10.1155/2015/632151

Research Article

The Effect of Land-Use Intensity on Surface Temperature in the Dongting Lake Area, China

Wenmin Hu,[1] Weijun Zhou,[1] and Hongshi He[2]

[1] *College of Resources and Environment, Hunan Agricultural University, Changsha 410128, China*
[2] *Institute of Applied Ecology, Chinese Academy of Sciences, Shenyang 110016, China*

Correspondence should be addressed to Wenmin Hu; wenmin115@163.com

Received 27 August 2014; Revised 30 October 2014; Accepted 8 December 2014

Academic Editor: Jinwei Dong

Land use and its environmental effects can be quantitatively expressed with land-use intensity. In this study, a land-use intensity metric was improved using a geographic mapping method. The relationships between observed rapid changes in land use and temperature in the Dongting Lake area from 2001 to 2010 were examined. The results revealed the following features: (1) The temperature increased when the land-use intensity increased via a hierarchical transition owing to grass and forest land reductions of 26.25% and 11.74%, respectively; built-up land increased by 48.45%. (2) The temperature increase was driven more by the external environment than by land-use intensity changes. Human activities produced larger effects in the western region than in the eastern or central region of the study area, according to the observed variations in the centres of gravity for temperature and land-use intensity. (3) The temperature response to land-use intensity changes was more sensitive in low-altitude areas than in high-altitude areas; the response presented a north-south gradient, possibly due to socioeconomic and urbanisation differences.

1. Introduction

With rapid social and economic development, the influence of human activities on the land surface temperature (LST) has intensified. Land-use intensity can convey the intensity of human activities and can provide a basis for discussing the relationship between land-use and environmental changes [1]. Changes in land-use intensity can be regarded as an extension of land-use/cover changes (LUCC) [2]. These changes are influenced by not only land cover but also policy measures [3], such as adjusting the structure of land use [4], regulating urban expansion, or optimising economic structures [5]. These changes impact environmental factors, such as the LST [6]. Therefore, the surface temperature could be affected by the variation in and intensity of land use.

Presently, the relationship between surface temperature and land-use intensity is difficult to determine because the quantitative expression for land-use intensity is complicated. Many studies have applied the land-use area [7], the landscape index [8], or particular quality control indexes, such as the intensity of a water supply and drainage, the amount of fertilisation, water consumption, or energy consumption [9–11]; however, these metrics are unable to embody the impacts of human activities on the land-use environment. Our study defines land-use intensity according to the "Study on China's Land Use of Temporal and Spatial Information on Remote Sensing" and seeks to improve the quantitative expression of land-use intensity using a GIS cartographic method. This new method might more reasonably explain the relationship between changes in land-use intensity and surface temperature.

Our study period was from 2001 to 2011 when the global temperature drastically changed [12, 13]. Many studies suggest that this period is indicative of a temperature spike. Foster and Rahmstorf [14] considered this period as having the most rapid global temperature increase. Solomon and Newman [15] emphasised that the thermal and atmospheric circulations in this period accelerated oceanic warming. Fall et al. [16] found that land-use and cover changes during the period resulted in greater warming compared with greenhouse gases. In addition, the study area around Dongting Lake, which is China's second largest interior lake, is a centre

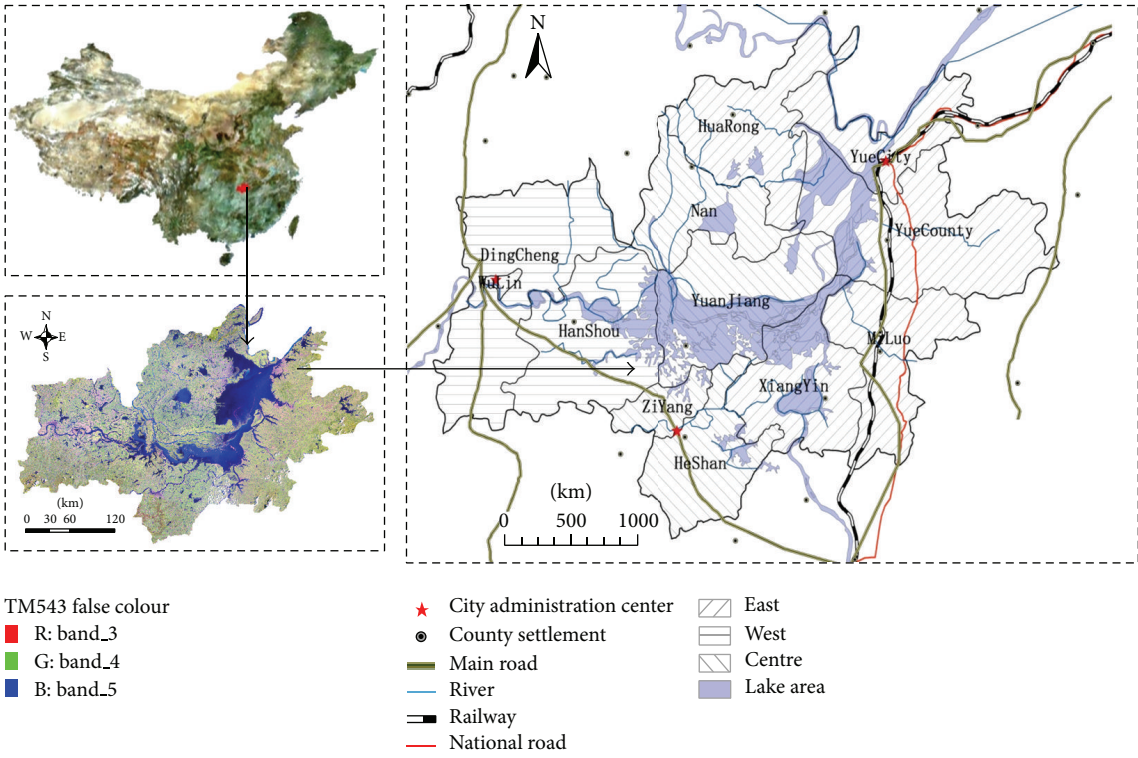

Figure 1: The location of the study area.

for the development of the national agricultural economy. Because of the influence of economic development and social activities, the surface temperatures were strongly affected by land-use changes.

Therefore, our research objectives were as follows: to determine the spatiotemporal differences between surface temperature changes and land-use intensity in the Dongting Lake area, to identify the intrinsic link between the landscape and gravitational and zonal changes in the macroenvironment, and to reveal the relationship between land-use intensity and land surface temperature from a geographical perspective. The results could lead to improvements in the ecological environment and provide a reference for rational land-use policy in the lake district.

2. Material and Methods

2.1. Study Area. The Dongting Lake District (28°03′–30°20′N, 110°40′–113°30′E), which is located in central China (Figure 1), encompasses approximately 21,000 km^2. Dongting is the second largest freshwater lake in China and is listed as one of the world's most substantial wetlands. The lake is divided into eastern, central, and western areas that are governed by three cities (Yueyang, Yiyang, and Changde, resp.). The average annual temperature is 16.6–17.6°C; the temperature is approximately 4.5°C in January and 30°C in July. The average annual precipitation is 1,303 mm. Approximately 16.63 million people live in the district (23.5% of the population of Hunan Province). The main landforms are plains and lakes that have abundant natural resources. The Dongting Lake District is an important economic production area in China. The economy has rapidly developed in recent years. In 2000, the urbanisation rate was 19%, and the regional GDP was 14.5 billion dollars. However, in 2011, the urbanisation rate increased to 38%, and the regional GDP was 56.3 billion dollar. The ratio of the industry, agriculture, and service sectors was 19 : 45 : 36. Agriculture has always played an important role in the district's economy.

2.2. Data Sources and Preprocessing. The land-use data were derived from TM/ETM+ images of LANDSAT5/7, which were downloaded from China's International Scientific Data Service Platform (http://www.gscloud.cn/). The data were obtained for the summers of 2001 and 2011, which correspond to the climate normal period. The images were preprocessed with radiation correction, geometric correction, and stripe elimination. According to the *State-Level Land-Use and Coverage Classification System* [17], the land was classified with a hierarchical decision tree using the supervised classification method [18]. Initially, the land was classified into thirteen land-use types: dry land, paddy field, high-coverage forested land, low-coverage forested land, high-coverage grassland, moderate-coverage grassland, low-coverage grassland, lakes, rivers, reservoirs, urban land, rural residential land, sand, and other lands. Then, the data were consolidated into six first-class types (Level II to Level I): cultivated land, forested land, built-up land, grassland, water body, and unused land (Table 1). The classification-precision assessment reached 83.5% using a land-use status map from 2006.

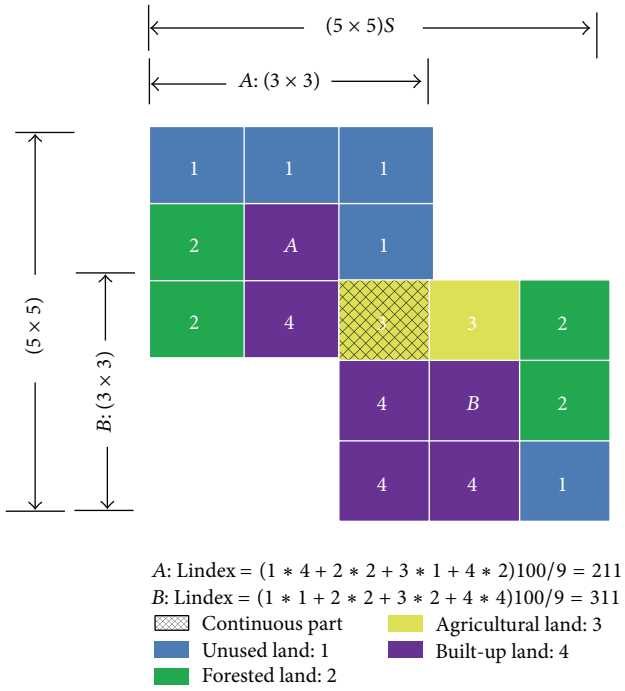

Figure 2: Spatial information of land-use intensity.

2.3. Optimisation of the Land-Use Intensity Expression. Land-use intensity varies according to the land-use type. Moreover, the consensus [19] is that built-up land has the highest intensity, followed by forested land, grassland, water bodies, and unused land. Therefore, the land-use intensity was classified into four grades, and each grade was assigned a value (Table 2). The land-use grades are the four ideal states in Table 1; however, the four states are actually unequally mixed within the same area. Using the grades, the land-use intensity forms a continuous-distribution composite index that ranges from 1 to 4. For the convenience of geographical calculations, the values were multiplied by 100; therefore, the land-use intensity is equivalent to the Weaver index.

The expression of land-use intensity is as shown in Table 2:

$$\text{Lindex} = 100 \times \sum_{i=1}^{n} A_i \times C_i. \quad (1)$$

Lindex is the comprehensive index of land-use intensity for which Lindex $\in$ [100, 400], A_i is the classification index of land use at the ith grade, C_i is the percentage of land-use intensity at the ith grade, and n is the classification number of the land-use intensity, $n = 4$.

An expression based on geographical radiative units (Figure 2) was developed. The weight coefficients mainly radiate outward from the basic units of A and B. The radius is one unit, and A and B represent the average land-use intensity of the region (3 × 3). The shaded areas are the mutual units connecting A and B. When A and B are calculated, their mutual units should be calculated repeatedly. Therefore, the average land-use intensity of the radiated areas in A and B was 211 and 311, respectively. This expression shows the influence of the surrounding land types and the continuity in geographical space; therefore, the expression is more scientific in practice.

Table 1: Land-use/cover classification in the Dongting Lake area.

Level I categories	Level II categories
Cultivated land	Dry land
	Paddy field
Forested land	High-coverage forested land
	Low-coverage forested land
Grassland	High-coverage grassland
	Moderate-coverage grassland
	Low-coverage grassland
Water body	Lakes
	Rivers
	Reservoirs
Built-up land	Urban land
	Rural residential land
Unused land	Sand
	Other lands

This method can effectively express the continuous characteristics of land-use intensity and the extent of land-use aggregation. The units were not subject to administrative partitions and were related to only the grid granularity (resolution) and scale (search radius). A higher unit resolution yields a more accurate expression. The unit value could also reflect the characteristics of the landscape. For example, a value within [300, 400] indicates that built-up land provided the greatest contribution, so built-up land was the dominant land-use type. In this research, 30 m resolution remote-sensing data were adopted; the radiative radius was 15 units or 930 m × 930 m. The value of each unit represented the average land-use intensity within an area of 8.4 hm^2. The total number of units was 5,877.

2.4. Land Surface Temperature Inversion. Table 3 showed the average surface temperature distribution in Dongting Lake, and the data in Table 3 was obtained from the China Statistical Yearbook. July, August, and September, which are the warmest months (summer) in the lake area, are chosen to facilitate intraseasonal comparisons.

The LSTs in July, August, and September of 2001 and 2011 in the Dongting Lake District were derived from NASA MODIS data (US). The image data were preprocessed with atmospheric corrections, radiometric calibrations, graphic clipping, and geometric corrections. The LST was calculated using the split-window algorithm (Figure 4) [20]. The process is as follows:

$$\text{TS} = A_0 + A_1 T_{31} - A_2 T_{32}, \quad (2)$$

where TS is the surface temperature (K), T_{31} and T_{32} are the satellite radiances of MODIS in the 31st and 32nd spectral

Table 2: Land-use intensity grade.

Land-use type	Unused land-use grade	Forested land, grassland, water-body use grade	Agricultural land-use grade	Urban land-use grade
Grading index	1	2	3	4

Table 3: Average surface temperature distribution in Dongting Lake in 2001 and 2011 (unit: ˚C).

Year	May	June	August	September	September	October
2001	23.0	24.9	29.2	27.3	26.1	18.9
2011	21.8	24.2	30.5	28.8	25.3	17.5

bands, respectively, and A_0, A_1, and A_2 are the split-window parameters, which are defined as follows:

$$\begin{aligned} A_0 &= E_1 a_{31} - E_2 a_{32}, \\ A_1 &= 1 + A + E_1 b_{31}, \\ A_2 &= A + E_2 b_{32}, \end{aligned} \tag{3}$$

where a_{31}, b_{31}, a_{32}, and b_{32} are constants. Within the surface temperature range of 0–50˚C, these constants are $a_{31} = -64.60363$, $b_{31} = 0.440817$, $a_{32} = -68.72575$, and $b_{32} = 0.473453$. The intermediate parameters of the abovementioned equations are calculated as follows:

$$\begin{aligned} A &= \frac{D_{31}}{E_0} \\ E_1 &= \frac{D_{32}\left(1 - C_{31} - D_{31}\right)}{E_0} \\ E_2 &= \frac{D_{31}\left(1 - C_{32} - D_{32}\right)}{E_0} \\ E_0 &= D_{32} C_{31} - D_{31} C_{32} \\ C_i &= \varepsilon \zeta_i(\theta) \\ D_i &= \left[1 - \zeta_i(\theta)\right]\left[1 + \left(1 - \varepsilon_i\right)\zeta_i(\theta)\right], \end{aligned} \tag{4}$$

where i is the spectral band of MODIS $i = 31$ or 32, $\zeta_i(\theta)$ is the atmospheric transmissivity when the visual angle is θ, and C is Earth's surface emissivity in spectral band i. Finally, the average monthly temperature was consolidated according to the inversion result. The average temperatures in the summers of 2001 and 2011 were obtained. The precision test of the measured temperatures from the station in 2011 indicated that the standard error of the inversion precision was 0.25˚C, which meets the general requirement.

2.5. Centre of Gravity Model. The relationship between the variation in the land-use and temperature centre of gravity was investigated using the centre of gravity model. This model, which has been widely applied to analyse correlations and extent of influence [21], is expressed as follows:

$$\begin{aligned} x &= \frac{\sum_{i=1}^{n} x_i \times M_i}{\sum_{i=1}^{n} M_i}, \\ y &= \frac{\sum_{i=1}^{n} y_i \times M_i}{\sum_{i=1}^{n} M_i}, \end{aligned} \tag{5}$$

where x and y are the centres of gravity of particular attributes in a region, x is the longitude, y is the latitude, x_i and y_i are the central longitude and latitude of the ith unit, respectively, and M_i is a particular attribute in the unit. In this study, the M_i attributes were land-use intensity or temperature. The variation in the centre of gravity of attributes was calculated for the eastern, middle, and western areas of the Dongting Lake District:

$$D_{W-j} = K \times \left[\left(x_w - x_j\right)^2 + \left(y_w - y_j\right)^2\right]^{1/2}, \tag{6}$$

where D_{w-j} represents the distance of the variation in the centre of gravity in different years, where w represents a previous time and j represents a later time, (x_w, y_w) and (x_j, y_j) represent the geographic position of the centre of gravity of a particular attribute at times w and j, respectively, or the longitude and latitude of the centre of gravity in the region, and K is a constant (111.111 km) for converting the longitude and latitude of the plan range.

3. Results and Discussion

3.1. Characteristics of Temperature Changes and Land-Use Intensity Changes. Figure 3 presents the results of the land-use classification and intensity expression in 2001 and 2011. Built-up land increased gradually, whereas forested land decreased due to a transition to agricultural and built-up land. The value of the land-use intensity in the Dongting Lake District varied between 100 and 400. A comparison of the land-use classification and intensity revealed that the land-use intensity varied with the land-use type, which was manifested as a continuous transitional feature. The colour gradually darkened from the water to the cultivated land and built-up land. Moreover, the land-use intensities were higher in locations close to urban centres (Figure 3). Therefore, the land-use intensity gradually increased towards urban centres, as represented by the scattered pattern from the urban centre to the suburbs. Additionally, the rapid urbanisation of the region is consistent with human activities.

Figure 4 displays the LST distribution in the summers of 2001 and 2011. High temperatures mainly occurred in urban centres, that is, the heat island effect. The regional average temperature exhibited an increase over the past decade;

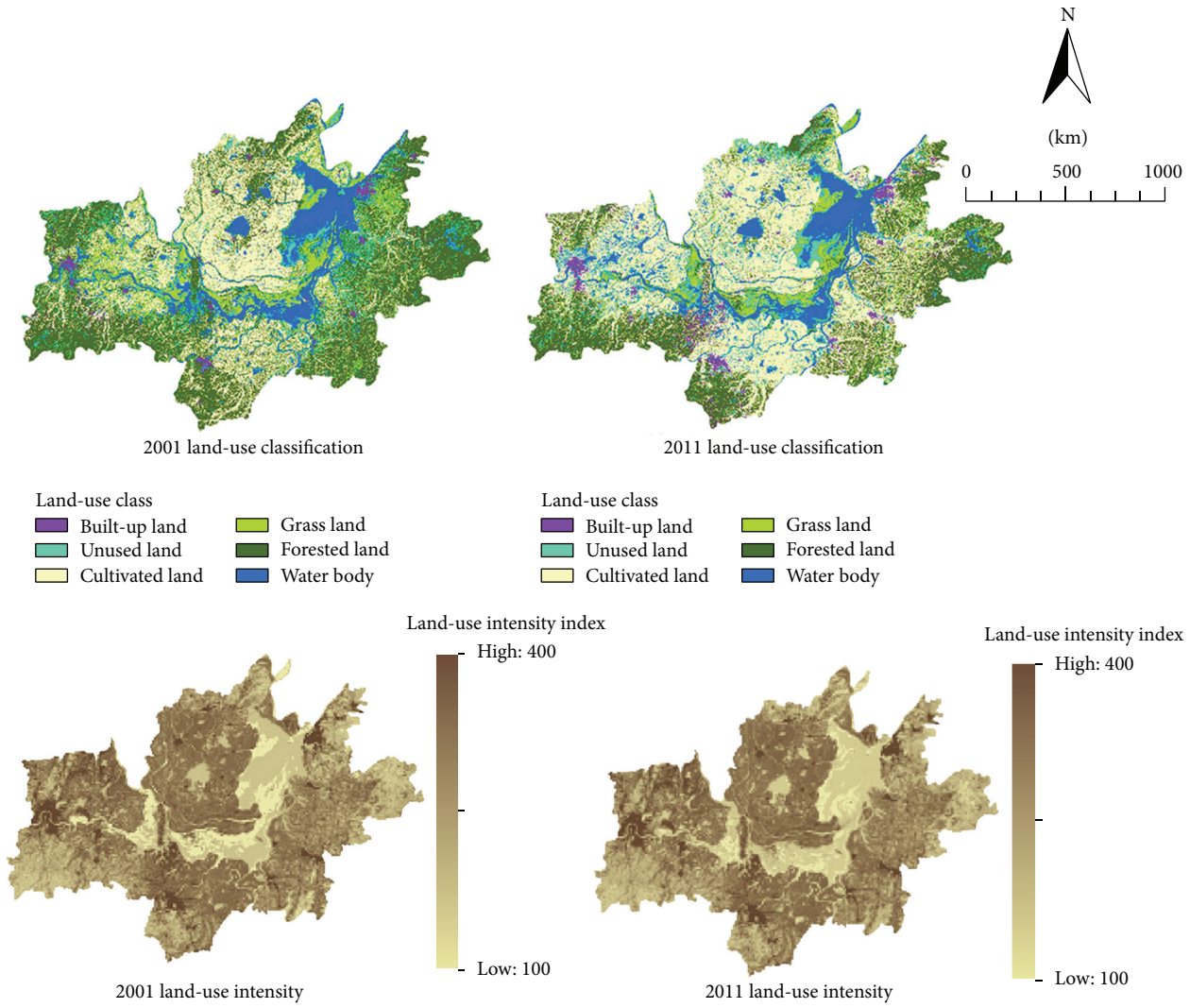

Figure 3: Spatial expression of the land-use classification and land-use intensity in 2001 and 2011.

the LST ranged from −0.458°C to 1.421°C. The temperature rise was higher in the south. The minimum, maximum, and average temperatures were, respectively, 29.411°C, 30.602°C, and 30.048°C in 2001 and 29.849°C, 30.983°C, and 30.422°C in 2011 (Figure 5). Over the ten years, the average temperature increased 0.374°C/10a (10a indicates 10 years), and the maximum and minimum temperatures increased 0.381°C/10a and 0.438°C/10a, respectively. The results suggest that the minimum temperature increase played a key role in the average temperature changes in the region.

The characteristics of the relationship between area and temperature at different land-use intensity levels are summarised in Table 4. The values of the land-use intensity were divided into three intervals (low, medium, and high). The low level was [100, 200], in which unused land, grassland, and water bodies were the dominant land-use types. The medium level was [200, 300], in which agricultural land, water bodies, and grassland were the dominant types. The high level was [300, 400], in which built-up land and agricultural land were the dominant land-use types. The overall temperature exhibited an increase; however, a significant difference was observed among the three land-use intensity levels. The low-level land area decreased by 492 km^2 (17.6%), which represented the best-case land-use intensity level; however, the temperature in the low-level land increased by 0.292°C (1.0%). The medium-level land area increased by 785 km^2 (5.5%), whereas the corresponding temperature increased by 0.372°C (1.2%). The high-level land area decreased by 293 km^2 (9.0%), whereas the temperature increased by 0.419°C (1.4%). Our results suggest that the increased land area of the medium level and the decreased land area of the low level were the primary causes of the temperature rise.

3.2. Response of the Temperature to Changes in the Land-Use Intensity. The study area was divided into 5,877 units, where each unit was 930 m × 930 m in size. The temperature and land-use intensity within the units were analysed with spatial statistics (Figure 6). The coefficient was -6×10^{-8} in 2001 and -3×10^{-8} in 2011. The results suggest that the sensitivity

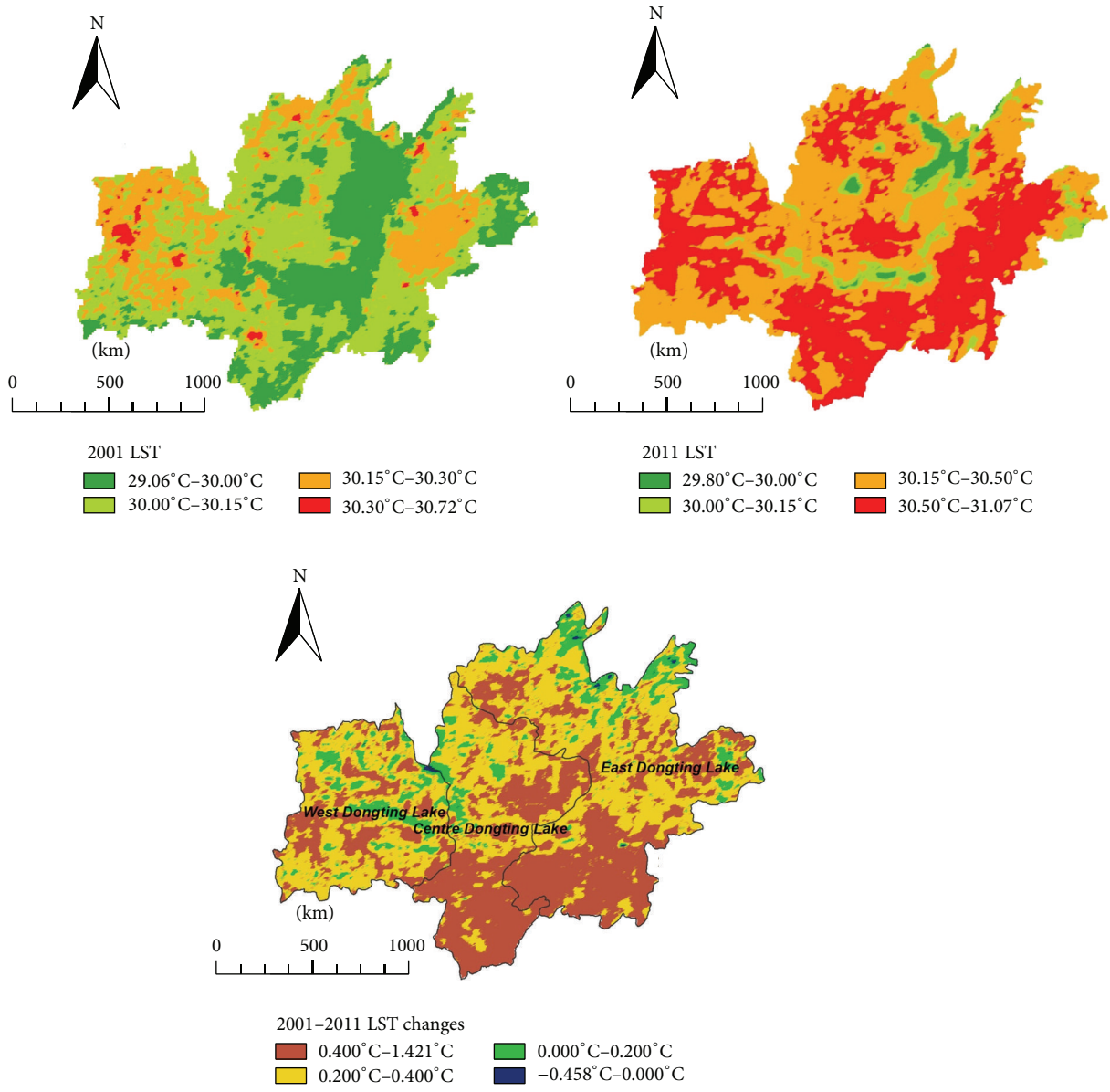

Figure 4: The average LSTs and changes in 2001 and 2011 (all figures depict summer: July, August, and September).

Table 4: Dynamic changes in the land-use intensity and temperature between 2001 and 2011.

Year	Low level [100, 200]		Medium level [200, 300]		High level [300, 400]	
	Area (km^2)	Temperature (°C)	Area (km^2)	Temperature (°C)	Area (km^2)	Temperature (°C)
2001	2798	29.862	14261	30.066	3264	30.127
2011	2306	30.154	15046	30.438	2971	30.546
Change	**−492**	0.292	**785**	0.372	**−293**	0.419
Rate of change	**−17.6%**	1.0%	**5.5%**	1.2%	**−9.0%**	1.4%

of temperature to the land-use intensity increased over the ten years. The inflection point of the curve appeared when the land-use intensity was 200 or 300, and the warming acceleration was relatively low when the land-use intensity was [100, 200] or [300, 400]; however, the temperature increased rapidly within [200, 300]. The scatter distribution shows that the temperature rise was concentrated within [200, 300], which suggests that the land-use intensity within [200, 300] was a major influence on the temperature rise and that the land-use intensity changes due to variations in agricultural land, water bodies, and grassland were the primary causes.

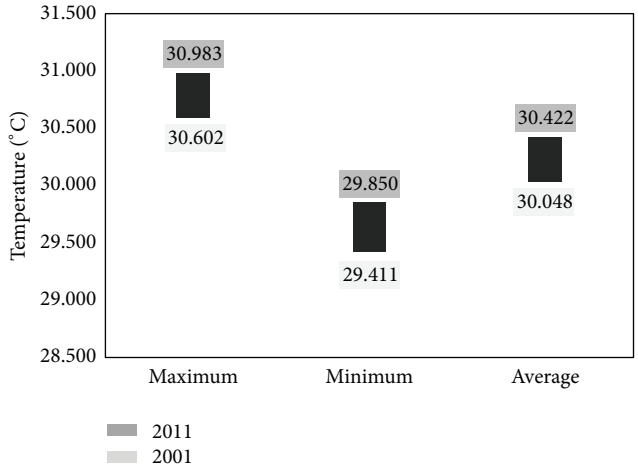

Figure 5: Changes in the surface temperature in the summers of 2001 and 2011.

The relationship between the temperature variations and land-use intensity over the past decade is illustrated in Figure 7. Small changes in the land-use intensity were concentrated within $[-50, 50]$. Moreover, the overall land-use intensity varied slightly, while the cross-level transition was infrequent. Thus, the main influence on the temperature variation was the transition between the first and second levels or between the second and third levels. The temperature decreased with increasing land-use intensity within $[-50, 50]$, indicating a negative correlation; however, when the land-use intensity was within $[-100, -50)$ and $(50, 100]$, the temperature revealed a positive correlation. This finding suggests that the temperature should increase when the land-use intensity sharply changes (i.e., a hierarchical transition), for example, when the unused land-use grade changes to the urban land-use grade.

3.3. Analysis of Influencing Factors

3.3.1. Landscape Effects. Table 5 presents the dynamic changes in the land-use type and temperature from 2001 to 2011. The area of built-up land increased by 50%, and the areas of cultivated land and water bodies increased by 4.6% and 13.6%, respectively. However, forested land, grassland, and unused land areas decreased by 26%, 12%, and 1.1%, respectively. The highest to lowest temperature increases were as follows: cultivated land (0.404°C), built-up land (0.383°C), forested land (0.352°C), water body (0.349°C), unused land (0.308°C), and grassland (0.290°C). The temperature increase over grassland was lower than that over water bodies. The results suggest that the temperature rise primarily resulted from the expansion of built-up land or cultivated land and the reduction of forested land or grassland. Accordingly, transitions to different landscapes may lead to changes in land-use intensity. For example, when forested land or grassland was transformed to built-up or cultivated land, the land-use intensity level may have changed in conjunction with an increase in temperature.

3.3.2. Centre of Gravity Effects. The changes in the centres of gravity of temperature and land-use intensity revealed the extent of interference by human activities. From the geographical perspective, a high correlation was observed when both changes were consistent, whereas a weak correlation or no correlation was observed when they were not consistent; consistency mainly refers to changes in the same direction [22, 23]. A_1, B_1, and C_1 are the variations in the centre of gravity of the temperature in Figure 8. A_2, B_2, and C_2 are the variations in the centre of gravity of the land-use intensity. A_1 and A_2 were highly consistent in terms of the direction of the change, whereas the directions of change for B_1 and B_2 and for C_1 and C_2 were inconsistent. These results suggest that a direct correlation exists between land-use intensity and temperature change in the western part of the lake, whereas the relationship was not obvious in the middle and eastern parts of the district.

These results reveal that the centre of gravity shift displayed a spatial difference that did not always vary consistently, and it could be due to other environmental factors, such as interannual and seasonal changes, global warming, and latent heat and sensible heat exchanges [24]. Therefore, the shift in the temperature's centre of gravity was affected by both land-use intensity and feedback from other environmental factors.

3.3.3. Latitudinal Effect. The latitudinal effect of temperature refers to the zonality variations from low latitudes to high latitudes. The latitude (28.27°N to 29.81°N) of the region was divided into 103 equal parts, in which each part represented approximately 0.015° of the latitudinal effect variation in the temperature. Figure 9 shows the correlation coefficients between the temperature and land-use intensity; the K value indicates the correlation coefficients. The temperature changes ranged within [0.158°C, 0.631°C], the land-use intensity changes ranged within $[-5, 24]$, and the K value changes ranged within $[0.581, 1.414]$.

Figure 9 illustrates that a significant linear relation was detected between the temperature variations and latitude. With increasing latitude, a distinct declining trend occurred. The phenomenon suggested that the temperature variation rate was greater in high-latitude areas and that the warming trend was more notable at high altitudes. The land-use intensity variation exhibited a fluctuating rising trend with increasing latitude.

However, no significant linear relationship was observed between variations in land-use intensity and increasing latitude. These results showed that the latitudinal rules of land-use intensity variations were not obvious, and no evident increasing or decreasing trend in the intensity occurred with latitude changes. Plausibly, the temperature was influenced by several human factors, such as land-use, development measures, and economic development orientations.

Similar to the temperature variation rules, the K value was characterised by zonality, which controlled the fluctuations and declines in the values. These results suggest that the temperature response range to the land-use intensity decreased gradually and that the influence of the land-use intensity on

Table 5: Land-use and temperature changes from 2001 to 2011.

Year	Built-up land		Cultivated land		Forested land		Water body		Grassland		Other/unused land	
	Area (km^2)	Average T (°C)	Area (km^2)	Average T (°C)	Area (km^2)	Average T (°C)	Area (km^2)	Average T (°C)	Area (km^2)	Average T (°C)	Area (km^2)	Average T (°C)
2001	1833	30.137	6691	30.083	5033	30.070	2706	29.890	1704	30.027	1178	30.012
2011	2721	30.520	6999	30.487	3712	30.422	3074	30.239	1504	30.317	1136	30.370
Change	888	0.383	308	0.404	**−1321**	**0.352**	368	0.349	**−200**	**0.290**	−42	0.308
Rate of change (%)	48.45%	1.27%	4.60%	1.34%	−26.25%	1.17%	13.60%	1.17%	−11.74%	0.97%	−3.57%	1.10%

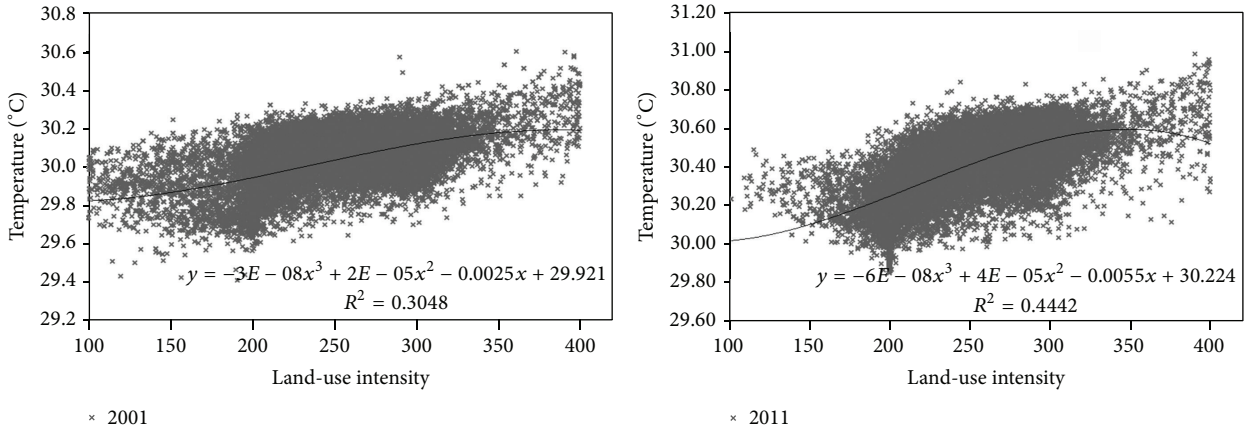

Figure 6: The static relationship of temperature and land-use intensity variations in 2001 and 2011.

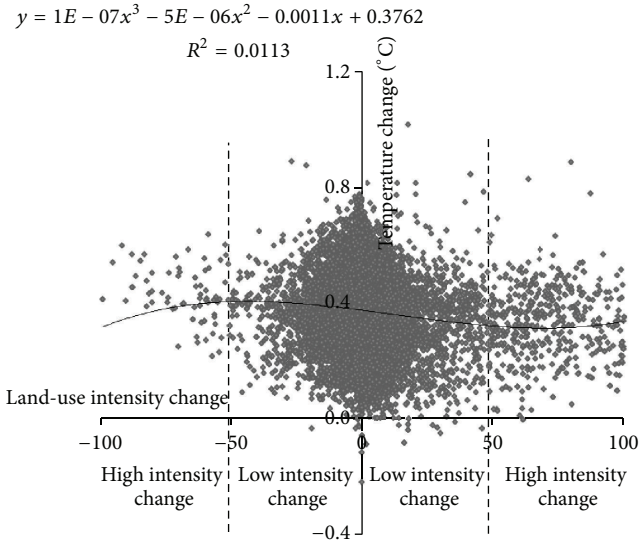

Figure 7: The dynamic relationship of temperature and land-use intensity variations over 10 years (2001–2011).

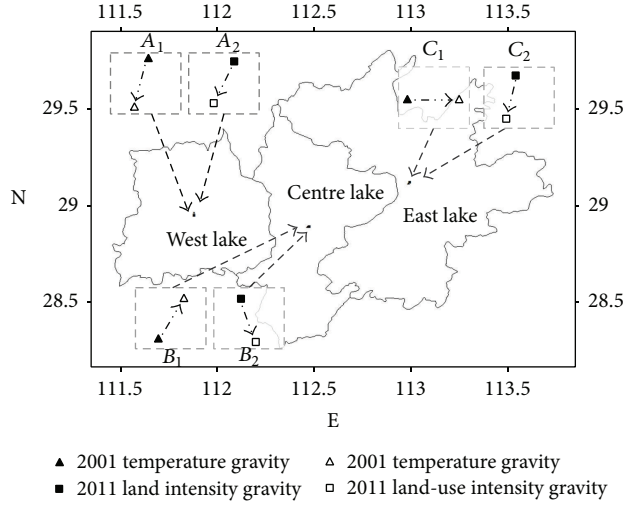

Figure 8: Change in the direction of the centre of gravity of the land-use intensity and temperature from 2001 to 2011.

the temperature gradually declined with increasing latitude. Therefore, the temperature response to the land-use intensity was more sensitive in low-altitude areas than in high-altitude areas in the Dongting Lake District.

4. Conclusions

(1) The average temperature increased from 30.048°C to 30.422°C in the Dongting Lake area between 2001 and 2011. This temperature rise in the Dongting Lake District was slightly higher than the background global warming [25]. The area of built-up land and cultivated land increased by approximately 50% and 4.6%, respectively, leading to an increase of 5.5% and a decrease of 9.0% in medium- and high-level land uses, respectively. These changes resulted in an increase in the land-use intensity. Built-up and cultivated lands were the major factors that accounted for the temperature increase. Therefore, the influence of human activities can be quantitatively expressed based on the land-use intensity.

(2) An increase in the land-use intensity generally corresponds to a temperature increase, such as the heat island effect. However, the results of this study suggest that the temperature increase was primarily caused by a change in the land-use intensity. This finding may be interpreted as land-cover change owing to a hierarchical transition and characteristics of temperature changes in the lake area. Therefore, in addition to the effects of greenhouse gases and radiative forcing, the regional land cover or land-use conversions must have enhanced the temperature change.

(3) The centre of gravity of temperature is inconsistent with the land-use intensity in most of the lake area. The shift in the temperature's centre of gravity was

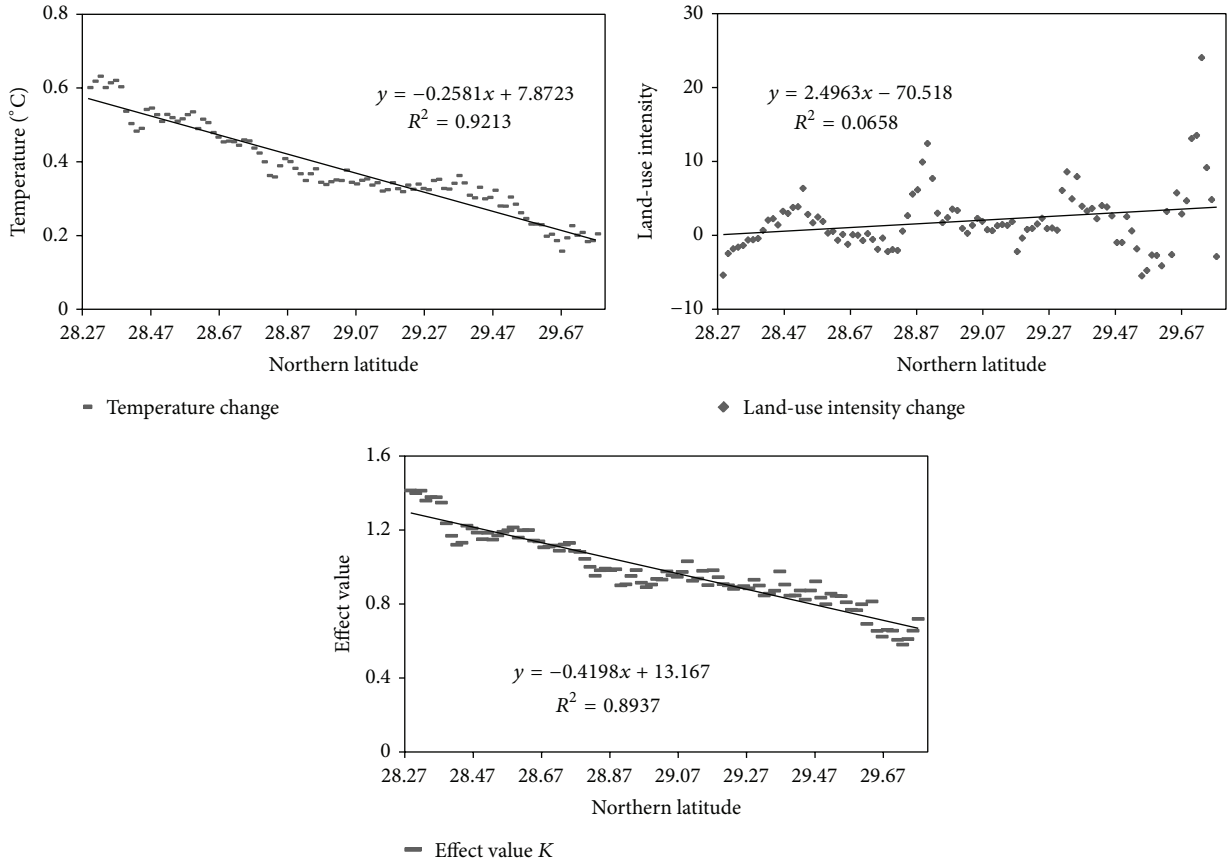

Figure 9: Latitudinal effects on land-use intensity and temperature from 2001 to 2011.

affected by both the land-use intensity and the external gas-water exchanges, suggesting that temperature changes in the region could be influenced by feedback from external environmental factors to an extent. For example, feedback from external environmental factors could have affected the regional atmospheric and water circulation. However, the centre of gravity of the temperature is consistent with the land-use intensity in the western region of the lake, and we can confirm that the land use and cover change strongly correlated with temperature in the west.

(4) The observed latitudinal effect showed that the extent of the temperature change gradually decreased while the land-use intensity gradually increased. Generally, the changes in temperature and land-use intensity exhibited a negative correlation. However, with increasing latitude, the degree of correlation gradually declined, suggesting that the temperature response to the land-use intensity changes was more sensitive in low-altitude areas than in high-altitude areas. In other words, the difference in the correlations between the temperature and land-use intensity did not significantly increase, possibly because the socioeconomics and urbanisation are more dominant in low-altitude areas than in high-altitude areas. Therefore, more guidance should be given to low-altitude areas.

Our study was conducted in a typical subtropical lake district between 2001 and 2011, when a rapid change in the global air temperature occurred. Moreover, the expression for land-use intensity was revised using a geographic method. This new formulation can accurately express the relationship between land-use and temperature changes and can be used to explore the relationship between land use and other climatic factors, such as rainfall, evapotranspiration, and aerosols. Because of the complexity of land-use and land-cover changes, the regional temperature change is related to many factors, such as global warming caused by the greenhouse effect, topographical factors, and modulations by ENSO [26], the PDO (Pacific Decadal Oscillation) [27], and the AMO (Atlantic Multidecadal Oscillation) [28]. Our study mainly considered the single factor of land use from the perspective of macrogeography. Further studies should consider multiple environmental factors and perspectives.

Conflict of Interests

The authors declare no conflict of interests.

Acknowledgments

The authors are grateful to NASA for their support in developing their study. They thank Jiyuan Liu and Liangfu

Chen (Chinese Academy of Sciences) for their insightful comments on the methodology. This research was funded by the National Natural Science Foundation of China (Foundation no. 41371228). They also appreciate the comments and suggestions by the anonymous reviewers.

References

[1] A. K. Mishraa, V. P. Singh, and S. K. Jain, "Impact of global warming and climate change on social development," *Journal of Comparative Social Welfare*, vol. 26, no. 2-3, pp. 239–260, 2010.

[2] B. L. Turner II, E. F. Lambin, and A. Reenberg, "The emergence of land change science for global environmental change and sustainability," *Proceedings of the National Academy of Sciences of the United States of America*, vol. 104, no. 52, pp. 20666–20671, 2007.

[3] S. Zhao, C. Peng, H. Jiang, D. Tian, X. Lei, and X. Zhou, "Land use change in Asia and the ecological consequences," *Ecological Research*, vol. 21, no. 6, pp. 890–896, 2006.

[4] S.-L. Lu, X.-H. Shen, and L.-J. Zou, "Land cover change in Ningbo and its surrounding area of Zhejiang Province, 1987–2000," *Journal of Zhejiang University: Science*, vol. 7, no. 4, pp. 633–640, 2006.

[5] X. Li, Z. Wang, K. Song, B. Zhang, D. Liu, and Z. Guo, "Assessment for salinized wasteland expansion and land use change using GIS and remote sensing in the west part of Northeast China," *Environmental Monitoring and Assessment*, vol. 131, no. 1–3, pp. 421–437, 2007.

[6] X. C. Yang, Y. L. Zhang, L. S. Liu, W. Zhang, M. J. Ding, and Z. F. Wang, "Sensitivity of surface air temperature change to land use/cover types in China," *Science in China, Series D: Earth Sciences*, vol. 52, no. 8, pp. 1207–1215, 2009.

[7] M. Dainese, "Impact of land use intensity and temperature on the reproductive performance of *Dactylis glomerata* populations in the Southeastern Alps," *Plant Ecology*, vol. 212, no. 4, pp. 651–661, 2011.

[8] C. P. Quine and K. Watts, "Successful de-fragmentation of woodland by planting in an agricultural landscape? An assessment based on landscape indicators," *Journal of Environmental Management*, vol. 90, no. 1, pp. 251–259, 2009.

[9] T. Rydberg and A. C. Haden, "Emergy evaluations of Denmark and Danish agriculture: assessing the influence of changing resource availability on the organization of agriculture and society," *Agriculture, Ecosystems and Environment*, vol. 117, no. 2-3, pp. 145–158, 2006.

[10] J. Liu, C. Li, and Y. Wan, "An agricultural land resource assessment study based on GIS-An example from Guiyang City," *Chinese Journal of Geochemistry*, vol. 21, no. 1, pp. 79–88, 2002.

[11] H. Daquan, W. Wei, D. Teqi, and L. Jinshe, "Assessment of industrial land use intensity: a case study of Beijing economic-technological development area," *Chinese Geographical Science*, vol. 21, no. 2, pp. 222–229, 2011.

[12] S. L. Martin, S. Cakmak, C. A. Hebbern, M.-L. Avramescu, and N. Tremblay, "Climate change and future temperature-related mortality in 15 Canadian cities," *International Journal of Biometeorology*, vol. 56, no. 4, pp. 605–619, 2012.

[13] C. Qian, Z. Yan, Z. Wu, C. Fu, and K. Tu, "Trends in temperature extremes in association with weather-intraseasonal fluctuations in Eastern China," *Advances in Atmospheric Sciences*, vol. 28, no. 2, pp. 297–309, 2011.

[14] G. Foster and S. Rahmstorf, "Global temperature evolution 1979–2010," *Environmental Research Letters*, vol. 6, no. 4, Article ID 044022, 8 pages, 2011.

[15] A. Solomon and M. Newman, "Decadal predictability of tropical indo-pacific ocean temperature trends due to anthropogenic forcing in a coupled climate model," *Geophysical Research Letters*, vol. 38, no. 2, Article ID L02703, 2011.

[16] S. Fall, D. Niyogi, A. Gluhovsky, R. A. Pielke, E. Kalnay, and G. Rochon, "Impacts of land use land cover on temperature trends over the continental United States: assessment using the North American Regional Reanalysis," *International Journal of Climatology*, vol. 30, no. 13, pp. 1980–1993, 2010.

[17] J. R. Anderson, E. E. Hardy, J. T. Roach et al., "A land use and land cover classification system for use with remote sensor data," Tech. Rep., United States Government Printing Office, 1976.

[18] B. Guindon, Y. Zhang, and C. Dillabaugh, "Landsat urban mapping based on a combined spectral-spatial methodology," *Remote Sensing of Environment*, vol. 92, no. 2, pp. 218–232, 2004.

[19] Z. Dafang and L. Jiyuan, "Study on the model of regional differentiation of land use degree in China," *Journal of Natural Resources*, vol. 12, no. 2, pp. 105–111, 1997 (Chinese).

[20] K. Mao, Z. Qin, J. Shi, and P. Gong, "The research of split-window algorithm on the MODIS," *Geomatics and Information Science of Wuhan University*, vol. 30, no. 8, pp. 703–707, 2005.

[21] J. Xu, J. Zhou, S. Luo, and H. Sun, "Study on characteristics of long-term gravity changes at Wuhan station," *Chinese Science Bulletin*, vol. 53, no. 13, pp. 2033–2040, 2008.

[22] S. Krätke, "A regulationist approach to regional studies," *Environment and Planning A*, vol. 31, no. 4, pp. 683–704, 1999.

[23] J.-M. Grether and N. A. Mathys, "Is the world's economic centre of gravity already in Asia?" *Area*, vol. 42, no. 1, pp. 47–50, 2010.

[24] M. Jung, M. Reichstein, H. A. Margolis et al., "Global patterns of land-atmosphere fluxes of carbon dioxide, latent heat, and sensible heat derived from eddy covariance, satellite, and meteorological observations," *Journal of Geophysical Research*, vol. 116, no. 3, 2011.

[25] J. Zhang, W. Dong, L. Wu, J. Wei, P. Chen, and D.-K. Lee, "Impact of land use changes on surface warming in China," *Advances in Atmospheric Sciences*, vol. 22, no. 3, pp. 343–348, 2005.

[26] H. Ronghui and W. Yifang, "The influence of ENSO on the summer climate change in China and its mechanism," *Advances in Atmospheric Sciences*, vol. 6, no. 1, pp. 21–32, 1989.

[27] H. Yang and Q. Zhang, "On the decadal and interdecadal variability in the Pacific ocean," *Advances in Atmospheric Sciences*, vol. 20, no. 2, pp. 173–184, 2003.

[28] M.-K. Kim and Y.-H. Kim, "Seasonal prediction of monthly precipitation in China using large-scale climate indices," *Advances in Atmospheric Sciences*, vol. 27, no. 1, pp. 47–59, 2010.

Hindawi Publishing Corporation
Advances in Meteorology
Volume 2015, Article ID 765472, 9 pages
http://dx.doi.org/10.1155/2015/765472

Research Article

Study on Clean Development Mechanism, Quantitative and Sustainable Mechanism

Donghai Yuan,[1] Lipeng Zheng,[1] Yuan Cao,[1] Xufeng Mao,[2] Xueju Huang,[3] Liansheng He,[4] Junqi Li,[1] and Mingshun Zhang[1]

[1] *Beijing Climate Change Response Research and Education Center, Key Laboratory of Urban Stormwater System and Water Environment, Ministry of Education, Beijing University of Civil Engineering and Architecture, Beijing 100044, China*
[2] *College of Life and Geography Sciences, Key Laboratory of Tibetan Plateau Environment and Resources (Ministry of Education), Qinghai Normal University, Qinghai, Xining 810000, China*
[3] *Research Institute of Forestry, Chinese Academy of Forestry, Beijing 100091, China*
[4] *Water Environment System Project Laboratory, Chinese Research Academy of Environmental Sciences, Beijing 100012, China*

Correspondence should be addressed to Xufeng Mao; maoxufeng@yeah.net

Received 19 September 2014; Accepted 12 February 2015

Academic Editor: Hongbo Su

Aiming at the system and market problem of clean development mechanism (CDM), this study is carried out to establish the feasibility of certified emission reduction (CER) quantitative evaluation method and reserve mechanism in host country at the United Nations Framework Convention on Climate Change (UNFCCC) level. After the introduction of CER quantitative and sustainable mechanism, the amount of CER that can enter the market was cut to a quarter, which reduces about 75% of the expected CER supply. Market CER from the technology types of higher CER market share and lower support for sustainable development appears to have different degrees of reduction. As for the technology types of lower CER market share and higher support for sustainable development, the amount of market CER is maintained in line with prevailing scenario, and market CER supply becomes more balanced.

1. Introduction

During the first Kyoto commitment period, the CDM emerged to be the global currency for emissions trading, avoided more than 1.5 billion tonnes of CO_2 by over 7000 projects, and granted 5–13.5 billion USD to developing countries till 2012 [1]. CDM linked developing and industrialized country emission reduction efforts and provided a governance and accounting framework to assess the environmental integrity of offset projects. However, the CDM has not been without its critics, who have raised questions with regard to the additionality of projects, the mechanism's bureaucracy and transaction costs, and the majority of projects being concentrated in a few primarily emerging economy countries. Efforts to reform the CDM are underway, but at the same time, the global carbon market shows more interest to develop new offset mechanism, even being very similar to CDM, instead of directly using CER as an offset unit [2, 3].

While the Doha decision on Second Commitment Period under the Kyoto Protocol (CP2) confirmed the existence of the CDM until 2020, it did not address the issue of low demand or the oversupply under current CDM framework, thereby questioning the role of the CDM as a catalyst for private sector investment in climate change mitigation [4, 5]. In order to better facilitate the reformation on supply side as well as promotion in demand side of CDM and also considering the protection of existing CDM projects in an interim measure, it is very necessary to explore more options to upgrade design of CDM [6]. In particular, new instrument and components are needed to evaluate divers cobenefit from each CDM projects and enable the cobenefit to become a part of the value of CERs, instead of only emission

Table 1: Demand forecast of national carbon offset in non-Annex I countries during the period 2008–2012 [13].

Potential demand from industrialized countries ($MtCO_2e$)		Potential supplies ($MtCO_2e$)		
Country or entity	Kyoto assets demand		Official target*	
EU	**1,293**	Potential GIS	**>1,500**	
Government (EU-15)	**428**	Ukraine	**500–700**	
Private sector (EU ETS)	**865**	Russian Federation	200	
		Czech Republic	120	
		Other EU-10	600	
Japan	**300**			
Government	100			
Private sector	200			
Rest of Annex B	51	CDM & JI	**1,573**	Range: **1,500–1,658**
Government	46	CDM	**1,273**	**1,250–1,301**
Private sector	5	JI	**300**	**250–357**
Total				
Government				
Private sector				

*These numbers correspond to the amounts of AAUs governments intend to sell. They are much lower than the whole amount of excess AAUs, now estimated at more than 10 billion tCO_2e over the first commitment period, with Russia accounting for half, Ukraine one-quarter, and Poland one-fifth.

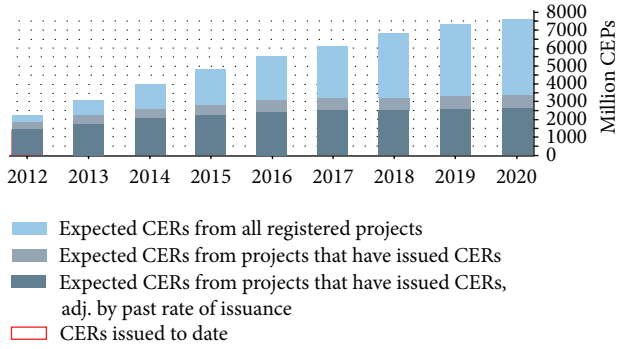

Figure 1: CER production forecast during the period 2013–2020 made by UNFCCC [14].

reduction. With such features, the amount of CER that is allowed to enter carbon market will be able to be adjusted in a quantitative way, according to its contributions to sustainable development and supply potentials [7–9].

Considering the limited capacity of carbon market for offset units, the share of CERs enlarged for those projects with higher cobenefit but lower potentials of supply. In the meanwhile, CDM under reformation should be considered to suit for demand in emerging ETS in both industrialized countries and developing countries. Following this concept, this paper is trying to develop such updated mechanism to enable us to differentiate between CERs as per their features, by dividing each CER issued into two parts, for reserve and for market. It is envisaged that the new mechanism is able to dynamically adjust the ratio of market CER from the issued CERs based on technology type, so that it is able to automatically control the supply potential of CER from different technologies according to its contributions to sustainable development and a real-time market share [10–12].

As a demonstration, this paper tested the effect of this new mechanism by using real data of CDM projects in CDM-pipeline. It can be found that the share of controversial CERs, for example, CER from destruction of chemical gases or large scale, hydro remarkably shrunk and the total volume of CER supply can be downsized.

2. Problem Analysis of CER Market

2.1. Absolute Overplus Risk of CER. According to supply and demand analysis of flexible mechanisms (CDM, joint implementation (JI), and assigned amount unit (AAU)) under the Kyoto Protocol during the period 2008–2012, the demand amount of the first commitment period is 1.64 billion tons, while the potential supply amount (CER, emission reduction unit (ERU), and AAU) has reached more than 3 billion tons (CER accounting for half of which, as shown in Table 1).

Considering that AAU cannot be used for the second commitment period of Kyoto Protocol, carbon offsets during the period 2013–2020 will be mainly based on CER and ERU. Combined with domestic emission reduction mechanisms of current non-Annex I countries, World Bank in the "2012 Global Carbon Market Trends Report" forecasts that during the period 2013–2020 the demand for carbon offset of non-Annex I countries worldwide can add up to approximately 2.7 billion tons, for which EU demand for carbon offsets accounts for 1.6 billion tons or less (as shown in Table 2).

According to the CER supply forecast made by UNFCCC in March 2013 for the second commitment period of Kyoto Protocol (from 2013 to 2020) up to 2020 CDM projects may generate CER accumulated up to an amount between 2.5 billion tons and 7.5 billion tons (as shown in Figure 1, not containing the program of activities (PoA)). Excluding the

Table 2: Demand forecast of national carbon offset in non-Annex I countries during the period 2013–2020 [13].

Country (group of)	Assumption	Potential demand ($MtCO_2e$)
Australia	Carbon price mechanism, cap in line with target of 5°/b below 2000	348
EU-27, Iceland, Liechtenstein, and Norway	20% below 1990, with differentiation EU ETS and effort sharing	1,635*
Japan	Between 25% and below 1990	≤539
New Zealand	NZ ETS: 10% below 1990	77
North America	Western climate initiative (WCI): limited to California and Québec, with international offsets allowed in California only	94
Switzerland	20% below 1990, with ETS and other measures	2.3–12.8
Total	≤2,706	

Notes: for detailed assumptions see Annex 8: assumptions for estimates of potential demand for offsets from non-Annex I countries.
* Already accounts for an inflow in the European Union Emission Trading Scheme (EU ETS) of 865 million CERs and ERUs during Phase II.

CER generated before 2012, the newly added CER supply of the second commitment period is expected to reach about 1 to 6 billion tons.

During the first commitment period of Kyoto Protocol (KP-1), CER supply and demand were basically balanced, with a slight excess subject to the impact of AAU. Due to the lack of existing demand, CER supply capacity will exceed demand in the second commitment period of Kyoto Protocol (KP-2). Theoretically the maximum amount of excess supply capacity can reach 3.3 billion tons.

According to the forecast of carbon emission scenarios in 2020 during the Copenhagen Climate Conference COP15, under different binding emission reduction scenarios, global greenhouse gas emissions will reach about 49–56 billion tons/year by 2020, which should be controlled at 40 billion tons under the 2°C target. Therefore, global emissions by 2020 should be decreased by 16 billion tons/year with the 2°C target (no binding emission reduction scenario). If more stringent binding emission reduction mechanisms are formed at Conference of COP15, global emissions by 2020 require further reduction of 9 billion tons/year or more (as shown in Figure 2).

Supposing 2013–2020 average emission reductions per year up to 9 billion tons/year, there have been totaled 72 billion tons of emission reductions during the eight years. On the supply side, in accordance with the UNFCCC forecast new supply of CER during 2013–2020 can reach 6 billion tons, accounting for 8% emission reduction mandate with the 2°C target (under strict-constraining mechanism scenario).

In a strict-constraining mechanism scenario, most of the emission reductions are required to carry out under the total carbon emissions control (cap-and-trade) in various regions, while the total control and carbon trading systems usually set an upper limit for the carbon offsets usage (about 8–10%). So even though a binding global emissions reduction agreement was formed in 2015 with a higher emission reduction target, the carbon offset demand may not be able to consume all of the CERs generated by CDM projects.

According to the emissions reduction assignment under the 2°C target, even though the broader and deeper global emissions reduction agreement can be formed before 2015, the global CER supply capacity is still difficult to be fully digested. Therefore, there is an absolute excess risk of CER.

2.2. Reflecting-Reduction-Cost Incompetency of CER. In addition to lack of demand, the CDM design also results in the current crisis of CDM. Existing CDM allows different types of projects to provide the market with undifferentiated credits (CER) in accordance with the CO_2 reduction equivalent, ignoring the key differences between different types of technology, such as emission reduction potential and cost differences, as well as different contribution to sustainable development.

Ignoring these differences leads to the domination of projects with the lowest emission reduction costs and largest emission reduction potential (e.g., hydrofluorocarbon (HFC)), which can only operate effectively with a large CER demand. Once the demand is insufficient, it will produce "bad money drives out good money" effect: the falling of CER price will result in the maximum damage to projects with higher additional emission reduction costs and smaller emission reductions, while projects with larger emission reduction and lower emission reductions costs can continue to generate CER. In the above scenario, except for a few projects receiving excessive subsidies, the emission reduction willingness of most participants including the host countries will be damaged, giving rise to the unsustainability of the current CDM system.

3. The Significance of CDM Quantifying to Sustainable Reform

3.1. Empowering CDM Host Countries to Intervene with International Carbon Market. In the market, developed countries have quota reserves such as EUR and control on trading rules, with the ability to dominate the CER prices and demand. As the supply side, host countries do not have the national CER reserves and are in the lack of market intervention to drastic fluctuations of CER prices, which is not beneficial for business and national CER revenue rights.

Although the UNFCCC is considering how to control the CER supply, political risk exists when certain methodological

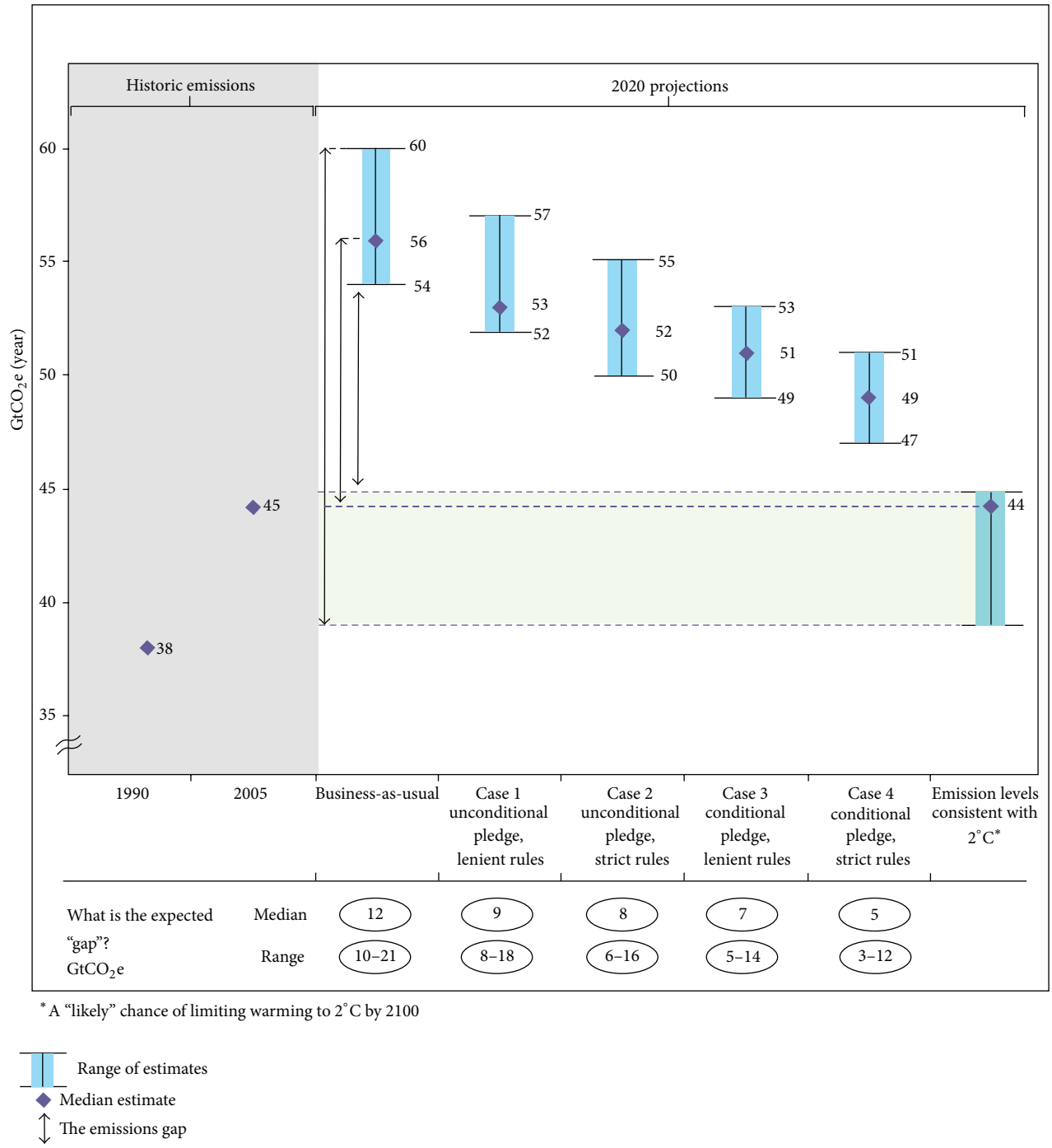

Figure 2: Comparison of expected emissions in 2020 with the emission levels consistent with a "likely" chance of meeting the 2°C limit [15]. The figure compares the expected emissions in 2020 resulting from the four pledge cases with the emission levels consistent with a "likely" chance of meeting the 2°C limit. The median estimates and range of estimates (20th to 80th percentile) are shown. The gap between expected emissions and the 2°C levels is given above in each case.

projects are prohibited to continue registering or issuing at the UNFCCC level. Especially for the chemical gas projects such as HFC, the management calls for further prudence. As these chemical gases have enormous greenhouse gas potential, if the ban of CDM leads to such projects ceasing the destruction of chemical gases and resuming direct emissions, global efforts to reduce emissions will be greatly weakened. Thus adopting tools to adjust and quantify CER supply at the UNFCCC level and recognizing the differences of various CER are not only much easier to implement compared to the administrative measures of "a clean cut," but also conducive to encouraging the promotion of more diversified emission

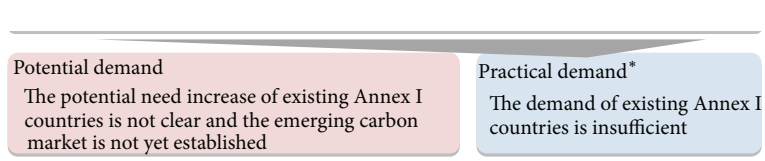

Figure 3: Relative excess scenario of current CER.

reduction technologies, thereby achieving the self-regulation and sustainability of CDM.

3.2. Enhancing Climate Negotiation Advantages of Host Countries by CER Reserves. CER reserves used for carbon offsets in domestic market by host countries or directly canceled as the quantified emission reduction contributions to host countries (similar to nationally appropriate mitigation actions (NAMAs)) can be taken as the measured, reported, and verified (MRV) responsibility for emissions reductions commitments to benefit developing countries in the climate negotiations [16]. Since CDM is a flexible mechanism that helps developed countries to offset emission reduction obligations and allows part of its reserves to be used in domestic market, it can provide a bargaining chip for developing countries in the climate negotiations, that is, to determine whether part of CER reserves would be used in domestic market based on the increase rate of emission reduction target committed by developed countries.

3.3. Empowering Host Countries to Interfere with CER Market by CER Reserves. Through this proposal, it is ensured that the large scale chemical gas projects will generate large CER reserves for host countries. When the quota/credit shortages lead to price rise in the future carbon market, host countries can supply CER reserves to the market. When there is an excess of quota/credit, host countries can continue reserving or use reserves for domestic emission trading scheme (ETS). Enabling host countries with reserve capacity can effectively restrain the speculative operations in the current buyer-country market and stabilize CER price volatility. This is a win-win outcome for the buyer and host countries.

3.4. Effectively Supporting Sustainable Development of Host Country by the Utilization of CDM. In addition, with the decreasing economic strength gap between developed and developing countries, differences of emission reduction obligations are being weakened. The role of CDM also needs to be adjusted, more suggestions declaiming that the CER should be transformed from cheap credits to offset emission reduction obligations of developed countries to a common emission reduction incentive tools. More than half of the CER amount is from chemical-gas-destruction projects, the majority of which is those CERs from relatively advanced developing countries, therefore, the disproportion of technology types and distribution of host countries cause that the CDM capability of supporting sustainability has being widely questioned. Support for sustainable development should be strengthened, and low-carbon technology transfer should be promoted. Only by CDM reformation that conforms to the trend of value foundation can the wider acceptance of CDM be strengthened.

Thus, by adding quantitative adjustment tools that can promote the contribution to sustainable development for current CDM system, host countries are able to comanage the CER market with Annex I countries at UNFCCC level and more capable of intervening with international market. Compared to maintaining the current situation of CDM, this improvement will be easy to accept within the framework of the UNFCCC.

3.5. Supporting the Emerging Carbon Market (ETS) by CER Reserves. There are currently more than twenty countries and regions establishing carbon markets (ETS), in which bilateral or multilateral trading mechanism with CER reserves can be introduced among host countries. That is, with excess CER, part of cheap CER can be used to start current emerging carbon markets in developed countries (e.g., Australia). In addition, when developed countries agree to increase the emission reduction commitments, host countries can provide initial liquidity for the domestic ETS to cover the illiquidity problem that brought about the single spot trading mode.

4. Design Concept of CDM Quantifying Sustainability Mechanism

The proposal intends to divide per ton CER into two parts based on CER shares of different types of technology and degree of contribution to sustainable development: CER directly accessing the market (market CER) and CER not directly entering the market and reserved by host countries (reserved CER). Excess short-term CER supply can be absorbed through the reserved CER mechanism of host countries; the ratio of reserved CER after issuance is decided by the adjustment factor at the UNFCCC level, thereby helping to enhance the advantages of host countries in the climate negotiations and establish the intervention capability to international carbon market.

The CER supply result is adjusted as shown in Figures 3 and 4.

After implementation of this proposal, international carbon market can help those CER generated by projects with greater contributions to sustainable development and lower

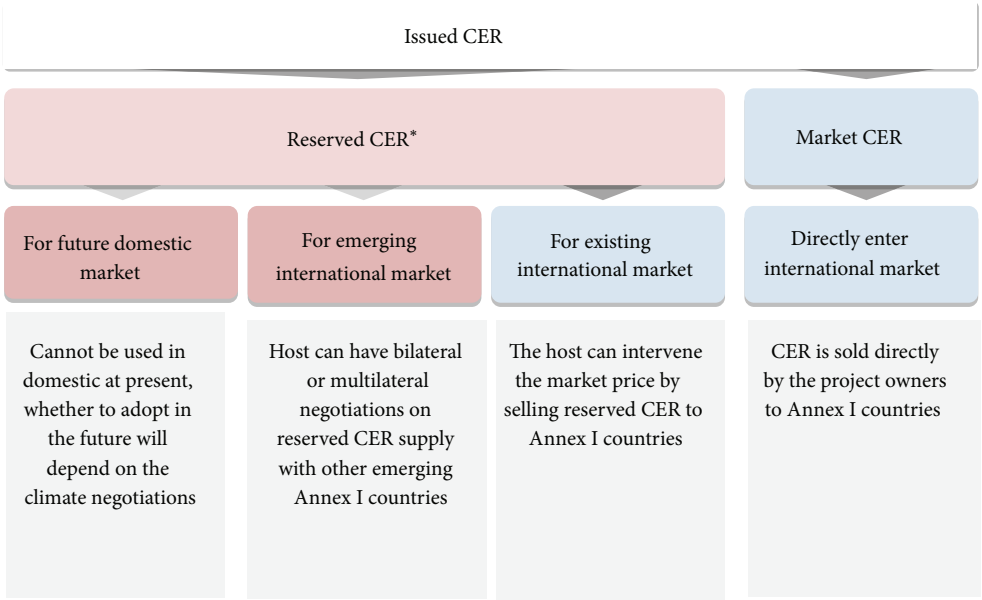

Figure 4: The scenario after implementation of this proposal.

share of CER to gain market advantage and to achieve long-term automatic adjustment. Due to more emphasis on technologies with larger contribution to sustainable development, this mechanism can enhance the value basis of CER.

In volume terms, the proposal will reduce CER market supply in the short run, while, in the long run, it will increase the intervention capability of the host CER reserves for the future international market. Moreover, it can improve and quantify the support of CDM to sustainable development and promote the equalization and diversification of CER in the technology distribution. The proposal design embodies the following ideas.

4.1. Proposal Principles at UNFCCC Level (Top-Down Approach). Implementation of this proposal reforms the quantitative and sustainable mechanism of CDM at UNFCCC level, to strengthen the status of UNFCCC and CDM and ensure the sustainability of CDM. The institutional reformation at the UNFCCC level (rather than the host country or the buyer country) is the most feasible way to limit the CER amount accessing markets by laws and regulations and to establish CER reserves of host countries.

4.2. Incentive Character of CDM in Limited Market Capacity. In this proposal, CDM market is seen as an incentive-subsidies market, which should emphasize the effectiveness and diversity of motivation. In a CER market with limited demand, CER market share among different countries and different types of technology should be more evenly distributed, avoiding long-term focus on a certain type of projects. Meanwhile, the occupied CDM market share of mature emission reduction technologies should be weakened, so that the international carbon market can better promote the new technologies. Therefore, this proposal has designed the project incentive levels of CDM for various emission reduction technologies.

4.3. Enhancing the Effect of Supporting Sustainable Development. Based on the compatibility of the existing methodology system (applicable to various types of emission reduction technology), to evaluate contribution of applicable technologies to sustainable development enables CDM to timely support those technologies with advantages in contributing to sustainable development.

4.4. Automatically Adjusting the Quantity of Various CER Entering the Market. Implementation of this proposal can automatically reduce CER market supply to mature project types (projects with large emission reductions and low emission reduction costs) and indirectly encourage projects with small emission reductions but great sustainable contribution to directly gain CER revenue through carbon markets, enabling emission reduction technologies gradually to decrease the proportion of CER entering the market with maturity improvement. Therefore, implementation of this proposal can automatically adjust the constitution of CER entering the market, thereby promoting the diversification and balanced development of CDM market.

4.5. Establishing CER Reserve Mechanism of Host Countries. The ratio of CER that is generated by each project type and can be used for reserving by host countries (the part that cannot directly enter the market) would be regulated at the UNFCCC level, with the host CER account established by the UNFCCC along the usage methods and conditions of this part of CER reserves. According to the emission reduction commitments of developed countries, host countries can set a proportion of CER reserves that can be used for host

Table 3: A test of the mechanism on current CERs issued from different technology types.

Parameters Rationale of parameters	M: marks (on contributions to sustainable development) Inputs values, based on objective evaluations or model	F_m: factor (derived from M ranking) $F_m = M_i/\text{average}\{M\, i\sim n\}$	V: volumes (of accumulated issued CER for each type) Input values, based on actual data from UNFCCC	S: share (of each type CER in the total) $S = V_i/\text{sum}\{V\, i\sim n\}$	F_s: factor (derived from S ranking) $F_s = F_m/\max\{S_i, \text{average}\{S\, i\sim n\}\}$	AF: adjusting factor (derived from F_m and F_s) $\text{AF} = \min\{1, F_{s_i}/\text{average}\{F_s\, i\sim n\}\}$	Volumes of market CER after adjusting	Shares of market CER from each type
Unit	**N.A.**	N.A.	$ktCO_2e$	%	N.A.	%	$ktCO_2e$	%
Wind	70	1.46	83,520	8.06%	18.06	78.9%	65922	26.35%
Hydro	20	0.42	107,682	10.39%	4.00	17.5%	18835	7.53%
Biomass energy	67	1.39	27,408	2.64%	33.44	100.0%	27408	10.96%
Methane avoidance	65	1.35	12,364	1.19%	32.44	100.0%	12364	4.94%
EE own generation	35	0.73	47,059	4.54%	16.03	70.0%	32961	13.18%
Landfill gas	40	0.83	30,074	2.90%	19.97	87.2%	26237	10.49%
Solar	70	1.46	166	0.02%	34.94	100.0%	166	0.07%
EE industry	40	0.83	2,089	0.20%	19.97	87.2%	1822	0.73%
Fossil fuel switch	35	0.73	35,598	3.44%	17.47	76.3%	27173	10.86%
EE supply side (power plants)	55	1.14	1,817	0.18%	27.45	100.0%	1817	0.73%
Coal bed/mine methane	50	1.04	16,559	1.60%	24.96	100.0%	16559	6.62%
EE households	100	2.08	135	0.01%	49.91	100.0%	135	0.05%
N_2O	5	0.10	217,632	21.00%	0.50	2.2%	4709	1.88%
Afforestation and reforestation	80	1.66	4,998	0.48%	39.93	100.0%	4998	2.00%
Fugitive	5	0.10	10,682	1.03%	2.50	10.9%	1165	0.47%
Cement	30	0.62	2,389	0.23%	14.97	65.4%	1563	0.62%
Transport	77	1.60	564	0.05%	38.43	100.0%	564	0.23%
EE service	90	1.87	6	0.00%	44.92	100.0%	6	0.00%
Geothermal	46	0.96	4,262	0.41%	22.96	100.0%	4262	1.70%
Energy distrib.	68	1.41	316	0.03%	33.94	100.0%	316	0.13%
HFCs	1	0.02	428,760	41.37%	0.05	0.2%	942	0.38%
PFCs and SF6	5	0.10	2,211	0.21%	2.50	10.9%	241	0.10%
CO_2 usage	20	0.42	10	0.00%	9.98	43.6%	4	0.00%
Tidal	80	1.66	—	0.00%	39.93	100.0%	0	0.00%
Total			1,036,302				250,169	

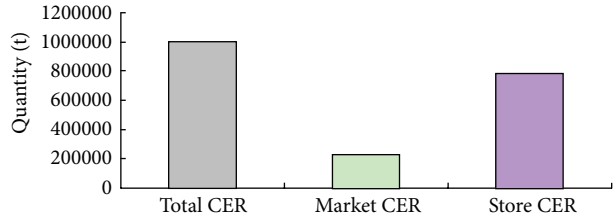

Figure 5: The scenario of reformed market CER and reserved CER [18].

Table 4: The CER proportion of all kinds of technology type before and after the reform.

Technology type	Issuance proportion before the reform	Issuance proportion after the reform
Wing power	8.06%	26.35%
Hydropower	10.39%	7.53%
Biomass	2.64%	10.96%
Waste-heat utilization	4.54%	13.18%
Landfill gas utilization	2.90%	10.49%
Alternative to fossil fuels	3.44%	10.86%
Coal mine methane utilization	1.60%	6.62%
N_2O	21.00%	1.88%
HFCs	41.37%	0.38%
Others	4.05%	11.76%

domestic market with the remaining reserves open for selling to international carbon market.

4.6. CER Reserves and the Intervention Capability of the Host Country in International Market. Host countries of CDM projects currently do not have CER reserve mechanism, so the CER pricing is entirely controlled by the buyer [17]. Thus, by UNFCCC-level rules, issued CER can be divided into two parts: CER entering the market and reserved CER by host countries. In that case, CER reserve mechanism of host countries can be established, which can transfer the current excess CER to national reserves, thereby transforming the current structure of CER solely being supplied by enterprises to the "dual track" of the state and enterprises. As the host governments reserve a large amount of CER, the interference on CER market price induced by speculation of buyer-market can be effectively curbed.

5. Expected Effect of CDM Quantifying Sustainability Mechanism

5.1. Significantly Cut the Traditional Expected CER under the Condition of Allowing Chemical Gas Projects to Enter the Market. After the introduction of CER quantitative and sustainable mechanism, the amount of CER that can enter the market was cut to a quarter, which reduces about 75% of the expected CER supply. The amount of cut CER is mainly from HFC and N_2O (reduced to 0.2% and 2.2%, resp.) destruction projects. However, HFC and N_2O destruction projects still can conduct CER trading in order to maintain necessary operation costs. Meanwhile, CER generated by those projects that cannot directly enter the market would be converted to reserved CER of the host country, which is managed by the host country (Figure 5).

5.2. Automatically Implementing the CER "Market Equilibrium Distribution" of Different Technologies. After introducing CER quantitative and sustainable mechanism, the amount of market CER from the technology types of higher CER market share and lower support for sustainable development appears to have different degrees of reduction. As for the technology types of lower CER market share and higher support for sustainable development, the amount of market CER is maintained in line with prevailing scenario. After the introduction of reform mechanism, market CER supply becomes more balanced. The expected change of share is shown in Table 3.

Among technologies in Table 3, those types in position of overwhelming majority are automatically adjusted, so that the market CER from those types declined differently according to their relative contribution to sustainable development. The effect of applying the mechanism in these technologies is summarized in Table 4.

Conflict of Interests

The authors declare no conflict of interests.

Acknowledgments

This work is supported by National Natural Science Foundation of China (nos. 51409144, 51209003, and 51478026), the National Water Pollution Control and Management Technology Major Project (nos. 2010ZX07320-002 and 2011ZX07301-004), and key projects in the National Science & Technology Pillar Program (no. 2012BAJ21B08).

References

[1] Executive board annual report 2013, UNFCCC, http://unfccc.int/resource/docs/publications/pub_cdm_eb_annualreport_2013.pdf.

[2] S. Q. Chen and B. Chen, "Network environ perspective for urban metabolism and carbon emissions: a case study of

Vienna, Austria," *Environmental Science & Technology*, vol. 46, no. 8, pp. 4498–4506, 2012.

[3] U. Raab, "Market mechanisms from CDM towards a global carbon market," FORES Study, 2012.

[4] H. Liming, "Financing rural renewable energy: a comparison between China and India," *Renewable and Sustainable Energy Reviews*, vol. 13, no. 5, pp. 1096–1103, 2009.

[5] Sustainable Prosperity, *British Columbia's Carbon Tax Shift: The First Four years*, Sustainable Prosperity, 2012, http://www.sustainableprosperity.ca/.

[6] D. Yuan, X. Guo, Y. Cao et al., "Case study on incentive mechanism of energy efficiency retrofit in coal-fueled power plant in China," *The Scientific World Journal*, vol. 2012, Article ID 841636, 7 pages, 2012.

[7] S. Chen and B. Chen, "Sustainability and future alternatives of biogas-linked agrosystem (BLAS) in China: an emergy synthesis," *Renewable & Sustainable Energy Reviews*, vol. 16, no. 6, pp. 3948–3959, 2012.

[8] M. I. Hoffert, K. Caldeira, G. Benford et al., "Engineering: advanced technology paths to global climate stability: energy for a greenhouse planet," *Science*, vol. 298, no. 5595, pp. 981–987, 2002.

[9] D. Mollicone, F. Achard, S. Federici et al., "An incentive mechanism for reducing emissions from conversion of intact and non-intact forests," *Climatic Change*, vol. 83, no. 4, pp. 477–493, 2007.

[10] Y. Y. Feng, S. Q. Chen, and L. X. Zhang, "System dynamics modeling for urban energy consumption and CO_2 emissions: a case study of Beijing, China," *Ecological Modelling*, vol. 252, no. 1, pp. 44–52, 2013.

[11] L. Zhang, Y. Feng, and B. Chen, "Alternative scenarios for the development of a low-carbon city: a case study of Beijing, China," *Energies*, vol. 4, no. 12, pp. 2295–2310, 2011.

[12] T. M. L. Wigley, R. Richels, and J. A. Edmonds, "Economic and environmental choices in the stabilization of atmospheric CO_2 concentrations," *Nature*, vol. 379, no. 6562, pp. 240–243, 1996.

[13] The World Bank, *Mapping Carbon Pricing Initiatives: Developments and Prospects*, The World Bank, Washington, DC, USA, 2013.

[14] UNFCCC, Total potential supply of CERs by host party from the end of the 1st Kyoto Protocol commitment period (31 Dec. 2012) to 2020, 2012, http://cdm.unfccc.int/Statistics/Public/files/201407/CER_potential.pdf.

[15] UNEP, "The emissions gap report: what 2020 emission levels are consistent with the 2°C and 1.5°C limits? The final plenary meeting at COP 15, Copenhagen, Denmark 19 December, 2009," Technical Summary, 2009, http://www.unep.org/publications/ebooks/emissionsgapreport/pdfs/EMISSIONS_GAP_TECHNICAL_SUMMARY.pdf.

[16] Bloomberg, *California Carbon Advances after Governor Approves Québec link*, Bloomberg, New York, NY, USA, 2013.

[17] R. S. J. Tol, "The marginal damage costs of carbon dioxide emissions: an assessment of the uncertainties," *Energy Policy*, vol. 33, no. 16, pp. 2064–2074, 2005.

[18] UNEP, *CDM Pipeline*, United Nations Environment Programme (UNEP), 2012, http://www.cd4cdm.org/.

Hindawi Publishing Corporation
Advances in Meteorology
Volume 2015, Article ID 518698, 7 pages
http://dx.doi.org/10.1155/2015/518698

Research Article

Stakeholders of Voluntary Forest Carbon Offset Projects in China: An Empirical Analysis

Derong Lin[1] and Yingzhi Lin[2]

[1] *School of Economics and Management, Qingdao Agricultural University, Qingdao 266109, China*
[2] *School of Mathematics and Physics, China University of Geosciences, No. 388 Rumo Road, Wuhan 430074, China*

Correspondence should be addressed to Yingzhi Lin; linyz.ccap@igsnrr.ac.cn

Received 18 July 2014; Accepted 20 September 2014

Academic Editor: Qun'ou Jiang

Climate change is one of the defining challenges facing the planet. Voluntary forest carbon offset project which has the potential to boost forest carbon storage and mitigate global warming has aroused the global concern. The objective of this paper is to model the game situation and analyze the game behaviors of stakeholders of voluntary forest carbon offset projects in China. A stakeholder model and a Power-Benefit Matrix are constructed to analyze the roles, behaviors, and conflicts of stakeholders including farmers, planting entities, communities, government, and China Green Carbon Foundation. The empirical analysis results show that although the stakeholders have diverse interests and different goals, a win-win solution is still possible through their joint participation and compromise in the voluntary forest carbon offset project. A wide governance structure laying emphasis on benefit balance, equality, and information exchanges and being regulated by all stakeholders has been constructed. It facilitates the agreement among the stakeholders with conflicting or different interests. The joint participation of stakeholders in voluntary forest carbon offset projects might change the government-dominated afforestation/reforestation into a market, where all participators including government are encouraged to cooperate with each other to improve the condition of fund shortage and low efficiency.

1. Introduction

According to the Intergovernmental Panel on Climate Change (IPCC) and World Meteorological Organization, the global climate is changing as the direct result of greenhouse gas (GHG) emissions from human activities including burning fossil fuels for energy, land clearing, and agriculture [1, 2]. While GHG emission reduction is called upon worldwide, a large body of evidence indicates that GHG emissions will continue increasing rapidly. It seems to be impossible to achieve the goal of the Copenhagen Accord of limiting the global temperature increase to 2°C [3]. Land use, land-use change, and forestry is regarded as one of the adequate and cost-effective measures that remove carbon dioxide from the atmosphere, therefore mitigating global warming [4–6]. The Fourth Assessment Report of IPCC indicates that afforestation will be an economical and feasible measure of mitigation and adaption climate change in the next 30 to 50 years. It is believed that the climate change mitigation goal will be hardly achieved if global deforestation cannot be reduced and afforestation cannot be accelerated in Post-Kyoto Times [7]. With the largest area of artificial forest (about 62 million hectares), China is still working on afforestation [8, 9]. Its experiences and challenges are of global significance.

Afforestation and sustainable forest management have been embodied in global strategies of climate change mitigation and adaption and proceeded to practice. A series of significant international climate change agreements have been established by United Nations Framework Convention on Climate Change, providing commercialization and marketization opportunities for forest carbon credits. The voluntary compensation of GHG emissions has become a new business domain which is increasingly arousing public interest [10]. Forest carbon market has become the most dynamic market for forest environmental services and might be the forestry market with the highest growth potential in

the future. It has become a new trend to develop forest carbon market to vitalize forest carbon offsets and forestry economy via forest carbon projects [11–13].

The decisions and behaviors of participants of forest carbon market are important factors that influence forest carbon transactions. The research of Cao et al. based on expert interview and structured questionnaire survey indicated that credit quality, common benefit, willingness to pay, and carbon-sink price/cost were the main determinants of forest carbon market in Asia [14]. Markowski-Lindsay et al. estimated the probability forest owners in Massachusetts would participate in carbon market and found that very few forest owners expressed interest in participating under a carbon scenario similar to the current voluntary scheme. They concluded that early withdrawal penalties, additionality requirements, and contract length are concerned by forest owners other than price, and harvesting plans, opinions about forest usage, and beliefs about climate change also play significant roles in the decision to participate [15]. Miller et al. assessed the forest owner interest in selling forest carbon credits in the Lake States, USA, and found that carbon credit payment amount, contract length, gender, value placed on other nonmarket forest amenities, need for additional income, attitude towards climate change, absentee status, land tenure, and total acres owned were all significant determinants [16].

The principal barriers and influencing factors of participation in the forest carbon market and projects have been discussed in previous researches, furnishing a lot of information for forest carbon market development [17–21]. Meanwhile, it is still undiscovered how those factors integrally motivate or prevent stakeholders to participate in the forest carbon market [22, 23]. The integrated effect of all the benefit-driving forces of different stakeholders is the focus of this paper. The major contribution of this paper is that it provides an analysis framework and some general conclusions of voluntary forest carbon offset projects. A comprehensive discussion on the roles, behaviors, and conflicts of stakeholders of voluntary forest carbon offset projects in China such as farmers, planting entities, communities, government, and China Green Carbon Foundation (CGCF) is carried out based on a stakeholder model and a Power-Benefit Matrix.

This paper is organized as follows. Section 2 briefly reviews the forest carbon offset projects and the status of forest carbon transactions in China and presents the proposed stakeholder model and Power-Benefit Matrix of CGCF voluntary forest carbon offset projects in China. Section 3 summarizes the role orientation and driving factors of key stakeholders and discusses their behaviors and conflicts, and Section 4 concludes the paper.

2. Materials and Methods

2.1. Forest Carbon Transaction in China. Attaching great importance to climate change, government of China made great efforts in forestry development. Forestry was regarded as one of the most important domains dealing with climate change by China's National Climate Change Program issued by the National Development and Reform Commission (NDRC) in 2007 [24]. The Outline of China's Forestry Action Plan to Address Climate Change released in 2009 intends to improve forest quality by forest management and protection. The concrete goal of forestry development announced by government of China is to expand its total forest area by 40 million hectares and increase the country's total forest inventory by 1.3 billion cubic meters by 2020 compared with those in 2005 [25].

Although its potential to be one of the most effective measures to address climate change by increasing forest carbon sink has been widely recognized, the development of forest carbon offset project is falling behind expectation. In China, the forest carbon offset projects are still in their infancy, which are fewer in quantity and smaller in scale compared with greenhouse gas emission reduction projects in industrial and energy sectors [26–28]. Concretely, there are two types of forest carbon offset projects in China, afforestation and reforestation (AR) projects under the clean development mechanism (CDM) and voluntary forest carbon offset projects [29, 30]. Since the first CDM reforestation project worldwide registered in Pearl River Basin, five CDM AR projects have been registered in China with a total transaction volume of about 440 million ton carbon dioxide according to statistics from the United Nations.

Volunteer actions of all levels of government, commodities, and individuals to reduce GHG emissions are also advocated besides CDM AR projects. The CGCF funding tree plantation and forest carbon sequestration by selling voluntary carbon offsets to firms and individuals is founded in 2010. All the voluntary forest carbon offset projects are carried out through CGCF in China ever since. By 2012, according to the statistics of CGCF, the foundation had raised about 600 million China Yuan (CNY) and set up 15 special funds according to donor intention and orientation, owning about 80 thousand hectares of carbon sink forest which spread over more than 20 provinces/municipalities all over China. On the whole, most of the voluntary forest carbon offset projects are located in comparatively developed districts such as Zhejiang Province, Fujian Province, Beijing Municipality, and Guangdong Province. The relatively complete markets and higher income levels and fiscal revenue there are beneficial to voluntary forest carbon offsets [11]. The nonprofit feature of CGCF determines that all the funds from firms and individuals are donations rather than investments, which significantly limits the funding sources. Consequently, CGCF and a majority of its donors expect the carbon credits can be traded in carbon markets and generate economic benefits [31]. A pilot project of domestic forest carbon transaction is launched by CGCF and Huadong Forestry Exchange in November 2011. Immediately after its launch, 148 thousand carbon credits (equivalent corresponds to 148 thousand ton of carbon dioxide) are subscribed [32]. However, this subscription becomes the only domestic forest carbon transaction of the pilot project so far.

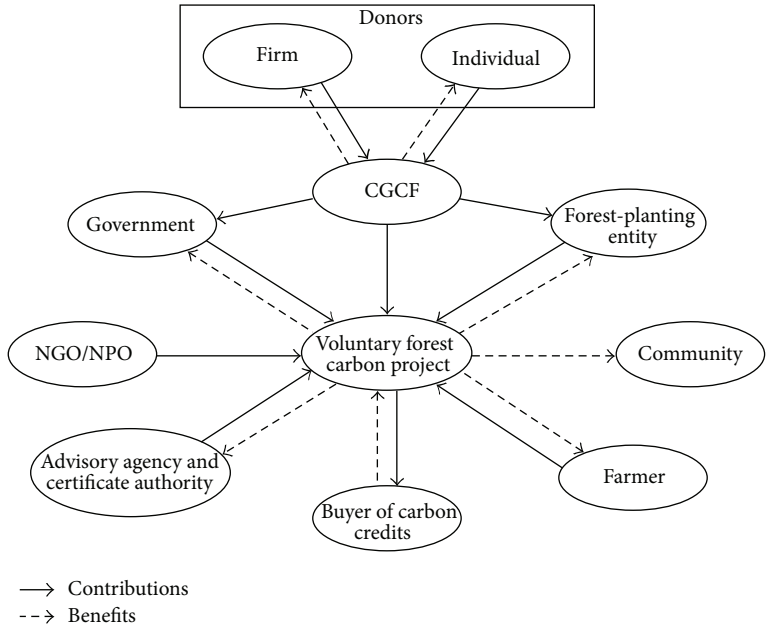

Figure 1: Stakeholder model of CGCF voluntary forest carbon offset projects in China.

2.2. Stakeholder Model. Stakeholder theory has been applied in many fields such as source management, business ethics, and even irregular warfare as a method of system analysis [33, 34]. According to the theory, all the individuals and groups influencing or influenced by the achievement of organization goals are counted as stakeholders [35]. Stakeholder model succeeds in challenging the usual analysis approaches because it takes all the stakeholders' needs into consideration [36]. It is applied in this research to describe the relationship and interaction of stakeholders of voluntary forest carbon offset projects in China.

By considering the management pattern of CGCF voluntary forest carbon offset projects, CGCF, donor (firm and individual), forest-planting entity, buyer of carbon credits, land user (mainly farmers after forest tenure reform), government, community, nongovernmental organization/nonprofit organization (NGO/NPO), advisory agency, and certificate authority are counted as stakeholders (Figure 1). CGCF is the core of project management, obtaining donations from the firms and individuals, cooperating with local government to promote and organize the project, and employing forest-planting entities. The firms and individuals donate money for CGCF voluntary forest carbon offset projects, restrain the use of the funds, and own the carbon credits generated by the project. Forest-planting entities are employed by CGCF to carry out the projects (afforestation/reforestation and forest management). The local government is involved because it is the competent authority of land use change in China and can promote the project by policy support and subsidies. In general, farmers transfer their land use right to CGCF and own the property right of lumbers. The carbon credits generated in the project are measured, monitored, certified and registered by advisory agency and certificate authority, and recorded in the social responsibility accounts of their donors. The NGO/NPO may provide aids and information for CGCF voluntary forest carbon offset projects. The generated carbon credits can circulate on the market and sell to the buyers of carbon credits.

2.3. Power-Benefit Matrix. Power-Benefit Matrix can be used to plot and analyze stakeholders. It displays how stakeholders express their expectations and whether they have the power to make an impact. The effectiveness of CGCF voluntary forest carbon offset projects are directly determined by the behaviors of stakeholders. Meanwhile, stakeholders' behaviors root in their willingness which depends on their rights and obligations (more concretely powers and benefits) in CGCF voluntary forest carbon offset projects. Consequently, the rights and obligations are the key factors in analyzing stakeholders in CGCF voluntary forest carbon offset projects.

3. Results and Discussion

3.1. Role Orientation of Key Stakeholders. With the stakeholder model of CGCF voluntary forest carbon offset projects in China, the role orientation and driving factors of stakeholders are summarized (Table 1). The various role orientations of stakeholders determine the decision makings and behavior choices to have different influences on CGCF voluntary forest carbon offset projects in China. Farmers and forest-planting entities are key stakeholders in China because their low participation willingness, participation capacity, and participation degree are major limits for the CGCF voluntary forest carbon offset project implementation. The role orientations and behavior choices of these two types of stakeholders are discussed in depth in this section.

According to ownerships, the forest land can be divided into two types in China, state-owned forest land and

Table 1: Role orientation and driving factors of stakeholders involved in CGCF voluntary forest carbon offset projects in China.

Stakeholder	Role orientation	Main driving factors
CGCF	Organizer and investor	Forest carbon sequestration increase
Firm	Donor	Carbon credits and good social image
Individual	Donor	Carbon credits and good social image
Forest-planting entity	Planter and forest manager	Revenue from forest planting and management
Buyer of carbon credits	Buyer	Social responsibility or carbon offsets
Farmer	Lumber owner and land supplier	Lumbers ownership, labor income, and training opportunities
Government	Policy and subsidy supporter	Ecological and social benefits
Community	—	Improvement in environment and infrastructure
NGO/NPO	Aids and information supporter	—
Advisory agency and certificate authority	Designer of project design document	Fees

collective-owned forest land. The latter is mainly used and managed by farmers because its use right had transferred to farmers since forest tenure reform [37]. This transition determined that the use right of all involved collective-owned forest land would belong to farmers in the next 50–70 years. Currently, the vast majority of forest land involved in CGCF voluntary forest carbon offset projects is collective-owned. Therefore farmers become the principal suppliers of forest land for forest carbon offset projects. For instance, the *Project Design Document* showed that, out of all the 4,196.8 hectares of forest land, 2,857.5 hectares (about 68%) was supplied by farmers in the CDM reforestation project in Pearl River Basin.

There exist two modes for farmers to participate in CGCF voluntary forest carbon offset projects. A few farmers would like to invest in afforestation/reforestation and take charge of daily forest management just as forest-planting entities do and finally turn into developers of CGCF voluntary forest carbon offset projects. These farmers will gain the benefits of forest carbon transaction besides selling lumber in the future. Others may directly entrust their land to CGCF for developing voluntary forest carbon offset projects, rather than directly undertaking the afforestation/reforestation as well as forest management themselves. These farmers only own the property right of lumbers on their forest land. Of course, they could be employed by forest-planting entities and then participated in afforestation/reforestation and forest management. Because of the small amount of own forest land, labor shortage, and lack of advanced technology for afforestation/reforestation and capacity for the effective forest management, the overwhelming majority of farmers participate in CGCF voluntary forest carbon offset projects with the later mode.

Actually not every farmer in project area is willing to participate in CGCF voluntary forest carbon offset projects. The farmer's participation willingness depends mainly upon the opportunity cost of land use and the chief industries the farmer's families engaged in. For example, the originally planned forest land area of one CGCF voluntary forest carbon offset project in Sichuan Province was 3,000 hectares; however only 2,300 hectares of forest land was finally involved. The low participation willingness of farmers is mainly due to the high opportunity cost of land use right transference. More economic benefits can be obtained if the land is used for planting tobacco, walnut, *Camellia oleifera,* and other commercial crops compared with forest carbon sequestration.

Forest-planting entities include the firms engaged in carbon sink forest plantation and management entrusted by CGCF. In CGCF voluntary forest carbon offset projects, forest-planting entities act as the operators of carbon credits generation. In particular, forest-planting entities are always one of the major donors of CGCF as well. Consequently, many voluntary forest carbon offset projects are driven by not only CGCF but also forest-planting entities. There may be totally four reasons for the forest-planting entities' participation in CGCF voluntary forest carbon offset projects. Firstly, the forest-planting entities can obtain benefit from CGCF by selling the service of forest plantation and management. Secondly, government subsidy for afforestation/reforestation is another major economic driver of forest-planting entities' participation. In most cases, the forest-planting entities are subsidized by government according to the standard of forestry ecological engineering (about 4,500 CNY per hectare). Thirdly, the high economic returns are always expected by donors when they also act as forest-planting entities. By directly participating in the forest plantation and management, donors can bring down the cost of generating carbon credits. Finally, most forest-planting entities believe that they can seize more opportunities in forest carbon credits transaction by accumulating more participation experience and management knowledge.

3.2. Power-Benefit Matrix Analysis of Stakeholders. According to the role orientation and driving factors of stakeholders involved in CGCF voluntary forest carbon offset projects in China, a Power-Benefit Matrix is established for stakeholders (Table 2).

3.2.1. Powers and Benefits of Stakeholders. Buyer of carbon credits may obtain relatively high economic and social benefit

Table 2: Power-Benefit Matrix of stakeholders in CGCF voluntary forest carbon offset projects in China.

	Benefit level	
	Low	High
Power level		
Low	NGO/NPO Advisory agency and certificate authority	Buyer of carbon credits
High	Donor (firm and individual) Community Government CGCF	Forest-planting entity Farmer

by purchasing carbon credits. Currently, the forest carbon transaction occurred in a buyer's market. The market is very competitive for suppliers of carbon credits. The price of carbon credits is determined by buyers' willingness under the regulation of the government's GHG reduction policies. Therefore, the supplier should pay close attention to policy changes and be conscious of willingness changes of the possible buyers. However, the buyer of carbon credits can hardly influence the launch, implementation, and effectiveness of CGCF voluntary forest carbon offset projects which is mainly determined by nonprofit factors.

Donor (firm and individual), community, government, and CGCF own a relatively high level of power in CGCF voluntary forest carbon offset projects. As important providers of funds, the donors exert significant influence on the launch of projects but may not care too much about the benefit. The behaviors or decisions of community, government, and CGCF are crucial to the projects though they hardly obtain any economic benefit in this process.

Forest-planting entities and farmers not only have high level of power but also benefit a lot from CGCF voluntary forest carbon offset projects. The effectiveness of the projects is directly affected by forest-planting entities which are the operators of afforestation/reforestation and forest management. By participating in the projects and selling their services, forest-planting entities can get corresponding profit. Farmers are the original owners of land use right and their willingness determines the projects' scale. They can obtain relatively high benefit because of owning lumber produced in the projects.

3.2.2. Farmers' Acceptance for Benefit Allocation. Payment for forest-based carbon sequestration may be an emerging opportunity to mitigate climate change while creating new income streams for farmers. As main suppliers of land and labor, farmers have the right to share the benefit of CGCF voluntary forest carbon offset projects with the forest-planting entities. Their acceptances of the projects are largely determined by the method of benefit allocation. However, they do not take part in the planning, budgeting, and managing and lack information about total benefit of the projects. Consequently, the acceptance for benefit allocation from farmers depends on the opportunity cost of the land including fertility, original use, location, road conditions, and government policy. The benefit gained from the projects should offset the opportunity cost of the land at least. The transaction cost would be huge if negotiation was conducted with each farmer for each piece of land. Therefore, it is a common practice to make negotiations between the forest-planting entities and representatives from the farmers and communities. Once a consensus is reached, most of the farmers may accept the pay from forest-planting entities for their land and labor.

3.2.3. Motivator of Forest-Planting Entity. The cost of CGCF voluntary forest carbon offset projects, including production cost and transaction cost, is the major obstacle for private landowners in participating in carbon credit market. In Eastern China especially in the developed areas such as Guangdong, Beijing, Tianjin, Shanghai, Zhejiang, and Fujian, the cost of forest carbon sequestration is much higher (an average of 2,042.62 CNY per ton of carbon) compared with those in southwest, northwest, and northeast regions (averaged at 819.42 CNY per ton of carbon) [38]. Meanwhile the carbon credits generated by CGCF voluntary forest carbon offset projects were priced at 18 CNY per ton, far below the carbon credits price of CDM AR projects ranging from 25 to 70 CNY per ton. Nevertheless, CDM AR projects are mainly located in the southwest and northeast of the country, and the CGCF voluntary forest carbon offset projects are concentrated in Guangdong, Beijing, Zhejiang, Fujian, and so forth. This phenomenon indicates that cost and price are not the decisive factors of CGCF voluntary forest carbon offset projects. The key lies in policy guidance and incentive measures of government under the condition of incomplete market. The carbon credits are actually appendages to afforestation and reforestation. The forest-planting entity will participate in a CGCF voluntary forest carbon offset project as long as its net benefit exceeds that of traditional forestry or the benefit from carbon credits is more than the extra cost incurred in carbon credits production and transaction.

3.2.4. Roles of CGCF, Government, and Community. CGCF, government, and community are more likely to win trust from other stakeholders due to their information superiority and having no apparent interest conflict with others. Meanwhile, their active participations are crucial to the successful implementation of CGCF voluntary forest carbon offset projects.

An effective governance mode is able to coordinate the stakeholders' interests through formal or informal institutions so as to avoid conflicts. The existence of CGCF is one of the major differences between voluntary forest carbon offset projects and CDM AR projects. Due to the absence of mature carbon credit market, CGCF actually plays the roles of leadership, demonstration, and medium, providing a communication platform for the buyers and sellers, which effectively reduces the information search cost and improves trading efficiency.

Policy clarity and perfection and regulation of institution are the keys to forest carbon market development [39, 40]. Experience shows that the implementation of prevenient

CGCF voluntary forest carbon offset projects is virtually impossible without effective participation and support of the government. The government departments and agencies involved in the projects mainly refer to the competent forestry departments and the municipal and township governments, which affect the implementation of CGCF voluntary forest carbon offset projects through three ways. Firstly, government helps to discover partners for the projects and directly or indirectly facilitates the forest carbon transactions between buyers and sellers. Secondly, government coordinates the beneficial relationships between the partners and ensures the smooth implementation of the projects and transactions. Thirdly, fund from government plays a guiding and substantive role that cannot be substituted. Take Wenzhou Carbon Credit Fund as an example, of all the raised funds of 74.3 million CNY, 40% (or 30.3 million CNY) come from the municipal government. Furthermore, most CGCF voluntary forest carbon offset projects could get afforestation subsidy from government. This is one of the main reasons that forest-planting entities are willing to take part in the projects and share more benefit out to farmers.

As a vital stakeholder of CGCF voluntary forest carbon offset projects, the community as well as its interests must be considered. Unlike forestry-planting entities and farmers who mainly focus on economic returns, community is more concerned with environmental and social benefit such as improvement in infrastructure, education and training, ecological environment, and access to the forest. Although these willingness can conflict with goals of economic benefit maximization of forestry-planting entities and farmers more or less, they have to be taken into account as much as possible. A real-world example is that the original plan had been altered in Wenzhou Carbon Credit Project because the community opposed planting too many fast-growing eucalypt trees.

4. Conclusions

The voluntary forest carbon offset projects are highly valued to boost forest carbon storage and mitigate global warming and will become the major form of forest carbon transaction in China. The empirical analysis of stakeholders indicates that a win-win solution is possible in CGCF voluntary forest carbon offset projects in China through stakeholders' joint participation and compromise, although the interests of government, forest-planting entities, farmers and community, and so forth are different. A wide governance structure laying emphasis on benefit balance, equality, and information exchanges and being regulated by all stakeholders has been constructed. It facilitates the agreement among the stakeholders with conflicting or different interests. Due to this governance structure, the functions such as carbon sequestration, environment conservation, and ecological restoration of forest are brought into play through financial subsidies, preferential taxations, and some other encouraging measures. In particular, the fund from government for voluntary forest carbon offset projects not only helps to increase the direct economic benefits of the forest-planting entities and farmers but also plays a substantive role in guiding donation. In sum, the joint participation of stakeholders in voluntary forest carbon offset projects might change the government-dominated afforestation/reforestation into a market, where all participators including government are encouraged to cooperate with each other to improve the condition of fund shortage and low efficiency. The analysis of stakeholders in this study is based on the hypothesis of ration while decisions of stakeholders are always influenced by psychology or belief. This is especially true for famers because they lack information. The irrationalities of stakeholders should be discussed in future studies.

Conflict of Interests

The authors declare that there is no conflict of interests regarding the publication of this paper.

Acknowledgments

This research was supported by China National Natural Science Funds for Distinguished Young Scholar (no. 71225005), the National Scientific Foundation of China (no. 41171434), and the Foundation for High-level Talents of Qingdao Agricultural University (no. 2017).

References

[1] B. Metz, O. R. Davidson, P. R. Bosch, R. Dave, and L. A. Meyer, *Climate Change 2007: Mitigation*, Cambridge University Press, Cambridge, UK, 2007.

[2] World Meteorological Organization, *World Meteorological Organization Statement on the Status of the Global Climate in 2003*, World Meteorological Organization, Geneva, Switzerland, 2003.

[3] D. J. Frame and D. A. Stone, "Assessment of the first consensus prediction on climate change," *Nature Climate Change*, vol. 3, no. 4, pp. 357–359, 2013.

[4] B. Schlamadinger, N. Bird, T. Johns et al., "A synopsis of land use, land-use change and forestry (LULUCF) under the Kyoto Protocol and Marrakech Accords," *Environmental Science and Policy*, vol. 10, no. 4, pp. 271–282, 2007.

[5] R. J. Zomer, A. Trabucio, D. A. Bossio, and L. V. Verchot, "Climate change mitigation: a spatial analysis of global land suitability for clean development mechanism afforestation and reforestation," *Agriculture, Ecosystems & Environment*, vol. 126, no. 1-2, pp. 67–80, 2008.

[6] J. Zhan, H. Yan, B. Chen, J. Luo, and N. Shi, "Decomposition analysis of the mechanism behind the spatial and temporal patterns of changes in carbon bio-sequestration in China," *Energies*, vol. 5, no. 2, pp. 386–398, 2012.

[7] W. M. Budzianowski and D. C. Budzianowska, "Allocation of ecologically allowable carbon emissions to countries as a key to more effective post–Kyoto Protocol climate change mitigation law," *International Journal of Global Warming*, vol. 4, no. 2, pp. 113–133, 2012.

[8] X. Deng, Q. Jiang, J. Zhan, S. He, and Y. Lin, "Simulation on the dynamics of forest area changes in Northeast China," *Journal of Geographical Sciences*, vol. 20, no. 4, pp. 495–509, 2010.

[9] J. Shi and L. Cui, "Soil carbon change and its affecting factors following afforestation in China," *Landscape and Urban Planning*, vol. 98, no. 2, pp. 75–85, 2010.

[10] S. Brinkel and R. Antes, "Voluntary carbon offsets—empirical findings of an international survey," in *Emissions Trading*, R. Antes, B. Hansjurgens, P. Letmathe, and S. Pickl, Eds., pp. 243–262, Springer, Berlin, Germany, 2011.

[11] L. Peskett, K. Schreckenberg, and J. Brown, "Institutional approaches for carbon financing in the forest sector: learning lessons for REDD+ from forest carbon projects in Uganda," *Environmental Science and Policy*, vol. 14, no. 2, pp. 216–229, 2011.

[12] C. S. Galik, D. M. Cooley, and J. S. Baker, "Analysis of the production and transaction costs of forest carbon offset projects in the USA," *Journal of Environmental Management*, vol. 112, pp. 128–136, 2012.

[13] S. Wu, "Forestry market perspective and transaction strategies for forestry CERs under CDM," *Scientia Silvae Sinicae*, vol. 46, no. 11, pp. 152–157, 2010 (Chinese).

[14] X. Cao, M. Seol, and Y. Yeo-Chang, "An exploratory study on forest carbon markets in Asia," *Forest Science and Technology*, vol. 8, no. 1, pp. 34–37, 2012.

[15] M. Markowski-Lindsay, T. Stevens, D. B. Kittredge, B. J. Butler, P. Catanzaro, and B. J. Dickinson, "Barriers to Massachusetts forest landowner participation in carbon markets," *Ecological Economics*, vol. 71, no. 1, pp. 180–190, 2011.

[16] K. A. Miller, S. A. Snyder, and M. A. Kilgore, "An assessment of forest landowner interest in selling forest carbon credits in the Lake States, USA," *Forest Policy and Economics*, vol. 25, pp. 113–122, 2012.

[17] R. Birdsey, K. Pregitzer, and A. Lucier, "Forest carbon management in the United States: 1600–2100," *Journal of Environmental Quality*, vol. 35, no. 4, pp. 1461–1469, 2006.

[18] J. C. Milder, S. J. Scherr, and C. Bracer, "Trends and future potential of payment for ecosystem services to alleviate rural poverty in developing countries," *Ecology and Society*, vol. 15, no. 2, p. 4, 2010.

[19] D. Wade and C. Moseley, "Foresters' perceptions of family forest owner willingness to participate in forest carbon markets," *Northern Journal of Applied Forestry*, vol. 28, no. 4, pp. 199–203, 2011.

[20] D. W. Thompson and E. N. Hansen, "Carbon storage on non-industrial private forestland: an application of the theory of planned behavior," *Small-Scale Forestry*, vol. 12, no. 4, pp. 631–657, 2013.

[21] S. L. Cook and Z. Ma, "Carbon sequestration and private rangelands: Insights from Utah landowners and implications for policy development," *Land Use Policy*, vol. 36, pp. 522–532, 2014.

[22] I. J. Visseren-Hamakers, B. Arts, and P. Glasbergen, "Interaction management by partnerships: the case of biodiversity and climate change," *Global Environmental Politics*, vol. 11, no. 4, pp. 89–107, 2011.

[23] P. Lamers and M. Junginger, "The "debt" is in the detail: a synthesis of recent temporal forest carbon analyses on woody biomass forenergy," *Biofuels, Bioproducts and Biorefining*, vol. 7, no. 4, pp. 373–385, 2013.

[24] Y. Ding, G. Ren, G. Shi et al., "National assessment report of climate change (I): climate change in China and its future trend," *Advances in Climate Change Research*, vol. 2, no. 1, pp. 3–8, 2006.

[25] NDRC, *China's Policies and Actions for Addressing Climate Change—The Progress Report 2009*, NDRC, Beijing, China, 2009.

[26] S. Thomas, P. Dargusch, S. Harrison, and J. Herbohn, "Why are there so few afforestation and reforestation Clean Development Mechanism projects?" *Land Use Policy*, vol. 27, no. 3, pp. 880–887, 2010.

[27] E. Liu and S. Liu, "Climate change mitigation through forest-based carbon sequestration projects in China: potential benefits and challenges," *Advanced Materials Research*, vol. 255—260, pp. 2949–2952, 2011.

[28] Y. Huang, "Policy experimentation and the emergence of domestic voluntary carbon trading in China," *East Asia*, vol. 30, no. 1, pp. 1–23, 2013.

[29] S. Wu, X. Zhang, and W. Song, "Carbon offset standard for international voluntary carbon sequestration market," *Scientia Silvae Sinicae*, vol. 45, no. 3, pp. 134–139, 2009.

[30] R. J. Zomer, A. Trabucco, L. V. Verchot, and B. Muys, "Land area eligible for afforestation and reforestation within the clean development mechanism: a global analysis of the impact of forest definition," *Mitigation and Adaptation Strategies for Global Change*, vol. 13, no. 3, pp. 219–239, 2008.

[31] X. Zhu, Y. Hou, and Y. Li, "A case study of forest carbon trade in China: Sino-forest funded protection of natural secondary forests in Heyuan City, Guangdong," *Forestry Science and Technology*, vol. 8, no. 2, pp. 38–45, 2009.

[32] Y. Ying and J. Li, "SWOT analysis of forest carbon-sink market transaction in China," in *Proceedings of the National Conference on Information Technology and Computer Science (CITCS '12)*, pp. 1065–1068, Lanzhou, China, November 2012.

[33] J. Sarkis, Q. Zhu, and K.-H. Lai, "An organizational theoretic review of green supply chain management literature," *International Journal of Production Economics*, vol. 130, no. 1, pp. 1–15, 2011.

[34] K. de Brucker, C. MacHaris, and A. Verbeke, "Multi-criteria analysis and the resolution of sustainable development dilemmas: a stakeholder management approach," *European Journal of Operational Research*, vol. 224, no. 1, pp. 122–131, 2013.

[35] M. C. Jensen, "Value maximization, stakeholder theory, and the corporate objective function," *Journal of Applied Corporate Finance*, vol. 22, no. 1, pp. 32–42, 2010.

[36] C. Connelley and P. Tripodi, *Aspects of Leadership: Ethics, Law, and Spirituality*, Marine Corps University Press, Quantico, Va, USA, 2012.

[37] Z. Zhu, Y. Shen, W. Wu, X. Xu, and C. Zeng, "Household optimal forest management decision and carbon supply: case from Zhejiang and Jiangxi provinces," *Acta Ecologica Sinica*, vol. 33, no. 8, pp. 2577–2585, 2013.

[38] W. Zhong and Z. Xing, "Analysis on cost and benefit of carbon sequestration in each province of China: based on afforestation and reforestation project," *China Population Resources and Environment*, vol. 22, no. 9, pp. 33–41, 2012 (Chinese).

[39] P. Dargusch, S. Harrison, and S. Thomas, "Opportunities for small-scale forestry in carbon markets," *Small-Scale Forestry*, vol. 9, no. 4, pp. 397–408, 2010.

[40] Z. Ying, M. Gao, J. Liu, Y. Wen, and W. Song, "Green accounting for forest and green policies in China—a pilot national assessment," *Forest Policy and Economics*, vol. 13, no. 7, pp. 513–519, 2011.

Hindawi Publishing Corporation
Advances in Meteorology
Volume 2015, Article ID 416728, 7 pages
http://dx.doi.org/10.1155/2015/416728

Research Article

The Impact Analysis of Water Body Landscape Pattern on Urban Heat Island: A Case Study of Wuhan City

Bohan Yang, Fen Meng, Xinli Ke, and Caixue Ma

College of Land Management, Huazhong Agricultural University, Wuhan 430079, China

Correspondence should be addressed to Xinli Ke; kexl@igsnrr.ac.cn

Received 17 September 2014; Revised 4 March 2015; Accepted 5 March 2015

Academic Editor: Hongbo Su

Based on the LST and the landscape metrics of water body with remote sensing technique and spatial analysis, the relationship between the mean LST and the attributes of water body was revealed via Pearson's correlation analysis and multiple stepwise regression analysis. Result showed that, in 32 class-based metrics we selected, the proportion of water body, average water body size, the isolation and fragmentation of water body, and other eight metrics have high correlation with the LST. As a resultant force, the quantity, shape, and spatial distribution of water body affect the forming of temperature. We found that the quantity and spatial pattern of city water body could be allocated reasonably to maximize its cooling effect.

1. Introduction

With the rapid development of urbanization since industrial revolution, land use and land cover (LULC) of the earth has changed dramatically because of human activities and natural disasters. At the same time, LULC not only changed the land surface condition, but also reduced the stability of the earth surface ecosystem. As a result, LULC has affected the climate change directly and indirectly [1] and hence has become more and more important study area for environmental researchers [2–4].

One relative mature research is the study of the relationship between LULC and urban heat island (UHI) [3, 4]. Studies have proved that the urban built-up land has positive influence on UHI [5], while green landscape has negative influence on UHI [3]. In addition, water body is another land use type with negative influence [6, 7] as the water bodies in city achieve cooling effect by transpiration and heat exchange with the surrounding environment. Compared with the studies of built-up, green landscape land use types, the research on urban water body is relatively less at present. There are three aspects in this research: (1) the relationship between water body and land surface temperature; the temperature of water is lower than other kinds of land uses [7]; (2) the impact of spatial characteristics (e.g., shape) on UHI [8]; (3) the configuration of water body, and its relationship with UHI [9].

The land surface temperature (LST), as one important indicator of the UHI [1], has been used in many researches to represent climate effects. This paper studies the relationship between the land surface temperature and the water body from the view of landscape pattern.

Wuhan, the capital of Hubei province, in central China, is famous for the title of "one of four furnaces in China." And it has another name: "the city of hundreds lakes," whose water area covers around 25% of the territory and the coverage of water area ranks first in the whole country. In recent years, Wuhan city has experienced rapid urbanization and economic development. As a result, many urban water bodies in Wuhan city have been disappeared because of the pressure to gain extra land profit in the process of urban development [10]. At the same time, the land use/cover change has a great effect on its local climate. Therefore, Wuhan city is chosen as the case area to estimate the relationship between LST and the water pattern from the view of landscape ecology.

Based on existing research, this paper used the Landsat Thematic Mapper (TM) data to retrieve LST and land use/cover for water. Then, considering the number of samples and computational burden, Wuhan city was divided into 736 sample areas whose size is 3000 m $*$ 3000 m. Then the landscape metrics of water and the mean LST of each sample area were calculated by using ArcGIS 10.0. With the help of

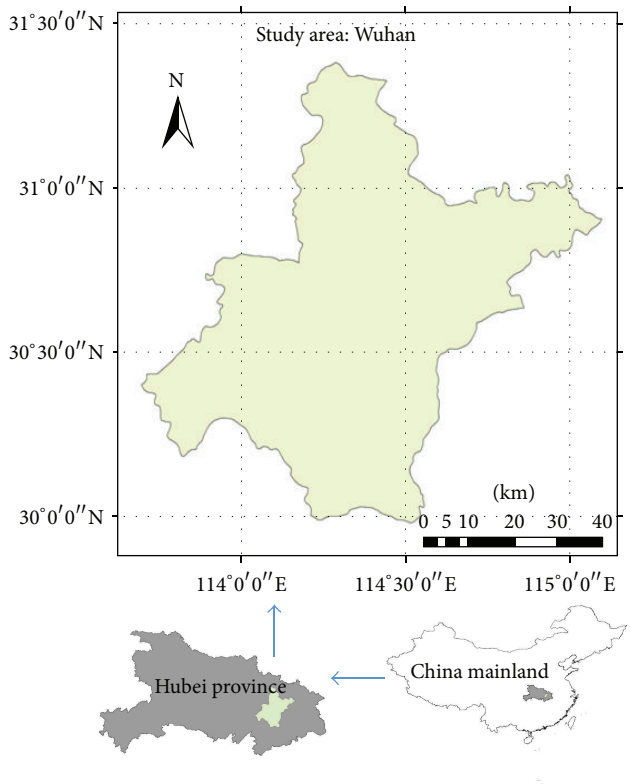

Figure 1: Wuhan city, the research area.

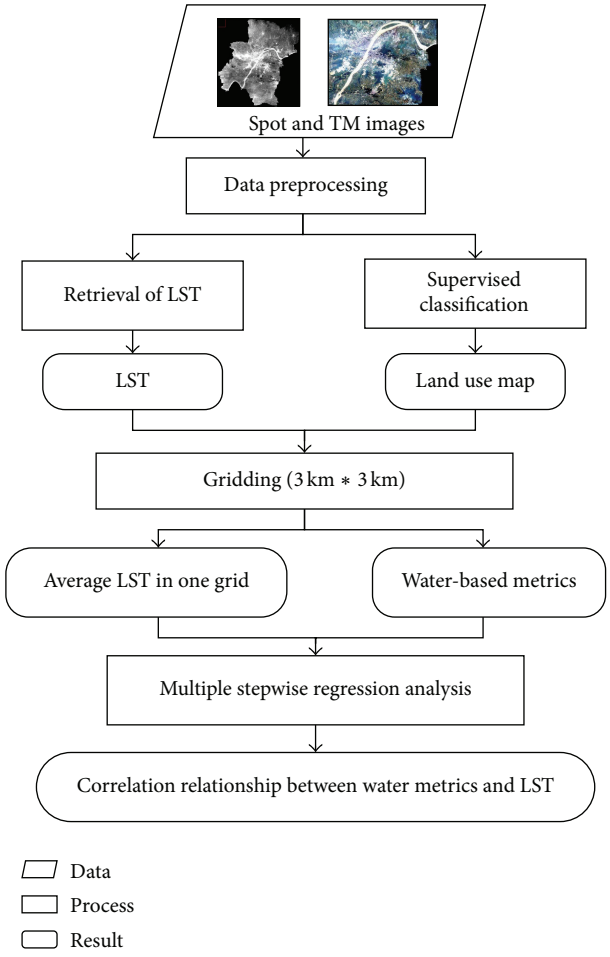

Figure 2: Research framework of landscape metrics of water on land surface temperature.

statistical analysis theory and methods, Pearson's correlation coefficients were used to determine the effect of the spatial structure of water on the LST. Finally, the computed experimental samples could be fitted to multiple linear regression model by stepwise regressions.

2. Study Area and Data Sources

2.1. Study Area. Wuhan city is situated in central China and located between 113°41′–115°05′ E and 29°58′–31°22′ N, shown in Figure 1. Wuhan is located at a subtropical humid monsoon climate zone, with an annual mean precipitation about 1096.1 mm. The average annual temperature ranges from 15.8°C to 17.5°C, and sometimes in summer the maximum temperature can soar to 40°C.

The total territorial area of Wuhan is about 8494.41 km^2, and the water area is about one-fourth of the city's total area. The famous rivers and lakes in Wuhan city are Yangtze River, Han River, East Lake, South Lake, and so on. These rivers/lakes mentioned above, together with other water bodies of Wuhan, are scattered and distributed in the study area. And they have a big influence on humidity, purifying atmosphere of Wuhan climate.

Wuhan's economy strength has grown rapidly, and levels of the industrialization and urbanization were improved as well. By the end of 2005, the resident population of Wuhan city was 8.58 million, and the annual GDP per capita reached 26238 Yuan.

2.2. Data Sources. This paper utilized three types of data: social-economy statistical data, Wuhan land use data, and LST data derived from remote sensing images. (1) The social-economy statistical data, such as population/annual GDP per capita in this paper, came from Wuhan Statistical Yearbook and Wuhan City Water Resources Bulletin. (2) A Landsat 5 TM imagery on September 11, 2005, (patch/row: 122/39) was selected to quantitatively measure LST and the situation of LULC. All bands of TM images except band 6 have a spatial resolution of 30 m, while band 6 (thermal infrared band) has a spatial resolution of 60 m. Before getting LULC information from the raw image, image preprocessing such as geometric rectification, relative radiometric correction, and atmospheric correction was completed. In addition, a Spot image on December 15, 2005, with a spatial resolution of 4 m was used to verify results of supervised classification in the study area.

3. Methods and Models

3.1. Research Framework. The basic idea of analysis for the impacts of landscape metrics of water on land surface temperature is illustrated in Figure 2. Based on the Landsat

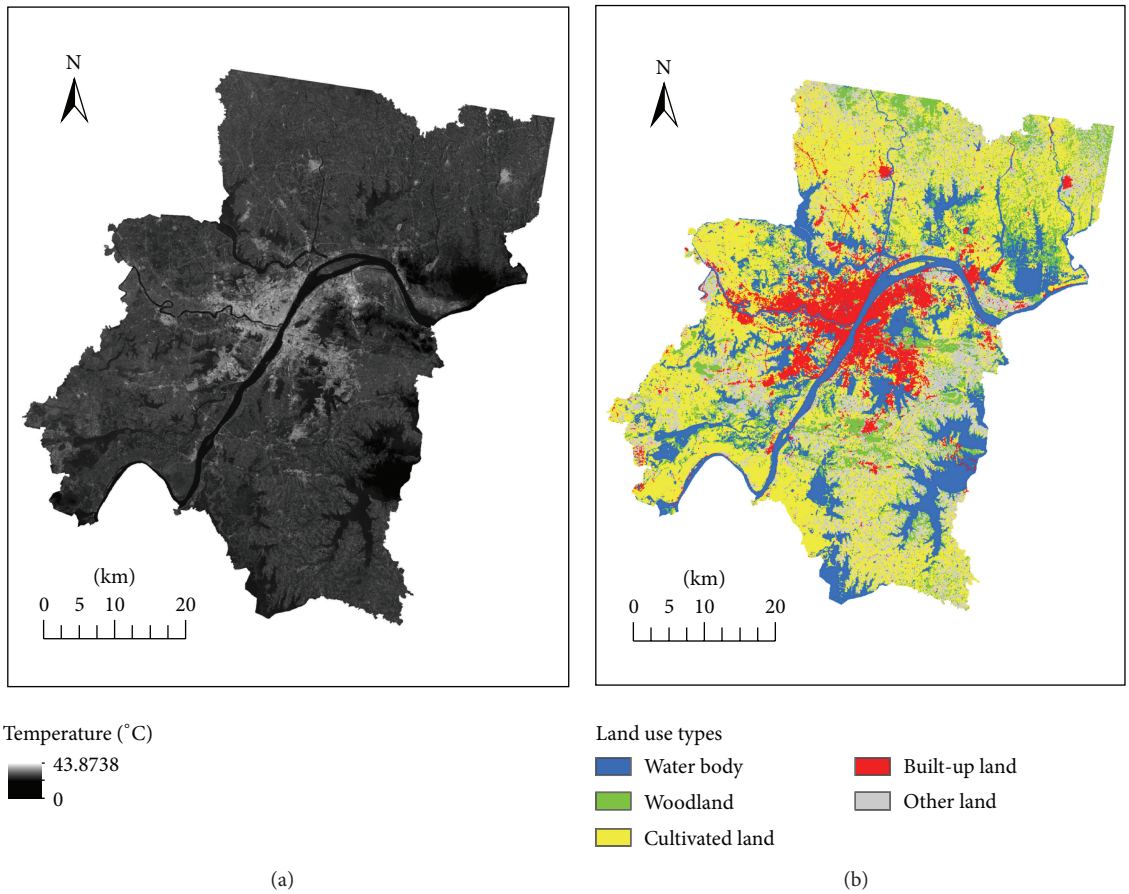

Figure 3: Land surface temperature (a) and land use map (b) in Wuhan city.

5 TM imagery, the land use information was extracted by the method of supervised classification, and the LST was retrieved by using the single-channel algorithm. Then considering number of statistical samples and the computational burden, Wuhan was divided into 736 sample regions. The mean LST and landscape metrics of water in each sample region as sample data would be used to do Pearson's correlation analysis and multiple stepwise regression analysis. By comparing relationship between the landscape metrics of water and the LST, it is meaningful to reveal the impacts of the spatial structure of water on LST, which can help improving urban environment through rational allocation of water resources.

3.2. Acquisition of Land Use Map. In order to calculate landscape metrics of water, a land cover classification is necessary to obtain the land use map in study area. In this paper, five land use classes were established: urban, forest, cropland, bare land, and water. It should be pointed out that water in here mainly includes rivers, lakes, and ponds. There are three steps to derive land use map. First, region of interest (ROI) was selected on the true color image, which was produced by combining bands 5, 4, and 3 of the TM images. They were used as training areas after passing separable test. Second, neural net classification was employed to perform the classification. Third, for each land category, at least 60 samples were selected randomly to check the accuracy of the classified maps by using confusion matrices. In addition, the true ROI was identified on the Spot image used as ground surveys in accuracy assessment. The overall accuracy is approximately 80%, and the overall kappa statistics value nearly reached 0.8, which met the recommended value. Fourthly, a $3 * 3$ moving window in clump process was used to do postclassification process, which can eliminate the unnecessary image noises from visual interpretation. After completing these above steps, the land use map was obtained as shown in Figure 3(b).

3.3. Retrieval of LST. In order to acquire the LST of Wuhan city, the brightness temperature should be derived first. A method composed by three equations was proposed by Qin et al. (2001) to derive brightness temperature from TM images [11].

The first equation can convert digital number of band 6 into radiation luminance (L_{TM6}, $m \times W \times cm^{-2} \times sr^{-1}$) as follows:

$$L_{TM6} = \frac{DN \times (L_{max} - L_{min})}{255} + L_{min}, \quad (1)$$

where DN is the digital number of TM image. L_{max} and L_{min} represent the maximum and minimum radiation luminance corresponding to the DN_{max} (255) and DN_{min} (0). According

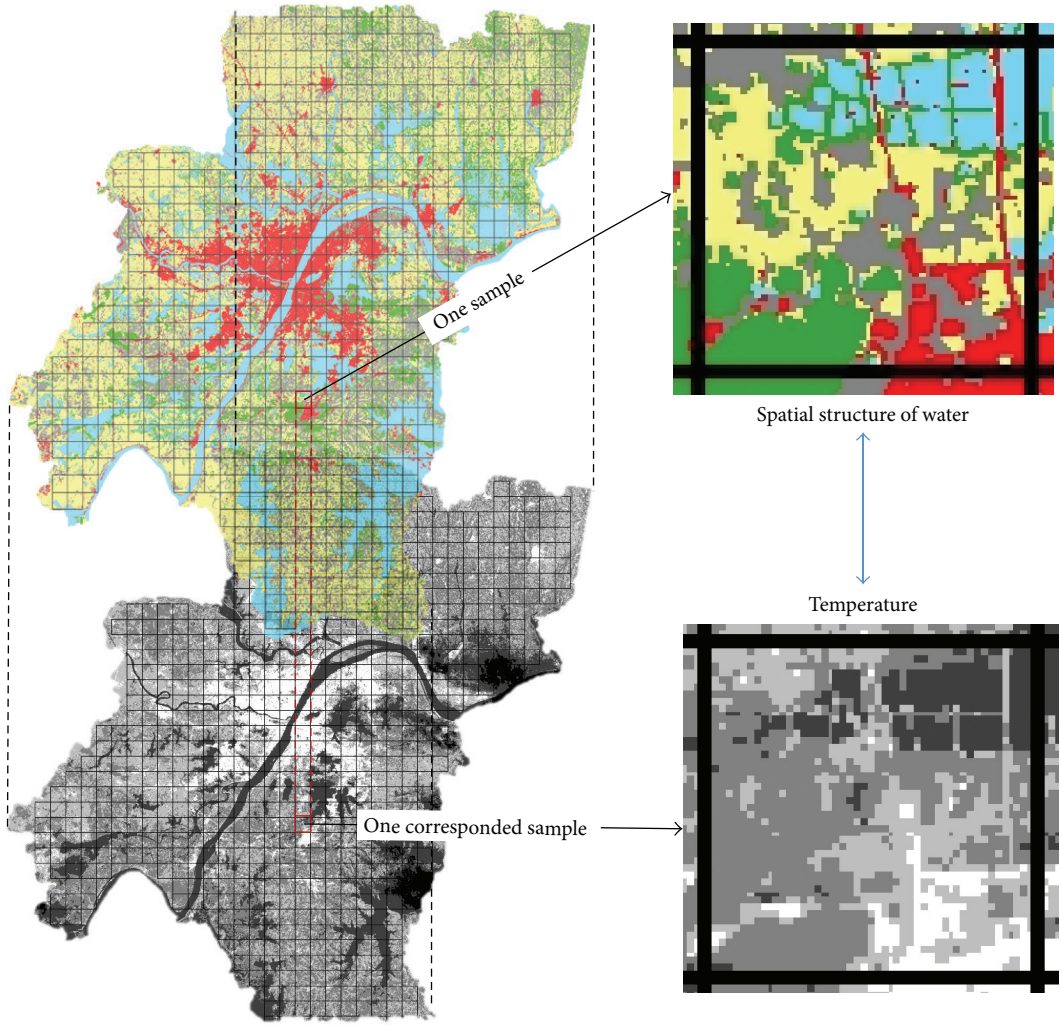

Figure 4: Water spatial structure and its corresponding mean temperature in sample areas.

to Li [12], the $L_{\max}$ is 1.896 m × W × cm^{-2} × sr^{-1} × μm^{-1} and $L_{\min}$ is 0.1534 m × W × cm^{-2} × sr^{-1} × μm^{-1}.

Then brightness temperature can be derived by two equations as follows:

$$L_\lambda = \frac{L_{\mathrm{TM6}}}{b},$$
$$T = \frac{k_2}{\ln\left(k_1/L_\lambda + 1\right)}, \tag{2}$$

where b is 1.239 μm and represents the effective spectral range; $K1$ = 60.766 m × W × cm^{-2} × sr^{-1} × μm^{-1} and $K2$ = 1260.56 K, and they are prelaunch calibration constants of Landsat TM5.

The brightness temperature obtained above just represents blackbody temperature. However, the blackbody is not existent in the real world. So it is necessary to convert the brightness temperature into LST by using the following formula [13]:

$$T_S = \frac{T}{1 + (\lambda * T/\rho)\ln\varepsilon}, \tag{3}$$

where T_s represents the LST, T represents brightness temperature, and λ is the effective wavelength whose value is 11.5 μm; $\rho = hc/\sigma = 1.438 * 10^{-2}$ mk; Boltzmann constant $\sigma = 1.38 * 10^{-23}$ J/K; Planck constant $h = 6.626 * 10^{-34}$ J * S; speed of light $c = 2.998 * 10^8$ m/s [14]. As emissivity is difficult to obtain, this paper uses Van's empirical formula [15]: when NDVI ≤ 0.157, ε = 0.923; when 0.157 < NDVI < 0.727, ε = 1.0094 + 0.047 ln(NDVI), and the emissivity of water is 0.9925.

After finishing these above steps, the LST image was retrieved, shown in Figure 3(a).

3.4. Calculation of Spatial Structure of Water Body by Using Landscape Metrics. From the land use map of Wuhan city, it can be intuitively identified that water body is evenly distributed in the whole study area. Unlike other metropolis in China, such as Beijing and Shanghai, the correlation between mean LST and water-based landscape metric is more significant in Wuhan because of the large quantity and special spatial structure of water body in study area [9], as it shown in Figure 4.

As we all know, landscape metrics are often used for quantitative spatial model building in biological, habitat, and landscape ecological contexts [16]. And they are used to analyze and characterize urban land use and structure types [17]. In this paper, 32 class-based metrics' landscape was used for quantitative expression of the spatial structure of water body.

Considering the relatively low time resolution of TM images, it is not convenient to get a series of sample data in the view of time, and the sample data would be chosen in space. Wuhan was divided into 736 sample regions whose size is 3000 m $*$ 3000 m (the value is determined by several experiments). The mean LST of each sample region was calculated by zonal statistics in ArcGIS 10.0 and the value of Moran's I was acquired to measure the spatial autocorrelation of the mean LST. Then the landscape metrics of water body were got using Patch Analyst 5. Patch Analyst 5 is an extension to ArcGIS system that can facilitate the spatial analysis of landscape patches and is used for spatial pattern analysis.

Then Pearson's correlation coefficients between the landscape metrics and mean LST were calculated. It is a significance test between spatial structure of water body and the mean LST.

Stepwise multiple regression analysis was designed to find the most parsimonious set of predictors which are most effective in predicting the dependent variable [18]. Analyses were performed using IBM SPSS Statistics.

4. Results and Discussion

4.1. The Land Use Types and Their Corresponding Mean LST. In this paper, in order to study the land surface temperature relationships of different land use types, the mean temperatures of different land use types were calculated by averaging all corresponding pixel values (Table 1).

The results shown in Table 1 suggested that the built-up area is corresponding to relatively high temperature, while the water body with lowest temperature may affect the LST, which will be considered as potential mitigating factors. Because the urban underlying surface is made up of different land use types, it is reasonable to analyze the relationship between land use and LST, through considering other land use types as potential factors.

4.2. Relationship between the LST and Landscape of Water Body. The mean temperature of each sample area is shown in Figure 5, and the value of Moran's I is 0.5969. Moran's I is a measure of spatial autocorrelation. Therefore, it was found that the temperature has a strong spatial autocorrelation. In this paper, we used a covariate to control the autocorrelation of the mean temperature.

Since we select 32 class-based metrics, not every landscape metric has high correlation with temperature. We choose the landscape metrics whose Pearson's correlation coefficient with temperature is higher than 0.4. The landscape metrics shown in Table 2 are highly related to the landscape metrics of water body.

Through multiple stepwise regression analysis, the most effective landscape metrics in predicting the dependent variable (the mean LST) were selected, and multiple linear regression equation was calculated:

$$y = 0.704x_1 - 0.557x_2 - 0.055x_3 + 0.128x_4 + 0.051x_5 + 0.064x_6 + 0.076x_7 + 0.036x_8, \quad (4)$$

where x_1 represents surrounding temperature accessed from the weight matrix via Generate Spatial Weight Matrix of ArcGIS tools. The threshold of its distance is 6000 m, double of spatial resolution. The weight matrix can be used to explain the impact of surrounding pixels' temperatures on the center pixel. In this study, it can also eliminate the spatial autocorrelation when analyzing the impact of water's factors on temperature. x_2–x_8 represent TCA, MCA, TCAI, CACVI, IJI, MPI, and MNN, respectively.

Table 1: Land use types and their corresponding mean LST in Wuhan city.

Land use types	Mean LST (°C)
Water body	25.29
Woodland	28.46
Cultivated land	28.33
Built-up land	32.78
Other land	29.94

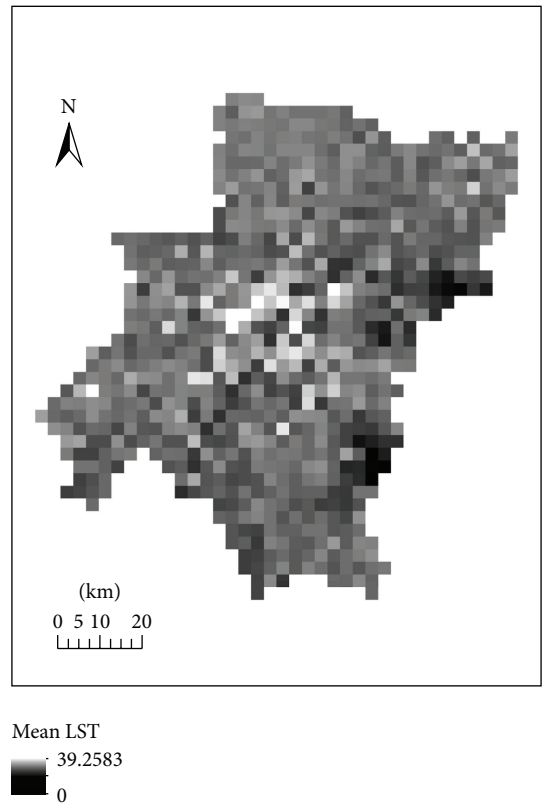

Figure 5: The mean land surface temperature in 3000 m $*$ 3000 m sample region in Wuhan city.

Table 2: Pearson's correlation coefficient between landscape metrics of water and LST.

Landscape metrics	Value
Class proportion	−0.604**
MPI	−0.46**
CA	−0.604**
MPS	−0.5**
PSSD	−0.515**
TCA	−0.613**
MCA	−0.436**
CASD	−0.515**
TCAI	−0.408**
LPI	−0.61**
MCAI	−0.474**

**Correlation is significant at the 0.01 level.

Table 3: Landscape metrics of water and their corresponding meaning, according to the Patch Analyst Help of ArcGIS.

Landscape metrics	Meaning
Class proportion	The proportion of class
MPI	Measure of the degree of isolation and fragmentation
CA	Sum areas of all patches belonging to a given class
MPS	Average patch size
PSSD	Patch size standard deviation
TCA	The total size of disjunct core patches
MCA	The average size of disjunct core patches
CASD	Measure of variability in core area size
TCAI	Measure of amount of core area in the landscape
LPI	The LPI is equal to the percent of the total landscape that is made up by the largest patch
MCAI	The average core area per patch
IJI	Measure of patch adjacency
MNN	Measure of patch isolation

The model is significant at the 0.05 level, and the adjusted R^2 reached 0.814. All independent variables are significant at 0.05 levels, whose meaning is shown in Table 3 [19, 20].

According to the result, it was found that the LST has spatial autocorrelation with water body. And the surrounding temperature calculated through weight matrix can help reduce the space correlation. The results of Pearson's correlation analysis show that the proportion of water body, average water body size, and the percent of the total landscape have relationship with the mean LST. They are made up by the largest water body patch and the isolation and fragmentation of water body. While the quantity, shape, and spatial distribution of water body affect the forming of temperature as resultant force, the result of multiple stepwise regression analysis reveals how the attributes of water body influence temperature.

5. Conclusions and Discussions

Rational allocation of land resources not only maintains the sustainable development of social economy, but also mitigates climate change. This research field has become one of the hottest issues in government and academy society. Despite the fact that Wuhan has abundant surface water resource, the amount of water resources is under severe threat. Meanwhile Wuhan is facing problems caused by urban heat island.

The UHI types can be generally categorized into air temperature UHI and surface UHI [21, 22]. Air temperature UHIs are generally stronger and exhibit greatest spatial variations at night, whereas the greatest difference in surface UHIs usually occurs during the daytime [21–23]. In this study, we focus on remotely sensed land surface temperature (LST): surface UHI.

Remotely sensed LST records the radiative energy emitted from the ground surface, including building roofs, paved surfaces, vegetation, bare ground, and water [21, 24]. Therefore, the pattern of land cover in urban landscapes may potentially influence LST [21, 25]. This study took Wuhan city as the case area and investigated the impact of water landscape pattern on UHI. Based on the mean LST and landscape metrics of water body via remote sensing technique and spatial analysis, the relationship between the mean LST and the attributes of water body was revealed by Pearson's correlation analysis and multiple stepwise regression analysis.

The results showed the following. (1) Compared to other land use types, water body is corresponding to lower LST. (2) In 32 class-based metrics we selected, the proportion of water body, average water body size, the isolation and fragmentation of water body, and other eight metrics have obvious correlation with the LST, whose Pearson's correlation coefficient with temperature is higher than 0.4. Among the 11 metrics, class proportion, CA, TCA, and LPI are of very high correlation with LST. The proportion of water body has a negative correlation with the mean LST. It means that in a fixed region, the lower the ratio of water body, the higher the mean LST. Meanwhile, the average water body size, the percent of the total landscape which is made up by the largest water body patch, and the isolation and fragmentation of water body all have negative correlation with the mean LST. (3) The LST is the result of comprehensive effects of multifactors. The result of multiple stepwise regression analysis indicated that the total size and amount of core water patches have a larger effect on the LST except for the variable of surrounding temperature calculated through weight matrix. The core water patches represent the interior water body with small external influence.

By analyzing the relationship between the LST and the attributes of water body, it was found that the spatial characteristics of water body have impact on LST, thus providing decision support for governments to allocate water resources.

Conflict of Interests

The authors declare that there is no conflict of interests regarding the publication of this paper.

Acknowledgments

This research was financially supported by the National Key Program for Developing Basic Science of China (Grant no. 2010CB950904), the National Science Foundation of China (Grant no. 41101098), the Ministry of Education Research of Social Sciences Youth funded Projects (Grant no. 10YJC790121), and the National Department Public Benefit Research Foundation of the Ministry of Land and Resources of China (Grant no. 201311001-5).

References

[1] H. Liu and Q. Weng, "Scaling effect on the relationship between landscape pattern and land surface temperature: a case study of Indianapolis, United States," *Photogrammetric Engineering and Remote Sensing*, vol. 75, no. 3, pp. 291–304, 2009.

[2] W. Zhang and B. Huang, "Land use optimization for a rapidly urbanizing city with regard to local climate change: Shenzhen as a case study," *Journal of Urban Planning and Development*, vol. 141, no. 1, Article ID 05014007, 2015.

[3] L. Huang, D. Zhao, J. Wang, J. Zhu, and J. Li, "Scale impacts of land cover and vegetation corridors on urban thermal behavior in Nanjing, China," *Theoretical and Applied Climatology*, vol. 94, no. 3-4, pp. 241–257, 2008.

[4] J. P. Connors, C. S. Galletti, and W. T. L. Chow, "Landscape configuration and urban heat island effects: assessing the relationship between landscape characteristics and land surface temperature in Phoenix, Arizona," *Landscape Ecology*, vol. 28, no. 2, pp. 271–283, 2013.

[5] X.-L. Chen, H.-M. Zhao, P.-X. Li, and Z.-Y. Yin, "Remote sensing image-based analysis of the relationship between urban heat island and land use/cover changes," *Remote Sensing of Environment*, vol. 104, no. 2, pp. 133–146, 2006.

[6] Y. Sun, Q. Guo, J. Liu, and R. Wang, "Scale effects on spatially varying relationships between urban landscape patterns and water quality," *Environmental Management*, vol. 54, no. 2, pp. 272–287, 2014.

[7] E. A. Hathway and S. Sharples, "The interaction of rivers and urban form in mitigating the Urban Heat Island effect: a UK case study," *Building and Environment*, vol. 58, pp. 14–22, 2012.

[8] W. Yue and L. Xu, "Thermal environment effect of urban water landscape," *Acta Ecologica Sinica*, vol. 33, no. 6, pp. 1852–1859, 2013.

[9] H. Wu, L.-P. Ye, W.-Z. Shi, and K. C. Clarke, "Assessing the effects of land use spatial structure on urban heat islands using HJ-1B remote sensing imagery in Wuhan, China," *International Journal of Applied Earth Observation and Geoinformation*, vol. 32, pp. 67–78, 2014.

[10] Y. Liu, Q. Wang, and H. Chen, "The development, protecting and planning envision of lakes in Wuhan City," *Economic Geography*, vol. 24, no. 2, pp. 192–196, 2004.

[11] Z.-H. Qin, M.-H. Zhang, A. Karnieli, and P. Berliner, "Mono-window algorithm for retrieving land surface temperature from Landsat TM6 data," *Acta Geographica Sinica*, vol. 56, no. 4, pp. 456–466, 2001.

[12] J. Li, "Study of relation between land cover condition and temperature based on Landsat/TM data," *Remote Sensing Technology and Application*, vol. 13, no. 1, pp. 18–28, 1998.

[13] W.-Z. Yue, J.-H. Xu, and L.-H. Xu, "An analysis on eco-environmental effect of urban land use based on remote sensing images: a case study of urban thermal environment and NDVI," *Acta Ecologica Sinica*, vol. 26, no. 5, pp. 1450–1460, 2006.

[14] B. L. Markham and J. L. Barker, "Spectral characterization of the Landsat thematic Mapper sensors," *International Journal of Remote Sensing*, vol. 6, no. 5, pp. 697–716, 1985.

[15] A. A. Van De Griend and M. Owe, "On the relationship between thermal emissivity and the normalized difference vegetation index for natural surfaces," *International Journal of Remote Sensing*, vol. 14, no. 6, pp. 1119–1131, 1993.

[16] N. Weber, D. Haase, and U. Franck, "Zooming into temperature conditions in the city of Leipzig: how do urban built and green structures influence earth surface temperatures in the city?" *Science of The Total Environment*, vol. 496, pp. 289–298, 2014.

[17] R. M. Chefaoui, "Landscape metrics as indicators of coastal morphology: a multi-scale approach," *Ecological Indicators*, vol. 45, pp. 139–147, 2014.

[18] R. F. Kokaly and R. N. Clark, "Spectroscopic determination of leaf biochemistry using band-depth analysis of absorption features and stepwise multiple linear regression," *Remote Sensing of Environment*, vol. 67, no. 3, pp. 267–287, 1999.

[19] K. McGarigal and B. J. Marks, *FRAGSTATS: Spatial Pattern Analysis Program for Quantifying Landscape Structure*, Forest Science Department, Oregon State University, Corvallis, Ore, USA, 1995.

[20] K. H. Riitters, R. V. O'Neill, C. T. Hunsaker et al., "A factor analysis of landscape pattern and structure metrics," *Landscape Ecology*, vol. 10, no. 1, pp. 23–39, 1995.

[21] A. J. Arnfield, "Two decades of urban climate research: a review of turbulence, exchanges of energy and water, and the urban heat island," *International Journal of Climatology*, vol. 23, no. 1, pp. 1–26, 2003.

[22] J. E. Nichol, W. Y. Fung, K.-S. Lam, and M. S. Wong, "Urban heat island diagnosis using ASTER satellite images and 'in situ' air temperature," *Atmospheric Research*, vol. 94, no. 2, pp. 276–284, 2009.

[23] C. M. Frey, E. Parlow, R. Vogt, M. Harhash, and M. M. Abdel Wahab, "Flux measurements in Cairo. Part 1: *in situ* measurements and their applicability for comparison with satellite data," *International Journal of Climatology*, vol. 31, no. 2, pp. 218–231, 2011.

[24] J. A. Voogt and T. R. Oke, "Thermal remote sensing of urban climates," *Remote Sensing of Environment*, vol. 86, no. 3, pp. 370–384, 2003.

[25] R. T. T. Forman, *Land Mosaics: The Ecology of Landscape and Regions*, Cambridge University Press, New York, NY, USA, 1995.

Hindawi Publishing Corporation
Advances in Meteorology
Volume 2015, Article ID 352360, 12 pages
http://dx.doi.org/10.1155/2015/352360

Research Article

A Comparison of Two Methods on the Climatic Effects of Urbanization in the Beijing-Tianjin-Hebei Metropolitan Area

Mingna Wang[1,2] and Xiaodong Yan[3]

[1]*Key Laboratory of Computational Geodynamics, Chinese Academy of Sciences, Beijing 100049, China*
[2]*College of Earth Science, University of Chinese Academy of Sciences, Beijing 100049, China*
[3]*State Key Laboratory of Earth Surface Processes and Resource Ecology, Beijing Normal University, Beijing 100875, China*

Correspondence should be addressed to Mingna Wang; wangmn@ucas.ac.cn

Received 28 September 2014; Revised 25 March 2015; Accepted 8 April 2015

Academic Editor: Charles Jones

Both the "urban minus rural" (UMR) and the "observation minus reanalysis" (OMR) methods were used to quantify the potential impacts of urbanization on regional temperature changes in the Beijing-Tianjin-Hebei metropolitan area in China. DMSP/OLS nighttime light imagery and population census data were used to classify stations into four classes: rural, small city, medium city, and large city groups. The regional average annual mean temperature was estimated to increase by 0.12°C decade^{-1} derived from urban warming, accounting for 40% of total climate warming from 1960 to 2009 using the UMR method. The OMR method also indicates that rapid urbanization has a significant influence on surface warming trend although the urban warming intensity is dependent on reanalysis dataset. The seasonal cycle patterns from all three datasets are consistent with each other, which is contrary to the UMR result owing to the cooling effect of agriculture activity in the rural stations confusing the UMR result. So in this paper we found a deficiency of the UMR method where it would underestimate the effects of urbanization in summer. In this regard, the results from the OMR method are relatively more convincing although we admit it still has many other problems.

1. Introduction

In addition to the climate change contributions from greenhouse gas concentrations and aerosol loading, anthropogenic changes in the large-scale character of land use/land cover change (LUCC) can also significantly influence climate change [1].

In terms of LUCC, urbanization has received much attention in climatic research. However, two divergent views on influence of urbanization on regional and global mean temperature trends currently exist. Many researchers support that urban heat island effects are real but local and have no biased large-scale trends; the second one holds the other view that urban heat island (UHI) effects contaminate the global and regional temperature time series, and urbanization is an important contribution to climate change by human activities. Both of these two views have many supporters.

IPCC proposed that the effects of urbanization on the land-based temperature record are negligible (0.006°C decade^{-1}); the release of heat from anthropogenic energy production can be significant over urban areas, but it is not globally significant [1]. Peterson et al. identified that well-known global temperature time series from in situ stations were not significantly impacted by urban warming (0.005°C decade^{-1}) [2], and no statistically significant impact of urbanization could be found in annual temperature in the contiguous United States [3]. Jones et al. studied station data from the Soviet Union, eastern Australia, and eastern China and then showed that urbanization influences have relatively minor contributions to regional warming trends [4]. Many papers also agreed with the viewpoint that the UHI effect in China during the last 50 years was minor compared to the background trend of increasing temperature [5, 6].

Nevertheless, some studies have employed the "urban minus rural" method (UMR) to indicate that urbanization may play a more significant role with regard to temperature trends on multiple geographic scales. Such results should be given more consideration for the mitigation of climate change [7]. Oke showed that even a city of 1000 people could have an UHI effect, and the magnitudes of UHI effects were linearly

Table 1: Results of recent studies of the urban heat island effects in China at regional and national scales.

Study area	Method	Time period	UHI warming (°C decade^{-1})	References
Mainland China	UMR	1954–2004	<0.012	[5]
Yangtze River Delta	UMR	1961–2005	0.069	[37]
North China	UMR	1961–2000	0.11	[10]
China	Comparison with SST	1951–2004	0.1	[38]
Northeast China	UMR	1954–2005	0.027	[6]
Southeast China	OMR	1979–1998	0.05	[26]
East of 110°E over China	OMR	1960–1999	0.12	[39]
China	OMR	1960–1999	0.14	[40]
East China	OMR and UMR	1981–2007	OMR: 0.398, 0.260, 0.214, 0.167 UMR: 0.285, 0.207, 0.135, 0.077 for stations from metropolises, large cities, medium cities, and small cities	[36]

correlated with the logarithm of the population [8]. Wang et al. chose 42 pairs of eastern China urban and rural stations to study UHI effects and revealed that the magnitude of UHI effects was 0.08°C decade^{-1} from 1954 to 1983 which must be carefully considered when attributing causes to observed trends [9]. Ren et al. found that the annual mean temperature of the national basic/reference stations in north China was significantly impacted by urban warming (0.11°C decade^{-1}) [10]. Therefore, they suggested that the urban warming bias for the regional average temperature anomaly series should be corrected.

A new method to estimate the effect of LUCC on air temperature changes that subtracts surface temperatures that are derived from the NCEP-NCAR reanalysis data from the trends that are observed at surface stations (observation minus reanalysis (OMR)) was proposed [11]. The rationale for the OMR method is that the reanalysis data represent large-scale climate changes due to greenhouse gases and atmospheric circulation but are insensitive to regional surface processes because little or no surface data or information (surface observations of temperature, moisture, and wind over land) about land surface changes has been utilized in the data assimilation process. Thus, Lim et al. studied the sensitivity of surface climate change to land types by the OMR method to reveal that warming over barren and urban areas is larger than most other land types [12]. The study of Fall et al. confirmed the robustness of the OMR method for detecting nonclimatic changes at the station level and provided robust results regarding the impact of LUCC on the temperature trends over the conterminous United States [13]. The results indicated that the regions converted into urban areas show a positive OMR trend which agreed well with those obtained by Lim et al. [12]. Hu et al. used the OMR method to estimate the impact of land surface forcing on mean and extreme temperatures in eastern China and found that LUCC impacts could explain one-third of the observed increase of the annual warm nights and nearly half of the observed decrease of the cold nights [14].

China has been experiencing a dramatic growth in urban areas and population since implementing the reform and open policy. All regions in China had more than a 20% expansion in urban areas during 1980–2005, and the Eastern Plain had the largest increase in urban area (2.5 million ha) [15], which could significantly change the land surface physical processes and surface heat flux. There could have been substantial impacts on local and regional climates as a result of the rapid urbanization. Therefore, determining how to estimate urban and land use contributions to the warming trends is a hot research topic currently.

Table 1 illustrates some results of recent studies on UHI effects in China at regional or national scales. Overall, the contribution of urban warming on temperature change, which was determined from the OMR method, has been more significant than the effect determined from the UMR approach. However, no papers explain that in detail, regardless of annual or seasonal changes.

Previous studies have predominantly focused on the UHI effect over a single large city [16, 17], and the study of urbanization in Beijing has attracted the most attention [18, 19]. Ren et al. showed that, with regard to the annual mean surface air temperature (SAT) at Beijing Station, the UHI contribution reached 80.4% during 1961–2000 and 61.3% during 1981–2000 [20]. However, with the increasing development and growth of the small and medium cities in Beijing-Tianjin-Hebei metropolitan area, the regional influence of urbanization should not be underestimated. The accurate detection and estimation of surface warming caused by urbanization in the Beijing-Tianjin-Hebei area may contribute significantly to the sustainable development and planning of orderly human activities in the region. Therefore, in the current study, we attempt to use both the UMR and the OMR methods to quantitatively determine the potential magnitude of UHI contributions to regional annual or seasonal temperature trends during a rapid urbanization period in the Beijing-Tianjin-Hebei metropolitan area. As far as the OMR is concerned, previous studies usually used one reanalysis dataset, but we know that each reanalysis may have some deficiencies in its model physics or assimilation process. So we conduct comparative studies with three independent reanalyses (NCEP/NCAR, NCEP/DOE, and ERA-interim) in order to show a fair and reasonable urban effect.

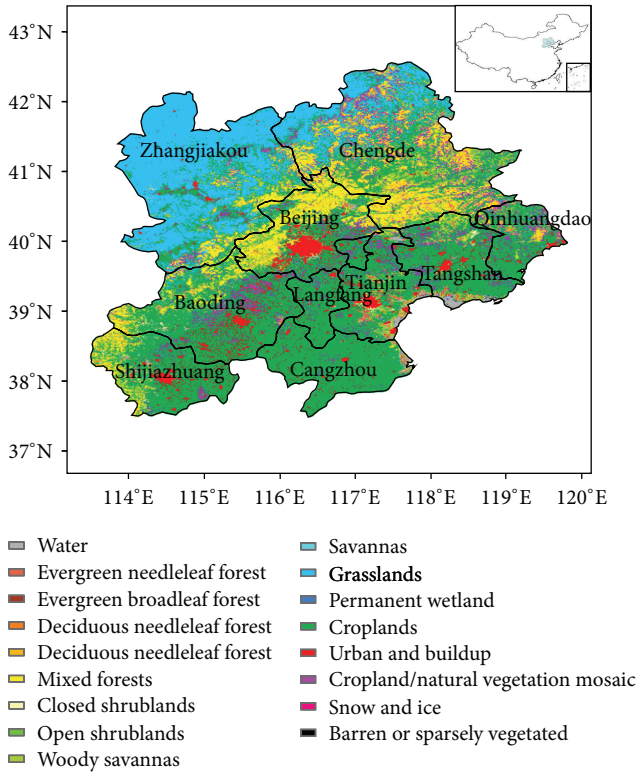

Figure 1: Study area and land cover types based on MODIS land cover product.

2. Region Definition, Data, and Analysis Methods

2.1. Study Area. The Beijing-Tianjin-Hebei metropolitan area refers to the center of Beijing and Tianjin and includes Shijiazhuang, Baoding, Qinhuangdao, Langfang, Cangzhou, Chengde, Tangshan, and Zhangjiakou, eight large cities in Hebei Province. The geographical location of these cities and land cover type are shown in Figure 1. The urban types are displayed in red in Figure 1. Hebei Province is named Ji for short in China, so the Beijing-Tianjin-Hebei metropolitan area is usually referred to as JING-JIN-JI area (JJJ area for short below). This region is defined as the political, cultural, and economic center of China. The JJJ regional plan is an important regional planning of the national Twelfth Five-Year Plan. Because of the rapid economic development, this region has been identified as the economic center of northern China.

According to the China City Statistical Yearbook (1985–2009), the total nonagricultural population in urban districts of the JJJ area doubled in about 20 years from 1984 to 2008. Undoubtedly, the large increase in the urban population due to the rapid urban expansion could considerably impact the local and regional climate and environment of the JJJ area.

2.2. Data. The meteorological data that were used in this study include the daily mean surface air temperature from 79 weather and climate observation stations in JJJ area, all covering 50 years from 1960 to 2009. The dataset included observations from all of the national reference climate stations and national basic weather stations in the study area as well as from some ordinary weather stations in Hebei Province. The inhomogeneity of the national reference climate stations and national basic weather stations that was caused by site relocation was adjusted [18, 21]. The data were also of good quality and were relatively evenly spatially distributed. All climate and weather stations in China are maintained by professional workers.

The U.S. Air Force Defense Meteorological Satellite Program's Operational Linescan System (DMSP/OLS) has provided a capable method for obtaining urban information at coarse spatial scales through its unique low-light imaging capability to detect persistent lights, even from small human settlements, gas fires, and vehicles in the dark background at night. The Version 4 stable nighttime light products (1992–2009) with 1 km spatial resolution were used to classify the stations. They are downloaded from the National Geophysical Data Center (http://www.ngdc.noaa.gov/eog/re_direct.html).

In addition, three widely used reanalysis datasets were used in our study. These included the National Centers for Environmental Prediction/National Center for Atmospheric Research (NCEP/NCAR) reanalysis data (NNR) [22], the National Centers for Environmental Prediction/Department of Energy (NCEP/DOE) Atmospheric Model Intercomparison Project- (AMIP-) II reanalysis data (NDR) [23], and the European Centre for Medium-Range Weather Forecasts (ECMWF) reanalysis data (ERA) [24]. The NNR and NDR datasets covered the period from 1948 and 1979 to the present, respectively, with the spatial resolution of the Global T62 Gaussian grid (192 × 94). There were some deficiencies in the model physics of the NNR; for example, the description of cloudiness and soil moisture is poor, which could bias the estimation of surface temperature [25]. Although based on the widely used NNR, the NDR has improved this quality by featuring newer physics and observed soil moisture forcing as well as fixing known errors of the NNR [23]. Consequently, the OMR for the NDR data should more accurately characterize near-surface temperature over land [26]. The latest extension reanalysis ERA-interim was also used in our analysis. It covers the period from 1979 to the present with a spatial resolution of 1.5° × 1.5°. In this work, we selected the same reference period that is used for comparison from 1979 to 2009. The ERA is somewhat more sensitive to land surface forcing than the NNR or NDR. However, results derived from the ERA would contain a portion of surface temperature variation due to land surface forcing [12, 27], and these results would strengthen our conclusions. Furthermore, an integrated study using a few types of reanalysis datasets may help to decrease the uncertainties brought about by data deficiencies, and a comparative analysis of three reanalyses may perhaps be helpful to confirm the results of the OMR. Following the same techniques put forward by Kalnay and Cai [11], we also interpolated the gridded reanalysis data to observational sites with bilinear interpolation.

2.3. Methods of Defining Types of Stations. The key issue of estimating the effect of urbanization on temperature trends is to define the reference or baseline stations. The stations located in rural areas could be assumed to be reference

Table 2: Numbers of stations for each station group in the JJJ area.

Station group name	Population criteria (million)	Number of stations
Large city station	≥0.5	11
Medium city station	0.1–0.5	31
Small city station	0.05–0.1	26
Rural station	≤0.05	11

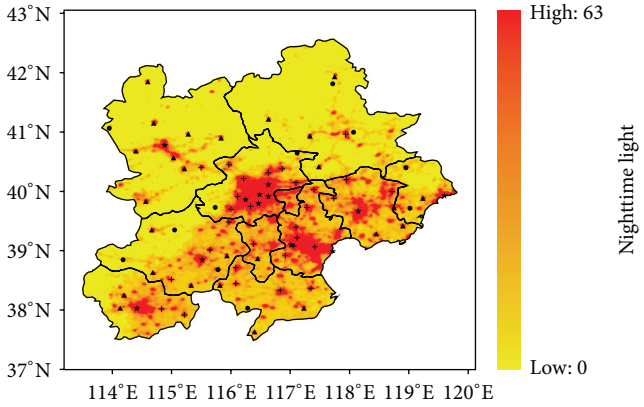

Figure 2: The distribution of the four types of stations in the JJJ area. The background is DMSP/OLS nighttime light data from 2009 (★ large city station; + medium city station; ▲ small city station; • rural station).

stations that have not been affected by urbanization and the temperature trends recorded at the rural stations would actually represent large-scale changes.

The stations were firstly classified into four types according to the population data provided by China City Statistical Yearbook (2009): large city stations with nonagricultural populations over 0.5 million; medium-sized city stations with nonagricultural populations of 0.1–0.5 million; small city stations with nonagricultural populations of 0.05–0.1 million; and rural stations with nonagricultural populations less than 0.05 million. This is consistent with Easterling et al. who considered a population of 0.05 million as the critical value between "urban" and "nonurban" stations [28].

Additionally, the DMSP/OLS nighttime light imagery was also applied to define the rural stations. The total number of stations with nonagricultural populations less than 50,000 was 17. Then the nighttime light data of these sites were analyzed. Among these 17 stations, the nighttime light values of six stations increased significantly, which indicated that these stations experienced a process of urbanization. These six sites were then classified as small city stations. Therefore, in the present study, a total of 11 rural stations were chosen. The definitions for the various categories of stations and the numbers of each station are listed in Table 2, which shows that the number of medium city stations was the largest, followed by the small city stations.

2.4. Calculation of Temperature Anomalies. Figure 2 illustrates the locations of all stations we analyzed in the JJJ area. Many factors, such as topography and altitude, could bias the research results when using average temperatures; therefore, we adopted temperature anomalies of the station observations and the reanalysis data to denote the interannual variation of the regional temperature for each station category. All trends were calculated using a simple linear regression, and the statistical significance of the linear trend was assessed using a t-test. The Mann-Kendall trend test [29, 30] was used to determine abrupt changes and the significance of urban warming [31, 32].

3. Results

3.1. Surface Air Temperature (SAT) Trends. The observed trends in the surface air temperature for the different station groups in the JJJ area are listed in Table 3. From 1960 to 2009, the trends in the annual mean temperature were all positive for the four station groups, with the largest increase occurring at the large city stations (0.43°C decade^{-1}), followed by the medium city stations (0.30°C decade^{-1}) and then the small city stations (0.28°C decade^{-1}). The weakest warming trend, only 0.19°C decade^{-1}, occurred at the rural stations, indicating that urbanization might have exerted a significant influence upon the observed temperature warming in the JJJ area. The annual mean temperature trends from 1979 to 2009 were even larger. The values for the seasonal trends are shown along with the annual means for each station group. The seasonal mean SAT trends for the various station groups all appeared to be largest in winter, followed by the spring. Relatively weak warming was observed during the autumn and summer. The rural stations even witnessed a slight cooling trend in the summertime. For the JJJ area as a whole, the annual mean SAT trend was 0.30°C decade^{-1}, which is similar to the results from northern China, 0.29°C decade^{-1} from 1961 to 2000 [10]. The regional averaged SAT warming trends during the winter, spring, summer, and autumn were 0.54, 0.46, 0.1, and 0.1°C decade^{-1}, respectively.

Figure 3 reveals the spatial distribution of the annual mean SAT trends from the observed station records and the reanalysis data in the JJJ area during 1979–2009. The station observations (Figure 3(a)) indicated that the spatial distribution of the warming trend was closely related to the intensity of the nighttime lights. The urban stations with relatively intense nighttime lights exhibited rapid increases in the temperature. Conversely, stations with weak warming trends were mainly rural or small city stations. A broad range of spatial difference existed in the observed SAT in the study area, with a minimum of 0.081 and a maximum of 1.012°C decade^{-1}. In contrast, the ERA (Figure 3(b)), NNR (Figure 3(c)), and NDR (Figure 3(d)) reanalysis data all showed the strongest warming trends from 1979 to 2009. However, the trend values did not reach the amplitude of the observed station records. The spatial difference ranged from 0.399 to 0.630°C decade^{-1} for the ERA, 0.284 to 0.510°C decade^{-1} for the NNR, and 0.227 to 0.346°C decade^{-1} for the NDR. The spatial differences of the reanalysis data were substantially less than that of the station observations, because the reanalysis data only reflected the atmospheric

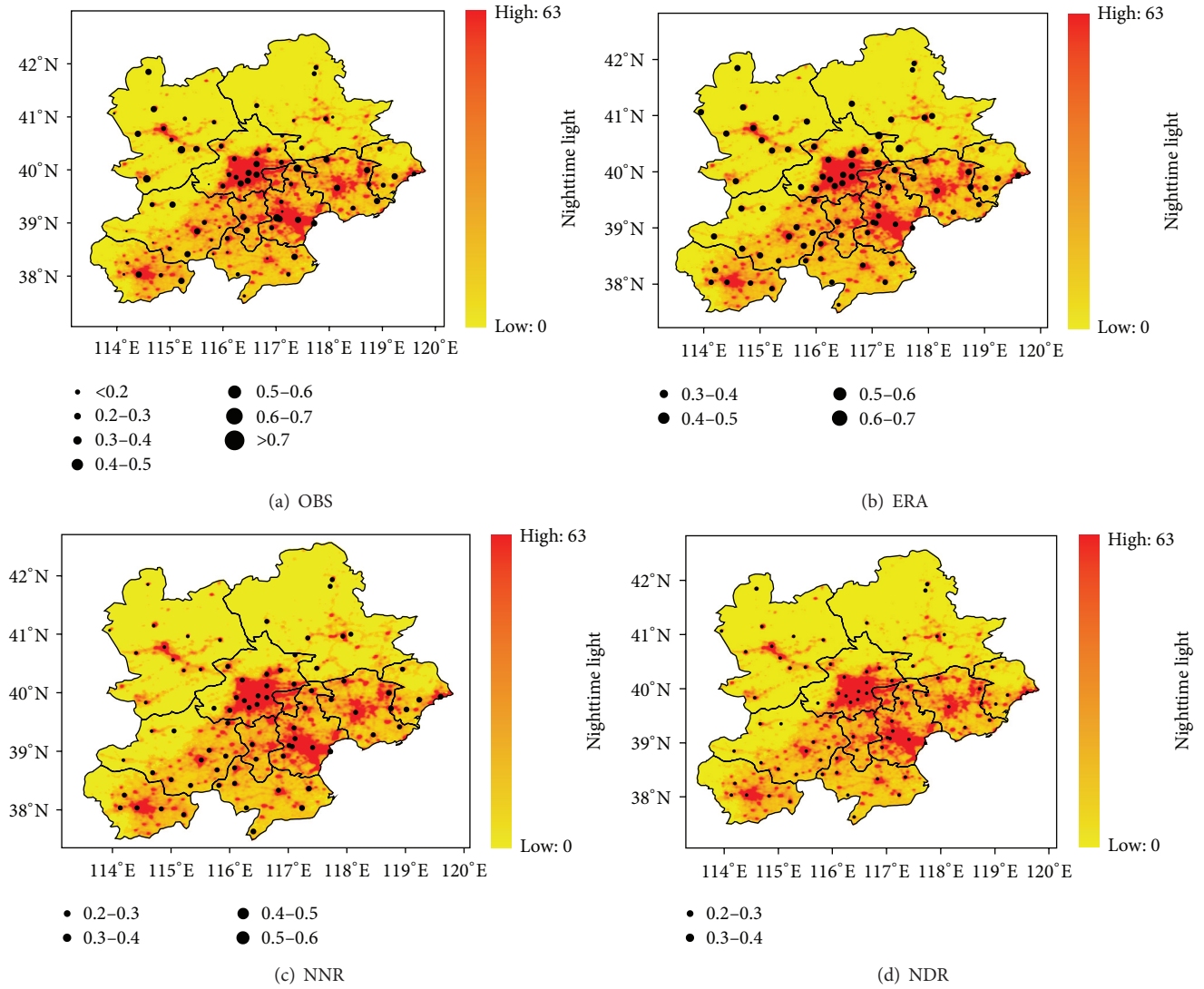

Figure 3: Annual mean SAT trends from (a) station observations (OBS), (b) ECMWF ERA-interim reanalysis data (ERA), (c) NCEP/NCAR reanalysis data (NNR), and (d) NCEP/DOE reanalysis data (NDR) during 1979–2009 (unit: $^{\circ}$C decade^{-1}). Also shown is the DMSP/OLS nighttime light imagery from 2009.

circulation and greenhouse gas concentrations but were insensitive to regional surface processes associated with different land types.

3.2. Effect of Urbanization on SAT Trends. Table 3 shows trends for the annual and seasonal mean SAT related to urbanization for various city station groups. The values in the parentheses are the SAT trend differences between the urban station groups and rural sites. From the difference in the observational temperature trends between the urban and rural stations (Table 3), the annual mean UMR trend was 0.24°C decade^{-1} for the large city station, 0.11°C decade^{-1} for the medium city station, and 0.09°C decade^{-1} for the small city station (statistically significant at the 0.01 confidence level for each city station group). The average annual urban warming in the JJJ area was 0.12°C decade^{-1} (statistically significant at the 0.01 confidence level). The effect of urbanization on the SAT trend for each city group after 1979 appeared to be slightly larger than that of 1960–2009. Among the four seasons, the urban warming in the summer was the largest (0.13°C decade^{-1}), followed by spring (0.11°C decade^{-1}) and autumn (0.10°C decade^{-1}). The annual SAT trend in winter was hardly affected by urbanization (0.04°C decade^{-1}). The contribution of urban warming to the total warming was largest in the summer, reaching 100% for all of the city station groups, whereas winter witnessed the lowest contribution. One reason may be attributed to the fact that the wind velocities during the summer are weaker than in winter in northern China, as many studies have reported that urban heat island intensity increases with decreasing wind speed [33–35]. The effects of UHI in the JJJ area did not significantly contribute to the observed rapid warming during the wintertime; therefore, the large-scale climate changes due to greenhouse gases and atmospheric circulation were likely

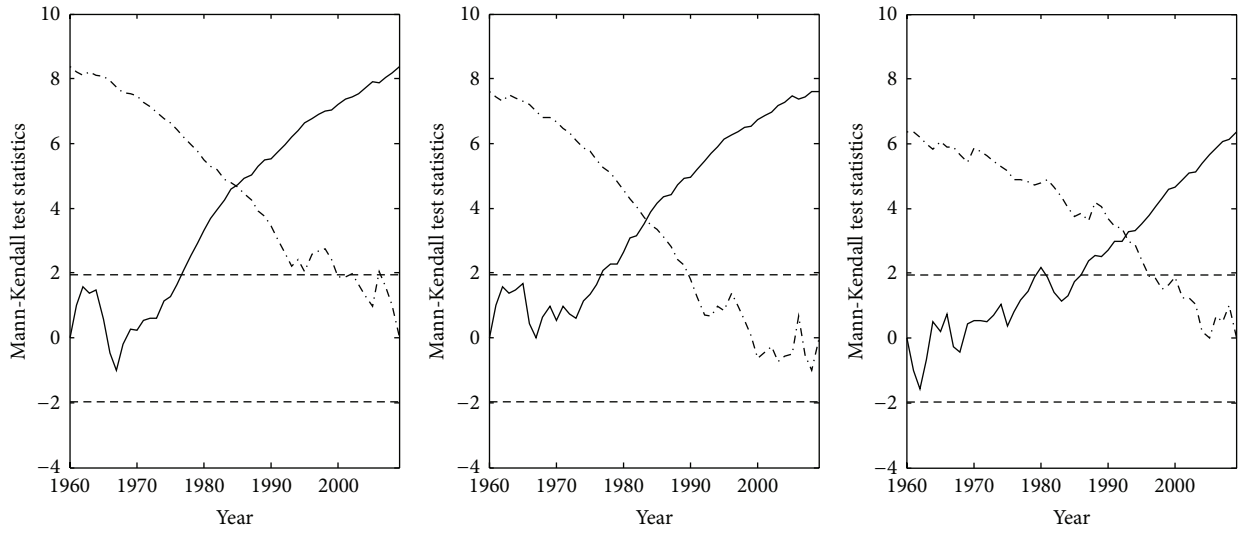

Figure 4: Sequential Mann-Kendall test applied to the observed annual mean temperature for the UMR of large city groups (a), medium city groups (b), and small city groups (c). The value ±1.96 (the 95% confidence level) is represented with horizontal dashed lines. The solid lines represent the MK trend for the time series, and the dash dotted lines represent the MK trend for the backward series.

Table 3: Observed trends of the annual and seasonal mean surface air temperature for different station groups in the JJJ area. The values in parentheses are the results of different urban station groups minus the rural station. Statistical significance is 0.05 (single asterisk) and 0.01 (double asterisk). The units for the values are °C decade^{-1}.

Station group name	Winter	Spring	Summer	Autumn	Annual (1960–2009)	Annual (1979–2009)
Large city station	0.75** (0.24**)	0.68** (0.31**)	0.21** (0.22**)	0.11** (0.09**)	0.43** (0.24**)	0.66** (0.27**)
Medium city station	0.54** (0.03)	0.49** (0.12*)	0.12** (0.13**)	0.06 (0.04)	0.30** (0.11**)	0.50** (0.11**)
Small city station	0.47** (−0.04)	0.34** (−0.03)	0.12* (0.13**)	0.24** (0.22**)	0.28** (0.09**)	0.51** (0.13**)
Urban station	0.55**	0.47**	0.12**	0.12	0.31**	0.53**
Rural station	0.51**	0.37**	−0.01	0.02	0.19**	0.39**
UMR	0.04	0.11*	0.13**	0.10**	0.12**	0.14**

Table 4: Linear trends of regional average annual, rural, and UMR temperature (°C decade^{-1}) and the contribution of urban warming to the total warming for different time periods. Statistical significance is 0.05 (single asterisk) and 0.01 (double asterisk).

	Total	Rural	UMR	UHI contribution
1960–1969	−1.10*	−1.13	0.03	0.30%
1970–1979	0.39	0.25	0.16*	41.03%
1980–1989	0.46	0.33	0.15*	32.61%
1990–1999	1.28**	1.14*	0.16*	12.50%
2000–2009	0.26	0.21	0.09	34.62%
1960–2009	0.30**	0.19**	0.12**	40.00%

the dominant contributors. This seasonal conclusion agrees with the results of Ren et al. for northern China [10] and Yang et al. in eastern China [36].

Table 4 shows the contribution of urban warming at different time periods. The contribution of urban warming to the overall warming was 40% for the 50 years from 1960 to 2009. The warming trends of the background (rural station) and urban stations were the strongest during the 1990s, followed by the 1980s and 1970s. The UMR trends in the 1970s, 1980s, and 1990s were the largest (all statistically significant at the 0.05 confidence level). This indicated that urbanization in the JJJ area was consistent with the Chinese progress of the reform and open policy since 1978. We know that the study area experienced rapid urban development after the Tangshan earthquake in 1976. Although the UMR in the 1990s was the largest, the contribution of urban warming to the overall warming was the largest in the 1970s (41.03%) because the background warming trend in the 1990s was so large.

Figure 4 shows the results of the sequential Mann-Kendall methods applied to the time series of the annual mean SAT for the UMR of different city groups. The sequential Mann-Kendall analysis indicated that the time series of the annual mean temperature differences between the city and rural sites all had very significant positive trends that exceeded the 99% confidence level. The abrupt changes in the trends of the time series of the annual mean SAT began in the early 1980s for the large city and medium city station groups (Figures 4(a) and 4(b)) and the early 1990s

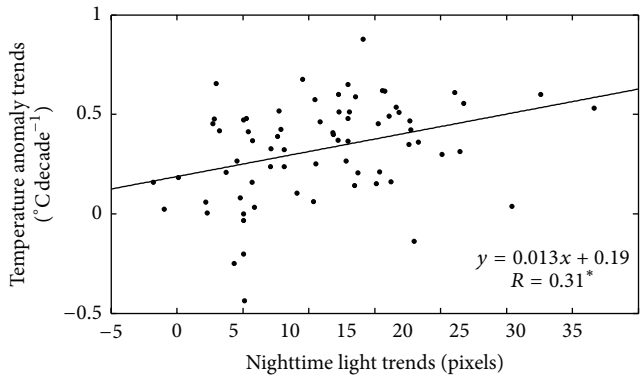

Figure 5: Correlation between the trends of the annual mean SAT and the intensity of the nighttime lights from 1992 to 2009.

for the small city groups (Figure 4(c)). The positive trends of the large city and medium city stations began to pass the 95% confidence level during the 1970s, while the small city stations passed the 95% confidence level during the late 1980s. Therefore, the small city stations clearly experienced weaker and slower urbanization progress than the large and medium city stations.

Figure 5 shows the trend of the annual mean SAT related to the intensity of the nighttime lights, and the correlation coefficient was 0.31, which is statistically significant at the 0.05 confidence level. It is notable that the observed SAT was somewhat affected by the urbanization in the JJJ area. Therefore, the increasing UHI effect amplified the trend of the observed SAT. Only when the urbanization effect is removed can these records be considered accurate and better represent the baseline temperature. The warming trend of the regional average annual SAT in the JJJ area decreased from 0.30°C decade^{-1} to 0.19°C decade^{-1} after the adjustment.

3.3. Observation Minus Reanalysis (OMR) Analysis. Compared with the progress of urbanization, the conversions of land use types caused by other human activities, such as agriculture, overgrazing, and deforestation, have been even more intense. China is one of the most obvious land use change regions, but the climatic effects from land use/cover changes and greenhouse gas emissions are difficult to distinguish. However, neglecting the role of land use changes could lead to the wrong assessment of human activities on contributions to surface warming. It is very important to reveal the contributions of urbanization and other land use changes to climate change. In this paper, we used the OMR method to analyze the contribution of urbanization and other land use changes to surface warming.

Figure 6 shows the observation and reanalysis time series of temperature anomalies for the four station groups from 1979 to 2009. Both the observed and the reanalysis annual mean temperatures showed increasing trends. The reanalysis dataset agreed best with the station observation from rural stations (Figure 6(a)), indicating that the rural stations were less affected by urbanization and that the background temperature changes were captured in both the observations and the reanalysis data. The warming trends of the station observations were stronger than the reanalysis data, with the strongest in the large city groups (Figure 6(d)), followed by the medium city groups (Figure 6(c)), small city groups (Figure 6(b)), and then the rural stations (Figure 6(a)).

The OMR values of the NDR were the largest (Figure 6). The ERA-interim [24] indirectly assimilated near-surface temperature observations [41], so the ERA was similar to the observed counterparts in China [42, 43]. This is shown in Figure 6, and the OMR of the ERA was the smallest (Figure 6). The most substantial increase in the OMR values occurred in the early 2000s in the small and medium city groups (Figures 6(b)-6(c)), indicating a significant effect of rapid urbanization on the SAT in the early 2000s. The largest increase of the OMR in the large city groups occurred during the late 1980s, implying that rapid urbanization developed during this period (Figure 6(d)), which is relatively consistent with the UMR abrupt changes tested by the Mann-Kendall method.

Table 5 presents the annual mean temperature trends from the station observation and three reanalysis datasets, along with the OMR and UMR values for each station group. The most significant increase in the station observed annual mean SAT occurred at the largest stations with an annual linear trend of 0.66°C decade^{-1}, and the weakest occurred at the rural stations with a trend of 0.39°C decade^{-1}. The trends of the reanalysis datasets among the various station groups were nearly uniform with a low range of 0.52 to 0.54°C decade^{-1} for the ERA, 0.43 to 0.50°C decade^{-1} for the NNR, and 0.24 to 0.26°C decade^{-1} for the NDR. This predominantly reflected changes in circulation and greenhouse warming. The annual OMR trends indicated strong warming in the large cities with 0.12, 0.19, and 0.42°C decade^{-1} for the ERA, NNR, and NDR, contributing 18.18%, 28.79%, and 63.64%, respectively. The annual OMR trends were weakest for the rural stations at 0.11, −0.06, and −0.15°C decade^{-1} for the ERA, NNR, and NDR, respectively. If these rural values were added to the UMR, the results would be consistent with those of the OMR. Accordingly, both methods showed that urbanization has imposed significant effects on the SAT in the JJJ area.

The seasonal mean temperature trends from three reanalysis datasets all present significant increasing trends, strongest in the winter and spring. In the four seasons, the trends of all the three reanalysis datasets among various station groups show little differences. In addition, the seasonal OMR values show strongest warming trends in the large city stations, followed by the medium and small city station groups. The OMR trends in the winter and spring are stronger than those in summer and autumn (Table 5), which agrees with the result obtained by Yang et al. [40] and Hu et al. [14] by the same method for eastern China, but no one had pointed out why it appeared contrary to the UMR result. The reason why it is contrary to the UMR result is difficult to explain.

The OMR values (Figure 7) exhibited a spatial pattern similar to the trends of the observational temperature (Figure 3(a)). On average, the OMR magnitudes for the NDR were largest, and those for the NNR and ERA were relatively small. The geographical distribution of both the OMR and

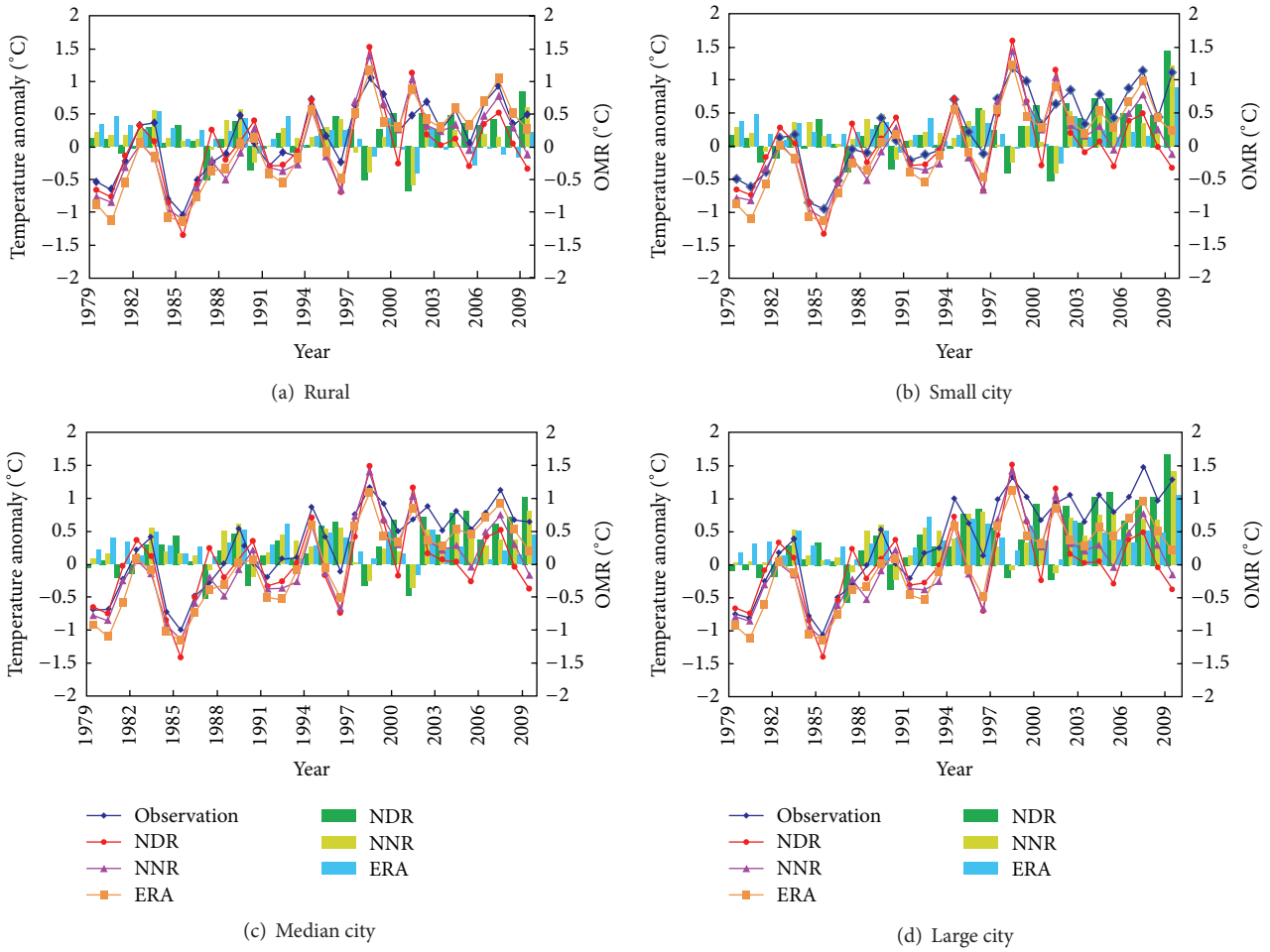

FIGURE 6: Observation and reanalysis time series of temperature anomalies (line graph) and OMR values (bar chart) for (a) rural, (b) small city, (c) medium city, and (d) large city groups from 1979 to 2009.

the observational temperature trends revealed that land surface change most likely affected the observed temperature and that the significant warming was affected by urbanization in the JJJ area, especially in Beijing, Tianjin, and other large cities with the most intense nighttime lighting and strongest UHI effects. We know that the OMR results reflect changes in land use rather than simply urbanization, so the negative OMR trends that were predominant found at the rural stations (Table 5 and Figure 7) could be caused by agricultural irrigation and increasing vegetation activity [44], especially in the summer and autumn season (Table 5) which reflected the climatic effects of both urbanization and increased agricultural planting around the cities. In terms of seasonal differences in Table 5, the urban warming effect from the OMR method in winter is the largest, but the contribution of urban warming is the largest in summer from the UMR result. This can be attributed to the fact that the rural stations were affected by agricultural irrigation and increasing vegetation activity in summer, so the cooling effects that we can see in Table 5 and Figure 7 enlarged the result of urban minus rural method.

4. Conclusion and Discussion

The above findings demonstrate that urbanization effects essentially exert positive promotions on the regional climate warming in the Beijing-Tianjin-Hebei metropolitan area. Using the UMR method, the urban warming of approximate 0.12°C decade^{-1} accounting for 40% of regional total climate warming (0.30°C decade^{-1}) from 1960 to 2009 and accounting for 25.69% of regional total climate warming from 1979 to 2009 could be found. Using the OMR method, the urban warming intensity is dependent on reanalysis dataset. A very slight UHI could be detected from the ERA, while the urban warming of 0.10°C decade^{-1} and 0.26°C decade^{-1} accounting for 18.77% and 51.19% of regional total warming from 1979 to 2009 could be calculated from the NNR and NDR, respectively. The differences might have partly resulted from diversities of assimilation systems and input datasets. For instance, ERA indirectly assimilated near-surface temperature observations [41], so a very slight UHI could be detected. Thus the ERA dataset is somewhat not optimal for the OMR method in the study area.

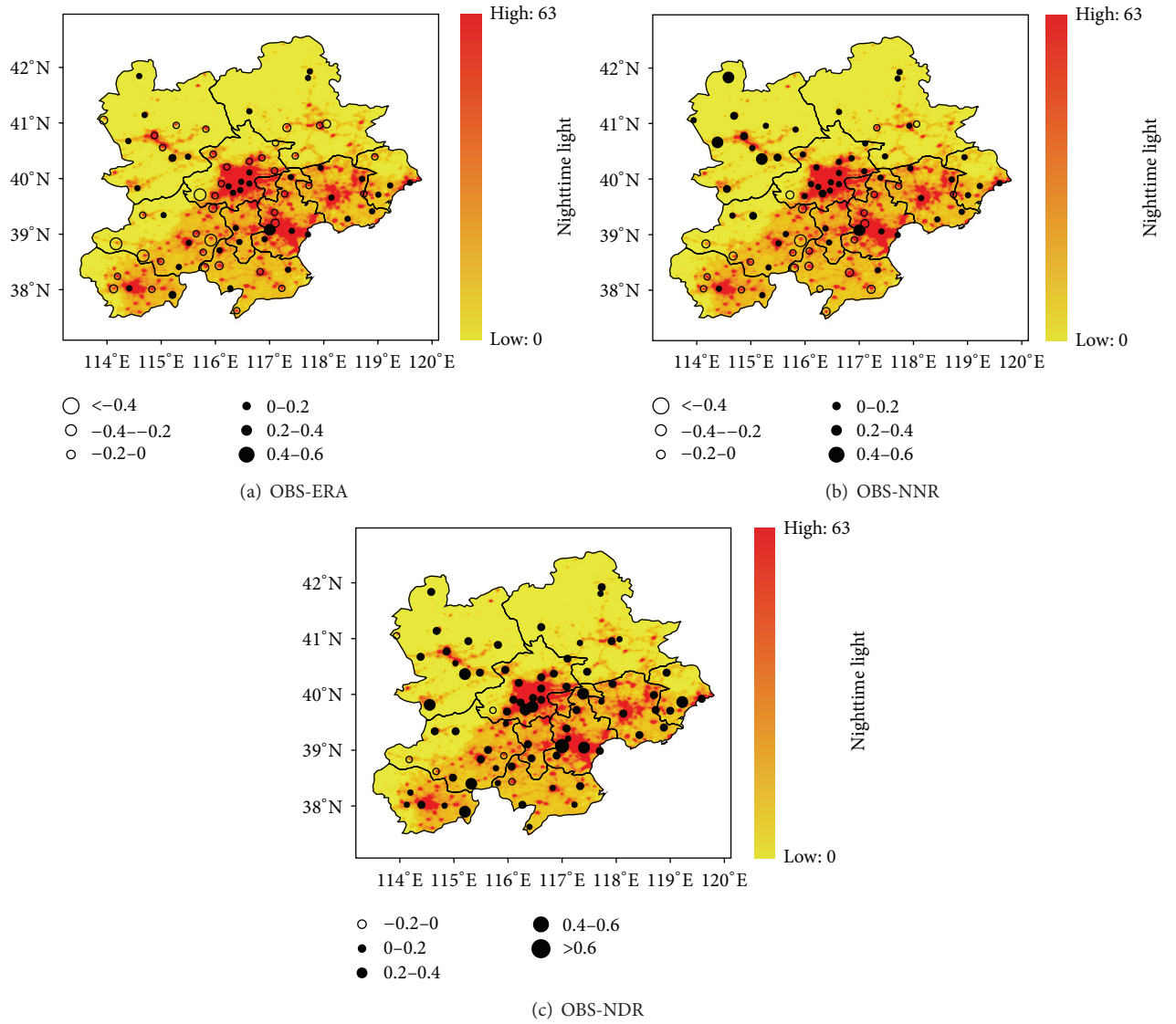

Figure 7: Annual mean temperature trends from the observation minus reanalysis method (°C decade^{-1}) for the (a) ERA, (b) NNR, and (c) NDR. The DMSP/OLS nighttime lights imagery from 2009 is also shown.

Although there are differences among the annual urban warming from ERA, NNR, and NDR, the seasonal cycle patterns from all three datasets are consistent with each other. A stronger UHI occurs in winter and it is weaker in summer from the OMR results, which may reflect strong anthropogenic heating effect in winter. However, the findings from the UMR method demonstrate that the urban warming contributes the largest in summer and smallest in winter. The reverse seasonal cycle pattern of urban warming from the UMR and OMR method implicates that our understanding of the seasonal cycle of urban effects has some uncertainties. As we know that the UMR used the observations entirely. The urban sites are influenced by UHI. Meanwhile, the rural sites are also influenced by other factors, such as vegetation transpiration and moisture evaporation from soil. Vegetation greening enhanced the transpiration and thus cooling of the climate [45]. This cooling effect of agriculture activities can also be found as suggested for the USA [13]. In our study area, vegetation has strong activities in summer. So the strongest urban warming effect in summer from the UMR method might be larger than actual UHI effect. Winter witnessed the lowest contribution from the UMR method that may be attributed to the stronger wind speed in winter in northern China, as UHI intensity decreases with increasing wind speed [33–35].

Therefore, we found some deficiencies of the UMR method that the results from the UMR overestimate the urban warming effect in winter and underestimate it in summer. On the other hand, the results from the OMR method are relatively more convincing although we admit its accuracy depends on the quality of reanalysis dataset.

We used nighttime light data to classify the station groups, but nighttime light can only provide objective urban development information, not details on the physical features

Table 5: Annual and seasonal mean temperature trends from station observation and three reanalysis datasets. Shown are the differences between the observations and the reanalysis datasets (OMR) as well as the differences between the urban and rural sites (UMR) for the different station groups from 1979 to 2009 (°C decade^{-1}). Statistical significance is 0.05 (single asterisk) and 0.01 (double asterisk).

Station group name	Datasets	Winter	Spring	Summer	Autumn	Annual
Large city station	OBS	1.06**	1.00**	0.37**	−0.09*	0.66**
	NDR	0.22**	0.32**	0.21**	0.25**	0.24**
	NNR	0.68**	0.39**	0.34**	0.32**	0.47**
	ERA	0.72**	0.50**	0.49**	0.36**	0.54**
	OMR (NDR)	0.84**	0.68**	0.16**	−0.44**	0.42**
	OMR (NNR)	0.38**	0.61**	0.03	−0.51**	0.19**
	OMR (ERA)	0.34**	0.50**	−0.12**	−0.55**	0.12**
	UMR	0.17**	0.26**	0.42**	−0.02	0.29**
Medium city station	OBS	0.83**	0.86**	0.27**	0.08	0.50**
	NDR	0.24**	0.33**	0.19**	0.24**	0.24**
	NNR	0.68**	0.39**	0.33**	0.30**	0.50**
	ERA	0.73**	0.48**	0.45**	0.36**	0.53**
	OMR (NDR)	0.59**	0.53**	0.08	−0.16**	0.26**
	OMR (NNR)	0.15**	0.47**	−0.06	−0.22**	0.00
	OMR (ERA)	0.10*	0.38**	−0.18**	−0.28**	−0.03
	UMR	−0.06	0.12**	0.32**	0.15**	0.13**
Small city station	OBS	0.64**	0.64**	0.36**	0.43**	0.51**
	NDR	0.21**	0.33**	0.22**	0.26**	0.25**
	NNR	0.64**	0.40**	0.33**	0.32**	0.43**
	ERA	0.65**	0.51**	0.51**	0.32**	0.52**
	OMR (NDR)	0.43**	0.31**	0.14**	0.17**	0.26**
	OMR (NNR)	0.00	0.24**	0.03	0.11**	0.08
	OMR (ERA)	−0.01	0.13**	−0.15**	0.11**	−0.01
	UMR	−0.25**	−0.10*	0.41**	0.50**	0.14**
Rural station	OBS	0.89**	0.74**	−0.05	−0.07	0.37**
	NDR	0.44**	0.33**	0.23**	0.25**	0.26**
	NNR	0.65**	0.41**	0.34**	0.32**	0.43**
	ERA	0.71**	0.51**	0.51**	0.34**	0.52**
	OMR (NDR)	0.45**	0.41**	−0.28**	−0.32**	0.11*
	OMR (NNR)	0.24**	0.33**	−0.39**	−0.39**	−0.06
	OMR (ERA)	0.18**	0.23**	−0.56**	−0.41**	−0.15**

of the sites and surroundings. Urban meteorological observations are more likely to be made within park cool islands than in industrial regions [3]. Therefore, more detailed information of the station locations and their surroundings or extensive remote sensing observation of the stations is needed in future works. Obviously, a more realistic treatment of the land surface and vegetation-climate interaction in models would be helpful for improving our understanding of the effects of LUCC on the climate [46]. Moreover, the surface observed data did not give any information about how high urbanization affects the overlying atmosphere [31]. To seek answers to these issues, the impact of UHI effect on the observed regional climate change needs more in-depth research, so integrated application of the observation analysis and numerical simulation methods will make the conclusions more convincing.

Although there still exist some uncertainties, the results presented in this paper suggest that a large portion of the current surface climate warming over the Beijing-Tianjin-Hebei metropolitan area is caused by urbanization. The results presented in this work suggest that the climatic effects of LUCC should be considered in climate change mitigation strategies during the rapid urbanization of China.

Conflict of Interests

The authors declare that there is no conflict of interests regarding the publication of this paper.

Acknowledgments

This research was sponsored by the Major State Basic Research Development Program of China (973 Program, no. 2010CB950900) and the National Natural Science Foundation of China (41405072).

References

[1] Intergovernmental Panel on Climate Change (IPCC), *Climate Change 2007: The Physical Science Basis: Contribution of Working Group I to the Fourth Assessment Report of the Intergovernmental Panel on Climate Change*, Cambridge University Press, Cambridge, UK, 2007.

[2] T. C. Peterson, K. P. Gallo, J. Lawrimore, T. W. Owen, A. Huang, and D. A. McKittrick, "Global rural temperature trends," *Geophysical Research Letters*, vol. 26, no. 3, pp. 329–332, 1999.

[3] T. C. Peterson, "Assessment of urban versus rural in situ surface temperatures in the contiguous United States: no difference found," *Journal of Climate*, vol. 16, no. 18, pp. 2941–2959, 2003.

[4] P. D. Jones, P. Y. Groisman, M. Coughlan, N. Plummer, W.-C. Wang, and T. R. Karl, "Assessment of urbanization effects in time series of surface air temperature over land," *Nature*, vol. 347, no. 6289, pp. 169–172, 1990.

[5] Q. Li, H. Zhang, X. Liu, and J. Huang, "Urban heat island effect on annual mean temperature during the last 50 years in China," *Theoretical and Applied Climatology*, vol. 79, no. 3-4, pp. 165–174, 2004.

[6] Q. Li, W. Li, P. Si et al., "Assessment of surface air warming in northeast China, with emphasis on the impacts of urbanization," *Theoretical and Applied Climatology*, vol. 99, no. 3-4, pp. 469–478, 2010.

[7] R. A. Pielke Sr., "Land use and climate change," *Science*, vol. 310, no. 5754, pp. 1625–1626, 2005.

[8] T. R. Oke, "City size and the urban heat island," *Atmospheric Environment (1967)*, vol. 7, no. 8, pp. 769–779, 1973.

[9] W. C. Wang, Z. Zeng, and T. R. Karl, "Urban heat islands in China," *Geophysical Research Letters*, vol. 17, no. 13, pp. 2377–2380, 1990.

[10] G. Y. Ren, Y. Q. Zhou, Z. Y. Chu et al., "Urbanization effects on observed surface air temperature trends in North China," *Journal of Climate*, vol. 21, no. 6, pp. 1333–1348, 2008.

[11] E. Kalnay and M. Cai, "Impact of urbanization and land-use change on climate," *Nature*, vol. 423, no. 6939, pp. 528–531, 2003.

[12] Y. K. Lim, M. Cai, E. Kalnay, and L. M. Zhou, "Observational evidence of sensitivity of surface climate changes to land types and urbanization," *Geophysical Research Letters*, vol. 32, no. 22, Article ID L22712, 2005.

[13] S. Fall, D. Niyogi, A. Gluhovsky, R. A. Pielke, E. Kalnay, and G. Rochon, "Impacts of land use land cover on temperature trends over the continental United States: assessment using the North American Regional Reanalysis," *International Journal of Climatology*, vol. 30, no. 13, pp. 1980–1993, 2010.

[14] Y. Hu, W. Dong, and Y. He, "Impact of land surface forcings on mean and extreme temperature in eastern China," *Journal of Geophysical Research: Atmospheres*, vol. 115, no. D19, Article ID D19117, 2010.

[15] M. Liu and H. Tian, "China's land cover and land use change from 1700 to 2005: estimations from high-resolution satellite data and historical archives," *Global Biogeochemical Cycles*, vol. 24, no. 3, Article ID GB3003, 2010.

[16] L. Chen, W. Zhu, X. Zhou, and Z. Zhou, "Characteristics of the heat island effect in Shanghai and its possible mechanism," *Advances in Atmospheric Sciences*, vol. 20, no. 6, pp. 991–1001, 2003.

[17] M. Sachweh and P. Koepke, "Radiation fog and urban climate," *Geophysical Research Letters*, vol. 22, no. 9, pp. 1073–1076, 1995.

[18] Z. Li and Z. Yan, "Application of multiple analysis of series for homogenization to Beijing daily temperature series (1960–2006)," *Advances in Atmospheric Sciences*, vol. 27, no. 4, pp. 777–787, 2010.

[19] Z. Yan, Z. Li, Q. Li, and P. Jones, "Effects of site change and urbanisation in the Beijing temperature series 1977–2006," *International Journal of Climatology*, vol. 30, no. 8, pp. 1226–1234, 2010.

[20] G. Y. Ren, Z. Y. Chu, Z. H. Chen, and Y. Y. Ren, "Implications of temporal change in urban heat island intensity observed at Beijing and Wuhan stations," *Geophysical Research Letters*, vol. 34, no. 5, Article ID L05711, 2007.

[21] Z. Li and Z. Yan, "Homogenized daily mean/maximum/minimum temperature series for China from 1960–2008," *Atmospheric and Oceanic Science Letters*, vol. 2, no. 4, pp. 237–243, 2009.

[22] E. Kalnay, M. Kanamitsu, R. Kistler et al., "The NCEP/NCAR 40-year reanalysis project," *Bulletin of the American Meteorological Society*, vol. 77, no. 3, pp. 437–471, 1996.

[23] M. Kanamitsu, W. Ebisuzaki, J. Woollen et al., "NCEP-DOE AMIP-II reanalysis (R-2)," *Bulletin of the American Meteorological Society*, vol. 83, no. 11, pp. 1631–1559, 2002.

[24] A. Simmons, S. Uppala, D. Dee, and S. Kobayashi, "ERA-interim: new ECMWF reanalysis products from 1989 onwards," *ECMWF Newsletter*, vol. 110, pp. 25–35, 2007.

[25] K. E. Trenberth, "Rural land-use change and climate," *Nature*, vol. 427, no. 6971, p. 213, 2004.

[26] L. Zhou, R. E. Dickinson, Y. Tian et al., "Evidence for a significant urbanization effect on climate in China," *Proceedings of the National Academy of Sciences of the United States of America*, vol. 101, no. 26, pp. 9540–9544, 2004.

[27] O. W. Frauenfeld, T. Zhang, and M. C. Serreze, "Climate change and variability using European Centre for Medium-Range Weather Forecasts reanalysis (ERA-40) temperatures on the Tibetan Plateau," *Journal of Geophysical Research D: Atmospheres*, vol. 110, no. 2, Article ID D02101, 2005.

[28] D. R. Easterling, B. Horton, P. D. Jones et al., "Maximum and minimum temperature trends for the globe," *Science*, vol. 277, no. 5324, pp. 364–367, 1997.

[29] M. G. Kendall, *Rank Correlation Methods*, Charles Griffin and Company, London, UK, 1948.

[30] H. B. Mann, "Nonparametric tests against trend," *Econometrica*, vol. 13, no. 3, pp. 245–259, 1945.

[31] Y. Ezber, O. L. Sen, T. Kindap, and M. Karaca, "Climatic effects of urbanization in Istanbul: a statistical and modeling analysis," *International Journal of Climatology*, vol. 27, no. 5, pp. 667–679, 2007.

[32] M. Tayanç, M. Karaca, and O. Yenigün, "Annual and seasonal air temperature trend patterns of climate change and urbanization effects in relation to air pollutants in Turkey," *Journal of Geophysical Research*, vol. 102, no. D2, pp. 1909–1919, 1997.

[33] A. J. Arnfield, "Two decades of urban climate research: a review of turbulence, exchanges of energy and water, and the urban heat island," *International Journal of Climatology*, vol. 23, no. 1, pp. 1–26, 2003.

[34] G. T. Johnson, T. R. Oke, T. J. Lyons, D. G. Steyn, I. D. Watson, and J. A. Voogt, "Simulation of surface urban heat islands under 'IDEAL' conditions at night part 1: theory and tests against field data," *Boundary-Layer Meteorology*, vol. 56, no. 3, pp. 275–294, 1991.

[35] T. R. Oke, G. T. Johnson, D. G. Steyn, and I. D. Watson, "Simulation of surface urban heat islands under 'ideal' conditions at night part 2: diagnosis of causation," *Boundary-Layer Meteorology*, vol. 56, no. 4, pp. 339–358, 1991.

[36] X. Yang, Y. Hou, and B. Chen, "Observed surface warming induced by urbanization in east China," *Journal of Geophysical Research: Atmospheres*, vol. 116, no. D14, Article ID D14113, 2011.

[37] Y. Du, Z. Xie, Y. Zeng, Y. Shi, and J. Wu, "Impact of urban expansion on regional temperature change in the Yangtze River Delta," *Journal of Geographical Sciences*, vol. 17, no. 4, pp. 387–398, 2007.

[38] P. Jones, D. Lister, and Q. Li, "Urbanization effects in large-scale temperature records, with an emphasis on China," *Journal of Geophysical Research*, vol. 113, Article ID D16122, 2008.

[39] Z. Jingyong, D. Wenjie, W. Lingyun, W. Jiangfeng, C. Peiyan, and D. K. Lee, "Impact of land use changes on surface warming in China," *Advances in Atmospheric Sciences*, vol. 22, no. 3, pp. 343–348, 2005.

[40] X. C. Yang, Y. L. Zhang, M. J. Ding, L. S. Liu, Z. F. Wang, and D. W. Gao, "Observational evidence of the impact of vegetation cover on surface air temperature change in China," *Chinese Journal of Geophysics*, vol. 53, no. 4, pp. 261–269, 2010.

[41] A. J. Simmons, P. D. Jones, V. da Costa Bechtold et al., "Comparison of trends and low-frequency variability in CRU, ERA-40, and NCEP/NCAR analyses of surface air temperature," *Journal of Geophysical Research D: Atmospheres*, vol. 109, no. 24, pp. 1–18, 2004.

[42] G. Huang, "The assessment and difference of the interdecadal variations of climate change in Northern part of China with the NCEP-NCAR and ERA-40 reanalysis data," *Climatic and Environmental Research*, vol. 11, no. 3, pp. 310–320, 2006 (Chinese).

[43] T. B. Zhao and C. B. Fu, "Preliminary comparison and analysis between ERA-40, NCEP-2 reanalysis and observations over China," *Climatic and Environmental Research*, vol. 11, no. 1, pp. 14–32, 2006 (Chinese).

[44] J. Fang, S. Piao, J. He, and W. Ma, "Increasing terrestrial vegetation activity in China, 1982–1999," *Science in China Series C: Life Sciences*, vol. 47, no. 3, pp. 229–240, 2004.

[45] S. J. Jeong, C. H. Ho, K. Y. Kim, and J. H. Jeong, "Reduction of spring warming over East Asia associated with vegetation feedback," *Geophysical Research Letters*, vol. 36, no. 18, Article ID L18705, 2009.

[46] R. Mahmood, R. A. Pielke Sr., K. G. Hubbard et al., "Impacts of land use/land cover change on climate and future research priorities," *Bulletin of the American Meteorological Society*, vol. 91, no. 1, pp. 37–46, 2010.

Hindawi Publishing Corporation
Advances in Meteorology
Volume 2015, Article ID 142036, 6 pages
http://dx.doi.org/10.1155/2015/142036

Research Article

How Long, Narrowly Constructed Wetlands Purify Irrigation Return Water: A Case Study of Ulansuhai Lake, China

Xufeng Mao,[1] Donghai Yuan,[2] Liansheng He,[3] Xiaoyan Wei,[1] Qiong Chen,[1] Libo Bian,[2] and Junqi Li[2]

[1]*College of Life and Geography Sciences, Key Laboratory of Tibetan Plateau Environment and Resources, Ministry of Education, Qinghai Normal University, Qinghai, Xining 810000, China*
[2]*Key Laboratory of Urban Stormwater System and Water Environment, Ministry of Education, Beijing Climate Change Response Research and Education Center, Beijing University of Civil Engineering and Architecture, Beijing 100044, China*
[3]*Water Environment System Project Laboratory, Chinese Research Academy of Environmental Sciences, Beijing 100012, China*

Correspondence should be addressed to Donghai Yuan; yuandonghai@aliyun.com and Liansheng He; heliansheng08@126.com

Received 18 September 2014; Revised 11 March 2015; Accepted 20 April 2015

Academic Editor: Jinwei Dong

The use of constructed wetlands (CWs) in the treatment of raw wastewater in China has proved to be very successful in recent decades. However, it is not known whether surface-flow constructed wetlands can effectively purify irrigation return water. To investigate the performance of a constructed wetland in terms of meeting the goals of pollutant purification, the 8th drainage of Ulansuhai Lake was used for this study. Pollutant removal performances, as well as hydrological characteristic variations in relation to specific characteristics of plants, were investigated utilizing two years of monthly average data. The results indicated that surface-flow constructed wetlands can effectively change the physical characteristics of return water and lead to a sharp decrease in pollutant concentrations. The 1200 m long, narrowly constructed wetland resulted in the average reduction rates of total nitrogen (TN) and total phosphorus (TP) of up to 22.1% and 21.5%, respectively. The overall purification efficient of the constructed wetland presented seasonal variations in four different monitoring periods (May, July, September, and November). Constructed wetlands with multiple types of plants exhibited higher efficiencies in pollutants removal than those with a single type of plant. The current study can provide meaningful information for the treatment of agricultural wastewater.

1. Introduction

Lake eutrophication has become a significant ecological environmental problem facing freshwater lakes in China [1]. High levels of nitrogen in water bodies are a crucial factor contributing to lake eutrophication [2–5]. The exogenous pollution of lakes is primarily caused by large amounts of fertilizer in the agricultural return water [6–8]. Therefore, educing exogenous pollutants has become the key measure in controlling the eutrophication of lakes.

Constructed wetlands serve as a valid treatment measure because investment and running costs are low, and maintenance and management are easy [9]. A CW is an artificial soil-plant-microbe system created as a new or restored habitat for native and migratory wildlife and for anthropogenic discharge, such as wastewater, stormwater runoff, or sewage treatment, for land reclamation after mining and other ecological disruptions [10–15]. Of the various types of CWs [16–19], such as surface- and subsurface-flow wetlands and vertical flow wetlands, each has a different technical characteristic and function [20–23]. Despite their advantages, CWs struggle to remove nutrients such as nitrogen and phosphates [24]. However, a higher pollutants removal efficiency has been demonstrated in constructed wetlands with continuous and intermittent artificial aeration [25–27].

CWs, which are designed to return irrigation water, have certain boundary conditions to meet [6]. For example, compared to general wastewater, irrigation return water flows faster and has a shorter hydraulic detention time. Whether a CW can work effectively in handling fast-flowing irrigation

Table 1: Detailed information of the three segments of the CW.

Segment	Segment I (400 m)	Segment II (400 m)	Segment III (400 m)
Types of plants	*Phragmites communis* *Typha angustifolia* *Iris tectorum Maxim*	*Phragmites communis* *Typha angustifolia*	*Phragmites communis*
Dominant plant	*Phragmites communis*	*Phragmites communis*	*Phragmites communis*
Plant density	30–35/m^2	30–35/m^2	30–35/m^2

return water remains to be seen. Vegetation types, plant density, and the landform may be the decisive factors in the success of return water treatment. To investigate the effects of CWs with irrigation return water, a long, narrow CW was constructed in a drainage system of Ulansuhai Lake in Inner Mongolia. The data of two years' worth of hydrologic and chemical characteristics of the irrigation return water were collected for an accurate assessment of the efficiency of constructed wetlands.

2. Study Area Selection

Ulansuhai Lake (N40°36′–41°03′, E108°43′–108°57′) is located in Ulate County, Inner Mongolia, China. It covers an area of 292 km^2 (Figure 1). Historically, Ulansuhai Lake has played an important role in maintaining the ecological balance of the surrounding region. However, for the past decade, it has faced severe eutrophication due to large amounts of input nutrients in the return water from farmland irrigation. Through nearly ten drainages from the upstream agricultural region, an average of 1088.59×10^3 kg nitrogen and 65.75×10^3 kg phosphor are discharged into the lake each year [28, 29]. The lake is now facing a serious ecosystem health challenge [28, 29].

3. Methods

3.1. The CW and Sampling Sites. The CW analyzed for this study is situated in the 8th drainage. The primary source of the drainage is from spring irrigation (April) and autumn irrigation (October) return water from the upstream region. The largest flowing velocity of these return flows reaches 0.3 m/s. The dimensions of the constructed wetland are 1200 m (L) × 5.0 m (W). The substrates are primarily at a depth of 0.3 m in the natural sediments on the bottom with sparse submerged plants (*Potamogeton pectinatus*). The CW is divided into three segments, according to the dominant aquatic plants. Aquatic plants, including *Phragmites communis, Typha angustifolia, and Iris tectorum Maxim*, were chosen for the current study because they are a dominant species in the region. After nearly two years of cultivation, these plants were growing well in the CW. Detailed information is depicted in Table 1.

A total number of 12 sampling sites were set in the CW at 100 m intervals. Three parallel samples were collected weekly from each segment and stored at −18°C until analysis.

3.2. Physical and Chemical Analyses. Water flow velocity (FV) was measured with a velocimeter, and the suspended solids (SS) were measured using the gravimetric method. TN concentrations were measured using the alkaline potassium persulfate digestion-UV spectrophotometric method, and TP concentrations were measured by the ammonium molybdate spectrophotometric method.

3.3. Removal Ratio and Purification Efficiency Analysis. The removal ratios (RRs) of the total N and P were calculated by (1), in which C_{in} (mg/L) is the N (P) concentration of inflows and C_{out} (mg/L) is the N (P) concentration of outflows:

$$\mathrm{RR} = \frac{C_{in} - C_{out}}{C_{in}} \times 100\%. \quad (1)$$

To determine the removal efficiency (RE) of nutrients at different locations, (2) was developed and applied to calculate RE mg $(\mathrm{L{\cdot}m})^{-1}$:

$$\mathrm{RE}_j = \left| \frac{C_j - C_i}{L} \right|, \quad (2)$$

where C_j is the nutrient concentration at site j; C_i is the nutrient concentration at site i (both in units of mg/L); and L (m) is the straight-line distance between site i and the next site j.

4. Results and Discussion

4.1. Flow Velocity and Suspended Solids Changes in the CW. As depicted in Figure 2, there were obvious changes in the FV (m/s) and SS (mg/L) after entering the CW. The average FV decreased from 0.23 m/s to 0.09 m/s, a decline of 59.4%. The return water was slowed in the CW by the dense aquatic plants. The biggest drop appeared in July (70.23%), which may have been related to the vigorous growth of the aquatic plants in that month. Moreover, a low inflow velocity in July (0.16 m/s) versus the average inflow velocity (0.23 m/s) also proved this theory. No obvious differences were observed in the velocity drop percentages during the other three months, which averaged 55%. Basically, the first part (before 600 m) of the CW had a slightly higher drop (an average of 40%) than that of the back part (an average of 36%).

The average SS levels decreased from 41.0 mg/L to 21.4 mg/L, a total of 48%, indicating that the CW was working well in controlling water quality. The largest concentration (55 mg/L) of SS was observed in May due to the large amounts of fine solids that were brought by the return water of spring irrigation. The largest drop (59%) appeared in July. This was attributed to the vigorous growth of the aquatic plants, as well

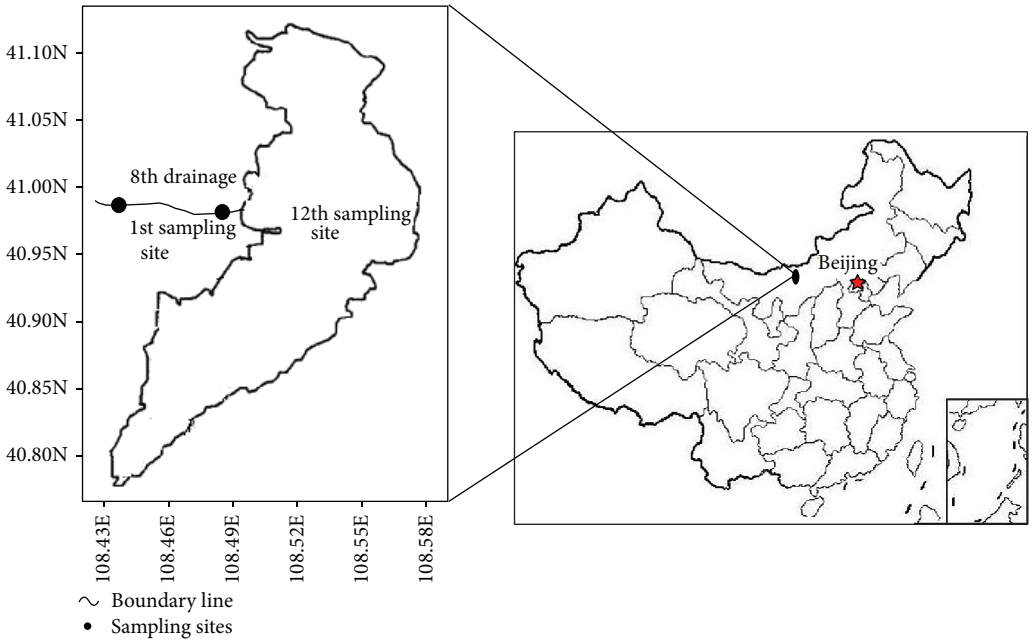

Figure 1: Location of the Ulansuhai Lake.

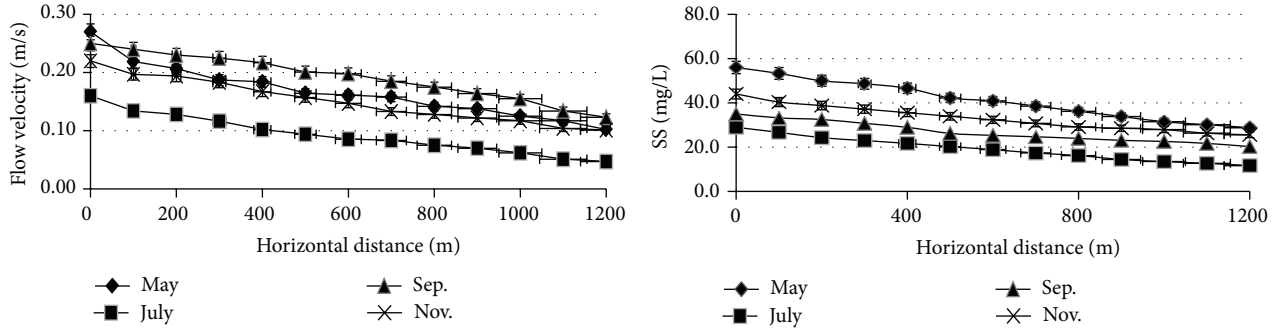

Figure 2: Flow velocity and suspended solids distribution in the CW.

Table 2: Average removal ratio of N and P in four monitoring periods.

	May	July	Sep.	Nov.	Average
RR_N	0.235	0.282	0.203	0.164	22.1%
RR_P	0.224	0.313	0.211	0.113	21.5%

as the lower initial inflow velocity in this region. The average drops in the SS level in the four periods were 48.5%, 59.6%, 42.0%, and 46.8%. The lowest removal ratio of SS appeared in November, when many plants withered up. During the months of May and July, the first part (before 500 m) of the CW had lower removal ratios (an average of 27.5%) than those of the back part (an average of 34%). Conversely, September and November showed higher removal ratios in the front part of the CW (an average of 24%) than those of the back part (an average of 20%). Therefore, the growth conditions of the aquatic plants are thought to be a decisive factor in the removal ratios of suspended solids.

4.2. Removal Ratios of N and P. The average removal ratios of N and P in the four monitored periods are listed in Table 2.

The average RR_{TN} and RR_{TP} were 22.1% and 21.5%, respectively, indicating the CW performed well in handling fast-flowing return wastewater from agricultural irrigation. The RR_{TN} of the four monitored periods was 23.5%, 28.2%, 20.3%, and 16.4%. The largest RR of TN appeared in July and the least RR appeared in November. The RR_{TP} of the four periods was 22.4%, 31.3%, 21.1%, and 11.3%. In consideration of the temporal distribution, July had the largest RR of total N and total P, which was closely related to the exuberant growth of the aquatic plants in that season. Contrarily, a peak removal ratio appeared in November, when most of the aquatic plants were in a stage of growth retardation. Compared to RV of 60%–80%, or higher, in other constructed wetlands [30], the RV of the current study is not high: 22%. However, considering the fast flow of the water, the current CW appeared to be successful in treating pollutants.

The temporal and spatial distributions of RRs in the 8th drainage are depicted in Figure 3. The average RR_{TN} and

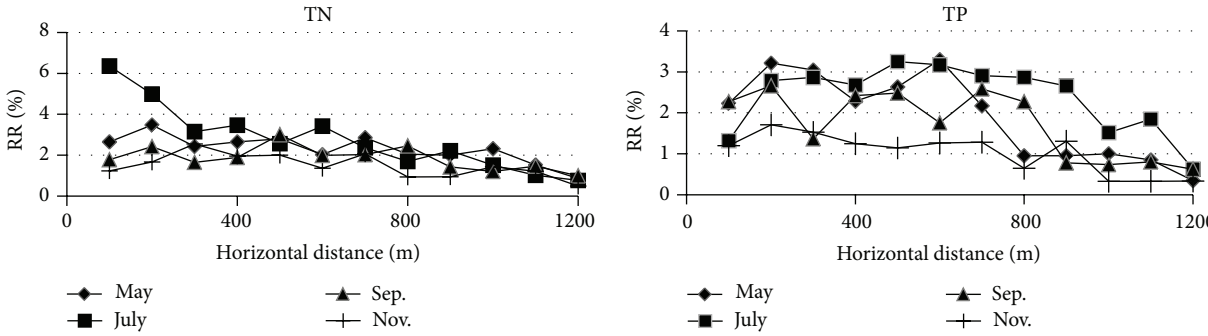

Figure 3: Temporal and spatial distribution of RRs in the 8th drainage.

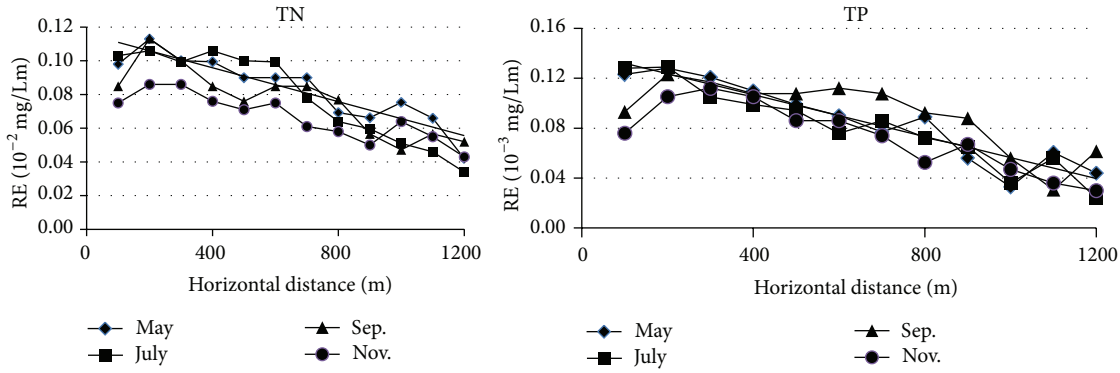

Figure 4: Temporal and spatial distribution of REs in the 8th drainage.

RR_{TP} were 1.96% and 1.79% for each segment, respectively. In general, the RR_{TN} and RR_{TP} decreased with an increased length of the CW. There were no significant differences in the RR_{TN} in the different seasons. The average RRs for the four seasons were 2.11%, 2.51%, 1.76%, and 1.49%, respectively. The average RR_{TN} of each segment in July was slightly higher than the corresponding values of the other three seasons. A similar trend was observed in the temporal distribution of the average RR_{TP}, and the average RR_{TP} in July was slightly higher than that of the other three seasons.

4.3. Temporal and Spatial Distribution of REs. Due to variations in water depth, vegetation, sediments, and so forth, each same-length CW presented a different level of removal efficiency. The results of the t-test ($P < 0.01$) also verified that there were significant differences among the different segments. The temporal and spatial distributions of the REs in the 8th drainage are depicted in Figure 4.

The average RE_{TN} was 0.08×10^{-2} mg (L·m)$^{-1}$ with a slight decreasing tendency. For example, the RE in the first segment was 1.2×10^{-2} mg (L·m)$^{-1}$, which was almost triple the amount in the last segment 0.44×10^{-2} mg (L·m)$^{-1}$. However, the largest RE appeared in the second segment. The high FV of the return water was thought to have contributed to this result. In consideration of temporal distribution of REs, July exhibited the highest average RE_{TN} among the four monitored periods. That was in accordance with the variation law of RVs. A similar variation tendency was observed in the REs of TP. The average RE_{TP} was 0.083×10^{-3} mg (L·m)$^{-1}$ with a slight decreasing tendency. The peak and valley values of RE_{TP} appeared in July (0.13×10^{-3} mg (L·m)$^{-1}$) and November (0.03×10^{-3} mg (L·m)$^{-1}$), respectively. Dissimilarly, the seasonal variation of the RE_{TP} was smaller than the RE_{TN}. Generally, both regularities and complexities existed in the temporal and spatial distributions of the REs. Many factors, including flow flux, velocity, and landform, produced different influences on the experimental results.

4.4. Absorption of N and P by Aquatic Plants. Absorption by aquatic plants is the primary way of reducing N and P in a surface-flow CW [31]. To test the absorption efficiency of different types of aquatic plants, the average percentage concentrations (PC) of TN and TP in the leaves of each plant were analyzed. Related results are illustrated in Figure 5.

The average percentage concentration (APC) of TN in the *Phragmites communis* (2.46% average) was slightly higher than the *Typha angustifolia* (2.08%) and *Iris tectorum* Maxim (2.19%). The seasonal variations of the PC_{TN}, in descending order, were July (3.68%), September (2.65%), May (2.12%), and November (1.39%), which was in accordance with the seasonal order of *Iris tectorum* Maxim. The descending order of the *Typha angustifolia* was slightly different: July (3.18%), May (2.07%), September (1.84%), and November (1.21%). The APC of TP in the *Typha angustifolia* is (3.07%) was slightly higher than in the *Phragmites communis* (2.75%)

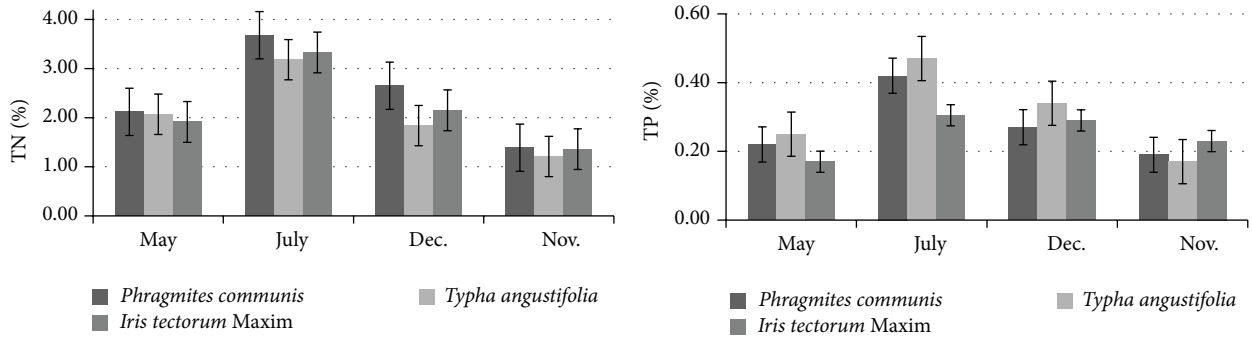

Figure 5: Nutrient concentration in the leaves of tree types of aquatic plants.

and *Iris tectorum* Maxim (2.48%). The APC-TP in July (4.0%) was significantly higher than the other three seasons (2.5%). Different types of plants have different capabilities of absorbing nutrients in different seasons, and further scientific research is needed to obtain more accurate conclusions.

4.5. Correlation between Related Indicators. The Pearson correlation index was used to analyze the simple correlations among five environmental indicators (Table 3).

The FV presented a strong positive correlation with TN ($a = 0.953$, $P < 0.01$) and TP ($a = 0.983$, $P < 0.01$), indicating the high flowing velocity has serious purification effects in CWs. Thus, a smaller drainage gradient (longer hydraulic detention time for water) contributes to a higher RR of pollutants. Additionally, the faster the FV, the higher the SS ($a = 0.987$, $P < 0.01$). Negative correlations existed between the CW length and TN ($a = -0.956$, $P < 0.01$), TP ($a = -0.972$, $P < 0.01$), FV ($a = -0.975$, $P < 0.01$), and SS ($a = -0.989$, $P < 0.01$), indicating the current CW performs well in treating fast-flowing return water. If the surface flow of the CW could be spread to the entire drainage, better purification results would be achieved. Due to the limited data, more quantitative conclusions with respect to the relations among different indicators cannot be provided. For example, if the plant density of each segment for each month were provided, then it could be quantitatively concluded whether the density of the aquatic plants or the type of aquatic plant was the decisive factor of the RR of SS. More experimental data will be collected in future work.

Table 3: Correlation analysis among five environmental indicators.

	TN	TP	FV	SS	CW length
TN	1	.970**	.953**	.954**	−.956**
TP	.970**	1	.983**	.988**	−.972**
FV	.953**	.983**	1	.987**	−.975**
SS	.954**	.988**	.987**	1	−.989**
CW length	−.956**	−.972**	−.975**	−.989**	1

**With a significance level of 0.01.

5. Conclusion

In the current study, a 1200 m long CW was constructed to detect the effectiveness of surface-flow CWs in the treatment of fast-flowing water in Ulansuhai Lake in Northern China. With monitoring and experimental data, the performances of surface-flow CWs were investigated. A preliminary conclusion was that the current CW effectively reduces the nutrient concentrations of the irrigation return water, even with a relatively high water flow velocity. Plant types and the CW length obviously affected the removal ratio of nutrients, and different types of plants had different capabilities of absorbing various nutrients. Moreover, the performance of the CW fluctuated with the seasonal fluctuations of aquatic plants. Overall, there were strong positive correlations among the TN, TP, FV, and SS, suggesting these indicators present similar variation trends in CWs. The length of the CW was an important factor in the RR of TN, TP, and SS. Moreover, plant density had a significant effect on the RE of various pollutants.

A limitation of the current study was the absence of daily, or even hourly, monitoring data. More accurate conclusions can be drawn only after a longer test and operation period. Future work should focus on plant configurations, plant density, and substrate construction in this field. The present study exhibits the great potential of CWs in dealing with agricultural wastewater.

Conflict of Interests

The authors declare no conflict of interests.

Acknowledgments

This work is supported by National Natural Science Foundation of China (no. 51409144, 51209003, and 51478026), the National Water Pollution Control and Management Technology Major Project (no. 2010ZX07320-002 and 2011ZX07301-004), and key projects in the National Science & Technology Pillar Program (no. 2012BAJ21B08).

References

[1] B. Q. Qin, G. Gao, G. Zhu et al., "Lake eutrophication and its ecosystem response," *Chinese Science Bulletin*, vol. 58, no. 9, pp. 961–970, 2013.

[2] J. Vymazal, "Constructed wetlands for wastewater treatment: five decades of experience," *Environmental Science and Technology*, vol. 45, no. 1, pp. 61–69, 2011.

[3] E. M. Seeger, U. Maier, P. Grathwohl, P. Kuschk, and M. Kaestner, "Performance evaluation of different horizontal subsurface flow wetland types by characterization of flow behavior, mass removal and depth-dependent contaminant load," *Water Research*, vol. 47, no. 2, pp. 769–780, 2013.

[4] D. F. Xu, Y. X. Li, A. Howard, and Y. Guan, "Effect of earth worm *Eisenia fetida* and wetland plants on nitrification and denitrification potentials in vertical flow constructed wetland," *Chemosphere*, vol. 92, no. 2, pp. 201–206, 2013.

[5] Y. H. Wang, X. S. Song, Y. Ding, R. Niu, X. Zhao, and D. Yan, "The impact of influent mode on nitrogen removal in horizontal subsurface flow constructed wetlands: a simple analysis of hydraulic efficiency and nutrient distribution," *Ecological Engineering*, vol. 60, pp. 271–275, 2013.

[6] B. C. Braskerud, "Factors affecting nitrogen retention in small constructed wetlands treating agricultural non-point source pollution," *Ecological Engineering*, vol. 18, no. 3, pp. 351–370, 2002.

[7] F. J. Díaz, A. T. O'Geen, and R. A. Dahlgren, "Agricultural pollutant removal by constructed wetlands: implications for water management and design," *Agricultural Water Management*, vol. 104, pp. 171–183, 2012.

[8] A. Sharpley and X. Y. Wang, "Managing agricultural phosphorus for water quality: lessons from the USA and China," *Journal of Environmental Sciences*, vol. 26, no. 9, pp. 1770–1782, 2014.

[9] J. Vymazal, "Removal of nutrients in various types of constructed wetlands. Contaminants in natural and constructed wetlands: pollutant dynamics and control—wetland pollution and control special issue," *Science of the Total Environment*, vol. 380, no. 1–3, pp. 48–65, 2007.

[10] D. J. Spieles and W. J. Mitsch, "The effects of season and hydrologic and chemical loading on nitrate retention in constructed wetlands: a comparison of low- and high-nutrient riverine systems," *Ecological Engineering*, vol. 14, no. 1-2, pp. 77–91, 1999.

[11] M. Scholz, P. Höhn, and R. Minall, "Mature experimental constructed wet-lands treating urban water receiving high metal loads," *Biotechnology Progress*, vol. 18, no. 6, pp. 1257–1264, 2002.

[12] D. P. Mungasavalli and T. Viraraghavan, "Constructed wetlands for stormwater management: a review," *Fresenius Environmental Bulletin*, vol. 15, no. 11, pp. 1363–1372, 2006.

[13] Y. H. Zhang, H. F. Jia, Y. J. Yao, and X. G. Chen, "Evaluating the evolution of the old urban river system of the plain river network in Southern Jiangsu Province, China," *Journal of Food, Agriculture and Environment*, vol. 11, no. 3-4, pp. 2556–2560, 2013.

[14] W. J. Mitsch, "Wetland creation and restoration," in *Encyclopedia of Biodiversity*, S. Levin, Ed., Elsevier, Amsterdam, The Netherlands, 2nd edition, 2013.

[15] H. F. Jia, Z. X. Sun, and G. H. Li, "A four-stage constructed wetland system for treating polluted water from an urban river," *Ecological Engineering*, vol. 71, pp. 48–55, 2014.

[16] H. Wang and J. W. Jawitz, "Hydraulic analysis of cell-network treatment wetlands," *Journal of Hydrology*, vol. 330, no. 3-4, pp. 721–734, 2006.

[17] Y. J. Zhao, B. Liu, W. G. Zhang, Y. Ouyang, and S. Q. An, "Performance of pilot-scale vertical-flow constructed wetlands in responding to variation in influent C/N ratios of simulated urban sewage," *Bioresource Technology*, vol. 101, no. 6, pp. 1693–1700, 2010.

[18] C. Ávila, M. Garfí, and J. García, "Three-stage hybrid constructed wetland system for wastewater treatment and reuse in warm climate regions," *Ecological Engineering*, vol. 61, pp. 43–49, 2013.

[19] J. Vymazal and T. Březinová, "Long term treatment performance of constructed wetlands for wastewater treatment in mountain areas: four case studies from the Czech Republic," *Ecological Engineering*, vol. 71, pp. 578–583, 2014.

[20] M. M. Spacil, J. H. Rodgers Jr., J. W. Castle, and W. Y. Chao, "Performance of a pilot-scale constructed wetland treatment system for selenium, arsenic, and low-molecular-weight organics in simulated fresh produced water," *Environmental Geosciences*, vol. 18, no. 3, pp. 145–156, 2011.

[21] N. Badhe, S. Saha, R. Biswas, and T. Nandy, "Role of algal biofilm in improving the performance of free surface, up-flow constructed wetland," *Bioresource Technology*, vol. 169, pp. 596–604, 2014.

[22] J. Vymazal and L. Kropfelova, *Wastewater Treatment in Constructed Wetlands with Horizontal Subsurface Flow*, vol. 14 of *Series of Environmental Pollution*, Springer, Berlin, Germany, 2008.

[23] E. Ranieri, A. Gorgoglionea, and A. Solimeno, "A comparison between model andexperimental hydraulic performances in a pilot-scale horizontal subsurface flow constructed wetland," *Ecological Engineering*, vol. 60, pp. 45–49, 2013.

[24] J. Vymazal, "The use of hybrid constructed wetlands for wastewater treatment with special attention to nitrogen removal: a review of a recent development," *Water Research*, vol. 47, no. 14, pp. 4795–4811, 2013.

[25] J. L. Fan, W. G. Wang, B. Zhang et al., "Nitrogen removal in intermittently aerated vertical flow constructed wetlands: impact of influent COD/N ratios," *Bioresource Technology*, vol. 143, pp. 461–466, 2013.

[26] P. Foladori, A. R. C. Ortigara, J. Ruaben, and G. Andreottola, "Influence of high organic loads during the summer period on the performance of hybrid constructed wetlands (VSSF + HSSF) treating domestic wastewater in the Alps region," *Water Science and Technology*, vol. 65, no. 5, pp. 890–897, 2012.

[27] M. Tao, F. He, D. Xu, M. Li, and Z. Wu, "How artificial aeration improved sewage treatment of an integrated vertical-flow constructed wetland," *Polish Journal of Environmental Studies*, vol. 19, no. 1, pp. 183–191, 2010.

[28] X. F. Mao, X. W. Wang, Q. Chen, and X. A. Yin, "A PSR-model-based regional health assessment of the lake Ulansuhai," *Polish Journal of Environmental Studies*, vol. 23, no. 6, pp. 2093–2012, 2014.

[29] X. Mao, C. Wang, X. Wei, and Q. Chen, "The distribution of Chlorophyll-a and its' correlation with related indicators in the Ulansuhai Lake, China," *Journal of Environmental Accounting and Management*, vol. 2, no. 2, pp. 123–131, 2014.

[30] X. X. Ju, S. Wu, X. Huang, Y. Zhang, and R. Dong, "How the novel integration of electrolysis in tidal flow constructed wetlands intensifies nutrient removal and odor control," *Bioresource Technology*, vol. 169, pp. 605–613, 2014.

[31] C. H. House, S. W. Broome, and M. T. Hoover, "Treatment of nitrogen and phosphorus by a constructed upland-wetland wastewater treatment system," *Water Science & Technology*, vol. 29, no. 4, pp. 177–184, 1994.